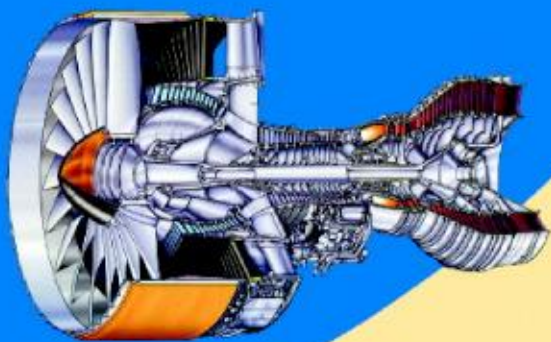


*Fundamentals
of Jet Propulsion
with Applications*

Ronald D. Flack



CAMBRIDGE AEROSPACE SERIES

Fundamentals of Jet Propulsion with Applications

This introductory text on air-breathing jet propulsion focuses on the basic operating principles of jet engines and gas turbines. Previous coursework in fluid mechanics and thermodynamics is elucidated and applied to help the student understand and predict the characteristics of engine components and various types of engines and power gas turbines. Numerous examples help the reader appreciate the methods and differing, representative physical parameters. A capstone chapter integrates the text material in a portion of the book devoted to system matching and analysis so that engine performance can be predicted for both on- and off-design conditions. The book is designed for advanced undergraduate and first-year graduate students in aerospace and mechanical engineering. A basic understanding of fluid dynamics and thermodynamics is presumed. Although aircraft propulsion is the focus, the material can also be used to study ground- and marine-based gas turbines and turbomachinery and some advanced topics in compressors and turbines.

Ronald D. Flack is a Professor, former Chair of Mechanical and Aerospace Engineering, and former Director of the Rotating Machinery and Controls (ROMAC) Industrial Research Program at the University of Virginia. Professor Flack began his career as an analytical compressor design engineer at Pratt & Whitney Aircraft. He is an ASME Fellow and is actively involved in research on experimental internal flows in turbomachines and fluid film bearings.

Fundamentals of Jet Propulsion with Applications

RONALD D. FLACK

University of Virginia



CAMBRIDGE
UNIVERSITY PRESS

CAMBRIDGE UNIVERSITY PRESS
Cambridge, New York, Melbourne, Madrid, Cape Town, Singapore, São Paulo

Cambridge University Press
40 West 20th Street, New York, NY 10011-4211, USA

www.cambridge.org
Information on this title: www.cambridge.org/9780521819831

© Cambridge University Press 2005

This book is in copyright. Subject to statutory exception
and to the provisions of relevant collective licensing agreements,
no reproduction of any part may take place without
the written permission of Cambridge University Press.

First published 2005

Printed in the United States of America

A catalog record for this publication is available from the British Library.

Library of Congress Cataloging in Publication Data

Flack, Ronald D., 1947–

Fundamentals of jet propulsion with applications / Ronald D. Flack, Jr.

p. cm. – (Cambridge aerospace series ; 17)

Includes bibliographical references and index.

ISBN 0-521-81983-0 (hardback)

1. Jet engines. I. Title. II. Series.

TL709.F5953 2005

621.43'52 – dc22

2004020358

On the cover is the PW 4000 Series – 112-inch fan (courtesy of Pratt & Whitney)

ISBN-13 978-0-521-81983-1 hardback

ISBN-10 0-521-81983-0 hardback

Cambridge University Press has no responsibility for
the persistence or accuracy of URLs for external or
third-party Internet Web sites referred to in this book
and does not guarantee that any content on such
Web sites is, or will remain, accurate or appropriate.

Dedicated to Harry K. Herr, Jr.

(Uncle Pete)

who quietly helped me find the right career direction

Contents

<i>Preface</i>	<i>page xv</i>
<i>Foreword</i>	<i>xix</i>

Part I Cycle Analysis

1 Introduction	3
1.1 History of Propulsion Devices and Turbomachines	3
1.2 Cycles	10
1.2.1 Brayton Cycle	10
1.2.2 Brayton Cycle with Regeneration	13
1.2.3 Intercooling	14
1.2.4 Steam-Topping Cycle	15
1.3 Classification of Engines	16
1.3.1 Ramjet	16
1.3.2 Turbojet	17
1.3.3 Turbojet with Afterburner	19
1.3.4 Turbofan	20
1.3.5 Turbofan with Afterburner	25
1.3.6 Turboprop	27
1.3.7 Unducted Fan (UDF)	29
1.3.8 Turboshift	29
1.3.9 Power-Generation Gas Turbines	30
1.3.10 Comparison of Engine Types	32
1.4 Engine Thrust	34
1.4.1 Turbojet	35
1.4.2 Turbofan with a Fan Exhaust	38
1.4.3 Turboprop	40
1.5 Performance Measures	41
1.5.1 Propulsion Measures	41
1.5.2 Power-Generation Measures	42
1.6 Summary	42
2 Ideal Cycle Analysis	46
2.1 Introduction	46
2.2 Components	47
2.2.1 Diffuser	48
2.2.2 Compressor	51
2.2.3 Fan	53
2.2.4 Turbine	55
2.2.5 Propeller	56

4.2.4	Combined Area Changes and Friction	215
4.3	Supersonic	216
4.3.1	Shocks	216
4.3.2	Internal Area Considerations	225
4.3.3	Additive Drag	229
4.3.4	“Starting” an Inlet	232
4.4	Performance Map	235
4.5	Summary	236
5	Nozzles	244
5.1	Introduction	244
5.2	Nonideal Equations	244
5.2.1	Primary Nozzle	244
5.2.2	Fan Nozzle	245
5.2.3	Effects of Efficiency on Nozzle Performance	245
5.3	Converging Nozzle	246
5.4	Converging–Diverging Nozzle	247
5.5	Effects of Pressure Ratios on Engine Performance	256
5.6	Variable Nozzle	258
5.7	Performance Maps	260
5.7.1	Dimensional Analysis	260
5.7.2	Trends	261
5.8	Thrust Reversers and Vectoring	265
5.8.1	Reversers	265
5.8.2	Vectoring	267
5.9	Summary	270
6	Axial Flow Compressors and Fans	276
6.1	Introduction	276
6.2	Geometry	277
6.3	Velocity Polygons or Triangles	283
6.4	Single-Stage Energy Analysis	286
6.4.1	Total Pressure Ratio	287
6.4.2	Percent Reaction	287
6.4.3	Incompressible Flow	288
6.4.4	Relationships of Velocity Polygons to Percent Reaction and Pressure Ratio	289
6.5	Performance Maps	299
6.5.1	Dimensional Analysis	299
6.5.2	Trends	300
6.5.3	Experimental Data	301
6.5.4	Mapping Conventions	302
6.5.5	Surge Control	303
6.6	Limits on Stage Pressure Ratio	303
6.7	Variable Stators	307
6.7.1	Theoretical Reasons	307
6.7.2	Turning Mechanism	312
6.8	Twin Spools	312
6.8.1	Theoretical Reasons	312

6.8.2	Mechanical Implementation	314
6.8.3	Three Spools	315
6.9	Radial Equilibrium	316
6.9.1	Differential Analysis	316
6.9.2	Free Vortex	317
6.9.3	Constant Reaction	318
6.10	Streamline Analysis Method	320
6.10.1	Flow Geometry	321
6.10.2	Working Equations	322
6.11	Performance of a Compressor Stage	331
6.11.1	Velocity Polygons	332
6.11.2	Lift and Drag Coefficients	335
6.11.3	Forces	340
6.11.4	Relationship of Blade Loading and Performance	341
6.11.5	Effects of Parameters	342
6.11.6	Empiricism Using Cascade Data	346
6.11.7	Further Empiricism	351
6.11.8	Implementation of General Method	354
6.12	Summary	355
7	Centrifugal Compressors	374
7.1	Introduction	374
7.2	Geometry	374
7.3	Velocity Polygons or Triangles	378
7.4	Single-Stage Energy Analysis	380
7.4.1	Total Pressure Ratio	381
7.4.2	Incompressible Flow (Hydraulic pumps)	381
7.4.3	Slip	382
7.4.4	Relationships of Velocity Polygons to Pressure Ratio	386
7.5	Performance Maps	390
7.5.1	Dimensional Analysis	390
7.5.2	Mapping Conventions	390
7.6	Impeller Design Geometries	391
7.6.1	Eye Diameter	392
7.6.2	Basic Blade Shapes	392
7.6.3	Blade Stresses	392
7.6.4	Number of Blades	393
7.6.5	Blade Design	394
7.7	Vaned Diffusers	394
7.8	Summary	397
8	Axial Flow Turbines	406
8.1	Introduction	406
8.2	Geometry	407
8.2.1	Configuration	407
8.2.2	Comparison with Axial Flow Compressors	409
8.3	Velocity Polygons or Triangles	413
8.4	Single-Stage Energy Analysis	416
8.4.1	Total Pressure Ratio	417

8.4.2	Percent Reaction	417
8.4.3	Incompressible Flow (Hydraulic Turbines)	418
8.4.4	Relationships of Velocity Polygons to Percent Reaction and Performance	419
8.5	Performance Maps	425
8.5.1	Dimensional Analysis	425
8.5.2	Mapping Conventions	425
8.6	Thermal Limits of Blades and Vanes	427
8.6.1	Blade Cooling	428
8.6.2	Blade and Vane Materials	429
8.6.3	Blade and Vane Manufacture	430
8.7	Streamline Analysis Method	433
8.8	Summary	434
9	Combustors and Afterburners	440
9.1	Introduction	440
9.2	Geometries	441
9.2.1	Primary Combustors	441
9.2.2	Afterburners	445
9.3	Flame Stability, Ignition, and Engine Starting	447
9.3.1	Flame Stability	447
9.3.2	Ignition and Engine Starting	448
9.4	Adiabatic Flame Temperature	449
9.4.1	Chemistry	450
9.4.2	Thermodynamics	451
9.5	Pressure Losses	456
9.5.1	Rayleigh Line Flow	456
9.5.2	Fanno Line Flow	457
9.5.3	Combined Heat Addition and Friction	458
9.5.4	Flow with a Drag Object	459
9.6	Performance Maps	461
9.6.1	Dimensional Analysis	461
9.6.2	Trends	462
9.7	Fuel Types and Properties	463
9.8	Summary	465
10	Ducts and Mixers	471
10.1	Introduction	471
10.2	Total Pressure Losses	471
10.2.1	Fanno Line Flow	471
10.2.2	Mixing Process	473
10.2.3	Flow with a Drag Object	475
10.3	Summary	477
Part III System Matching and Analysis		
11	Matching of Gas Turbine Components	481
11.1	Introduction	481
11.2	Component Matching	482

11.2.1	Gas Generator	482
11.2.2	Jet Engine	484
11.2.3	Power-Generation Gas Turbine	486
11.2.4	Component Modeling	487
11.2.5	Solution of Matching Problem	492
11.2.6	Other Applications	499
11.2.7	Dynamic or Transient Response	499
11.3	Matching of Engine and Aircraft	508
11.4	Use of Matching and Cycle Analysis in Second-Stage Design	511
11.5	Summary	512
Part IV Appendixes		
Appendix A	Standard Atmosphere	527
Appendix B	Isentropic Flow Tables	530
Appendix C	Fanno Line Flow Tables	548
Appendix D	Rayleigh Line Flow Tables	558
Appendix E	Normal Shock Flow Tables	568
Appendix F	Common Conversions	583
Appendix G	Notes on Iteration Methods	585
	G.1 Introduction	585
	G.2 Regula Falsi	585
	G.3 Successive Substitutions	588
Appendix H	One-Dimensional Compressible Flow	591
	H.1 Introduction	591
	H.2 Ideal Gas Equations and Stagnation Properties	591
	H.3 Variable Specific Heats	593
	H.4 Isentropic Flow with Area Change	595
	H.5 Fanno Line Flow	597
	H.6 Rayleigh Line Flow	598
	H.7 Normal Shocks	600
	H.8 Oblique Planar Shocks	601
	H.9 Flow with a Drag Object	604
	H.10 Mixing Processes	605
	H.11 Generalized One-Dimensional Compressible Flow	607
	H.12 Combined Area Changes and Friction	608
	H.13 Combined Heat Addition and Friction	609
	H.14 Combined Area Changes, Heat Addition, and Friction	610
Appendix I	Turbomachinery Fundamentals	613
	I.1 Introduction	613
	I.2 Single-Stage Energy Analysis	613
	I.2.1 Total Pressure Ratio	613
	I.2.2 Percent Reaction	618
	I.2.3 Incompressible Flow	618

I.3	Similitude	620
I.3.1	Dimensional Analysis – Compressible Flow	620
	<i>References</i>	623
	<i>Answers to Selected Problems</i>	628
	<i>Index</i>	631



Preface

My goal with this project is to repay the gas turbine industry for the rewarding profession it has provided for me over the course of more than three decades. At this point in my career, student education is a real passion for me and this book is one way I can archive and share experiences with students. I have written this text thinking back to what I would have liked as an undergraduate student nearly 40 years ago. Thus, this work has been tailored to be a very student friendly text.

This book is intended to serve primarily as an introductory text in air-breathing jet propulsion. It is directed at upper-level undergraduate students in mechanical and aerospace engineering. A basic understanding of fluid mechanics, gas dynamics, and thermodynamics is presumed; however, thermodynamics is reviewed, and an appendix on gas dynamics is included for reference. Although the work is entitled *Jet Propulsion*, it can well be used to understand the fundamentals of “aeroderivative” ground- or marine-based gas turbines such as those used for marine propulsion, ground transportation, or power generation. Although turbomachinery is not the primary target of the text, it is the book’s secondary focus, and thus the fundamentals of, and some advanced topics in, compressors and turbines are also covered.

This text covers the basic operating principles of jet engines and gas turbines. Both the fundamental mathematics and hardware are addressed. Numerous examples based on modern engines are included so that students can grasp the methods and acquire an appreciation of different representative physical parameters. For this reason, development of “plug-and-chug” equations or “formulas” is de-emphasized, and the solutions of all examples are logically and methodically presented. The examples are an integral part of the presentation and are not intended to be side issues or optional reading. A student is expected to understand the individual steps of analyzing an entire engine or an individual component. By the use of examples and homework problems a student is also expected to develop an appreciation of trend analysis; that is, if one component is changed by a known amount, how will the overall engine performance change? Both British and SI units are used in the examples. A strong and unique feature of the book is a capstone chapter (Chapter 11) that integrates the previous 10 chapters into a section on component matching. From this integrated analysis, engine performance can be predicted for both on- and off-design conditions.

Subjects are treated with equal emphasis, and the parts of the book are interdependent in such a way that each step builds on the previous one. The presentation is organized into three basic areas as follows:

1. Cycle Analysis (Chapters 1 through 3) – In these chapters, different engines are defined, the fundamental thermodynamic and gas dynamic behavior of the various components are covered, and ideal and nonideal analyses are performed on each type of engine considered as a whole. Fundamental applicable thermodynamic principles are reviewed in detail. The performance of each individual component is assumed to be known at this point in the text. Trend studies and quantitative analysis methodologies are presented. The effects of nonideal characteristics are

demonstrated by comparing performance results with those that would occur if the characteristics were ideal.

2. **Component Analysis** (Chapters 4 through 10) – In these chapters the components are studied and analyzed individually using thermodynamic, fluid mechanical, and gas dynamic analyses. Diffusers, nozzles, axial flow compressors, centrifugal compressors, axial flow turbines, combustors and afterburners, ducts, and mixers are covered. Individual component performance can be predicted and analyzed, including on- and off-design performance and “maps,” thus expanding on the fundamentals covered in cycle analyses. The effects on component performance of different geometries for the various components are covered. Some advanced topics are included in these sections.
3. **System Analysis and Matching** (Chapter 11) – This chapter serves as a capstone chapter and integrates the component analyses and characteristic “maps” into generalized cycle analyses. Individual component performance and overall engine performance are predicted and analyzed simultaneously. Both on- and off-design analyses are included, and prediction of engine parameters such as the engine operating line and compressor surge margin is possible.

Every chapter begins with an introduction providing an historical overview and outlining the objectives of the chapter. At the end of every chapter, a summary reviews the important points and specifies which analyses a student should be able to perform. In addition, appendixes are included that review or introduce compressible flow fundamentals, general concepts of turbomachinery, and general concepts of iteration methods – all of which are a common thread throughout the text.

The text is well suited to independent study by students or practicing engineers. Several topics are beyond what a one-semester undergraduate course in gas turbines can include. For this reason, the book should also be a valuable reference text.

A suite of user-friendly computer programs is available to instructors through the Cambridge Web site. The programs complement the text, but it can stand alone without the programs. I have used the programs in a variety of ways. I have found the programs (especially the cycle analysis, turbomachinery, and matching programs) to be most useful for design problems, and this approach reduces the need for repetitious calculations. In general, I provide the programs to students once they have demonstrated proficiency at making the fundamental calculations. The programs are as follows:

Atmosphere – Table for standard atmosphere.

Simple1D – Compressible one-dimensional calculations or tables for Fanno line, Rayleigh line, isentropic, normal shock flow, or constant static temperature flows.

General1D – Computations for combined Fanno line, Rayleigh line, drag object, mixing flow, and area change.

Shock – Calculations for normal, planar oblique, or conical oblique shocks.

Nozzle – Calculations for shockless nozzle flow.

JetEngineCycle – Cycle analysis of ideal and real ramjets, turbojets, turbofans, and turboprops.

PowerGTCycle – Cycle analysis of power-generation gas turbines with regenerators.

Turbomachinery – Mean-line turbomachinery calculations for axial and radial compressors and axial and radial turbines.

SLA – Three-dimensional streamline analysis of axial flow compressors or turbines with radial equilibrium with several specifiable boundary condition types.

CompressorPerf – Fundamental prediction of compressor stage efficiency due to lift and drag characteristics and incidence flow.

Kerosene – Adiabatic flame temperature of n -decane for different fuel-to-air mix ratios.

JetEngineMatch – Given diffuser, compressor, burner, turbine, and nozzle maps are matched to find overall turbojet engine performance and airframe drag maps are used to match engines with an aircraft.

PowerGTMatch – Given inlet, compressor, burner, turbine, regenerator, and exhaust maps are matched to find overall power-generation gas turbine performance.

A solutions manual (PDF) to the more than 325 end-of-chapter problems is also available to instructors. Please email Cambridge University Press at: solutions@cambridge.org.

This book was primarily written in two stages: first from 1988 to 1993 and then from 2000 to 2004 – the void being while I was Chair of our department. The bulk of the writing was done at the University of Virginia, although a portion of the book was written at Universität Karlsruhe while I was on sabbatical (twice). Some chapters were used in my jet propulsion class starting in 1989, and I began to use full draft versions of the text starting in 1992. In the course of this extended use, students have suggested many changes, which I have included; more than 300 students have been very important to the development of the text. I have also used portions of draft versions of the text in a graduate-level turbomachinery course, and graduate students have also made very useful suggestions. Over the past 15 years, I have incorporated many comments from students, and I took such suggestions very seriously. I am indebted to the numerous students who contributed in this way.

This project has been most fulfilling and it has been a culminating point in my own life. Through the writing and the resulting input from students, I have become a better and more patient teacher in all aspects of my life. Acknowledgments and thanks are in order starting with Mac Mellor and Sigmar Wittig, back in 1968, and then Doyle Thompson, in 1971, who triggered my interest in gas dynamics and gas turbines with projects at Purdue – the concepts have been central to my professional life since then. Certainly, thanks are due to my colleagues at both the University of Virginia and Universität Karlsruhe for their collegiality. Special appreciation is due to all of my graduate students at the University of Virginia, Universität Karlsruhe, and Ruhr Universität Bochum, who helped keep me young through the years. Portions of the proceeds of this text are going back to the University of Virginia, Universität Karlsruhe, and Purdue to help further undergraduate gas turbine education.

My family has been a timeless inspiration to me. Missy and Todd are both great kids who allowed me to forget work when needed, and now my granddaughters Mya and Maddie enable me again to see how much fun little ones can be. And then there are Zell and Dieter – one could not want better companions.

I cannot say enough about Nancy, my soul mate and best friend since 1966. This book would never have come to fruition without her positive influence. She helped me to realize the true value of life and to keep the proper perspectives.

Ron Flack
2004

Foreword

The book entitled *Fundamentals of Jet Propulsion with Applications*, by Ronald D. Flack, will satisfy the strong need for a comprehensive, modern book on the principles of propulsion – both as a textbook for propulsion courses and as a reference for the practicing engineer.

Professor Flack has written an exciting book for students of aerospace engineering and design. His book offers a combination of theory, practical examples, and analysis utilizing information from actual aerospace databases to motivate students; illustrate, and demonstrate physical phenomena such as the principles behind propulsion cycles, the fundamental thermofluids governing the performance of – and flow mechanisms in – propulsion components, and insight into propulsion-system matching.

The text is directed at upper-level undergraduate students in mechanical and aerospace engineering, although some topics could be taught at the graduate level. A basic understanding of fluid mechanics, gas dynamics, and thermodynamics is presumed, although most principles are thoroughly reviewed early in the book and in the appendixes. Propulsion is the primary thrust, but the material can also be used for the fundamentals of ground- and marine-based gas turbines. Turbomachinery is a secondary target, and the fundamentals and some advanced topics in compressors and turbines are covered.

The specific and unique contributions of this book and its strengths are that fundamental mathematics and modern hardware are both covered; moreover, subjects are treated with equal emphasis. Furthermore, the author uses an integrated approach to the text in which each step builds on the previous one (cycle analyses and engine design are treated first, component analysis and design are treated next, and finally and uniquely, component matching and its influence on cycle analysis are addressed to bring all of the previous subjects together). The latter feature is a very great strength of the text. In contrast to most other texts, the author incorporates many numerical examples representing current engines and components to demonstrate the main points. The examples are a major component of the text, and the author uses them to stress important points. In working through these examples, the author de-emphasizes the use of “ready-made formulas.” Numerous trend analyses are performed and presented to give students a “feel” of what can be expected if engine or component parameters are varied. The book can be used as a text for a university course or as a self-learning reference text.

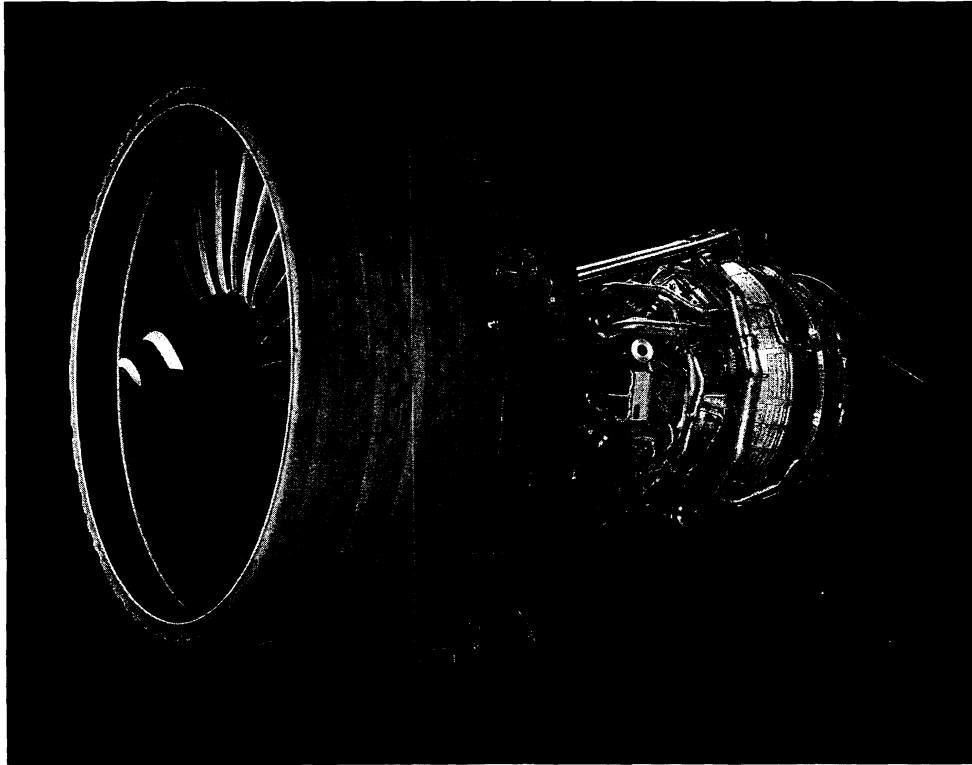
At the beginning of every chapter the author presents an introduction outlining some history as well as the objectives of the chapter. At the end of every chapter he provides a summary recalling the key points of the chapter and places the chapter in the context of other chapters. The text is well suited for independent study by students or practicing engineers. Several topics are covered that are beyond those typically included in a one-semester undergraduate gas turbine course. As a result, the book should also be a valuable reference text.

As a teacher of an aerospace engineering course, I strongly recommend the book to college engineering students and teachers, practicing engineers, and members of the general

public who want to think and be challenged to solve problems and learn the technical fundamentals of propulsion.

Abraham Engeda
Professor of Mechanical Engineering and
Director of Turbomachinery Laboratory
Michigan State University
2004

Cycle Analysis



GE90-94B
(courtesy of General Electric Aircraft Engines)

Introduction

1.1. History of Propulsion Devices and Turbomachines

Manmade propulsion devices have existed for many centuries, and natural devices have developed through evolution. Most modern engines and gas turbines have one common denominator: compressors and turbines or “turbomachines.” Several of the early turbomachines and propulsive devices will be described in this brief introduction before modern engines are considered. Included are some familiar names not usually associated with turbomachines or propulsion. Many of the manmade devices were developed by trial and error and represent early attempts at design engineering, and yet some were quite sophisticated for their time. Wilson (1982), Billington (1996), ASME (1997), Engeda (1998), St. Peter (1999), and others all present very interesting introductions to some of this history supplemented by photographs.

One of the earliest manmade turbomachines was the aeolipile of Heron (often called “Hero” of Alexandria), as shown in Figure 1.1. This device was conceived around 100 B.C. It operated with a plenum chamber filled with water, which was heated to a boiling condition. The steam was fed through tubes to a sphere mounted on a hollow shaft. Two exhaust nozzles located on opposite sides of the sphere and pointing in opposite directions were used to direct the steam with high velocity and rotate the sphere with torque (from the moment of momentum) around an axis – a reaction machine. By attaching ropes to the axial shaft, Heron used the developed power to perform tasks such as opening temple doors.

In about A.D. 1232, Wan Hu developed and tested the Chinese rocket sled, which was driven by an early version of the solid propulsion rocket. Fuel was burned in a closed container, and the resulting hot gases were exhausted through a nozzle, which produced high exit velocities and thus the thrust. Tragically, this device resulted in one of the earliest reported deaths from propulsion devices, for Hu was killed during its testing.

Leonardo da Vinci also contributed to the field of turbomachines with his chimney jack in 1500. This device was a turbine within the chimney that used the free convection of hot rising gases to drive a set of vanes rotationally. The rotation was redirected, using a set of gears, to turn game in the chimney above the fire. Thus, the game was evenly cooked. At the same time, da Vinci also contributed to turbomachinery development with his conception of a helicopter producing lift with a large “screw.”

From the conceptions of Robert Hooke and others, windmills (Fig. 1.2) – actually large wind turbines – were extensively used in the Netherlands for both water pumping and milling from the 1600s to the 1800s. These huge wind turbines (more than 50 m in diameter) made use of the flat terrain and strong and steady winds and turned at low rotational speeds. Through a series of wooden “bevel” gears and couplings, the torsional power was turned and directed to ground level to provide usable power. Some of the early pumping applications of “windmills” in the Netherlands used an inverse of a water wheel – that is, the “buckets” on the wheel scooped water up at a low level and dropped it over a dyke to a higher level, thus, recovering land below sea level from flooding.

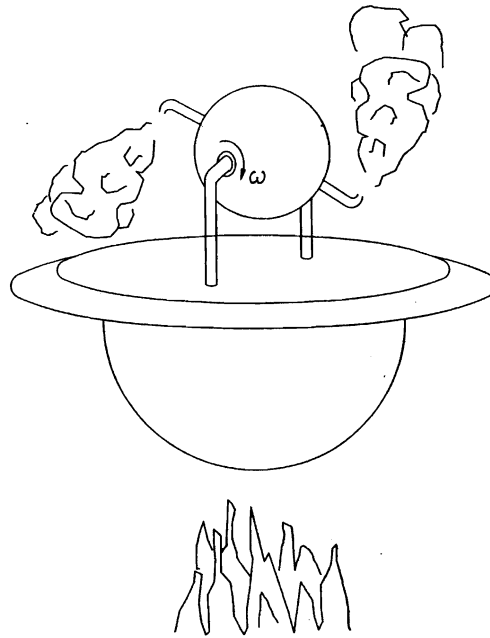


Figure 1.1 Hero's aeolipile, 100 B.C.

Giovanni de Branca developed a gas turbine in 1629 that was an early version of an impulse turbine. Branca used a boiling, pressurized vessel of steam and a nozzle to drive a set of radial blades on a shaft with the high-velocity steam. The rotation was then redirected with a set of bevel gears for a mechanical drive.

In 1687, Sir Isaac Newton contributed the steam wagon, which may be viewed as an early automobile. He used a tank of boiling water constantly heated by a fire onboard the wagon and a small nozzle to direct the steam to develop thrust. By adjusting the fire intensity, the valve on the nozzle, and the nozzle direction, he was able to regulate the exhaust velocity and thus the thrust level as well as thrust direction. Although the concept was viable, the required power exceeded that available for reasonable vehicle speeds. Thus, the idea was abandoned.

Denis Papin developed the first scientific conceptions of the principles of a pump impeller in a volute in 1689, although remains of early wooden centrifugal pumps from as early as the fifth century A.D. have been found. In 1754, Leonhard Euler, a well-known figure in mathematics and fluids, further developed the science of pumps and today has the ideal pump performance named after him – “Euler head.” Much later, in 1818, the first centrifugal pumps were produced commercially in the United States.

Garonne developed a water-driven mill in 1730. This mill was an early venture with a water (or hydraulic) turbine. Water at a high hydrostatic head from a dammed river was used to direct water onto a conoid (an impeller) with a set of conical vanes and turn them. The rotating shaft drove a grinding mill above the turbine for grain preparation. The same concept was applied in 1882 in Wisconsin, where a radial inflow hydraulic turbine was used to generate electricity.

Gifford was the first to use a controlled propulsion device successfully to drive an “aircraft.” In 1851, he used a steam engine to power a propeller-driven dirigible. The total load



Figure 1.2 Dutch windmill (R. Flack).

required to generate power was obviously quite large because of the engine size, combustion fuel, and water used for boiling, making the idea impractical.

In 1883, Carl de Laval developed the so-called Hero-type *reaction* turbine shown in Figure 1.3 utilized for early water turbines. Water flowed through hollow spokes, formed high-velocity jets normal to, and at the end of, the spokes, and was used to turn a shaft. This is the basic type of rotating sprinkler head used to convert potential energy from a static body of water to a rotating shaft with torque.

As another example, in 1897 de Laval developed the *impulse* steam turbine (Fig. 1.4). This utilized jets of steam and turning vanes or blades mounted on a rotating shaft. The high-speed steam impinged on the blades and was turned, thus imparting momentum to the blades and therefore rotating the shaft and providing torque.

Over the next quarter century, rapid developments took place. Gas and steam turbines came into wide use for ships and power generation. For example, in 1891 the first steam turbine was developed by Charles Parsons. This device was a predecessor to the modern gas turbine. It had two separate components: the steam generator-combustor and the turbine.

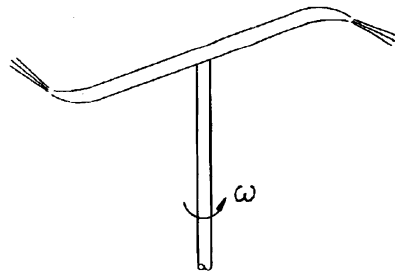


Figure 1.3 DeLaval "Hero" reaction turbine, 1883.

The generator-combustor developed a high-pressure steam, which was directed as a high-velocity jet into the steam turbine. In the early 1800s, ship propellers or "screws," which are themselves a variety of turbomachines, were invented by Richard Trevithick and others. Parsons' steam turbine, rated at 2100 hp (1570 kW), was used to power such a propeller directly on the 100-ft (30.5-m)-long ocean vessel *Turbinia* in 1897 and drove it at 34 kt, which was a true feat if one considers that most seaworthy vehicles were slow-moving sail craft.

In 1912, a large (64-stage) steam turbine facility was installed in Chicago and ran at 750 rpm to deliver 25 MW of electrical power. In the 1920s, several General Electric 40-MW units were put in service. These ran at 1800 rpm and had 19 stages. Although many refinements and advancements have been made to steam-turbine technology since this installation, the same basic design is still in use in power plants throughout the world.

In the 1930s, simultaneous and strictly independent research and development were performed in Great Britain and Germany on gas turbines. In 1930, Sir Frank Whittle (Great Britain) patented the modern propulsion gas turbine (Fig. 1.5). The engine rotated at almost 18,000 rpm and developed a thrust of 1000 lbf (4450 N). It had a centrifugal flow compressor and a reverse-flow combustion chamber; that is, the flow in the burner was opposite in direction to the net flow of air in the engine – a concept still used for small engines to conserve space. This gas turbine was first installed on an aircraft in 1941 after several years of development. Meher-Homji (1997a) reviews this early effort in great detail. Dunham (2000) reviews the efforts of A. R. Howell, also of Great Britain, which complemented the work of Whittle.

In 1939, the first flight using a gas turbine took place in Germany. Hans von Ohain patented the engine for this aircraft in 1936 (Fig. 1.6), which developed 1100 lbf (4890 N) of thrust. This engine had a combination of axial flow and centrifugal compressor stages. In general, this gas turbine and further developmental engines were superior to the British counterparts in efficiency and durability. A few years later the German Junkers Jumo

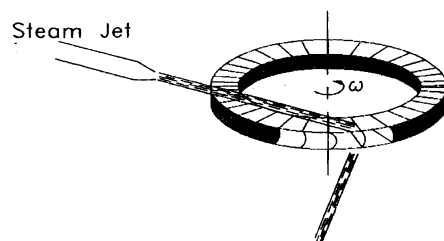


Figure 1.4 DeLaval impulse turbine, 1897.

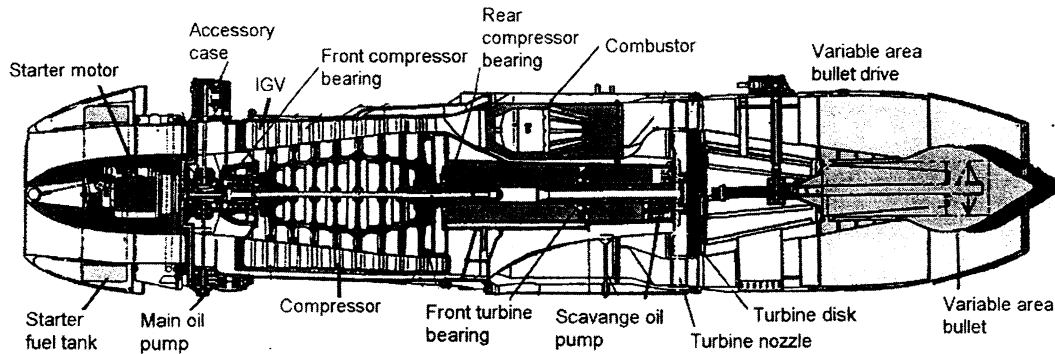


Figure 1.7 Junkers' Jumo 004 (courtesy of Cyrus Meher-Homji).

004 (Fig. 1.7), designed by Anselm Franz, was the first engine to be mass produced. Meher-Homji (1996, 1997b, and 1999) also presents an interesting review of these early developments. Other historical perspectives on turbomachines and propulsion are offered by Heppenheimer (1993), St. Peter (1999), and Wilson (1982). Today both Whittle and von Ohain are credited equally with the invention of the jet engine.

Also during the 1930s, the first high-speed turbopumps for rocket propulsion were developed in Germany for the V2. Hot exhaust gases from a combustor were expanded by turbines and drove the high-speed oxygen and hydrogen cryopumps, which in turn pumped or compressed the cryofluids, readying them for the combustor. The maiden voyage of the V2 occurred in 1940, and its introduction allowed for previously unattainable long-range delivery of warheads. This type of propulsion inspired modern rocket technology and is still the basic operating principle for modern rocketry.

In 1942, General Electric (GE) developed what is considered the first American jet engine, the GE I-A. This was a small engine that generated 1300 lbf of thrust and was a copy of the early Whittle engine. The GE I-A was developed into the larger GE J-31 (or I-16), which

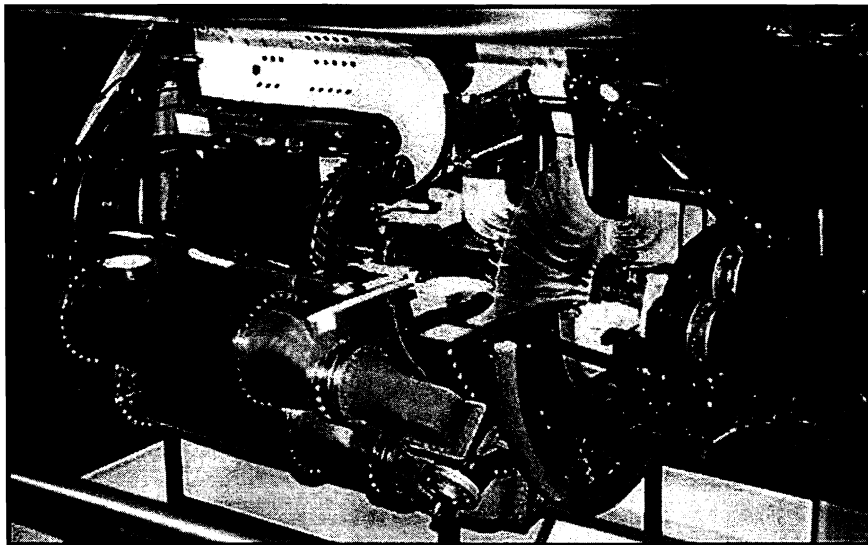


Figure 1.8 General Electric J-31 (courtesy of Wright Patterson Air Force Base (WPAFB)).

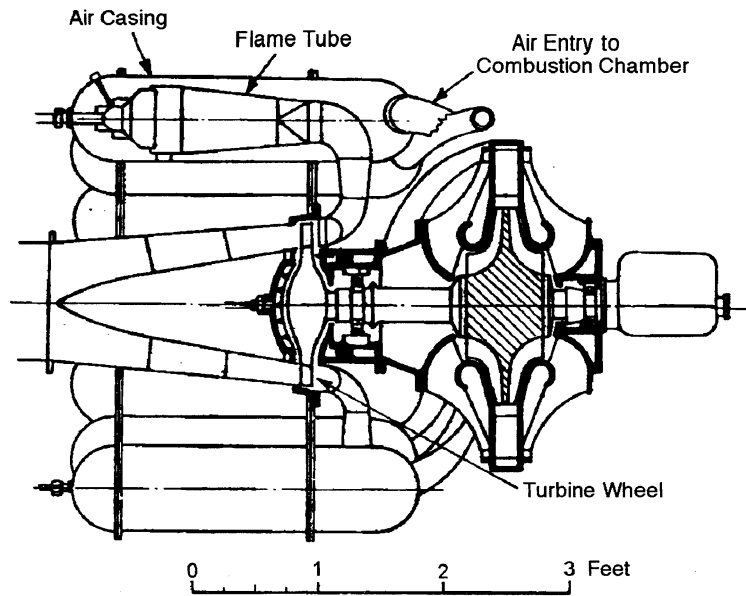


Figure 1.5 Whittle's WU1 jet engine (from Fig. 105 Lloyd [1945] reproduced with permission of the Council of the Institution of Mechanical Engineers).

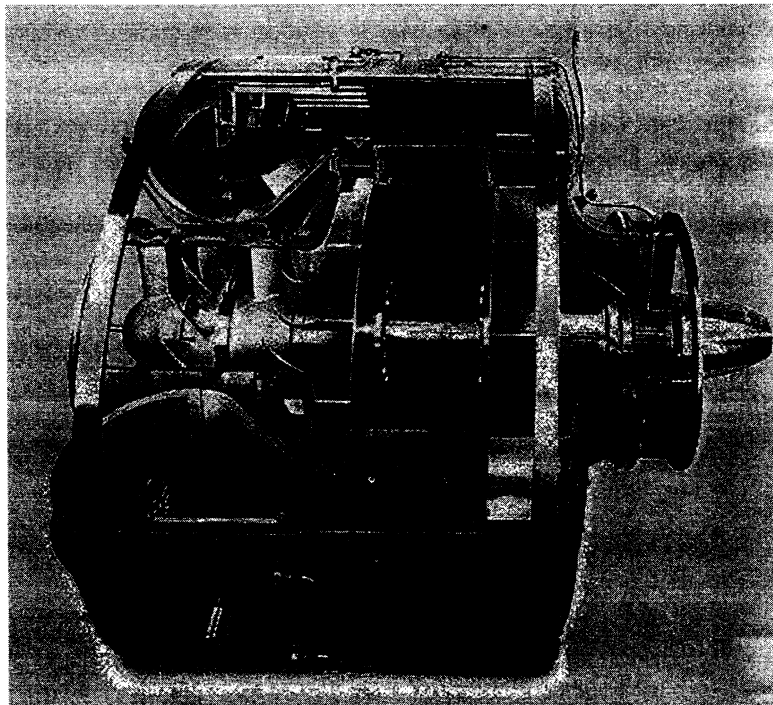
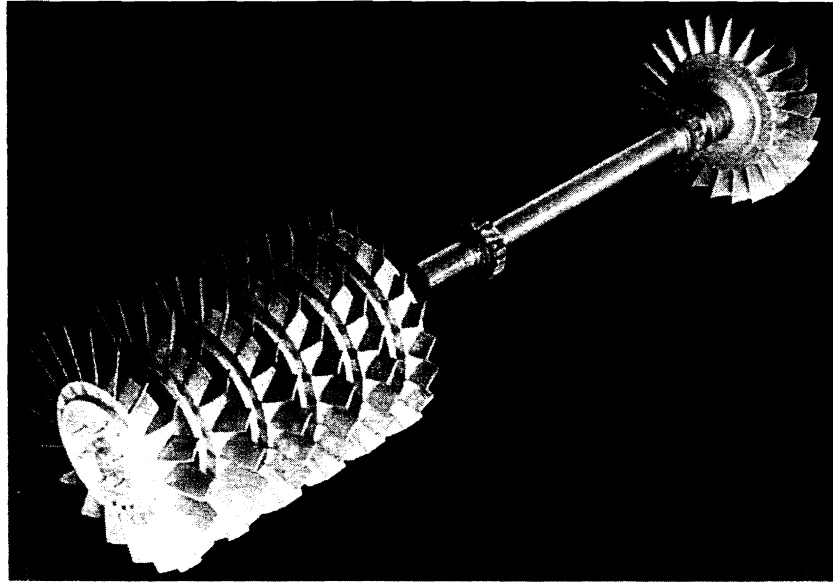
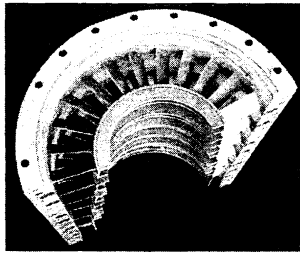


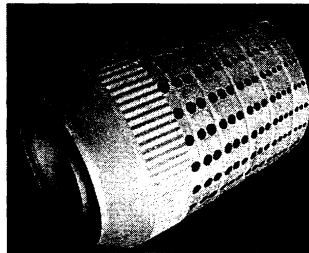
Figure 1.6 Ohain's jet engine (© Deutsches Museum Bonn photographer: Hans-Jochum Becker).



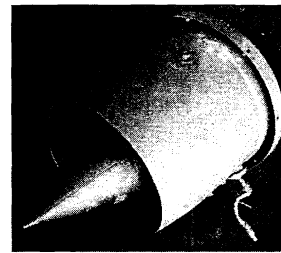
Rotor (Compressor, Shaft, and Turbine)



Compressor "Can"



Burner



Nozzle

Figure 1.9 Disassembled Westinghouse J30 (photos by R. Flack).

ran at 16,500 rpm, weighed 850 lb (385 kg), and developed 1650 lbf (7340 N) of thrust (Fig. 1.8). After this engine became commercially available, several standing manufacturers of other power-generation equipment rapidly began developing such jet engines: Pratt & Whitney, Allison, Honeywell, Garrett, Avco, Solar, Volvo, Westinghouse, and Rolls-Royce, among others. Another very early engine in the United States was the Westinghouse J30 (Fig. 1.9), which had a six-stage axial compressor and a single-stage turbine and developed 1560 lbf (6940 N) of thrust.

Today the largest engines are built by Pratt & Whitney (PW 4098), General Electric (GE 90), and Rolls-Royce (Trent), and all of these manufacturers produce engines that develop thrusts in excess of 100,000 lbf (445,000 N). The Rolls-Royce Trent turbofan series is one in such a series of engines (Fig. 1.10). Since the 1950s, gas turbines, which are derivatives of jet engines, have found their way into automobiles (Parnelli Jones almost won the 1967 Indianapolis 500 with an Andy Granatelli turbine), trains (the Union Pacific BoBoBoBo 4500-hp [3360-kW] oil-burning gas turbine and other trains in Europe and Japan), naval and commercial ships and boats, and many electric-power generation units.

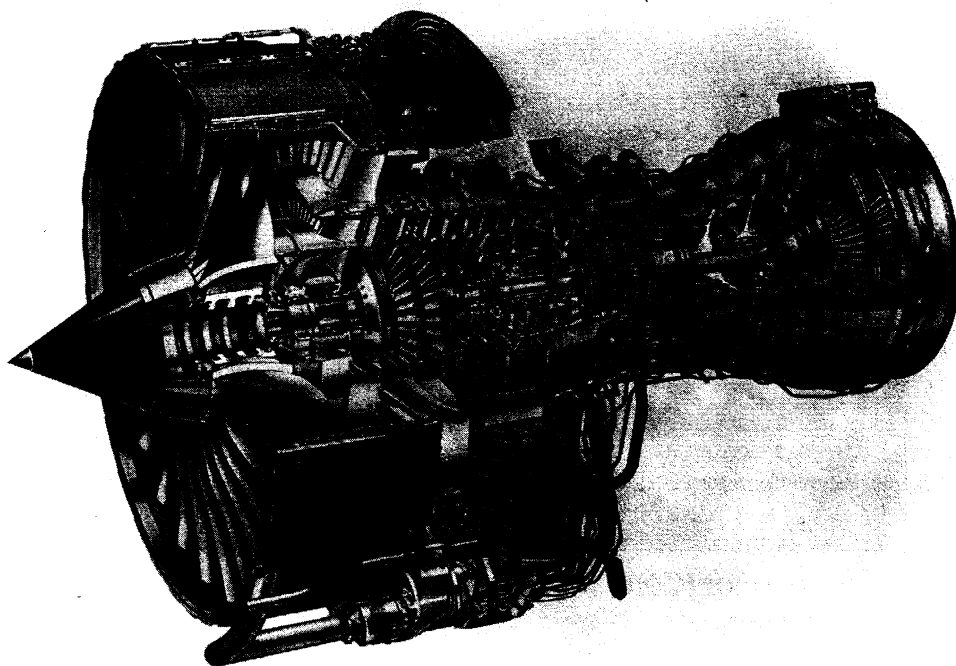


Figure 1.10 Rolls-Royce Trent turbofan (courtesy of Rolls-Royce).

Before proceeding it is important to note that other very respectable books and references, provide complimentary material and sometimes different perspectives of analysis for both gas turbines and components thereof and have in fact provided inspiration for this book. These include Cumpsty (1997), Cohen et al (1996), Hesse and Mumford (1964), Hill and Peterson (1992), Kerrebrock (1992), Mattingly (1996), Oates (1985, 1997), Pratt & Whitney (1988), Rolls-Royce (1996), Treager (1979), and Whittle (1981).

1.2. Cycles

1.2.1. *Brayton Cycle*

A Brayton cycle is the basis for the operation of a gas turbine and can be used to approximate the cycle of all such units. A jet engine operates with an open cycle, which means fresh gas is drawn into the compressor and the products are exhausted from the turbine and not reused. A typical ideal system is illustrated in Figure 1.11a. Shown are the compressor, combustor, and turbine. It is important to remember that the compressor and turbine are on the same shaft, and thus power is extracted from the fluid by the turbine and used to drive the compressor. Also shown in Figures 1.11b and c are the h-s and p-v diagrams for the cycle. The compression process, in which work is performed on the fluid mechanically and the pressure and enthalpy ideally increase isentropically (at constant entropy), is from 2 to 3. The combustion process, in which a fuel burns with the air, increases the enthalpy significantly from 3 to 4, and the process (3 to 4) is ideally isobaric.

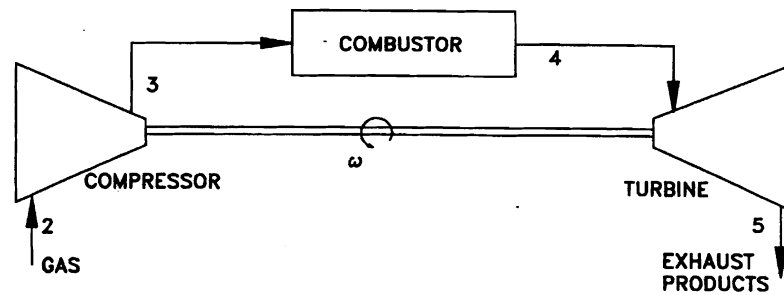


Figure 1.11a Geometry of open Brayton cycle.

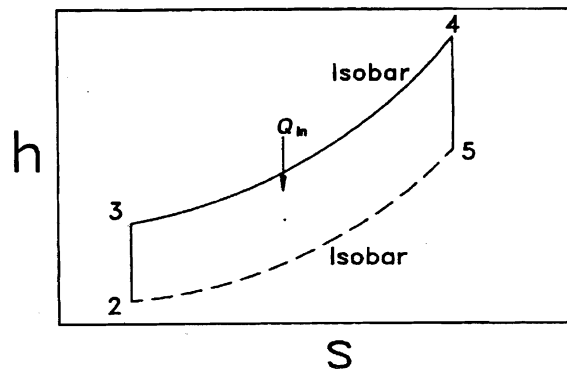


Figure 1.11b h-s diagram for Brayton cycle.

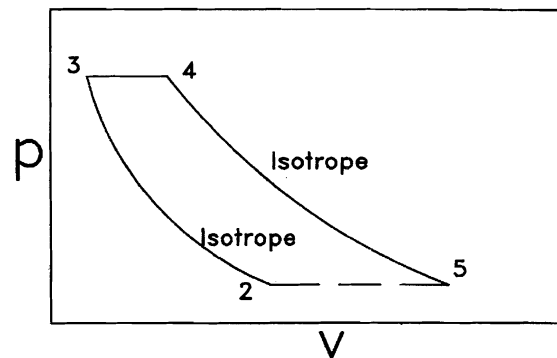


Figure 1.11c p-v diagram for Brayton cycle.

The expansion process, in which the pressure and enthalpy ideally decrease isentropically and energy is mechanically extracted from the fluid, is from 4 to 5.

Some ground or power-generation applications use closed Brayton cycles. In this process, the same gas is continually used in a recirculating process. Such a cycle is shown in Figure 1.12. The h-s and p-v diagrams are also shown in Figures 1.11b and c. For a closed cycle, the gas is heated with a heat exchanger from 3 to 4 (not a combustion process), and hot gas products from the turbine are cooled with a heat exchanger and fed back into the compressor for process 5 to 2. Typically, the heat exchanger is very heavy, which makes the closed cycle inappropriate for jet engines and results in an exhaust temperature that is too cool for propulsion purposes. For the closed cycle, the compression

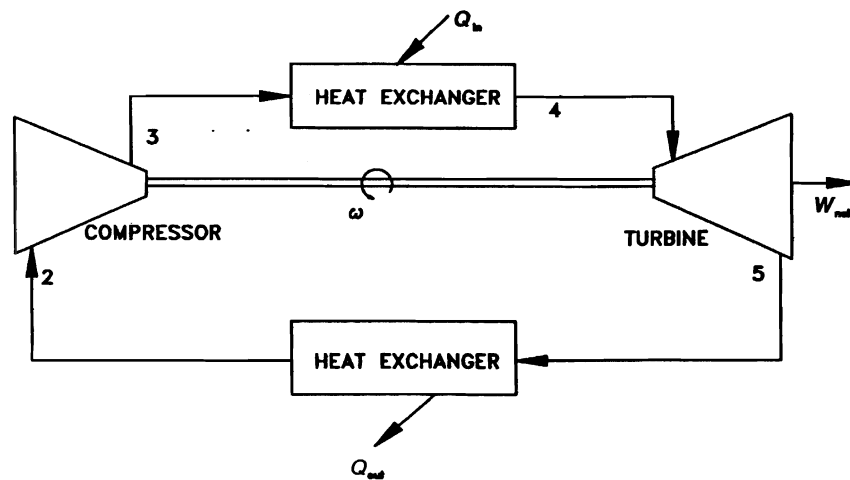


Figure 1.12 Geometry of closed Brayton cycle.

and expansion processes are ideally isentropic and the heat exchanger processes are ideally isobaric.

A very important parameter used to evaluate the overall performance of a cycle is the thermodynamic efficiency. For a closed cycle this is given by

$$\eta_{\text{th}} = \dot{W}_{\text{net}} / \dot{Q}_{\text{in}}, \quad 1.2.1$$

where \dot{W}_{net} is the net usable power from the system, as shown in Figure 1.12, and \dot{Q}_{in} is the heat that is input to the heat exchanger in process 3 to 4. Or for the ideal case

$$\eta_{\text{th}} = 1 - \frac{h'_5 - h_2}{h_4 - h'_3}, \quad 1.2.2$$

where h is the static enthalpy. For an ideal gas, this becomes

$$\eta_{\text{th}} = 1 - \frac{T'_5 - T_2}{T_4 - T'_3}, \quad 1.2.3$$

where T is the static temperature and the primes (') serve as reminders that the processes are ideal. This is also equal to

$$\eta_{\text{th}} = 1 - \left[\frac{v_3}{v_2} \right]^{\gamma-1} = 1 - \left[\frac{p_2}{p_3} \right]^{\frac{\gamma-1}{\gamma}}, \quad 1.2.4$$

where v is the specific volume, p is the pressure, and γ is the ratio of specific heats. It is important to note that, as the pressure ratio increases across the compressor, the thermodynamic efficiency increases. This will be discussed and demonstrated at many points throughout this book. However, note that, as the compressor's pressure ratio is increased, the size of the compressor becomes larger, adding to both the cost and weight. Thus, a trade-off study is usually required for a given design.

Now that we have presented the engineering definition of a Brayton cycle and reviewed the very basic thermodynamics, one question may challenge the reader: How can the general

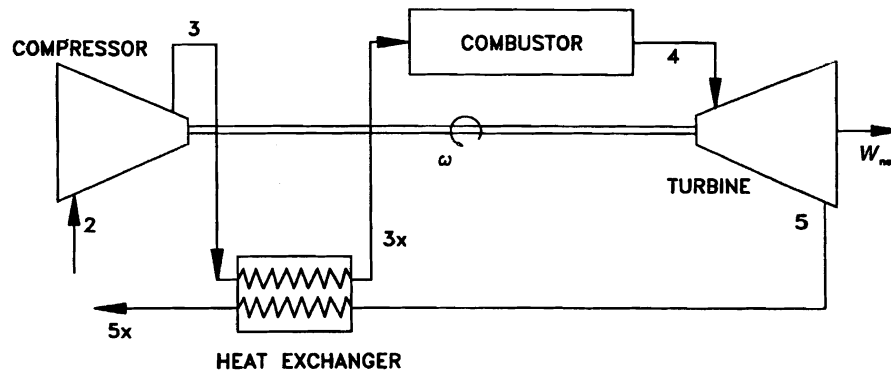


Figure 1.13a Geometry for Brayton cycle with regeneration.

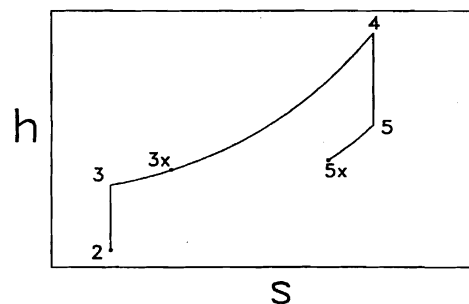


Figure 1.13b h-s diagram for Brayton cycle with regeneration.

principle of a jet engine be explained in layman's terms? One explanation is as follows. A high nozzle pressure is required to develop high momentum or thrust. The compressor initially works on the working fluid and increases the pressure of the fluid. Next, energy is added as heat in the combustor. Third, some energy is extracted mechanically by the turbine (thus reducing the temperature of the fluid) to drive the compressor, which also reduces the pressure of the fluid. However, more energy is added by the combustor than is extracted by the turbine. Consequently, the pressure exiting the turbine remains higher than the inlet pressure to the compressor. As a result, enough internal energy remains in the fluid to be converted to a high-velocity fluid (with high momentum) or thrust.

1.2.2. *Brayton Cycle with Regeneration*

A variation of the Brayton cycle is a cycle with the addition of "regeneration." A diagram for this hardware is shown in Figure 1.13a, and the h-s diagram is shown in Figure 1.13b. This process utilizes the hot gas that is "thrown away" at the turbine exit with a simple open Brayton cycle. Using the warm air at station 5, a heat exchanger is used to warm the gas exiting from the compressor (station 3) before it reaches the inlet of the combustor. Thus, for the same amount of fuel, this cycle allows the exit temperature from the combustor to be higher than the burner exit temperature of the simple open Brayton cycle. The thermodynamic efficiency is therefore improved. However, because of the heat

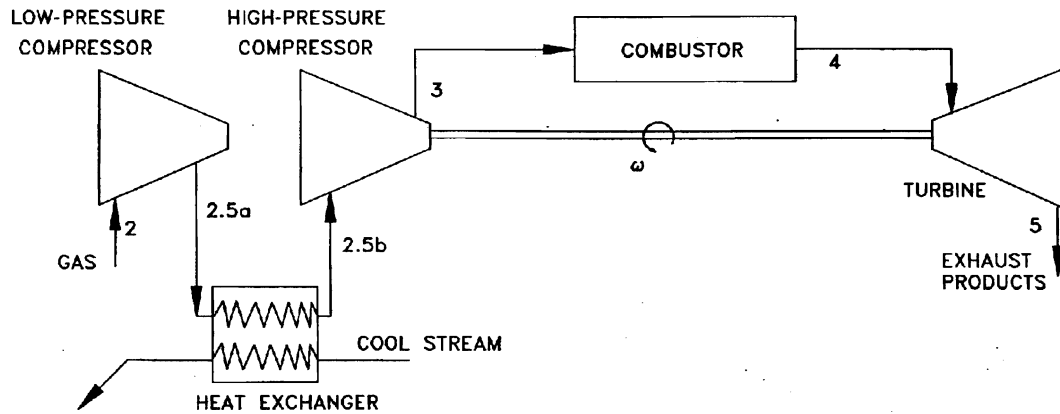


Figure 1.14a Brayton cycle with intercooling.

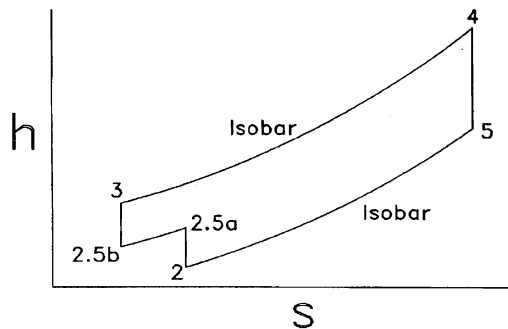


Figure 1.14b h-s diagram for Brayton cycle with intercooling.

exchanger, the weight is increased significantly. As a result, this type of gas turbine is not used for aircraft, although it has many important ground applications, including electric power generation.

1.2.3. Intercooling

Another variation of the Brayton cycle that is often used for power generation involves the addition of "intercooling." Such a cycle is shown in Figure 1.14. For this cycle, the working gas is first compressed by a "low-pressure" compressor, which increases the pressure to an intermediate value. Next, the gas is cooled, reducing the temperature of the gas. The gas is then further compressed until it reaches the nominal pressure. As will be shown through cycle analyses (Chapters 2 and 3) as well as a consideration of compressor design fundamentals (Chapter 6), decreasing the temperature of the gas reduces the power required to increase the pressure to a given level. Consequently, intercooling reduces the compressor power required for the cycle, thus increasing the net power as well as enhancing the net thermal efficiency. Intercooling and regeneration are almost always used together to improve thermal efficiency.

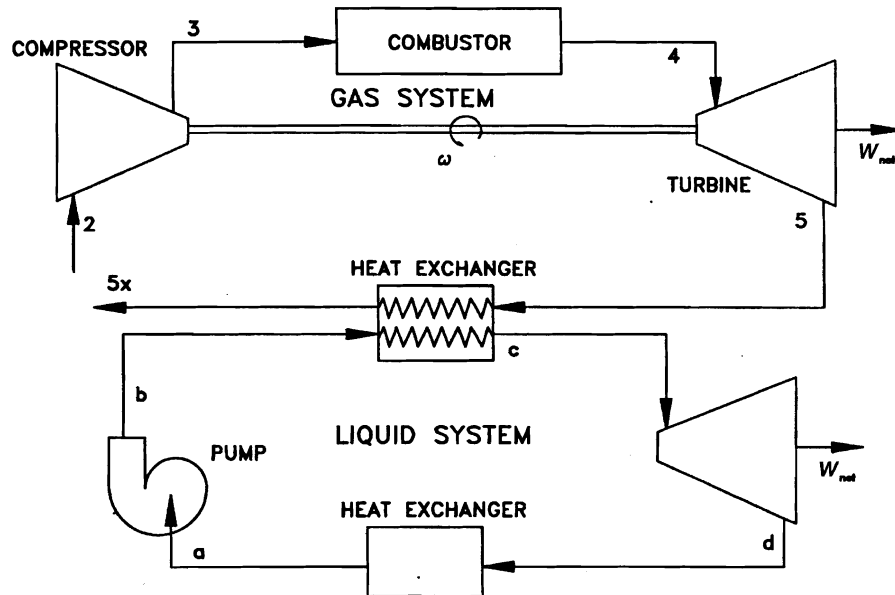


Figure 1.15a Geometry for a steam-topping cycle.

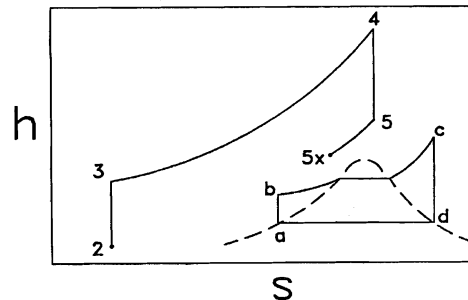


Figure 1.15b h-s diagram for steam-topping cycle.

1.2.4. Steam-Topping Cycle

Another cycle that improves the performance of a simple Brayton cycle is the steam-topping cycle. This cycle is also used with some stationary ground application gas turbines. The diagram for this system is shown in Figure 1.15a. Like the regeneration cycle, this cycle is used because it takes advantage of the very hot gases that are dumped or thrown away in a normal open Brayton cycle. The exhaust hot gases are used to heat water in a second or “topping” cycle. Thus, a certain amount of the energy is recovered and used to drive a second turbine. This in fact produces two connected cycles. The first is an open Brayton cycle, and the second is a steam or Rankine cycle, which is a cycle of two phases. The h-s diagram for the two dependent cycles is shown in Figure 1.15b. The Brayton cycle operates with two isentropic and two isobaric processes. The Rankine cycle ideally

operates with two isentropic processes, one of which is nearly isovolumetric, and two isobaric processes.

1.3. Classification of Engines

Historically, engines have evolved from simple conceptions to very complex designs. Yet, several different types of engines continue to be used. For a given application, one particular type may be significantly better than another. For example, one might expect a short-range “puddle jumper” to have different needs than a supersonic fighter. In this section, different types of engines will be defined and described. In the following chapters, the basic principles (including thermodynamics and gas dynamics) of the components and of these engines are covered. Diagrams (such as h-s and p-v) will be included. From these principles, one can predict and compare the different operating characteristics of the various engines and determine what parameters make some engines more appropriate for some applications than others. In the following sections, example details of some current and previously used engines are presented; some outdated engines are discussed for historic purposes. Many of the engines have different submodels or “builds” for different applications, and for these cases typical characteristics are presented. Information was collected from engine data in *Aviation Week & Space Technology*, *Flight International*, Mattingly (1996), Treager (1979) engine and airframe manufacturers’ materials, brochures, Web pages, and military publications. Although, every effort has been made by to be accurate cross-checking information as much as possible, accuracy cannot be guaranteed because some engines and manufacturers are forever changing.

1.3.1. Ramjet

The “simplest” jet engine is the ramjet, which is shown in Figure 1.16. This engine is only used in very high speed applications and is not capable of self-propelled takeoff. The ramjet is simple because it has no moving parts. Basically, the engine moves relative to the air with a velocity u_a . Air enters the diffuser, where the air pressure is significantly increased owing to the high air speed. Air enters the combustor next and mixes with the fuel and burns, thus increasing the temperature. Finally, the hot and expanded gases are accelerated and leave the engine through the nozzle, producing thrust. Because the engine must move relative to the ambient air to develop a pressure rise in front of the burner, this engine cannot operate statically. The ramjet is also the basis for a scramjet (supersonic combustion ramjet). Although no rotating parts are included in a scramjet, the combustion is far from simple, and significant research has been dedicated to this process. Similarly, the diffuser is not a simple device. The overall performance depends heavily on both of these components.

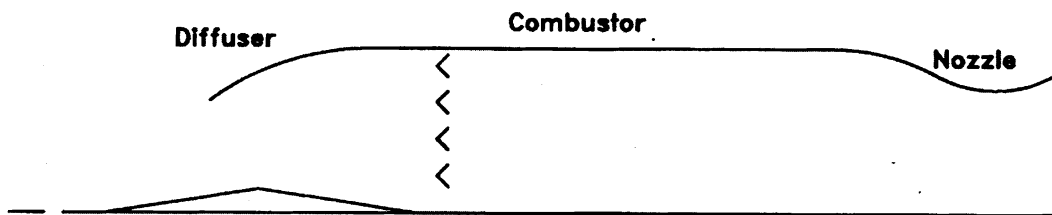


Figure 1.16 Ramjet.

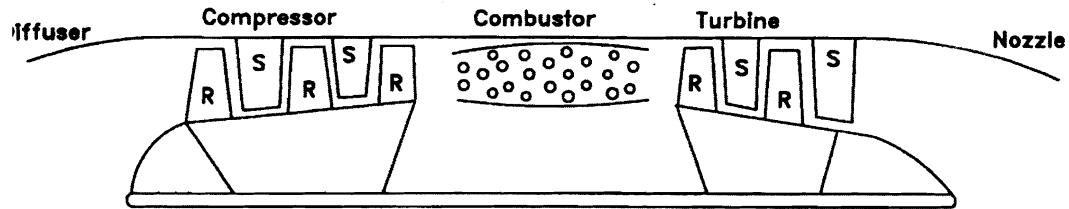


Figure 1.17 Single-spool turbojet.

1.3.2. Turbojet

The turbojet represents the next level of engine complexity. Such an engine is shown in Figure 1.17. The turbojet also has a diffuser, which decreases the fluid velocity and increases the incoming air pressure. Air enters the compressor next, where the fluid is worked on and the density is increased, and this process is accompanied by an elevation in pressure and a moderate increase in temperature. The air then enters the combustor, where the injected fuel burns with the air. The temperature and specific volume of the gas increase significantly. The turbine is used to extract some of the energy from the air, and this energy is used to drive the compressor; the turbine and compressor are on the same shaft. Finally, the hot and expanded air, which is still at moderate pressure, flows through the nozzle and is accelerated to a high velocity to produce thrust.

One such configuration is shown in Figure 1.18. This is called a single-shaft or single-spool engine, which represents an older design. An example of this type is the GE J85-21 (Fig. 1.18). This engine weighs 684 lb (310 kg), develops 3500 lbf (15,600 N) of thrust at

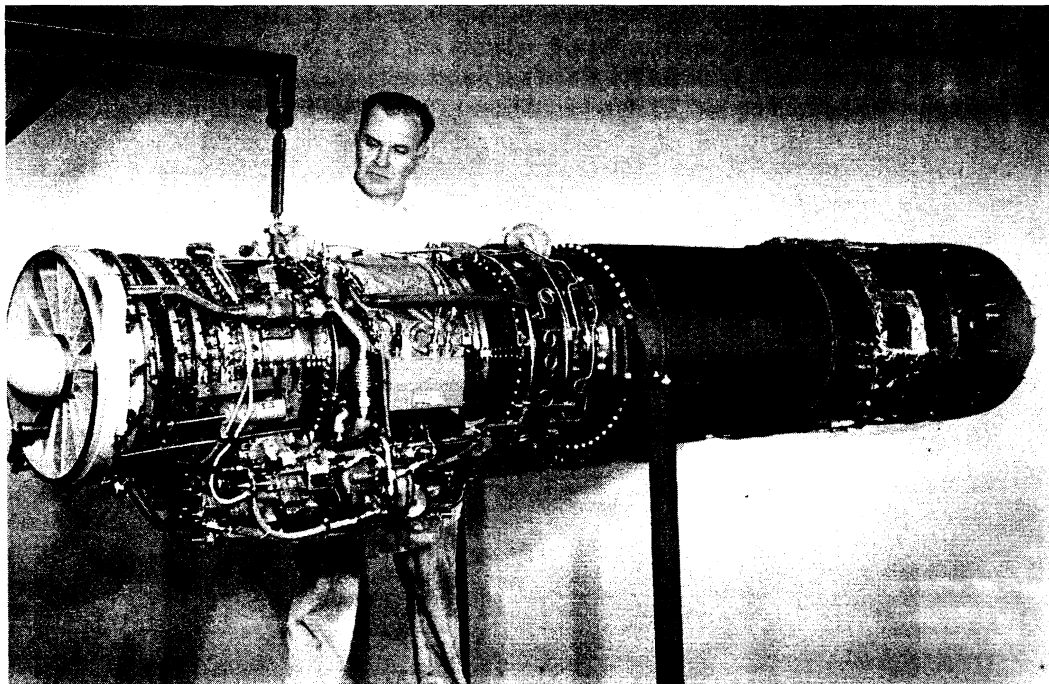


Figure 1.18 General Electric J85-21 single-spool turbojet (photo courtesy of General Electric Aircraft Engines).

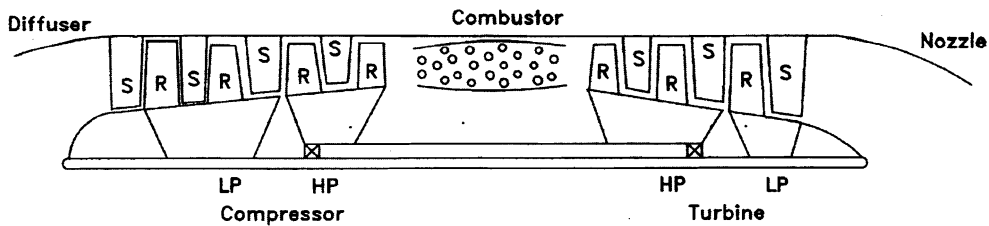


Figure 1.19 Two-spool turbojet.

maximum power (without the afterburner; see next section), ingests 52 lbm/s (24 kg/s) of air, and uses 1.24 lbm of fuel per hour to generate each lbf of thrust (lbm-fuel/lbf-thrust-h will later be defined as the thrust-specific fuel consumption [*TSFC*] or 0.126 kg/N-h). One of the smallest turbojets is the Williams WR24-7 (used on a drone). This engine weighs 44 lb (20 kg), develops 160 lbf (710 N) of thrust, ingests only 3 lbm/s (1.4 kg/s) of air, and uses 1.2 lbm-fuel/lbf-thrust-h (0.12 kg/N-h).

A second turbojet configuration is shown in Figure 1.19. This is a two-spool or twin-spool engine. This type of engine is more complex than the single-spool engine but has better operating characteristics at off-design conditions. This configuration has, in fact, two separate consecutive compressors and two separate consecutive turbines on two different shafts, one of which is hollow. One turbine is used to drive one compressor, and the second turbine is used to drive the other compressor. The first compressor that works on the air is called the low-pressure compressor and is driven by the last turbine – the low-pressure turbine – which extracts energy from the air. The second compressor that works on the air is called the high-pressure compressor, and it is driven by the high-pressure turbine. Typically, the high-pressure shaft or spool rotates considerably faster than the low-pressure spool. An example of this type of engine is the Pratt & Whitney J52 (Fig. 1.20). The J52-P408 version of this engine develops 11,200 lbf (49,800 N) of thrust, weighs 2320 lb (1050 kg), and uses 140 lbm/s (63 kg/s) of air and 2.1 lbm-fuel/lbf-thrust-h (0.21 kg-fuel/N-thrust-h).

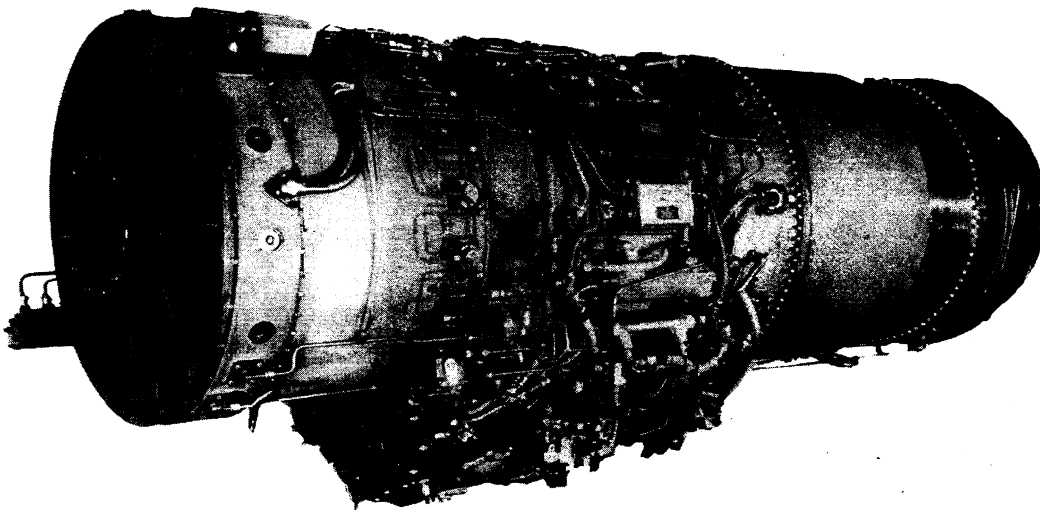


Figure 1.20 Pratt & Whitney J52 twin-spool turbojet (courtesy Pratt & Whitney).

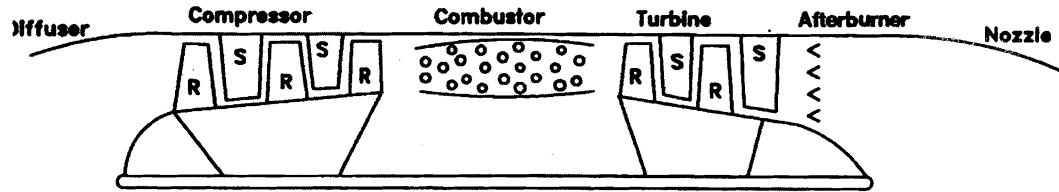


Figure 1.21 Turbojet with afterburner.

Current turbojet developments include interesting miniapplications to model aircraft (van den Hout and Koullen 1997). These small engines develop 9 lbf (40 N) of thrust, consume 0.33 lbf/s (0.15 kg/s) of air, and weigh 4 lb (1.8 kg).

1.3.3. Turbojet with Afterburner

A turbojet with an afterburner is an engine with an additional combustion chamber after the turbine. Such an engine is shown in Figure 1.21. The additional combustor adds the capability for nearly instantaneous additional thrust and acceleration. The process is sometimes called thrust augmentation. This is very important in military fighter craft applications. As a result, almost all fighter aircraft include afterburners in their engines. Basically, the additional burning increases the temperature and volume of the engine air and allows for more velocity in the exhaust nozzle, thus producing more thrust. However, using an afterburner is very inefficient thermodynamically. Therefore, afterburners are only used for short-term needs (e.g., for aircraft carrier takeoff or when a fighter is being tailed by an enemy aircraft). Afterburners are not usually found on transport aircraft with the exception of the Rolls-Royce/Snecma Olympus 593 for the Concorde, which is one of the largest of this category (thrust: 31,350 lbf [139,500 N] with the afterburner off and 38,050 lbf [169,200 N] with the afterburner on; weight: 6600 lb [3000 kg]; total airflow: 415 lbf/s [189 kg/s] fuel usage: 0.70 lbf-fuel/lbf-thrust-h [0.070 kg/N-h] with the afterburner off and 1.18 lbf-fuel/lbf-thrust-h [0.120 kg/N-h] with the afterburner on). Afterburners can be found on all basic types of turbojets (single-shaft, twin-shaft, etc.). Another example of a twin-shaft afterburning turbojet is the Pratt & Whitney J57. The schematic in Figure 1.22 clearly shows the two shafts and also identifies internal temperatures and pressures. Another example of this type of engine is the Pratt & Whitney J58 (Fig. 1.23). This engine develops up to 34,000 lbf (151,000 N) with the afterburner on (sometimes called “wet” thrust, whereas “dry” thrust is with the afterburner off) and is used on the SR-71 Blackbird, a Mach 3 fighter. The GE single-shaft J85-21 (Fig. 1.18) develops 5000 lbf (22,200 N) of

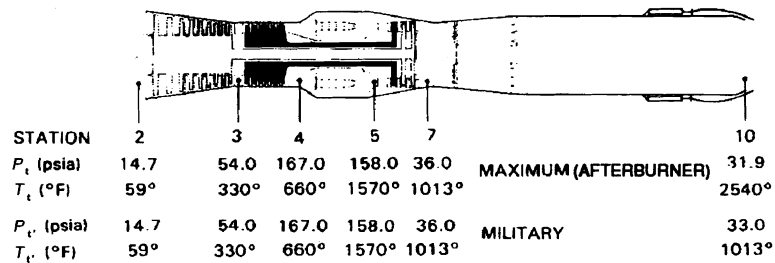


Figure 1.22 Pratt & Whitney J57 afterburning turbojet showing internal conditions (courtesy of Pratt & Whitney).



Figure 1.23 Pratt & Whitney J58 afterburning turbojet (courtesy of Pratt & Whitney).

thrust at maximum power (with the afterburner) and uses 2.1 lbf-fuel/lbf-thrust-h (0.21 kg/N-h).

1.3.4. Turbofan

The turbofan is at one level of complexity above a turbojet engine. It is a heavier powerplant but has better fuel economy than a turbojet. Two fundamental types of turbofans are used. Each will be described separately.

a. Turbofan with Fan Exhausted

A turbofan engine with fan exhausted is shown in Figure 1.24. Turbofans are always multispool engines. In the front of the engine, the air is first diffused. The air enters the fan, which compresses the air and increases the pressure somewhat. The air is then split at the “splitter,” and a portion of it enters the low-pressure compressor and continues down the “core” of the engine. Eventually this “core” air exhausts through the primary exhaust nozzle and produces thrust. The second stream of air is called the “bypass” air. In

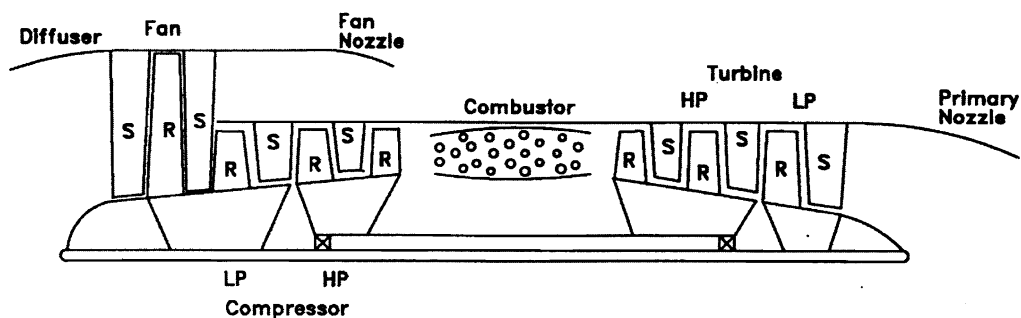


Figure 1.24 Turbofan with fan exhausted.

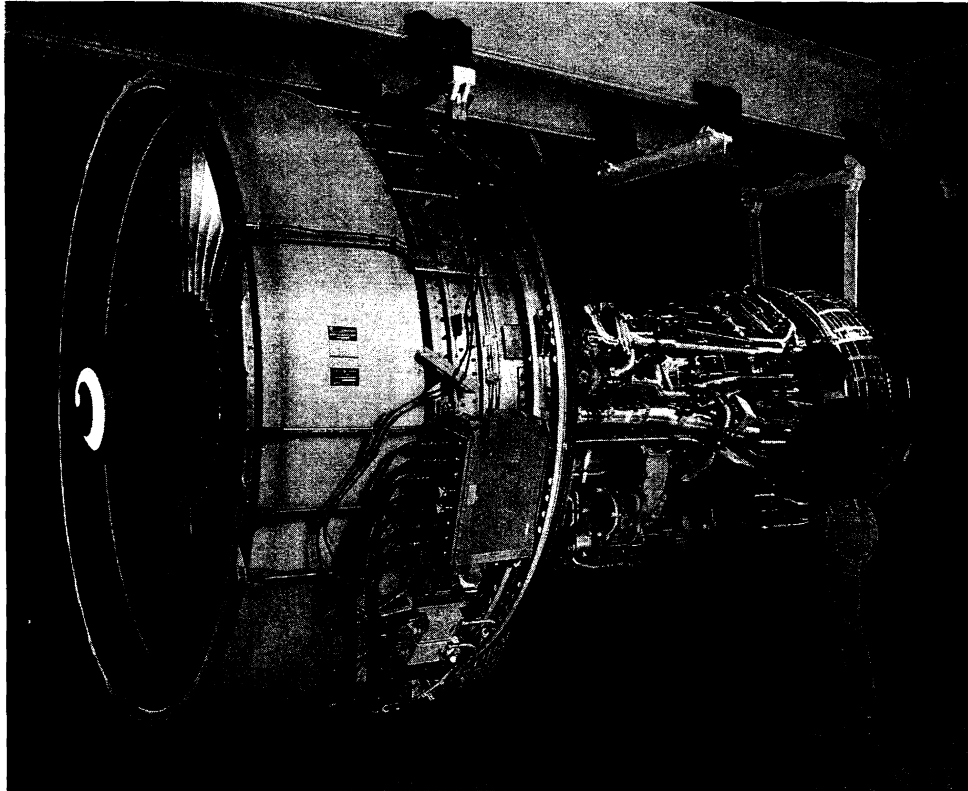


Figure 1.25 General Electric CF6-80C2 exhausted turbofan (photo courtesy of General Electric Aircraft Engines).

this engine type, the “bypass” air is accelerated in the fan nozzle, producing a second or additional thrust. The fan and usually the first few stages of the low-pressure compressor are driven by the low-pressure turbine. The high-pressure compressor extracts its energy from the high-pressure turbine. In a few cases, three shafts are used.

The GE CF6-80C2 (Fig. 1.25) is an example of a twin-shaft fanjet and is used on the Boeing 767. The low- and high-pressure shafts rotate at about 3800 and 10,300 rpm, respectively. For the CF6-80E1A2 version (used on the Airbus 330), the developed thrust is 65,800 lbf (293,000 N), and the engine uses about 0.33 lbf-fuel/lbf-thrust-h (0.034 kg/N-h). The engine has a weight of 11,162 lb (5060 kg). The airflow rate for the engine is about 1950 lbf/s (885 kg/s). Another example of this type of engine is the Rolls-Royce RB211 series (Fig. 1.26). This engine develops up to about 60,000 lbf (267,000 N), but the thrust varies according to the particular model. Next, a schematic of the Pratt & Whitney PW4000 is shown with representative internal temperatures and pressures in Figure 1.27, and the materials for the PW4084 (also on the text cover) are illustrated in Figure 1.28. Furthermore, one of the smallest engines in this category is the Williams/Rolls-Royce FJ44-1C, which weighs 45 lb (20 kg), develops 1600 lbf (7100 N) of thrust, ingests 58 lbf/s (26 kg/s) of air, and uses 0.46 lbf-fuel/lbf-thrust-h (0.047 kg/N-h). On the other end of the scale is the huge GE 90-115B, which generates commissioned thrusts up to 115,000 lbf (512,000 N) (recent tests have pushed this up to about 130,000 lbf [578,000 N]), has a maximum diameter of

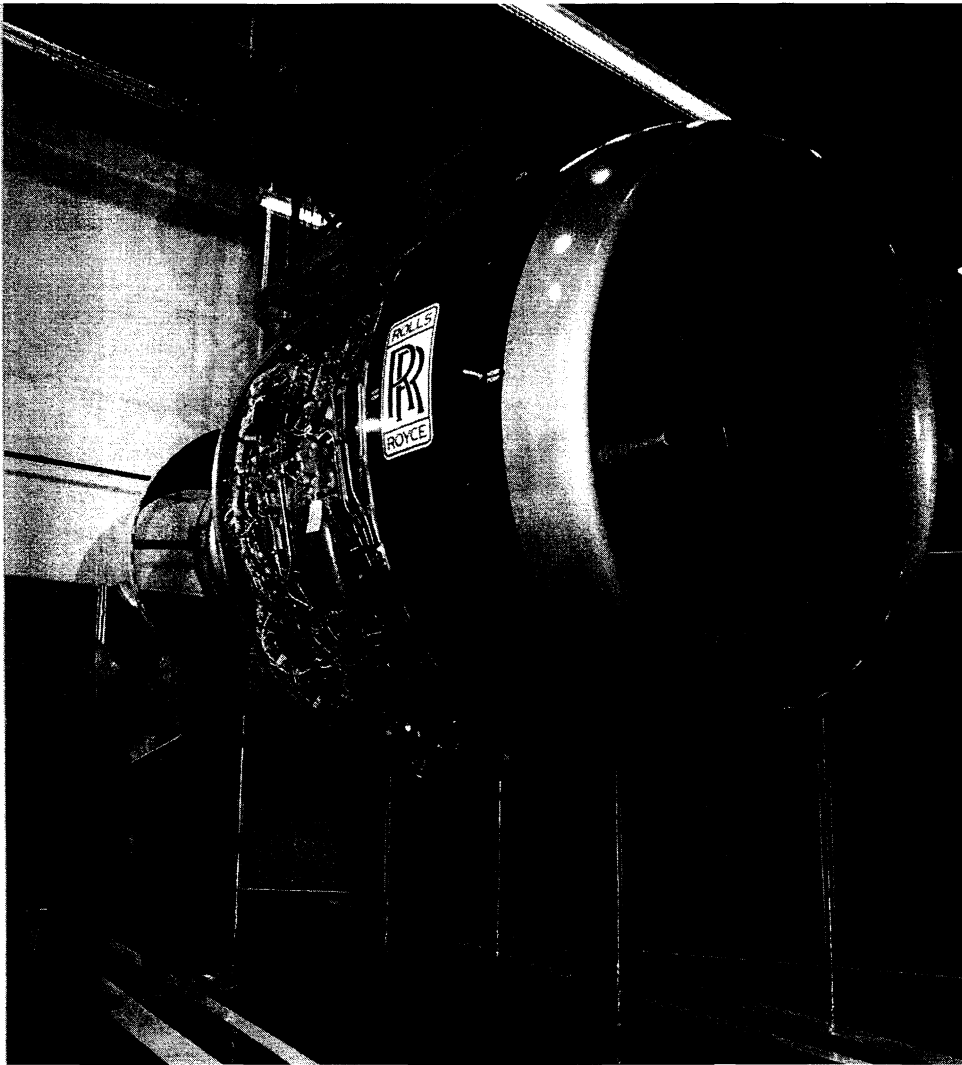
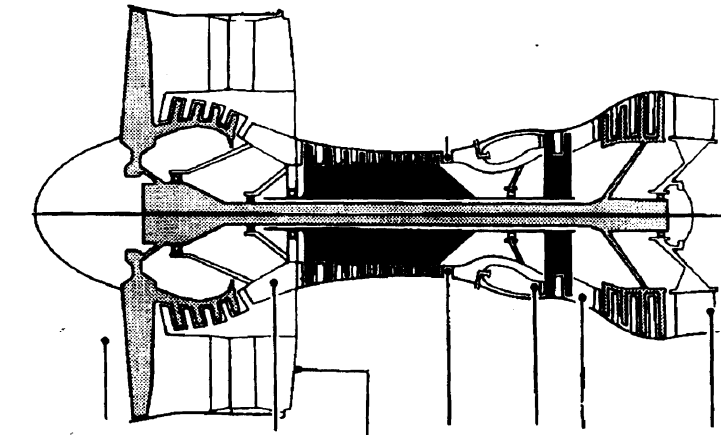


Figure 1.26 Rolls-Royce RB211-535 exhausted turbofan (courtesy of Rolls-Royce).

136 in. (3.45 m), and weighs 18,260 lb (8280 kg). As will be discussed in the following two chapters, commercial engines such as these operate with “high bypass ratios” (mass flow rate of the bypassed air to mass flow rate through the core); the GE 90-115B has a bypass ratio of about 9. Namely, the major portion of total air goes through the fan and fan nozzle. Such engines use fuel very efficiently. They tend to be heavier than low-bypass engines or turbojets with similar thrusts, however.

As indicated earlier in this section, in a few applications one engine manufacturer has gone to a design with three spools. Thus, a low-pressure compressor is driven by a low-pressure turbine, an intermediate-pressure compressor is driven by an intermediate-pressure turbine, and a high-pressure compressor is driven by a high-pressure turbine. The three spools operate at different speeds, and a three-spool engine has better off-design operating characteristics than a twin spool engine. However, such an engine is more complex. An



STATION	2	2.5	14	3	4	4.5	5
P_t (psia)	14.7	38	25	440	422	96	22
T_t (°F)	59°	245°	150°	1035°	2280°	1420°	860°

Figure 1.27 Pratt & Whitney PW4000 exhausted turbofan showing internal conditions (courtesy of Pratt & Whitney).

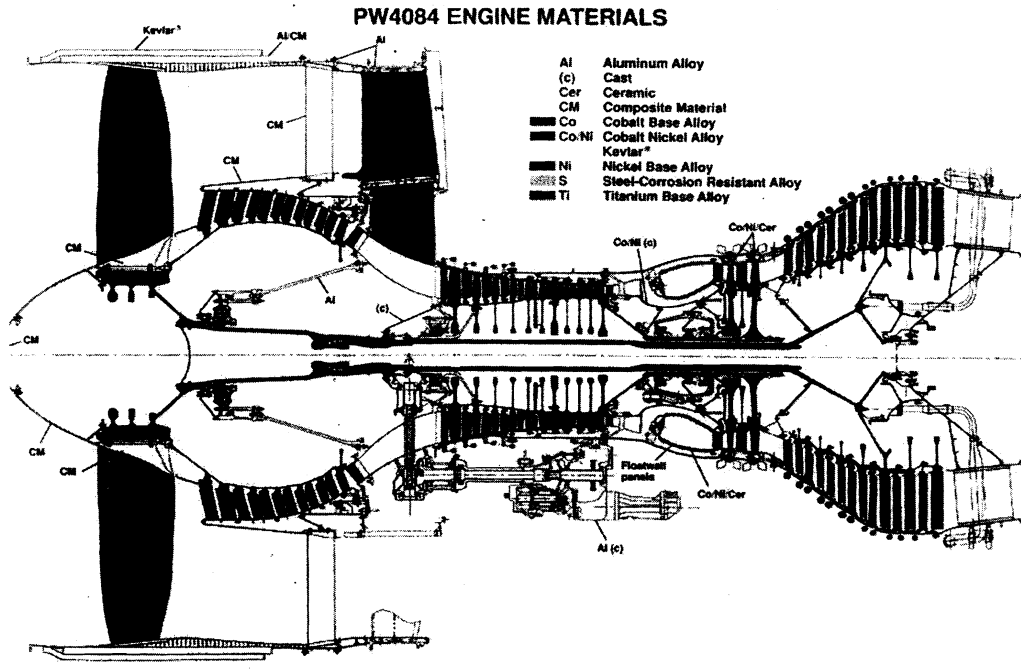


Figure 1.28 Pratt & Whitney PW4084 exhausted turbofan showing materials (courtesy of Pratt & Whitney).

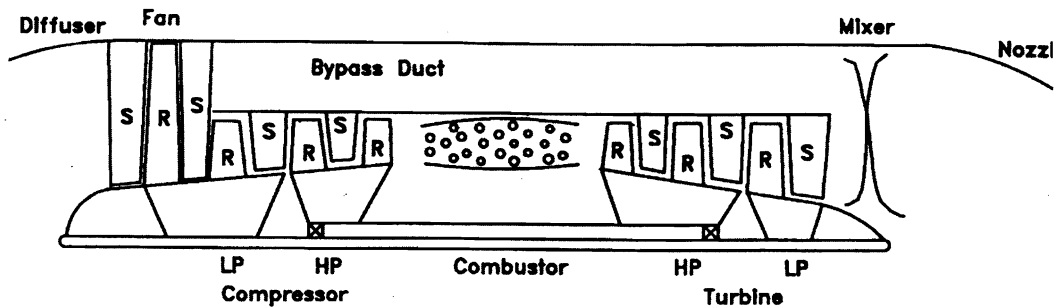


Figure 1.29 Turbofan with fan mixed.

example, of a very successful three-spool engine is the Rolls-Royce Trent series (Fig. 1.10), which is an enlarged version of the RB211 series. The three shafts typically rotate at 3,000, 7,500, and 10,000 rpm. The thrust developed is up to 104,000 lbf (463,000 N) as determined by the particular engine “build.”

b. Turbofan with Fan Mixed

A turbofan with fan mixed is shown in Figure 1.29. It is similar to the previous type, but the bypass air is not directly exhausted. The secondary air is bypassed around the low- and high-pressure compressors, combustor, and the low- and high-pressure turbines through a duct. The secondary air is then mixed with the turbine exhaust in a “mixer.” The mixed air is then accelerated through the nozzle to produce the thrust. The Pratt & Whitney JT8D (Fig. 1.30) is an example of this type. The JT8D-209 develops 18,500 lbf (82,300 N) of thrust, weighs 4410 lb (2000 kg), and uses 0.51 lbm-fuel/lbf-thrust-h (0.052 kg/N-h). The fan and primary air flow rates are about 300 and 170 lbm/s (136 and 77 kg/s), respectively

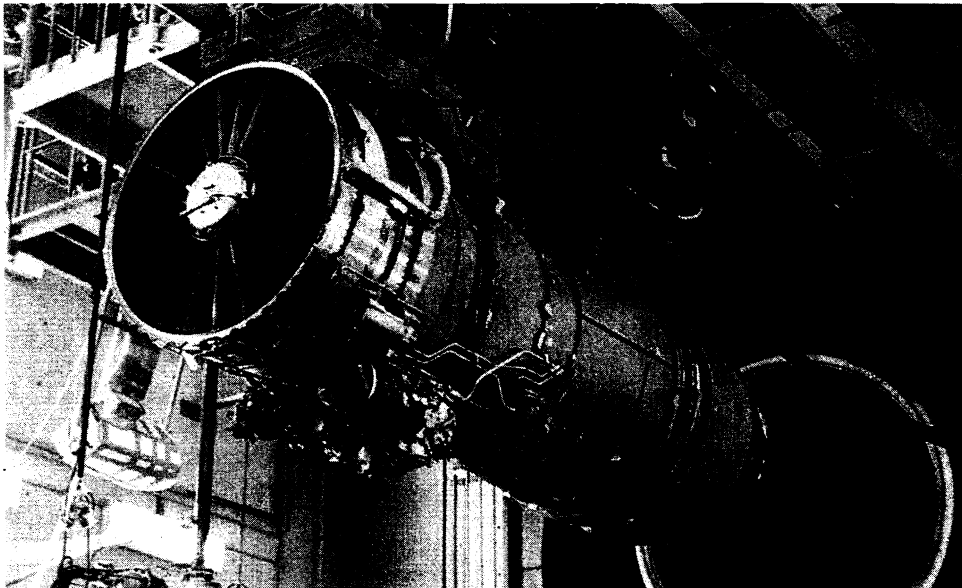


Figure 1.30 Pratt & Whitney JT8D mixed turbofan (courtesy of Pratt & Whitney).

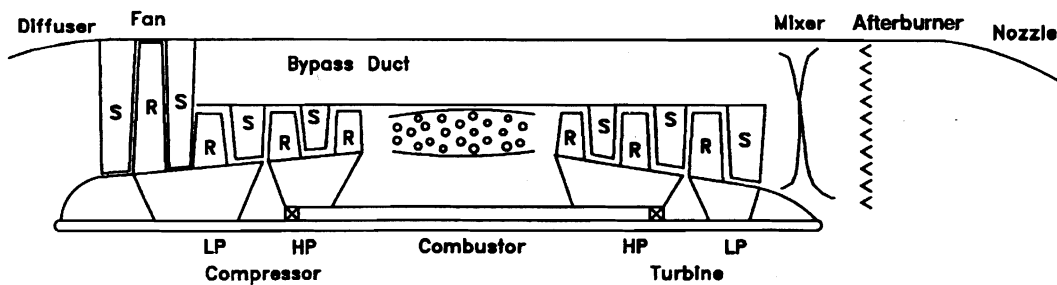


Figure 1.32 Turbofan with fan mixed and afterburner.

Of course, these specifications vary from model to model in the F100 series. Another example of this configuration is the GE F110-GE-129 (an engine that is also used on the F-15 and F-16), which produces 17,000 and 32,000 lbf of thrust with the afterburner off and on, respectively (75,600 and 142,000 N). The bypass ratio is 0.76, and the engine weighs 3980 lb (1805 kg). The fuel usage is 1.9 lbm/lbf-h with the afterburner on (0.19 kg/N-h). A smaller engine in this category is the F404-GE-400 (used on the Mach 1.8 F/A-18 Hornet), which produces 10,600 and 16,000 lbf (47,100 and 71,200 N) of thrust with the afterburner off and on, respectively. The bypass ratio is 0.32, and the engine weighs 2195 lb (995 kg). The fuel usage is 1.85 lbm/lbf-h with the afterburner on (0.189 kg/N-h). An even smaller engine of this type is the Rolls-Royce Adour MK815, which produces 5500 and 8400 lbf (24,500 and 37,400 N) of thrust with the afterburner off and on, respectively. The bypass ratio is 0.75, and the engine weighs 1630 lb (739 kg). Another engine of this variety is the Pratt & Whitney F135 (see Fig. 1.34) for the joint strike fighter (JSF). This engine, which is under development, combines vertical takeoff with supersonic flight and has the highest thrust-to-weight ratio of any engine.

Once again, as with the turbojet, turbofan afterburners are used for rapid increases in thrust. They are thermodynamically inefficient and are thus not used in commercial aircraft. Fan-mixed engines with afterburners are very often used for military fighter applications. They operate with lower bypass ratios than commercial engines and thus are lighter in weight, but a large amount of air enters the afterburner, allowing for very large increases in thrust.

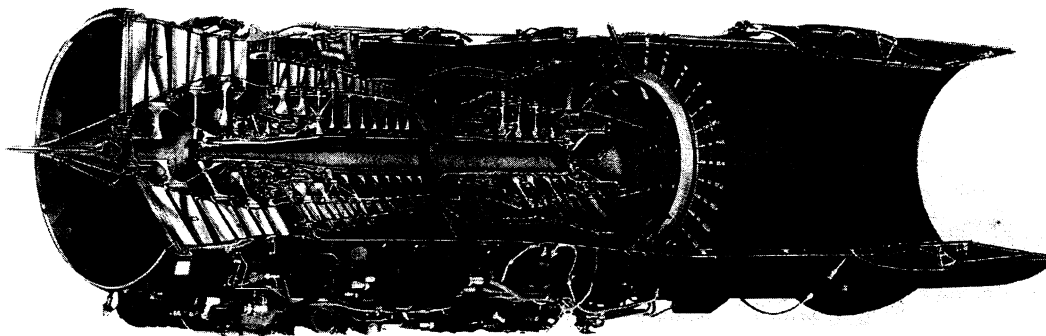


Figure 1.33 Pratt & Whitney F100 afterburning mixed turbofan (courtesy of Pratt & Whitney).

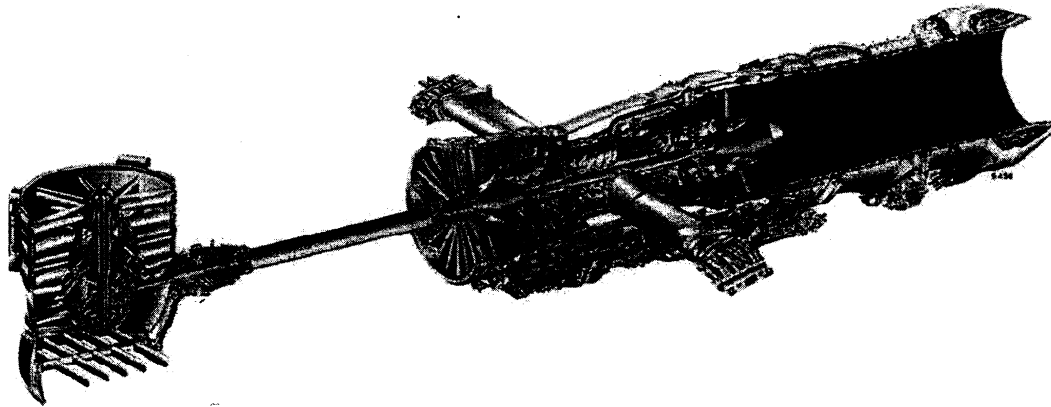


Figure 1.34 Pratt & Whitney F135 JSF engine (courtesy of Pratt & Whitney).

1.3.6. Turboprop

Another engine type is the turboprop, which is shown in Figure 1.35. For this type, the core of the engine is similar to a turbojet – namely, a diffuser, compressor, and turbine – are used. The core airflow is accelerated through the exhaust nozzle, which produces one component of thrust. A second component of thrust, and usually the largest, is obtained from the propeller. The power for the propeller is extracted from the turboshaft in the core – that is a part of the turbine work drives the propeller. A gearbox reduces the speed so

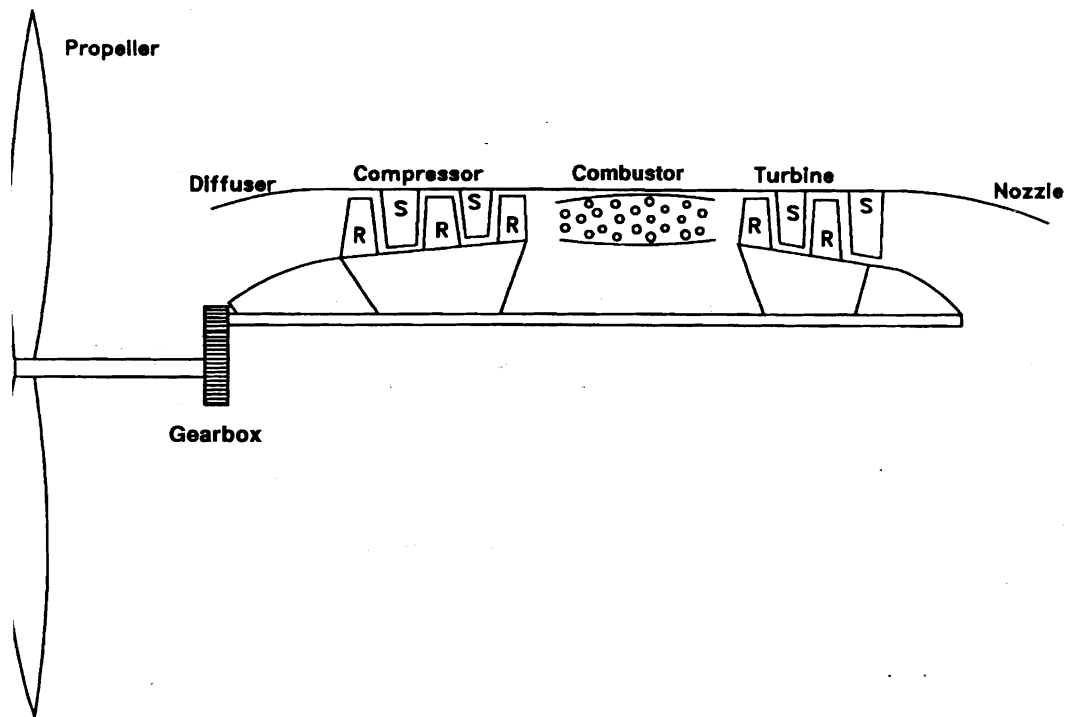


Figure 1.35 Turboprop.

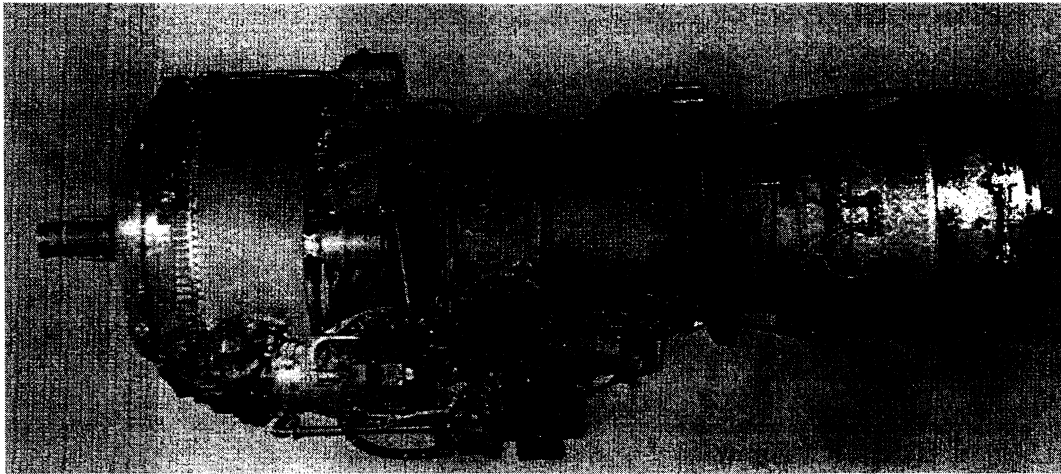


Figure 1.36 Rolls-Royce Tyne turboprop (courtesy of Rolls-Royce).

that the propeller spins at a lower speed than the compressor. An example of a turboprop is the Rolls-Royce Tyne shown in Figure 1.36. Model 512 of this series produces 5500 total horsepower (4100 kW) and ingests 47 lbm/s (21 kg/s) of air. Another example is the Garrett TPE331 shown in a cutaway view in Figure 1.37 revealing the complex gear system. Model 12B of this series develops up to 1100 hp (820 kW), weighs 400 lb (180 kg), and uses 0.52 lbm of fuel per hour to generate 1 hp (later defined as specific fuel consumption [*SFC*], which is also equal to 0.32 kg-fuel/kW-h). A third, smaller unit is the Rolls-Royce

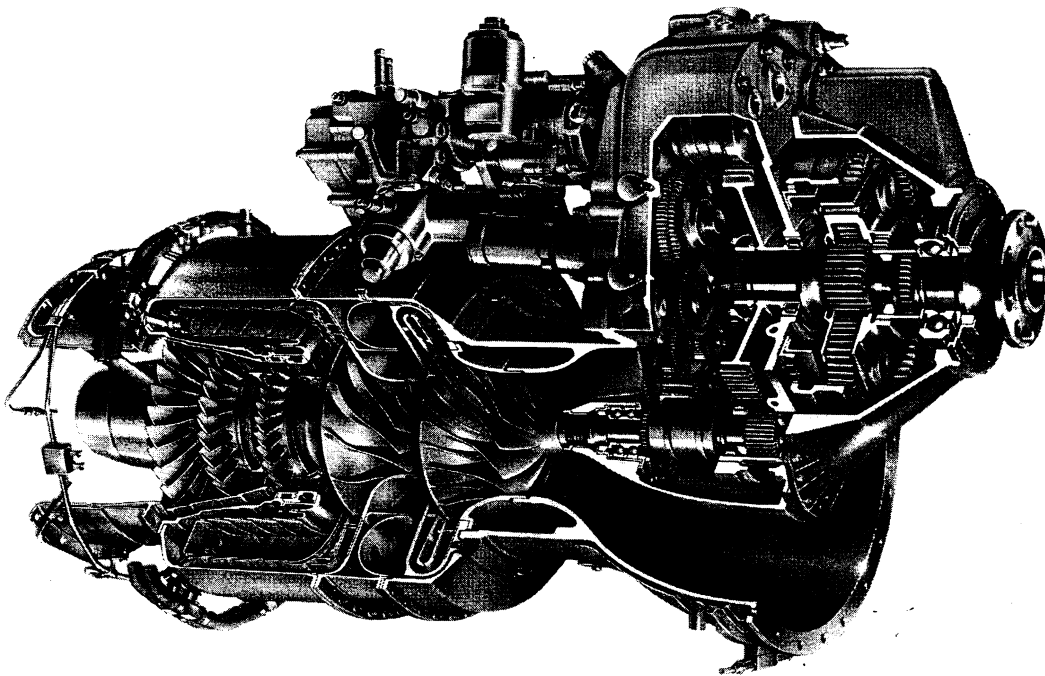


Figure 1.37 TPE331 turboprop (courtesy of Honeywell).

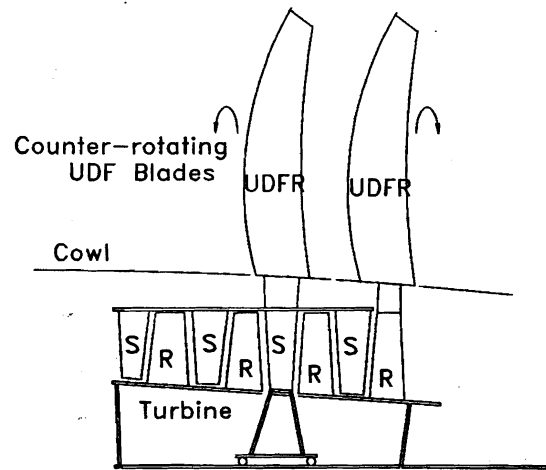


Figure 1.38 Schematic of an unducted fan.

Allison 250-B17F, which weighs 205 lb (93 kg), ingests 3.6 lbm/s (1.6 kg/s) of air, produces 450 hp (336 kW), and uses 0.613 lbm/hp-h (0.37 kg/kW-h) of fuel.

Because of the size and low speed of the propeller, turboprops cannot be used at high air speeds. They are very efficient thermodynamically, however. As a result, turboprops are used on many light aircraft designed for short journeys.

1.3.7. Unducted Fan (UDF)

The fundamental configuration of the turboprop engine is also used for the unducted fan (UDF), external fan engine, or prop-fan, which received considerable attention in the 1980s and early 1990s. This is an alternative to a turboprop, which has long propeller blades and is thus limited to low rotational speeds and has the drawback of a heavy gearbox. The UDF was developed during this period by NASA in concept with General Electric, Pratt & Whitney, Rolls-Royce, and others (Figs. 1.38 and 1.39). This engine never went into production in the United States but was produced in the former Soviet Union. This engine type is a crossbreed between the turboprop, which demonstrates excellent low-aircraft-speed efficiency, and the conventional exhausted turbofan. The blades of a UDF are shorter than propeller blades and thus can be directly attached to the shaft without the need for a gearbox. More complexly designed blades are used as well, and they are highly “swept” (curved and twisted). Such designs can effectively operate at higher Mach numbers than turboprops. As noted, this engine never went into production in the United States (largely owing to decreased fuel prices in the early 1990s), and much of the advanced technology that was developed went into other advanced engine designs. For example, General Electric directly used such technologies in the GE 90 engine development.

1.3.8. Turboshaft

The last aircraft engine type is the turboshaft. It is basically the same as the turboprop except that thrust is not derived from the exhaust. The gas from the core exhausts at a low velocity, and consequently additional thrust is not obtained. These engines are used largely for helicopter applications, although it is noteworthy that turboshaft engines

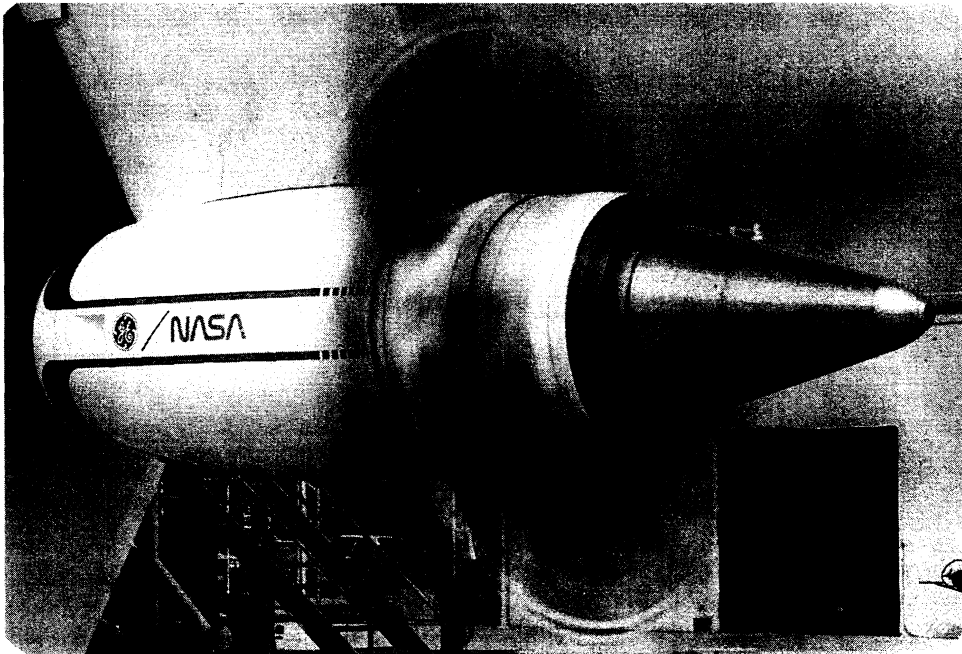


Figure 1.39 General Electric/NASA unducted fan (photo courtesy of General Electric Aircraft Engines).

are used to drive tanks and other ground vehicles with a transmission attached to the shaft in lieu of the rotating blades. An example of this engine is the Rolls-Royce/Turbomeca RTM322 shown in Figure 1.40. Depending on particular sub-model, this engine develops up to 2800 hp (2090 kW) and weighs up to 540 lb (245 kg). The Pratt & Whitney Canada PW206A develops 621 hp (463 kW), and the output shaft rotates at 6240 rpm. Lastly, the GE T700-401 weighs up to 458 lb (208 kg), develops up to 1800 hp (1340 kW), and uses 0.46 lbm/hp-h (0.28 kg/kW-h) of fuel. Many turboshafts have been developed concurrently with turboprops, and thus different designs of the same basic engine are used for fixed-wing and rotary aircraft.

1.3.9. Power-Generation Gas Turbines

The next category of gas turbines to be discussed is not for aircraft applications but for power generation. A power-generation unit of typical design is shown in Figure 1.41. As one can see, the unit is very much like a turbojet engine, although subtle differences exist in the design. The turbine consists of the high- and low-pressure turbines, which drive the compressor, and a “free” turbine, which is used for power generation. An inlet bell replaces the diffuser, and the nozzle is replaced by an exhaust. A power-extracting device is attached to one of the primary shafts or an auxiliary shaft. This device may be an electrical generator (which must run at constant rotational speed), ship propeller, offshore equipment, or another mechanical power-extracting device. Until 2001, aircraft engines dominated the gas turbine industry; however, in that year sales of power-generation gas turbines exceeded those for aircraft engines. One example of this type of unit is the Rolls-Royce Industrial RB211,

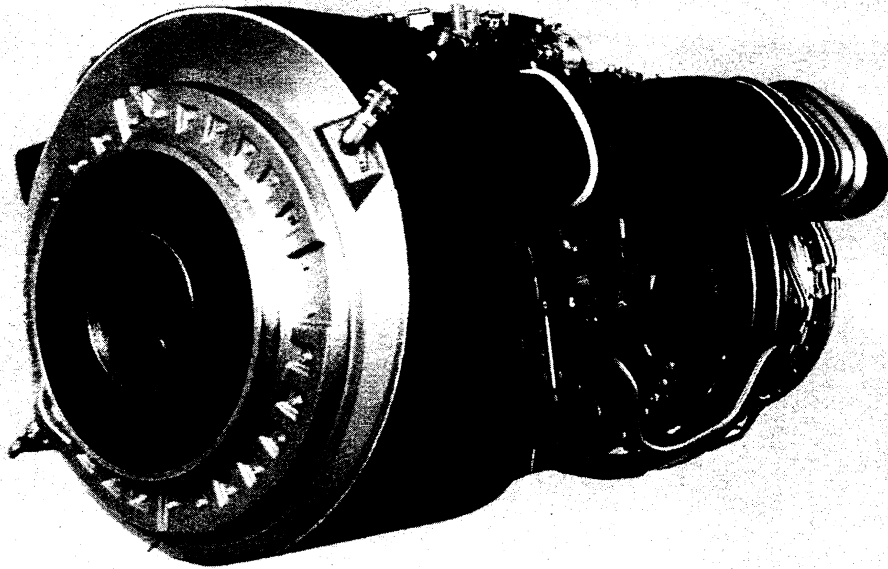


Figure 1.40 Rolls-Royce/Turbomeca RTM322 turboshaft (courtesy of Rolls-Royce).

which is shown in Figure 1.42. As its designation implies, this electrical power-generation unit is in fact a derivative of the aircraft engine (Fig. 1.26). One can see many similarities between this gas turbine and the aircraft engine. This type of unit tends to be slightly heavier, for weight is not a concern. The GE LM2500 is another example of this type of gas turbine and is shown in Figure 1.43. Such gas turbines generate up to 33,600 hp (25,000 kW) on the output shaft, ingest about 150 lbm/s of air (68 kg/s), have a weight of 10,300 lb (4670 kg), and use 0.373 lbm-fuel/hp-h (0.227 kg/kW-h) with a thermodynamic efficiency of 37 percent. A larger unit, the LM 6000 (about 55,000 hp or 41,000 kW), is a derivative of the GE CF6 aircraft engine. In Figure 1.44 the Rolls-Royce Marine Tyne is shown. Once again, as indicated by the name, this seaworthy unit is a modification of an aircraft turboprop (Fig. 1.36). The Rolls-Royce Trent is one of the largest power units and delivers up to 69,800 hp (52,000 kW) with over 350 lbm/s (160 kg/s) of air ingested. This gas turbine runs at about 42 percent thermodynamic efficiency. One of the smallest is the Capstone C30, which delivers 39 hp (29 kW) with an air consumption of 0.7 lbm/s (0.32 kg/s) at 25 percent efficiency. As implied earlier in this section, many modern power-generation units are “aero-derivatives” of the aircraft engines; namely, the core of the engine is essentially

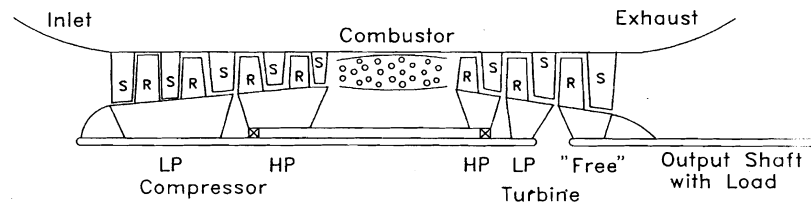


Figure 1.41 Power-generation gas turbine.



Figure 1.42 Rolls-Royce industrial RB211 gas turbine (courtesy of Rolls-Royce).

the same as that of a jet engine. Thus, much of the development engineering costs entailed in the design of a new power-generation unit are reduced because the original development was already completed for a propulsion unit (and sometimes paid for by a government). The cost of such a power-generation unit can therefore be significantly reduced. Furthermore, because many parts are the same for both power-generation and propulsion gas turbines, manufacturing needs and costs are reduced.

New applications of power-generation units include the development of miniaturized and microminiaturized gas turbines to replace small household-size electrical generators and batteries. Some units under development are as small as 1 in. (25 mm) and produce a mere 50W (0.067 hp) (Ashley (1997)).

1.3.10. Comparison of Engine Types

Typical weights, powers, thrusts, and other parameters have been presented in the preceding sections for a spectrum of applications. Applications are presented so that one can appreciate the different uses. As noted, many of the engines have different submodels or “builds” for different applications. The reader is encouraged to routinely consult *Aviation Week and Space Technology* and *Flight International*, which both have approximately annual reviews of engine specifications as well as the Pratt & Whitney, Rolls-Royce, General Electric, Snecma, and other web sites detailed in the reference list. One particularly convenient Web site is <www.jet-engine.net>, which categorizes specifications for turbfans, turbojets, and turboshafts for both commercial and military applications. An interesting observation on engine development and manufacture is that large corporations that were in competition a decade ago now are partners in some large engine development and manufacturing projects. For example, CFM is a venture between General Electric and Snecma;

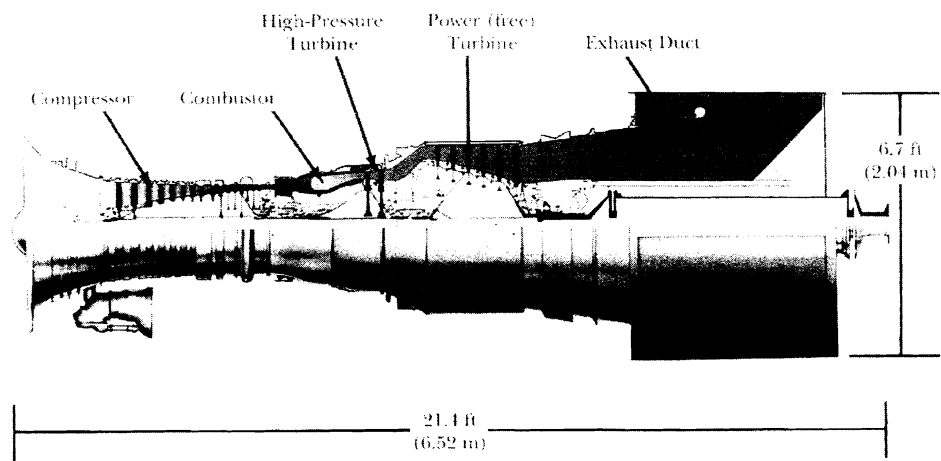
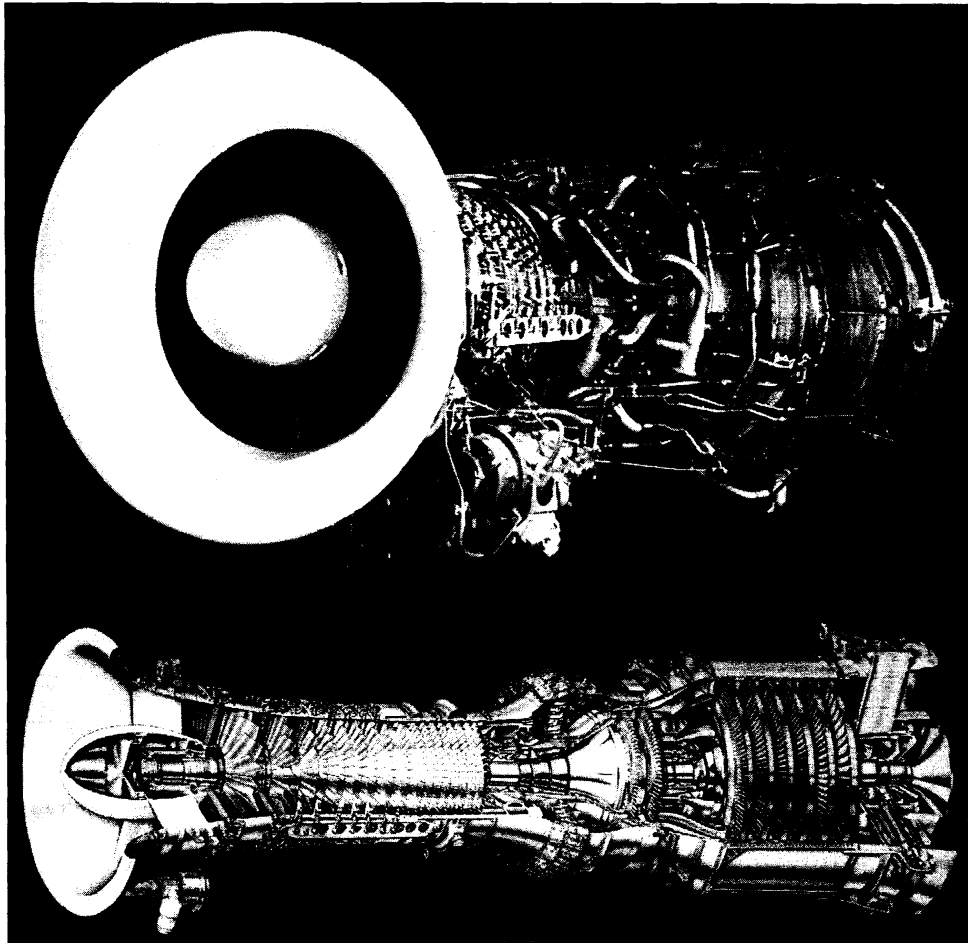


Figure 1.43 General Electric LM2500 gas turbine (courtesy General Electric Power Systems).

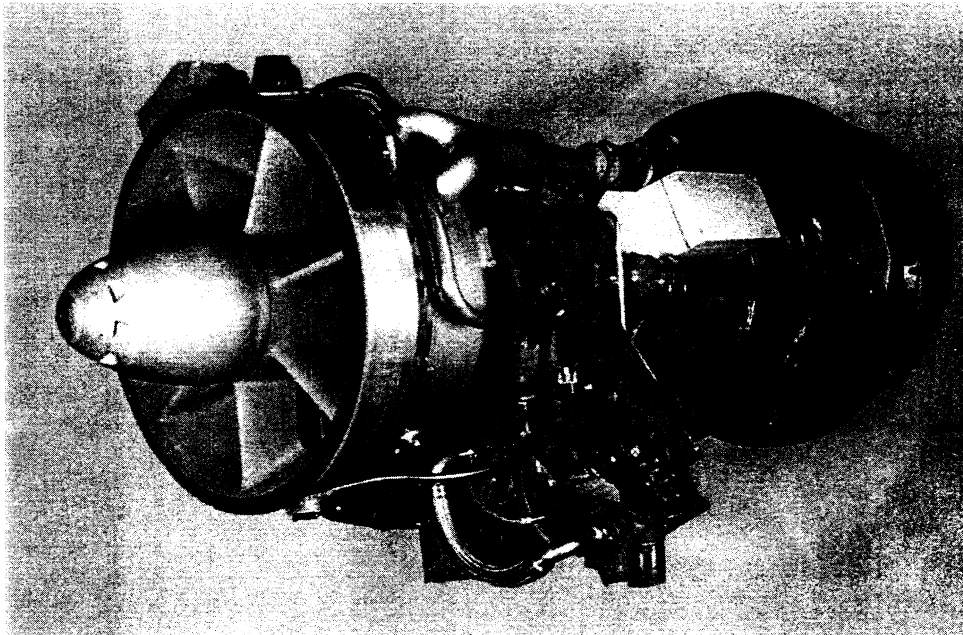


Figure 1.44 Rolls-Royce marine Tyne gas turbine (courtesy of Rolls-Royce).

MTR is a joint effort with MTU (Motoren und Turbinen Union, Div. of Daimler-Chrysler), Turbomeca, and Rolls-Royce; IAE is International Aero Engines (Pratt & Whitney, Rolls-Royce, Japanese Aero, and MTU); and the Engine Alliance is a cooperative effort with Pratt & Whitney and General Electric. Furthermore, companies have cooperated on individual engines: MTU has worked individually with General Electric, Pratt & Whitney Aircraft, and Rolls-Royce; IHI (Isakawajima-Harima Heavy Industries) has worked with Pratt & Whitney Aircraft and Rolls-Royce; BMW and Rolls-Royce have teamed, and so on. Furthermore, many companies have merged or been bought out, and thus the list of manufacturers changes annually. Companies have adopted the healthy strategy that engineering efforts should not be developed independently and that effective design ideas and research can be effectively transferred between corporations. The best example is probably the Engine Alliance for which advanced technologies from the large GE 90 and PW 4000 engines are merged and each member is engaged in building different parts of engines.

In Table 1.1, a comparison of the different engine types is made. The table is self-explanatory, and one can make comparisons based on the different criteria. For example, it can be seen that a turboprop has the best fuel economy at low speeds and the turbojet has the best thrust-to-weight ratio. The information in this table is demonstrated with different applications and examples in the following two chapters on cycle analysis.

1.4. Engine Thrust

The most important characteristic of a jet engine is its thrust-producing capability. In this section, the basic equations that will allow the reader to calculate engine thrust are developed. These equations are developed based on the simple control volume approach in which the incoming and exiting properties are known and are used in Chapters 2, 3, and 11. Details of the internal flow are included in Chapters 4 through 10. The thrust equations are

Table 1.1. Comparison of Engine Types

	Ramjet	Turbojet*	Turbofan*	Turboprop
Speed	Very High	High	Moderate	Low
Thrust/weight	Moderate	High	Moderate/Low	Low
Fuel use/thrust	High	Moderate	Low	Low
Thrust/air flow	High	High	Moderate	Moderate
Ground Clearance	NA	Good	Moderate	Poor

* Afterburners: Increase Speed
 Increase Thrust/weight
 Increase Fuel use/thrust
 NA = Not applicable

developed for two different engine types: the turbojet and the turbofan with an exhausted fan. The thrust for all other engine types can be found from one of these two cases, but proving this will be left as an exercise for the reader.

1.4.1. Turbojet

Figure 1.45 shows a turbojet. At this point in the analysis, only the inlet and exit conditions of the engine are considered. The calculations of the different internal component processes are not undertaken, although they are obviously extremely important to the overall

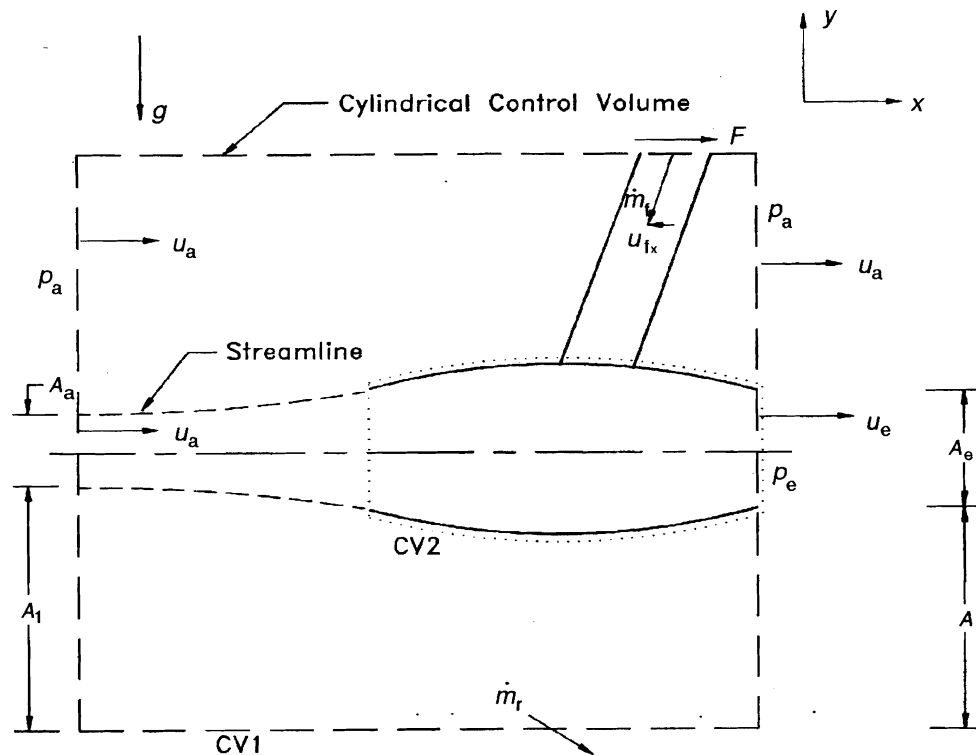


Figure 1.45 Control volume definition for a turbojet.

design and performance. A control volume is drawn around the engine as shown. The engine is moving in air to the left with velocity u_a . The large-diameter cylindrical control volume (CV1), which is fixed to the engine and thus is moving, cuts through the engine strut. Fuel is also injected into the engine through the control volume. One surface is at the exit plane of the engine, and the front plane is far from the inlet.

Writing the general linear momentum equation in rectangular coordinates yields

$$\sum \mathbf{F}_s + \sum \mathbf{F}_b = \frac{\partial}{\partial t} \int_{CV} \mathbf{V} \rho d\mathcal{V} + \int_{CS} \mathbf{V} \rho \mathbf{V} \cdot d\mathbf{A}. \quad 1.4.1$$

However, if the flow is considered to be steady, the unsteady term ($\partial/\partial t$) disappears. Next, one should consider applying the equation in the thrust (x) direction. The surface forces are due to pressures on the control volume and to the cutting of the strut, F , which is the force holding the engine in place. Thus, the force, F , represents the developed thrust. Because the front surface is far from the engine, the pressure is uniform and at atmospheric conditions, p_a , at this surface. At the front surface, the air flows at velocity u_a across an area $A_a + A_1$. Also, at the engine exit, the pressure in the engine is uniformly p_e , and the pressure outside of the engine is the atmospheric pressure, p_a . The velocity of the engine exhaust is uniformly u_e . The area of the engine exhaust is A_e . At the rear of the control volume, air exits at uniform velocity u_a across area A_2 . The fuel is injected at a mass flow rate of \dot{m}_f with velocity $-u_{fx}$ in the x -direction, but it does not usually contribute significantly to the flux portion of the momentum equation. A mass flow term, \dot{m}_r , can exit from the sides of the control volume owing to displacement of air by the engine, which must be evaluated and included in the analysis. Thus, evaluating each of the terms and rewriting the momentum equation yields

$$\begin{aligned} F + p_a A_a + p_a A_1 - p_e A_e - p_a A_2 + F_{bx} \\ = -u_a \rho_a A_a u_a + u_e \rho_e A_e u_e - u_a \rho_a A_1 u_a + u_a \rho_a A_2 u_a + \dot{m}_r u_a - \dot{m}_f u_{fx}. \end{aligned} \quad 1.4.2$$

Next, one should realize that no body forces exist in the x -direction. Also, uniform flow is assumed across areas A_e and A_a . The mass fluxes across these inlet and exit surfaces, which are the gas flows into and out of the engine, respectively, are

$$\dot{m}_a = \rho_a A_a u_a \quad 1.4.3$$

and

$$\dot{m}_e = \rho_e A_e u_e. \quad 1.4.4$$

Also, by inspecting the control volume one can see the areas are related by

$$A_1 + A_a = A_2 + A_e \quad 1.4.5$$

Using the previous three equations with Eq. 1.4.2 yields

$$\begin{aligned} F + p_a A_2 + p_a A_e - p_e A_e - p_a A_2 \\ = \dot{m}_e u_e - \dot{m}_a u_a + \dot{m}_r u_a - u_a^2 \rho_a (A_1 - A_2) - \dot{m}_f u_{fx}. \end{aligned} \quad 1.4.6$$

Because the flow is steady, the continuity equation yields (using a second control volume, CV2, for the engine only)

$$\dot{m}_e = \dot{m}_a + \dot{m}_f, \quad 1.4.7$$

and CV1 yields

$$\dot{m}_e + \rho_a u_a A_2 + \dot{m}_r = \dot{m}_a + \rho_a u_a A_1 + \dot{m}_f; \quad 1.4.8$$

thus, using the preceding two equations, we obtain

$$\dot{m}_r = \rho_a u_a (A_1 - A_2). \quad 1.4.9$$

Or, using Eqs. 1.4.6 and 1.4.9 and combining terms, we obtain

$$F = (\dot{m}_e u_e - \dot{m}_a u_a) + A_e (p_e - p_a) - \dot{m}_f u_{fx}. \quad 1.4.10$$

Using this with Eq. 1.4.7 yields

$$F = \dot{m}_f u_a + \dot{m}_e (u_e - u_a) + A_e (p_e - p_a) - \dot{m}_f u_{fx}. \quad 1.4.11$$

Often, the x -component of fuel velocity is negligible, resulting in

$$F = \dot{m}_f u_a + \dot{m}_e (u_e - u_a) + A_e (p_e - p_a). \quad 1.4.12$$

This is the general equation for a turbojet engine. One further simplifying assumption can often be made. Usually the fuel flow is much smaller than the airflow ($\dot{m}_f \ll \dot{m}_a$). As a result,

$$\dot{m}_e = \dot{m}_a = \dot{m}. \quad 1.4.13$$

Thus, Eq. 1.4.12 becomes

$$F = \dot{m}(u_e - u_a) + A_e (p_e - p_a). \quad 1.4.14$$

It is important to note that the resulting thrust has two contributions. One is due to the mass flux and flow acceleration. The second results from pressure differences between the engine exit and atmosphere. In Chapter 5, an engine will be shown to operate most efficiently (i.e., maximum thrust) when the pressures are equalized for the ideal case (no losses) and nearly equalized for the nonideal case.

One should note that, although derived for a turbojet, the preceding equations apply for a fully mixed turbofan as well, for only one inlet and one exit exists. Deriving the equations is left as an exercise for the reader.

Example 1.1: A turbojet operates at sea level and moves at 800 ft/s (243.8 m/s). It ingests 250 lbm/s (113.4 kg/s) of air and has negligible fuel flow. The diameter of the exit is 30 in. (0.762 m). The exit pressure is 22 psia (151.7 kPa), and the exit velocity is 1300 ft/s (396.2 m/s). Find the developed thrust.

SOLUTION:

From the problem statement,

$$p_a = 14.7 \text{ psia (101.3 kPa)}$$

$$p_e = 22 \text{ psia (151.7 kPa)}$$

$$\dot{m} = 250 \text{ lbm/s (113.4 kg/s),}$$

and because 32.17 lbm = 1 slug, $\dot{m} = 7.8 \text{ slugs/s,}$

$$A_e = \pi D_e^2 / 4 = 706 \text{ in.}^2 \text{ (0.4554 m}^2\text{)}$$

$$u_a = 800 \text{ ft/s (243.8 m/s)}$$

$$u_e = 1300 \text{ ft/s (396.2 m/s).}$$

Thus, using Eq. 1.4.14, we obtain

$$F = \dot{m}(u_e - u_a) + A_e (p_e - p_a)$$

$$F = 7.8 \text{ slugs/s (1300 - 800) ft/s} + 706 \text{ in.}^2 \text{ (22 - 14.7) lbf/in.}^2;$$

therefore, because $\text{lbf} = \text{slug}\cdot\text{ft}/\text{s}^2$ and $\text{lbf} = \text{in.}^2 \text{ lbf}/\text{in.}^2$,

$$F = 3900 + 5153 = 9053 \text{ lbf (40, 270 N)} \quad <\text{ANS}$$

As one can see, 3900 lbf (17,350 N) is due to mass flux, and 5153 lbf (22,920 N) is due to pressure differences.

1.4.2. Turbofan with a Fan Exhaust

In Figure 1.46, a turbofan with a fan exhaust is shown. The analysis applies for either a turbofan with all of the fan air exhausted or for the hybrid turbofan (a part of the bypassed air separately exhausted). A cylindrical control volume is once again drawn that moves with the engine (CV1). The front surface is far away from the inlet, and the control volume has been drawn so that the rear control surface is at the core exhaust as well as the fan exit. The control volume once again cuts through the strut.

The general momentum equation is the same as for that of the turbojet (Eq. 1.4.1). For the turbofan, applying this equation is slightly more complicated, however. The surface forces are again due to pressures acting on the surfaces, and the force F is due to cutting the strut. The pressure on the front surface of the control volume is uniform because it is far from the engine and at atmospheric conditions p_a . At the front surface, air moves at velocity u_a , uniformly across area $A_a + A_1$. Part of this air enters the core, and part enters the fan. In the most general case (hybrid turbofan), the portion of air that enters the fan can be divided so that a portion exits through the fan exhaust and another part of it is mixed into the core and exits through the primary nozzle. Two exit areas must be considered. At the core exit, the pressure is p_e and the gas velocity is u_e . At the fan exhaust, the pressure is p_s and the air

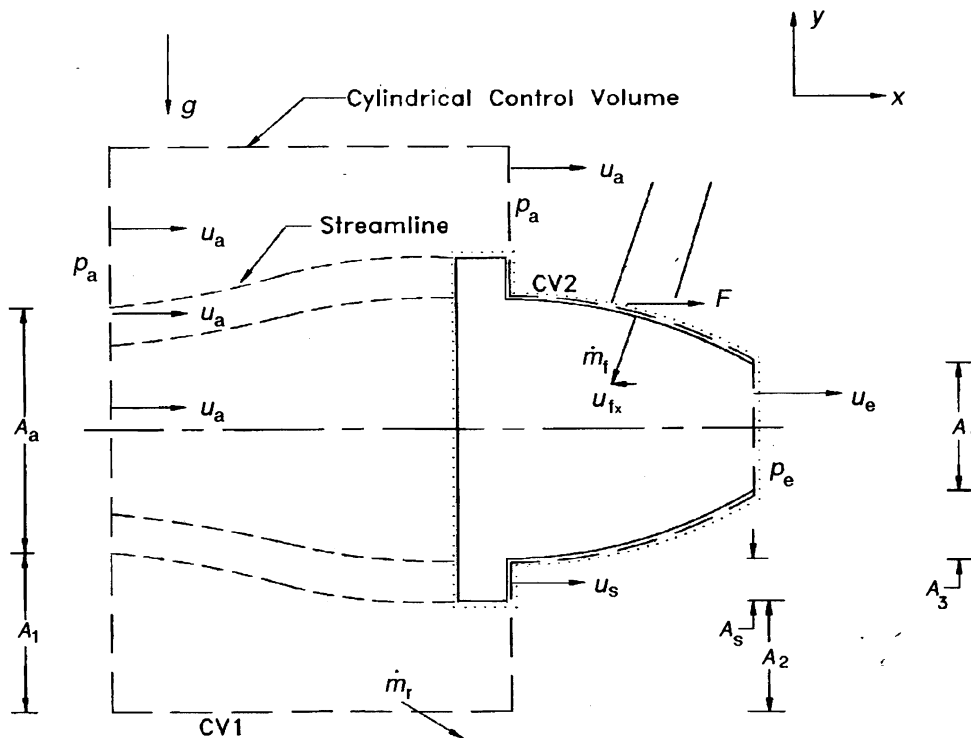


Figure 1.46 Control volume definition for a turbofan with fan exhausted.

velocity is u_s . The areas of the core and fan exits are A_e and A_s , respectively. The pressure on other portions of the rear surface of the control volume is p_a . At the back of the control volume, air exits at velocity u_a across area A_2 . Fuel is once again injected at a flow rate of \dot{m}_f . Once again, the body force in the x -direction is zero. Evaluating each of the terms in Eq. 1.4.1 for steady flow yields

$$\begin{aligned} F + p_a A_1 + p_a A_a - p_a A_2 - p_s A_s - p_e A_e - p_a A_3 + F_{bx} \\ = -u_a \rho_a A_a u_a + u_e \rho_e A_e u_e + u_s \rho_s A_s u_s - u_a \rho_a A_1 u_a + u_a \rho_a A_2 u_a \\ + \dot{m}_f u_a - \dot{m}_f u_{fx}. \end{aligned} \quad 1.4.15$$

By examination of the control volume, one can see that

$$A_1 + A_a = A_2 + A_3 + A_s + A_e \quad 1.4.16$$

Also, three different mass flow rates can be found as follows:

$$\dot{m}_a = \rho_a A_a u_a \quad 1.4.17$$

$$\dot{m}_e = \rho_e A_e u_e \quad 1.4.18$$

$$\dot{m}_s = \rho_s A_s u_s, \quad 1.4.19$$

where \dot{m}_a is the total flow entering the engine, \dot{m}_e is the primary exhaust air flow, and \dot{m}_s is the fan (or secondary) exhaust airflow. Thus, Eq. 1.4.15 becomes

$$\begin{aligned} F = A_e(p_e - p_a) + A_s(p_s - p_a) - \dot{m}_a u_a + \dot{m}_e u_e + \dot{m}_s u_s \\ + \dot{m}_f u_a - u_a^2 \rho_a (A_1 - A_2) - \dot{m}_f u_{fx}. \end{aligned} \quad 1.4.20$$

The continuity equation can be used to show that using a second control volume, CV2, only around the engine

$$\dot{m}_e + \dot{m}_s = \dot{m}_a + \dot{m}_f, \quad 1.4.21$$

and CV1 yields

$$\dot{m}_e + \dot{m}_s + \rho_a u_a A_2 + \dot{m}_r = \dot{m}_a + \dot{m}_f + \rho_a u_a A_1; \quad 1.4.22$$

thus,

$$\dot{m}_r = \rho_a u_a (A_1 - A_2). \quad 1.4.23$$

Using this with Eq. 1.4.20 yields

$$\begin{aligned} F = A_e(p_e - p_a) + A_s(p_s - p_a) + \dot{m}_e(u_e - u_a) \\ + \dot{m}_s(u_s - u_a) + \dot{m}_f u_a - \dot{m}_f u_{fx}. \end{aligned} \quad 1.4.24$$

If the x -component of the fuel velocity is small,

$$F = A_e(p_e - p_a) + A_s(p_s - p_a) + \dot{m}_e(u_e - u_a) + \dot{m}_s(u_s - u_a) + \dot{m}_f u_a. \quad 1.4.25$$

This is the general equation of the thrust of a turbofan engine with the fan exhausted. If the fuel flow is very small ($\dot{m}_f \ll \dot{m}_a$),

$$\dot{m}_a = \dot{m}_e + \dot{m}_s. \quad 1.4.26$$

Equation 1.4.24 for this case reduces to

$$F = A_e(p_e - p_a) + A_s(p_s - p_a) + \dot{m}_e(u_e - u_a) + \dot{m}_s(u_s - u_a). \quad 1.4.27$$

As can be seen, four terms arise from this equation. The first is thrust generated by pressure differences at the primary exhaust. The second is due to pressures at the fan exhaust. The

third and fourth are due to mass fluxes in the primary exhaust and fan exhaust, respectively. A limiting case that could be considered is the fan becoming very small with a reduced flow rate, which is a turbojet. By examining Eq. 1.4.27, one can see that this does indeed reduce to Eq. 1.4.14, for $A_s = 0$ and $\dot{m}_s = 0$.

Example 1.2: A turbofan (approximately the same size as a commercial turbofan engine) operates at sea level and moves at 269.7 m/s (885 ft/s). It ingests 121.1 kg/s (267 lbm/s) of air into the core and five times this amount into the fan (the bypass ratio), which all exhausts through the fan exhaust. The fuel flow is negligible. The exit areas of the fan and core are 1.580 and 1.704 m² (2450 and 2642 in.²), respectively. The exit pressures from the fan and core are 154.4 and 144.8 kPa (22.4 and 21 psia), respectively. The exhaust velocities from the fan and core are 328.6 and 362.7 m/s (1078 and 1190 ft/s), respectively. Find the thrust.

SOLUTION:

From the problem statement,

$$p_a = 101.3 \text{ kPa (14.7 psia)} \quad u_a = 269.7 \text{ m/s (885 ft/s)}$$

$$p_s = 154.4 \text{ kPa (22.4 psia)} \quad u_s = 328.6 \text{ m/s (1078 ft/s)}$$

$$p_e = 144.8 \text{ kPa (21 psia)} \quad u_e = 362.7 \text{ m/s (1190 ft/s)}$$

$$\dot{m}_e = 121.1 \text{ kg/s (267 lbm/s)} = 8.3 \text{ slugs/s}$$

$$\dot{m}_s = 5 \times 121.1 \text{ kg/s} = 605.4 \text{ kg/s (41.7 slugs/s)}$$

$$A_s = 1.580 \text{ m}^2 \text{ (2450 in.}^2\text{)} \quad A_e = 1.704 \text{ m}^2 \text{ (2642 in.}^2\text{)}$$

Therefore, using Eq. 1.4.27, we obtain

$$F = A_e(p_e - p_a) + A_s(p_s - p_a) + \dot{m}_e(u_e - u_a) + \dot{m}_s(u_s - u_a)$$

$$F = 1.704 \text{ m}^2 (144.8 - 101.3) \text{ kPa} + 1.580 \text{ m}^2 (154.4 - 101.3) \text{ kPa} \\ + 121.1 \text{ kg/s (362.7 - 269.7) m/s} + 605.4 \text{ kg/s (328.6 - 269.7) m/s,}$$

and so, because $\text{N} = \text{kg}\cdot\text{m/s}^2$ and $\text{N} = \text{Pa}\cdot\text{m}^2$ and $1000 \text{ Pa} = \text{kPa}$,

$$F = \underset{\text{p-core}}{74,120} + \underset{\text{p-fan}}{83,900} + \underset{\text{m-core}}{11,260} + \underset{\text{m-fan}}{35,660} \\ = \underset{\text{core}}{85,380} + \underset{\text{fan}}{119,560}$$

$$F = 204,940 \text{ N (46,075 lbf)} \quad <\text{ANS}$$

By examining the four different terms, one can see that 85,380 N (19,200 lbf) of thrust is generated by the core, and 119,560 N (26,880 lbf) comes from the fan.

1.4.3. Turboprop

As indicated in the previous section, a turboprop is essentially a turbojet with a propeller. As a result, the derivation of the thrust equation is very similar to that for the turbojet. That is, the thrust is given by

$$F = \dot{m}_f u_a + \dot{m}_e (u_e - u_a) + A_e (p_e - p_a) + F_p, \quad 1.4.28$$

where F_p is the additional thrust due to the propeller. Once again, the fuel flow is often much smaller than the airflow ($\dot{m}_f \ll \dot{m}_a$). As a result,

$$F = \dot{m} (u_e - u_a) + A_e (p_e - p_a) + F_p. \quad 1.4.29$$

1.5. Performance Measures

1.5.1. Propulsion Measures

One of the most important parameters quantifying aircraft engine performance is obviously thrust, F . If an engine does not generate enough thrust to overcome airframe drag, a given aircraft cannot fly. However, a quantity that is just as important as thrust is the thrust-specific fuel consumption ($TSFC$), which is defined as

$$TSFC = \dot{m}_f / F, \quad 1.5.1$$

where \dot{m}_f is the total mass flow rate of fuel (primary burner and afterburner). The $TSFC$ is a measure of how much fuel is used for given thrust and allows for efficiency comparisons between different engines and engine types. It is comparable to the inverse of the miles-per-gallon (mpg) rating of an automobile. A well-suited engine will have a small value for $TSFC$. For a nonafterburning engine, this becomes

$$TSFC = \dot{m}_f / F, \quad 1.5.2$$

where \dot{m}_f is the mass flow rate of the primary burner fuel. The $TSFC$ can conveniently be nondimensionalized using the ambient sound speed:

$$\overline{TSFC} = TSFC \times a_a. \quad 1.5.3$$

A second quantity sometimes used to evaluate fuel economy (but is more often used for rocket engines) is the specific impulse I . This is defined as

$$I = F / (g \times \dot{m}_f), \quad 1.5.4$$

where g is the gravitational constant. One can relate the specific impulse to $TSFC$ by

$$I = 1 / (g \times TSFC). \quad 1.5.5$$

For the remainder of this book, $TSFC$ (or the nondimensional value) will be used to evaluate fuel consumption.

Another dimensionless parameter used to characterize an engine's performance is the dimensionless thrust. This quantity is defined as

$$\overline{F} = \frac{F}{\dot{m}_t a_a}, \quad 1.5.6$$

where \dot{m}_t is the total air mass flow rate into the engine and a_a is again the local speed of sound. This dimensionless thrust represents the inverse to the physical size of an engine, including the diameter and weight. That is, for a given dimensional thrust, the dimensionless thrust decreases as the required mass flow (or physical size) increases and vice versa. In a sense, this nondimensional parameter represents the trends of the thrust-to-weight ratio.

Another performance characteristic for a jet engine that is sometimes used is the propulsive efficiency. This is the ratio of thrust power to the rate of production-of-propellant kinetic energy. In equation form, this is defined as

$$\eta_k = \frac{F u_a}{\sum \dot{m}_{\text{exit}} u_{\text{exit}}^2 - \dot{m}_a u_a^2}. \quad 1.5.7$$

For a turbojet or a mixed turbofan only, one exit stream is present; however, for an unmixed turbofan, two exit streams are exhausted. Note that this efficiency is not an overall thermal efficiency because the enthalpy change is not included. This equation has limited practicality. For example, for a simple turbojet, if the fuel flow is negligible and the exit pressure and

ambient pressure are the same, the thrust is $F = \dot{m}(u_e - u_a)$. The efficiency parameter then becomes $\frac{u_a}{u_a + u_{\text{exit}}}$. One can maximize this (to unity) by setting u_{exit} equal to zero, which results in a negative thrust! Furthermore, if one sets $u_{\text{exit}} = u_a$, the efficiency is 50 percent, but the thrust is zero! Thus, this parameter is identified but will not be used in this book.

To evaluate the overall performance of an aircraft engine, the thrust, *TSFC*, nondimensional thrust, and sometimes the propulsive efficiency must all be considered. The four parameters cannot be treated independently. For different aircraft applications, various objectives will have to be satisfied. For example, for fighter aircraft the fuel consumption is less important than for a commercial carrier, but the engine weight is extremely important. An optimization of the different parameters for a given application can only be accomplished with detailed cycle analyses, as will be shown in chapters 2 and 3.

1.5.2. Power-Generation Measures

For comparison, the most common evaluators for power-generation gas turbines are the net power (\mathcal{P}_{net}), thermodynamic efficiency (η_{th}), heat rate (HR), and specific fuel consumption (SFC). The latter three are given as

$$\eta_{\text{th}} = \mathcal{P}_{\text{net}} / \dot{Q}_{\text{in}} \quad 1.5.8$$

$$HR = \dot{Q}_{\text{in}} / \mathcal{P}_{\text{net}} = \dot{m}_f \Delta H / \mathcal{P}_{\text{net}} \quad 1.5.9$$

$$SFC = \dot{m}_f / \mathcal{P}_{\text{net}} \quad 1.5.10$$

To evaluate the overall performance of a power-generation unit, one must consider the net power, *SFC*, and thermodynamic efficiency. The three parameters also cannot be treated independently. For different applications, various objectives will have to be satisfied. As for an aircraft, an optimization of the different parameters for a given application can only be accomplished through detailed cycle analyses.

1.6. Summary

In this chapter, a brief historical review of turbomachine and propulsion development was first presented and then the different types of aircraft jet engines were introduced. Early developments culminated in the 1930s and 1940s simultaneously in Great Britain and Germany with the patents and operating prototypes of the basic modern jet engine designs. The fundamental thermodynamic concepts of the Brayton cycle which is the basis for a gas turbine, and three complementing cycles were reviewed. The different types of aircraft jet engines and gas turbines were introduced, including ramjets, turbojets, turbofans (two types), turboprops and unducted fans, turboshafts, and power-generation units. Afterburners for thrust augmentation are used on turbojets and turbofans. Typical sizes and thrust or power levels were discussed for both modern and outdated engines to give the reader an appreciation of the variety of applications and historical trends. Cross-sectional views and photographs of engines and gas turbines were also presented. General comparisons were made to indicate which engines are best under different operating conditions. Many modern power-generation gas turbines were shown to be “aero-derivatives” of aircraft engines; that is, the core of the units is essentially the same. Equations were also derived for turbojet and turbofan thrust if all of the inlet and exit conditions are known. Other parameters that allow overall evaluation of a propulsion gas turbine performance were defined: the thrust-specific fuel consumption *TSFC*, nondimensional thrust, and propulsive efficiency. Also, parameters that allow overall evaluation of a power-generation gas turbine performance were defined: the net power, *SFC*, and thermodynamic efficiency.

In the following chapters, thermodynamic and gas dynamic details of the individual components and internal flows are covered in increasing detail so that the operating conditions can be determined. First, an ideal analysis is presented in which the components perform ideally, and the overall operating characteristics (thrust, *TSFC*, etc.) of the engine are found. Second, losses are included (but specified a priori) so that the overall nonideal performance of an engine can be determined. From the cycle analyses, trends are evident that can be used to compare the performances of different engine types. Similarly, engine parameters are varied so that trends in overall performance can be maximized for a given engine type for a given application. Third, detailed component analyses are performed with which component losses can be predicted for the different component geometries and operating conditions (each component is covered in a separate chapter). Lastly, as a capstone, component matching is included so that the dynamic interaction of the different nonideal components with variable losses can be found and the overall engine performance can be predicted for both on-design and off-design conditions.

List of Symbols

A	Area
F	Force
g	Gravitational constant
h	Specific enthalpy
HR	Heat rate
I	Specific impulse
\dot{m}	Mass flow rate
p	Pressure
\mathcal{P}	Power
\dot{Q}	Heat transfer rate
s	Entropy
<i>SFC</i>	Specific fuel consumption
T	Temperature
<i>TSFC</i>	Thrust-specific fuel consumption
u	Velocity
v	Specific volume
\dot{W}	Power
γ	Specific heat ratio
η	Efficiency
ρ	Density

Subscripts

a	Freestream
e	Primary exit
f	Fuel
in	Into component
k	Propulsive
out	Out-of component
net	Net out-of cycle
p	Propeller
r	Rejected
s	Secondary (bypassed)
t	Total (summation)

t_h	Thermal
x	x -direction
1,2,3	Areas of control volume
1...5	Stations in cycle

Problems

- 1.1 A turbojet operates at sea level and moves at 728 ft/s. It ingests 175 lbm/s of air and has negligible fuel flow. The diameter of the exit is 29 in. The exit pressure is 6.75 psia, and the exit velocity is 2437 ft/s. Find the developed thrust.
- 1.2 A turbojet operates at 20,000 ft and moves at 728 ft/s. It ingests 175 lbm/s of air and has negligible fuel flow. The diameter of the exit is 29 in. The exit pressure is 6.75 psia, and the exit velocity is 2437 ft/s. Find the developed thrust.
- 1.3 A turbofan operates at sea level and moves at 893 ft/s. It ingests 150 lbm/s of air into the core and 2.2 times this amount into the fan, which all exits through the fan exhaust. The fuel flow is negligible. The exit areas of the fan and core are 336 and 542 in.², respectively. The exit pressures from the fan and core are 14.7 and 15.8 psia, respectively. The exhaust velocities from the fan and core are 2288 and 1164 ft/s, respectively. Find the thrust. What proportions arise from the fan and core?
- 1.4 A turbofan operates at sea level and moves at 893 ft/s. It ingests 150 lbm/s of air into the core and 2.2 times this amount into the fan, which all is mixed into the core flow. The fuel flow is negligible. The exit area is 851 in.². The exit pressure is 18.4 psia, and the exhaust velocity is 1435 ft/s. Find the thrust.
- 1.5 A turboprop operates at sea level and moves at 783 ft/s. It ingests 30 lbm/s of air and has negligible fuel flow. The area of the exit is 290 in.². The exit pressure is 14.7 psia, and the exit velocity is 625 ft/s. The thrust from the propeller is 2517 lbf. Find the total developed thrust.
- 1.6 Show that a turbofan with all of the bypassed air mixed into the core flow results in the same equation for thrust as for a turbojet.
- 1.7 A turbofan operates at 30,000 ft and moves at Mach 0.75. It ingests 190 lbm/s of air into the core and 1.2 times this amount into the fan, which all exits through the fan exhaust. The fuel flow is 4.66 lbm/s. The exit areas of the fan and core are 936 and 901 in.², respectively. The exit pressures from the fan and core are 4.36 and 9.42 psia, respectively. The exhaust velocities from the fan and core are 1350 and 1880 ft/s, respectively. Find the thrust. What proportions arise from the fan and core? Do this problem for two conditions: first consider the fuel flow to be negligible; then, include the effect of finite fuel flow.
- 1.8 A turbojet operates at 18,000 ft and moves at Mach 0.80. The area of the exit is 361 in.². The exit pressure is 22.40 psia, and the exit velocity is 1938 ft/s. The developed thrust is 11,666 lbf and the fuel flow rate is 4.04 lbm/s. Find the air mass flow rate. Do this problem for two conditions: first consider the fuel flow to be negligible; then, include the effect of finite fuel flow.
- 1.9 A turbofan operates at 24,000 ft and moves at Mach 0.70. It has a bypass ratio of 3.00, and all of this air exhausts through the fan nozzle. The fuel flow is 3.77 lbm/s. The exit areas of the fan and core are 1259 and 1302 in.²,

- respectively. The exit pressures from the fan and core are 9.74 and 5.69 psia, respectively. The exhaust velocities from the fan and core are 1146 and 1489 ft/s, respectively. The thrust is 15,536 lbf. Find the air mass flow rate in the core. Do this problem for two conditions: first consider the fuel flow to be negligible; then, include the effect of finite fuel flow.
- 1.10** A turboprop operates at 9000 ft and moves at 487 ft/s. The exit pressure is 10.5 psia, the exit velocity is 1137 ft/s, and the exit density is $0.000453 \text{ slugs/ft}^3$. The fuel flow rate is 0.95 lbm/s. The thrust from the propeller is 4243 lbf, and the total developed thrust is 4883 lbf. (a) What is the ingested air mass flow rate? (b) If the exit nozzle is round, what is the nozzle exit diameter?
- 1.11** A turbojet operates at 20,000 ft and moves at Mach 0.75. The nozzle exit pressure is 19.70 psia, the exit velocity is 1965 ft/s, and the exit density is $0.000979 \text{ slugs/ft}^3$. The developed thrust is 8995 lbf, and the fuel flow rate is 3.16 lbm/s. (a) Find the ingested air mass flow rate. (b) If the exit nozzle is round, what is the nozzle exit diameter?
- 1.12** A ramjet operates at 50,000 ft and moves at Mach 4. It ingests 90 lbm/s of air and has a fuel flow of 3.74 lbm/s. The diameter of the exit is 31.7 in. The exit pressure is 1.60 psia, and the exit velocity is 5726 ft/s. Find the developed thrust and *TSFC*.
- 1.13** A turbofan operates at 25,000 ft and moves at 815 ft/s. It ingests 1.2 times the amount of air into the fan than into the core, which all exits through the fan exhaust. The fuel-flow-to-core airflow ratio is 0.0255. The exit densities of the fan and core are 0.00154 and $0.000578 \text{ slugs/ft}^3$, respectively. The exit pressures from the fan and core are 10.07 and 10.26 psia, respectively. The developed thrust is 10,580 lbf, and the exhaust velocities from the fan and core are 1147 and 1852 ft/s, respectively. (a) Find the ingested air mass flow rate for the core and *TSFC*. (b) What are the exit areas of the fan and core nozzles?
- 1.14** A turbofan operates at sea-level takeoff (SLTO). It has a bypass ratio of 8.00, and all of the secondary air exhausts through the fan nozzle. The fuel flow is 9.00 lbm/s. The exit areas of the fan and core are 6610 and 1500 in.^2 , respectively. The exit pressures from the fan and core are 14.69 and 14.69 psia, respectively. The exhaust velocities from the fan and core are 885 and 1255 ft/s, respectively. The core mass flow rate is 375 lbm/s. Find the thrust and *TSFC*.

Ideal Cycle Analysis

2.1. Introduction

Chapter 1 identified the basic engine types and defined the important operating performance parameters of gas turbines. That chapter also reviewed the fundamental thermodynamics of cycles and established that gas turbines consist of several important components. Although the operation and design of each component are essential for the efficient operation of the entire jet engine, such details will not be covered yet. Instead, the overall engine will be analyzed for given components with given characteristics. Later chapters address component operation and design. This chapter considers the ideal components. Its objective is to review the fundamental ideal thermodynamic processes (e.g., from Keenan 1970 or Wark and Richards 1999) and the gas dynamic processes (e.g., from Anderson 1982, Zucrow and Hoffman 1976, or Shapiro 1953) and to explain the physical processes for each of the components. Components are assembled in a “cycle analysis” to make it possible to predict the overall engine performance. This chapter presents quantitative examples to demonstrate the analysis and to give the reader a physical understanding of characteristics. Trend studies are also discussed to show the dependence of the overall characteristics on individual parameters. In Chapter 3, nonideal components in which losses occur are used to evaluate the overall performance of an engine. Chapters 2 and 3 each cover all basic engine configurations. As will be seen, the ideal cycle analysis results in relatively short closed-form equations for the engine characteristics. Developing these equations serves three purposes. First, doing so allows the reader to see how the equations are assembled to model an engine without having to deal with numerical details. Second, and more importantly, developing the equations allows the reader to observe how detail parameters affect the overall performance of an engine without parametrically varying numbers. Third, in some cases, analytically optimizing a performance characteristic is possible. On the other hand, nonideal cycle analysis does not result in closed-form equations owing to the increased complexity of the engine.

The adjective “ideal” implies that no losses occur in any of the components. It also suggests that a component is designed to operate at given conditions. An adiabatic process has no heat transfer, whereas an isentropic process is at constant entropy. In all cases in this book, an isentropic process is accomplished through an adiabatic and reversible process. Thus, in this section the components are assumed to have the following ideal characteristics:

External to inlet	– Isentropic and adiabatic flow
Inlet or diffuser	– Isentropic and adiabatic flow
Compressor	– Isentropic and adiabatic flow
Fan	– Isentropic and adiabatic flow
Propeller	– All propeller power generates thrust
Combustor	– Constant static and total pressure Very low velocities
Turbine	– Isentropic and adiabatic flow
Bypass duct	– Isentropic and adiabatic flow

Bypass mixer	– Isentropic and adiabatic flow
Afterburner	– Constant static and total pressure Very low velocities
Exhaust nozzle or exhaust stack	– Isentropic and adiabatic flow <i>And Exit Pressure Matches Atmospheric Pressure</i>
Overall	– Thermally and calorically perfect gas steady state constant c_p , c_v , (and γ) throughout engine Negligible fuel flow No power loss by shaft

First, the reader is encouraged to review the ideal gas equations and stagnation properties in Appendix H, for they will be used extensively in the analysis. Also note that a perfect gas assumption has been used in this chapter. This means that not only is the gas ideal, but the specific heats and the specific heat ratio are not functions of temperature. Lastly, in this and following chapters, standard conditions will be used occasionally. Appendix A contains information on a standard atmosphere at different altitudes. Thus, for reference, standard conditions are $p_{\text{stp}} = 14.69$ psia or 101.33 kPa and $T_{\text{stp}} = 518.7$ °R or 288.2 K. Having reviewed a few of the important concepts of gas dynamics, we now proceed to discuss the operating characteristics of ideal components followed by ideal cycle analyses of the different engines.

2.2. Components

This section covers each component separately as modules with the idea that a group of components will be analytically assembled to analyze a particular engine. In Figure 2.1, a sectional view of the Pratt & Whitney F100 is shown illustrating most of the components covered in this section. Enlargements of the components from this particular engine are shown throughout this section. A few other engine components are also shown and discussed. The basic physical processes are discussed, and enthalpy–entropy (h – s) and pressure–volume (p – v) diagrams are used to reinforce the thermodynamic fundamentals.

A general engine is presented in Figure 2.2. No engine with this geometry exists in the current market because of the many features it incorporates. As will be seen, however, all engines are simplifications of this general engine. In the most general case, three individual flow paths exist. The primary path goes through the propeller, diffuser, fan and compressor, burner, turbine, mixer, afterburner, and primary nozzle. The second path includes the propeller, diffuser, fan, bypass duct, mixer, afterburner, and primary nozzle. In the third path, air flows through the propeller, diffuser, fan, and fan nozzle. In Figure 2.2, position a is the ambient condition, station 1 is the inlet to the diffuser, and position 2 is the exit of the diffuser and entrance to the fan–compressor. Position 3 is the exit of the compressor and entrance to the combustor, and station 4 is the exit of the burner and entrance to the turbine. Station 5 is the exit of the turbine and primary flow entrance to the mixer. Position 7 is the exit of the fan and the entrance to both the fan nozzle and bypass duct. Station 9 is the fan nozzle exit. Position 7.5 is the bypass duct exit and the bypass flow entrance to the mixer. Position 5.5 is the exit of the mixer and entrance to the afterburner, and station 6 is the exit of the afterburner and entrance to the primary nozzle. Lastly, station 8 is the primary nozzle exit. For consistency between engine types, the nomenclature established here will be used for all engine types, each of which will be viewed as a simplification of this general engine.

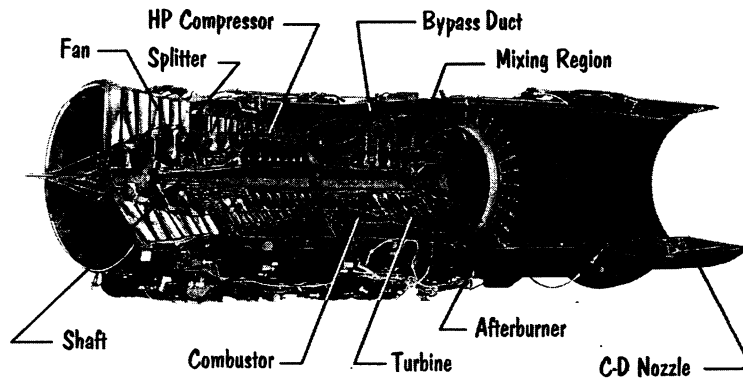


Figure 2.1 Sectional view of Pratt & Whitney F100 (courtesy of Pratt & Whitney).

The purpose of this section is to define the basic thermodynamic operating characteristics of each of the components in a general engine shown in Figure 2.2 and to introduce a few basic definitions.

2.2.1. Diffuser

The first component to be considered is the diffuser or inlet. The purpose of the diffuser is to slow the fluid and to increase the pressure. Figure 2.3 shows the diffuser of a large Pratt & Whitney turbofan. An ideal diffuser is depicted in Figure 2.4. As can be seen, the flow area increases – and thus the flow velocity decreases – from station 1 to 2. Recall that, for ideal cycle analyses, adiabatic and isentropic flows are assumed both outside (stations a to 1) and inside (stations 1 to 2) the diffuser. The overall operation of the ideal diffuser is best illustrated on the h - s and p - v diagrams shown in Figure 2.5. The freestream air is at pressure p_a and can be decelerated adiabatically to total enthalpy h_{ta} and isentropically to total pressure p_{ta} . Processes a to 1 and 1 to 2 are both on the same isentropic process line. As can be seen, because the flow velocity is decreasing, the static enthalpy will increase from ambient enthalpy to that at station 2. Similarly, the static pressure will increase from ambient pressure to that at station 2. Stagnation conditions are also shown. Because all stagnation processes are by definition isentropic, the stagnation properties can be seen to also be on the same isentropic process line. Next, inasmuch as all processes are

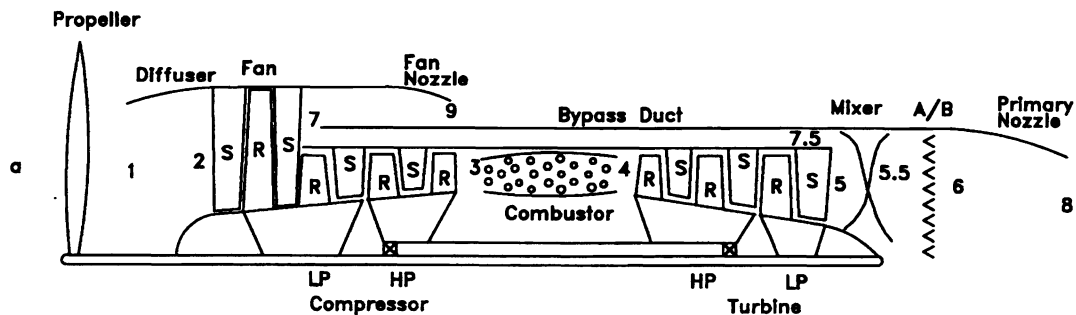


Figure 2.2 General engine description.

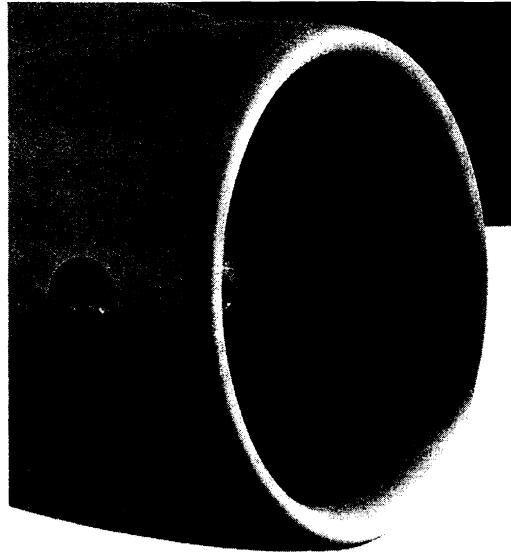


Figure 2.3 Pratt & Whitney inlet or diffuser (courtesy of Pratt & Whitney).

adiabatic, for the flow outside of the diffuser the stagnation enthalpy is constant:

$$h_{t_1} = h_{t_a}, \quad 2.2.1$$

which for an ideal gas reduces to

$$T_{t_1} = T_{t_a}, \quad 2.2.2$$

and for isentropic flow outside of the diffuser the total pressure is constant:

$$p_{t_1} = p_{t_a}. \quad 2.2.3$$

Furthermore, outside of the diffuser, for the definition of stagnation temperature,

$$\frac{T_{t_a}}{T_a} = \left[1 + \frac{\gamma - 1}{2} M_a^2 \right], \quad 2.2.4$$

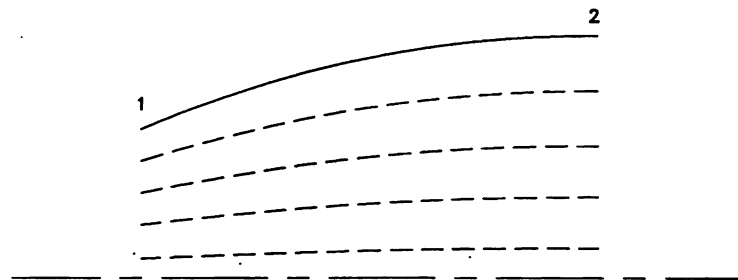


Figure 2.4 Ideal diffuser with streamlines.

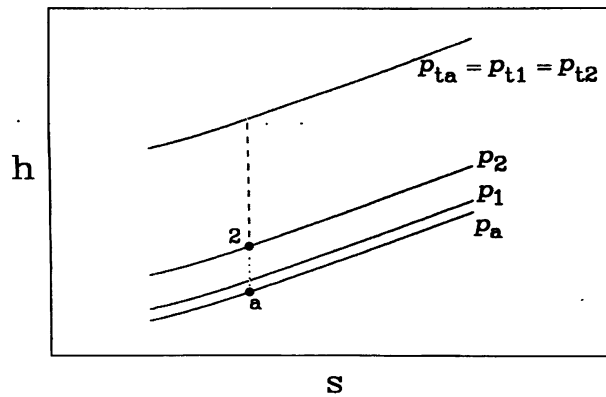


Figure 2.5a h-s diagram for an ideal diffuser.

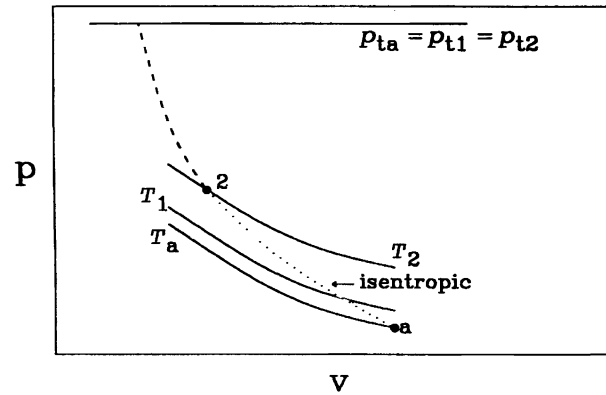


Figure 2.5b p-v diagram for an ideal diffuser.

and from the definition of stagnation pressure,

$$\frac{T_{ta}}{T_a} = \left[\frac{p_{ta}}{p_a} \right]^{\frac{\gamma-1}{\gamma}} \quad 2.2.5$$

Thus, for isentropic flow up to the diffuser,

$$\frac{p_{ta}}{p_a} = \left[1 + \frac{\gamma-1}{2} M_a^2 \right]^{\frac{\gamma}{\gamma-1}} \quad 2.2.6$$

Once again, because the flow is adiabatic inside of the diffuser, the total enthalpy is constant:

$$T_{t2} = T_{t1}; \quad 2.2.7$$

the flow is also isentropic, and thus the stagnation pressure is constant:

$$p_{t2} = p_{t1}. \quad 2.2.8$$

Therefore, for an ideal diffuser,

$$\frac{T_{t2}}{T_a} = \left[1 + \frac{\gamma-1}{2} M_a^2 \right], \quad 2.2.9$$

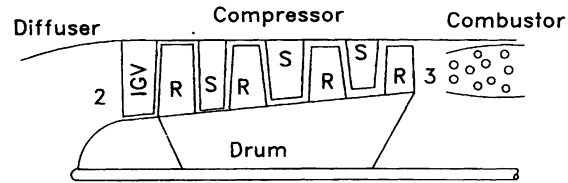


Figure 2.6 Schematic of compressor section.

and

$$\frac{p_{t2}}{p_a} = \left[1 + \frac{\gamma - 1}{2} M_a^2 \right]^{\frac{\gamma}{\gamma - 1}} \quad 2.2.10$$

Thus, by knowing the freestream Mach number and freestream static properties, the stagnation (or total) temperature and pressure at the exit of the diffuser can be found.

2.2.2. Compressor

The next component to be considered is the compressor. A schematic is presented in Figure 2.6, and the Pratt & Whitney F100 compressor is shown in Figure 2.7. In these figures, sets of stationary airfoils are shown (called stator vanes). Directly downstream of these vanes are rotating or moving airfoils (called rotor blades), which are attached to the drum and shaft. The vanes are used to turn the flow in a compressor locally. The rotating blades turn the flow and add energy to the fluid, as will be discussed in Chapter 6. As is the case for any airfoil, air ideally flows across a vane or blade without incidence at the leading edge and is turned smoothly by the vane or blade. A compressor typically consists of 5 to 25 of such sets of rotor blades and stator vanes or stages. One should remember that, in general, as the compressor total pressure ratio increases, the performance of a gas turbine increases. However, as the compressor pressure ratio is increased, the number of compressor stages increases, which adds to the cost and weight of the compressor. Furthermore, the burner needs a high inlet pressure (high compressor exit pressure) for a stable combustion.

The h - s and p - v diagrams for an ideal compressor are presented in Figure 2.8. Process 2 to 3 is isentropic, and both the enthalpy (and temperature) and pressure increase. Also

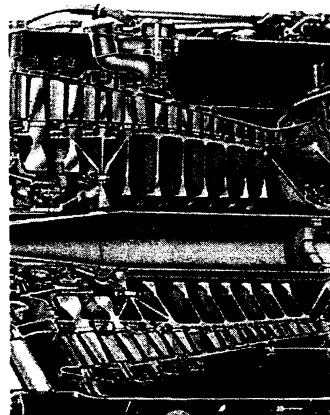


Figure 2.7 F100 Ten-stage compressor (from Fig. 2.1).

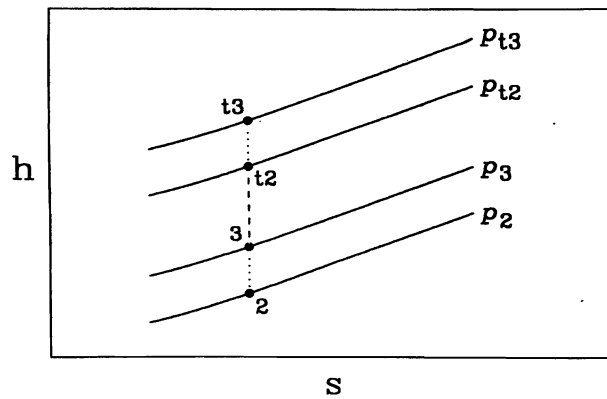


Figure 2.8a h-s diagram for an ideal compressor.

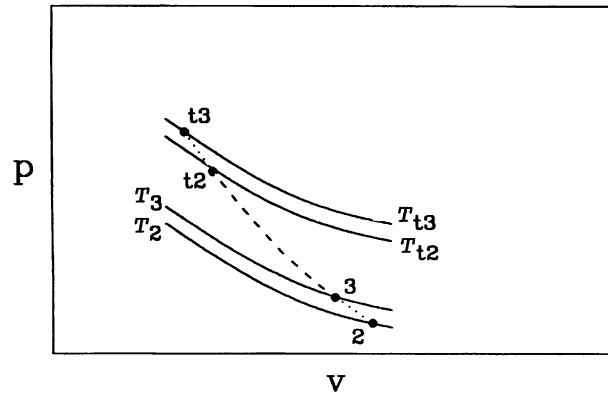


Figure 2.8b p-v diagram for an ideal compressor.

shown are the total (or stagnation) pressures and total enthalpies (and temperatures) at conditions t_2 and t_3 . Because energy is added to the flow, the total pressures and enthalpies also increase from stations 2 to 3. By definition, the stagnation processes are isentropic. Thus, as can be seen, conditions 2, 3, t_2 , and t_3 are all on the same isentropic process line. Next, one can define two quantities for the compressor, the total pressure and temperature ratios across the compressor (stations 2 to 3), as follows:

$$\pi_c = \frac{P_{t3}}{P_{t2}} \quad 2.2.11$$

$$\tau_c = \frac{T_{t3}}{T_{t2}} \quad 2.2.12$$

As will be demonstrated later in this chapter and in Chapter 3, the total pressure ratio is a very important design parameter. Furthermore, because the flow is isentropic in an ideal compressor, the total pressure and total temperature ratios can be related as follows:

$$\pi_c = [\tau_c]^{\frac{\gamma}{\gamma-1}} \quad 2.2.13$$

Thus, if the inlet conditions are known for a compressor and the total pressure ratio is specified, the exit conditions can be determined.

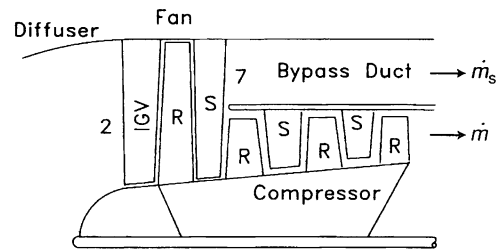


Figure 2.9 Schematic of a fan.

2.2.3. Fan

For a turbofan, a portion of the gas passes through the core of the engine (compressor, combustor, and turbine, see Fig. 2.2), and a portion of the gas is “bypassed”, which passes through the fan and then through the bypass duct and/or fan nozzle. Such a fan section is shown in Figures 2.9 and 2.10. The h - s and p - v diagrams for a fan are identical in nature to those for a compressor except for station numbers. The only differences are in the relative increases in pressure and temperature for a compressor and fan; they are much higher for a compressor. Process 2 to 7 is isentropic, and both the temperature and pressure increase. Also, the stagnation pressures and total temperatures are conditions t_2 and t_7 , and these also increase from stations 2 to 7. Because the stagnation processes are isentropic, conditions 2, 7, t_2 , and t_7 all are on the same isentropic process line.

The core gas flow will be referred to as \dot{m} , and the bypassed flow, or secondary flow, will be termed \dot{m}_s . Thus, the bypass ratio is the ratio of airflow through only the fan to that of the core and is defined by

$$\alpha = \frac{\dot{m}_s}{\dot{m}} \quad 2.2.14$$

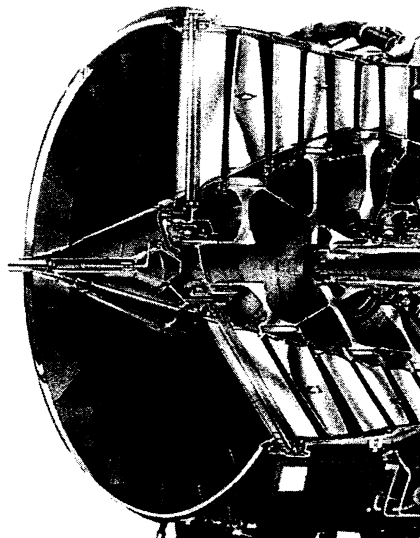


Figure 2.10 Three-stage F100 Fan (from Fig. 2.1).

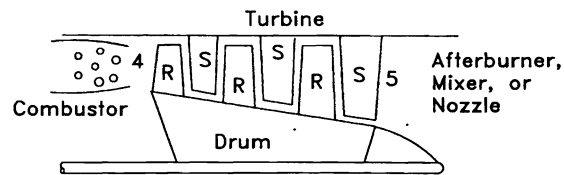


Figure 2.11 Schematic of a turbine.

This ratio is a very important design parameter. For modern aircraft, typical bypass ratios are 0.5 to 9. The next quantities to be defined are the fan total pressure and total temperature ratios (stations 2 to 7). These are given by

$$\pi_f = \frac{p_{t7}}{p_{t2}} \quad 2.2.15$$

and

$$\tau_f = \frac{T_{t7}}{T_{t2}}, \quad 2.2.16$$

which for the ideal case can be related by the isentropic relationship

$$\pi_f = [\tau_f]^{\frac{\gamma}{\gamma-1}}. \quad 2.2.17$$

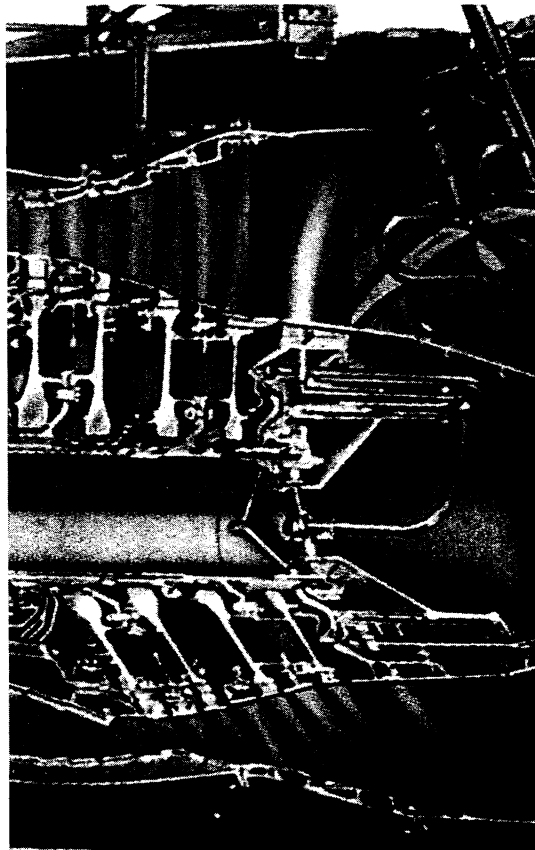


Figure 2.12 F100 Four-stage turbine (from Fig. 2.1).

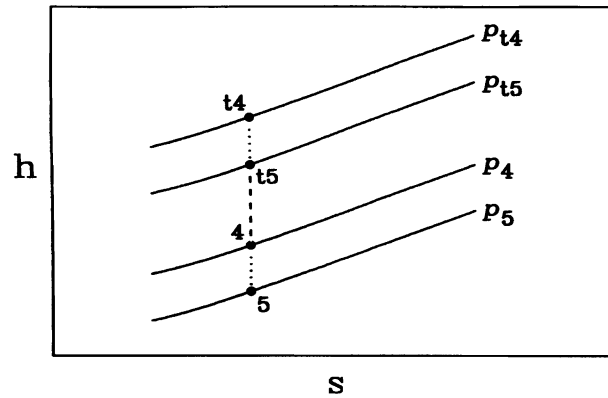


Figure 2.13a h-s diagram for an ideal turbine.

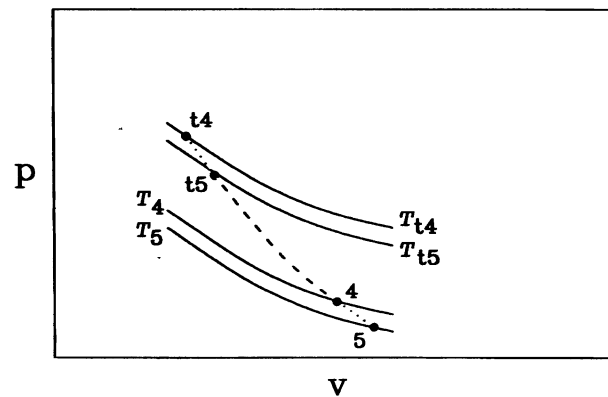


Figure 2.13b p-v diagram for an ideal turbine.

It is very important to note that the total pressure and temperature ratios for the compressor (π_c and τ_c) include the property rises in both the compressor and fan. That is, the fan is also acting as the first stage(s) of the low-pressure compressor.

2.2.4. Turbine

The next component to be considered is the turbine. A schematic is shown in Figure 2.11, and the F100 turbine is shown in Figure 2.12. Like a compressor, a turbine consists of a series airfoils: stator vanes (stationary) and rotating rotor blades. For this component, power is derived from the fluid with the rotor blades. The number of turbine stages is considerably less than for a compressor. The h-s and p-v diagrams for an ideal turbine are shown in Figure 2.13. As is true for an ideal compressor, processes 4 to 5 are isentropic. For the turbine, however, the pressure and temperature drop as do the total pressure and temperature because energy is removed from the fluid. Once again, the static and total conditions at stations 4 and 5 all occur on the same isentropic process line. Two quantities can be defined for the turbine that are similar to those of a compressor: the total pressure and temperature ratios across the turbine (stations 4 to 5):

$$\pi_t = \frac{P_{t5}}{P_{t4}} \quad 2.2.18$$

$$\tau_t = \frac{T_{t5}}{T_{t4}} \quad 2.2.19$$

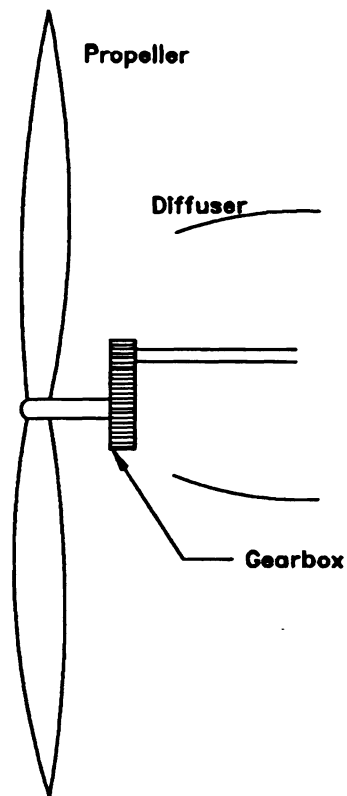


Figure 2.14 Schematic of a propeller.

Once again, because the flow is isentropic in an ideal turbine one can relate the total pressure and total temperature ratios:

$$\pi_t = [\tau_t]^{\frac{\gamma}{\gamma-1}}. \quad 2.2.20$$

2.2.5. Propeller

Propellers are used on turboprop engines (Figs. 2.14 and 2.15) and behave somewhat like very large bypass ratio (~ 20 to 100) fans. The basic operating principle of a propeller entails taking the axial flow of air into the propeller and accelerating that flow to a somewhat higher velocity by adding power derived from the turbine. Because the airflow through the propeller is large, considerable thrust is generated. Power is added to the flow by the rotating propeller blades, which are basically airfoils designed to efficiently accelerate the flow without any leading edge incidence (Theodorsen 1948). Propellers are usually designed so that the blades can be turned or twisted at the hub to adjust the leading edge angle of the blades. Thus, a propeller can be used at various speeds and altitudes with minimal leading edge incidence by rotating the blades through various angles at different conditions. Blade settings at particular conditions are called “schedules.” Blades can also be rotated to produce a negative thrust or reverse thrust for runway braking on landing. Propellers have large aspect ratios; that is, the tip diameter is much larger than the hub diameter. As a result, large stresses can be developed in a propeller because of the centrifugal forces. Propellers could not withstand the stresses if they were attached directly to the compressor shaft. Thus,

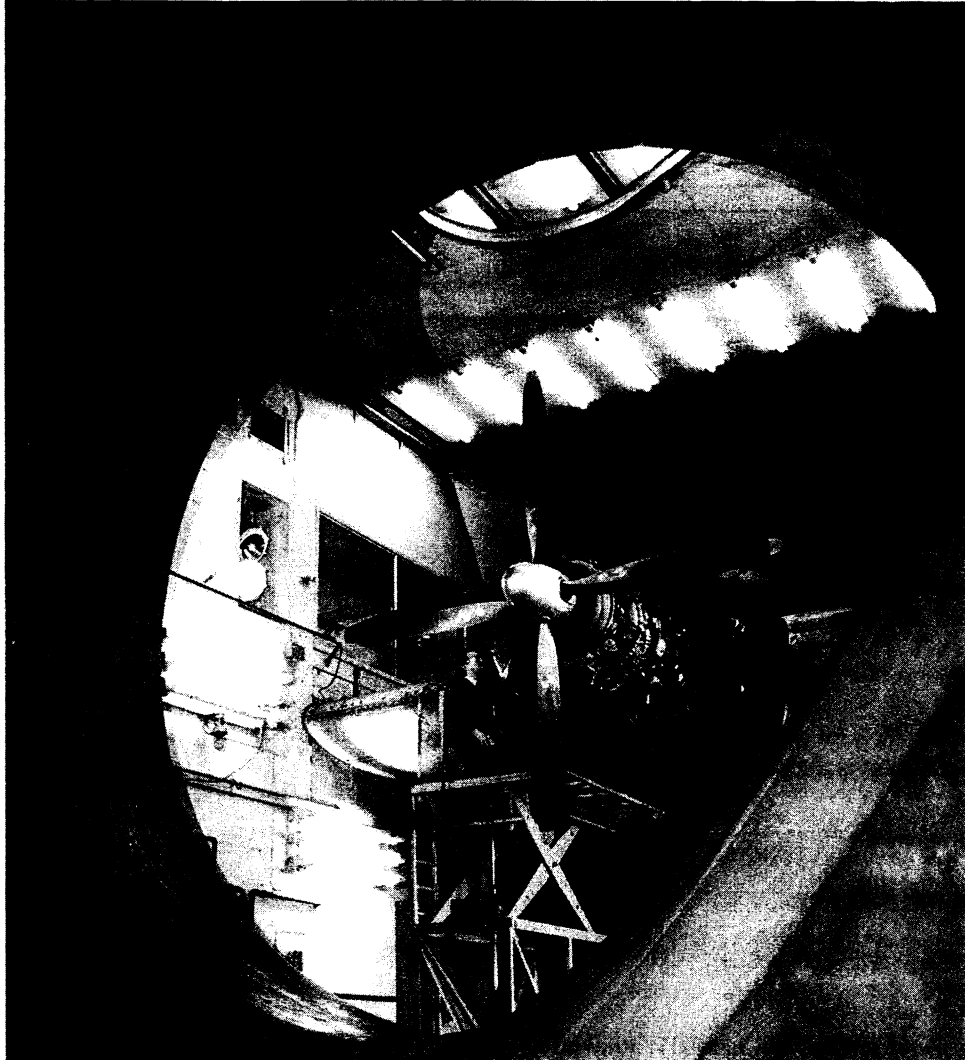


Figure 2.15 Rolls-Royce Dart turboprop with a propeller on a test stand (courtesy of Rolls-Royce).

gearboxes are used to reduce the rotational speed of the propeller – usually by a factor of 10 to 20.

For a turboprop engine, the propeller generates a major portion of the thrust, although some thrust is also derived from the jet. Also, the propeller requires a significant amount of power to generate this thrust. For the analysis of the propeller, power delivered to the propeller, \mathcal{P}_p , will be related to the propeller thrust F_p by

$$\mathcal{P}_p = F_p u_a. \quad 2.2.21$$

A convenient dimensionless quantity is the propeller work coefficient (C_{w_p}), which was defined by Kerrebrock (1992) and is used in this text by

$$C_{w_p} = \frac{\mathcal{P}_p}{\dot{m} c_p T_a}. \quad 2.2.22$$

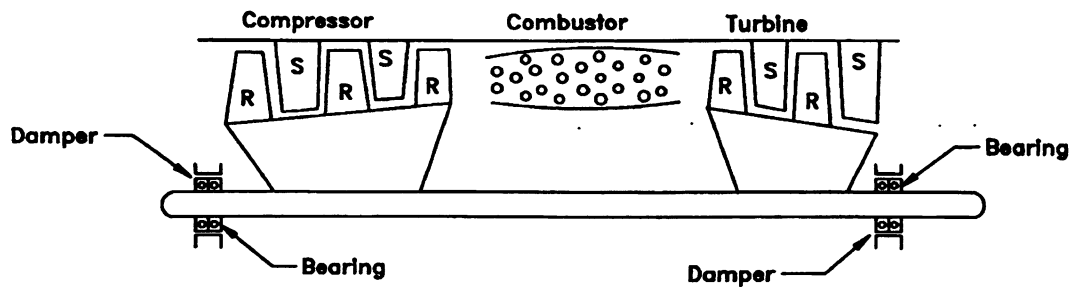


Figure 2.16 Schematic of the turbojet engine shaft.

Thus, if the propeller work coefficient, core mass flow rate, and aircraft speed are known, the thrust can be found.

Two other characteristics are often used to correlate propeller data. The first is the thrust coefficient, which is defined by

$$C_T = \frac{F_p}{\frac{1}{2} \rho_a u_a^2 A_p}, \quad 2.2.23.a$$

where A_p is the circular frontal area swept by the rotating propeller. This is sometimes defined as

$$C_T = \frac{F_p}{\rho_a N_p^2 D_p^4}, \quad 2.2.23.b$$

where N_p is the propeller rotational speed and D_p is the diameter of the impeller. The second coefficient is the power coefficient defined by

$$C_P = \frac{\mathcal{P}_p}{\frac{1}{2} \rho_a u_a^3 A_p} \quad 2.2.24.a$$

or sometimes by

$$C_P = \frac{\mathcal{P}_p}{\rho_a N_p^3 D_p^5}. \quad 2.2.24.b$$

As discussed in Chapter 1, an alternative to a turboprop with long propeller blades is the unducted fan (UDF) or propfan, which was developed in the 1980s and early 1990s by NASA and General Electric, Pratt & Whitney, Rolls-Royce, and others (Figs. 1.36 and 1.37), although this engine never went into production in the United States. Such an engine is a crossbreed between the turboprop, which demonstrates excellent low-aircraft-speed efficiency, and the conventional exhausted turbofan. The blades are shorter than a propeller and thus can be directly attached to the shaft without the need for a gearbox. More blades, which are highly swept, are used as well. Such designs can also effectively operate at higher flight Mach numbers than conventional turboprops.

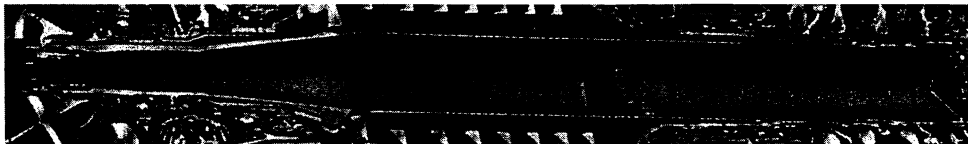


Figure 2.17 F100 shaft (from Fig. 2.1).

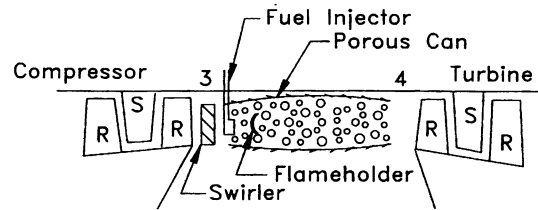


Figure 2.18 Schematic of a combustor.

2.2.6. Shaft

In all engines, except for a ramjet, power is derived from a turbine and delivered to drive all of the compressive devices (namely, a compressor and possibly a fan or propeller). In Figures 2.16 and 2.17, a turbojet shaft is shown. Ideally, all of the derived power will be delivered to the compressive devices. Also, ideally, the mass flow rate remains constant through the engine core (i.e., the fuel flow rate is negligible), and thus the mass flow rate through the turbine is the same as in the compressor. Therefore, with the compressor, fan, propeller, and turbine power taken into consideration, an energy balance on the shaft for the most general ideal case (Fig. 2.2) yields

$$\dot{m}_p (T_{13} - T_{12}) + \dot{m}_s c_p (T_{17} - T_{12}) + C_{w_p} \dot{m}_p T_a = \dot{m}_p (T_{14} - T_{15}), \quad 2.2.25$$

compressor fan propeller turbine

where \dot{m}_s is the bypassed air, which, when used with Eq. 2.2.14 yields

$$\dot{m}_p (T_{13} - T_{12}) + \alpha \dot{m}_p (T_{17} - T_{12}) + C_{w_p} \dot{m}_p T_a = \dot{m}_p (T_{14} - T_{15}) \quad 2.2.26$$

2.2.7. Combustor

A schematic of a primary combustor is shown in Figure 2.18, and the F100 burner is shown in Figure 2.19. The design is complex and empirical. Fuel is injected into the air stream and gradually mixed and burned with the oxidant. The combustor or burner is often the only method by which energy is added to the engine (the only other location is the afterburner). Thus, an energy balance is necessary for the combustor (stations 3 to 4). The h - s and p - v diagrams for an ideal combustor are shown in Figure 2.20. The process 3 to 4 is isobaric (constant pressure) for an ideal process; the process is certainly not isentropic because the entropy increases owing to the irreversible combustion process. Also, for low

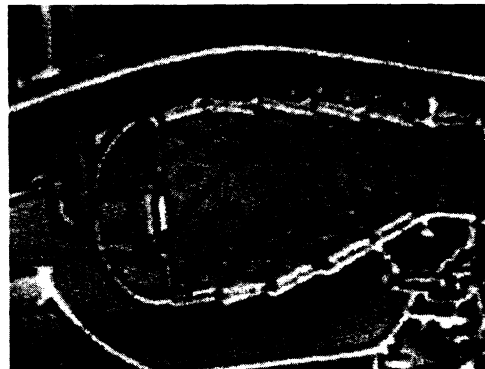


Figure 2.19 F100 primary combustor (from Fig. 2.1).

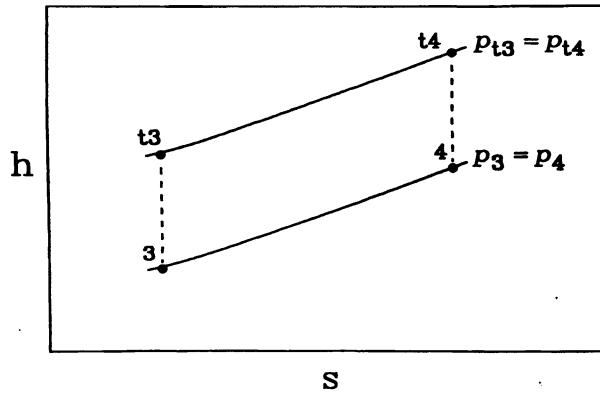


Figure 2.20a h-s diagram for an ideal combustor.

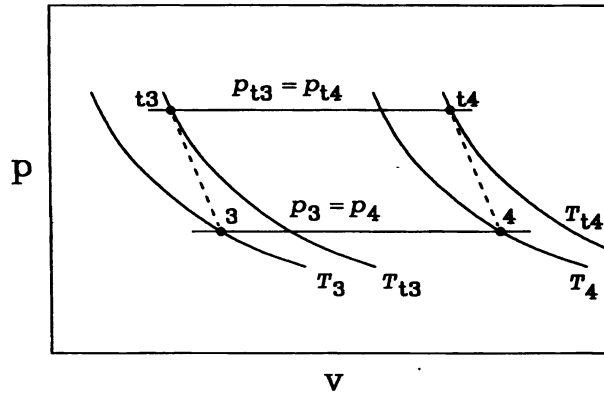


Figure 2.20b p-v diagram for an ideal combustor.

gas velocities (as assumed), process 3 to 4 is at constant total pressure (isobaric) and is also not isentropic. Obviously, the static and total temperatures increase significantly in the combustor. As a result, the static and total specific volumes increase for process 3 to 4, and the fluid density decreases significantly across the combustor.

One needs first to examine the steady-state energy equation for the combustor:

$$\dot{Q} - \mathcal{P} = \Delta \dot{h}, \quad 2.2.27$$

where \dot{Q} is the heat energy rate added to the flow by combustion, \mathcal{P} is the power derived from the flow, and $\Delta \dot{h}$ is the rate change in total enthalpy of the flow. The quantity $\Delta \dot{h}$ contains two contributions. The first is for the air passing through the burner. The second is for the fuel injected into the combustor. The entering air and exiting gas from the burner are both assumed to have specific heat c_p , which will be evaluated based on pure air. This assumption is valid for low fuel flow rates, as will be shown in Chapter 9. The fuel has specific heat c_{pf} . All gases leaving the burner are at T_{t4} . The air entering is at T_{t3} , whereas the fuel enters at T_{tf} . Applying this equation across positions 3 and 4 and realizing no work is produced by the burner, we find that

$$\dot{m}_f \Delta H = \dot{m} (h_{t4} - h_{t3}) + \dot{m}_f (h_{t4} - h_{tf}) \quad 2.2.28.a$$

or

$$\dot{m}_f \Delta H = \dot{m} (c_p T_{t4} - c_p T_{t3}) + \dot{m}_f (c_p T_{t4} - c_{pf} T_{tf}). \quad 2.2.28.b$$

In this equation, ΔH is the heating value of the fuel, and \dot{m}_f is the flow rate of the fuel injected into the burner. Rewriting this equation, using $dh = c_p dT$ and defining the engine parameter τ_b by

$$\tau_b = \frac{T_{t4}}{T_{t3}} \quad 2.2.29$$

yields

$$\frac{\dot{m}_f}{\dot{m}} \Delta H = c_p T_{t3} [\tau_b - 1] + \frac{\dot{m}_f}{\dot{m}} c_p T_{t3} \left[\tau_b - \frac{c_{pf}}{c_p} \right]. \quad 2.2.30$$

Next, the fuel ratio for a nonafterburning engine is defined as

$$f \equiv \frac{\dot{m}_f}{\dot{m}}. \quad 2.2.31$$

For many engines this quantity is very small (on the order of 0.02). Thus, for the ideal analysis it will be assumed to be negligible. Therefore, using Eq. 2.2.30 and solving for \dot{m}_f , we obtain

$$\dot{m}_f = \frac{\dot{m} c_p T_{t3} [\tau_b - 1]}{\Delta H}. \quad 2.2.32$$

The final equation for the burner is given by

$$\pi_b = \frac{p_{t4}}{p_{t3}}, \quad 2.2.33$$

which for the ideal case is unity because the total pressure is constant across the combustor:

$$p_{t4} = p_{t3}. \quad 2.2.34$$

The combustion analysis is greatly simplified at this point so that it can easily be incorporated into an ideal cycle analysis. A more refined and much more accurate analysis referred to as the adiabatic flame temperature will be covered in Chapter 9. A chemical balance (tracking of all the reactants and products) as well as the thermodynamics analysis will later be covered in detail in Chapter 9. For an initial engine cycle analysis, the heating value method is sufficient.

2.2.8. Afterburner

Figure 2.21, presents a schematic of an afterburner, and the F100 afterburner is shown in Figure 2.22. The design is much simpler than that for a primary combustor. Basically, fuel is injected and burned upstream of the nozzle. The process 5.5 to 6 is isobaric for an ideal afterburner and not isentropic. As is the case for a primary combustor, the entropy increases owing to the irreversible combustion process. Also, the process 5.5 to 6 is ideally at constant stagnation pressure. The static temperature and total temperatures increase markedly in the afterburner. As a result, the static and total specific volumes increase for process 5.5 to 6, and the fluid density decreases significantly across the afterburner. As

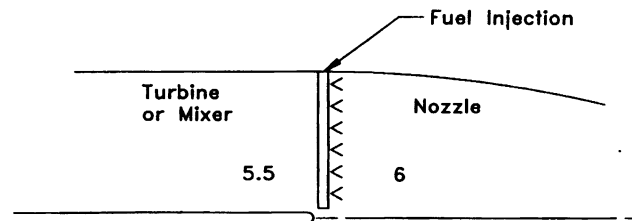


Figure 2.21 Schematic of an afterburner.

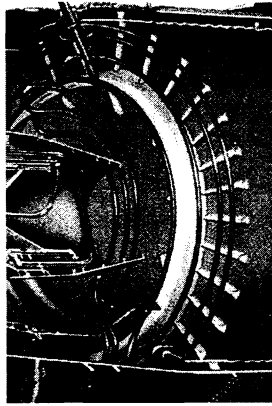


Figure 2.22 F100 afterburner (from Fig. 2.1).

is the case for the primary burner, an energy balance is needed for the afterburner so that the fuel rate can be related to the change in gas temperature. Following a procedure similar to that used for the combustor, one finds for stations 5.5 to 6 that

$$\dot{m}_{f_{ab}} \Delta H = \dot{m}_{5.5} (c_p T_{t6} - c_p T_{t5.5}) + \dot{m}_{f_{ab}} (c_p T_{t6} - c_{p_{f_{ab}}} T_{t_{f_{ab}}}). \quad 2.2.35$$

In this equation, $\dot{m}_{f_{ab}}$ is the flow rate of the fuel injected into the afterburner, and $\dot{m}_{5.5}$ is the mass flow rate of the gas entering the afterburner. Note that $\dot{m}_{5.5}$ will simply be \dot{m} for an ideal turbojet or exhausted turbofan and will be $(\dot{m} + \alpha \dot{m})$ for an ideal mixed turbofan. Also remember that the fuel flow rate is assumed small in the primary burner in deriving Eq. 2.2.35. Rewriting this equation and defining

$$\tau_{ab} = \frac{T_{t6}}{T_{t5.5}} \quad 2.2.36$$

yield

$$\frac{\dot{m}_{f_{ab}}}{\dot{m}_{5.5}} \Delta H = c_p T_{t5.5} [\tau_{ab} - 1] + \frac{\dot{m}_{f_{ab}}}{\dot{m}_{5.5}} c_p T_{t5.5} \left[\tau_{ab} - \frac{c_{p_{f_{ab}}}}{c_p} \right]. \quad 2.2.37$$

One can next examine the quantity $\frac{\dot{m}_{f_{ab}}}{\dot{m}_{5.5}}$ and determine that for many engines this quantity is very small. Thus, for the ideal analysis, it will be assumed negligible. Therefore, using Eq. 2.2.37 and solving for $\dot{m}_{f_{ab}}$ yield

$$\dot{m}_{f_{ab}} = \frac{\dot{m}_{5.5} c_p T_{t5.5} [\tau_{ab} - 1]}{\Delta H}. \quad 2.2.38$$

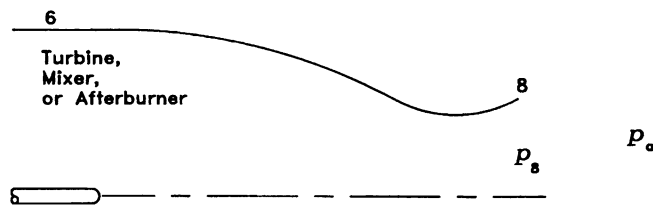


Figure 2.23 Schematic of a primary nozzle.

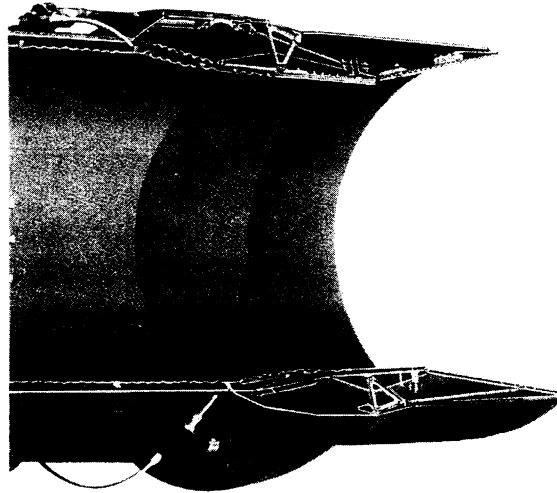


Figure 2.24 F100 nozzle (From Fig. 2.1).

Also, the afterburner fuel ratio is defined by

$$f_{ab} \equiv \frac{\dot{m}_{f_{ab}}}{\dot{m}}. \quad 2.2.39$$

The final equation for the afterburner is given by

$$\pi_{ab} = \frac{p_{t6}}{p_{t5.5}}, \quad 2.2.40$$

which for the ideal case is unity because the total pressure is constant across the afterburner:

$$p_{t6} = p_{t5.5}. \quad 2.2.41$$

2.2.9. Primary Nozzle

The purpose of the primary nozzle (stations 6 to 8) is to convert the moderate temperature and moderate pressure gas to a high-velocity gas that will produce thrust. Figure 2.23 presents a schematic of a primary nozzle and Figure 2.24 displays the F100 nozzle. In Figure 2.25, the h - s and p - v diagrams are depicted for an ideal nozzle. Basically, the flow is accelerated from 6 to 8. As a result, the static temperature and pressure decrease through the nozzle. The specific volume markedly increases (density decreases) through the nozzle, which gives rise to the increase in fluid velocity. The acceleration process is ideally isentropic and adiabatic as is the stagnation process. Thus, once again the conditions 6 and 8 and the stagnation conditions all occur on the same isentropic process line, and the total pressure and temperature are constant through the nozzle. One can first consider the total temperature at the exit:

$$T_{t8} = T_8 \left[1 + \frac{\gamma - 1}{2} M_8^2 \right] \quad 2.2.42$$

For the ideal case the nozzle is adiabatic; thus,

$$T_{t8} = T_{t6}. \quad 2.2.43$$

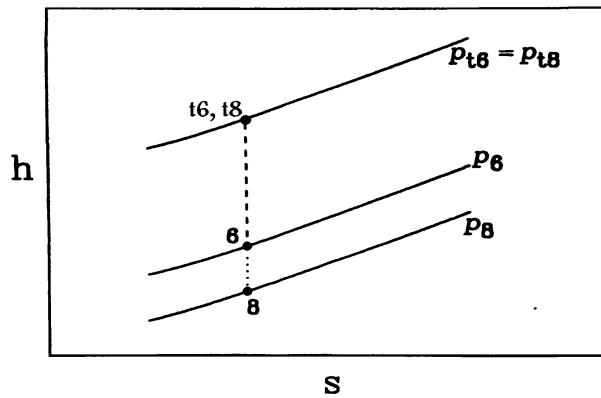


Figure 2.25a a h-s diagram for an ideal nozzle.

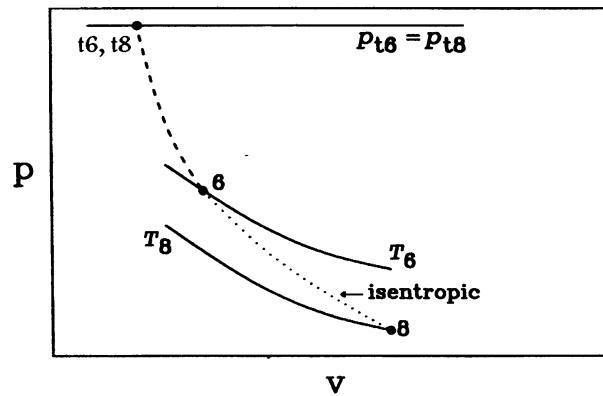


Figure 2.25b a p-v diagram for an ideal nozzle.

Therefore,

$$T_{t6} = T_8 \left[1 + \frac{\gamma - 1}{2} M_8^2 \right]. \quad 2.2.44$$

The exit total pressure can be considered as follows:

$$p_{t8} = p_8 \left[1 + \frac{\gamma - 1}{2} M_8^2 \right]^{\frac{\gamma}{\gamma - 1}} \quad 2.2.45$$

For the ideal case, the nozzle is also isentropic; thus,

$$p_{t8} = p_{t6}. \quad 2.2.46$$

Therefore,

$$p_{t6} = p_8 \left[1 + \frac{\gamma - 1}{2} M_8^2 \right]^{\frac{\gamma}{\gamma - 1}}. \quad 2.2.47$$

Also, for an ideal engine case the nozzle exit pressure “matches,” or is equal to, the ambient pressure. That is,

$$p_8 = p_a. \quad 2.2.48$$

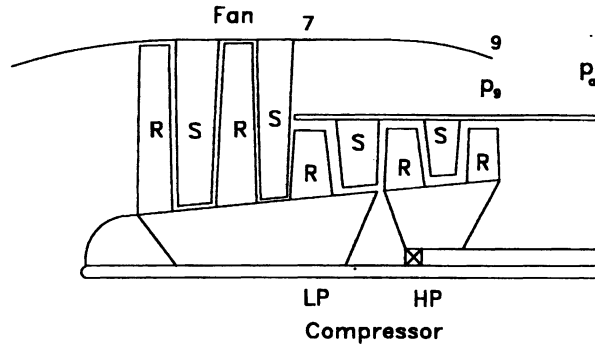


Figure 2.26 Schematic of a fan nozzle.

Thus,

$$p_{t6} = p_a \left[1 + \frac{\gamma - 1}{2} M_8^2 \right]^{\frac{\gamma}{\gamma - 1}} \quad 2.2.49$$

Therefore, if the inlet total pressure and ambient pressure are known, the exit Mach number can be found. Using the exit Mach number, one can find the exit temperature from Eq. 2.2.44 if the inlet total temperature is known. Finally, the exit velocity can be found from the speed of sound (Eq. H.2.8) and Mach number:

$$u_8 = M_8 \sqrt{\gamma \mathcal{R} T_8}. \quad 2.2.50$$

Also, using the energy equation (Eq. H.2.6) across the nozzle for adiabatic flow yields

$$u_8 = \sqrt{2c_p (T_{t6} - T_8)}. \quad 2.2.51$$

Equations 2.2.50 and 2.2.51 will yield identical results.

The reader should recognize that two separate and independent assumptions are made here. First, the *nozzle* is ideal – namely isentropic and adiabatic, which means the efficiency (to be defined in Chapter 3) is unity. Second, the *engine* is operating at the exit ideally, namely p_8 is equal to p_a . These two assumptions can be independently varied, and this will be done in Chapters 3 and 5.

2.2.10. Fan Nozzle

Figure 2.26 is a schematic of a fan nozzle. The fundamental fluid mechanics and thermodynamics of an adiabatic and ideal fan nozzle (stations 7 to 9) are exactly the same as those for an adiabatic and ideal primary nozzle. That is, the flow is accelerated from 7 to 9. The static temperature and pressure decrease through the fan nozzle. The specific volume significantly increases through the nozzle, so to increase the fluid velocity. The acceleration process is ideally isentropic and adiabatic as is the stagnation process. Thus, once again, the conditions 7 and 9 and the stagnation conditions all occur on the same isentropic process line, and the stagnation pressure and temperature are constant through the nozzle. Because the operation is similar to the primary nozzle, the details of the equation development will not be covered. The equations of interest are listed below.

$$T_9 = T_7 \left[1 + \frac{\gamma - 1}{2} M_9^2 \right] \quad 2.2.52$$

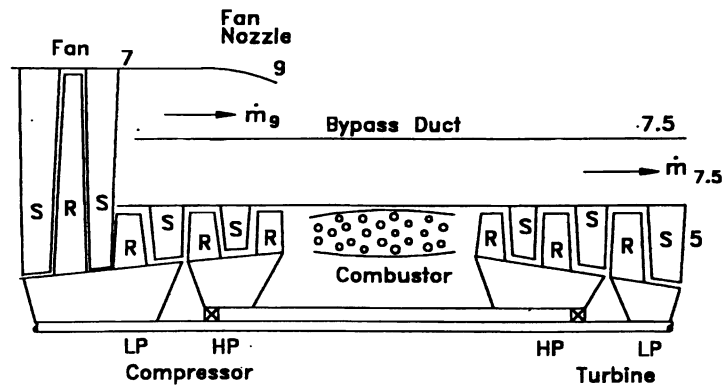


Figure 2.27 Schematic of a bypass duct.

$$T_{t9} = T_{t7} \quad 2.2.53$$

$$T_{t7} = T_9 \left[1 + \frac{\gamma - 1}{2} M_9^2 \right] \quad 2.2.54$$

$$p_{t9} = p_9 \left[1 + \frac{\gamma - 1}{2} M_9^2 \right]^{\frac{\gamma}{\gamma - 1}} \quad 2.2.55$$

$$p_{t9} = p_{t7} \quad 2.2.56$$

$$p_{t7} = p_9 \left[1 + \frac{\gamma - 1}{2} M_9^2 \right]^{\frac{\gamma}{\gamma - 1}} \quad 2.2.57$$

$$p_9 = p_a \quad 2.2.58$$

$$p_{t7} = p_a \left[1 + \frac{\gamma - 1}{2} M_9^2 \right]^{\frac{\gamma}{\gamma - 1}} \quad 2.2.59$$

$$u_9 = M_9 \sqrt{\gamma \mathcal{R} T_9} \quad 2.2.60$$

or

$$u_9 = \sqrt{2c_p (T_{t7} - T_9)} \quad 2.2.61$$

2.2.11. Bypass Duct

When a fan is present, and when at least a part of the flow is mixed into the turbine exit flow, a bypass duct (Figs. 2.27 and 2.28) is used to direct the bypassed air. For the ideal cases, all of the bypassed air is assumed to be either all exhausted or all bypassed through the bypass duct before being mixed back into the primary flow. This latter bypass process is from stations 7 to 7.5. For an ideal bypass duct, the process is adiabatic, and thus the stagnation temperature is constant through the duct:

$$T_{t7.5} = T_{t7}. \quad 2.2.62$$

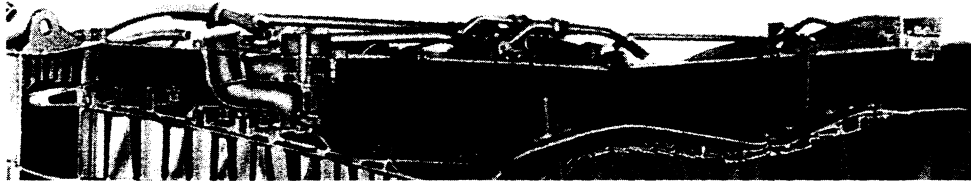


Figure 2.28 F100 Bypass duct (from Fig. 2.1).

The process is also isentropic, and consequently the total pressure is constant:

$$p_{t7.5} = p_{t7}. \quad 2.2.63$$

Now, for a stable condition at the mixer inlet the static pressures from the bypassed and core streams must be equal. If they are not, backflow will occur in either the fan or core, which is impossible. Thus, the static pressures must match:

$$p_{7.5} = p_5. \quad 2.2.64$$

Applying this condition for the analysis at the mixer would require knowledge of the flow velocities or cross-sectional areas because the analyses of all of the other component analyses use total pressures. However, if the Mach numbers are approximately the same for the two streams – that is, $M_5 \cong M_{7.5}$ – or if both Mach numbers are well below about 0.3, where compressibility effects can be ignored, an alternative condition can be used as follows:

$$p_{t7.5} = p_{t5}. \quad 2.2.65$$

This is a simpler condition and will be used herein because it facilitates the cycle analysis considerably.

2.2.12. Bypass Mixer

For a fully mixed turbofan, a mixer is used to fold the ducted (and bypassed) air stream (stream 7.5) and the core gas flow stream (out of the turbine, stream 5) together. The average properties after the mixer are stream 5.5. A schematic is presented in Figure 2.29, and the F100 mixing region is shown in Figure 2.30. The mixer can be a series of blades to “fold” the cool bypassed air into the warmer gas from the turbine to induce a uniform flow. Ideally, the process is isentropic; thus, the stagnation pressure remains constant across the mixer. For the conditions just cited, from Eq. 2.2.65,

$$p_{t5.5} = p_{t5} = p_{t7.5}. \quad 2.2.66$$

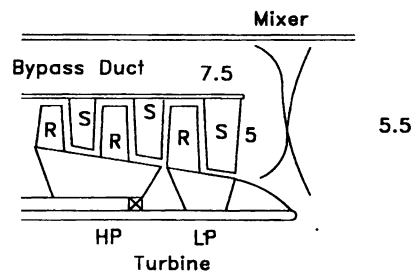


Figure 2.29 Mixer schematic.



Figure 2.30 F100 mixing region (from Fig. 2.1).

Next, for adiabatic flow, the summation of total enthalpy remains constant across the mixer. Also, ideally, the flow exiting the mixer is uniform in static and total temperatures. If one considers the mixing streams at station 5.5, the energy equation yields

$$(\dot{m} + \dot{m}_s) h_{15.5} = \dot{m}_s h_{17.5} + \dot{m} h_{15}, \quad 2.2.67$$

where \dot{m} is the core mass flow rate and \dot{m}_s is the secondary airflow rate through the duct. Now, from the definition of the bypass ratio (Eq. 2.2.14), this becomes

$$h_{15.5} = \frac{\alpha h_{17.5} + h_{15}}{\alpha + 1}. \quad 2.2.68$$

But, for an ideal gas, this reduces to

$$T_{15.5} = \frac{\alpha T_{17.5} + T_{15}}{\alpha + 1}. \quad 2.2.69$$

Thus, once the properties of the incoming streams are known, the exit conditions can be found.

2.2.13. Exhaust for a Power-Generation Gas Turbine

The primary focus of this book is jet propulsion. However, power-generation gas turbines are closely related. In fact, as discussed in Chapter 1, many power gas turbines for electric generation or marine applications are aero-derivatives. That is, much of the development work for such gas turbines was carried out as a part of jet engine design research. One of the largest differences between a power gas turbine and a jet engine is that a power-generation gas turbine has an exhaust with very low velocity compared with a nozzle and does not generate thrust. Thus, because a nozzle and exhaust operate with different functions, they are treated differently and separately.

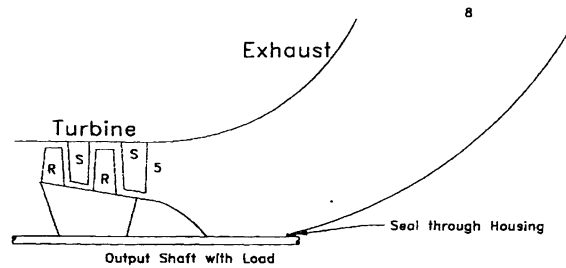


Figure 2.31 Schematic of a power-generation gas turbine exhaust.

A simple schematic of an exhaust is shown in Figure 2.31. Figure 2.32 presents the Coberra 6000 gas turbine. The reader should identify two major differences between this geometry and that of a jet engine. First, the exhaust section primarily takes axial flow out of the turbine and turns it mainly in a radial direction. The exhaust has a series of large vanes that smoothly direct the flow to the remainder of the exhaust system. Second, the bell inlet accelerates the flow axially into the compressor. Note also the large, two-stage auxiliary or free turbine used to generate mechanical power on this unit. An exhaust system is often quite long and may extend, for example, through ducting to a stack or tower. The velocity at the exit of the exhaust system is very low, and consequently the static and total pressures are nearly identical. The design of an exhaust should include smooth walls and gentle curves.

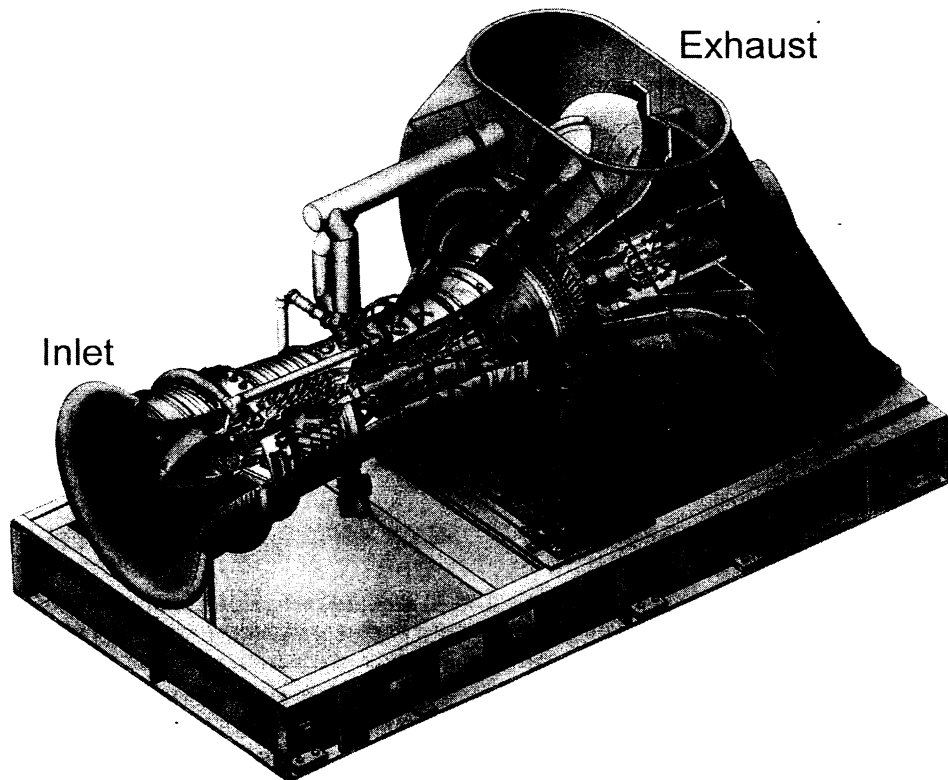


Figure 2.32 Coberra 6000 series gas turbine (courtesy of Rolls-Royce).

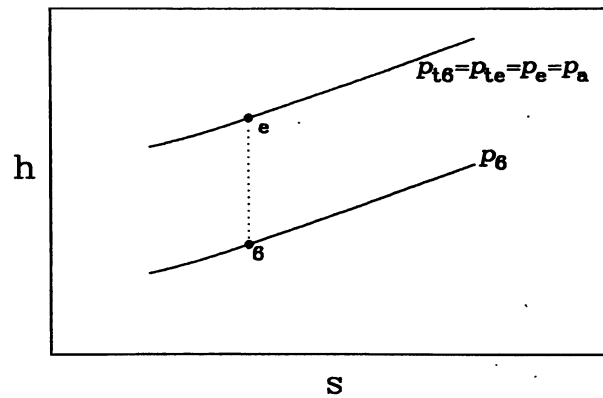


Figure 2.33a h-s diagram for an ideal exhaust.

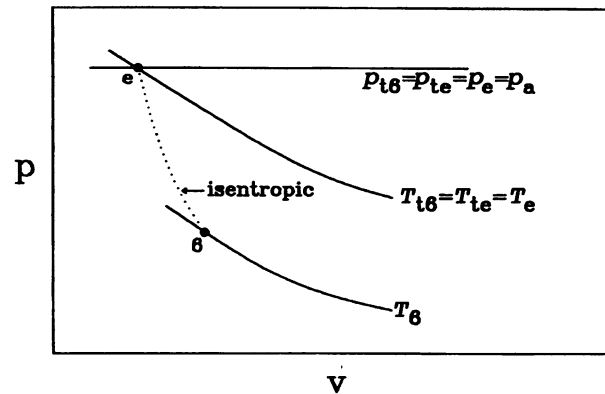


Figure 2.33b p-v diagram for an ideal exhaust.

Figure 2.33a displays an h-s diagram for an ideal exhaust, and Figure 2.33b shows the p-v diagram. An ideal exhaust is assumed to be adiabatic and isentropic. The static pressure and temperature increase through the exhaust since the velocity is decreasing. Because the velocity is low at the exit, the exit static pressure matches atmospheric pressure. Thus, one can write a set of working equations:

$$P_{t8} = P_8 = P_{t5} = P_a \quad 2.2.70$$

$$T_{t8} = T_8 = T_{t5}. \quad 2.2.71$$

2.3. Cycle Analysis

The previous section has described ideal components. This section covers the analysis of different engines with ideal components. Different combinations of the various components are used as determined by the engine type of concern, and they are assembled in two ways. First, for the different jet engine types, analytical, closed-form equations for thrust and *TSFC* are derived based on the component equations developed in Section 2.2. Kerrebrock (1992) presented some of the following resulting equations but did not completely present the development. This chapter will allow the reader to see how the equations are assembled to model an engine without being encumbered by numerical details. A similar

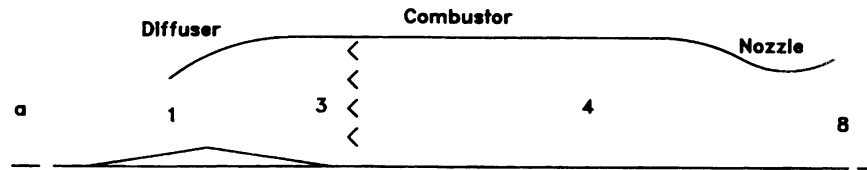


Figure 2.34 Ramjet.

procedure is used for a power-generation gas turbine. More importantly, this approach will allow the reader to observe directly how detail parameters affect the overall performance of an engine without having to vary numbers parametrically. In some cases, analytical optimizations will be possible based on the performance equations. Second, examples will be worked in which each component will be analyzed and treated independently with step-by-step numerical computations. Solutions for different gas turbine types and conditions can also be obtained using the software, “JETENGINECYCLE” and “POWERGTCYCLE”.

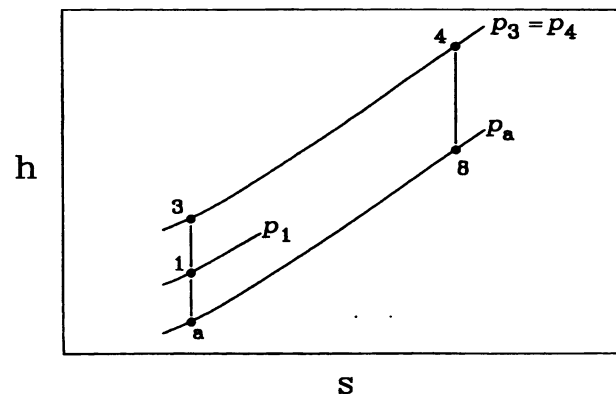
2.3.1. Ramjet

A general ramjet is considered in Figure 2.34. As indicated earlier, this is the simplest of jet engines because it does not have any rotating shafts. In Figure 2.34, position “a” is the ambient condition, position 1 is the inlet to the diffuser, position 3 is the exit of the diffuser and inlet to the combustor, position 4 is the exit of the burner and inlet to the nozzle, and lastly position 8 is the exit of the nozzle. Figure 2.35 presents the h - s diagram for an ideal ramjet system. Process “a” to 1 to 3 is an isentropic compression in which the pressure is increased by the “ram” effect. Process 3 to 4 is an isobaric combustion process. Finally, process 4 to 8 is an isentropic expansion process that accelerates the flow velocity and decreases the pressure. Both states “a” and 8 are on the same pressure line but do not constitute a process as in a closed cycle.

The objective now is to determine the thrust for given component characteristics. Thus, Eq. 1.4.14 is used because the fuel flow rate has been assumed to be small for the ideal case:

$$F = \dot{m}(u_e - u_a) + A_e(p_e - p_a) \quad 2.3.1$$

The airflow rate (\dot{m}) is presumably known for an engine. Also, the aircraft speed, u_a , is presumed to be known. Furthermore, because the nozzle exit pressure matches atmospheric pressure for the ideal case, $p_e = p_a$. Thus, the only quantity that needs to be found for

Figure 2.35 h - s diagram for an ideal ramjet.

calculation of the thrust is u_e , which for the ramjet is also labeled u_8 . Nondimensionalizing the thrust by $\dot{m} u_a$ results in

$$\frac{F}{\dot{m} u_a} = \left(\frac{u_8}{u_a} - 1 \right). \quad 2.3.2$$

Thus, to find this parameter it is first necessary to identify the nozzle exit gas velocity u_8 or the ratio u_8/u_a . Thus, the objective of the next several steps is to find F and $TSFC$ eventually in terms of the engine operating parameters. As indicated, u_8/u_a must be determined. First, this ratio can be identified as

$$\frac{u_8}{u_a} = \frac{M_8 a_8}{M_a a_a} = \frac{M_8 \sqrt{\gamma \mathcal{R} T_8}}{M_a \sqrt{\gamma \mathcal{R} T_a}} = \frac{M_8 \sqrt{T_8}}{M_a \sqrt{T_a}}, \quad 2.3.3$$

where M_a and M_8 are the free-stream and exit Mach numbers, respectively, and a_a and a_8 are the free-stream and exit sound speeds, respectively. Next, the total pressures at positions a and 8 can be considered:

$$\frac{p_{ta}}{p_a} = \left[1 + \frac{\gamma - 1}{2} M_a^2 \right]^{\frac{\gamma}{\gamma - 1}} \quad 2.3.4$$

$$\frac{p_{t8}}{p_8} = \left[1 + \frac{\gamma - 1}{2} M_8^2 \right]^{\frac{\gamma}{\gamma - 1}}. \quad 2.3.5$$

However, from the ideal assumption that the exit pressure matches ambient conditions, it follows that

$$p_8 = p_a. \quad 2.3.6$$

Also, processes “a” to 1 (external flow), 1 to 3 (diffuser), and 4 to 8 (nozzle) are all isentropic, whereas process 3 to 4 (combustor) is isobaric (constant total pressure, not to be confused with isobaric). Thus, the total pressure is constant throughout an ideal ramjet:

$$p_{ta} = p_{t1} = p_{t3} = p_{t4} = p_{t8}. \quad 2.3.7$$

Therefore, from Eqs. 2.3.6 and 2.3.7,

$$\frac{p_{ta}}{p_a} = \frac{p_{t8}}{p_8}. \quad 2.3.8$$

Thus, from Eqs. 2.3.4, 2.3.5 and 2.3.8, one finds that

$$M_a = M_8. \quad 2.3.9$$

At first, this may look surprising. The Mach numbers at the freestream and exhaust are the same, but not the velocities. The gas entering the nozzle is very hot since it is just exiting from the burner. The exhaust velocity can be found using Eqs. 2.3.9 and 2.3.3:

$$\frac{u_8}{u_a} = \frac{\sqrt{T_8}}{\sqrt{T_a}}. \quad 2.3.10$$

Now, for the total temperatures at locations a and 8 , one finds the ratio from Eq. H.2.9 as follows:

$$\frac{T_{t8}}{T_{ta}} = \frac{T_8 \left[1 + \frac{\gamma - 1}{2} M_8^2 \right]}{T_a \left[1 + \frac{\gamma - 1}{2} M_a^2 \right]}. \quad 2.3.11$$

However, since the Mach numbers are the same,

$$\frac{T_8}{T_a} = \frac{T_{t8}}{T_{ta}}. \quad 2.3.12$$

Processes a to 3 (external and diffuser) and 4 to 8 (nozzle) are both adiabatic; thus, the total temperatures are constant for these processes:

$$T_{t3} = T_{ta} \quad 2.3.13$$

$$T_{t8} = T_{t4}. \quad 2.3.14$$

Thus,

$$\frac{T_{t8}}{T_{ta}} = \frac{T_{t4}}{T_{t3}} = \tau_b, \quad 2.3.15$$

which is the burner total temperature ratio. Using Eqs. 2.3.15, 2.3.12, and 2.3.10 yields

$$\frac{u_8}{u_a} = \sqrt{\tau_b}. \quad 2.3.16$$

And so, from Eq. 2.3.2, a dimensionless quantity is

$$\frac{F}{\dot{m}u_a} = (\sqrt{\tau_b} - 1). \quad 2.3.17$$

Alternatively, if the value of the free-stream velocity is expressed in terms of the Mach number and speed of sound ($u_a = M_a a_a$), the dimensionless thrust is

$$\frac{F}{\dot{m}a_a} = M_a(\sqrt{\tau_b} - 1). \quad 2.3.18$$

Thus, this represents half of the objective. By examining this simple equation, one can see that the dimensional thrust is directly proportional to the mass flow rate. It is also directly proportional to the Mach number if all of the other parameters are constant. One limiting case is for a Mach number of zero; this equation indicates that the thrust is zero for this case. A ramjet is unique in this respect and is not capable of takeoff on its own as are all other engines. Moreover, as the burner total temperature ratio increases, so does the thrust. One should remember, however, that $\tau_b = T_{t4}/T_{t3}$ and that T_{t3} is related to the free-stream Mach number; consequently, independently varying M_a and τ_b is difficult.

The thrust has been found, but the *TSFC* remains to be determined. Because this quantity depends on the fuel flow rate, the steady-state energy equation needs to be examined for the combustor (Eq. 2.2.32) with Eqs. 2.3.13 and 2.2.31. The fuel ratio (\dot{m}_f/\dot{m}) is

$$f = \frac{c_p T_{ta} (\tau_b - 1)}{\Delta H}. \quad 2.3.19$$

Finally, using Eqs. 2.3.18, 2.3.19, and 1.7.3 yields the nondimensional *TSFC*:

$$TSFC \ a_a = \frac{c_p T_{ta} (\tau_b - 1)}{M_a \Delta H (\sqrt{\tau_b} - 1)}. \quad 2.3.20$$

From this equation, the *TSFC* can be evaluated based on the engine characteristics. By examining this equation, one can see that the *TSFC* is directly proportional to the total ambient temperature, but it must be remembered that T_{ta} is related to the Mach number. Also, as the burner total temperature ratio increases, so does the *TSFC*. Thus, equations for both of the desired performance quantities (thrust and *TSFC*) have been determined. For a typical ramjet, the values of *TSFC* range from 1.5 to 3 lbm/h/lbf.

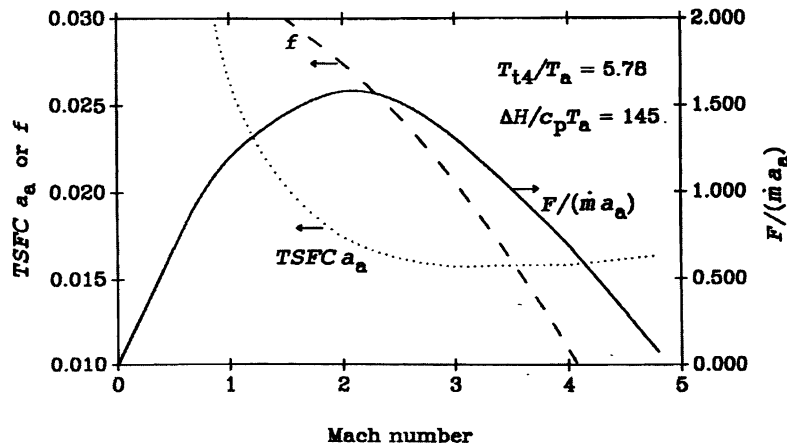


Figure 2.36 Effect of Mach number on dimensionless $TSFC$, dimensionless thrust, and fuel ratio of an ideal ramjet.

Using Eq. 2.2.4 to find T_{ta} , one can differentiate Eq. 2.3.20 with respect to M_a set to zero and easily show that, for constant altitude, heating value, and τ_b , the minimum value of $TSFC$ occurs for

$$M_{a,opt} = \sqrt{\frac{2}{\gamma - 1}}. \quad 2.3.21$$

It is now possible to perform the first of many trend studies. Before proceeding however, note an important operating characteristic of all engines. One of the limiting quantities in modern jet engines is the thermal limit of the materials. Thus, T_{t4} is essentially fixed by this consideration because this is the hottest region in the engine. For a ramjet this constitutes the nozzle, and for engines with rotating components the turbine inlet temperature is the limit. As a result, T_{t4}/T_a for a given altitude is fixed. Of primary importance for any engine are the developed thrust and $TSFC$. In Figure 2.36, the dimensionless thrust and $TSFC$ for an ideal ramjet are shown as functions of Mach number for a fixed value of T_{t4}/T_a (i.e., $T_{t4} = 3000^\circ\text{R}$ and $T_a = 519^\circ\text{R}$). The fuel ratio is also shown. For this trend study and all others to follow, the specific heat ratio is 1.4 and the quantity $\Delta H/(c_p T_a)$ is 144.62. As can be seen, the thrust is maximized for one particular value of Mach number. On the other hand, the $TSFC$ is minimized at a somewhat higher Mach number. This indicates that, for a given fuel and material operating limits, two optimum flight conditions exist as determined by which quantity is to be optimized. Note that, at low Mach numbers, the value of $TSFC$ rapidly increases and the thrust rapidly decreases, which indicates that this engine should not be used at low velocities because the total pressure into it is too small owing to the lack of “ram” effect. As the Mach number becomes large, the exhaust velocity approaches the free-stream velocity if T_{t4} is held constant; consequently, the resulting thrust decreases. These are very important findings. Although the current analysis is ideal, similar trends would be found for a nonideal cycle analysis.

A special case, namely the *stoichiometric* condition, is now considered. For this condition, exactly the right proportion of fuel and air will be used so that *all* of the fuel and air are consumed in the combustion process and neither is left in the combustion products. This subject will be covered in more detail later but is identified now. Basically, for a given fuel, the stoichiometric condition fixes τ_b and f , which are defined as τ_{bst} and f_{st} , respectively. Typically, the stoichiometric fuel ratio is 0.06 to 0.07 for jet fuels, which results in very high

temperatures – too high for engines with turbines, as will be shown in Chapter 9. However, ramjets can tolerate much higher temperatures because of the lack of rotating parts. Thus, Eq. 2.3.19 becomes

$$\tau_{b, \text{st}} - 1 = \frac{f_{\text{st}} \Delta H}{c_p T_{\text{ta}}} \quad 2.3.22$$

Using eq. 2.3.20 yields

$$TSFC_{\text{st}} = \frac{f_{\text{st}}}{M_a a_a (\sqrt{\tau_b} - 1)} \quad 2.3.23$$

Thus, Eqs. 2.3.22 and 2.3.23 yield

$$TSFC_{\text{st}} = \frac{f_{\text{st}}}{M_a a_a \left(\sqrt{\frac{f_{\text{st}} \Delta H \left(\frac{T_a}{T_{\text{ta}}} \right)}{c_p T_a} + 1} - 1 \right)} \quad 2.3.24$$

Note that the quantity T_{ta}/T_a is solely a function of the free-stream Mach number and is given by Eq. 2.3.4. Thus, for a given fuel at stoichiometric conditions, the value of $TSFC$ is *only* a function of the Mach number and T_a (or a_a for a given γ). Using these facts, one can perform another trend study. In Figure 2.37, the dimensionless $TSFC$ is plotted against the Mach number under stoichiometric conditions. As can be seen, a minimum $TSFC$ is attained at one particular Mach number. For this condition, the maximum thrust is developed at the same Mach number. By comparing Figures 2.36 and 2.37, one can observe several characteristics. For example, under stoichiometric conditions, the optimum $TSFC$ is higher

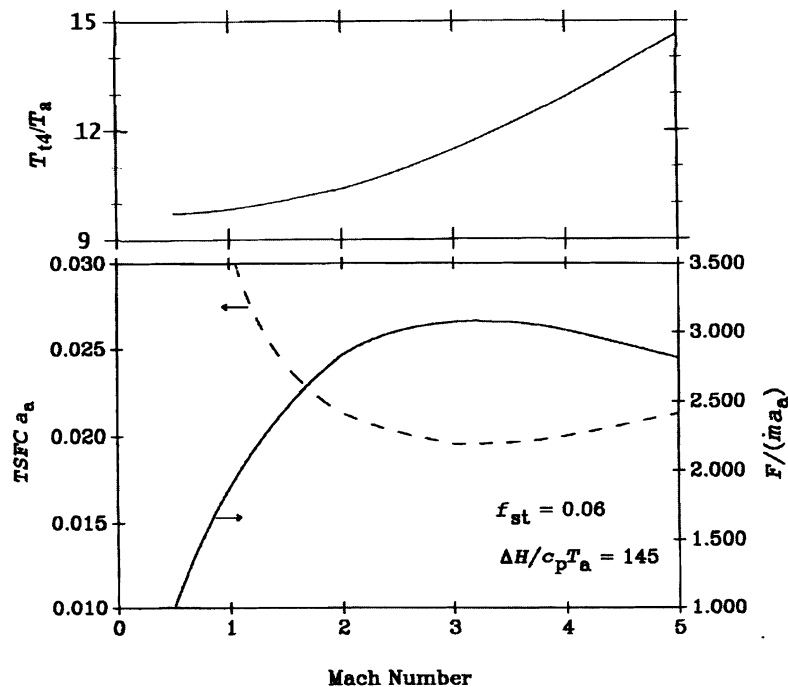


Figure 2.37 Effect of Mach number on dimensionless temperature, dimensionless $TSFC$ and dimensionless thrust of an ideal ramjet operating stoichiometrically.

than for fuel ratios that are below the stoichiometric condition. Therefore, this condition is less fuel efficient. However, the maximum thrust is higher than the previous value. An engine can thus develop more thrust when operated stoichiometrically. The optimum Mach number is different than either of the values found for the nonstoichiometric case. It is also important to recognize that as the Mach number increases, the burner exit temperature increases significantly for the stoichiometric condition.

Example 2.1: A ramjet is traveling at Mach 3 at an altitude of 4572 m (15,000 ft), the external static temperature is 258.4 K (465.2 °R), and the external static pressure is 57.1 kPa (8.29 psia) as determined from Appendix A. The heating value of the fuel is 46,520 kJ/kg (20,000 Btu/lbm). Air flows through the engine at 45.35 kg/s (100 lbm/s). The burner exit total temperature is 1944 K (3500 °R). Find the thrust, fuel ratio, and *TSFC*. The specific heat ratio can be assumed to be 1.40.

SOLUTION

For the solution, one could simply use Eqs. 2.3.18 and 2.3.20. However, these equations do not allow an engineer to obtain a “feel” for any of the internal numbers. Thus, for the solution, all of the intermediate steps through all of the components will be performed in detail.

DIFFUSER

First, because the Mach number is given, $M_a = 3$, and the ambient temperature is $T_a = 258.4 \text{ K} (465.2 \text{ °R})$, one can find the speed of sound a_a :

$$\begin{aligned} a_a &= \sqrt{\gamma \mathcal{R} T_a} \\ &= \sqrt{1.4 \times 287.1 \frac{\text{J}}{\text{kg-K}} \times 258.4 \text{ K} \times \frac{\text{N-m}}{\text{J}} \times \frac{\text{kg-m}}{\text{s}^2\text{-N}}} \\ &= 322.2 \text{ m/s} (1057 \text{ ft/s}) \end{aligned}$$

Thus, the ramjet velocity is

$$u_a = M_a a_a = 3 \times 322.2 \text{ m/s} = 967.1 \text{ m/s} (3172 \text{ ft/s}).$$

Next, for the stagnation temperature T_{ta} ,

$$\frac{T_{ta}}{T_a} = \left[1 + \frac{\gamma - 1}{2} M_a^2 \right],$$

and so

$$T_{ta} = 258.4 \text{ K} \left[1 + \frac{1.4 - 1}{2} 3^2 \right] = 723.9 \text{ K} (1303 \text{ °R})$$

Thus, because the diffuser is adiabatic the total temperature at the diffuser exit is

$$T_{t3} = T_{ta} = 723.9 \text{ K} (1303 \text{ °R}).$$

Also, for the stagnation pressure p_{ta} ,

$$\frac{p_{ta}}{p_a} = \left[1 + \frac{\gamma - 1}{2} M_a^2 \right]^{\frac{\gamma}{\gamma - 1}},$$

and so $p_{ta} = 57.1 \text{ kPa} \left[1 + \frac{1.4 - 1}{2} 3^2 \right]^{\frac{1.4}{1.4 - 1}} = 2099 \text{ kPa} (304.4 \text{ psia})$.

Thus, because the diffuser, combustor, and nozzle are ideal, the stagnation pressure is constant through the entire engine:

$$p_{t8} = p_{t4} = p_{t3} = 2099 \text{ kPa} (304.4 \text{ psia}).$$

BURNER

It is given that the burner exit total temperature is $T_{t4} = 1944 \text{ K}$ ($3500 \text{ }^\circ\text{R}$) and the heating value of the fuel is $46,520 \text{ kJ/kg}$. The specific heat at constant pressure is $1.005 \text{ kJ/(kg}\cdot\text{K)}$ for $\gamma = 1.40$.

Thus, the fuel flow is given by the first law of thermodynamics:

$$\begin{aligned}\dot{m}_f &= \frac{\dot{m}c_p [T_{t4} - T_{t3}]}{\Delta H} \\ &= \frac{45.35 \frac{\text{kg}}{\text{s}} \times 1.005 \frac{\text{kJ}}{\text{kg}\cdot\text{K}} \times [1944 - 723.9] \text{ K}}{46520 \frac{\text{kJ}}{\text{kg}}} \\ &= 1.195 \text{ kg/s (2.636 lbm/s)}\end{aligned}$$

or

$$f = \frac{\dot{m}_f}{\dot{m}} = \frac{1.195}{45.35} = 0.02636,$$

which is small and consistent with the ideal assumption of negligible fuel flow rates

NOZZLE

For an ideal analysis, the total temperature is constant from the burner through the nozzle (adiabatic):

$$T_{t8} = 1944 \text{ K (3500 }^\circ\text{R)}.$$

Next, at the nozzle exit, because for the ideal case the exit pressure matches the ambient pressure,

$$p_8 = p_a = 57.1 \text{ kPa (8.29 psia)},$$

and from the definition of stagnation pressure,

$$p_{t8} = p_8 \left[1 + \frac{\gamma - 1}{2} M_8^2 \right]^{\frac{\gamma}{\gamma - 1}};$$

thus, solving for the nozzle exit Mach number M_8 yields

$$\begin{aligned}M_8 &= \sqrt{\left[\frac{2}{\gamma - 1} \right] \left[\left[\frac{p_{t8}}{p_8} \right]^{\frac{\gamma - 1}{\gamma}} - 1 \right]} = \sqrt{\left[\frac{2}{1.4 - 1} \right] \left[\left[\frac{2099}{57.1} \right]^{\frac{1.4 - 1}{1.4}} - 1 \right]}, \\ &= 3.000\end{aligned}$$

which is identical to the inlet Mach number (as shown by Eq. 2.3.9)

Therefore, the nozzle exit temperature is

$$T_8 = \frac{T_{t8}}{\left[1 + \frac{\gamma - 1}{2} M_8^2 \right]} = \frac{3500}{\left[1 + \frac{1.4 - 1}{2} 3.000^2 \right]} = 694.4 \text{ K (1250 }^\circ\text{R)},$$

and the nozzle exit gas velocity is

$$\begin{aligned}u_8 &= M_8 a_8 \\ &= M_8 \sqrt{\gamma \mathcal{R} T_8} \\ &= 3.000 \sqrt{1.4 \times 287.1 \frac{\text{J}}{\text{kg}\cdot\text{K}} \times 694.4 \text{ K} \times \frac{\text{N}\cdot\text{m}}{\text{J}} \times \frac{\text{kg}\cdot\text{m}}{\text{s}^2\cdot\text{N}}} \\ &= 1585 \text{ m/s (5199) ft/s}.\end{aligned}$$

TOTAL THRUST AND *TSFC*

Finally, the ideal thrust does not have a pressure thrust component, and so

$$F = \dot{m}(u_e - u_a) = 45.35 \frac{\text{kg}}{\text{s}} (1585 - 967.1) \frac{\text{m N-s}^2}{\text{s kg-m}}$$

$$= 28,030 \text{ N (6302 lbf)}.$$

Thus, the *TSFC* is

$$TSFC = \frac{\dot{m}_f}{F} = \frac{1.195 \frac{\text{kg}}{\text{s}} \times 3600 \frac{\text{s}}{\text{h}}}{28,030 \text{ N}}$$

$$TSFC = 0.1538 \frac{\text{kg}}{\text{h-N}} \left(1.506 \frac{\text{lbm}}{\text{h-lbf}} \right). \quad < \text{ANS}$$

Once again, simply using Eqs. 2.3.18 and 2.3.20 could have eliminated all of these intermediate steps. However, the details of the internal operating conditions would be missing. For example, the supersonic exit Mach number would not have been seen nor any of the intermediate pressures and temperatures. Furthermore, as will be observed in Chapter 3, for nonideal analyses, performing these steps will be necessary because the equations will not reduce to closed-form equations as they do for an ideal case.

2.3.2. Turbojet

A general turbojet is shown in Figure 2.38. This is a much more complex machine than the ramjet because of the rotating shaft. Eight stations are identified. The free stream is position *a*. The inlet is position 1. Position 2 is the exit of the diffuser and compressor inlet. Station 3 is the compressor exit and burner inlet. The burner exit and turbine inlet are denoted as station 4. Station 5 is the turbine exit and afterburner inlet. The afterburner exit and nozzle inlet are at position 6. Finally, station 8 is the nozzle exhaust. For an ideal analysis, single or multispool engines will yield exactly the same results because only the overall effects of the components are of importance. The *h-s* diagram for the general ideal turbojet is presented in Figure 2.39. Process *a* to 1 to 2 is an isentropic compression during the diffusion. Process 2 to 3 is an isentropic compression while power is required by the compressor. Process 3 to 4 is an isobaric combustion process. The isentropic expansion through the turbine is process 4 to 5, during which power is removed from the flow. The afterburner process (5 to 6) is also isobaric. And finally, process 6 to 8 is an isentropic expansion in the nozzle where the flow velocity is accelerated. States *a* and 8 are once again on the same pressure line but do not constitute a process. For the analysis both nonafterburning and afterburning configurations will be considered separately.

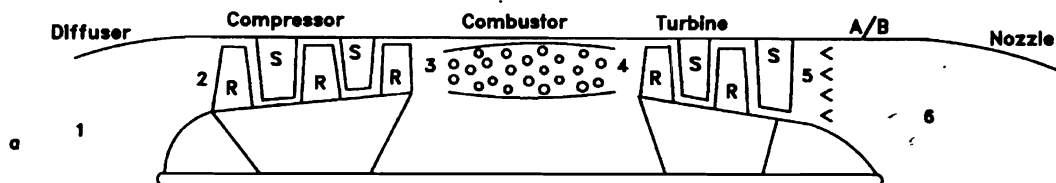


Figure 2.38 General turbojet.

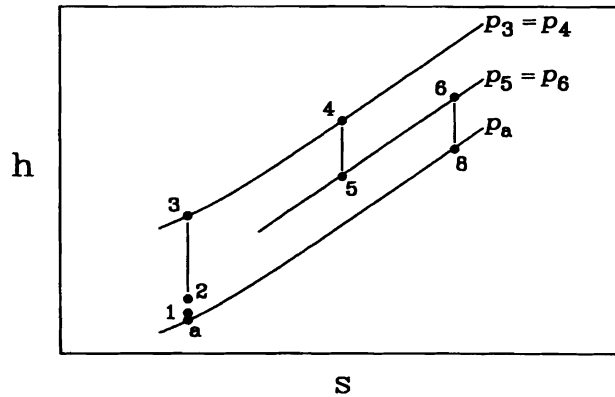


Figure 2.39 h-s diagram for an ideal turbojet with an afterburner.

a. Nonafterburning

For this configuration, stations 5 and 6 are identical (Fig. 2.40). For the ideal analysis, Eq. 2.3.1 once again applies. For the turbojet engine, the dimensionless quantity is (recall that for the ideal case \dot{m}_f is small and that $p_e = p_a$):

$$\frac{F}{\dot{m}u_a} = \left(\frac{u_8}{u_a} - 1 \right). \quad 2.3.25$$

Thus, once again, the velocity ratio u_8/u_a is needed to proceed. If one considers the exit total temperature and by multiplies and divides by the same terms, realizing that the diffuser and nozzle are adiabatic ($T_{t2} = T_{ta}$ and $T_{t8} = T_{t5}$) for the ideal case, the exit total temperature is

$$T_{t8} = T_a \frac{T_{ta}}{T_a} \frac{T_{t3}}{T_{t2}} \frac{T_{t4}}{T_{t3}} \frac{T_{t5}}{T_{t4}}. \quad 2.3.26$$

Therefore,

$$T_{t8} = T_a \frac{T_{ta}}{T_a} \tau_c \tau_t, \quad 2.3.27$$

where τ_c and τ_t are the total temperature ratios for the compressor and turbine, respectively. Also, given the exit total pressure and because, for the ideal case, the diffuser and nozzle are isentropic ($p_{t2} = p_{ta}$ and $p_{t8} = p_{t5}$), the nozzle exit total pressure is

$$p_{t8} = p_a \frac{p_{ta}}{p_a} \frac{p_{t3}}{p_{t2}} \frac{p_{t4}}{p_{t3}} \frac{p_{t5}}{p_{t4}}. \quad 2.3.28$$

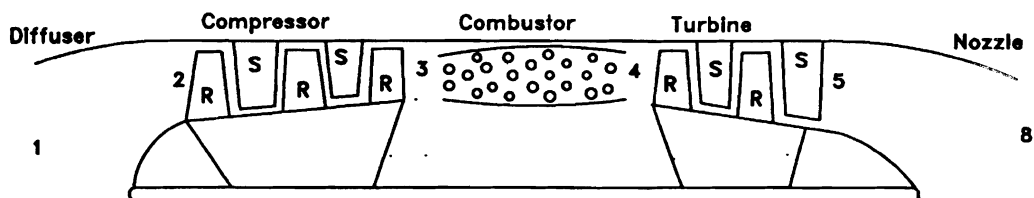


Figure 2.40 Nonafterburning turbojet.

Also, for the ideal case the total pressure is constant across the combustor ($p_{t4} = p_{t3}$). Thus, the nozzle exit total pressure is

$$p_{t8} = p_a \frac{p_{t4}}{p_a} \pi_c \pi_t \quad 2.3.29$$

However, for the ideal case the nozzle exit static pressure matches the free-stream pressure ($p_8 = p_a$). Thus, from Eqs. 2.2.45 and 2.3.29 one obtains

$$1 + \frac{\gamma - 1}{2} M_8^2 = \left[\frac{p_{t4}}{p_a} \pi_c \pi_t \right]^{\frac{\gamma-1}{\gamma}} \quad 2.3.30$$

Next, from Eqs. 2.2.42, 2.3.27 and 2.3.30,

$$\frac{T_{t8}}{T_a} = \frac{\frac{T_{t4}}{T_a} \tau_c \tau_t \tau_t}{\left[\frac{p_{t4}}{p_a} \pi_c \pi_t \right]^{\frac{\gamma-1}{\gamma}}} \quad 2.3.31$$

Thus, using Eqs. 2.2.6, 2.2.13, and 2.2.20 with Eq. 2.3.31 yields the temperature ratio

$$\frac{T_8}{T_a} = \tau_b. \quad 2.3.32$$

Next, u_8/u_a can be found in the same way as for the ramjet:

$$\frac{u_8}{u_a} = \frac{M_8 a_8}{M_a a_a} = \frac{M_8 \sqrt{\gamma \mathcal{R} T_8}}{M_a \sqrt{\gamma \mathcal{R} T_a}} = \frac{M_8 \sqrt{T_8}}{M_a \sqrt{T_a}}. \quad 2.3.33$$

Now, from Eqs. 2.2.42, 2.3.27, and 2.3.32, the square of the exit Mach number is

$$M_8^2 = \frac{2}{\gamma - 1} \left[\frac{T_{t4}}{T_a} \tau_c \tau_t - 1 \right] \quad 2.3.34$$

And by solving for the square of the free-stream Mach number, M_a^2 , from Eq. 2.2.4 we obtain

$$M_a^2 = \frac{2}{\gamma - 1} \left[\frac{T_{t4}}{T_a} - 1 \right]. \quad 2.3.35$$

Next, using Eqs. 2.3.32 to 2.3.35 yields

$$\frac{u_8}{u_a} = \sqrt{\tau_b \frac{\frac{T_{t4}}{T_a} \tau_c \tau_t - 1}{\frac{T_{t4}}{T_a} - 1}}. \quad 2.3.36$$

Finally, using this with Eq. 2.3.25 yields

$$\frac{F}{\dot{m} a_a} = M_a \left[\sqrt{\tau_b \frac{\frac{T_{t4}}{T_a} \tau_c \tau_t - 1}{\frac{T_{t4}}{T_a} - 1}} - 1 \right]. \quad 2.3.37$$

This equation may appear to represent the finished product because it yields the thrust in terms of engine parameters. However, one simplification can yet be accomplished. That is, the compressor and turbine are not acting independently because they are on the same shaft. In fact for the ideal analysis, all of the power derived from the turbine drives the compressor. The energy equation applied to the shaft (Eq. 2.2.26) under steady and ideal conditions reduces to

$$\dot{m} c_p (T_{t3} - T_{t2}) = \dot{m} c_p (T_{t4} - T_{t5}). \quad 2.3.38$$

Or solving for the turbine total temperature ratio τ_t , one obtains

$$\tau_t = 1 - \frac{T_{t4}}{T_a} \frac{T_a}{T_{t4}} (\tau_c - 1). \quad 2.3.39$$

Thus, using this with Eq. 2.3.37 yields the dimensionless thrust:

$$\frac{F}{\dot{m}a_a} = M_a \left[\sqrt{\left[\frac{\frac{T_{t4}}{T_a}}{\frac{T_{t4}}{T_a} - 1} \right] \left[\frac{T_{t4}}{T_a} \frac{T_a}{T_{t4}} \frac{1}{\tau_c} - 1 \right] [\tau_c - 1] + \left[\frac{\frac{T_{t4}}{T_a}}{\frac{T_{t4}}{T_a} \tau_c} \right] - 1} \right]. \quad 2.3.40$$

This equation therefore, represents the ideal thrust equation for a turbojet. By examining this equation, one can see that, as is the case for a ramjet, the dimensional thrust is directly proportional to the mass flow rate. It is also directly proportional to the Mach number if all of the other parameters are constant. However, one should remember that T_{t4}/T_a is strictly a function of Mach number and γ ; that is, $\frac{T_{t4}}{T_a} = 1 + \frac{\gamma-1}{2} M_a^2$. Also, as the burner total temperature increases, so does the thrust. However, as the ambient static temperature decreases, the thrust increases.

Also in Eq. 2.3.40, the compressor total temperature ratio, which is directly related to the total pressure ratio, is seen to influence the thrust performance strongly. By differentiating this equation with respect to τ_c and setting to zero, one finds that the nondimensional thrust is maximized for a value of

$$\tau_{c\text{opt}} = \sqrt{\left(\frac{T_{t4}}{T_a} \right)} / \left(\frac{T_{t4}}{T_a} \right), \quad 2.3.41$$

which can be related to the total pressure ratio by Eq. 2.2.13.

Next, to find the *TSFC* one must again use the energy equation for the burner as is done for the ramjet and recognizing that the total temperature ratio across the burner can be written as

$$\frac{T_{t4}}{T_{t3}} = \frac{T_{t4}}{T_a} \frac{T_a}{T_{t2}} \frac{T_{t2}}{T_{t3}}. \quad 2.3.42$$

And next, with Eq. 2.2.12, for the ideal case ($T_{t2} = T_{t4}$),

$$\tau_b \equiv \frac{T_{t4}}{T_{t3}} = \frac{T_{t4}}{T_a} \frac{T_a}{T_{t4}} \frac{1}{\tau_c}. \quad 2.3.43$$

Finally, using Eq. 2.2.32 for the first law of combustion process with Eqs. 1.5.3, 2.3.39, and 2.3.43 yields

$$TSFC a_a = \frac{\left[\frac{T_{t4}}{T_a} - \frac{T_{t4}}{T_a} \tau_c \right] \left[\frac{c_p T_a}{\Delta H M_a} \right]}{\left[\sqrt{\left[\frac{\frac{T_{t4}}{T_a}}{\frac{T_{t4}}{T_a} - 1} \right] \left[\frac{T_{t4}}{T_a} \frac{T_a}{T_{t4}} \frac{1}{\tau_c} - 1 \right] [\tau_c - 1] + \left[\frac{T_{t4}}{T_a} \frac{T_a}{T_{t4}} \frac{1}{\tau_c} \right] - 1} \right]}. \quad 2.3.44$$

This equation thus is the nondimensionalized *TSFC* for an ideal turbojet. Once again, for both Eqs. 2.3.40 and 2.3.44, the quantity (T_{t4}/T_a) is strictly a function of the free-stream Mach number. One can see that, as the ambient static temperature decreases, the *TSFC* decreases. Careful examination also shows that the *TSFC* decreases as τ_c (or π_c) increases. Typical values of *TSFC* for a turbojet range from 0.75 to 1.0 lbm/h/lbf.

Various parametric studies can be made for an ideal turbojet. For example, one can study the effect of compressor pressure ratio on the overall performance. In Figure 2.41, a general study of this type is made. It can see that, for given operating conditions (M_a , T_{t4}/T_a , and \dot{m}), one particular value of π_c will maximize or optimize the thrust. The general trend of

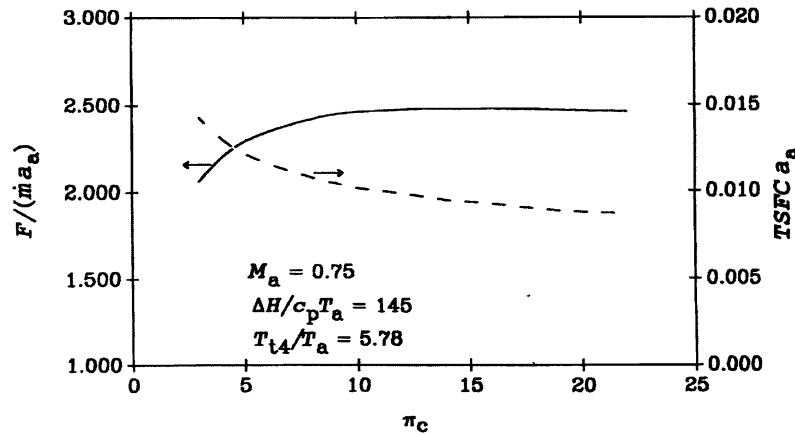


Figure 2.41 Effect of compressor total pressure ratio on the performance of an ideal turbojet.

$TSFC$ is also shown in this figure. As can be seen, this value always decreases with the compressor pressure ratio. This general information could be used in a design process, for example, because it indicates that, for a given engine size, the thrust can be optimized but the $TSFC$ may be improvable. A designer would have to examine the specific information on the engine application before deciding to maximize the thrust or decrease $TSFC$.

A second investigation is presented in Figure 2.42. The nondimensionalized thrust and $TSFC$ are shown as functions of the nondimensionalized inlet temperature. As can be seen, as the inlet temperature decreases (at constant inlet pressure and Mach number), the thrust increases and the $TSFC$ decreases. This indicates that the engine operates more effectively at low inlet temperatures and that the thrust of a given engine will be different as determined by the operating location. For example, the thrust at sea level will be higher at a pole than at the equator. Also, many engines are designed with an inlet water-spray injection system to take advantage of this phenomenon. As water is sprayed in the inlet, the air temperature decreases owing to the vaporization of the water and the $TSFC$ decreases. This behavior can be explained by referring to Eqs. 2.2.13 and 2.2.25. That is, as a given amount of energy is extracted from the fluid by the turbine and transferred to the compressor (a given

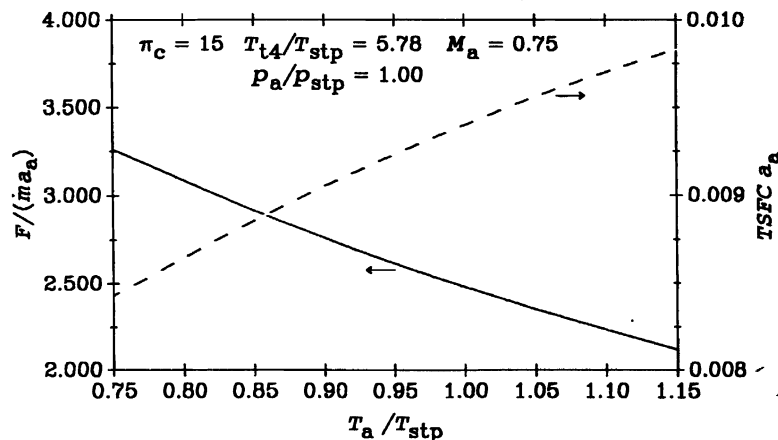


Figure 2.42 Effect of inlet static temperature on the performance of an ideal turbojet.

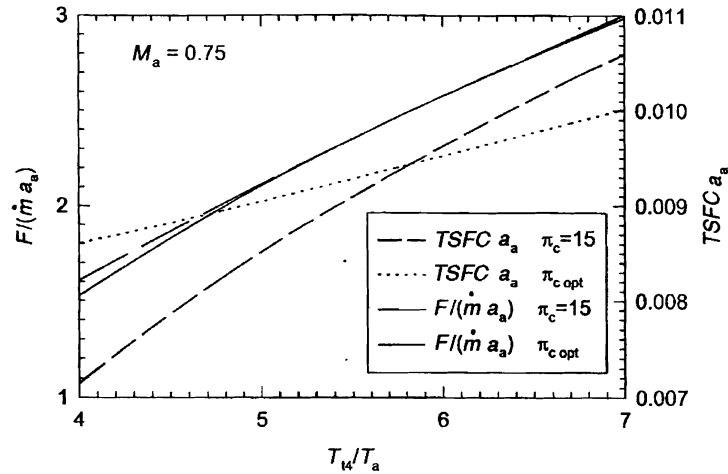


Figure 2.43 Effect of turbine inlet total temperature on the performance of an ideal turbojet.

compressor total temperature difference), the total temperature ratio will increase as the inlet temperature decreases. As the total temperature ratio increases, so does the total pressure ratio. As discussed in Chapter 1, as the total pressure ratio increases, the thermal efficiency increases. For the case of a jet engine, this translates into a lower *TSFC*.

Altitude also has a related effect on thrust. For example, as the altitude increases, the pressure and temperature decrease, but pressure decreases faster than temperature. As a result, the density decreases as the altitude increases, which decreases the intake air flow. The thrust directly decreases as the mass flow decreases as evidenced by Eq. 2.3.40. However, the thrust increases as the temperature decreases as discussed in the preceding paragraph. However, this effect is not as great as the effect of the density change, and, as a result, thrust decreases with altitude increase. Furthermore, the temperature decreases until 36,000 ft (11,000 m) in a standard atmosphere (as shown in Appendix A) after which it remains constant. However, the pressure and density continue to decrease as the altitude increases. Thus, after 36,000 ft, the thrust decreases with altitude faster than at lower altitudes. As a result, many aircraft operate at around 36,000 ft.

A second study on the effects of temperature is presented in Figure 2.43. For this investigation, the turbine inlet total temperature was varied for a simple turbojet. The Mach number was constant, and two different variations of compressor pressure ratio were considered. First, π_c was held constant at 15. As can be seen, the nondimensional thrust and *TSFC* monotonically increase. This implies that the thrust-to-weight ratio improves significantly, but unfortunately the *TSFC* also increases significantly. The second consideration is to optimize the pressure ratio of the compressor by Eq. 2.3.41. As can be seen for this case, once again, the nondimensional thrust increases dramatically, but now the *TSFC* still increases – albeit much less than for the constant π_c case. This implies that, in the design stage, simply increasing the turbine inlet temperature is not optimal and that the compressor must be matched to the turbine inlet temperature.

Another possible study is the effect of flight Mach number on performance. Such a general study is shown in Figure 2.44. In this figure, the thrust and *TSFC* are shown as functions of the Mach number for given values of T_{t4}/T_a and \dot{m} and for the optimum compressor pressure ratio (which varies with M_a , as is also shown in Fig. 2.44). As can be seen, the thrust always decreases with the Mach number and *TSFC* increases. Also, at a particular

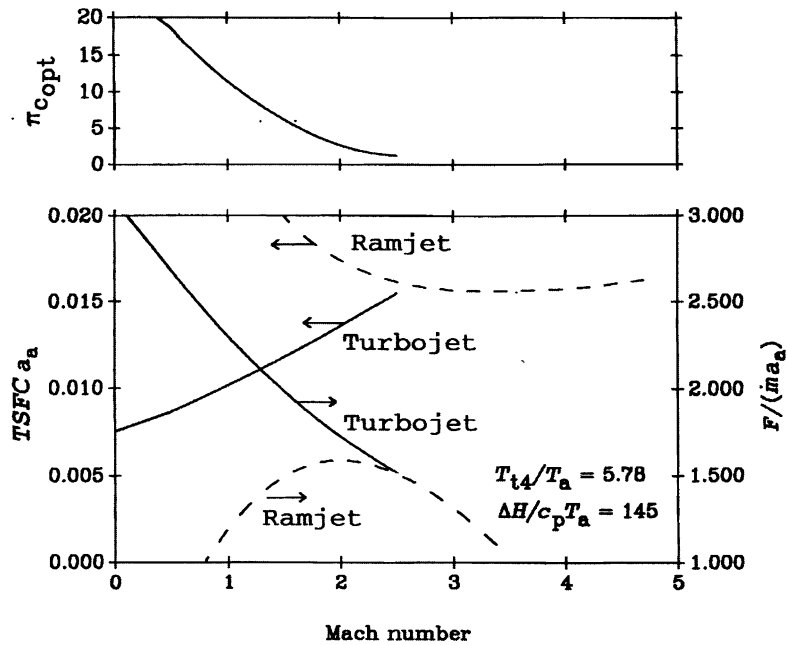


Figure 2.44 Effect of Mach number on the performance of an ideal turbojet with optimum compressor pressure ratio.

value of M_a , the pressure ratio in the compressor becomes unity (for this case $M_a \cong 2.65$). This indicates that the compressor is not energizing the fluid and the analysis is not valid for larger Mach numbers. In fact, at this point the engine is acting like a ramjet because the compressor is not being powered. One should also note as well that the thrust is much lower and the $TSFC$ is much higher than for lower Mach numbers. Thus, lower speeds are better suited for a turbojet. Also shown on this figure are general results for a ramjet. As can be seen, for high speeds the ramjet is preferred.

b. Afterburning

Next, an afterburning turbojet will be considered. This engine is also shown in Figure 2.38. Much of the analysis is the same as for the nonafterburning type. For example, the diffuser is the same, and the energy balance of the shaft (compressor and turbine) is identical. Some portions are of course different because of the additional energy input.

If one expands the total temperature at the nozzle exit, T_{t8} , the following equation results:

$$T_{t8} = T_a \frac{T_{t1a}}{T_a} \frac{T_{t3}}{T_{t2}} \frac{T_{t4}}{T_{t3}} \frac{T_{t5}}{T_{t4}} \frac{T_{t6}}{T_{t5}} \quad 2.3.45$$

By identifying the different ratios, one obtains

$$T_{t8} = T_a \frac{T_{t1a}}{T_a} \tau_c \tau_b \tau_t \tau_{ab}, \quad 2.3.46$$

where τ_{ab} is the total temperature ratio for the afterburner. This equation replaces Eq. 2.3.27, which was derived for the nonafterburning case. One can use this with Eqs. 2.2.42, 2.3.30,

2.2.6, 2.2.13, and 2.2.20 to find the ratio of static temperatures T_8/T_a :

$$\frac{T_8}{T_a} = \tau_b \tau_{ab}, \quad 2.3.47$$

which replaces Eq. 2.3.32. The velocity ratio is obtained similarly as follows:

$$\frac{u_8}{u_a} = \sqrt{\tau_b \tau_{ab} \frac{\frac{T_{t6}}{T_a} \tau_c \tau_t - 1}{\frac{T_{t6}}{T_a} - 1}}. \quad 2.3.48$$

Next, using this with Eq. 2.3.46 results in

$$\frac{u_8}{u_a} = \sqrt{\frac{T_{t6}}{T_a} \left[\frac{1 - \frac{1}{\frac{T_{t6}}{T_a} \tau_c \tau_t}}{\frac{T_{t6}}{T_a} - 1} \right]}, \quad 2.3.49$$

which replaces Eq. 2.3.36. Next, the energy balance on the combustion process in the afterburner (Eq. 2.2.38) can be used, and this can be added to the equation for the main burner (Eq. 2.2.32) to yield

$$(\dot{m}_f + \dot{m}_{fab})\Delta H = \dot{m}c_p [T_{t4} - T_{t3} + T_{t6} - T_{t5}], \quad 2.3.50$$

but for the ideal analysis from the energy balance of the shaft, one finds from Eq. 2.3.38 that

$$T_{t3} - T_{t2} = T_{t4} - T_{t5}. \quad 2.3.51$$

Using this with the fact that the diffuser and nozzle are adiabatic yields

$$\dot{m}_f \Delta H = \dot{m}c_p (T_{t8} - T_{ta}), \quad 2.3.52$$

where \dot{m}_f is the total fuel flow in the engine ($\dot{m}_f + \dot{m}_{fab}$). It is now possible to solve for the total fuel ratio:

$$f = \frac{\dot{m}_f}{\dot{m}} = \frac{c_p T_{t8}}{\Delta H} \left[1 - \frac{T_{ta}}{T_{t8}} \right]. \quad 2.3.53$$

Finally, Eq. 2.3.49 can be combined with previously derived Eqs. 2.3.39 and 2.3.25 to obtain the thrust as follows:

$$\frac{F}{\dot{m}a_a} = M_a \left[\sqrt{\left[\frac{\frac{T_{t8}}{T_a}}{\frac{T_{t6}}{T_a} - 1} \right]} \left[1 - \frac{\frac{T_{t4}}{T_a} \frac{T_a}{T_{ta}}}{\tau_c \left(\frac{T_{t4}}{T_a} - \frac{T_{t6}}{T_a} (\tau_c - 1) \right)} \right] - 1 \right]. \quad 2.3.54$$

This can be compared with the nonafterburning case (Eq. 2.3.40). One can see that, as is true for a simple turbojet, the dimensional thrust is directly proportional to the mass flow rate. It is also directly proportional to the Mach number if all of the other parameters are constant. As the burner or afterburner total temperature increases, or both total temperatures increase so does the thrust. Again, in Eq. 2.3.54, the compressor total temperature ratio is seen to influence the thrust performance strongly. By differentiating this equation relative to τ_c for a given value of T_{t8} , and setting to zero, one finds that the nondimensional thrust is maximized for a value of

$$\tau_{c,opt} = \left[\left(\frac{T_{t4}}{T_a} \right) + \left(\frac{T_{t6}}{T_a} \right) \right] / \left[2 \left(\frac{T_{t6}}{T_a} \right) \right], \quad 2.3.55$$

which can be related to the total pressure ratio by Eq. 2.2.13. The optimum value for the afterburning turbojet is considerably higher than for the nonafterburning case.

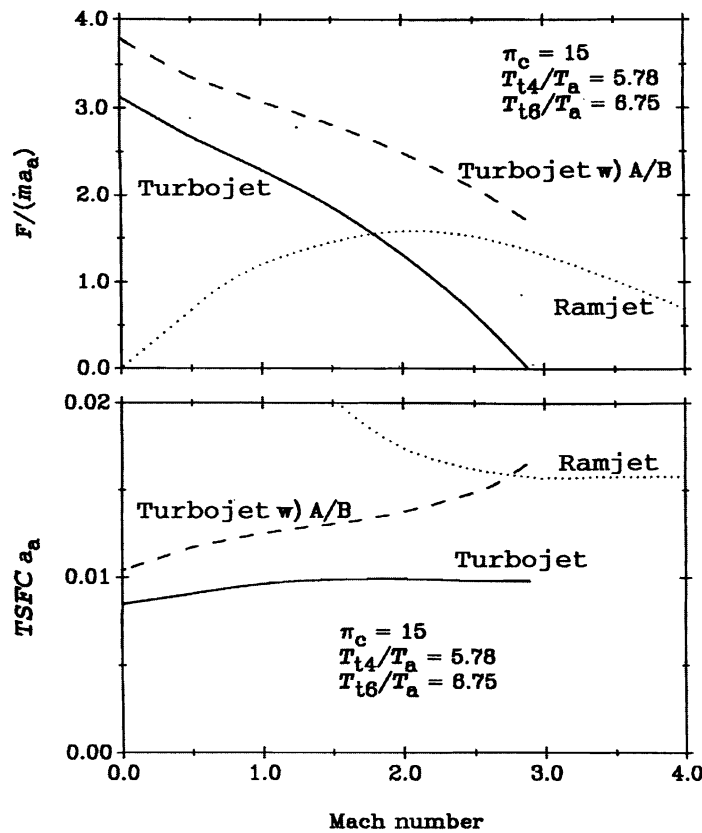


Figure 2.45 Comparison of thrust and $TSFC$ versus Mach number trends for an ideal turbojet, turbojet with an afterburner, and ramjet.

To determine the nondimensional $TSFC$, one now uses Eqs. 2.3.53 and 2.3.54 with previously derived Eqs. 1.5.1 and 2.3.43 to find

$$TSFC a_a = \frac{\left[\frac{T_{t8}}{T_a} - \frac{T_{t4}}{T_a} \tau_c \right] \left[\frac{c_p T_a}{\Delta H M_a} \right]}{\left[\sqrt{\left[\frac{T_{t8}}{T_a} - 1 \right]} \left[1 - \frac{T_{t4} T_a}{T_a T_{t4}} \right] - 1 \right]} \quad 2.3.56$$

Thus, this represents the nondimensionalized $TSFC$ for an afterburning turbojet and replaces Eq. 2.3.44. Once again, studies can be performed to determine the overall performance of an afterburning turbojet with a fixed compressor pressure ratio. Two general trends are presented in Figure 2.45. The thrust is presented as a function of the Mach number and is compared with a turbojet with no afterburner and a ramjet. All engines have the same airflow rate. One can see that the thrust for the afterburning case is always higher than for the nonafterburning case. Also in Figure 2.45, it can be seen that the $TSFC$ is likewise higher than for the nonafterburning case. This indicates that the extra fuel injected into the afterburner is not being used optimally. As indicated in Chapter 1, however, this is generally not of importance when immediate extra thrust is required. In comparison with the ramjet, one finds that the turbojet thrust can be higher at high Mach numbers, but this

will depend on how much afterburner fuel is used. At low Mach numbers, the *TSFC* for an afterburning turbojet is usually lower than for a ramjet but is once again less efficient at high Mach numbers. Note that at some Mach number ($M_a \cong 2.887$ for this case) the thrust for the nonafterburning turbojet becomes zero. This is due to the increased total temperature entering the compressor; all of the added enthalpy is extracted from the fluid by the turbine to drive the compressor. As a result, sufficient enthalpy is not delivered to the nozzle to generate any thrust. One should be careful and not directly compare the results from Figure 2.45 with those of Figure 2.44; in Figure 2.45 the compressor pressure ratio is fixed at 15, whereas in Figure 2.44 the optimum value of π_c is used, which, except for one particular Mach number, is different than 15.

Example 2.2: An ideal turbojet flies at sea level at a Mach number of 0.75. It ingests 165 lbm/s (74.83 kg/s) of air, and the compressor operates with a total pressure ratio of 15. The fuel has a heating value of 17,800 Btu/lbm (41,400 kJ/kg), and the burner exit total temperature is 2500 °R (1389 K). Find the developed thrust and the *TSFC*. One can assume that the specific heat ratio is 1.40.

SOLUTION

For the solution, one could simply use Eqs. 2.3.40 and 2.3.44. Once again, all of the intermediate steps will be performed so that some of the internal parameter values can be appreciated.

DIFFUSER

First since the turbojet flies at sea level, it can be determined from Appendix A that $p_a = 14.69$ psia (101.3 kPa) and $T_a = 518.7$ °R (288.2 K).

Thus, the speed of sound is

$$\begin{aligned} a_a &= \sqrt{\gamma \mathcal{R} T_a} = \sqrt{1.4 \times 53.35 \frac{\text{ft}\cdot\text{lbf}}{\text{lbm}\cdot\text{°R}} \times 32.17 \frac{\text{lbm}}{\text{slug}} \times 518.7 \text{°R} \times \frac{\text{slug}\cdot\text{ft}}{\text{s}^2\cdot\text{lbf}}} \\ &= 1116 \text{ ft/s (340.1 m/s),} \end{aligned}$$

and the jet velocity is $u_a = M_a a_a = 837.3$ ft/s (255.2 m/s).

Now $\frac{T_{ta}}{T_a} = [1 + \frac{\gamma-1}{2} M_a^2]$.

Thus, the inlet total temperature is

$$T_{ta} = 518.7 \text{°R} \left[1 + \frac{1.4-1}{2} 0.75^2 \right] = 577.1 \text{°R (320.6 K)}.$$

Also, for an ideal analysis that is adiabatic: $T_{t2} = T_{ta}$

Thus, the diffuser exit total temperature is $T_{t2} = 577.1$ °R (320.6 K).

Similarly, $\frac{p_{ta}}{p_a} = [1 + \frac{\gamma-1}{2} M_a^2]^{\frac{\gamma}{\gamma-1}}$.

Therefore, the inlet total pressure is

$$p_{ta} = 14.69 \text{ psia} \left[1 + \frac{1.4-1}{2} 0.75^2 \right]^{\frac{1.4}{1.4-1}} = 21.33 \text{ psia (147.1 kPa)}.$$

And for an ideal analysis that is isentropic: $p_{t2} = p_{ta}$.

Thus, the diffuser exit total pressure is $p_{t2} = 21.33$ psia (147.1 kPa).

Also, for an ideal gas,

$$\begin{aligned} \rho_a &= \frac{p_a}{\mathcal{R} T_a} = \frac{14.69 \frac{\text{lbf}}{\text{in}^2} \times 144 \frac{\text{in}^2}{\text{ft}^2}}{53.35 \frac{\text{ft}\cdot\text{lbf}}{\text{lbm}\cdot\text{°R}} \times 518.7 \text{°R} \times 32.17 \frac{\text{lbm}}{\text{slug}}}; \\ &= 0.002376 \text{ slug/ft}^3 \text{ (1.225 kg/m}^3\text{)} \end{aligned}$$

thus, if (not necessarily the case) the gas velocity at the diffuser inlet is the same as the jet velocity, the diffuser inlet area is

$$\begin{aligned} A_{in} &= \frac{\dot{m}}{\rho_a u_a} = \frac{165 \frac{\text{lbm}}{\text{s}} \times 144 \frac{\text{in.}^2}{\text{ft}^2}}{0.002376 \frac{\text{slugs}}{\text{ft}^3} \times 837.3 \frac{\text{ft}}{\text{s}} \times 32.17 \frac{\text{lbm}}{\text{slug}}}, \\ &= 371.3 \text{in.}^2 (0.2395 \text{m}^2) \end{aligned}$$

which yields an inlet diameter of 21.74 in. (0.5522 m). For this calculation the gas velocity at the diffuser inlet was assumed to be the same as the jet velocity. This may not, however, be the case, and the gas velocity can be higher or lower than the freestream velocity as determined by the engine operating point. More on this topic will be discussed in Chapter 4 (*Diffusers*).

COMPRESSOR

The compressor total pressure ratio is given as 15. Thus, the compressor exit total pressure is

$$p_{t3} = \pi_c p_{t2} = 15 \times 21.33 \text{ psia} = 320.0 \text{ psia} (2206 \text{ kPa}).$$

Also, because the compressor is isentropic for an ideal case,

$$\tau_c = \pi_c^{\frac{\gamma-1}{\gamma}} = 15^{\frac{0.4}{1.4}} = 2.168.$$

Thus, the total temperature at the exit of the compressor is

$$T_{t3} = T_{t2} \tau_c = 577.1^\circ\text{R} \times 2.168 = 1251^\circ\text{R} (695.0 \text{ K})$$

BURNER

Also, because the burner is ideal, the total pressure is constant across the burner:

$$p_{t4} = p_{t3}.$$

Consequently, the exit total pressure is $p_{t4} = 320.0 \text{ psia} (2206 \text{ kPa})$.

The exit total temperature is given as $T_{t4} = 2500^\circ\text{R} (1389 \text{ K})$, and the heating value of the fuel is 17,800 Btu/lbm. The specific heat at constant pressure is 0.24 Btu/(lbm \cdot °R) for $\gamma = 1.40$.

The fuel flow is given by

$$\begin{aligned} \dot{m}_f &= \frac{\dot{m} c_p [T_{t4} - T_{t3}]}{\Delta H} \\ &= \frac{165 \frac{\text{lbm}}{\text{s}} \times 0.24 \frac{\text{Btu}}{\text{lbm}\cdot^\circ\text{R}} \times [2500 - 1251]^\circ\text{R}}{17,800 \frac{\text{Btu}}{\text{lbm}}} \\ &= 2.778 \text{ lbm/s} (1.260 \text{ kg/s}), \end{aligned}$$

or $f = \frac{\dot{m}_f}{\dot{m}} = \frac{2.778}{165} = 0.01684$, which again is small and consistent with the ideal assumption.

TURBINE

Now, from the shaft energy balance for the ideal case,

$$\dot{m} c_p (T_{t4} - T_{t5}) = \dot{m} c_p (T_{t3} - T_{t2}).$$

Thus, solving for the turbine exit total temperature yields

$$T_{t5} = T_{t4} - (T_{t3} - T_{t2}) = 2500 - (1251 - 577) = 1826^\circ\text{R} (1014 \text{ K}),$$

which for an ideal analysis is also T_{t8} because the nozzle is adiabatic.

For the ideal (isentropic) turbine, the exit total pressure is

$$\begin{aligned} p_{t5} &= p_{t4}\pi_t = p_{t4} [\tau_t]^{\frac{\gamma}{\gamma-1}} = 320.0 \left[\frac{1826}{2500} \right]^{\frac{1.4}{0.4}} = 320.0 \times 0.333 \\ &= 106.6 \text{ psia (735.0 kPa)}. \end{aligned}$$

NOZZLE

For an ideal (isentropic) nozzle the total pressure is constant: $p_{t8} = p_{t5} = 106.6 \text{ psia (735.0 kPa)}$.

Thus, at the exit, because for the ideal case the exit pressure matches the ambient pressure,

$$p_8 = p_a = 14.69 \text{ psia (101.3 kPa)}.$$

Consequently, the nozzle exit Mach number can be found from

$$p_{t8} = p_8 \left[1 + \frac{\gamma-1}{2} M_8^2 \right]^{\frac{\gamma}{\gamma-1}}:$$

$$\begin{aligned} M_8 &= \sqrt{\left[\frac{2}{\gamma-1} \right] \left[\left[\frac{p_{t8}}{p_8} \right]^{\frac{\gamma-1}{\gamma}} - 1 \right]} = \sqrt{\left[\frac{2}{1.4-1} \right] \left[\left[\frac{106.6}{14.69} \right]^{\frac{0.4}{1.4}} - 1 \right]} \\ &= 1.951 \text{ (very supersonic)} \end{aligned}$$

Also, the exit nozzle temperature can be found from

$$T_8 = \frac{T_{t8}}{1 + \frac{\gamma-1}{2} M_8^2} = \frac{1826}{1 + \frac{1.4-1}{2} 1.951^2} = 1037^\circ\text{R (576.1 K)}$$

And the exit velocity is

$$\begin{aligned} u_8 &= M_8 a_8 = M_8 \sqrt{\gamma \mathcal{R} T_8} \\ &= 1.951 \sqrt{1.4 \times 53.35 \frac{\text{ft}\cdot\text{lbf}}{\text{lbf}\cdot^\circ\text{R}} \times 32.17 \frac{\text{lbfm}}{\text{slug}} \times 1037^\circ\text{R} \times \frac{\text{slug}\cdot\text{ft}}{\text{s}^2\cdot\text{lbf}}} \\ &= 1.951 \times 1579 \\ &= 3080 \text{ ft/s (938.7 m/s)}. \end{aligned}$$

From the ideal gas law,

$$\begin{aligned} \rho_8 &= \frac{p_8}{\mathcal{R} T_8} = \frac{14.69 \frac{\text{lbf}}{\text{in}^2} \times 144 \frac{\text{in}^2}{\text{ft}^2}}{53.35 \frac{\text{ft}\cdot\text{lbf}}{\text{lbfm}\cdot^\circ\text{R}} \times 1037^\circ\text{R} \times 32.17 \frac{\text{lbfm}}{\text{slug}}}; \\ &= 0.001189 \text{ slug/ft}^3 \text{ (0.6127 kg/m}^3\text{)} \end{aligned}$$

thus, the nozzle exit area is

$$\begin{aligned} A_8 &= \frac{\dot{m}}{\rho_8 u_8} = \frac{165 \frac{\text{lbfm}}{\text{s}} \times 144 \frac{\text{in}^2}{\text{ft}^2}}{0.001189 \frac{\text{slugs}}{\text{ft}^3} \times 3080 \frac{\text{ft}}{\text{s}} \times 32.17 \frac{\text{lbfm}}{\text{slug}}}, \\ &= 201.7 \text{ in}^2 \text{ (0.1301 m}^2\text{)} \end{aligned}$$

which is smaller than the inlet and yields a diameter of 16.02 in. (0.4070 m).

THRUST AND TSFC

Finally, because the nozzle exit pressure is the same as the ambient pressure, the ideal thrust is

$$\begin{aligned} F &= \dot{m}(u_e - u_a) = 165 \frac{\text{lbfm}}{\text{s}} (3080 - 837.3) \frac{\text{ft}}{\text{s}} \frac{\text{slug}}{32.17 \text{ lbfm}} \frac{\text{lbf}\cdot\text{s}^2}{\text{slug}\cdot\text{ft}} \\ &= 11,502 \text{ lbf (51,160 N)} \end{aligned}$$

< ANS

and the nondimensional thrust is

$$\frac{F}{a_a \dot{m}} = \frac{11,502 \text{ lbf} \times 32.17 \frac{\text{lbm}}{\text{sl}} \times \frac{\text{slug-ft}}{\text{s}^2\text{-lbf}}}{1116 \frac{\text{ft}}{\text{s}} \times 165 \frac{\text{lbm}}{\text{s}}} = 2.009$$

Thus, the *TSFC* is

$$\begin{aligned} TSFC &= \frac{\dot{m}_f}{F} = \frac{2.778 \frac{\text{lbm}}{\text{s}} \times 3600 \frac{\text{s}}{\text{h}}}{11,502 \text{ lbf}} \\ &= 0.870 \text{ lbm/h/lbf} (0.08866 \text{ kg/h/N}). \end{aligned} \quad < \text{ANS}$$

As before, all of these steps could have been eliminated. However, the details would again be missing. Furthermore, in the next chapter this same example is repeated for nonideal effects.

Example 2.3: The ideal turbojet, as examined in the previous example, now has an afterburner with an afterburner exit total temperature of 3200 °R (1778 K). Once again, find the developed thrust and *TSFC*.

SOLUTION

Much of the work has already been performed for this analysis. All calculations up through the turbine exit are still valid.

AFTERBURNER

The additional fuel flow for the afterburner is given by

$$\begin{aligned} \dot{m}_{f_{ab}} &= \frac{\dot{m} c_p [T_{t6} - T_{t5}]}{\Delta H} = \frac{165 \frac{\text{lbm}}{\text{s}} \times 0.24 \frac{\text{Btu}}{\text{lbm} \cdot \text{R}} \times [3200 - 1826] \text{ }^\circ\text{R}}{17,800 \frac{\text{Btu}}{\text{lbm}}}, \\ &= 3.055 \text{ lbm/s} (1.385 \text{ kg/s}) \end{aligned}$$

and thus the total fuel mass flow is

$$\dot{m}_f = \dot{m}_f + \dot{m}_{f_{ab}} = (2.778 + 3.055) \frac{\text{lbm}}{\text{s}} = 5.833 \frac{\text{lbm}}{\text{s}} \left(2.645 \frac{\text{kg}}{\text{s}} \right).$$

NOZZLE

Because the inlet total pressure to the nozzle is the same, the nozzle exit Mach number is once again 1.951. However, since the nozzle inlet total temperature is much higher, the exit temperature is higher. That is, since the nozzle is adiabatic ($T_{t8} = T_{t6} = 3200 \text{ }^\circ\text{R}$) and so

$$\begin{aligned} T_8 &= \frac{T_{t8}}{1 + \frac{\gamma-1}{2} M_8^2} = \frac{3200}{1 + \frac{1.4-1}{2} 1.951^2} \\ &= 1817 \text{ }^\circ\text{R} (1009 \text{ K}) \end{aligned}$$

As a result, the exit speed of sound and exit velocity are much higher, and thus

$$\begin{aligned} u_8 &= M_8 a_8 = M_8 \sqrt{\gamma \mathcal{R} T_8} \\ &= 1.951 \sqrt{1.4 \times 53.35 \frac{\text{ft-lbf}}{\text{lbm} \cdot \text{R}} \times 32.17 \frac{\text{lbm}}{\text{slugs}} \times 1817 \text{ }^\circ\text{R} \times \frac{\text{slug-ft}}{\text{s}^2\text{-lbf}}} \\ &= 4077 \text{ ft/s} (1234 \text{ m/s}) \end{aligned}$$

$$\begin{aligned} \rho_8 &= \frac{p_8}{\mathcal{R} T_8} = \frac{14.69 \frac{\text{lbf}}{\text{in}^2} \times 144 \frac{\text{in}^2}{\text{ft}^2}}{53.35 \frac{\text{ft-lbf}}{\text{lbm} \cdot \text{R}} \times 1817 \text{ }^\circ\text{R} \times 32.17 \frac{\text{lbm}}{\text{slug}}} \\ &= 0.0006783 \text{ slug/ft}^3 (0.3497 \text{ kg/m}^3) \end{aligned}$$

Therefore, the required nozzle exit area is

$$A_8 = \frac{\dot{m}}{\rho_8 u_8} = \frac{165 \frac{\text{lbm}}{\text{s}} \times 144 \frac{\text{in.}^2}{\text{ft}^2}}{0.0006783 \frac{\text{slug}}{\text{ft}^3} \times 4077 \frac{\text{ft}}{\text{s}} \times 32.17 \frac{\text{lbm}}{\text{slug}}}$$

$$= 267.1 \text{ in.}^2 (0.1723 \text{ m}^2)$$

Thus, with the afterburner a larger nozzle diameter is needed. A fixed geometry cannot accommodate the flows with a higher exit temperature. Consequently, a variable geometry would be needed. This topic is considered in detail in Chapters 3 and 5.

THRUST AND *TSFC*

Because the exit pressure again matches the ambient pressure, the ideal thrust is thus

$$F = \dot{m}(u_e - u_a) = 165 \frac{\text{lbm}}{\text{s}} (4077 - 837.3) \frac{\text{ft}}{\text{s}} \frac{\text{slug}}{32.17 \text{ lbm slug-ft}} \frac{\text{lbf-s}^2}{\text{slug-ft}}$$

$$= 16,616 \text{ lbf} (73,910 \text{ N}) \quad < \text{ANS}$$

$$TSFC' = \frac{\dot{m}_f}{F} = \frac{5.833 \frac{\text{lbm}}{\text{s}} \times 3600 \frac{\text{s}}{\text{h}}}{16,616 \text{ lbf}}$$

$$= 1.264 \text{ lbm/h/lbf} (0.1288 \text{ kg/h/N}). \quad < \text{ANS}$$

One can compare the results to the previous example and see that the thrust has been increased by 44.5 percent. The *TSFC* has been increased by 45.4 percent. Thus, although the thrust is much higher, the fuel economy is relatively poor.

2.3.3. Turbofan

The general diagram for a turbofan is shown in Figure 2.2. As indicated earlier in this chapter, this engine has up to three basic flow paths. Two simplifications of the general turbofan are covered for the ideal analysis: the fully exhausted fan and the ducted and mixed fan. Both nonafterburning and afterburning cases are considered. The following chapter on real cycles covers the hybrid fan (in which a portion of the secondary flow is mixed while the remainder is exhausted).

a. Fan Exhausted

The first type of a turbofan is shown in Figure 2.46. For this configuration two flow paths exist. For one path, the air enters the diffuser, flows through the core, and exhausts through the primary nozzle. For the second path, air enters the diffuser, flows through the

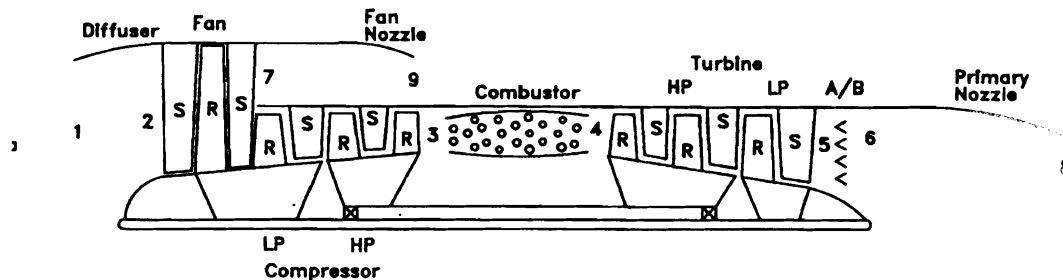


Figure 2.46 General turbofan with exhausted fan.

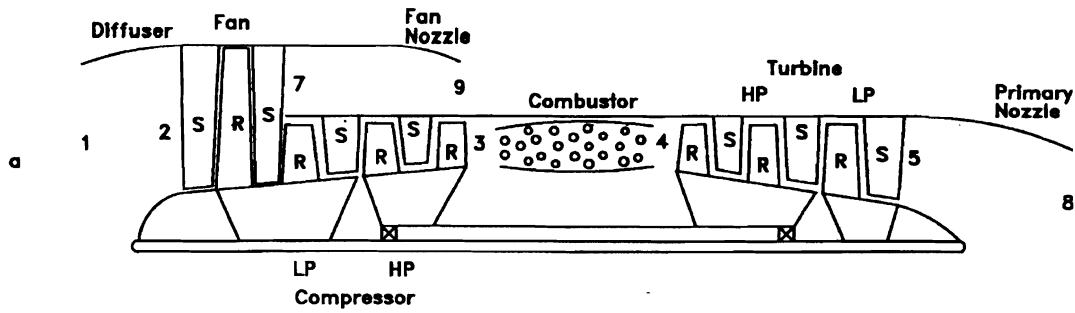


Figure 2.47 Nonafterburning turbofan with exhausted fan.

fan, and exits through the fan nozzle. Two separate subcases are considered here: without and with the afterburner. In Figure 2.46, an afterburner is present in the core between stations 5 and 6. Analyses for the two subcases are performed separately.

Nonafterburning: For the nonafterburning case, stations 5 and 6 are one and the same and will be termed station 5, as shown in Figure 2.47. For this case, the thrust is generated by two separate gas streams and found from Eq. 1.6.27 as follows:

$$F = \dot{m}(u_8 - u_a) + \dot{m}_s(u_9 - u_a), \quad 2.3.57$$

where u_9 is the gas velocity at the fan nozzle exit. Or this can be written as

$$F = \dot{m}u_a \left(\frac{u_8}{u_a} - 1 \right) + \dot{m}_s u_a \left(\frac{u_9}{u_a} - 1 \right), \quad 2.3.58$$

where \dot{m} is the airflow rate into the core and \dot{m}_s is the bypassed airflow rate (the air that flows only through the outer section of the fan and fan nozzle – or secondary flow rate). The flow path from station a to station 8 is exactly the same as for the turbojet, and thus u_8/u_a is already known. However, for the fan the quantity u_9/u_a is needed. The ratio u_9/u_a can be written as

$$\frac{u_9}{u_a} = \frac{M_9 a_9}{M_a a_a} = \frac{M_9 \sqrt{\gamma \mathcal{R} T_9}}{M_a \sqrt{\gamma \mathcal{R} T_a}} = \frac{M_9 \sqrt{T_9}}{M_a \sqrt{T_a}}, \quad 2.3.59$$

but for the ideal analysis the fan nozzle exit pressure matches the ambient pressure

$$p_9 = p_a. \quad 2.3.60$$

Next one can recall that the processes a–1, 1–2, 2–7, and 7–9 are all isentropic. Therefore, the entire process a–9 is also isentropic. Thus, for process a–9, Eq. H.2.10 applies. Consequently, from Eqs. 2.3.60 and H.2.10, the nozzle exit static temperature matches the atmospheric temperature:

$$T_9 = T_a. \quad 2.3.61$$

Also, by expanding on the nozzle total exit temperature T_{t9} , one obtains

$$T_{t9} = T_a \frac{T_{ta}}{T_a} \frac{T_{t7}}{T_{t2}} = T_a \frac{T_{ta}}{T_a} \tau_f. \quad 2.3.62$$

Thus, from Eqs. 2.3.62 and 2.2.54, the square of the fan nozzle exit Mach number is

$$M_9^2 = 2 \left[\frac{\frac{T_{ta}}{T_a} \tau_f - 1}{\gamma - 1} \right], \quad 2.3.63$$

where τ_f is the total temperature ratio for the fan. Also from Eq. 2.2.4, the square of the freestream Mach number is

$$M_a^2 = 2 \left[\frac{\frac{T_{1a}}{T_a} - 1}{\gamma - 1} \right]. \quad 2.3.64$$

Therefore, from Eqs. 2.3.59, 2.3.61, 2.3.63, and 2.3.64 one finds the ratio

$$\frac{u_9}{u_a} = \sqrt{\frac{\frac{T_{1a}}{T_a} \tau_f - 1}{\frac{T_{1a}}{T_a} - 1}}. \quad 2.3.65$$

Next, the energy equation applied to the rotating shaft (Eq. 2.2.26) reduces to

$$\dot{m}c_p(T_{14} - T_{15}) = \dot{m}c_p(T_{13} - T_{12}) + \alpha \dot{m}c_p(T_{17} - T_{12}), \quad 2.3.66$$

which reduces to

$$\frac{T_{14}}{T_a} \left(1 - \frac{T_{15}}{T_{14}} \right) = \frac{T_{12}}{T_a} \left(\frac{T_{13}}{T_{12}} - 1 \right) + \alpha \frac{T_{12}}{T_a} \left(\frac{T_{17}}{T_{12}} - 1 \right). \quad 2.3.67$$

Or, by using Eqs. 2.2.20, 2.2.12, and 2.2.16, one obtains

$$\frac{T_{14}}{T_a} (1 - \tau_t) = \frac{T_{12}}{T_a} (\tau_c - 1) + \alpha \frac{T_{12}}{T_a} (\tau_f - 1), \quad 2.3.68$$

and solving for the turbine total temperature ratio τ_t yields

$$\tau_t = 1 - \left[\frac{T_{1a}}{T_a} \times \frac{T_a}{T_{14}} \right] [(\tau_c - 1) + \alpha (\tau_f - 1)]. \quad 2.3.69$$

Because the core is essentially a simple turbojet and $p_8 = p_a$, one can use Eq. 2.3.36 to find u_8/u_a . Thus, Eqs. 2.3.36, 2.3.43, 2.3.58, 2.3.65, and 2.3.69 are used to yield the dimensionless thrust:

$$\begin{aligned} \frac{F}{\dot{m}a_a} = M_a \left[\sqrt{\left[\frac{\left[\frac{T_{14}}{T_a} \frac{T_a}{T_{1a}} \frac{1}{\tau_c} \right] \left[\frac{T_{1a}}{T_a} \tau_c \left[1 - \left[\frac{T_{1a}}{T_a} \times \frac{T_a}{T_{14}} \right] [(\tau_c - 1) + \alpha (\tau_f - 1)] \right] - 1 \right]}{\frac{T_{1a}}{T_a} - 1} \right] - 1 \right] \\ + \alpha M_a \left[\sqrt{\left[\frac{\left[\frac{T_{1a}}{T_a} \tau_f - 1 \right]}{\frac{T_{1a}}{T_a} - 1} \right] - 1 \right]. \end{aligned} \quad 2.3.70$$

Thus, the thrust is a strong function of the compressor total pressure ratio, the fan total pressure ratio, the exit total temperature from the burner, and the bypass ratio. Next, the value of *TSFC* is desired. The combustion energy balance is exactly the same as for the turbojet and is given by Eq. 2.2.32. Thus, using the definition of nondimensional *TSFC* with Eqs. 2.2.32, 2.3.43, and 2.3.70 yields

TSFC a_a

$$= \frac{\left[\frac{T_{13}}{T_a} - \frac{T_{1a}}{T_a} \tau_c \right] \left[\frac{c_p T_a}{\Delta H} \right]}{M_a \left[\sqrt{\left[\frac{\left[\frac{T_{14}}{T_a} \frac{T_a}{T_{1a}} \frac{1}{\tau_c} \right] \left[\frac{T_{1a}}{T_a} \tau_c \left[1 - \left[\frac{T_{1a}}{T_a} \times \frac{T_a}{T_{14}} \right] [(\tau_c - 1) + \alpha (\tau_f - 1)] \right] - 1 \right]}{\frac{T_{1a}}{T_a} - 1} \right] - 1 \right] + \alpha M_a \left[\sqrt{\left[\frac{\left[\frac{T_{1a}}{T_a} \tau_f - 1 \right]}{\frac{T_{1a}}{T_a} - 1} \right] - 1 \right]}. \quad 2.3.71$$

Therefore, both the thrust and *TSFC* have been determined for the turbofan with an exhausted fan. Typical *TSFC* values for this engine are 0.35 to 0.7 lbm/h/lbf. For a turbofan with the fan exhausted, one should realize that the temperature ratios across both the fan

and compressor are independent. For example, in a design stage, both τ_c and τ_f can be specified.

If the thrust is to be maximized, one can differentiate F with respect to the fan total temperature ratio (which is directly related to the fan total pressure ratio) τ_f in Eq. 2.3.70, set equal to zero, and show that (which is left as an exercise to the reader) τ_f is specified as

$$\tau_{f_{\text{opt}}} = \frac{1 + \frac{T_{t4}}{T_a} + \frac{T_{t3}}{T_a} [1 + \alpha - \tau_c] - \frac{\frac{T_{t4}}{T_a}}{\frac{T_{t3}}{T_a} \tau_c}}{\frac{T_{t3}}{T_a} [1 + \alpha]}, \quad 2.3.72$$

which can be used to find the optimum total pressure ratio from Eq. 2.2.17. This condition interestingly results in the two nozzle exit velocities being the same:

$$u_8 = u_9. \quad 2.3.73$$

Similarly, one can maximize the thrust by differentiating F with respect to the bypass ratio α , set equal to zero, and solve for α , which yields

$$\alpha_{\text{opt}} = \frac{1}{(\tau_f - 1)} \left\{ \frac{\frac{T_{t4}}{T_a}}{\frac{T_{t3}}{T_a}} \left(1 - \frac{1}{\tau_c \frac{T_{t3}}{T_a}} - \frac{1}{4 \frac{T_{t4}}{T_a}} \left[\sqrt{\frac{T_{t4}}{T_a} \tau_f - 1} + \sqrt{\frac{T_{t3}}{T_a} - 1} \right]^2 \right) - (\tau_c - 1) \right\}. \quad 2.3.74$$

It is also possible to perform a series of parametric studies to compare engine types under different operating conditions. For example, the dimensionless thrust is plotted versus the flight Mach number in Figure 2.48. As can be seen, the thrust decreases with the Mach number but is higher than that of a turbojet. This is somewhat misleading however. That is, the total airflow for a turbofan is considerably higher than the primary flow, which is used to nondimensionalize the thrust. Bypass ratios up to 9 are used in modern designs, which means that the total flow can be as much as eight times the core flow. Thus, a better parameter to nondimensionalize the thrust is the total flow rate ($\dot{m}_t = \dot{m}(1 + \alpha)$). If this is used and the analysis is again performed, one obtains the right-hand axis in Figure 2.48. Now it can be seen that the dimensionless thrust is lower than that for the turbojet case. Thus, for the same total flow, which is represented by the physical size of the engine, the turbojet produces more thrust. Next, one should consider the *TSFC*, which is also characterized in Figure 2.48. In this respect the turbofan outperforms the turbojet. The turbofan produces more thrust per fuel flow than does the turbojet. This explains why most commercial craft, use turbofans with large bypass ratios. Fighter craft, on the other hand, use turbojets or turbofans with low bypass ratios to reduce engine size and weight.

Figure 2.49 presents a study in which the thrust and *TSFC* are treated as functions of the fan total pressure ratio. As can be seen, a maximum thrust is realized as well as a minimum *TSFC*. These optimums occur at the total pressure ratio corresponding to the total temperature ratio given by Eq. 2.3.73.

Another trend study that can be performed is the effect of compressor pressure ratio on the overall performance. In Figure 2.50, such a study is shown. This is for a fixed Mach number, bypass ratio, fan pressure ratio, flow rate, and turbine inlet temperature. As for the simple turbojet, an optimum pressure ratio is found if the objective is to maximize the thrust. However, one can also see that the value of *TSFC* continuously decreases with increasing the compressor pressure ratio.

Figure 2.51 demonstrates the relationship of nondimensional thrust on both the compressor and fan pressure ratios. As can be seen from the three-dimensional plot, a maximum occurs for one particular combination of π_c and π_f . The counterpart performance plot

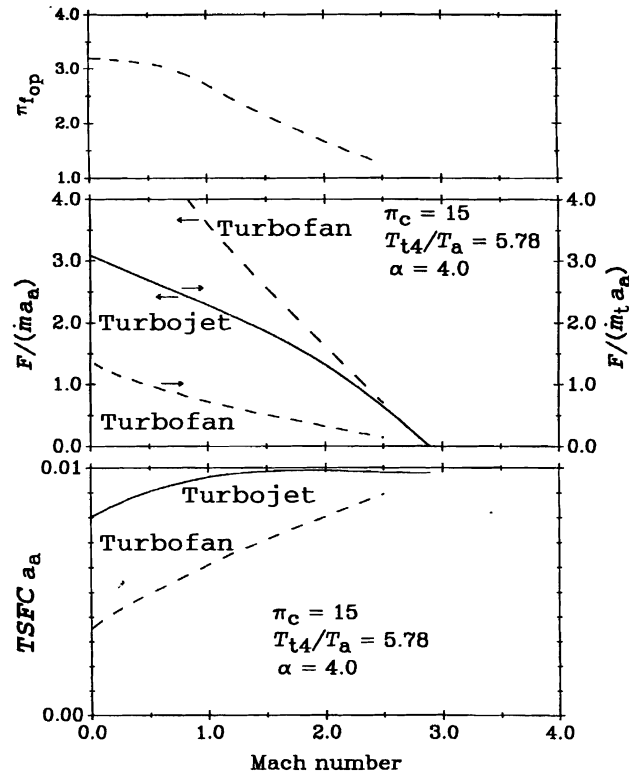


Figure 2.48 Dimensionless thrust (based on core flow), dimensionless thrust (based on total flow), and dimensionless $TSFC$ versus Mach number for an ideal exhausted fan and turbojet.

(nondimensional $TSFC$) is presented in Figure 2.52. The $TSFC$ can be minimized in the π_f direction; however, it decreases monotonically in the π_c direction.

To expand on fan performance, one can study the effect of bypass ratio on the overall performance. Figure 2.53 illustrates the general dimensionless thrust and $TSFC$ trends as

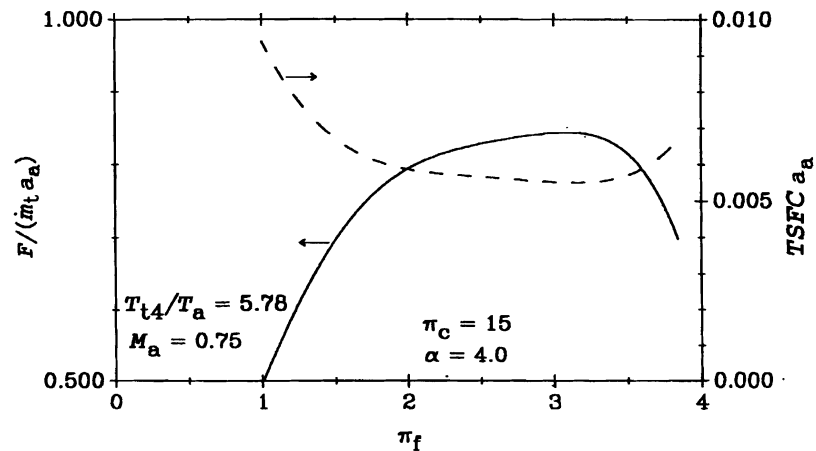


Figure 2.49 Effect of fan total pressure ratio on performance of ideal exhausted turbofan.

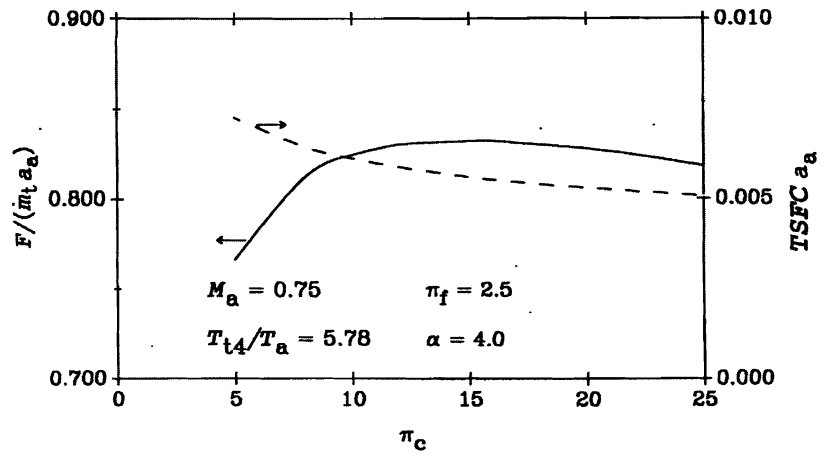


Figure 2.50 Effect of compressor total pressure ratio on performance of an ideal exhausted turbofan.

functions of the bypass ratio. These are for fixed fan and compressor pressure ratios, Mach number, core flow rates, and turbine exit temperatures. When the thrust is nondimensionalized by the core flow rate, it can be seen from the Figure that an optimum thrust is attained for one particular bypass ratio. Note that a bypass ratio of zero represents a simple turbojet. When nondimensionalized by the total flow rate, the thrust always decreases with the bypass ratio. For this type of turbofan with the parameters fixed as stated, a maximum bypass ratio exists. If an attempt is made to operate above this, too much energy is required from the turbine to drive both the fan and the compressor and the engine will drop to a lower flow rate, different pressure ratios, or both. The $TSFC$ trend is also shown in Figure 2.53.

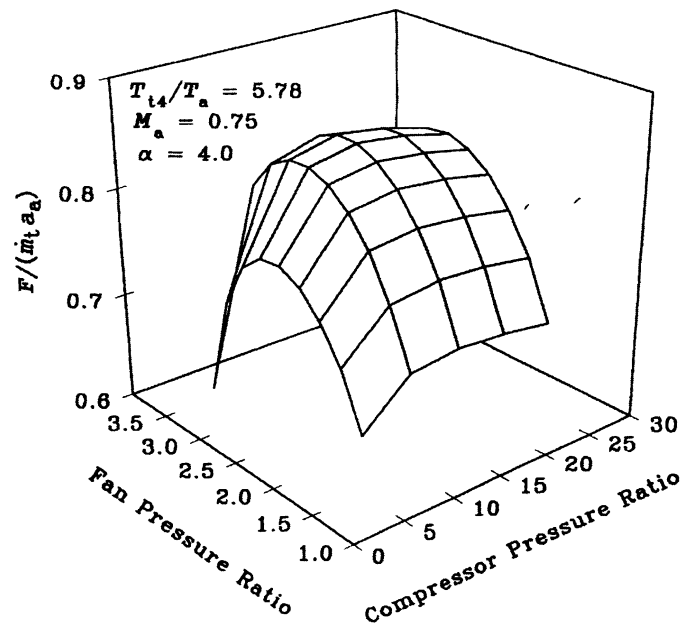


Figure 2.51 Effect of fan total pressure ratio and compressor total pressure ratio on dimensionless thrust of an ideal exhausted turbofan.

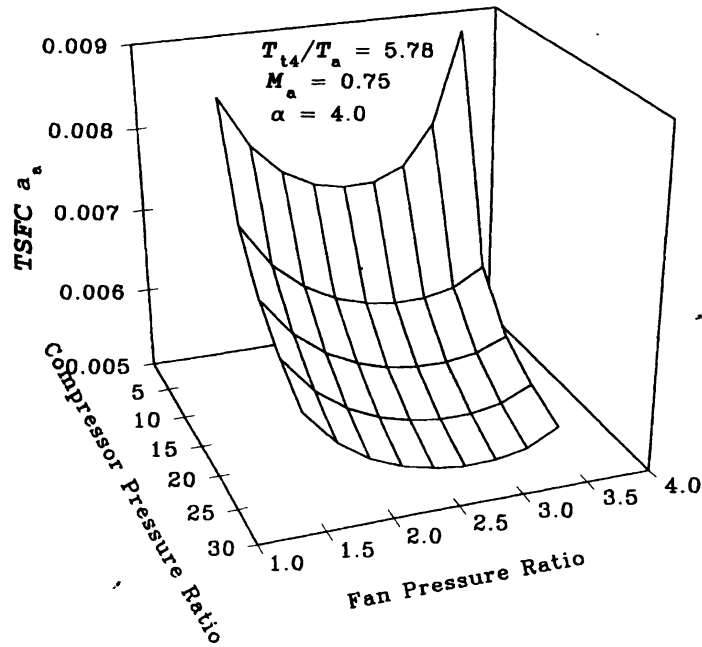


Figure 2.52 Effect of fan total pressure ratio and compressor total pressure ratio on dimensionless TSFC of an ideal exhausted turbofan.

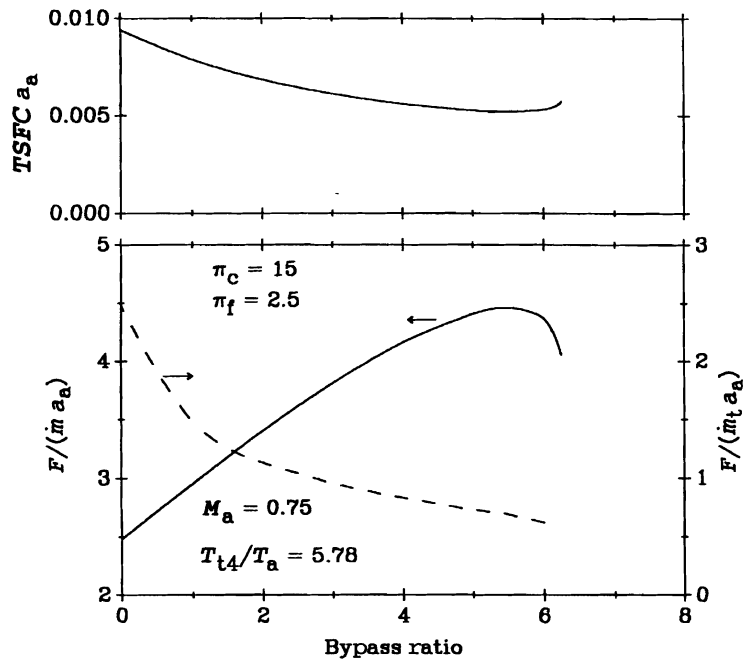


Figure 2.53 Effect of bypass ratio on dimensionless thrust and dimensionless TSFC of an ideal exhausted turbofan.

As one can see, a minimum *TSFC* is realized at the same bypass ratio that the maximum thrust (based on only the core mass flow rate) was obtained.

Afterburning: Next, the afterburning exhausted fan is considered. Figure 2.46 depicts this geometry. As can be seen, the afterburner is strictly in the core region and near the primary exhaust. In general, a second afterburner could be located near the fan exhaust. This geometry is seldom used, however, and will not be covered here. Several of the equations used for the nonafterburning exhausted fan and the afterburning turbojet apply, but a few new derivations are needed. For example, Eq. 2.3.58 still applies. Thus, once again, finding u_9/u_a and u_8/u_a is necessary. However, u_9/u_a will be exactly as it was for the nonafterburning case and is given by Eq. 2.3.65. Also, the flow through the core is the same as for the afterburning turbojet case. Thus, one can use Eq. 2.3.49 to find u_8/u_a . Therefore, the dimensionless thrust can be found through the following equation:

$$\begin{aligned} \frac{F}{\dot{m}a_a} = M_a \left[\sqrt{\left[\frac{T_{16}}{T_a} \right]} \left[1 - \frac{1}{\left(\frac{T_{1a}}{T_a} \tau_c \left(1 - \left[\frac{T_{1a}}{T_a} \times \frac{T_a}{T_{14}} \right] [(\tau_c - 1) + \alpha(\tau_f - 1)] \right)} \right)} - 1 \right] \right. \\ \left. + \alpha M_a \left[\sqrt{\left[\frac{T_{1a} \tau_f - 1}{\frac{T_{1a}}{T_a} - 1} \right]} - 1 \right] \right]. \end{aligned} \quad 2.3.75$$

The thrust is a strong function of burner exit temperature, afterburner exit temperature, compressor pressure ratio, fan pressure ratio, and bypass ratio. Of course the Mach number and mass flow rate are strong influences as well for all other engines. Next, to find the total fuel burned (\dot{m}_f) one can apply Eqs. 2.2.32 and 2.2.38. However, an easier method is to apply the energy equation to the entire engine. Note that no shaft power crosses the control volume if it is drawn around the entire engine and also that, ideally, \dot{m}_f is much smaller than \dot{m} . Thus, the total fuel flow rate (primary plus afterburner) is

$$\dot{m}_f \Delta H = \sum \dot{m}_{out} h_{t_{out}} - \sum \dot{m}_{in} h_{t_{in}} \quad 2.3.76$$

or

$$\dot{m}_f \Delta H = (\dot{m} c_p T_{16} + \dot{m}_s c_p T_{17}) - c_p T_{1a} (\dot{m} + \dot{m}_s), \quad 2.3.77$$

which, using eqs. 2.2.16 and 2.2.14 and realizing that ideally $T_{12} = T_{1a}$ reduces to

$$\dot{m}_f = \left[\frac{\dot{m} c_p T_a}{\Delta H} \right] \left[\frac{T_{16}}{T_{1a}} + \alpha \tau_f - (1 + \alpha) \right]. \quad 2.3.78$$

Finally, using the definition of nondimensional *TSFC*, one finds with Eq. 2.3.78 that

$$\begin{aligned} TSFC a_a \\ = \frac{\left[\frac{T_{16}}{T_a} \times \frac{T_a}{T_{1a}} + \alpha \tau_f - (1 + \alpha) \right] \left[\frac{c_p T_a}{\Delta H} \right] \left[\frac{T_{1a}}{T_a} \right]}{M_a \left[\sqrt{\left[\frac{T_{16}}{T_a} \right]} \left[1 - \frac{1}{\left(\frac{T_{1a}}{T_a} \tau_c \left(1 - \left[\frac{T_{1a}}{T_a} \times \frac{T_a}{T_{14}} \right] [(\tau_c - 1) + \alpha(\tau_f - 1)] \right)} \right)} - 1 \right] + \alpha M_a \left[\sqrt{\left[\frac{T_{1a} \tau_f - 1}{\frac{T_{1a}}{T_a} - 1} \right]} - 1 \right]}. \end{aligned} \quad 2.3.79$$

For the exhausted fan with an afterburner, the *TSFC* is significantly higher than for the turbofan without an afterburner.

In Figure 2.54, the thrust and *TSFC* for an exhausted fan with an afterburner are depicted as functions of the Mach number for the optimum fan pressure ratio (maximum thrust).

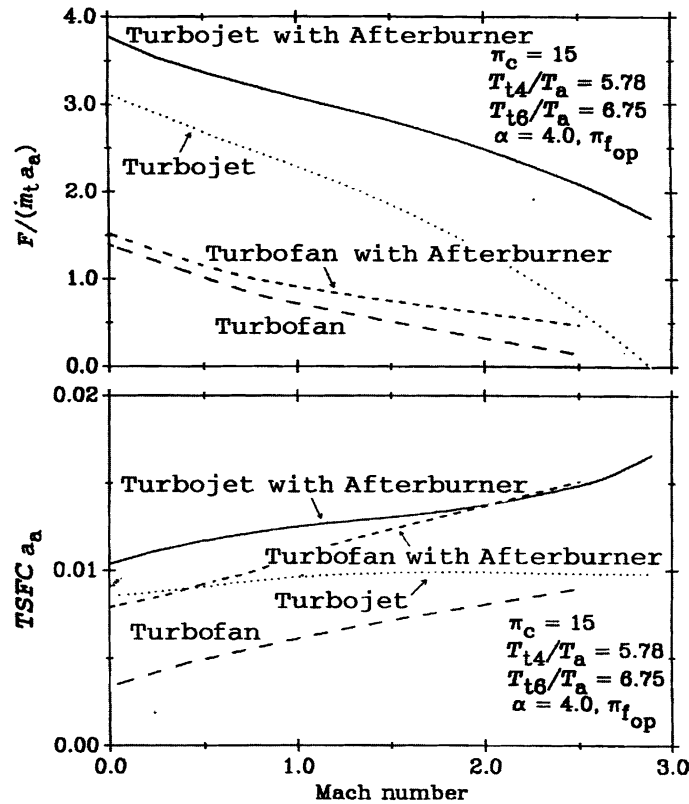


Figure 2.54 Dimensionless thrust (based on total flow) and dimensionless $TSFC$ versus Mach number for an ideal exhausted fan with an optimum total pressure ratio and turbojet with and without afterburners.

The fan pressure ratio is given in Figure 2.48. As should be expected, the thrust and $TSFC$ are higher than for a nonafterburning case. Also, these trends are compared with those for a turbojet. As can be seen, the $TSFC$ for the afterburning turbofan is lower than that for the afterburning turbojet at low Mach numbers. The dimensionless thrust (by total flow rate) is higher for a turbojet without afterburning than for a turbofan with an afterburner.

Example 2.4: An ideal turbofan with an exhausted fan flies at sea level at a Mach number of 0.75. The primary flow is 74.83 kg/s (165 lbm/s), and the bypass ratio is 1.20. The compressor pressure ratio is 15, whereas that of the fan is 3. The fuel has a heating value of 41,400 kJ/kg (17,800 Btu/lbm), and the burner exit total temperature is 1389 K (2500 °R). Find the developed thrust and the $TSFC$ if $\gamma = 1.40$.

SOLUTION:

If this example is compared with the previous ones for the turbojet, it can be seen that the only difference is the addition of the exhausted fan. All of the given conditions are identical. Once again, a step-by-step solution is presented because it allows determination of internal differences between this example and the plain turbojet example.

Many of the values are the same as in the previous example. These will simply be listed as follows:

$$\begin{aligned} p_a &= 101.3 \text{ kPa (14.69 psia)} & T_a &= 288.2 \text{ K (518.7 }^\circ\text{R)} \\ u_a &= 255.2 \text{ m/s (837.3 ft/s)} & a_a &= 340.1 \text{ m/s (1116 ft/s)} \\ T_{1a} &= 320.6 \text{ K (577.1 }^\circ\text{R)} = T_{12} & p_{1a} &= 147.1 \text{ kPa (21.33 psia)} = p_{12} \\ p_{13} &= 2206 \text{ kPa (320.0 psia)} = p_{14} & T_{13} &= 695.0 \text{ K (1251 }^\circ\text{R)} \end{aligned}$$

DIFFUSER

As was the case for the turbojet, $\rho_a = 1.225 \text{ kg/m}^3$ (0.002376 slug/ft³); thus, if (not necessarily the case) the gas velocity at the diffuser inlet is the same as the jet velocity, the diffuser inlet area is

$$A_{\text{in}} = \frac{\dot{m}(1 + \alpha)}{\rho_a u_a} = \frac{74.83 \frac{\text{kg}}{\text{s}} \times (1 + 1.20)}{1.225 \frac{\text{kg}}{\text{m}^3} \times 255.2 \frac{\text{m}}{\text{s}}} = 0.5269 \text{ m}^2 \text{ (816.9 in.}^2\text{)},$$

which yields an inlet diameter of 32.24 in. (0.8191 m), which is 48 percent larger than that for the simple turbojet.

FAN

From the fan pressure ratio, the fan exit total pressure is

$$p_{17} = \pi_f p_{12} = 3 \times 147.1 = 441.3 \text{ kPa (64.00 psia)}.$$

Because the fan is isentropic, the fan exit total temperature is

$$T_{17} = T_{12} \tau_f = T_{12} [\pi_f]^{\frac{\gamma-1}{\gamma}} = 320.6 [3]^{\frac{0.4}{1.4}} = 438.8 \text{ K (789.8 }^\circ\text{R)}.$$

FAN NOZZLE

For the ideal fan nozzle, the exit pressure matches the ambient pressure; that is,

$$p_9 = p_a = 101.3 \text{ kPa (14.69 psi)},$$

and since the nozzle is isentropic the total pressure remains constant through the nozzle:

$$p_{19} = p_{17} = 441.3 \text{ kPa (64.00 psia)} \text{ and } p_{19} = p_9 \left[1 + \frac{\gamma-1}{2} M_9^2 \right]^{\frac{\gamma}{\gamma-1}}.$$

Thus, solving for the exit Mach number yields

$$\begin{aligned} M_9 &= \sqrt{\left[\frac{2}{\gamma-1} \right] \left[\left[\frac{p_{19}}{p_9} \right]^{\frac{\gamma-1}{\gamma}} - 1 \right]} \\ &= \sqrt{\left[\frac{2}{1.4-1} \right] \left[\left[\frac{441.3}{101.3} \right]^{\frac{0.4}{1.4}} - 1 \right]} \\ &= 1.617. \end{aligned}$$

Consequently, the exit static temperature is

$$T_9 = \frac{T_{19}}{1 + \frac{\gamma-1}{2} M_9^2} = \frac{438.8}{1 + \frac{1.4-1}{2} 1.617^2} = 288.2 \text{ K (518.7 }^\circ\text{R)},$$

and the exit velocity is

$$\begin{aligned} u_9 &= M_9 a_9 = M_9 \sqrt{\gamma \mathcal{R} T_9} \\ &= 1.617 \sqrt{1.4 \times 287.1 \frac{\text{J}}{\text{kg-K}} \times 288.2 \text{ K} \times \frac{\text{N-m}}{\text{J}} \times \frac{\text{kg-m}}{\text{s}^2\text{-N}}} \\ &= 550.1 \text{ m/s (1805 ft/s)}. \end{aligned}$$

TURBINE

For power balance on the shaft:

$$\dot{m} c_p (T_{14} - T_{15}) = \dot{m} c_p (T_{13} - T_{12}) + \alpha \dot{m} c_p (T_{17} - T_{12})$$

or

$$(T_{14} - T_{15}) = (T_{13} - T_{12}) + \alpha (T_{17} - T_{12});$$

thus, $(1389 - T_{15}) = (695.0 - 320.6) + 1.20(438.8 - 320.6)$.

Solving instead for the turbine exit total temperature yields $T_{15} = 872.8 \text{ K}$ (1571°R). Note that, because the turbine is also driving the fan, the turbine exit temperature is lower than that for the turbojet.

Since the ideal turbine is isentropic, it is possible to find the turbine exit total pressure

$$\begin{aligned} p_{15} &= p_{14} \pi_t = p_{14} [\tau_t]^{\frac{\gamma}{\gamma-1}} = 2206 \left[\frac{872.8}{1389} \right]^{\frac{1.4}{0.4}} \\ &= 2206 \times 0.197 = 433.8 \text{ kPa (62.92 psia)}. \end{aligned}$$

PRIMARY NOZZLE

Because the nozzle is isentropic, $p_{18} = p_8 [1 + \frac{\gamma-1}{2} M_8^2]^{\frac{\gamma}{\gamma-1}}$.

Or, solving for the exit Mach number yields

$$\begin{aligned} M_8 &= \sqrt{\left[\frac{2}{\gamma-1} \right] \left[\left[\frac{p_{18}}{p_8} \right]^{\frac{\gamma-1}{\gamma}} - 1 \right]} = \sqrt{\left[\frac{2}{1.4-1} \right] \left[\left[\frac{433.8}{101.3} \right]^{\frac{0.4}{1.4}} - 1 \right]} \\ &= 1.605 \end{aligned}$$

Thus, the exit static temperature is

$$T_8 = \frac{T_{18}}{1 + \left[\frac{\gamma-1}{2} \right] M_8^2} = \frac{872.8}{1 + \left[\frac{1.4-1}{2} \right] 1.605^2} = 576.1 \text{ K (1037}^\circ \text{R)},$$

and the exit gas velocity is

$$\begin{aligned} u_8 &= M_8 a_a = M_8 \sqrt{\gamma \mathcal{R} T_8} \\ &= 1.617 \sqrt{1.4 \times 287.1 \frac{\text{J}}{\text{kg-K}} \times 576.1 \text{ K} \times \frac{\text{N-m}}{\text{J}} \times \frac{\text{kg-m}}{\text{s}^2\text{-N}}} \\ &= 772.2 \text{ m/s (2533 ft/s)}. \end{aligned}$$

Note here that u_8 and u_9 are not identical; thus, the thrust is not maximized.

THRUST AND *TSFC*

Finally, because both nozzle exit pressures are atmospheric, the thrust is given by

$$\begin{aligned} F &= \dot{m}(u_8 - u_a) + \dot{m}_s(u_9 - u_a) = \dot{m}(u_8 - u_a) + \alpha \dot{m}(u_9 - u_a) \\ &= \left[74.83 \frac{\text{kg}}{\text{s}} (772.2 - 255.2) \frac{\text{m}}{\text{s}} + 1.2 \times 74.83 \frac{\text{kg}}{\text{s}} (550.1 - 255.2) \frac{\text{m}}{\text{s}} \right] \times \frac{\text{N}\cdot\text{s}^2}{\text{kg}\cdot\text{m}} \\ &= 38,690 \text{ N (primary)} + 26,480 \text{ N (fan)} \\ &= 65,170 \text{ N (14,653 lbf)}. \end{aligned} \quad < \text{ANS}$$

This thrust is 27 percent more than for the turbojet, but the total airflow rate is 2.2 times that of the turbojet. Thus, the thrust-to-weight ratio will be considerably higher for the turbojet. The nondimensional thrust is

$$\frac{F}{a_a \dot{m} (1 + \alpha)} = \frac{65,170 \text{ N} \times \frac{\text{kg}\cdot\text{m}}{\text{s}^2\cdot\text{N}}}{340.1 \frac{\text{m}}{\text{s}} \times 74.83 \frac{\text{kg}}{\text{s}} \times (1 + 1.20)} = 1.164,$$

which is considerably less than that for the turbojet (2.009), again showing that the thrust-to-weight ratio for the turbofan is less than that for the turbojet.

The fuel flow rate is exactly the same as for the turbojet; that is,

$$\dot{m}_f = 1.260 \text{ kg/s (2.778 lbm/s)}$$

Thus,

$$\begin{aligned} TSFC &= \frac{\dot{m}_f}{F} = \frac{1.260 \frac{\text{kg}}{\text{s}} \times 3600 \frac{\text{s}}{\text{h}}}{65,170 \text{ N}} \\ &= 0.06960 \text{ kg/h/N (0.683 lbm/h/lbf)}, \end{aligned} \quad < \text{ANS}$$

which is 22 percent less than for the turbojet.

As an afterthought, to maximize the thrust one could find the optimum value of τ_f and then π_f . These values are 1.576 and 4.912, respectively, but their determination is left as an exercise for the reader. This optimization yields a thrust of 66,710 N (14,998 lbf) and a *TSFC* of 0.06797 kg/h/N (0.667 lbm/h/lbf).

b. Fan Mixed

The second type of fan is shown in Figure 2.55. For this configuration, the fan exit bypassed air passes through a bypass duct and is mixed with the turbine exhaust before station 5.5. Two separate subcases are considered here: without and with afterburner. In Figure 2.55, the afterburner exists between stations 5.5 and 6. Analyses for the two engines are performed separately in the following sections:

Nonafterburning. For the nonafterburning case, stations 5.5 and 6 are one and the same and are termed station 6, as shown in Figure 2.56. For the turbojet, because only one exhaust-gas stream or nozzle is present, the following is obtained:

$$\frac{F}{\dot{m}_8 u_a} = \left(\frac{u_8}{u_a} - 1 \right), \quad 2.3.80$$

where \dot{m}_8 is the total exiting gas flow from the nozzle and given by

$$\dot{m}_8 = (1 + \alpha) \dot{m}; \quad 2.3.81$$

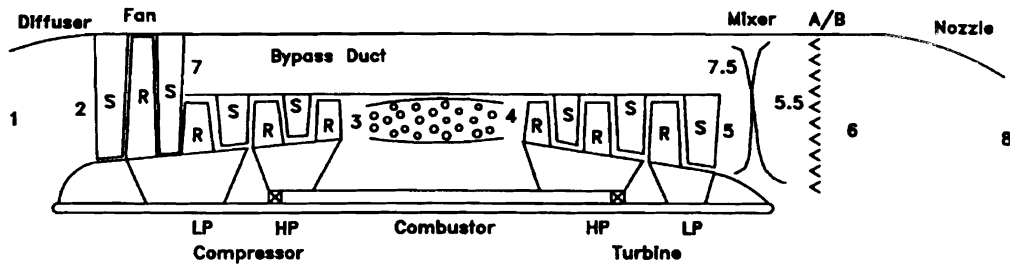


Figure 2.55 General turbofan with mixed fan.

thus, once again, it is necessary to find the velocity ratio u_8/u_a . For the ramjet,

$$\frac{u_8}{u_a} = \frac{M_8 \sqrt{T_8}}{M_a \sqrt{T_a}} \quad 2.3.82$$

Therefore, using Eqs. 2.2.4 and 2.2.42 yields

$$\frac{u_8}{u_a} = \sqrt{\frac{\frac{T_{18}}{T_8} - 1}{\frac{T_{1a}}{T_a} - 1}} \sqrt{\frac{T_8}{T_a}}, \quad 2.3.83$$

which reduces to

$$\frac{u_8}{u_a} = \sqrt{\frac{\frac{T_{18}}{T_a} - \frac{T_8}{T_a}}{\frac{T_{1a}}{T_a} - 1}} \quad 2.3.84$$

Thus, the ratios T_{18}/T_a and T_8/T_a are needed to find the thrust. Next, if one considers the enthalpy of the ideal uniform mixing streams at station 6 (Eq. 2.2.69) and expands on the total temperature exiting the mixer, T_{t6} , the following equation is obtained:

$$T_{t6} = \frac{\alpha T_a \left[\frac{T_{1a}}{T_a} \right] \left[\frac{T_{17}}{T_2} \right] + T_a \left[\frac{T_{14}}{T_a} \right] \left[\frac{T_{15}}{T_{14}} \right]}{\alpha + 1}, \quad 2.3.85$$

which can be reduced to

$$T_{t6} = \frac{\alpha T_a \left[\frac{T_{1a}}{T_a} \right] \tau_f + T_a \left[\frac{T_{14}}{T_a} \right] \tau_t}{\alpha + 1}. \quad 2.3.86$$

For a stable condition at the mixer inlet, Eq. 2.2.64 indicates that the static pressures are equal ($p_{7.5} = p_5$). However, as discussed earlier in this chapter, it can be assumed that the

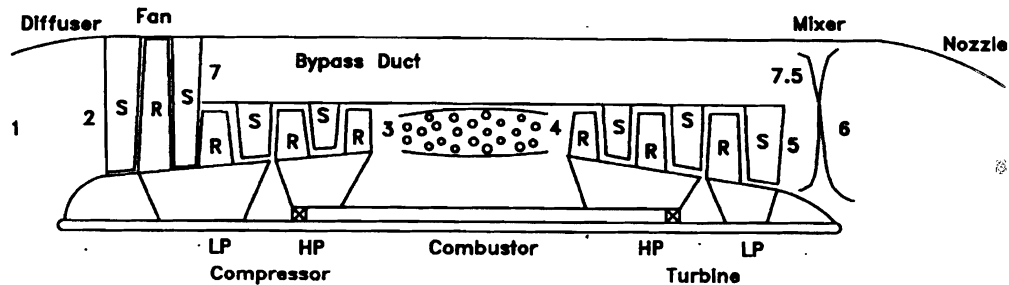


Figure 2.56 Nonafterburning mixed turbofan.

Mach numbers for streams 5, 7.5, and 5.5 are equal ($M_{7.5} = M_{15} = M_{15.5}$) or small, the total pressures will also be equal ($p_{7.5} = p_{15}$). Furthermore, since the mixing is ideal, the total pressures are constant across the mixer:

$$p_{7.5} = p_{15} = p_{15.5}. \quad 2.3.87$$

Thus, the total pressure ratio across the fan is

$$\frac{p_{17}}{p_{12}} = \frac{p_{15} p_{13}}{p_{13} p_{12}}. \quad 2.3.88$$

Note that if the Mach numbers are not equal for the two streams, the relationship of p_{17} and p_{15} can be obtained from Eq. H.2.11. For the ideal case, Eq. 2.3.88 reduces to

$$\pi_f = \pi_1 \pi_c, \quad 2.3.89$$

which for the ideal case (isentropic for all three components and constant γ) also implies (from Eq. H.2.10) that

$$\tau_f = \tau_1 \tau_c. \quad 2.3.90$$

Using this with Eq. 2.3.86 yields

$$T_{16} = \frac{\alpha T_a \left[\frac{T_{1a}}{T_a} \right] \tau_f + T_a \left[\frac{T_{1d}}{T_a} \right] \frac{\tau_f}{\tau_c}}{\alpha + 1}, \quad 2.3.91$$

which for the ideal case is also T_{18} because the nozzle is adiabatic. Therefore,

$$\frac{T_{18}}{T_a} = \left[\frac{T_{1a}}{T_a} \right] \tau_f \left[\frac{\alpha + \frac{1}{\tau_c} \left[\frac{T_a}{T_{1a}} \right] \left[\frac{T_{1d}}{T_a} \right]}{\alpha + 1} \right]. \quad 2.3.92$$

One can find the total pressure at station 8, which is also (from Eq. 2.3.87)

$$p_{18} = p_a \left[\frac{p_{1a}}{p_a} \right] \left[\frac{p_{13}}{p_{12}} \right] \left[\frac{p_{15}}{p_{14}} \right]. \quad 2.3.93$$

From Eq. 2.3.89 this becomes

$$p_{18} = p_a \left[\frac{p_{1a}}{p_a} \right] \left[\frac{p_{17}}{p_{12}} \right] = p_a \left[\frac{p_{1a}}{p_a} \right] \pi_f. \quad 2.3.94$$

Now, since for the ideal case the exit pressure matches the ambient pressure ($p_8 = p_a$), Eq. 2.2.45 yields

$$\left[1 + \frac{\gamma - 1}{2} M_8^2 \right] = \left[\left[\frac{p_{1a}}{p_a} \right] \pi_f \right]^{\frac{\gamma - 1}{\gamma}}. \quad 2.3.95$$

Finally, from Eqs. 2.3.92, 2.2.42, and 2.3.95 and solving for T_8/T_a one obtains

$$\frac{T_8}{T_a} = \left[\frac{T_{1a}}{T_a} \right] \tau_f \left[\frac{\alpha + \frac{1}{\tau_c} \left[\frac{T_a}{T_{1a}} \right] \left[\frac{T_{1d}}{T_a} \right]}{(\alpha + 1) \left[\left[\frac{p_{1a}}{p_a} \right] \pi_f \right]^{\frac{\gamma - 1}{\gamma}}} \right], \quad 2.3.96$$

which for the ideal case (from Eqs. H.2.10 and 2.2.17) becomes

$$\frac{T_8}{T_a} = \left[\frac{\alpha + \frac{1}{\tau_c} \left[\frac{T_a}{T_{1a}} \right] \left[\frac{T_{1d}}{T_a} \right]}{\alpha + 1} \right]. \quad 2.3.97$$

The shaft energy equation is exactly the same for the mixed and exhausted cases. Thus, using Eqs. 2.3.90 and 2.3.69 and solving for the fan total temperature ratio τ_f yields

$$\tau_f = \frac{\tau_c + \left[\frac{T_{t4}}{T_a} \right] \left[\frac{T_a}{T_{t4}} \right] \tau_c (1 + \alpha - \tau_c)}{1 + \left[\frac{T_{t4}}{T_a} \right] \left[\frac{T_a}{T_{t4}} \right] \tau_c \alpha} \quad 2.3.98$$

From this one can see that, as soon as T_{t4}/T_a , τ_c (or π_c) and the Mach number are specified, τ_f (and thus π_f) can be calculated. Note that the fan total pressure ratio is not independent as it was for the exhausted case. Thus, during the design phase this parameter cannot be independently varied and must be appropriately chosen at the design stage! Finally, using Eqs. 2.3.80, 2.3.81, 2.3.84, 2.3.91, 2.3.96 and remembering that Eq. 2.3.98 must hold, one obtains the following equation for the dimensionless thrust:

$$\frac{F}{\dot{m} a_a} = M_a (1 + \alpha) \left[\sqrt{\left[\frac{\alpha + \left[\frac{T_{t4}}{T_a} \right] \left[\frac{T_a}{T_{t4}} \right] \frac{1}{\tau_c}}{1 + \alpha} \right] \left[\frac{\left[\frac{T_{t4}}{T_a} \right] \left[\frac{T_a}{T_{t4}} \right] \tau_c (1 + \alpha - \tau_c)}{1 + \left[\frac{T_{t4}}{T_a} \right] \left[\frac{T_a}{T_{t4}} \right] \tau_c \alpha} \right] - 1} \right] - 1 \quad 2.3.99$$

The thrust is a strong function of the burner exit temperature, compressor pressure ratio, and bypass ratio. As is the case for all other engines, the Mach number and mass flow rate are of course strong influences as well. The procedure for finding the nondimensionalized *TSFC* for the ducted fan is similar to that for the exhausted fan and again uses the definition of the *TSFC* as follows:

$$TSFC a_a = \frac{\left[\frac{T_{t4}}{T_a} - \frac{T_{t4}}{T_a} \tau_c \right] \left[\frac{c_p T_a}{\Delta H} \right]}{M_a (1 + \alpha) \left[\sqrt{\left[\frac{\alpha + \left[\frac{T_{t4}}{T_a} \right] \left[\frac{T_a}{T_{t4}} \right] \frac{1}{\tau_c}}{1 + \alpha} \right] \left[\frac{\left[\frac{T_{t4}}{T_a} \right] \left[\frac{T_a}{T_{t4}} \right] \tau_c (1 + \alpha - \tau_c)}{1 + \left[\frac{T_{t4}}{T_a} \right] \left[\frac{T_a}{T_{t4}} \right] \tau_c \alpha} \right] - 1} \right] - 1} \quad 2.3.100$$

Once again, for the ducted and mixed fan typical *TSFC* values are 0.35 to 0.7 lbm/h/lbf.

A representative trend study is presented in Figure 2.57. Here the trends of thrust and *TSFC* are shown for a given compressor pressure ratio, Mach number, turbine inlet temperature, and core flow rate as functions of bypass ratio. Unlike the exhausted fan case, both the dimensionless thrust (by \dot{m}_t) and *TSFC* continuously decrease with increasing bypass ratio. Because the fan pressure ratio is not specified, a limiting or maximum bypass ratio value does not exist as it did for the exhausted fan case. As just noted, as the bypass ratio increases, the value of *TSFC* monotonically decreases, which is good from a fuel economy standpoint. However, as the bypass ratio increases, the value of $F/\dot{m}_t a_a$ decreases. Keeping in mind that the physical size of the engine increases as \dot{m}_t increases, one should realize that, as the bypass ratio increases, the thrust-to-size or, more importantly, the thrust-to-weight ratio decreases. Thus, for a given needed thrust, if a large bypass ratio is used, a large and heavy engine will be required. However, if a low bypass ratio is used, a smaller, lighter

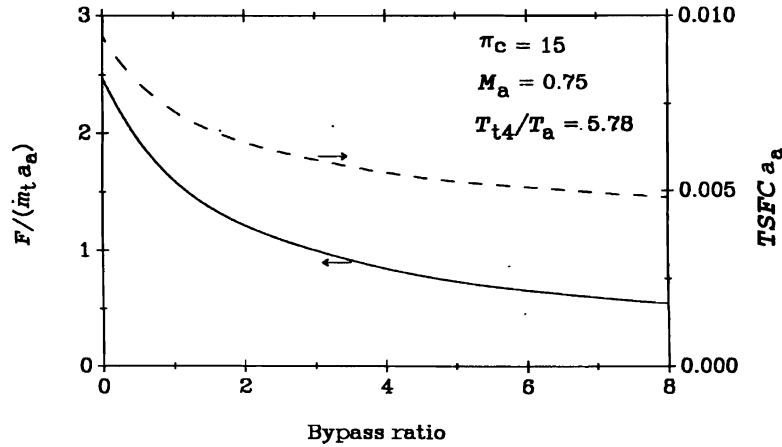


Figure 2.57 Effect of bypass ratio on performance of an ideal mixed turbofan.

engine can be used. As a result, for military (fighter) applications, where weight is a primary concern, low bypass ratios are used (often less than unity). On the other hand, for commercial applications in which fuel economy is the primary concern, high bypass ratios up to 9 are used (and with the exhausted fan design).

Afterburning: The afterburning mixed fan is now considered. Figure 2.55 depicts this geometry. Many of the equations from the nonafterburning case, apply but several new derivations will be required. Equations 2.3.80 through 2.3.84 apply. The mixer energy equation (Eq. 2.2.69), after being expanded on the exit uniform total temperature from the mixer, $T_{t5.5}$, ideally becomes

$$T_{t5.5} = \frac{\alpha T_a \left[\frac{T_{t6}}{T_a} \right] \left[\frac{T_{t7}}{T_2} \right] + T_a \left[\frac{T_{t6}}{T_a} \right] \left[\frac{T_{t3}}{T_2} \right] \left[\frac{T_{t4}}{T_{t3}} \right] \left[\frac{T_{t5}}{T_{t4}} \right]}{\alpha + 1}, \quad 2.3.101$$

which can be reduced to

$$T_{t5.5} = \frac{\alpha T_a \left[\frac{T_{t6}}{T_a} \right] \tau_f + T_a \left[\frac{T_{t6}}{T_a} \right] \tau_c \tau_b \tau_t}{\alpha + 1}. \quad 2.3.102$$

Using this with Eq. 2.3.90 yields

$$T_{t5.5} = T_a \left[\frac{T_{t6}}{T_a} \right] \tau_f \left[\frac{\alpha + \tau_b}{\alpha + 1} \right]. \quad 2.3.103$$

The total temperature at the afterburner exit (station 6) is given by

$$T_{t6} = T_{t5.5} \left[\frac{T_{t6}}{T_{t5.5}} \right] = T_{t5.5} \tau_{ab}, \quad 2.3.104$$

where τ_{ab} is again the afterburner total temperature ratio, which, again for the ideal case (adiabatic nozzle), is the same as for T_{t8} . Thus, from this and Eq. 2.3.103,

$$\frac{T_{t8}}{T_a} = \tau_{ab} \tau_f \left[\frac{T_{t6}}{T_a} \right] \left[\frac{\alpha + \tau_b}{\alpha + 1} \right]. \quad 2.3.105$$

From Eqs. 2.3.105, 2.3.92, and 2.2.42 one therefore obtains

$$\frac{T_8}{T_a} = \frac{\tau_{ab} \tau_f \left[\frac{T_{t6}}{T_a} \right] \left[\frac{\alpha + \tau_b}{\alpha + 1} \right]}{\left[\left(\frac{p_{t8}}{p_a} \right) \pi_f \right]^{\frac{\gamma-1}{\gamma}}}, \quad 2.3.106$$

which for the ideal case (from Eqs. 2.2.6 and 2.2.17) becomes

$$\frac{T_8}{T_a} = \tau_{ab} \left[\frac{\alpha + \tau_b}{\alpha + 1} \right]. \quad 2.3.107$$

One can now solve for the burner total temperature ratio τ_b from Eq. 2.3.103 as follows:

$$\tau_b = \frac{\left[\frac{T_{t5.5}}{T_a} \right] \left[\frac{T_a}{T_{ta}} \right]}{\tau_f} [1 + \alpha] - \alpha. \quad 2.3.108$$

Thus, from this and Eq. 2.3.107,

$$\frac{T_8}{T_a} = \frac{\tau_{ab}}{\tau_f} \left[\frac{T_{t5.5}}{T_a} \right] \left[\frac{T_a}{T_{ta}} \right] \quad 2.3.109$$

or

$$\frac{T_8}{T_a} = \frac{\left[\frac{T_{t6}}{T_a} \right] \left[\frac{T_a}{T_{ta}} \right]}{\tau_f}. \quad 2.3.110$$

Now, expanding on T_{t8}/T_8 :

$$\frac{T_{t8}}{T_8} = \left[\frac{T_{t8}}{T_a} \right] \left[\frac{T_a}{T_8} \right], \quad 2.3.111$$

which, when Eq. 2.3.110 is used, becomes

$$\frac{T_{t8}}{T_8} = \left[\frac{T_{t8}}{T_a} \right] \tau_f. \quad 2.3.112$$

Therefore, the velocity ratio is obtained from Eqs. 2.3.83, 2.3.10, and 2.3.112 as follows:

$$\frac{u_8}{u_a} = \sqrt{\frac{\left[\frac{T_{ta}}{T_a} \right] \tau_f - 1}{\frac{T_{ta}}{T_a} - 1}} \sqrt{\frac{\left[\frac{T_{t8}}{T_a} \right]}{\tau_f \left[\frac{T_{ta}}{T_a} \right]}}. \quad 2.3.113$$

Using this with Eqs. 2.3.80, 2.3.81, and 2.3.98 yields

$$\frac{F}{\dot{m}a_a} = M_a (1 + \alpha) \left[\sqrt{\frac{\left[\frac{T_{ta}}{T_a} \right] \left[\frac{\tau_c + \left[\frac{T_{tb}}{T_a} \right] \left[\frac{T_a}{T_{t4}} \right] \tau_c (1 + \alpha - \tau_c)}{1 + \left[\frac{T_{tb}}{T_a} \right] \left[\frac{T_a}{T_{t4}} \right] \tau_c \alpha} \right] - 1}{\left[\frac{T_{ta}}{T_a} - 1 \right] \left[\frac{\tau_c + \left[\frac{T_{tb}}{T_a} \right] \left[\frac{T_a}{T_{t4}} \right] \tau_c (1 + \alpha - \tau_c)}{1 + \left[\frac{T_{tb}}{T_a} \right] \left[\frac{T_a}{T_{t4}} \right] \tau_c \alpha} \right] \left[\frac{T_{t8}}{T_a} \right] - 1} \right]. \quad 2.3.114$$

This expression is the dimensionless thrust equation for the mixed afterburning turbofan. The thrust is a strong function of burner exit temperature, afterburner exit temperature, compressor pressure ratio, and bypass ratio. Next, to find the total fuel burned, \dot{m}_f , one can apply the energy equation to the entire engine. Recall that no shaft power crosses the control volume and that, ideally, \dot{m}_f is much smaller than \dot{m} . Thus, very simply,

$$\dot{m}_f \Delta H = \dot{m} (1 + \alpha) c_p (T_{t6} - T_{ta}). \quad 2.3.115$$

Thus, solving for \dot{m}_f and using the definition of dimensionless *TSFC*, Eqs. 2.3.98 and 2.3.114, and the fact that $T_{t6} = T_{t8}$ yields

$$TSFC a_a = \frac{\left[\left(\frac{T_{t8}}{T_a} \right) - \left(\frac{T_{t4}}{T_a} \right) \right] \left[\frac{c_p T_a}{\Delta H M_a} \right]}{\sqrt{\left[\frac{T_{t4}}{T_a} \right] \left[\frac{\tau_c + \left[\frac{T_{t4}}{T_a} \right] \left[\frac{T_a}{T_{t4}} \right] \tau_c (1 + \alpha - \tau_c)}{1 + \left[\frac{T_{t4}}{T_a} \right] \left[\frac{T_a}{T_{t4}} \right] \tau_c \alpha} \right] - 1} \left[\frac{T_{t8}}{T_a} \right] - 1} \left[\frac{T_{t4}}{T_a} - 1 \right] \left[\frac{\tau_c + \left[\frac{T_{t4}}{T_a} \right] \left[\frac{T_a}{T_{t4}} \right] \tau_c (1 + \alpha - \tau_c)}{1 + \left[\frac{T_{t4}}{T_a} \right] \left[\frac{T_a}{T_{t4}} \right] \tau_c \alpha} \right] \left[\frac{T_{t4}}{T_a} \right]}. \quad 2.3.116$$

This is the *TSFC* for the mixed fan with an afterburner. Values for this are much higher than for the nonafterburning case. The same result (although by a longer derivation) would have been obtained if the energy equation had been applied to both the primary burner and afterburner to find the total flow rate. For example, Eqs. 2.2.31 and 2.2.32 give the primary burner fuel ratio. The afterburner fuel ratio for the mixed turbofan can be found by the following analysis. Applying the energy equation to only the afterburner (Eq. 2.2.38) and solving for the fuel ratio (Eq. 2.2.39) yields

$$f_{ab} = \frac{\dot{m}_{f,ab}}{\dot{m}} = \frac{(1 + \alpha) c_p (T_{t6} - T_{t5.5})}{\Delta H}, \quad 2.3.117$$

where $T_{t5.5}$ is given by Eq. 2.3.102.

Once again, a series of parametric studies can be performed for this type of engine. The ideal afterburning version of the mixed fan operates with characteristics similar to those for the exhausted version of a turbofan. That is, the dimensionless thrust (by \dot{m}_t) is lower than that of a turbojet; however, the *TSFC* is also lower. The addition of the afterburner increases the thrust and *TSFC* significantly, but both thrust and *TSFC* are below those for a similar turbojet with an afterburner. Typical trends are shown in Figure 2.58.

The characteristics of mixed and exhausted turbofans can be compared from Figures 2.58 and 2.54. One important conclusion is that ideal (and only ideal) nonafterburning models operate identically when (and only when) the exhausted fan operates with the optimum pressure ratio. Another very important conclusion is that the ideal mixed turbofan has markedly more thrust than the ideal exhausted fan when the afterburner is lit. This finding is true because of the much larger airflow rate $((1 + \alpha)\dot{m})$ and consequently a much larger fuel flow) present in the afterburner for the mixed configuration. However, on the basis of the same reasoning the *TSFC* is much larger for the mixed version. This partially explains why mixed turbofans are usually used in military applications. That is, military craft usually have afterburners and thus need an increase in thrust levels as large as possible when the afterburner is lit but also need to be fuel efficient when cruising. On the other hand, exhausted turbofans are usually used in commercial aircraft, and these do not usually have afterburners. Ideally, both types of turbofans without afterburners have been demonstrated in this chapter to operate identically. However, as discussed in Chapter 3, the ducts and mixers in mixed turbofans are quite nonisentropic and thus incur significant losses to the flow. As a result, if an afterburner is not to be used, an exhausted fan is more efficient than a mixed turbofan owing to reduced nonideal effects or losses.

Example 2.5: An ideal turbofan with a mixed fan flies at sea level at a Mach number of 0.75. The primary flow is 165 lbm/s (74.83 kg/s), and the bypass ratio is 1.20. The compressor pressure ratio is 15. The fuel has a heating value of 17,800 Btu/lbm (41,400 kJ/kg), and the burner exit total temperature is 2500 °R (1389 K).

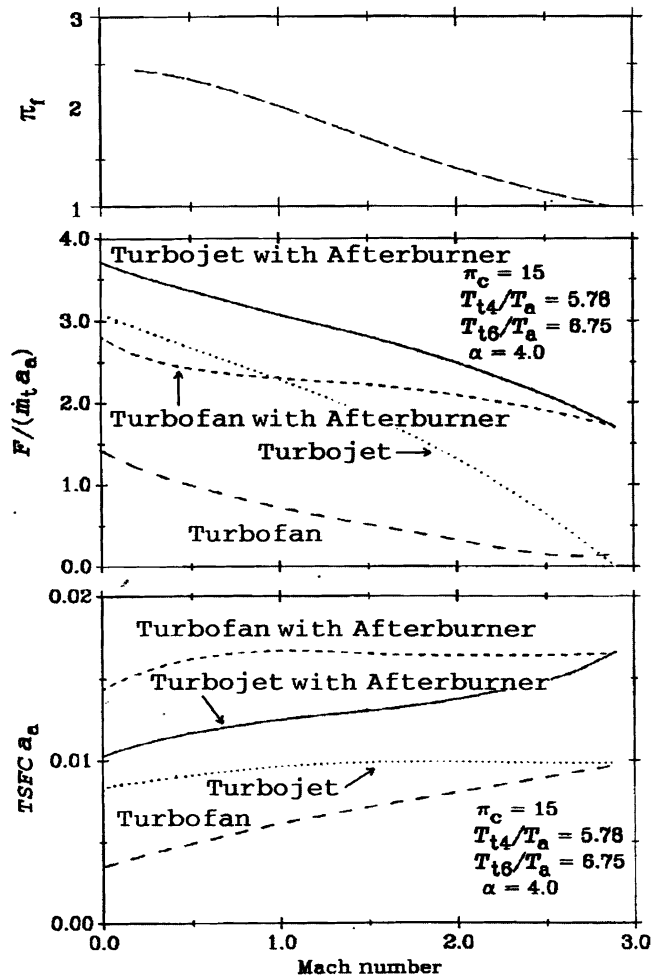


Figure 2.58 Dimensionless thrust (based on total flow) and dimensionless $TSFC$ versus Mach number for an ideal mixed fan and turbojet with and without afterburners.

The Mach numbers at the turbine and duct exits are the same. Find the developed thrust and the $TSFC$ for $\gamma = 1.40$.

SOLUTION:

If this example is compared with the previous example for the turbojet, it can readily be seen that the only difference is the addition of the mixed fan. All of the given conditions are identical. Once again, a step-by-step solution is presented, for it allows internal differences between this example and the simple turbojet and the exhausted fan examples to be determined.

Many of the parameter values are the same as in the previous turbojet example and are as follows:

$$\begin{aligned}
 p_a &= 14.69 \text{ psia (101.3 kPa)} & T_a &= 518.7^\circ\text{R (288.2 K)} \\
 u_a &= 837.3 \text{ ft/s (255.2 m/s)} & T_{ta} &= 577.1^\circ\text{R (320.6 K)} = T_{t2} \\
 a_a &= 1116 \text{ ft/s (340.1 m/s)} \\
 p_{ta} &= 21.33 \text{ psia (147.1 kPa)} = p_{t2} & p_{t3} &= 320.0 \text{ psia (2206 kPa)} = p_{t4} \\
 T_{t3} &= 1251^\circ\text{R (695.0 K)} & \tau_c &= 2.168
 \end{aligned}$$

FAN

First, the fan total pressure ratio, π_f , must be found. Obtaining this requires that the total temperature ratio, τ_f , be known:

$$\begin{aligned}\tau_f &= \frac{\tau_c + \left[\frac{T_{13}}{T_a}\right] \left[\frac{T_a}{T_{14}}\right] \tau_c (1 + \alpha - \tau_c)}{1 + \left[\frac{T_{13}}{T_a}\right] \left[\frac{T_a}{T_{14}}\right] \tau_c \alpha} \\ &= \frac{2.168 + \left[\frac{577.1}{518.7}\right] \left[\frac{518.7}{2500}\right] \times 2.168 \times (1 + 1.20 - 2.168)}{1 + \left[\frac{577.1}{518.7}\right] \left[\frac{518.7}{2500}\right] \times 2.168 \times 1.20} \\ &= 1.365.\end{aligned}$$

Thus, for the ideal (isentropic) fan, $\pi_f = [\tau_f]^{\frac{\gamma}{\gamma-1}} = [1.365]^{\frac{1.4}{0.4}} = 2.968$, which is very close to the exhausted fan case (but not exactly the same).

The total temperature exiting the fan is $T_{17} = \tau_f \times T_{12} = 1.365 \times 577.1 = 787.4^\circ\text{R}$ (437.4 K) = $T_{17.5}$. Also, the total pressure exiting the fan is $p_{17} = \pi_f \times p_{12} = 2.968 \times 21.33 = 63.32$ psia (436.6 kPa) = $p_{17.5}$.

DUCT

Because the duct is ideal (adiabatic), the total temperature is constant; that is, $T_{17.5} = T_{17} = 787.4^\circ\text{R}$ (437.4 K). Inasmuch as the duct is ideal (isentropic), the total pressure is also constant; that is, $p_{17.5} = p_{17} = 63.32$ psia (436.6 kPa)

TURBINE

The power balance on the shaft is determined as follows:

$$\dot{m}c_p(T_{14} - T_{15}) = \dot{m}c_p(T_{13} - T_{12}) + \alpha\dot{m}c_p(T_{17} - T_{12})$$

or

$$(T_{14} - T_{15}) = (T_{13} - T_{12}) + \alpha(T_{17} - T_{12});$$

thus, $(2500 - T_{15}) = (1251 - 577.1) + 1.20 \times (787.4 - 577.1)$,

and solving for the turbine exit total temperature yields $T_{15} = 1573^\circ\text{R}$ (873.9 K).

For the isentropic turbine,

$$\begin{aligned}p_{15} &= p_{14} [\tau_t]^{\frac{\gamma}{\gamma-1}} = p_{14} \left[\frac{T_{15}}{T_{14}}\right]^{\frac{\gamma}{\gamma-1}} = 320.0 \left[\frac{1573}{2500}\right]^{\frac{1.4}{0.4}} \\ &= 63.32 \text{ psia (436.6 kPa)} = p_{15.5},\end{aligned}$$

which, one should note, matches the value of $p_{17.5}$ found in the preceding discussion of the duct (as it should).

MIXER

For the mixer, the exit total temperature is found from a balance on the energy equation on the assumption that the exit temperature is uniform:

$$T_{15.5} = \frac{\alpha T_{17.5} + T_{15}}{\alpha + 1} = \frac{1.20 \times 787.4 + 1573}{1.20 + 1} = 1145^\circ\text{R} (636.1 \text{ K}).$$

The total pressure remains constant in an ideal mixer, and thus

$$p_{15.5} = p_{15} = 63.32 \text{ psia (436.6 kPa)}.$$

NOZZLE

For the ideal nozzle, the exit total temperature is the same as that of the inlet value:

$$T_{18} = T_{15.5} = 1145^\circ\text{R} (636.1 \text{ K})$$

For an ideal nozzle, $p_{t8} = p_8 \left[1 + \frac{\gamma-1}{2} M_8^2 \right]^{\frac{\gamma}{\gamma-1}}$.
Solving for the exit Mach number thus yields

$$M_8 = \sqrt{\left[\frac{2}{\gamma-1} \right] \left[\left[\frac{p_{t8}}{p_8} \right]^{\frac{\gamma-1}{\gamma}} - 1 \right]} = \sqrt{\left[\frac{2}{1.4-1} \right] \left[\left[\frac{63.32}{14.69} \right]^{\frac{0.4}{1.4}} - 1 \right]}$$

$$= 1.609.$$

Therefore the exit temperature is

$$T_8 = \frac{T_{t8}}{1 + \left[\frac{\gamma-1}{2} \right] M_8^2} = \frac{1145}{1 + \left[\frac{1.4-1}{2} \right] 1.609^2} = 754.1 \text{ }^\circ\text{R} (418.9 \text{ K}),$$

and the exit gas velocity is

$$u_8 = M_8 a_8 = M_8 \sqrt{\gamma \mathcal{R} T_8}$$

$$= 1.609 \sqrt{1.4 \times 53.35 \frac{\text{ft}\cdot\text{lbf}}{\text{lbm}\cdot^\circ\text{R}} \times 32.17 \frac{\text{lbm}}{\text{slug}} \times 754.1 \text{ }^\circ\text{R} \times \frac{\text{slug}\cdot\text{ft}}{\text{s}^2\cdot\text{lbf}}}$$

$$= 2166 \text{ ft/s} (660.2 \text{ m/s}).$$

THRUST AND *TSFC*

Finally, since the nozzle exit pressure matches the ambient pressure, the thrust is given by

$$F = F = \dot{m}_t (u_8 - u_a) = (1 + \alpha) \dot{m} (u_8 - u_a)$$

$$= 2.20 \times 165 \frac{\text{lbm}}{\text{s}} \times (2166 - 837.3) \frac{\text{ft}}{\text{s}} \times \left[\frac{\text{slug}}{32.17 \text{ lbm}} \right] \left[\frac{\text{lbf}\cdot\text{s}^2}{\text{slug}\cdot\text{ft}} \right]$$

$$= 14,998 \text{ lbf} (66,710 \text{ N}). \quad < \text{ANS}$$

This thrust is 2.4 percent higher than in the fan exhausted case.

The fuel flow rate is the same as for the turbojet once again:

$$\dot{m}_f = 2.778 \text{ lbm/s} (1.260 \text{ kg/s})$$

Thus

$$TSFC = \frac{\dot{m}_f}{F} = \frac{2.778 \frac{\text{lbm}}{\text{s}} \times 3600 \frac{\text{s}}{\text{h}}}{14,998 \text{ lbf}}$$

$$= 0.667 \text{ lbm/h/lbf} (0.06799 \text{ kg/h/N}), \quad < \text{ANS}$$

which is 2.4 percent lower than in the exhausted fan case

Note that the thrust and *TSFC* match the *optimized* exhausted case. This is not a coincidence and can be shown to always be the case for an ideal fan. Proving this is left as an exercise for the reader.

Example 2.6: The ideal turbofan with a mixed fan in the previous example now has an afterburner. All other conditions are the same, and the afterburner exit total temperature is $3200 \text{ }^\circ\text{R}$ (1779 K). The same fuel is used for both the primary burner and afterburners. Find the developed thrust and the *TSFC*.

SOLUTION:

If this example is compared with the previous one for the turbofan, the only difference that will be observed is the addition of the afterburner. All of the given conditions are identical. Once again a step-by-step solution is presented because it

allows the internal differences between this example and the nonafterburning case to be determined.

Many of the values are the same as in the previous nonafterburning example and are simply listed as follows:

$$\begin{aligned}
 p_a &= 14.69 \text{ psia (101.3 kPa)} & T_a &= 518.7^\circ\text{R (288.2 K)} \\
 u_a &= 837.3 \text{ ft/s (255.2 m/s)} \\
 T_{1a} &= 577.1^\circ\text{R (320.6 K)} = T_{12} & p_{1a} &= 21.33 \text{ psia (147.1 kPa)} = p_{12} \\
 p_{13} &= 320.0 \text{ psia (2206 kPa)} = p_{14} & T_{13} &= 1251^\circ\text{R (695.0 K)} \\
 \tau_c &= 2.168 & \tau_f &= 1.365 \\
 \pi_f &= 2.968 & T_{17.5} &= 787.4^\circ\text{R (437.4 K)} \\
 p_{15} &= p_{15.5} = p_{17.5} & M_8 &= 1.609 \\
 &= 63.32 \text{ psia (436.6 kPa)} \\
 T_{15} &= 1573^\circ\text{R (873.9 K)} & T_{15.5} &= 1145^\circ\text{R (636.1 K)}
 \end{aligned}$$

AFTERBURNER

The total temperature at station 8 is the same as that of the afterburner exit (T_{16}), which is given as follows:

$$T_{16} = T_{18} = 3200^\circ\text{R (1779 K)}.$$

And the total pressure at the exit of the afterburner is the same as the total pressure at the turbine exit:

$$p_{16} = p_{15} = 63.32 \text{ psia (436.6 kPa)}.$$

The primary fuel flow rate is the same as for the nonafterburning case and is $\dot{m}_f = 2.778 \text{ lbm/s (1.260 kg/s)}$,

but the afterburning fuel flow rate is needed and is given by

$$\begin{aligned}
 \dot{m}_{f_{ab}} &= \frac{\dot{m}_{1c_p} [T_{16} - T_{15.5}]}{\Delta H} = \frac{(1 + \alpha) \dot{m}_{c_p} [T_{16} - T_{15.5}]}{\Delta H} \\
 &= \frac{2.20 \times 165 \frac{\text{lbm}}{\text{s}} \times 0.24 \frac{\text{Btu}}{\text{lbm}^\circ\text{R}} \times [3,200 - 1145]^\circ\text{R}}{17,800 \frac{\text{Btu}}{\text{lbm}}} \\
 &= 10.06 \text{ lbm/s (4.562 kg/s)},
 \end{aligned}$$

which is 3.62 times the primary burner rate! The afterburner is consuming large amounts of fuel, and it is obvious that not much time will be required to drain the fuel tank. Thus, the total fuel flow rate is

$$\dot{m}_{f_t} = \dot{m}_f + \dot{m}_{f_{ab}} = 2.788 + 10.06 = 12.84 \text{ lbm/s (5.823 kg/s)}.$$

NOZZLE

Because the gas is expanding between the same pressures, the Mach number will be the same as in the previous example. The exit temperature will be higher as follows:

$$T_8 = \frac{T_{18}}{1 + \left[\frac{\gamma-1}{2}\right] M_8^2} = \frac{3200}{1 + \left[\frac{1.4-1}{2}\right] 1.609^2} = 2108^\circ\text{R (1171K)}$$

And the gas exit velocity is

$$\begin{aligned}
 u_8 &= M_8 a_8 = M_8 \sqrt{\gamma \mathcal{R} T_8} \\
 &= 1.609 \sqrt{1.4 \times 53.35 \frac{\text{ft-lbf}}{\text{lbm}^\circ\text{R}} \times 32.17 \frac{\text{lbm}}{\text{slug}} \times 2108^\circ\text{R} \times \frac{\text{slug-ft}}{\text{s}^2\text{-lbf}}} \\
 &= 3622 \text{ ft/s (1104 m/s)}.
 \end{aligned}$$

THRUST AND *TSFC*

Finally, the nozzle exit pressure and atmospheric pressure are ideally the same, and thus the thrust is given by

$$\begin{aligned} F &= \dot{m}_t (u_g - u_a) = (1 + \alpha) \dot{m} (u_g - u_a) \\ &= 2.20 \times 165 \frac{\text{lbf}}{\text{s}} \times (3622 - 837.3) \frac{\text{ft}}{\text{s}} \times \left[\frac{\text{slug}}{32.17 \text{ lbf}} \right] \left[\frac{\text{lbf}}{\text{slug-ft}} \right] \\ &= 31,424 \text{ lbf} (139,800 \text{ N}). \end{aligned} \quad <\text{ANS}$$

This thrust is 110 percent higher than the nonafterburning case.

Thus, the *TSFC* is

$$\begin{aligned} TSFC &= \frac{\dot{m}_t}{F} = \frac{12.84 \frac{\text{lbf}}{\text{s}} \times 3600 \frac{\text{s}}{\text{h}}}{31,424 \text{ lbf}} \\ &= 1.470 \text{ lbf/h/lbf} (0.1500 \text{ kg/h/N}), \end{aligned} \quad <\text{ANS}$$

which is 110 percent higher than in the nonafterburning case.

By comparing this example with the afterburning turbojet example, one can see that the thrust has been increased by 89 percent but the *TSFC* has only been increased by 16 percent – this is a large increase in thrust and only a moderate decrease in fuel economy. This partially explains why low-bypass-ratio turboprops are used in military applications.

2.3.4. Turboprop

As indicated in Chapter 1, a turboprop is aimed at a different group of aircraft than the engines already covered. This geometry is somewhat different than that of the previous engines and is shown in Figure 2.59. Propellers tend to be relatively large; propeller tip speeds can be quite high. As a result, this engine type in the past was only used primarily on low-speed aircraft so that the tip speeds would not become prohibitively large. Current technologies are allowing higher aircraft speeds with turboprops – for example, with unducted fan engines. The geometry is somewhat similar to a turbofan with the propeller replacing the fan; however, the flow through the propeller is not as well defined as in a fan. Also, the pressure ratio across the propeller is very nearly unity. In some respects, this engine behaves like a turbofan with a very high bypass ratio (approximately 25 to 100); that is, a considerable flow of air goes through the propeller to generate thrust. The remainder of the engine (stations 2 through 8) is fundamentally identical to a turbojet. A portion of the flow fanned by the propeller enters the compressor (station 2). The thrust from this engine type is developed from two sources: the propeller and the turbojet nozzle. Thus, this engine is similar to the exhausted turbofan in this respect, which also has two components of thrust. Because of the less defined nature of the propeller flow (mass flow, pressure rise, and flow direction), a somewhat different approach to the analysis is needed.

First, the total power generated for thrust of an ideal turboprop is given by

$$\mathcal{P}_t = F u_a + \mathcal{P}_p, \quad 2.3.118$$

where F is the thrust of a turbojet, which can be found from the analysis from Section 2.3.2.a, and \mathcal{P}_p is the propeller power. Next, a work coefficient for the engine can conveniently be defined as

$$C_{w_c} \equiv \frac{\mathcal{P}_t}{\dot{m} h_a}, \quad 2.3.119$$

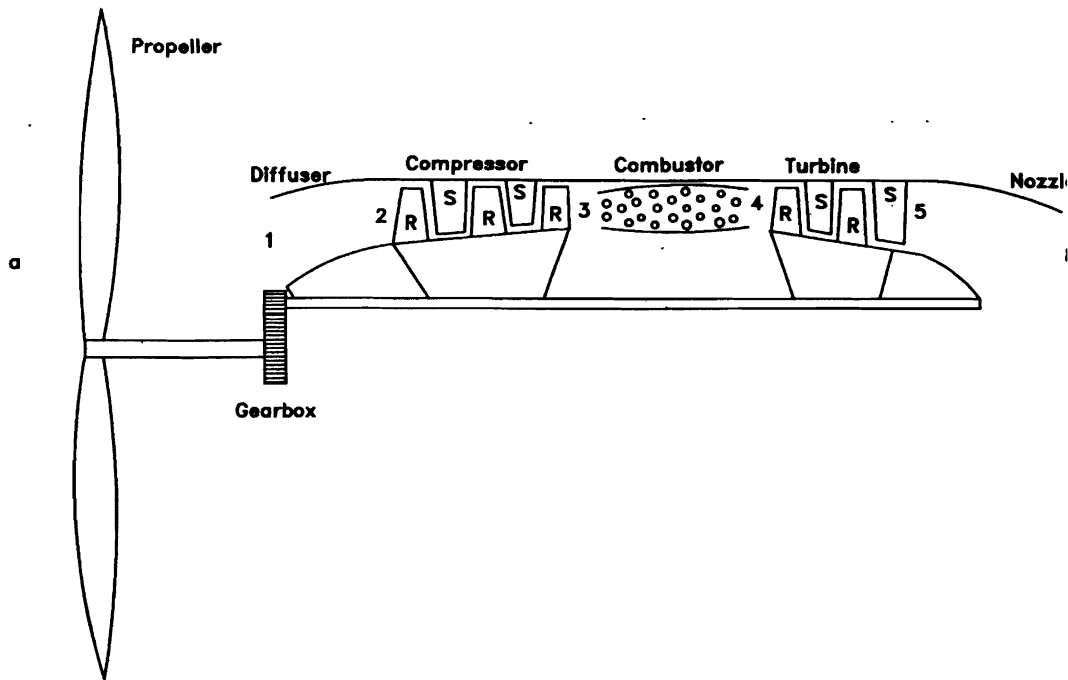


Figure 2.59 General turbojet.

where \dot{m} is the airflow through the turbojet core. This now can be applied to Eq. 2.3.118

$$C_{w_e} = C_{w_p} + \frac{u_a F}{\dot{m} c_p T_a}, \quad 2.3.120$$

where C_{w_p} is the propeller work coefficient given by Eq. 2.2.22. Next, applying the energy equation to the shaft (Eq. 2.2.26) and reducing yield

$$\frac{\mathcal{P}}{p} + \dot{m} c_p (T_{t3} - T_{t2}) = \dot{m} c_p (T_{t4} - T_{t5}). \quad 2.3.121$$

Assuming that the air entering the compressor has the same total properties as the freestream (i.e., the pressure and temperature have not increased significantly by traversing the propeller) and solving for the propeller power, one obtains

$$\frac{\mathcal{P}}{\dot{m} c_p T_a} = \left[\frac{T_{t4}}{T_a} \right] \left[1 - \frac{\tau_5}{\left[\frac{T_{ta}}{T_a} \right] \tau_c} \right] - \left[\frac{T_{ta}}{T_a} \right] (\tau_c - 1), \quad 2.3.122$$

where τ_5 is a new parameter and is defined by

$$\tau_5 \equiv \left[\frac{T_{ta}}{T_a} \right] \tau_c \tau_t. \quad 2.3.123$$

This equation ideally (isentropically) reduces to (recall that $p_{t4} = p_{t3}$)

$$\tau_5 = \left[\left[\frac{p_{ta}}{p_a} \right] \pi_c \pi_t \right]^{\frac{\gamma-1}{\gamma}} = \left[\frac{p_{ta} p_{t3} p_{t5}}{p_a p_{t2} p_{t4}} \right]^{\frac{\gamma-1}{\gamma}} = \left[\frac{p_{t5}}{p_a} \right]^{\frac{\gamma-1}{\gamma}} \quad 2.3.124$$

or

$$\tau_5 = [\pi_5]^{\frac{\gamma-1}{\gamma}}, \quad 2.3.125$$

where

$$\pi_5 \equiv \left[\frac{p_{t5}}{p_a} \right], \quad 2.3.126$$

which is a nozzle parameter and is directly related to the exit Mach number for the ideal case by Eq. 2.2.44 and will be discussed in more detail in Chapter 5. One should not make the error of equating τ_5 to T_{t5}/T_a , for the equality does not hold ($T_{t4} \neq T_{t3}$)! Also, recall that for the ideal case the total pressure is constant through the nozzle; thus, p_{t8} is equal to p_{t5} . Because p_{t5}/p_a must be greater than unity, by Eq. 2.3.125 τ_5 must also be greater than unity. Next, the work coefficient for the turboprop is considered using Eq. H.2.2; that is,

$$\frac{u_a F}{\dot{m} c_p T_a} = \frac{u_a F}{\dot{m} \left[\frac{\gamma \mathcal{R}}{\gamma-1} \right] T_a} = \frac{(\gamma-1) u_a F}{\dot{m} \gamma \mathcal{R} T_a} = \frac{(\gamma-1) u_a F}{\dot{m} a_a^2}, \quad 2.3.127$$

or finally

$$\frac{u_a F}{\dot{m} c_p T_a} = \frac{(\gamma-1) M_a F}{\dot{m} a_a}. \quad 2.3.128$$

Next, using Eqs. 2.3.37, 2.3.43, and 2.3.123, one finds the jet thrust as follows:

$$\frac{F}{\dot{m} a_a} = M_a \left[\sqrt{\frac{\left[\frac{T_{t4}}{T_a} \right] \left[\frac{T_a}{T_{ta}} \right] \left[\frac{\tau_5-1}{\tau_c} \right]}{\left[\frac{T_{ta}}{T_a} \right] - 1}} - 1 \right]. \quad 2.3.129$$

Now, using Eqs. 2.3.120, 2.2.22, 2.3.122, 2.3.128, and 2.3.129 results in

$$\begin{aligned} C_{we} &= \left[\frac{T_{t4}}{T_a} \right] \left[1 - \frac{\tau_5}{\left[\frac{T_{ta}}{T_a} \right] \tau_c} \right] - \left[\frac{T_{ta}}{T_a} \right] (\tau_c - 1) \\ &+ (\gamma-1) M_a^2 \left[\sqrt{\frac{\left[\frac{T_{t4}}{T_a} \right] \left[\frac{T_a}{T_{ta}} \right] \left[\frac{\tau_5-1}{\tau_c} \right]}{\left[\frac{T_{ta}}{T_a} \right] - 1}} - 1 \right]. \end{aligned} \quad 2.3.130$$

Once the work coefficient is found, the total thrust can be found by

$$F_t = \frac{\mathcal{P}_t}{u_a}, \quad 2.3.131$$

or the dimensionless thrust can be found by

$$\frac{F_t}{\dot{m} a_a} = \frac{\mathcal{P}_t}{\dot{m} a_a u_a}, \quad 2.3.132$$

which, when used with Eqs. 2.3.119, H.2.7, H.2.8, and H.2.2, yields

$$\frac{F_t}{\dot{m} a_a} = \frac{C_{we}}{(\gamma-1) M_a}. \quad 2.3.133$$

The thrust is a strong function of burner exit temperature, afterburner exit temperature, compressor pressure ratio, and the nozzle parameter. Of course, the Mach number and mass

flow rate are strong influences for the turboprop just as they are for all other engines. Next, the fuel consumption needs to be determined. For a turboprop, a different fuel parameter is sometimes used and is identical to that used for a power-generation unit. This is the specific fuel consumption and is defined by

$$SFC \equiv \frac{\dot{m}_f}{\dot{Q}_1} = \frac{\dot{m}_f}{F_1 u_a} = \frac{\dot{m}_f}{\dot{m} c_p T_a C_{w_e}} \quad 2.3.134$$

Thus, using Eqs. 2.2.32 and 2.2.29, one obtains

$$SFC = \frac{\left[\frac{T_{t4}}{T_a} \right] - \left[\frac{T_{t3}}{T_a} \right] \tau_c}{\Delta H C_{w_e}}, \quad 2.3.135$$

where C_{w_e} is given above in Eq. 2.3.130. The definition of $TSFC$ can also be used to find that

$$TSFC = SFC u_a. \quad 2.3.136$$

Thus, the $TSFC$ is

$$TSFC = u_a \left[\frac{\left[\frac{T_{t4}}{T_a} \right] - \left[\frac{T_{t3}}{T_a} \right] \tau_c}{\Delta H C_{w_e}} \right]. \quad 2.3.137$$

For a turboprop, typical values of $TSFC$ are 0.3 to 0.4 lbm/h/lbf.

The thrust may be maximized by using Eq. 2.3.130 because the thrust is proportional to the work coefficient. That is, if one differentiates C_{w_e} with respect to τ_5 , holding all other parameters fixed, and sets the result to zero, the following equation is obtained with the aid of Eq. 2.2.4:

$$\tau_{5,opt} = 1 + \tau_c \left[\frac{T_{t3}}{T_a} \right] \left[\frac{T_a}{T_{t4}} \right] \left[\left[\frac{T_{t3}}{T_a} \right] - 1 \right]. \quad 2.3.138$$

Although the analytical operations are on τ_5 , in actuality the turbine operation is being optimized to deliver the best balanced performance between the propeller and exhaust. Through this equation, one can find the optimum value of π_5 from Eq. 2.3.125 and the resulting temperature and pressure ratios in the turbine. With the aid of Eqs. 2.3.36 and 2.3.123, this ideally results in $u_8 = u_a$, which implies that the thrust from the turbojet optimally is zero (Eq. 2.3.25) and that all of the thrust is provided from the propeller!

Also, a set of studies can once again be performed. For example, the independent effect of both the compressor pressure ratio and the nozzle parameter π_5 on the work coefficient (or thrust) can be studied. Such a general study is presented in Figure 2.60 for a fixed freestream Mach number and temperature ratio T_{t4}/T_a . From this figure, it can be seen that optimum values of both π_c and π_5 exist if the thrust is to be maximized. That is, for a fixed value of π_5 , one can optimize the compressor pressure ratio π_c or vice versa. Furthermore, by choosing optimum values of both π_5 and π_c , one can maximize the thrust. For this case, the optimum values are $\pi_{5-opt} = 1.08$ and $\pi_{c-opt} = 13$.

Example 2.7: An ideal turboprop powers an aircraft at sea level at a Mach number of 0.7. The compressor has a pressure ratio of 6.5 and an airflow of 13.61 kg/s (30 lbm/s). The burner exit total temperature is 1389 K (2500 °R), and the nozzle exit Mach number is 0.95. The heating value of the fuel is 43,960 kJ/kg (18,900 Btu/lbm). Find the thrust and $TSFC$.

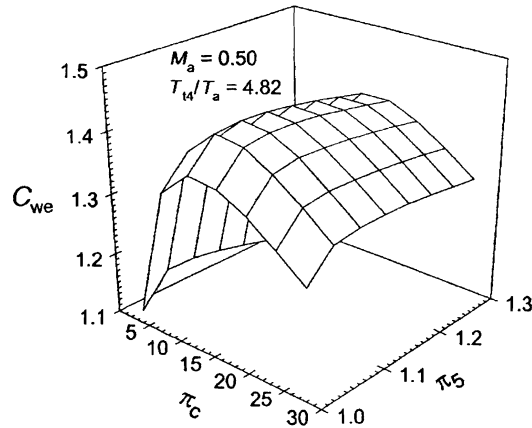


Figure 2.60 Effect of compressor total pressure ratio and nozzle parameter π_5 on the work coefficient of an ideal turboprop.

SOLUTION:

The known quantities are as follows:

$$\begin{aligned} T_a &= 288.2 \text{ K (518.7}^\circ\text{R)} & p_a &= 101.3 \text{ kPa (14.69 psia)} \\ T_{t4} &= 1389 \text{ K (2500}^\circ\text{R)} & p_8 &= 101.3 \text{ kPa (14.69 psia)} \\ M_a &= 0.7 & M_e &= 0.95 \end{aligned}$$

DIFFUSER

The freestream velocity is

$$\begin{aligned} u_a &= M_a a_a = M_a \sqrt{\gamma_a \mathcal{R} T_a} \\ &= 0.7 \sqrt{1.400 \times 287.1 \frac{\text{J}}{\text{kg}\cdot\text{K}} \times 288.2 \text{ K} \times \frac{\text{N}\cdot\text{m}}{\text{J}} \times \frac{\text{kg}\cdot\text{m}}{\text{N}\cdot\text{s}^2}} \\ &= 238.2 \text{ m/s (781.5 ft/s)}, \end{aligned}$$

and the total temperature at the inlet is

$$\begin{aligned} T_{ta} &= T_a \left[1 + \frac{\gamma - 1}{2} M_a^2 \right] = T_a \left[1 + \frac{1.4 - 1}{2} 0.7^2 \right] \\ &= 1.098 \times T_a = 316.4 \text{ K (569.5}^\circ\text{R)}, \end{aligned}$$

which is also equal to T_{t2} because the process is adiabatic. The total pressure at the inlet is

$$p_{ta} = p_a \left[1 + \frac{\gamma - 1}{2} M_a^2 \right]^{\frac{\gamma}{\gamma - 1}} = p_a \left[\frac{T_{ta}}{T_a} \right]^{\frac{\gamma}{\gamma - 1}},$$

and thus $p_{ta} = p_a [1.098]^{\frac{1.4}{0.4}} = 140.5 \text{ kPa (20.38 psia)}$.

COMPRESSOR

Since the compressor total pressure ratio, π_c , is given,

the total pressure at the compressor exit is $p_{t3} = \pi_c \times p_{t2}$,

but because the process is isentropic for an ideal diffuser, $p_{t2} = p_{ta}$,

$p_{t3} = 6.5 \times 140.5 \text{ kPa} = 912.9 \text{ kPa (132.4 psia)}$.

For an isentropic compressor, $\tau_c = [\pi_c]^{\frac{\gamma - 1}{\gamma}} = [6.5]^{\frac{0.4}{1.4}} = 1.707$,

and thus the total temperature at the compressor exit is $T_{t3} = \tau_c \times T_{t2} = 1.707 \times 316.4 \text{ K} = 540.2 \text{ K} (972.3 \text{ }^\circ\text{R})$.

BURNER

The fuel flow rate is given by

$$\begin{aligned} \dot{m}_f &= \frac{\dot{m}c_p [T_{t4} - T_{t3}]}{\Delta H} = 13.61 \frac{\text{kg}}{\text{s}} \times 1.005 \frac{\text{kJ}}{\text{kg}\cdot\text{K}} \times \frac{(1389 - 540.2)\text{K}}{43,960 \frac{\text{kJ}}{\text{kg}}} \\ &= 0.2639 \text{ kg/s} (0.5819 \text{ lbm/s}), \end{aligned}$$

and the exit total pressure is the same as that for the inlet of an ideal burner: $p_{t4} = p_{t3} = 912.9 \text{ kPa} (132.4 \text{ psia})$.

NOZZLE

Because $\frac{p_{t8}}{p_8} = [1 + \frac{\gamma-1}{2} M_8^2]^{\frac{\gamma}{\gamma-1}}$,

the exit Mach number is known, and the nozzle exit pressure ideally matches atmospheric pressure, the total pressure at the exit can be found as follows:

$$p_{t8} = 101.3 \text{ kPa} \left[1 + \frac{1.4-1}{2} 0.95^2 \right]^{\frac{1.4}{0.4}} = 181.1 \text{ kPa} (26.26 \text{ psia}).$$

For an ideal nozzle, the total pressure is constant (isentropic flow), and thus $p_{t5} = p_{t8} = 181.1 \text{ kPa} (26.26 \text{ psia})$, which is also the exit pressure for the turbine.

TURBINE

The total pressure ratio for the turbine can be found directly by

$$\pi_t = \frac{p_{t5}}{p_{t4}} = \frac{181.1 \text{ kPa}}{912.9 \text{ kPa}} = 0.1982,$$

and thus the total temperature ratio for the isentropic case can be found:

$\tau_t = [\pi_t]^{\frac{\gamma-1}{\gamma}} = [0.1982]^{\frac{0.4}{1.4}} = 0.6298$. The turbine total temperature is therefore $T_{t5} = \tau_t \times T_{t4} = 0.6298 \times 1389 \text{ K} = 875.0 \text{ K} (1575 \text{ }^\circ\text{R})$.

PROPELLER

The nozzle temperature parameter is

$$\tau_5 = \left[\frac{T_{t5}}{T_a} \right] \tau_c \tau_t = (1.098) \times (1.707) \times (0.6298) = 1.181,$$

and the work coefficient is

$$\begin{aligned} C_{w_e} &= \left[\frac{T_{t4}}{T_a} \right] \left[1 - \frac{\tau_5}{\left[\frac{T_{t4}}{T_a} \right] \tau_c} \right] - \left[\frac{T_{t4}}{T_a} \right] (\tau_c - 1) \\ &\quad + (\gamma - 1) M_a^2 \left[\sqrt{\frac{\left[\frac{T_{t4}}{T_a} \right] \left[\frac{T_a}{T_{t4}} \right] \left[\frac{\tau_5 - 1}{\tau_c} \right]}{\left[\frac{T_{t4}}{T_a} \right] - 1}} - 1 \right]; \end{aligned}$$

thus,

$$\begin{aligned} C_{w_e} &= \left[\frac{1389}{288.2} \right] \left[1 - \frac{1.181}{1.908 \times 1.707} \right] - [1.098] \times (0.707) \\ &\quad + (0.4) \times 0.7^2 \left[\sqrt{\frac{\left[\frac{1389}{288.2} \right] \left[\frac{1}{1.098} \right] \left[\frac{0.181}{1.707} \right]}{0.098}} - 1 \right] \end{aligned}$$

$$C_{w_e} = 1.0078 + 0.2305 = 1.2384,$$

$\begin{matrix} \text{prop} & \text{jet} \end{matrix}$

which means that 81.4 percent of the thrust work or power comes from the propeller. The total thrust power is therefore

$$\begin{aligned}\mathcal{P}_t &= C_{w_e} \dot{m} h_a = C_{w_e} \dot{m} c_p T_a \\ &= 1.2384 \times 13.61 \frac{\text{kg}}{\text{s}} \times 1.005 \frac{\text{kJ}}{\text{kg-K}} \times 288.2 \text{ K} \times 10^{-3} \frac{\text{MW}}{\text{kJ}} \\ &= 4.878 \text{ MW (6542 hp)}.\end{aligned}$$

The thrust is then

$$\begin{aligned}F_t &= \frac{\mathcal{P}_t}{u_a} = \frac{4.878 \text{ MW}}{238.2 \frac{\text{m}}{\text{s}}} \times 10^6 \frac{\text{W}}{\text{MW}} \times \frac{\text{J}}{\text{W-s}} \times \frac{\text{N-m}}{\text{J}} \\ &= 20,480 \text{ N (4605 lbf)},\end{aligned} \quad < \text{ANS}$$

and thus the *SFC* is

$$SFC \equiv \frac{\dot{m}_f}{\mathcal{P}_t} = \frac{0.2639 \frac{\text{kg}}{\text{s}} \times 3600 \frac{\text{s}}{\text{h}}}{4.878 \text{ MW}} = 194.7 \frac{\text{kg}}{\text{MW-h}} \left(0.320 \frac{\text{lbm}}{\text{hp-h}} \right).$$

The *TSFC* is

$$TSFC = \frac{\dot{m}_f}{F_t} = \frac{0.2639 \frac{\text{kg}}{\text{s}} \times 3600 \frac{\text{s}}{\text{h}}}{20,480 \text{ N}} = 0.04639 \frac{\text{kg}}{\text{N-h}} \left(0.455 \frac{\text{lbm}}{\text{h-lbf}} \right). \quad < \text{ANS}$$

As a complementary study, one can maximize the thrust. The optimum value of τ_5 is

$$\begin{aligned}\tau_{5_{\text{opt}}} &= 1 + \tau_c \left[\frac{T_{t4}}{T_a} \right] \left[\frac{T_a}{T_{t4}} \right] \left[\left[\frac{T_{t4}}{T_a} \right] - 1 \right] \\ &= 1 + 1.707 \times [1.098] \times \left[\frac{288.2}{1389} \right] \times [0.098] = 1.0381.\end{aligned}$$

This results in an engine work coefficient $C_{w_e} = 1.374$.

The total power is thus $\mathcal{P}_t = 5.413 \text{ MW (7259 hp)}$.

The total thrust is $F_t = 22,720 \text{ N (5109 lbf)}$ and is *all* from the propeller, and the *TSFC* = 0.04180 kg/h/N (0.410 lbm/h/lbf).

Also, for the ideal case,

$$\frac{p_{t8}}{p_a} = \frac{p_{t5}}{p_a} = [\tau_5]^{\frac{\gamma}{\gamma-1}} = [1.0381]^{\frac{1.4}{0.4}} = 1.1399,$$

which yields an exit Mach number of 0.437, a turbine total temperature ratio of 0.554, a turbine exit total temperature of 769.6 K (1385 °R), a nozzle exit static temperature of 741.1 K (1334 °R), and an exhaust velocity of 238.2 m/s (781.5 ft/s).

2.3.5. Power-Generation Gas Turbine

The next category of gas turbines to be analyzed is for power generation and not aircraft applications. A power-generation unit of general design is shown in Figure 2.61. As discussed in Chapter 1, the unit is very much like a turbojet engine, and one can see many similarities between this gas turbine and the aircraft engine; much of the cycle analysis is therefore identical. However, an inlet bell, with a decreasing area along the flow path, replaces the diffuser, which has an increasing area, and an exhaust, in which the gas flow has a very low velocity, replaces the nozzle, which has a high gas velocity. Also, a power-extracting device is attached to the shaft. This device may be an electrical generator, ship propeller, or one of several other power-extracting devices. Many modern power-generation units are aero-derivatives of the aircraft engines; that is, the core of the engine is essentially

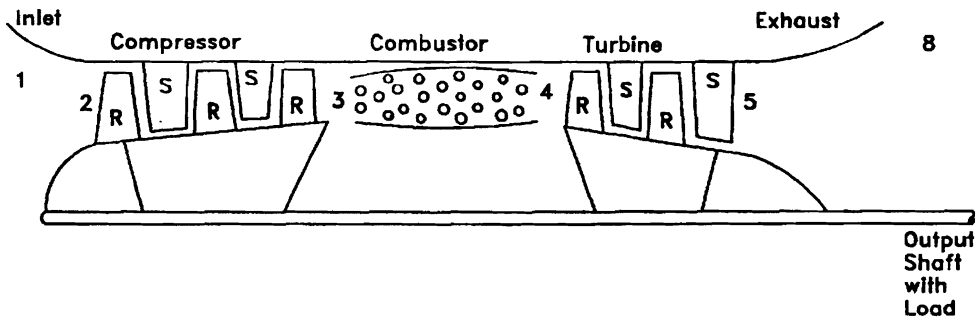


Figure 2.61 General power-generation gas turbine.

the same as that of a jet engine, thus reducing costs and manufacturing needs. This type of unit tends to be slightly heavier because weight is not as much of a concern as it is for aircraft applications. Since the net power output is of primary concern (and not thrust), derivation of the fundamental equations is somewhat different.

First, for the ideal case, the shaft power balance yields

$$\mathcal{P}_{\text{net}} = \dot{m}c_p(T_{14} - T_{15}) - \dot{m}c_p(T_{13} - T_{12}), \quad 2.3.139$$

where \mathcal{P}_{net} is the net or derived power. Nondimensionalizing results in

$$\frac{\mathcal{P}_{\text{net}}}{\dot{m}c_p T_a} = \left(\frac{T_{14}}{T_a} - \frac{T_{15}}{T_a} \right) - \left(\frac{T_{13}}{T_a} - \frac{T_{12}}{T_a} \right). \quad 2.3.140$$

If one recognizes that, for the ideal case, the diffuser is adiabatic ($T_{12} = T_{1a} = T_a$) and rearranges terms,

$$\frac{\mathcal{P}_{\text{net}}}{\dot{m}c_p T_a} = \left(\frac{T_{14} - T_{13}}{T_a} \right) - \left(\frac{T_{15}}{T_a} - 1 \right), \quad 2.3.141$$

but for the compressor the exit total temperature is

$$T_{13} = \tau_c T_{12} = T_{12} [\pi_c]^{\frac{\gamma-1}{\gamma}} \quad 2.3.142$$

and for the turbine the exit total temperature is

$$T_{15} = \tau_t T_{14} = [\pi_t]^{\frac{\gamma-1}{\gamma}} T_{14} = \left[\frac{p_{15}}{p_{14}} \right]^{\frac{\gamma-1}{\gamma}} T_{14}. \quad 2.3.143$$

For the ideal case, however, the total pressure is constant through the exhaust and the exit pressure is ambient; thus, $p_{15} = p_a$. Also for the ideal case the total pressure across the combustor is constant ($p_{14} = p_{13}$); consequently, from Eq. 2.3.139, if one recognizes that $\pi_c = p_{13}/p_{12}$ and recalls for the ideal case that the total pressure remains constant across the inlet and is equal to the ambient pressure because the inlet velocity is low ($p_{12} = p_{1a} = p_a$),

$$T_{15} = T_{14} \left[\frac{p_a}{\pi_c p_a} \right]^{\frac{\gamma-1}{\gamma}} = T_{14} [\pi_c]^{-\frac{\gamma-1}{\gamma}}. \quad 2.3.144$$

Therefore, using Eqs. 2.3.144 and 2.2.13 yields

$$T_{15} = \frac{T_{14}}{\tau_c}. \quad 2.3.145$$

Now, using Eqs. 2.3.141, 2.3.142, and 2.3.145 results in

$$\frac{\mathcal{P}_{\text{net}}}{\dot{m}c_p T_a} = \left(\frac{T_{t4}}{T_a}\right) \left(1 - \frac{1}{\tau_c}\right) - (\tau_c - 1). \quad 2.3.146$$

Thus, this nondimensional power output is a function of only two variables. The first is the compressor total temperature ratio (or total pressure ratio), and the second is the ratio of the combustor exit total temperature to the ambient temperature.

One can examine Eq. 2.3.146 for the dependence of net power on the compressor total temperature ratio. By differentiating the equation with respect to the total temperature ratio of the compressor, τ_c (which is directly related to the total pressure ratio), it is possible to optimize the output power. This results in

$$\tau_{c,\text{opt}} = \sqrt{\frac{T_{t4}}{T_a}}. \quad 2.3.147$$

The fuel flow rate for the ideal case is

$$\dot{m}_f = \frac{\dot{m}c_p}{\Delta H_f} (T_{t4} - T_{t3}) = \frac{\dot{m}c_p T_a}{\Delta H_f} \left(\frac{T_{t4}}{T_a} - \frac{T_{t3}}{T_a}\right), \quad 2.3.148$$

which, when Eq. 2.3.142 is used with ($T_{t2} = T_{ta} = T_a$), becomes

$$\dot{m}_f = \frac{\dot{m}c_p T_a}{\Delta H_f} \left(\frac{T_{t4}}{T_a} - \tau_c\right). \quad 2.3.149$$

The specific fuel consumption is

$$SFC = \frac{\dot{m}_f}{\mathcal{P}_{\text{net}}}; \quad 2.3.150$$

using Eqs. 2.3.146, 2.3.149, and 2.3.150 results in

$$SFC = \frac{1}{\Delta H_f} \frac{\left(\frac{T_{t4}}{T_a} - \tau_c\right)}{\left(\frac{T_{t4}}{T_a}\right) \left(1 - \frac{1}{\tau_c}\right) - (\tau_c - 1)}, \quad 2.3.151$$

which reduces to

$$SFC = \frac{1}{\Delta H_f} \left(\frac{\tau_c}{\tau_c - 1}\right). \quad 2.3.152$$

The reduced dimensional variable is a function of only two variables. The first is the compressor total temperature ratio (or total pressure ratio in as much as they are directly related), and the second is the heating value of the fuel. Typical values for such modern gas turbines are $0.35 \frac{\text{lbm}}{\text{hp-h}}$ ($0.20 \frac{\text{kg}}{\text{kW-h}}$). Lastly one can find the thermal efficiency by

$$\eta_{\text{th}} = \frac{\mathcal{P}_{\text{net}}}{\dot{Q}_{\text{in}}} = \frac{\mathcal{P}_{\text{net}}}{\dot{m}_f \Delta H_f} = \frac{1}{SFC \Delta H_f}, \quad 2.3.153$$

and thus

$$\eta_{\text{th}} = \frac{\left(\frac{T_{t4}}{T_a}\right) \left(1 - \frac{1}{\tau_c}\right) - (\tau_c - 1)}{\left(\frac{T_{t4}}{T_a} - \tau_c\right)}, \quad 2.3.154.a$$

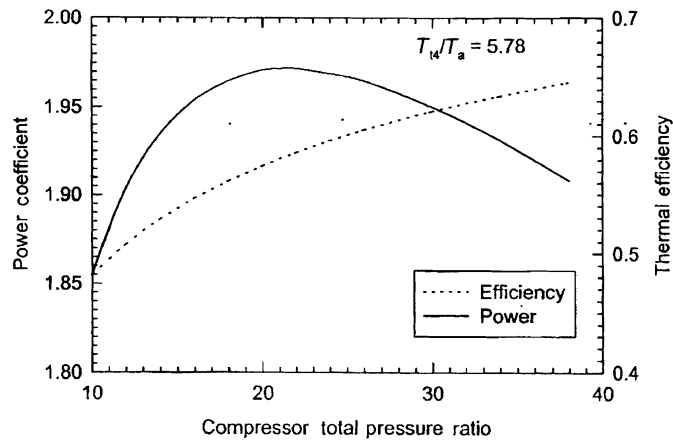


Figure 2.62 Effect of compressor total pressure ratio on net power and thermal efficiency.

which reduces to

$$\eta_{th} = \frac{\tau_c - 1}{\tau_c} \quad 2.3.154.b$$

The reduced nondimensional variable is a function of only one variable – the compressor total temperature ratio (or total pressure ratio). Examination of this equation shows that, as the total temperature ratio (or pressure ratio) increases, so does the efficiency. Typical values of thermal efficiency for modern power-generation units are 40 to 45 percent.

A typical trend study is presented in Figure 2.62 for a temperature ratio, T_{t4}/T_a , of 5.78. In this figure, the net nondimensional power and efficiency are plotted as functions of the compressor total pressure ratio. As predicted by Eq. 2.3.147, the net power is maximized at a total pressure ratio value of 21.55. Very importantly, however, note that the thermal efficiency continues to increase as the compressor total pressure ratio increases past the optimum value based on power.

Example 2.8: An ideal power-generation gas turbine with characteristics approximating those of a modern moderate size unit operates at sea level. It ingests 66.67 kg/s (147 lbm/s) of air. The compressor operates with a pressure ratio of 18. The fuel has a heating value of 42,800 kJ/kg (18,400 Btu/lbm), and the burner exit total temperature is 1456 K (2620 °R). Find the net output power, *SFC*, and net thermal efficiency for $\gamma = 1.40$.

SOLUTION:

INLET

First, flow is drawn into the gas turbine and accelerated to the inlet velocity from a stagnant condition far from the inlet. Because the velocity is zero far from the inlet, the ambient static and total pressures are equal ($p_{ta} = p_a = 101.3$ kPa), and the ambient static and total temperatures are equal ($T_{ta} = T_a = 288.2$ K). The process is also adiabatic; thus, ideally, the exit total temperature is $T_{t2} = T_{ta} = 288.2$ K (518.7 °R), and since the flow in the inlet is isentropic, the exit total pressure is $p_{t2} = p_{ta} = 101.3$ kPa (14.69 psia).

COMPRESSOR

The total pressure ratio of the compressor is given as $\pi_c = 18$.

The total pressure exiting the compressor is therefore

$$p_{t3} = \pi_c p_{t2} = 18 \times 101.3 \text{ kPa} = 1823 \text{ kPa} (264.4 \text{ psia}).$$

Ideally, the compressor total temperature ratio is

$$\tau_c = [\pi_c]^{\frac{\gamma-1}{\gamma}} = [18]^{\frac{1.4-1}{1.4}} = 2.2838 \quad \text{for } \gamma = 1.40;$$

therefore, the compressor total exit temperature is

$$T_{t3} = \tau_c T_{t2} = 2.2838 \times 288.2 \text{ K} = 658.1 \text{ K} (1185 \text{ }^\circ\text{R}).$$

COMBUSTOR

The ideal burner exit pressure is $p_{t4} = p_{t3} = 1823 \text{ kPa} (264.4 \text{ psia})$, and the first law of thermodynamics yields

$$\Delta H \dot{m}_f = \dot{m} c_{pb} (T_{t4} - T_{t3}),$$

where the fuel heating value is 42,800 kJ/kg; thus, solving for the fuel mass flow rate yields

$$\begin{aligned} \dot{m}_f &= 66.67 \frac{\text{kg}}{\text{s}} \times 1.004 \frac{\text{kJ}}{\text{kg-K}} \times \frac{(1456 - 658.1)\text{K}}{42,800 \frac{\text{kJ}}{\text{kg}}} \\ &= 1.248 \text{ kg/s} (2.752 \text{ lbm/s}). \end{aligned}$$

Note that $\dot{m}_f/\dot{m} = 0.01938$, which is again small.

EXHAUST

The gas velocity at the exhaust exit is small, and thus the static and total pressures are equal ($p_{t8} = p_8$). Furthermore, since the velocity is small (subsonic), the exit and ambient pressures are the same ($p_8 = p_a$). Thus, $p_{t8} = p_a = 101.3 \text{ kPa}$.

Therefore, ideally (isentropic), the inlet total pressure to the exhaust is

$$p_{t5} = p_{t8} = 101.3 \text{ kPa} (14.69 \text{ psia}).$$

TURBINE

Because the inlet total pressure to the exhaust is the same as the exit total pressure for the turbine, the turbine total pressure ratio is

$$\pi_t = p_{t5}/p_{t4} = 101.3 \text{ kPa}/1823 \text{ kPa} = 0.05556.$$

Ideally, the total temperature ratio is $\tau_t = [\pi_t]^{\frac{\gamma-1}{\gamma}} = [0.05556]^{\frac{1.4-1}{1.4}}$,

and thus $\tau_t = 0.4379$ for $\gamma = 1.40$.

The turbine exit total temperature is therefore

$$T_{t5} = \tau_t T_{t4} = 0.4379 \times 1456 \text{ K} = 637.3 \text{ K} (1147 \text{ }^\circ\text{R}).$$

NET POWER AND THERMAL EFFICIENCY

The power balance on the shaft is

$$\begin{aligned} \mathcal{P}_{\text{net}} &= \dot{m} c_p (T_{t4} - T_{t5}) - \dot{m} c_p (T_{t3} - T_{t2}) \\ \mathcal{P}_{\text{net}} &= \left[66.67 \frac{\text{kg}}{\text{s}} \times 1.004 \frac{\text{kJ}}{\text{kg-K}} \times (1456 - 637.3) \text{K} \right. \\ &\quad \left. - 66.67 \frac{\text{kg}}{\text{s}} \times 1.004 \frac{\text{kJ}}{\text{kg-K}} \times (658.1 - 288.2) \text{K} \right] \times \frac{\text{kW}}{\text{kJ/s}}, \end{aligned}$$

or the net power from the gas turbine, which can be used for electric generation or other applications, is

$$\mathcal{P}_{\text{net}} = 30,030 \text{ kW} = 30.03 \text{ MW} (40,270 \text{ hp}).$$

The overall thermal efficiency is $\eta_{\text{th}} = \frac{\mathcal{P}_{\text{net}}}{Q_{\text{in}}}$, where the heat in is

$$\begin{aligned} Q_{\text{in}} &= \dot{m}_f \Delta H = 1.248 \frac{\text{kg}}{\text{s}} \times 42,800 \frac{\text{kJ}}{\text{kg}} \times \frac{\text{kW}}{\text{kJ/s}} \\ &= 53,410 \text{ kW} = 53.41 \text{ MW} (71,620 \text{ hp}) \end{aligned}$$

or $\eta_{\text{th}} = 30,030 \text{ kW} / 53,410 \text{ kW} = 0.562$ or 56.2 percent.

The heat rate is defined as $HR = \frac{\dot{m}_f \Delta H}{P_{\text{net}}}$; thus,

$$HR = \frac{1.248 \frac{\text{kg}}{\text{s}} \times 42,800 \frac{\text{kJ}}{\text{kg}} \times 3600 \frac{\text{s}}{\text{h}}}{30,030 \text{ kW}} = 6403 \frac{\text{kJ}}{\text{kW-h}} \left(4527 \frac{\text{Btu}}{\text{hp-h}} \right)$$

and finally the specific fuel consumption is defined as $SFC = \frac{\dot{m}_f}{\mathcal{P}_{\text{net}}}$; thus,

$$SFC = \frac{1.248 \frac{\text{kg}}{\text{s}}}{30,030 \text{ kW}} \times 3600 \frac{\text{s}}{\text{h}} = 0.1496 \frac{\text{kg}}{\text{kW-h}} \left(0.2460 \frac{\text{lbm}}{\text{hp-h}} \right)$$

As a final exercise, one can find the optimum operating total temperature ratio for the compressor from $\tau_{\text{c,opt}} = \sqrt{\frac{T_{t4}}{T_3}}$, which yields $\tau_{\text{c,opt}} = 2.248$, which is very close to the actual ratio of 2.284. This yields an optimum compressor total pressure ratio of 17.02, which is also very close to the actual value. On the basis of these characteristics, this is a well-designed power unit.

2.4. Summary

In this chapter the ideal gas turbine cycle analyses were presented to facilitate calculation of the ideal overall engine performance. Components (inlet or diffuser, compressor, fan, propeller, combustor, turbine, bypass duct, bypass mixer, afterburner, nozzle, and power gas turbine exhaust) were first discussed, and the characteristics of the ideal components were defined. The thermodynamic concepts were reviewed in detail, and the enthalpy–entropy (h–s) and pressure–volume (p–v) diagrams and operating equations were presented for each of the components.

Next, ideal cycle analyses were performed by assembling the ideal components for different engine types: ramjet, turbojet, turbofan with exhausted fan, turbofan with mixed fan, turboprop, and power-generation gas turbine. A component station numbering identification scheme was also established that is used throughout the book. Component equations were used with equations from Chapter 1 to determine overall engine performance. Afterburners were included for the turbojet and turbofan. All of the components were assumed to operate without any losses, and the gas was assumed to behave ideally and with constant properties throughout the engine. Three performance parameters were demonstrated as being important comparative measures of a propulsive engine: thrust, nondimensional thrust, and *TSFC*. Similar quantities were found for power-generation gas turbines. Relatively short closed-form expressions were obtained for these parameters for the different engine types.

Assembling the component models to develop these equations served two purposes. First, the reader was able to see how the equations are assembled to model an entire engine without being encumbered by numerical details. Second, and most importantly, the reader was permitted to observe the dependence of the overall performance of an engine on detail parameters conveniently and directly without having to resort to numerical parametric studies. Third, for some cases the approach used allowed analytical optimization or further analysis of performance characteristics. Typical trend studies were also presented for different engine types. For example, some important trend studies showed that the thrust can be maximized for a turbojet or turbofan at fixed given conditions with a prudent choice of compressor pressure ratio, that decreasing the inlet temperature of the incoming air improves the *TSFC*, and that increasing the flight Mach number increases the *TSFC*. Although the analyses are now ideal, the trend studies also generally hold for nonideal cases. For a power-generation unit, the output power was maximized for a particular value of compressor pressure ratio, but it was found that the overall thermal efficiency monotonically increased with increasing compressor pressure ratio.

Along with the trend studies, different engine types were compared. For example, a ramjet was shown to operate with a lower *TSFC* than a turbojet or a turbofan at very high Mach numbers. Also, afterburning in an engine was shown to increase the thrust significantly; however, the *TSFC* was also significantly increased. Thus, afterburning is good for short-term, sudden thrust increases but degrades fuel economy. Turbofans were shown to operate with lower *TSFCs* than turbojets and better fuel economy; however, for the same thrust as a turbojet, the air mass flow rate is larger for a turbofan, thus increasing the required physical engine diameter or size (or weight). Also, as the bypass ratio of the turbofan was increased, the *TSFC* decreased but the engine size, including weight, increased for a given thrust level. For these reasons, military fighter craft are outfitted with low-bypass-ratio engines and commercial craft are designed with large-bypass-ratio engines. It was demonstrated ideally, that both types of turbofans (exhausted and mixed) operate identically at the optimum conditions. If an afterburner is used with a turbofan, a mixed turbofan is usually utilized so that more airflow is available for afterburning than for an exhausted turbofan, thus increasing the possible thrust boost. The *TSFC* of a turboprop for a relatively slow aircraft is lower than for any of the other engines.

Several quantitative examples were also presented. The objective of the examples was not simply to use the final equations but to step through each representative problem so that the individual steps could be understood and appreciated. This also gives the reader a “feel” for some of the different internal parameter values (pressures and temperatures) usually seen in engines.

In Chapter 3, nonideal components are used, and thus the ideal assumptions are relaxed. Losses and nonideal effects are identified and specified for these components. The added complexity does not allow for closed-form expressions for the engine parameters but does permit more realistic predictions of the overall engine performance. Sufficient details are included in Chapter 3 to allow the entire group of the previously discussed engine types to be analyzed with reduced efficiencies for each of the different components and to determine the reduced efficiency of the engine.

List of Symbols

A	Area
a	Speed of sound
c_p	Specific heat at constant pressure

c_v	Specific heat at constant volume
C	Coefficient (4 for propeller/turboprop)
F	Force or thrust
f	Fuel ratio
h	Specific enthalpy
ΔH	Heating value
HR	Heat rate
\dot{m}	Mass flow rate
M	Mach number
p	Pressure
\mathcal{P}	Power
\dot{Q}	Heat transfer rate
\mathcal{R}	Ideal gas constant
s	Entropy
SFC	Specific fuel consumption
T	Temperature
$TSFC$	Thrust-specific fuel consumption
u	Specific internal energy
v	Specific volume
α	Bypass ratio
ρ	Density
γ	Specific heat ratio
η	Efficiency
π	Total pressure ratio
τ	Total temperature ratio

Subscripts

a	Freestream
ab	Afterburner
b	Primary burner
c	Compressor
e	Exit
e	Engine
f	Fan
f	Fuel
in	Inlet
opt	Optimum
p	Propeller
p	Power
s	Secondary (bypassed)
st	Stoichiometric
t	Total (stagnation)
t	Total (summation)
t	Turbine
T	Thrust
th	Thermal
w	Work
1...9	Positions in engine

Problems

- 2.1 The Mach number of an ideal ramjet is 2.88, and the external temperature is 400°R . The flow rate of air through the engine is 85 lbm/s. Because of thermal limits of the materials, the burner exit total temperature is 3150°R . The heating value of the fuel is 17,900 Btu/lbm. What are the developed thrust, dimensionless thrust, fuel ratio, and *TSFC* for this engine?
- 2.2 An ideal ramjet engine is being designed for a Mach 3.2 aircraft at an altitude of 33,000 ft. The fuel has a heating value of 18,600 Btu/lbm, and the burner exit total temperature is 3400°R . A thrust of 9500 lbf is needed. What is the required airflow? What is the resulting nozzle exit diameter? What is the resulting *TSFC* and dimensionless thrust?
- 2.3 An ideal ramjet is to fly at 20,000 ft at a yet-to-be determined Mach number. The burner exit total temperature is to be 3200°R and the engine will use 145 lbm/s of air. The heating value of the fuel is 18,500 Btu/lbm. At what Mach number will the *TSFC* be optimized? What is the optimum *TSFC*? What is the thrust and dimensionless thrust at this condition?
- 2.4 An ideal ramjet is to fly stoichiometrically at 20,000 ft. The fuel ratio is 0.050 for the stoichiometric combustion of this fuel. The heating value is 18,500 Btu/lbm. At what Mach number will the *TSFC* be optimized? What is the optimum *TSFC*?
- 2.5 The airflow through an ideal ramjet is 156 lbm/s. The aircraft flies at a Mach number of 2.5 at an altitude of 35,000 ft. The heating value of the fuel is 17,900 Btu/lbm. Study how the thrust varies with the burner exit total temperature. That is, plot the thrust versus T_{t4} . Also, plot the fuel ratio and *TSFC* versus T_{t4} .
- 2.6 An ideal turbojet ingests 192 lbm/s of air at an altitude of 22,000 ft. It flies at a Mach number of 0.88, and the compressor pressure ratio is 17. The fuel has a heating value of 17,900 Btu/lbm, and the burner exit total temperature is 2350°R . Find the developed thrust, dimensionless thrust, and *TSFC*.
- 2.7 An ideal turbojet powers a Mach 0.92 aircraft that requires 15,500 lbf of thrust at sea level. The compressor ratio is 16.4, and the exit total temperature from the combustor is 2450°R . The heating value of the fuel is 18,100 Btu/lbm. Find the required airflow. How large will the nozzle exit diameter be? What is the resulting *TSFC* and dimensionless thrust?
- 2.8 The Mach number of an ideal turbojet that flies at 27,000 ft is 0.82. The airflow is 205 lbm/s, and the burner total temperature is 2550°R . The heating value of the fuel is 17,700 Btu/lbm. If the thrust is to be maximized, find the resulting compressor ratio and *TSFC*. How sensitive is the thrust to this pressure ratio that is, if the pressure ratio is increased by 4 percent, how much will the thrust drop? How much will the *TSFC* drop? Comment.
- 2.9 An ideal turbojet with an afterburner flies at 22,000 ft with a Mach number of 0.88. It ingests 192 lbm/s of air, and the compressor pressure ratio is 17. The fuel has a heating value of 17,900 Btu/lbm. The primary burner and afterburner exit total temperatures are 2350 and 2980°R , respectively. (a) Find the developed thrust, dimensionless thrust, and *TSFC*. (b) Compare these parameters with those of the nonafterburning case.

- 2.10** An ideal turbojet with an afterburner is being designed for an aircraft that flies at sea level at Mach 0.92. The compressor ratio is 16.4. With the afterburner unlit, 15,500 lbf of thrust are needed. The total temperature at the turbine inlet is 2450 °R. The heating value of the fuel is 18,100 Btu/lbm. With the afterburner lit, 21,000 lbf of thrust are needed. What is the required air mass flow? What is the required afterburner total exit temperature? What are the *TSFC* and dimensionless thrust for the engine with the afterburner on and off?
- 2.11** An ideal turbofan with the fan exhausted operates at 20,000 ft at Mach 0.82. The compressor pressure ratio is 16 and the fan pressure ratio is 2.2. The fuel has a heating value of 17,700 Btu/lbm, and the exit total temperature from the burner is 2450 °R. The core airflow is 144 lbm/s, and the bypass ratio is 1.4. Find the developed thrust, dimensionless thrust, and the *TSFC*.
- 2.12** An ideal turbofan with an exhausted fan is being designed to operate at 25,000 ft and at a Mach number of 0.78. It is to operate at maximum or optimum thrust. The compressor pressure ratio is to be 14.5. The developed thrust is to be 16,800 lbf, and the bypass ratio is to be 4.4. The fuel has a heating value of 18,100 Btu/lbm, and the exit total temperature from the combustor is to be 2600 °R. What is the fan pressure ratio? What is the core flow rate? What are the *TSFC* and dimensionless thrust?
- 2.13** An ideal turbofan with the fan exhausted operates at 15,000 ft at a Mach number of 0.93. The compressor and fan pressure ratios are 17 and 2.3, respectively. The core airflow rate is 143 lbm/s, and the bypass ratio is 1.1. The fuel has a heating value of 17,900 Btu/lbm, and the combustor exit total temperature is 2550 °R. An afterburner is on the core and when lit results in a total temperature of 3200 °R in the nozzle. Find the thrust, dimensionless thrust, and *TSFC* for both the nonafterburning and afterburning cases.
- 2.14** Two engine types are being considered for a commercial application. Both have core airflow rates of 133 lbm/s. Both use a fuel with a heating value of 17,800 Btu/lbm, and both have turbine inlet total temperatures of 2469 °R. Both have a compressor pressure ratio of 13. The altitude will be 27,000 ft, and the Mach number will be 0.77. Engine “A” is a turbojet. Engine “B” is a turbofan with the fan exhausted and has a fan pressure ratio of 2.2 and a bypass ratio of 3.2. The total thrust required for the aircraft is 30,000 lbf. How many of the two ideal engine types will be needed to power the aircraft? What will the *TSFC* and dimensionless thrust be of the two engine types?
- 2.15** An ideal turbofan with the fan mixed operates at 22,000 ft at Mach 0.89. The compressor pressure ratio is 13. The fuel has a heating value of 18,100 Btu/lbm, and the exit total temperature from the burner is 2475 °R. The core airflow is 124 lbm/s, and the bypass ratio is 1.15. Find the developed thrust, dimensionless thrust, and the *TSFC*. What is the fan pressure ratio?
- 2.16** An ideal turbofan with a mixed fan is being designed to operate at 31,000 ft and at a Mach number of 0.86. The compressor pressure ratio is to be 16.5. The developed thrust is to be 18,800 lbf, and the bypass ratio is to be 3.6. The fuel has a heating value of 18,300 Btu/lbm, and the exit total temperature from the combustor is to be 2650 °R. What is the fan pressure ratio? What is the core flow rate? What is the *TSFC*?

- 2.17 An ideal turbofan with the fan mixed operates at 27,500 ft at Mach 0.93. The compressor pressure ratio is 17. The fuel has a heating value of 18,100 Btu/lbm, and the exit total temperature from the burner is 2230 °R. The core airflow is 157 lbm/s, and the bypass ratio is 1.60. An afterburner is also used. When lit, the afterburner total exit temperature is 3300 °R. Find the developed thrust, dimensionless thrust, and the *TSFC* when the afterburner is on and when it is off. What is the fan pressure ratio?
- 2.18 An ideal turbofan (mixed) with an afterburner is being designed for an aircraft that flies at sea level at Mach 0.90. The compressor ratio is 14.6, and the bypass ratio is 1.35. Without the afterburner lit, 12,000 lbf of thrust is needed. The total temperature at the turbine inlet is 2340 °R. The heating value of the fuel is 18,200 Btu/lbm. With the afterburner lit, 27,000 lbf of thrust are needed. What is the required air mass flow? What is the resulting fan pressure ratio? What is the required afterburner total exit temperature? What are the *TSFC*, dimensionless thrust, and exit diameter for the afterburner on and off?
- 2.19 An ideal turboprop is used to propel an aircraft at 5000 ft. The craft flies with a Mach number of 0.4. The compressor pressure ratio is 4.8, and the airflow through the core is 24 lbm/s. The burner exit total temperature is 2200 °R, and the exit Mach number is 0.7. The heating value of the fuel is 17,800 Btu/lbm. Find the developed thrust, dimensionless thrust, and *TSFC*.
- 2.20 An ideal turboprop is used to propel an aircraft at 5000 ft. The craft flies with a Mach number of 0.4. The compressor pressure ratio is 4.8, and the airflow through the core is 24 lbm/s. The burner exit total temperature is 2200 °R, and the heating value of the fuel is 17,800 Btu/lbm. Find the optimum developed thrust, dimensionless thrust, *TSFC*, and exit Mach number.
- 2.21 An aircraft is to fly at 10,000 ft with a Mach number of 0.5. It is to be propelled with a turboprop and requires 7000 lbf of thrust per engine. The compressor pressure ratio is 7.5, and the exit total temperature from the burner is 2340 °R. The fuel has a heating value of 17,800 Btu/lbm. The engine is to operate optimally at the preceding conditions. How much airflow is required? What are the resulting horsepower of the engine, dimensionless thrust, and *TSFC*?
- 2.22 An ideal turboprop is used to power an aircraft at 7000 ft. It flies at a Mach number of 0.45, and the compressor pressure ratio is 5.4. The airflow rate is 19 lbm/s. The turbine inlet total temperature is 2278 °R, and the heating value of the fuel is 18,400 Btu/lbm. The work coefficient of the propeller is 0.85. Find the thrust, dimensionless thrust, horsepower, exit Mach number, and *TSFC*.
- 2.23 A transport craft with an ideal engine is to fly at a Mach number of 0.80 at sea level on a standard day. The burner exit total temperature is 2400 °R, and the core airflow rate is 180 lbm/s. The fuel has a heating value of 17,900 Btu/lbm.
- (a) Find the thrust, dimensionless thrust, and *TSFC* for the following engines:
- (1) Ramjet
 - (2) Turbojet $\pi_c = 13$

- (3) Turbojet with afterburner $\pi_c = 13$
Total A/B exit temperature is 3800 °R
- (4) Turbofan with mixed auxiliary air $\pi_c = 13$, $\alpha = 1.4$
What is π_f ?
- (5) Turbofan with the fan all exhausted $\pi_c = 13$, $\alpha = 1.4$
 π_f is the same as for the mixed case
- (6) Turbofan with an afterburner and mixed auxiliary air
 $\pi_c = 13$, $\alpha = 1.4$
Total A/B exit temperature is 3800 °R
- (b) Which engine would you pick and why?
- 2.24** An ideal turbojet flies at sea level on a standard day. The airflow rate is 180 lbm/s. The total pressure ratio for the compressor is 13, and the fuel has a heating value of 17,900 Btu/lbm.
- (a) Consider the following cases and find the thrust, dimensionless thrust, and *TSFC*:
- (1) Mach number is 0.80 and
burner exit total temperature is 2400 °R
 - (2) Mach number is 1.20 and
burner exit total temperature is 2400 °R
 - (3) Mach number is 0.80 and
burner exit total temperature is 3000 °R
- (b) Comment on the effect of M_a and burner exit total temperature on performance.
- 2.25** The Mach number of an ideal ramjet is 2.80 at an external pressure of 2.71 psia and a temperature of 376.1 °R. The flow rate of air through the engine is unknown. Owing to thermal limits of the materials, the burner exit total temperature is 3300 °R. The heating value of the fuel is 18,100 Btu/lbm. The developed thrust is 9127 lbf. What are the mass flow rate, fuel ratio, dimensionless thrust, and *TSFC* for this engine?
- 2.26** An ideal ramjet is to fly at an external pressure of 2.71 psia and a temperature of 376.1 °R at a yet-to-be-determined Mach number. The burner exit total temperature is to be 3300 °R, and the engine will use 130 lbm/s of air. The heating value of the fuel is 18,100 Btu/lbm. At what Mach number will the *TSFC* be optimized? What is the optimum *TSFC*? What are the fuel ratio, thrust, and dimensionless thrust at this condition?
- 2.27** An ideal turbojet with an afterburner is being designed for an aircraft that flies at 15,000 ft at Mach 0.87. The compressor ratio is 18.2. With the afterburner unlit, 10,860 lbf of thrust are needed. The total temperature at the turbine inlet is 2600 °R. The heating value of the fuel is 18,000 Btu/lbm. With the afterburner lit, 15,740 lbf of thrust are needed. What is the required air mass flow? What is the required afterburner total exit temperature? What are the *TSFC* and dimensionless thrust for the engine with the afterburner on and off?
- 2.28** An ideal turbofan with an exhausted fan is being designed to operate at 32,000 ft and at a Mach number of 0.80. It is to operate at maximum or optimum thrust. The compressor pressure ratio is to be 19.0. The developed thrust is to be 20,660 lbf, and the bypass ratio is to be 3.5. The fuel has a heating value of 17,850 Btu/lbm, and the exit total temperature from the combustor is to

- be 2520 °R. What is the fan pressure ratio? What is the core flow rate? What is the *TSFC*? What is the dimensionless thrust?
- 2.29** An ideal turbofan with the fan mixed operates at 29,200 ft at Mach 0.80. The compressor pressure ratio is 19.3. The fuel has a heating value of 17,750 Btu/lbm, and the exit total temperature from the burner is 2460 °R. The core airflow is 164 lbm/s, and the bypass ratio is 2.50. An afterburner is also used. When lit, the afterburner total exit temperature is 3350 °R and the aircraft travels at Mach 1.5. Find the developed thrust, dimensionless thrust, and *TSFC* for the engine with the afterburner on and off. What is the fan total pressure ratio?
- 2.30** An ideal turboprop is used to propel an aircraft at 3500 ft. The craft flies with a Mach number of 0.44. The compressor pressure ratio is 4.3, and the airflow through the core is 26 lbm/s. The burner exit total temperature is 2150 °R, and the propeller work coefficient is 0.97. The heating value of the fuel is 17,940 Btu/lbm. Find the developed thrust, dimensionless thrust, and *TSFC*.
- 2.31** An ideal turboprop is used to propel an aircraft at 3500 ft. The craft flies with a Mach number of 0.44. The compressor pressure ratio is 4.3, and the airflow through the core is 26 lbm/sec. The burner exit total temperature is 2150 °R. The heating value of the fuel is 17,940 Btu/lbm. Find the optimum developed thrust, dimensionless thrust, *TSFC*, and propeller work coefficient.
- 2.32** You are to pick an engine for a transport aircraft flying at $M_a = 0.8$ at sea level on a standard day. The exit burner total temperature is 3000 °R and $\Delta H = 18,000$ Btu/lbm. The air mass flow rate in the core is 180 lbm/s. Use an ideal cycle analysis.
- (a) Find the dimensionless quantity, $F/\dot{m}_a a_a$, and the dimensional quantities F and *TSFC* for the following engines:
- (1) Ramjet
 - (2) Turbojet $\pi_c = 16$
 - (3) Turbojet with afterburner $\pi_c = 16$;
total afterburner temperature is 4200 °R
 - (4) Turbofan with exhausted fan $\pi_c = 16$, $\pi_f = 4.0$, $\alpha = 1$
 - (5) Turbofan with mixed secondary flow and with afterburner
 $\pi_c = 16$, $\alpha = 1$; total afterburner temperature is 4200 °R. What is π_f ?
- (b) Which engine will you choose and why?
- 2.33** You are to pick an engine for takeoff from an aircraft carrier on a standard day. The exit burner total temperature is 2600 °R, and $\Delta H = 179,00$ Btu/lbm. The air mass flow rate in the core is 230 lbm/s. Use an ideal cycle analysis with $\gamma = 1.40$.
- (a) Find the dimensionless quantity $F/\dot{m}_a a_a$ and the dimensional quantities F and *TSFC*, for the following engines:
- (1) Ramjet
 - (2) Turbojet $\pi_c = 23.5$
 - (3) Turbojet with afterburner $\pi_c = 23.5$;
total afterburner temperature is 3900 °R
 - (4) Turbofan with exhausted fan $\pi_c = 23.5$, $\pi_f = 1.98$, $\alpha = 5.0$

- (5) Turbofan with mixed secondary flow and with afterburner
 $\pi_c = 23.5$, $\alpha = 0.7$ total afterburner temperature is 3900°R .
 What is π_f ?

(b) Which engine will you choose and why?

- 2.34 An ideal ramjet cruises at 251°R and 0.324 psia (local sound speed is 754 ft/s), and the Mach number is 4.0 . The flow rate of air through the engine is 190 lbm/s. The fuel ratio is 0.0457 and is used because of the thermal limits of the nozzle materials. The heating value of the fuel is $18,000$ Btu/lbm. The average specific heat ratio for the engine is 1.320 , and the average specific heat at constant pressure is 0.2828 Btu/lbm- $^\circ\text{R}$. Find the

- (a) Burner exit total temperature
 (b) Developed thrust
 (c) *TSFC*

For comparison, consider a nonideal ramjet having burner and fixed converging nozzle efficiencies of 91 and 95 percent, respectively, total pressure ratios for the diffuser and burner of 0.92 and 0.88 , respectively, and for a variable specific heat, a burner exit total temperature, thrust, and *TSFC* of 3500°R , 9950 lbf, and 3.15 lbm/h/lbf, respectively.

- 2.35 Draw a general h - s diagram for an ideal turbofan engine with a totally exhausted fan and which has an afterburner for the core flow (Fig. 2.46). Draw this to scales showing the correct relative magnitudes – that is, be careful to show reasonable relative pressures and enthalpies for the different components. Show all points (a, 1, 2, 3, 4, 5, 6, 7, 8, and 9) as well as the static and total pressures.
- 2.36 Draw a general h - s diagram for an ideal turbofan engine with a totally mixed fan and an afterburner (Fig. 2.57). Draw this to scales showing the correct relative magnitudes – that is, be careful to show reasonable relative pressures and enthalpies for the different components. Show all points (a, 1, 2, 3, 4, 5, 5.5, 6, 7, 7.5, and 8) and show only the total (stagnation) conditions.
- 2.37 A new commercial aircraft is to be designed to fly routinely at $36,000$ ft at an air speed of 826 ft/s. Owing to expected drag characteristics of the airframe, two engines are required, the required thrust is $42,500$ lbf per engine or more, and fuel economies dictate that the engines are to operate with *TSFC* values of 0.62 lbm/h-lbf or less. The limit on the exit temperature of the burner is 2950°R . Design an ideal engine for this application.
- 2.38 A new military fighter aircraft is to be designed to fly routinely at a variety of altitudes. One particular condition is at $20,000$ ft at an air speed of 935 ft/s. Owing to expected drag characteristics of the airframe, two engines are required, the required thrust is $16,500$ lbf per engine, and engine weight considerations dictate that the engines are to operate with nondimensional thrusts of about 1.90 and with *TSFC* values of 0.92 lbm/h-lbf or less. Furthermore, because the aircraft is a fighter craft, short increases in thrust for rapid acceleration to supersonic speeds are required to a total of $31,500$ lbf per engine. The limits on the exit temperatures of the primary burner and afterburner are 3000 and 3600°R , respectively. Design an ideal engine for this application and these conditions.
- 2.39 For an ideal turbojet (no losses, properties are constant throughout, and the fuel ratio is negligible), start with Eq. 1.4.14 and analytically show that the

maximum thrust is obtained when the exit pressure of the nozzle matches the ambient pressure. Consider the flight Mach number, altitude, core mass flow rate, compressor total pressure ratio, burner exit total temperature, and fuel properties to be known.

- 2.40** An ideal turbojet cruises at an altitude at which the conditions are 430°R and 5.45 psia (local sound speed is 994 ft/s) and the Mach number is 0.85 . The flow rate of air through the engine is 150 lbm/s . The compressor total pressure ratio is 18.0 . The fuel ratio is 0.0265 . The turbine exit total temperature is 2228°R . The heating value of the fuel is $17,800\text{ Btu/lbm}$. The average specific heat ratio for the engine is 1.340 , and the average specific heat at constant pressure is $0.270\text{ Btu/lbm}\cdot^\circ\text{R}$. Find the
- Burner exit total temperature
 - Nozzle exit velocity
- 2.41** An ideal turbojet ingests 200 lbm/s of air at SLTO (sea level takeoff). The compressor pressure ratio is 20 . The fuel has a heating value of $17,800\text{ Btu/lbm}$, and the burner exit total temperature is 2700°R . Find the developed thrust, dimensionless thrust, and *TSFC*.
- 2.42** An ideal air standard Brayton cycle (power generation) operates with a maximum temperature of 1500°C . The inlet air temperature and pressure to the compressor are 40°C and 120 kPa , respectively, and the compressor pressure ratio is 18 . Assume constant specific heats and $\gamma = 1.40$. The airflow rate is 20 kg/s . Find
- Net power output
 - System thermal efficiency

Nonideal Cycle Analysis

3.1. Introduction

Chapter 2 has included a review of the ideal thermodynamic processes of different components, ideal cycle analyses for various types of engines, and a discussion of performance trends. All of the components were assumed to operate without any losses, and the gas was assumed to be perfect and to have constant specific heats throughout the entire engine. The objectives of this chapter are to relax these assumptions, to explain the physical conditions that lead to losses, and to review the nonideal thermodynamic processes from, for example, Keenan (1970) or Wark and Richards (1999) and the gas dynamic processes from, for example, Anderson (1982), Zucrow and Hoffman (1976), or Shapiro (1953). Efficiency levels and losses are included for the different components so that more realistic predictions can be made for overall engine performance. Even though most components operate with individually with relatively high efficiencies (upwards from 90%), when all the components are coupled the overall engine performance can be reduced drastically. However, in general, the performance trends do not change. Also, note that simple single- or two-term expressions are used to model the losses in each component in this chapter for simplicity. Each component is covered separately and in detail. At this stage these loss terms are specified a priori even though, in a real engine, the different component losses are dependent on the engine operating point and are thus dependent on each other. This advanced topic is the subject of Chapter 11, which addresses component matching. More complex and refined analyses of the component losses are presented in each of the component chapters (Chapters 4 through 10).

3.1.1. Variable Specific Heats

The first assumption to be relaxed is the constant specific heat assumption. Specific heats are approximated in this chapter to be constant across each component; however, they are different for each component through the engine. The specific heats for a particular component are found based on the average temperature of that component. In Appendix H, tables and equations are presented that allow the specific heats to be evaluated at a given temperature and pressure. In applying the equations, the reader should evaluate the specific heats for each component independently.

An ideal gas approximation is still used in that $dh = c_p dT$. If the ideal gas assumption were to be eliminated, it would be necessary to use tabular data for the enthalpy as a function of both temperature and pressure as is done in the JANAF tables from, for example, Chase (1998) or Keenan, Chao, and Kaye (1983). Also, note that the gas is assumed to be pure air. With a combustor, this is obviously not the case. To perform a more accurate evaluation of the properties, one would need to find the enthalpy of the combustion products (which change as air goes through the engine) and then the mixed enthalpy of the air and other products. Once again, JANAF tables would be required for the combustion products. This is covered in detail in Chapter 9.

Thus, for the remainder of this chapter, c_p and γ will be assumed to be constant across each component and evaluated at the average temperature of the component; this yields the best approximation for evaluating the change in properties between the end states.

3.2. Component Losses

As stated in the previous section, simple one- and two-term parameters will be introduced for each of the engine components so that losses and nonideal effects can be included in the cycle analyses. Methods of determining these losses will not be covered; the losses and efficiencies are assumed to be known. The determination of these parameters is the partial focus of future chapters. Herein, each component will be modularly covered separately with the idea that a group of components will be assembled numerically to analyze a particular engine. The physical phenomena behind the losses are discussed and enthalpy–entropy diagrams (h – s) are presented to reinforce the thermodynamic fundamentals.

3.2.1. Diffuser

Previously, the diffuser or inlet was assumed to operate isentropically – both internally and externally. Unfortunately, this is not the case. Losses can occur both before the air reaches the diffuser and also once it enters the diffuser. The diffuser does essentially operate adiabatically; this assumption will not be relaxed. The losses inside and outside the diffuser are discussed separately.

The overall operation of the diffuser is best shown on an h – s diagram (Fig. 3.1) for two basic different operating conditions. For example in Figure 3.1 (a) the flow is shown to accelerate from a to 1. Both the ideal and nonideal processes are shown in this figure. The freestream air is at pressure p_a and can be decelerated isentropically to total enthalpy, h_{ta} and total pressure, p_{ta} . Ideally, this results in a total exit pressure $p'_{t2} = p_{ta}$. However, losses in the diffuser, the entropy increases from station a to station 2. Because the process is very nearly adiabatic, the total enthalpy (and total temperature) does not change from a to 2, thus, $h_{t2} = h_{ta}$ and $T_{t2} = T_{ta}$. As a result of losses, however, the total pressure at station 2 is p_{t2} , which is less than p'_{t2} , as shown in the figure. Similar conclusions are drawn when Figure 3.1(b) is considered for flow decelerating from a to 1.

The concept of total pressure recovery is introduced to quantify this loss. This is defined as

$$\pi_d = \frac{p_{t2}}{p_{ta}}. \quad 3.2.1$$

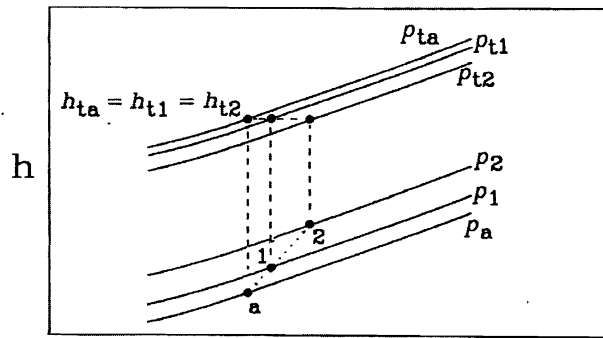
Note that this recovery factor represents the loss from the freestream to the diffuser exit and can be expanded to

$$\pi_d = \frac{p_{t2} p_{t1}}{p_{t1} p_{ta}}. \quad 3.2.2$$

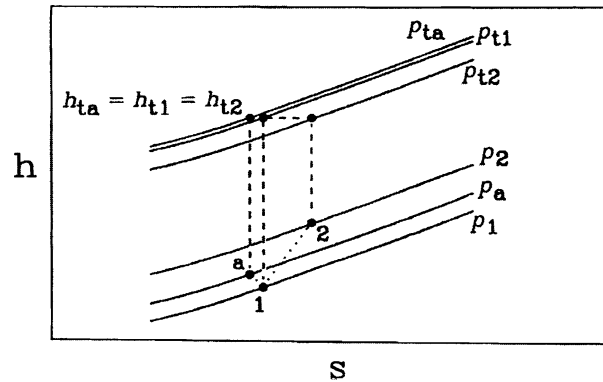
The first term, or loss, is often defined to identify internal diffuser losses. This is the diffuser pressure recovery factor and is defined as

$$\pi_r = \frac{p_{t2}}{p_{t1}}. \quad 3.2.3$$

This expression represents losses only within the diffuser. Ideally, the flow in the diffuser is uniform and the streamlines are smooth, as shown in Figure 2.4. However, given the unfavorable pressure gradient, the boundary layer on the walls tends to grow quickly and can separate (Fig. 3.2). This can have three effects. First, owing to the wall shear, boundary



(a) Subsonic operation at low air flow rate or high aircraft speed



(b) Subsonic operation at high air flow rate or low aircraft speed or supersonic operation

Figure 3.1 h - s diagram for a diffuser.

layer turbulence, and internal freestream turbulence, the flow is nonisentropic because of viscous effects; thus, the total pressure is reduced as indicated by π_r . Second, if the flow separates, the flow area is decreased. Thus, the mainstream flow velocity remains high, and the static pressure does not increase as much as in the ideal case. Third, as the result of any separation that occurs, the flow is highly nonuniform as it enters the compressor. As a result, compressor performance is compromised.

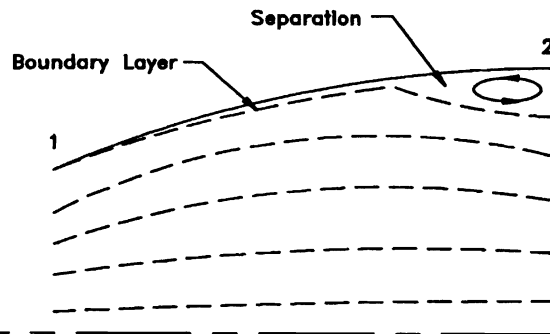


Figure 3.2 Streamlines for a nonideal diffuser.

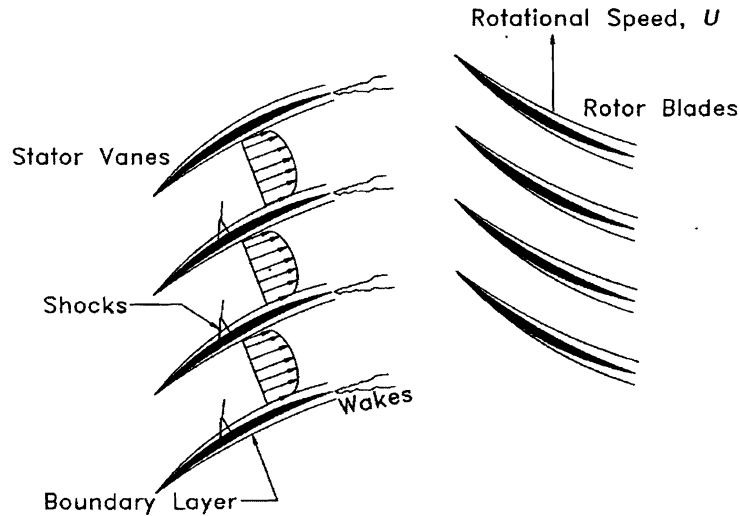


Figure 3.3 Top view of the rotor blades and stator vanes in a compressor stage.

Losses can also occur before the flow enters the diffuser. These are usually due to supersonic flow and ensuing shocks outside of, or in the plane of, the diffuser inlet. Determining these losses will be deferred until Chapter 4. However, this loss is the second term in Eq. 3.2.2 and is defined by

$$\pi_o = \frac{P_{t1}}{P_{ta}}, \quad 3.2.4$$

which represents the loss from the far freestream to the diffuser inlet. For subsonic flow this quantity is usually unity or very close to unity. However, as the freestream Mach number increases past unity, this loss can increase quickly if design precautions are not taken. Thus, from Eqs. 3.2.2, 3.2.3, and 3.2.4 one finds that

$$\pi_d = \pi_r \pi_o. \quad 3.2.5$$

Consequently by specifying either π_d or both π_o and π_r , the losses associated with the diffuser can be included in the analysis.

3.2.2. Compressor

The next component to be covered is the compressor. Once again, in the ideal case the flow was assumed to operate isentropically (see Figs. 2.6, 2.7, and 3.3). Isentropic flow does not occur in the compressor to boundary layers on the blades and case, turbulence, and other frictional losses. In fact, because the pressure increases as the air passes through the compressor, each row of blades acts like a diffuser (as will be discussed in Chapter 6). That is, an unfavorable pressure gradient is developed, which can lead to separation, viscous wakes, and reduced performance. Also, since the flow can be nonuniform both radially and circumferentially, it is not entirely incidence free to the leading edges of the rotor blades and stator vanes, which can also lead to separation on the blades, thus reducing compressor performance. Incidence increases, and so do the losses, if compressor operation deviates from the design point. The flow is also not steady within the compressor because of the wakes generated by every blade. For example, as a rotor blade passes behind every stator blade, the inlet velocity to the rotor blade fluctuates because of the wakes (called a jet-wake

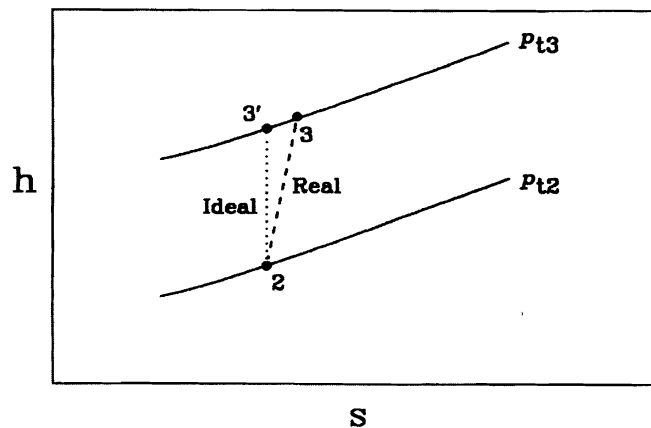


Figure 3.4 h-s diagram for a compressor.

effect), which again can lead to flow incidence. Next, because the flow velocities can be high, regions of transonic or supersonic flow can occur. These can lead to partial choking in some of the passages or shocks. Shocks are highly nonisentropic. Also, because the blades have finite lengths, tip flows (and vortices) are generated. These secondary flows once again result in increased friction, which dissipates the energy and thus reduces performance. Lastly, as noted, any nonuniformities from the inlet will reduce compressor performance because of flow incidence to the blades. The details of these losses will be covered in Chapter 6.

A single parameter is introduced for the entire compressor to characterize all of these losses. This is the efficiency (η_c) and is defined for the compressor as the ratio of the ideal power to actual power delivered to the fluid for a given total pressure rise. This is best illustrated by an h-s diagram (Figure 3.4). Shown on this diagram are the ideal and real processes. *Both processes are operating between the same total pressures (p_{t2} and p_{t3}), which is an important consideration. The ideal case operates between total enthalpies h_{t2} and h'_{t3} , whereas the real case operates between total enthalpies h_{t2} and h_{t3} . As one can see, as a result of the losses and increase in entropy, the increase in total enthalpy for the nonideal case is more than for the ideal case. That is, more power is required for the real case than for the ideal case. Thus, h'_{t3} is greater than h_{t3} . It is very important to note that the efficiency is defined as the ratio of ideal power to the actual power for the same increase in total pressure. Thus, the efficiency is*

$$\eta_c \equiv \frac{\text{ideal power}}{\text{actual power}} = \frac{h'_{t3} - h_{t2}}{h_{t3} - h_{t2}} \quad 3.2.6$$

If the specific heats are constant across the compressor, this reduces to

$$\eta_c = \frac{T'_{t3} - T_{t2}}{T_{t3} - T_{t2}} \quad 3.2.7$$

Typically, modern compressors operate at design with peak efficiencies of 85 to 93 percent, although the efficiency is a function of the pressure ratio and other parameters. A compressor with a design efficiency of 80 percent would be considered poor. After great strides in the 1950s and 1960s to improve the peak compressor efficiencies, this number has only gradually improved over the past 15 years. Also, one should realize that the efficiency is a strong function of the operating conditions. At low or high flow rates, or at high or low

rotational speeds, or both, the efficiency can be reduced significantly from the design value. This is discussed in detail in Chapter 6.

Combining Eqs. 3.2.7 and 2.2.13 yields

$$\pi_c \equiv \frac{p_{t3}}{p_{t2}} = \left\{ 1 + \eta_c \left[\frac{T_{t3}}{T_{t2}} - 1 \right] \right\}^{\frac{\gamma}{\gamma-1}} = \left\{ 1 + \eta_c [\tau_c - 1] \right\}^{\frac{\gamma}{\gamma-1}}. \quad 3.2.8$$

Equation 3.2.8 thus defines the total pressure ratio of the compressor in terms of the total temperature ratio (which is related to the input work) and the efficiency of the compressor. If the efficiency is specified, this equation will allow the analysis to proceed. Note that, as for all of the components, γ will be determined based on the average temperature in the particular component of interest – in this case the compressor. Thus, the value of γ for the compressor will in general be different than that for the diffuser or any other component.

a. Polytropic Efficiency

A second method for quantifying the performance of a compressor is sometimes used. This method will not be used for the analyses in this book. However, the reader should be aware of the method because several other texts and some manufacturers use it. This method, which determines what is described as the polytropic efficiency, basically entails separating the dependence of the efficiency from the pressure ratio so that different compressors can be better compared. The advantage of using this approach is that the polytropic efficiency is approximately the same for all modern engines at the design point and is determined by the design of the single stages; this measurement is thus independent of the number of stages. One can therefore directly compare the polytropic efficiencies for compressors of different sizes. The polytropic efficiency is often used in regulatory specifications. For example, the American Petroleum Institute (API) uses polytropic efficiency as the basis for a regulation to oversee the petroleum processing and other industries using compressor “trains” in the United States.

First, consider a single stage as shown in Figure 3.5. The inlet to the stage is station x and the exit is station y . For this single stage, the total pressure and total temperature ratios can be related by

$$\frac{p_{ty}}{p_{tx}} = \left\{ 1 + \eta_{ss} \left[\frac{T_{ty}}{T_{tx}} - 1 \right] \right\}^{\frac{\gamma}{\gamma-1}}, \quad 3.2.9$$

where η_{ss} is the efficiency for the single stage. If one assumes that the entire compressor is composed of n identical stages and that all stages have the same single-stage efficiency and total pressure ratios, the following equation results for the total pressure ratio of the entire compressor:

$$\frac{p_{t3}}{p_{t2}} = \left[\frac{p_{ty}}{p_{tx}} \right]^n. \quad 3.2.10$$

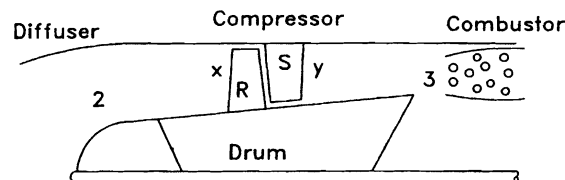


Figure 3.5 Single stage of a compressor.

Table 3.1. *Variation of single stage efficiency with number of stages for $\eta_c = 0.88$ and $\pi_c = 25$*

n	η_{ss}
1	0.880
2	0.902
4	0.912
6	0.915
10	0.917
20	0.919
100	0.921

The total temperature rise for the compressor is described similarly as follows:

$$\frac{T_{t3}}{T_{t2}} = \left[\frac{T_{ty}}{T_{tx}} \right]^n \quad 3.2.11$$

Thus, using Eqs. 3.2.9 through 3.2.11 and solving for η_{ss} , one obtains

$$\eta_{ss} = \frac{\left[\frac{p_{t3}}{p_{t2}} \right]^{\frac{\gamma-1}{\gamma}} - 1}{\left[\frac{T_{t3}}{T_{t2}} \right]^{\frac{1}{n}} - 1} \quad 3.2.12$$

For example, if a compressor has an overall efficiency of 0.88 and a total pressure ratio (p_{t3}/p_{t2}) of 25 – and thus a total temperature ratio of 2.7142 – it is possible to determine the effect of the number of stages from Table 3.1. As can be seen, the most pronounced changes occur for values of n between 1 and 10. Lastly, one can now hypothetically allow the number of stages to become infinite. This results in the definition of the so-called compressor polytropic or small-stage efficiency:

$$\eta_{pc} = \frac{\gamma - 1}{\gamma} \frac{\ln \left[\frac{p_{t3}}{p_{t2}} \right]}{\ln \left[\frac{T_{t3}}{T_{t2}} \right]} \quad 3.2.13$$

This equation can also be written as

$$\frac{p_{t3}}{p_{t2}} = \left[\frac{T_{t3}}{T_{t2}} \right]^{\eta_{pc} \frac{\gamma}{\gamma-1}} \quad 3.2.14$$

Using Eqs. 3.2.8 and 3.2.14, one can relate the overall efficiency and polytropic efficiency as follows:

$$\eta_c = \frac{[\pi_c]^{\frac{\gamma-1}{\gamma}} - 1}{[\pi_c]^{\gamma \eta_{pc}} - 1} \quad 3.2.15$$

As noted, polytropic efficiency is a second and equally valid method for including compressor losses. To include the losses for a compressor, one must either specify the compressor efficiency (η_c) or the small-stage compressor efficiency (η_{pc}). If η_c is known it is possible to find η_{pc} , and vice versa. The value of η_c is always less than that of η_{pc} . As stated earlier in this section, all modern engines demonstrate approximately the same η_{pc} at the peak design condition, and this is about 90 percent to 92 percent. The compressor efficiency is thus a function of the total pressure ratio of the compressor.

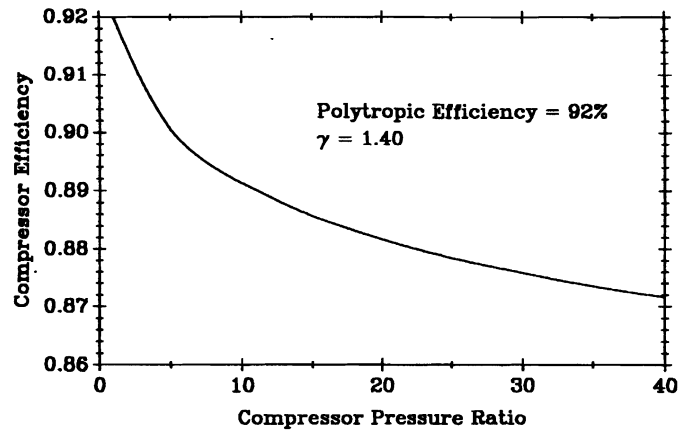


Figure 3.6 Compressor efficiency variation with pressure ratio.

For example, the compressor efficiency is presented in Figure 3.6 for the total pressure ratio range of 1 to 40 for a polytropic efficiency of 92 percent and $\gamma = 1.40$. As can be seen, the compressor efficiency decreases with increasing pressure ratio i.e., the number of stages increase. The polytropic efficiency is an alternative method and is confused with the first approach by some because of the definition and the ensuing derivation. If one remembers that η_c and η_{pc} are dependent and that only one of these parameters needs to be specified, however, the method is straightforward. For the remainder of this book, the first approach (η_c) will be used.

3.2.3. Fan

The physical losses and thermodynamic fundamentals of a fan are essentially those for a compressor with a low total pressure ratio and very long blade lengths. As a result, the methodology for incorporating the losses into the fan analysis is exactly the same as that for the compressor. The h - s diagram is very similar except for the station numbers. With reference to Figure 2.9, the stations before and after the fan are 2 and 7, respectively. Thus, one obtains

$$\frac{p_{t7}}{p_{t2}} = \left\{ 1 + \eta_f \left[\frac{T_{t7}}{T_{t2}} - 1 \right] \right\}^{\frac{\gamma}{\gamma-1}} \quad 3.2.16$$

This equation is used to characterize the fan, where η_f is the fan efficiency. The value of γ is determined by the average of the temperatures in the fan and will in general be different than the value for the compressor or any other component. As was true for the compressor, a polytropic efficiency for the fan can be defined. Although the fundamental thermodynamics for a fan are similar to those for a compressor owing to the large blade lengths of the fan, the blade design is considerably different, as is discussed in Chapter 6.

3.2.4. Turbine

Ideally, a turbine (Figs. 2.11 and 2.12) operates isentropically. As is true for a compressor, several losses contribute to the overall loss in a turbine. Among these losses are viscous effects due to the boundary layers on the vanes and blades, freestream turbulence, secondary flows, and incidence angles to the vanes and blades (because of inlet

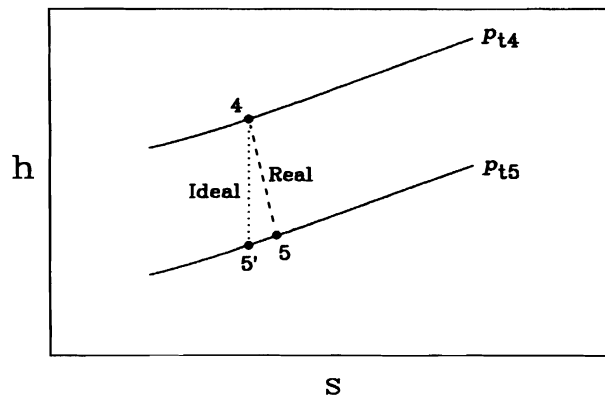


Figure 3.7 h-s diagram for a turbine.

conditions, jet-wakes, and three-dimensional flows). Because the pressure drops through a turbine, it is more prone to partial choking (and ensuing shocks) than a compressor. Furthermore, because a turbine is directly downstream of the very hot combustor, cool air is often bled through and around the vanes and blades to avoid failures (called blade cooling). This injected cool air lowers the enthalpy of the fluid. An h-s diagram is presented in Figure 3.7. Both the ideal and nonideal processes are shown. As is the case for the compressor, both processes are shown to operate between the same two total pressures. The ideal case operates between total enthalpies h_{t4} and h'_{t5} , whereas the nonideal case operates between h_{t4} and h_{t5} . Because of the losses and increase in entropy, *the drop in enthalpy for the nonideal case is less than for the ideal case*. That is, less power is derived from the fluid for the nonideal case as compared with the ideal case. For the turbine, the efficiency is defined as the ratio of actual power to ideal power *for the same total pressure ratio*. This results in

$$\eta_t = \frac{\text{actual power}}{\text{ideal power}} = \frac{h_{t4} - h_{t5}}{h_{t4} - h'_{t5}} \quad 3.2.17$$

If the specific heats are constant across the turbine, the equation reduces to

$$\eta_t = \frac{T_{t4} - T_{t5}}{T_{t4} - T'_{t5}} \quad 3.2.18$$

Typically, because the pressure decreases in turbines, they operate with slightly higher efficiencies than do compressors. Typical peak values for turbine efficiencies at the design condition are 85 percent to 95 percent, but these depend on the pressure ratio and operating conditions. Finally, from Eqs. 3.2.18 and 2.2.49, one finds

$$\pi_t \equiv \frac{p_{t5}}{p_{t4}} = \left\{ 1 - \frac{\left[1 - \frac{T_{t5}}{T_{t4}} \right]}{\eta_t} \right\}^{\frac{\gamma}{\gamma-1}} = \left\{ 1 - \frac{[1 - \tau_t]}{\eta_t} \right\}^{\frac{\gamma}{\gamma-1}} \quad 3.2.19$$

Equation 3.2.19 thus relates the total pressure and total temperature ratios for the nonideal case, which can be used for the total engine analysis with losses. Once again, the specific heat ratio is to be determined based on the average turbine temperature. The value of γ for the turbine is usually considerably lower than for a compressor owing to the higher operating temperature. A turbine polytropic efficiency, η_{pt} , can be defined for the turbine in the same

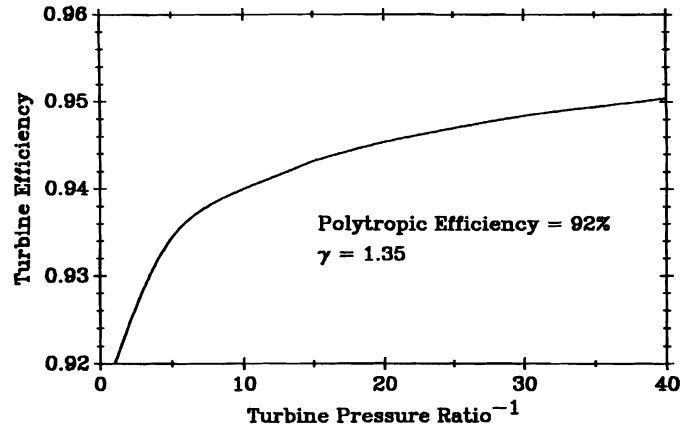


Figure 3.8 Turbine efficiency variation with pressure ratio.

way as for the compressor basically to separate the efficiency from its dependence on the pressure ratio. Thus, different turbines can effectively be compared. This definition yields

$$\eta_t = \frac{1 - [\pi_t]^{\eta_{pt} \frac{\gamma-1}{\gamma}}}{1 - [\pi_t]^{\frac{\gamma-1}{\gamma}}} \quad 3.2.20$$

Again, for a given total pressure ratio, if the polytropic efficiency is known, the overall efficiency can be found and vice versa. For this case, the polytropic efficiency is less than the overall turbine efficiency. As is the case for compressors, all modern engines demonstrate approximately the same η_{pt} at the design condition, and this is again about 90 percent. The turbine efficiency is thus a function of the total pressure ratio of the turbine. For example, the turbine efficiency is presented in Figure 3.8 for the pressure ratio range of 1 to 40⁻¹ for a polytropic efficiency of 92 percent and $\gamma = 1.35$. As can be seen, turbine efficiency increases with increasing pressure ratio, whereas the efficiency of a compressor decreases with increasing pressure ratio.

3.2.5. Propeller

In the ideal analysis, the assumption was made that all of the propeller power is used to generate thrust. In the real case, this is not true. For example, because of the unbounded nature of the propeller and long blade lengths some of the flow exits the propeller with a radial component of velocity, whereas most of the flow enters the propeller with no radial velocity. Thus, some power is used to accelerate the flow from the axial direction to the radial direction without deriving any axial thrust. Second, because a diffuser is not used to direct the flow axially into the propeller, wind fluctuations and crossflows will result in incidence angles to the propeller blades, causing local separation and thus detracting from the propeller performance. Third, also because of the unbounded nature of the flow, more mixing and turbulence are generated; again power is wasted. Fourth, some of the power is used to generate noise, although this is much smaller than the other losses.

Thus, one can define the propeller efficiency as

$$\eta_p = \frac{\mathcal{P}_p}{\mathcal{P}'_p}, \quad 3.2.21$$

where \mathcal{P}_p is the power used for thrust and \mathcal{P}_p' is the total power delivered to the propeller. Thus, the thrust from the propeller is given by

$$F_p = \eta_p C_{w_p} c_p T_a \dot{m} / u_a, \quad 3.2.22$$

where C_{w_p} is the propeller work coefficient as practically defined in Chapter 2. Other coefficients for the propeller are the thrust and power coefficients. Efficiencies vary widely owing to operating conditions, but maximum efficiencies are typically 70 to 90 percent. Propeller efficiencies are of course dependent on the particular designs and settings – especially the variable incidence. Efficiencies for propellers with fixed blades are compromised much faster when they are operated off of the design point (rotational speed, air speed, or both) than are propellers with variable blades as the result of increased leading edge incidence. More generally, propeller efficiencies are a function of (i) the propeller power coefficient, (ii) the “advance ratio” (freestream velocity to blade velocity) of the propeller at an operating speed, and (iii) the freestream Mach number. Some correlations are presented by Haines, MacDougall, and Monaghan (1946) and others. Such dependence is determined for particular designs and twist settings (or “schedules”) from wind tunnel tests. A simple and practical model for propeller efficiency is presented by Mattingly, Heiser, and Daley (1987), who in general show in practice that, for a variable pitch propeller, the efficiency is at a maximum over a range of Mach numbers but deteriorates quickly as the freestream velocity goes to zero and also as the freestream Mach number approaches unity. When a nonideal analysis for an engine with a propeller is conducted, Eq. 3.2.22 becomes the working equation.

3.2.6. Shaft

In all shaft engines, power is derived from a turbine and delivered to a compressive device. Previously, all of the derived power was assumed to be delivered to other components. A shaft (Figs. 2.16 and 2.17), however, does rotate – often at high rotational speeds. Shafts are mounted in bearings and often a damping device called a squeeze film damper to control shaft vibrations passively. Rolling element bearings are incorporated for aircraft applications, and hydrodynamic bearings are usually used in power gas turbines. Low-viscosity synthetic lubricants provide lubrication for the rolling element bearings, and mineral light turbine oils are used for the hydrodynamic bearings. As a result, these bearings and dampers parasitically dissipate some of the power due to viscous lubricant and surface friction. Also, in a turboprop engine, gears and associated bearings are usually used to reduce the speed of the propeller as discussed in Chapter 1. Gears also demonstrate parasitic losses because of surface friction. In summary, not all of the power derived from the turbine is delivered to the compressive devices.

These losses can be accommodated in the analysis through the following definition of mechanical efficiency:

$$\eta_m = \frac{\mathcal{P}_c}{\mathcal{P}_t}, \quad 3.2.23$$

where \mathcal{P}_t is the power derived from the turbine and \mathcal{P}_c is the total power delivered to all of the compressive devices (compressor, fan, propeller). The general power equation is thus

$$\underbrace{\dot{m} c_{p_c} (T_{13} - T_{12})}_{\text{compressor}} + \alpha \underbrace{\dot{m} c_{p_f} (T_{17} - T_{12})}_{\text{fan}} + \underbrace{C_{w_p} \dot{m} c_{p_a} T_a}_{\text{propeller}} = \eta_m \dot{m} (1 + f) \underbrace{c_{p_t} (T_{14} - T_{15})}_{\text{turbine}}. \quad 3.2.24$$

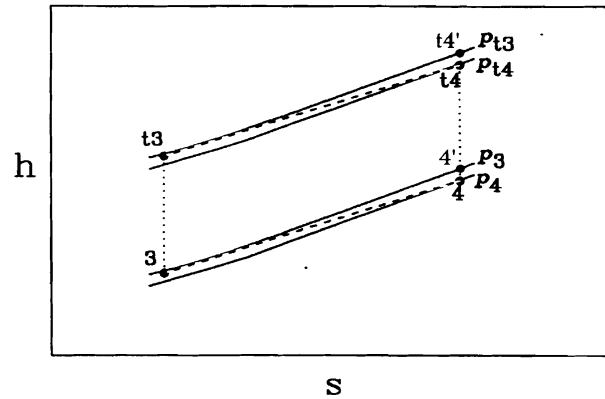


Figure 3.9 h - s diagram for a combustor.

This mechanical efficiency is usually high (between 98 and 100 percent). Thus, Eq. 3.2.24 can be used to include shaft losses in the nonideal analysis.

3.2.7. Combustor

Previously, all of the fuel was assumed to be burned and the total pressure was assumed to be constant across the primary burner. The combustors (Figs. 2.18 and 2.19) have two separate nonideal effects that must be included in the real analysis. Figure 3.9 presents the h - s diagram. First, the combustion is not perfect and not all of the fuel is burned. As a result, the combustor exit temperature will not be as high as in the ideal case and some of the fuel will be wasted. That is the total enthalpy h_{t4} , as shown in Figure 3.9, is less than the ideal value h'_{t4} , and the static enthalpy h_4 is less than the ideal value h'_4 . Second, because of the mixing and combustion processes in the combustor, which are both highly nonreversible and nonisentropic, the total pressure drops and the exit total pressure p_{t4} is less than the inlet value p_{t3} , as shown in Figure 3.9. The two effects are somewhat independent in that two terms must be used to identify the combustor losses. However, as is shown in Chapter 9, in reality the two effects are somewhat inversely dependent. That is, if one wants to decrease the amount of wasted fuel, more mixing is required, which further reduces the total pressure, and vice versa.

a. Imperfect Combustion

As indicated in the preceding paragraph, not all of the fuel is burned. Ideally, the gas goes to complete combustion. In actuality, however, four nonidealities cause losses in the total temperature. First, the combustion is not complete because of poor or ineffective mixing or the fact that the mean velocity in the primary combustor is too high and the mixture thus leaves the chamber before it has completely burned. Second, if cold fuel is injected that must therefore be warmed within the combustion chamber before burning, this again can result in fuel exiting the combustion region before it has burned. Third, because the temperatures are very high, some heat transfer can take place in the combustor and the total temperature can drop. Fourth, the fuel composition is not ideal. It is not strictly combustible because of additives and the presence of impurities. A simple, single parameter is introduced at this point to account for these four effects. This is called the primary burner

efficiency η_b and is defined by, and used with, the simple heating value analysis:

$$\eta_b \dot{m}_f \Delta H = \dot{m}(h_{t4} - h_{t3}) + \dot{m}_f(h_{t4} - h_{t4f}), \quad 3.2.25$$

where \dot{m}_f is the fuel flow rate. As is often the case, the heating value of the fuel is given for its inlet temperature. Thus, this equation reduces to

$$\eta_b \dot{m}_f \Delta H = \dot{m}(h_{t4} - h_{t3}) + \dot{m}_f h_{t4}. \quad 3.2.26$$

By assuming that the incoming and exiting gases are air, by using the value of c_p at the average temperature, and by assuming the value of c_p for the fuel is approximately that of air, one finds that

$$\eta_b \dot{m}_f \Delta H = \dot{m} c_p (T_{t4} - T_{t3}) + \dot{m}_f c_p T_{t4}. \quad 3.2.27$$

Typical values for the primary burner efficiency range from 90 to 95 percent. Note that the combustion analysis is greatly simplified at this point so that it can easily be incorporated into a cycle analysis. In Chapter 9, a more refined and much more accurate analysis referred to as the adiabatic flame temperature is covered. This method requires a chemical analysis (and tracking of all the reactants and products) as well as thermodynamics and will be covered in detail. For an initial engine cycle analysis, the heating value method is sufficient.

b. Pressure Losses

The second effect that must be considered is the loss in total pressure in the primary combustor. This occurs for four reasons. First, a combustion process is taking place, which is in itself a highly irreversible (and nonisentropic) process. This reduces the total pressure. Second, the primary combustor has swirlers, flame holders (obstructions), and turbulence generators to encourage mixing between the fuel and air and induce regions of low velocity. Thus, more losses occur owing to increases in viscous effects. Third, within the primary burner itself, small holes (orifices) are used to distribute the air evenly in the combustion zone. Because air is forced through these small orifices, total pressure is lost. Fourth, the combustion process, which, because of the rapid density decrease is in itself a turbulence generator, induces more losses. As a result of these four factors, p_{t4} is less than p_{t3} . This effect is taken into account by the primary burner pressure ratio. It is defined as

$$\pi_b = \frac{p_{t4}}{p_{t3}}. \quad 3.2.28$$

Typical values for this ratio are 0.92 to 0.98. As implied above, at the beginning of Section 3.2.7 as the mixing is increased, generally π_b decreases and η_b increases.

3.2.8. Afterburner

When an afterburner is present (Figs. 2.21 and 2.22), two additional losses must be included. An afterburner is essentially a simple burner without most of the complex hardware of a primary burner. Fuel is injected into the flow upstream of the nozzle – usually with a series of spokes and circumferential rings to generate immediate increased thrust. The same two types of losses for a burner are also present for an afterburner. The physical processes and fundamental thermodynamic behavior are the same, although the actual designs are much different. For example, the afterburner efficiency is defined by

$$\eta_a \dot{m}_{f,ab} \Delta H = \dot{m}_{5.5} c_p (T_{t6} - T_{t5.5}) + \dot{m}_{f,ab} c_p T_{t6}. \quad 3.2.29$$

where \dot{m}_{fab} is the afterburner fuel flow rate and $\dot{m}_{5.5}$ is the total mass flow rate into the afterburner. The total fuel flow rate for an engine can also be realized as the sum of the primary and afterburner fuel flow rates, $\dot{m}_f = \dot{m}_f + \dot{m}_{\text{fab}}$. Also, the afterburner total pressure ratio is

$$\pi_{\text{ab}} = \frac{p_{16}}{p_{15.5}}. \quad 3.2.30$$

However, for most of the engine operating time, an afterburner is not used. Thus, the added large pressure loss associated with a primary burner is not desired because this would also detract from the nominal operation of the engine. Thus, the design of an afterburner is simpler than that of a primary burner without most of the flow blockages used to induce good mixing. As a result, the efficiency is not as high as that of a primary burner. On the other hand, the pressure loss is not as large. Typical efficiencies are 80 to 90 percent, whereas typical total pressure ratios are 0.95 to 0.99 when the afterburner is ignited.

As noted earlier, afterburners are present on almost all military fighter craft but receive limited use. For normal engine operation (no afterburner fuel flow or combustion), a total pressure loss (Eq. 3.2.30 but not Eq. 3.2.29) must still be included because the additional length of the engine and the presence of the fuel nozzles and struts in the flow path generate more viscous losses. However, when afterburner combustion is not occurring, this pressure ratio is usually higher than stated in the previous paragraph and is typically 0.98 to 1.00.

3.2.9. Primary Nozzle

For the ideal analysis, two assumptions were made for the nozzle flow. First, the flow was assumed to be frictionless and adiabatic. Second, the exit pressure was assumed to match the ambient pressure. For the nonideal analysis, these two assumptions will be relaxed (Fig. 3.10).

a. Exit Pressure

During actual operation, the exit pressure may not match the ambient pressure. The nozzle areas may not be in the correct proportion, and thus the resulting exit and ambient pressures will be unequal. As is demonstrated in Chapter 5, for an efficient nozzle the maximum thrust is derived when these two pressures are the same.

If the exit pressure is greater than the ambient pressure, the flow is considered to be underexpanded. A positive thrust is thus derived from the pressure terms in the thrust equation. However, the exit velocity will not be as high as it would be the properly expanded case, and thus the momentum component of thrust will be lower than ideal. As a result, the two effects complement each other, but total thrust will be lower than ideal. On the other

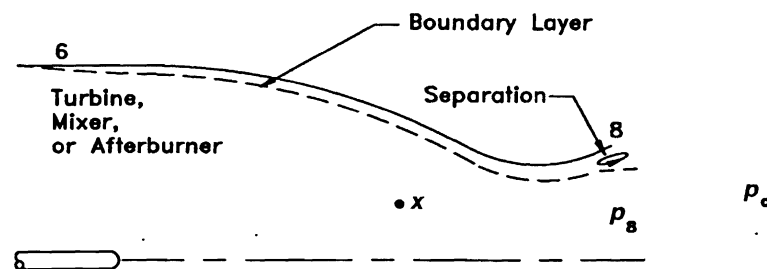


Figure 3.10 Schematic of a primary nozzle section.

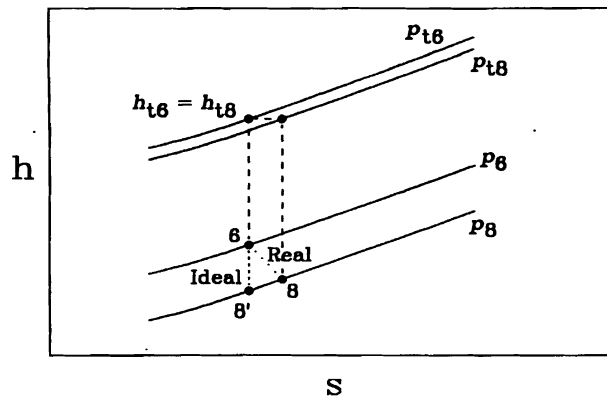


Figure 3.11 h - s diagram for a nozzle.

hand, if the exit pressure is lower than the ambient pressure, the flow is considered to be overexpanded, and negative thrust is derived from the pressure terms in the thrust equation. Now, the exit velocity will be higher than it would be in the properly expanded case, and thus the momentum component of thrust will be higher than ideal. Again, the two effects complement each other, but total thrust will again be lower than ideal. For the nonideal analysis, all three cases will be considered.

b. Losses

For the ideal case the flow was assumed to be isentropic. For the nonideal case, frictional losses will be included, although the flow is still considered to be adiabatic. An h - s diagram is shown in Figure 3.11. The ideal case operates between end states 6 and 8', whereas the nonideal case operates between states 6 and 8. For the definition of nozzle efficiency presented in this section, both cases operate between the inlet total pressure p_{t6} and the exit static pressure p_8 . For the ideal case, the entropy remains constant for the nozzle process. However, for the nonideal case the entropy increases owing to friction in the boundary layer, freestream turbulence, secondary flows, shocks in the nozzle, and possible flow separation. Because the flow is adiabatic, the total enthalpy remains constant in the nozzle; that is, h_{t6} is equal to h_{t8} . However, the entropy increase in the nozzle results in a drop in total pressure from inlet to exit (p_{t6} to p_{t8}), as shown in Figure 3.11. As a result, the nonideal static exit enthalpy, h_8 , is greater than the ideal enthalpy h'_8 , which leads to a reduced exit velocity and in turn to a reduced thrust.

A nozzle efficiency is introduced to include these losses and is defined (only for adiabatic flow) by

$$\eta_n = \frac{h_{t6} - h_8}{h_{t6} - h'_8}, \quad 3.2.31$$

which for the constant specific heat case results in

$$\eta_n = \frac{T_{t6} - T_8}{T_{t6} - T'_8}. \quad 3.2.32$$

Now, by applying the energy equation between states $t6$ and 8, one finds

$$u_8 = \sqrt{2(h_{t6} - h_8)}, \quad 3.2.33$$

or, for the constant specific heat case

$$u_8 = \sqrt{2c_p(T_{t6} - T_8)}, \quad 3.2.34$$

which is also

$$u_8 = \sqrt{2 c_p \eta_n (T_{t6} - T'_8)}. \quad 3.2.35$$

This is obviously less than the ideal value and leads to reduced thrust. Since the flow is still considered to be adiabatic,

$$\frac{T_8}{T_{t6}} = \frac{1}{1 + \frac{\gamma-1}{2} M_8^2}, \quad 3.2.36$$

and for the ideal case

$$\frac{p_8}{p_{t6}} = \left[\frac{T'_8}{T_{t6}} \right]^{\frac{\gamma}{\gamma-1}}. \quad 3.2.37$$

Thus, Eqs. 3.2.32, 3.2.36, and 3.2.37 yield

$$\frac{p_8}{p_{t6}} = \left[\frac{\frac{1}{1 + \frac{\gamma-1}{2} M_8^2} - 1 + \eta_n}{\eta_n} \right]^{\frac{\gamma}{\gamma-1}}. \quad 3.2.38$$

Thus, if the exit pressure is known, the exit Mach number can be found (on the assumption that the nozzle efficiency and upstream total pressure are known).

Another effect that should be considered is nozzle choking. Before proceeding, one should realize that all of the preceding equations can be applied to an arbitrary location in the nozzle such as axial position x in Figure 3.10. Or, now Eq. 3.2.38 can be used when p_8 is replaced with p_x and M_8 is replaced with M_x . Therefore, Eq. 3.2.38 can be applied at the condition where the Mach number is unity. One should also realize that this sonic condition may or may not exist in a nozzle. For example, an unchoked converging nozzle will not have a sonic condition. Yet, one can still apply Eq. 3.2.38 with a Mach number of unity to determine what the conditions would be if the nozzle were choked and use this as a reference condition. Thus, by letting $M_x = 1.00$, one obtains

$$\frac{p^*}{p_{t6}} = \left[1 + \frac{1 - \gamma}{\eta_n (1 + \gamma)} \right]^{\frac{\gamma}{\gamma-1}}, \quad 3.2.39$$

where the superscript * indicates the sonic condition. This equation can thus be used to check a converging nozzle for choking. For example, if p_a is less than p^* , the nozzle is choked, $p_8 = p^*$, and $M_8 = 1$. In actuality for a choked converging nozzle with an efficiency less than unity, the nozzle exit Mach number is slightly less than one. However, to simplify the analyses in this book, the sonic condition will be used for the choked case because the difference has minimal effect on the engine thrust and *TSFC* (typically less than 0.1 percent and conservative). However, if p_a is greater than p^* , the nozzle is not choked, M_8 is less than unity, and $p_8 = p_a$. Furthermore, when considering the temperature at the exit of a choked nozzle, from Eq. 3.2.36 one finds the following for a Mach number of unity:

$$\frac{T^*}{T_{t6}} = \frac{2}{1 + \gamma}. \quad 3.2.40$$

A relationship may also be desired between the area and the Mach number. Because mass flow is conserved between the sonic condition (if it exists in reality or not) and the exit condition,

$$\dot{m}_8 = \dot{m}^*. \quad 3.2.41$$

Thus,

$$\rho^* u^* A^* = \rho_8 u_8 A_8, \quad 3.2.42$$

or solving for A_8/A^* and using the ideal gas equation (Eq. H.2.1). Yield

$$\frac{A_8}{A^*} = \frac{T_8 p^* u^*}{T^* p_8 u_8}. \quad 3.2.43$$

By realizing that $u^* = a^*$ and that $u_8 = M_8 a_8$, one obtains

$$\frac{A_8}{A^*} = \frac{T_8 p^* a^*}{T^* p_8 M_8 a_8}. \quad 3.2.44$$

Using Eq. H.2.8 results in

$$\frac{A_8}{A^*} = \frac{T_8 p^* \sqrt{T^*}}{T^* p_8 M_8 \sqrt{T_8}}. \quad 3.2.45$$

Combining terms and multiplying and dividing by similar terms yield

$$\frac{A_8}{A^*} = \sqrt{\frac{T_8}{T_{16}} \left[\frac{p^*}{p_{16}} \right]} \frac{1}{M_8}. \quad 3.2.46$$

Finally, one can apply Eqs. 3.2.46 with 3.2.38, 3.2.39, 3.2.36, and 3.2.40 to yield

$$\frac{A_8}{A^*} = \frac{1}{M_8} \sqrt{\frac{\gamma + 1}{2 + (\gamma - 1) M_8^2}} \left[\eta_n \frac{1 + \frac{1-\gamma}{\eta_n(1+\gamma)}}{1 + \frac{\gamma-1}{2} M_8^2} - 1 + \eta_n \right]^{\frac{\gamma}{\gamma-1}}. \quad 3.2.47$$

This section has presented the equations that will both include losses and allow the nozzle to operate at off-design conditions. Typical nozzle efficiencies are 90 to 97 percent. The application of these equations requires careful thought on the part of the reader. One single, final equation cannot be derived because the operating conditions govern the form of the equations. For example, the application of the equations will be different for a choked converging nozzle than for an unchoked converging nozzle. For another example, the application of the equations will be different for a choked converging nozzle than for a supersonic converging-diverging nozzle. Some of the differences will be discussed in Example 3.1.

3.2.10. Fan Nozzle

In the case of an exhausted fan, a second nozzle must be analyzed. The fluid mechanics of this secondary nozzle, including physical losses, thermodynamics, and definitions, are fundamentally the same as for the primary nozzle. Thus, only the important equations will be listed below for the fan nozzle. The fan nozzle operates between stations 7 and 9 (Fig. 3.12) with an efficiency of η_{fn} .

$$\eta_{fn} = \frac{h_{17} - h_9}{h_{17} - h'_9} \quad 3.2.48$$

$$u_9 = \sqrt{2c_p(T_{17} - T_9)} \quad 3.2.49$$

$$u_9 = \sqrt{2c_p\eta_{fn}(T_{17} - T'_9)} \quad 3.2.50$$

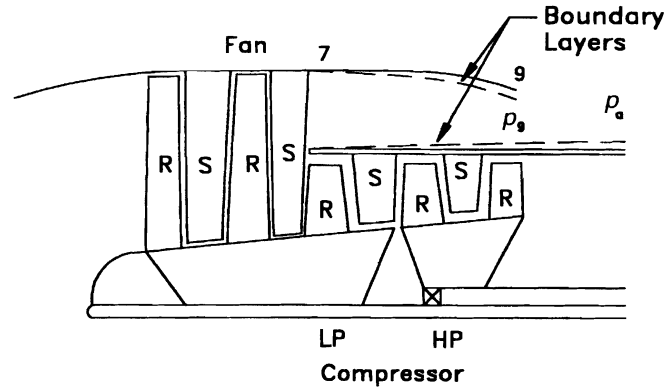


Figure 3.12 Schematic of a fan nozzle section.

$$\frac{T_9}{T_{t7}} = \frac{1}{1 + \frac{\gamma-1}{2} M_9^2} \quad 3.2.51$$

$$\frac{p_9}{p_{t7}} = \left[\frac{T_9'}{T_{t7}} \right]^{\frac{\gamma}{\gamma-1}} \quad 3.2.52$$

$$\frac{p_9}{p_{t7}} = \left[\frac{\frac{1}{1 + \frac{\gamma-1}{2} M_9^2} - 1 + \eta_{fn}}{\eta_{fn}} \right]^{\frac{\gamma}{\gamma-1}} \quad 3.2.53$$

$$\frac{p^*}{p_{t7}} = \left[1 + \frac{1-\gamma}{\eta_{fn}(1+\gamma)} \right]^{\frac{\gamma}{\gamma-1}} \quad 3.2.54$$

$$\frac{A_9}{A^*} = \frac{1}{M_9} \sqrt{\frac{\gamma+1}{2 + (\gamma-1)M_9^2}} \left[\eta_{fn} \frac{1 + \frac{1-\gamma}{\eta_{fn}(1+\gamma)}}{\frac{1}{1 + \frac{\gamma-1}{2} M_9^2} - 1 + \eta_{fn}} \right]^{\frac{\gamma}{\gamma-1}} \quad 3.2.55$$

3.2.11. Bypass Duct

When a fan is present, and when at least a part of the flow is mixed into the turbine exit flow, a bypass duct (Fig. 3.13) is used to direct the bypassed air. For the ideal cases, all of the bypassed air was assumed to be either all exhausted or all mixed back into the primary flow. In practice, a portion of the air is sometimes bled and mixed. A new parameter, termed the duct split ratio, is defined as the ratio of secondary air that is mixed to the total secondary air. This is given by

$$\sigma = \frac{\dot{m}_{7.5}}{\dot{m}_{7.5} + \dot{m}_9}. \quad 3.2.56$$

The quantities $\dot{m}_{7.5}$ and \dot{m}_9 are the mass fluxes at stations 7.5 and 9, respectively, as shown in Figure 3.13. The ratio σ is to unity for the fully mixed case and to zero for the totally exhausted case.

Also ideally, the exit conditions of the duct were assumed to be identical to the inlet conditions. In actuality, however, this flow has frictional losses, as in any duct or pipe, including wall shear and freestream shear and turbulence. The flow is thus nonisentropic

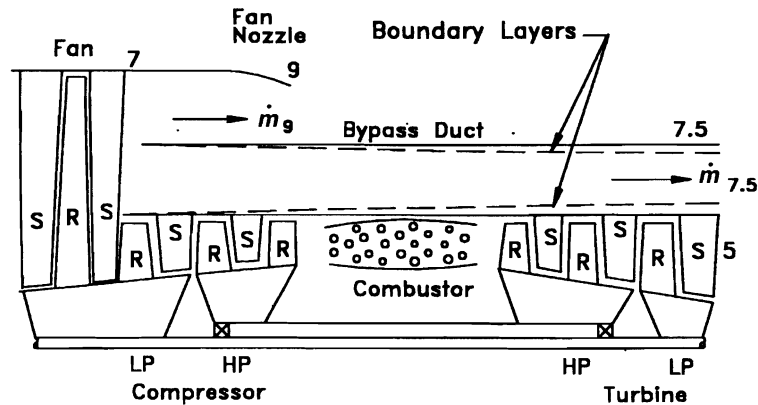


Figure 3.13 Schematic of a fan bypass duct.

and has a drop in total pressure but is still considered to be adiabatic; thus, $h_{t7} = h_{t7.5}$. The loss is simply included in the cycle analysis as the ratio of the total pressures as follows:

$$\pi_u = \frac{p_{t7.5}}{p_{t7}} \quad 3.2.57$$

This ratio is typically high and near unity because bypass ducts are relatively smooth and short. Nonetheless, it should be included for completeness.

As in the ideal case, a boundary condition is needed to match the bypassed air when it is mixed back into the primary flow. Once again, for flow stability, the physical process will naturally match the static pressures; that is,

$$p_{7.5} = p_5 \quad 3.2.58$$

Applying this condition for the analysis at the mixer would require knowledge of the flow velocities or cross-sectional areas because the analyses of all of the other components use total pressures. However, if the Mach numbers are approximately the same for the two streams ($M_5 \cong M_{7.5}$), or if both Mach numbers are well below about 0.3, where compressibility effects can be ignored, an alternative condition can be used as follows:

$$p_{t7.5} \cong p_{t5} \quad 3.2.59$$

This is a simpler condition and will be used herein because it facilitates the cycle analysis.

3.2.12. Bypass Mixer

As discussed in Chapters 1 and 2, for the turbofan, the mixer (Fig. 3.14) mixes the ducted and bypassed air (stream 7.5) into the turbine exit air (stream 5). The average properties before the mixer are labeled as 5.2 and those after the mixer are stream 5.5. This mixing process of the two streams is irreversible and nonisentropic. Furthermore, mix enhancers are often used to further improve the mixing efficiency. The introduction of such enhancers increases viscous losses due to increased surface areas, blockage, and increasing turbulence and thus increases the nonisentropic behavior of the process. Good mixing is desired to ensure uniform properties. However, with improved mixing and resulting high turbulence levels, the entropy increases and the total pressure drops. Once again, a total

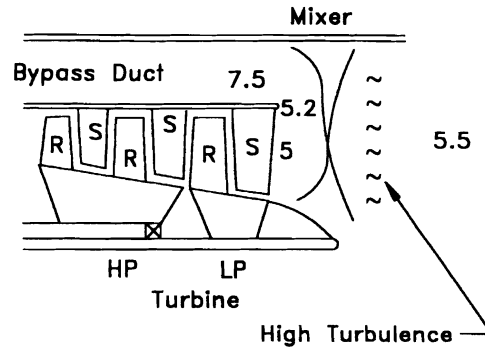


Figure 3.14 Schematic of a fan flow–primary flow mixer.

pressure ratio is included to account for the frictional and mixing losses:

$$\pi_m = \frac{p_{t5.5}}{p_{t5.2}} \quad 3.2.60$$

Typically, this ratio is between 0.97 to 0.99.

Also, one needs to find the total temperature of the exiting stream of gas from the mixer (into the afterburner or nozzle) because the two incoming streams are at different total temperatures. The energy equation is first applied to find

$$\dot{m}_5 h_{t5} + \dot{m}_{7.5} h_{t7.5} = \dot{m}_{5.5} h_{t5.5}, \quad 3.2.61$$

or using Eqs. H.3.8, 2.2.14, 2.2.29, and 3.2.56 results in

$$\dot{m}(1+f)c_{p_{mc}}T_{t5} + \dot{m}\sigma\alpha c_{p_{mu}}T_{t7.5} = \dot{m}((1+f)c_{p_{mc}} + \sigma\alpha c_{p_{mu}})T_{t5.5} \quad 3.2.62$$

or, finally,

$$T_{t5.5} = \frac{(1+f)c_{p_{mc}}T_{t5} + \sigma\alpha c_{p_{mu}}T_{t7.5}}{(1+f)c_{p_{mc}} + \sigma\alpha c_{p_{mu}}}, \quad 3.2.63$$

where $c_{p_{mu}}$ is evaluated at the average temperature from stations 7.5 to 5.5 and $c_{p_{mc}}$ is evaluated at the average temperature from stations 5 to 5.5.

3.2.13. Power Turbine Exhaust

Although the primary focus of this book is jet propulsion, power gas turbines are closely related. A power gas turbine has an exhaust with very low velocity compared with a nozzle. A nozzle and exhaust operate with different functions and losses are treated differently. A simple schematic of an exhaust is shown in Figure 3.15. In Figure 2.32, the exhaust of the Coberra 6000 gas turbine is shown. Because of low velocities at the exit of the exhaust, the static and total pressures are nearly identical at the exit. Total pressure is lost between the turbine and exit because of friction and internal dissipation in the fluid caused by turbulence and separation regions. As a result of this pressure drop, a turbine is not able to expand down to atmospheric pressure and thus is not able to derive as much power from the fluid as for the ideal case. The design of an exhaust should include smooth walls and gentle curves to reduce such losses. An h - s diagram for an exhaust is shown in Figure 3.16. An exhaust is assumed to be adiabatic and, as can be seen, a total pressure loss between station 5 and 8 is realized owing to the entropy increase. Because the velocity is

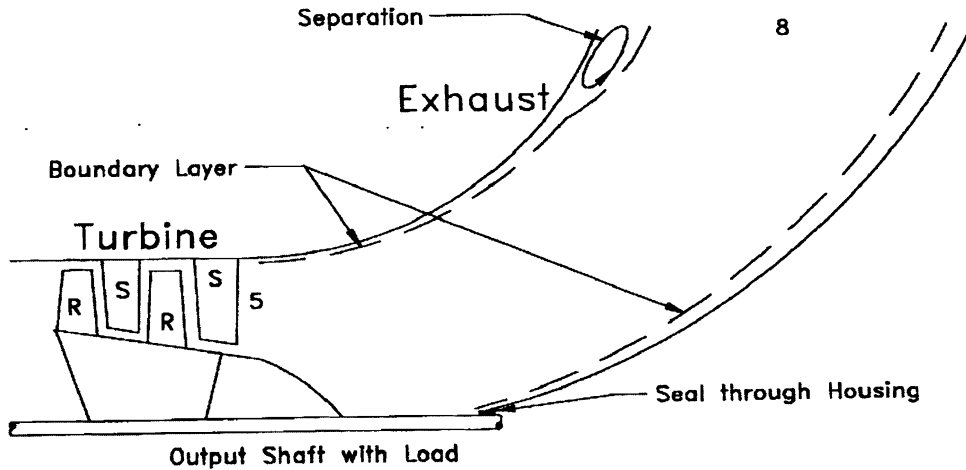


Figure 3.15 Schematic of a power gas turbine exhaust geometry.

low at the exit, the exit pressure matches atmospheric pressure. Thus, one can define an exhaust pressure ratio and write a working equation as follows:

$$\pi_e = \frac{p_{t8}}{p_{t5}} = \frac{p_8}{p_{t5}} = \frac{p_a}{p_{t5}} \quad 3.2.64$$

This pressure ratio is usually high – on the order of 0.98 to 0.99.

3.2.14. Summary of Nonideal Effects and Simple Parameter Models in Components

In the previous 13 sections, 13 components were covered and nonideal effects were discussed for each. For each component one- or two-term parameters were introduced to incorporate the different types of losses. Other parameters were introduced to include operating characteristics. To conclude this section, these parameters are summarized in Table 3.2.

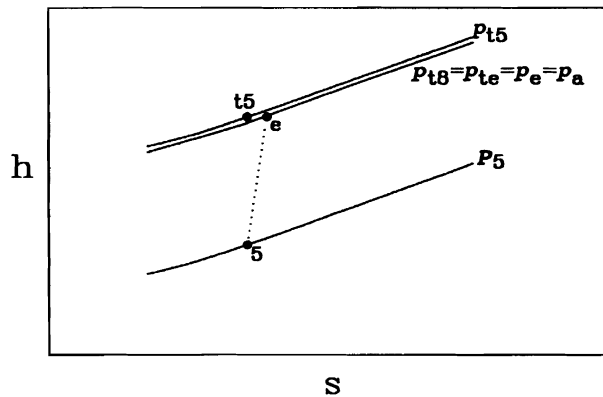


Figure 3.16 h-s diagram for power turbine exhaust.

Table 3.2. Component Parameters

Component	Effect	Symbol
Diffuser	Total pressure recovery	π_d
Compressor	Efficiency	η_c
Fan	Efficiency	η_f
	Bypass ratio	α
Turbine	Efficiency	η_t
Propeller	Efficiency	η_p
Shaft	Efficiency	η_m
Combustor	Efficiency	η_b
	Total pressure ratio	π_b
Afterburner	Efficiency	η_{ab}
	Total pressure ratio	π_{ab}
Primary nozzle	Efficiency	η_n
Fan nozzle	Efficiency	η_{fn}
Bypass duct	Total pressure ratio	π_u
	Split ratio	σ
Bypass mixer	Total pressure ratio	π_m
Exhaust	Pressure ratio	π_e

3.3. Cycle Analysis

3.3.1. General Approach

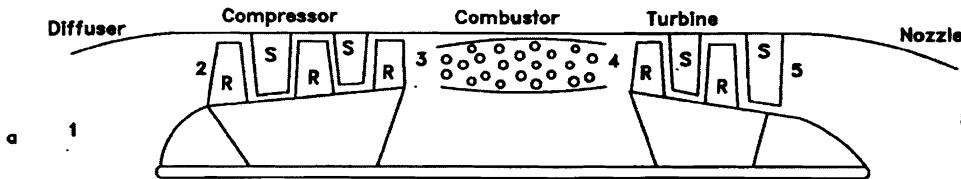
In Section 3.2 all of the different component losses were covered. For some components, single-term expressions were introduced that allowed nonideal effects to be included. For a few of the components, two-term expressions were required. For the ideal analyses, all of the component equations could be combined to yield single equations for both the thrust and *TSFC* for different engine types. However, because of the nonideal effects, combining equations would be a cumbersome, and in most cases impossible, task. Thus, each engine type must be considered separately to solve nonideal problems. To determine the thrust and *TSFC*, one must step through the engine component-by-component until all of the different parameters are determined. In some cases, iterative solutions are required in the step-by-step procedure because the nonideal effects do not allow the parameters to be directly determined. Solutions for different gas turbine types and conditions can also be obtained using the software, “JETENGINECYCLE” and “POWERGTCYCLE”

As was noted in section 3.2, the specific heat values for a given component should be evaluated at the average temperature of that component. This means that both the inlet and exit temperatures must be known. However, in practice this is not the case. Usually only one temperature is known when the component is analyzed. Only after the analysis is done is the average temperature known. Thus, iterations are required for nearly all components and the use of a computer becomes almost imperative. That is, a value of c_p is first guessed for a given component, and the analysis is completed for the component. Next, the average temperature is found, which is used to find c_p from a table or from Eq. H.3.1. The process is repeated until the assumed and calculated values of c_p agree within a small tolerance. As one would expect, such iterations require the aid of a personal computer for all of the examples herein, although the particular steps are not shown. Two general approaches to iterative solutions are presented in Appendix G. Also, in Appendix G, some examples of iterative solutions are presented that correspond to some of the following engine examples.

3.3.2. Examples

In this section, five examples are presented. They do not cover the entire range of possible combinations of the different components. These examples do, however, cover all of the important component concepts that may be encountered in real analyses. All of the examples will be compared with ideal analyses for the same engines. Some trend studies are presented to indicate that the basic trends shown for ideal components also apply for nonideal components. Also, complementary examples will be used for some examples to emphasize certain effects. The examples presented are an integral portion of the chapter and should not be treated as supplementary or complementary material.

Example 3.1: A turbojet flies at sea level at a Mach number of 0.75. It ingests 165 lbm/s (74.83 kg/s) of air. The compressor operates with a pressure ratio of 15 and an efficiency of 88 percent. The fuel has a heating value of 17,800 Btu/lbm (41,400 kJ/kg), and the burner total temperature is 2500°R (1389 K). The burner has an efficiency of 91 percent and a total pressure ratio of 0.95, whereas the turbine has an efficiency of 85 percent. A converging nozzle is used, and the nozzle efficiency is 96 percent. The total pressure recovery for the diffuser is 0.92, and the shaft efficiency is 99.5 percent. Find the developed thrust and $TSPC$. Note that this is the same engine as in Example 2.2 with the exception of the nonideal effects.



SOLUTION:

DIFFUSER

First, the standard conditions at sea level are $T_a = 518.7^\circ\text{R}$ and $p_a = 14.69$ psia (from Appendix A). The speed of sound is

$$\begin{aligned} a_a &= \sqrt{\gamma_a \mathcal{R} T_a} \\ &= \sqrt{1.4029 \times 53.35 \frac{\text{ft}\cdot\text{lbf}}{\text{lbm}\cdot^\circ\text{R}} \times 32.17 \frac{\text{lbm}}{\text{slug}} \times 518.7^\circ\text{R} \times \frac{\text{slug}\cdot\text{ft}}{\text{lbf}\cdot\text{s}^2}} \\ &= 1118 \text{ ft/s} (340.6 \text{ m/s}). \end{aligned}$$

Thus, the jet velocity is $u_a = M_a a_a = 0.75 \times 1118 \text{ ft/s} = 838.2 \text{ ft/s} (255.5 \text{ m/s})$.

Next,

$$\begin{aligned} \frac{T_{1a}}{T_a} &= 1 + \frac{\gamma_d - 1}{2} M_a^2 = 1 + \frac{1.3997 - 1}{2} \times 0.75^2 \\ &= 1.1124 \text{ for } \gamma_d = 1.3997 \text{ and } M_a = 0.75. \end{aligned}$$

Thus, since the diffuser is adiabatic, the total temperature at the diffuser exit is

$$T_{12} = T_{1a} = 1.1124 \times 518.7^\circ\text{R} = 577.0^\circ\text{R} (320.6 \text{ K}).$$

Also,

$$\frac{p_{ta}}{p_a} = \left[\frac{T_{ta}}{T_a} \right]^{\frac{\gamma_d}{\gamma_d - 1}} = [1.1124]^{\frac{1.3997}{1.3997 - 1}} = 1.4522.$$

The pressure recovery factor for the diffuser is 0.92;

hence,

$$\frac{p_{t2}}{p_a} = \frac{p_{t2}}{p_{ta}} \frac{p_{ta}}{p_a} = \pi_d \frac{p_{ta}}{p_a} = 0.92 \times 1.4522 = 1.3360.$$

Therefore, the diffuser exit total pressure is

$$p_{t2} = 1.3360 \times 14.69 \text{ psia} = 19.63 \text{ psia} (135.3 \text{ kPa}).$$

COMPRESSOR

The total pressure ratio of the compressor is given as $\pi_c = 15$, and thus the total pressure exiting the compressor is

$$p_{t3} = \pi_c p_{t2} = 15 \times 19.63 \text{ psia} = 294.4 \text{ psia} (2030 \text{ kPa}).$$

Ideally,

$$\tau'_c = [\pi_c]^{\frac{\gamma_c - 1}{\gamma_c}} = [15]^{\frac{1.3805 - 1}{1.3805}} = 2.1095 \quad \text{for } \gamma_c = 1.3805;$$

therefore, ideally,

$$T'_{t3} = \tau'_c T_{t2} = 2.1095 \times 577.0^\circ\text{R} = 1217^\circ\text{R} (676.2 \text{ K}),$$

but the compressor efficiency is given and

$$\eta_c = 0.88 = \frac{T'_{t3} - T_{t2}}{T_{t3} - T_{t2}} = \frac{1217^\circ\text{R} - 577.0^\circ\text{R}}{T_{t3} - 577.0^\circ\text{R}};$$

thus, solving for T_{t3} , one finds the compressor total exit temperature is

$$T_{t3} = 1305^\circ\text{R} (724.7 \text{ K}).$$

Note: This specific heat ratio for the compressor was evaluated at 941°R or 523 K , which is the resulting *average* total temperature of the compressor. As for all components, the average total temperature was not known a priori but was found by iteration. That is, the compressor exit temperature depends on the specific heat ratio, but this ratio depends on the exit temperature. Thus, one can find both values by a progressive iteration. Details of the "successive substitution" iteration are presented in Appendix G, Example G.3. Fortunately, the iteration process converges quickly (four iterations for this case) and is easily programmed. In actuality, two or three iterations could have been used with minimal effects on the net results. Also, note that, although precise values of the specific heat ratio are desired, it should not become the dominant feature of examples or chapter problems.

Note also that the static temperature would have best been used to evaluate the average temperature and resulting specific heat. However, because of the lack of information about the static temperatures, Mach numbers, velocities, or areas at the different sections that would have allowed a calculation of static values, the total temperatures were used.

PRIMARY COMBUSTOR

The total pressure ratio of the burner is given as 0.95.

The burner exit total pressure therefore is

$$p_{t4} = \pi_b p_{t3} = 0.95 \times 294.4 \text{ psia} = 279.7 \text{ psia} (1928 \text{ kPa}),$$

and the energy analysis is

$$\Delta H \eta_b \dot{m}_f = \dot{m} c_{pb} (T_{t4} - T_{t3}) + \dot{m}_f c_{pb} T_{t4};$$

however, the combustion efficiency is 91 percent and ΔH is 17,800 Btu/lbm.

Thus, solving for the fuel mass flow rate yields

$$\begin{aligned}\dot{m}_f &= 165 \frac{\text{lbm}}{\text{s}} \times 0.2731 \frac{\text{Btu}}{\text{lbm} \cdot ^\circ\text{R}} \frac{2500^\circ\text{R} - 1305^\circ\text{R}}{0.91 \times 17,800 \frac{\text{Btu}}{\text{lbm}} - 0.2731 \frac{\text{Btu}}{\text{lbm} \cdot ^\circ\text{R}} \times 2500^\circ\text{R}} \\ &= 3.472 \text{ lbm/s} (1.575 \text{ kg/s}),\end{aligned}$$

where the burner specific heat is evaluated at the average burner temperature, which for this case is not an iteration (T_{t3} and T_{t4} are known). Because no afterburner is present, this is also the total fuel flow rate (\dot{m}_f). Note also that $\dot{m}_f/\dot{m} = 0.02104$, which is small. The fuel flow rate can also be compared with that from the ideal case (2.778 lbm/s [1.260 kg/s]), which is 25 percent higher owing to combustor and compressor inefficiencies.

TURBINE

The mechanical efficiency is given as 0.995, and therefore the shaft power balance

$$\dot{m} c_{pc}(T_{t3} - T_{t2}) = \eta_m \dot{m}_t c_{pt}(T_{t4} - T_{t5})$$

becomes

$$\begin{aligned}165 \frac{\text{lbm}}{\text{s}} \times 0.2487 \frac{\text{Btu}}{\text{lbm} \cdot ^\circ\text{R}} (1305^\circ\text{R} - 577.0^\circ\text{R}) \\ = 0.995 \times \left(165 \frac{\text{lbm}}{\text{s}} + 3.472 \frac{\text{lbm}}{\text{s}} \right) \times 0.2807 \frac{\text{Btu}}{\text{lbm} \cdot ^\circ\text{R}} (2500^\circ\text{R} - T_{t5});\end{aligned}$$

thus, the turbine exit total temperature $T_{t5} = 1865^\circ\text{R}$ (1036 K).

Again, the specific heat of the turbine is iteratively found for the average turbine temperature.

However, the turbine efficiency is defined as $\eta_t = \frac{T_{t4} - T_{t5}}{T_{t4} - T'_{t5}}$ and given as 85 percent; therefore,

$$0.85 = \frac{2500^\circ\text{R} - 1865^\circ\text{R}}{2500^\circ\text{R} - T'_{t5}};$$

thus, if one solves for the ideal exit total temperature, $T'_{t5} = 1753^\circ\text{R}$ (974.1 K), and ideally

$$\tau'_t = \frac{T'_{t5}}{T_{t4}} = \frac{1753}{2500} = 0.7014.$$

From the definition of turbine efficiency and the total pressure ratio, $\tau'_t = [\pi_t]^{n-1}$.

The turbine total pressure ratio is thus

$$\pi_t = [\tau'_t]^{\frac{n}{n-1}} = (0.7014)^{\frac{1.3233}{1.3233-1}}$$

with $\pi_t = 0.2341$ for $\gamma_t = 1.3233$ (evaluated at average turbine temperature).

Finally, the turbine exit total pressure is

$$p_{t5} = \pi_t p_{t4} = 0.2341 \times 279.7 \text{ psia} = 65.46 \text{ psia} (451.4 \text{ kPa}).$$

Since no mixer is present, $T_{t5.5} = T_{t5} = 1865^\circ\text{R}$ (1036 K)

and $p_{t5.5} = p_{t5} = 65.46 \text{ psia} (451.4 \text{ kPa})$.

PRIMARY NOZZLE

Because no afterburner is present, the inlet total temperature for the nozzle is

$$T_{t6} = T_{t5.5} = 1865^\circ\text{R} (1036 \text{ K}),$$

and the inlet total pressure is $p_{t6} = p_{t5.5} = 65.46 \text{ psia} (451.4 \text{ kPa})$.

Since the engine has a fixed converging nozzle, one must first check to see if the nozzle is choked.

In the case of a choked nozzle, the nozzle exit pressure is

$$p_8^* = p_{t6} \left[1 + \frac{1 - \gamma_n}{\eta_n(1 + \gamma_n)} \right]^{\frac{\gamma_n}{\gamma_n - 1}};$$

thus, for $p_{t6} = 65.46$ psia, which represents a nozzle efficiency of 96 percent, and $\gamma_n = 1.3368$ (iteratively found for the average nozzle temperature),

$$\begin{aligned} p_8^* &= 65.46 \text{ psia} \times \left[1 + \frac{1 - 1.3368}{0.96 \times (1 + 1.3368)} \right]^{\frac{1.3368}{1.3368 - 1}} \\ &= 34.32 \text{ psia (236.6 kPa)}. \end{aligned}$$

However, since $p_a = 14.69$ psia (101.3 kPa), which is well below the choking condition p_8^* , the nozzle is choked and the exit Mach number is identically unity; therefore, the exit pressure is $p_8 = p_8^* = 34.32$ psia (236.6 kPa),

and $T_8 = \frac{2T_{t6}}{1 + \gamma_n}$ for $M_8 = 1$.

Thus, for $T_{t6} = 1865$ °R (1036 K), $T_8 = \frac{2 \times 1865 \text{ °R}}{1 + 1.3368} = 1597$ °R (887.0 K)

The nozzle exit velocity is given by $u_8 = \sqrt{2 c_{pn} (T_{t6} - T_8)}$.

The exit velocity is therefore

$$\begin{aligned} u_8 &= \sqrt{2 \times 0.2721 \frac{\text{Btu}}{\text{lbm} \cdot \text{°R}} \times (1865 \text{ °R} - 1597 \text{ °R}) \times 32.17 \frac{\text{lbm}}{\text{slug}} \times 778.16 \frac{\text{ft} \cdot \text{lb}}{\text{Btu}} \times \frac{\text{slug} \cdot \text{ft}}{\text{lb} \cdot \text{s}^2}} \\ &= 1914 \text{ ft/s (583.3 m/s)}. \end{aligned}$$

The speed of sound at the exit is $a_8 = \sqrt{\gamma_8 \mathcal{R} T_8}$;

thus,

$$\begin{aligned} a_8 &= \sqrt{1.3368 \times 53.35 \frac{\text{ft} \cdot \text{lb}}{\text{lbm} \cdot \text{°R}} \times 32.17 \frac{\text{lbm}}{\text{slug}} \times 1597 \text{ °R} \times \frac{\text{slug} \cdot \text{ft}}{\text{lb} \cdot \text{s}^2}} \\ &= 1914 \text{ ft/s (583.3 m/s)} \end{aligned}$$

As a check on the calculations, $M_8 = u_8/a_8 = 1$, as it should.

From the continuity equation, the exit area is given by $A_8 = \frac{\dot{m}_8}{\rho_8 u_8}$, where \dot{m}_8 is the total mass flow rate at 8 and is given by $\dot{m}_8 = \dot{m}_{a8} + \dot{m}_f$ and \dot{m}_{a8} is the air mass flow rate at 8 and is equal to \dot{m} , the ingested flow.

Thus, $\dot{m}_{a8} = 165$ lbm/s (74.83 kg/s),

and the total mass flow rate at the exit is therefore

$$\dot{m}_8 = 165 + 3.472 = 168.5 \text{ lbm/s (76.40 kg/s)}.$$

Since both T_8 and p_8 are known, ρ_8 is found from the ideal gas equation

$$\rho_8 = \frac{p_8}{\mathcal{R} T_8} = \frac{34.32 \frac{\text{lb}}{\text{in}^2} \times 144 \frac{\text{in}^2}{\text{ft}^2}}{53.35 \frac{\text{ft} \cdot \text{lb}}{\text{lbm} \cdot \text{°R}} \times 1597 \text{ °R} \times 32.17 \frac{\text{lbm}}{\text{slug}}}$$

which yields $\rho_8 = 0.001804$ slug/ft³ (0.9297 kg/m³);

thus, the nozzle exit area is

$$A_8 = \frac{168.5 \frac{\text{lbm}}{\text{s}} \times 144 \frac{\text{in}^2}{\text{ft}^2}}{0.001804 \frac{\text{slug}}{\text{ft}^3} \times 1914 \frac{\text{ft}}{\text{s}} \times 32.17 \frac{\text{lbm}}{\text{slug}}} = 218.5 \text{ in}^2 (0.1409 \text{ m}^2).$$

TOTAL THRUST AND TSFC

The thrust is given by

$$F = \dot{m}_8 u_8 - \dot{m}_{a8} u_a + A_8 (p_8 - p_a).$$

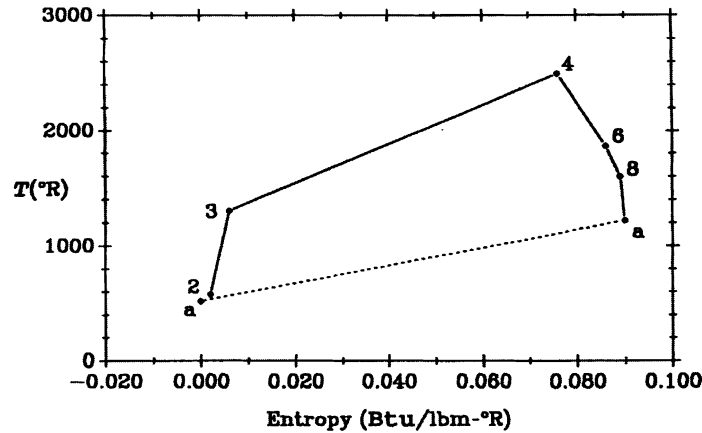


Figure 3.17 T - Δs diagram for the turbojet in Example 3.1.

Thus,

$$F = \frac{168.5 \frac{\text{lbm}}{\text{s}} \times 1914 \frac{\text{ft}}{\text{s}} \text{ lbf-s}^2}{32.17 \frac{\text{lbm}}{\text{slug}}} - \frac{165 \frac{\text{lbm}}{\text{s}} \times 838.2 \frac{\text{ft}}{\text{s}} \text{ lbf-s}^2}{32.17 \frac{\text{lbm}}{\text{slug}}} + 218.5 \text{ in.}^2 \times \left(34.32 \frac{\text{lbf}}{\text{in.}^2} - 14.69 \frac{\text{lbf}}{\text{in.}^2} \right);$$

therefore, $F = 5723 \text{ lbf (momentum)} + 4288 \text{ lbf (pressure)}$

or $F = 10,010 \text{ lbf (44,540 N)}$,

and 57 percent of the thrust is from momentum.

Finally, $TSFC = \dot{m}_R / F$,

and thus

$$\begin{aligned} TSFC &= \frac{3.472 \frac{\text{lbm}}{\text{s}}}{10,010 \text{ lbf}} \times 3600 \frac{\text{s}}{\text{h}} \\ &= 1.248 \frac{\text{lbm}}{\text{h-lbf}} \left(0.1273 \frac{\text{kg}}{\text{h-N}} \right) \end{aligned}$$

Comparing these results with those of the ideal case (Example 2.2) reveals that the thrust is 13 percent lower, but the $TSFC$ is 44 percent higher because of losses. In Figure 3.17, a scaled T - Δs diagram for this example is shown.

Complementary Example 3.1.a: As a complement to the preceding example, the parametric variation of the compressor pressure ratio was studied. Details of the calculations are exactly as in Example 3.1 except for the parameter values. Figure 3.18, in which the net thrust and $TSFC$ are plotted as functions of the compressor pressure ratio, presents the results of the study. As found for the ideal cases in Chapter 2, an optimum pressure ratio exists at which the thrust is maximized; for this case the optimum value of π_c is approximately 8.50 and the maximum thrust is 10,340 lbf. For a practical range of compressor pressure ratios (up to 40), the $TSFC$ always decreases with increasing pressure ratio. For large values of π_c , the $TSFC$ increases with increasing π_c . This trend was not seen for the ideal analysis and is due to the increasing importance of the losses in the compressor. Note also that for a compressor ratio of 20 the $TSFC$ is much lower than for the value of π_c that yielded the maximum thrust (1.192 versus 1.391 lbm/h-lbf). Thus, if this engine were in the design phase, the designer would need to balance the requirement for

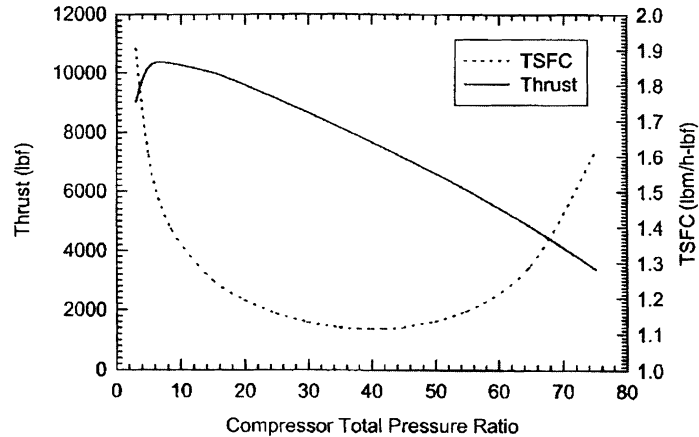


Figure 3.18 Effect of compressor pressure ratio on performance for the turbojet in Example 3.1a.

high thrust versus a low $TSFC$. The balance is further complicated by the fact that, as the compressor pressure ratio is increased, the number of compressor stages increases, which adds to the cost and weight of the compressor.

Note that, for this nonideal case, when a wider range of compressor ratio is considered, a minimum value of $TSFC$ (1.114 lbm/h-lbf) is realized at a compressor pressure ratio of 40 and the corresponding thrust level is only 7670 lbf. Such a trend was not seen for the ideal case; that is, the value of $TSFC$ always decreased with increasing compressor ratio. Thus, although a value of $\pi_c = 40$ does not make such a design worthy of consideration in this example (the ratio is too large and the thrust is much too low), such a trend study should not be precluded for other cases and conditions.

Complementary Example 3.1.b: Although it was not requested, one can replace the converging nozzle with a variable converging–diverging nozzle (to match the exit pressure to the ambient pressure) and repeat the preceding calculations to see how much improvement results. All of the computations are the same as those in Example 3.1 up to the nozzle.

PRIMARY NOZZLE

Because no afterburner is present, $T_{t6} = T_{t5.5} = 1865^\circ\text{R}$ (1036 K)

and $p_{t6} = p_{t5.5} = 65.46$ psia (451.4 kPa).

The nozzle is a variable C–D nozzle, and so the exit pressure matches the ambient pressure and there is no need to check for choking as in Example 3.1;

thus, $p_8 = 14.69$ psia (101.3 kPa).

Ideally,

$$T'_8 = T_{t6} \left[\frac{p_8}{p_{t6}} \right]^{\frac{\gamma_n - 1}{\gamma_n}} = 1865^\circ\text{R} \left[\frac{14.69 \text{ psia}}{65.46 \text{ psia}} \right]^{\frac{1.3368 - 1}{1.3368}} = 1280^\circ\text{R} (711.2 \text{ K})$$

for $\gamma_n = 1.3368$ (iterative).

The nozzle efficiency is again 96 percent, thus, the nozzle exit temperature is

$$\begin{aligned} T_8 &= T_{t6} - \eta_n(T_{t6} - T'_8) = 1865^\circ\text{R} - 0.96(1865^\circ\text{R} - 1280^\circ\text{R}) \\ &= 1304^\circ\text{R} (724.2 \text{ K}). \end{aligned}$$

Now the exit gas speed is $u_8 = \sqrt{2 c_{pn} (T_{t6} - T_8)}$;

thus,

$$u_8 = \sqrt{2 \times 0.2721 \frac{\text{Btu}}{\text{lbm} \cdot ^\circ\text{R}} \times (1865^\circ\text{R} - 1304^\circ\text{R}) \times 32.17 \frac{\text{lbm}}{\text{slugs}} \times 778.16 \frac{\text{ft} \cdot \text{lbf}}{\text{Btu}} \times \frac{\text{slug} \cdot \text{ft}}{\text{lbf} \cdot \text{s}^2}}$$

$$= 2767 \text{ ft/s (843.2 m/s),}$$

which is much higher than in the choked case in Example 3.1 (1914 ft/s).

The speed of sound at the exit is $a_8 = \sqrt{\gamma_8 \mathcal{R} T_8}$,

and so

$$a_8 = \sqrt{1.3368 \times 53.35 \frac{\text{ft} \cdot \text{lbf}}{\text{lbm} \cdot ^\circ\text{R}} \times 32.17 \frac{\text{lbm}}{\text{slug}} \times 1304^\circ\text{R} \times \frac{\text{slug} \cdot \text{ft}}{\text{lbf} \cdot \text{s}^2}}$$

$$= 1,729 \text{ ft/s (527.1 m/s);}$$

thus, $M_8 = u_8/a_8 = 2767 \text{ ft/s}/1729 \text{ ft/s} = 1.600$, which is considerably higher than in Example 3.1.

The exit area is given by $A_8 = \frac{\dot{m}_8}{\rho_8 u_8}$,

where \dot{m}_8 is the total mass flow rate at 8 and is given by $\dot{m}_8 = \dot{m}_{a8} + \dot{m}_f$,

and \dot{m}_{a8} is the air mass flow rate at 8 and is equal to \dot{m} ;

thus, $\dot{m}_{a8} = 165 \text{ lbm/s (74.83 kg/s)}$,

which results in $\dot{m}_8 = 165 + 3.472 = 168.5 \text{ lbm/s (76.40 kg/s)}$, as in Example 3.1.

Since both T_8 and p_8 are known, ρ_8 is again found from the ideal gas equation:

$$\rho_8 = 0.0009455 \text{ slug/ft}^3 (0.4874 \text{ kg/m}^3);$$

thus, the exit area is

$$A_8 = \frac{168.5 \frac{\text{lbm}}{\text{s}} \times 144 \frac{\text{in}^2}{\text{ft}^2}}{0.0009455 \frac{\text{slug}}{\text{ft}^3} \times 2767 \frac{\text{ft}}{\text{s}} \times 32.17 \frac{\text{lbm}}{\text{slug}}} = 288.3 \text{ in}^2 (0.1860 \text{ m}^2).$$

TOTAL THRUST AND TSFC

The thrust is given by

$$F = \dot{m}_8 u_8 - \dot{m}_{a8} u_a + A_8 (p_8 - p_a).$$

Thus,

$$F = \frac{168.5 \frac{\text{lbm}}{\text{s}} \times 2767 \frac{\text{ft}}{\text{s}}}{32.17 \frac{\text{lbm}}{\text{slug}}} \frac{\text{lbf} \cdot \text{s}^2}{\text{slug} \cdot \text{ft}} - \frac{165 \frac{\text{lbm}}{\text{s}} \times 838.2 \frac{\text{ft}}{\text{s}}}{32.17 \frac{\text{lbm}}{\text{slug}}} \frac{\text{lbf} \cdot \text{s}^2}{\text{slug} \cdot \text{ft}}$$

$$+ 288.3 \text{ in}^2 \times \left(14.69 \frac{\text{lbf}}{\text{in}^2} - 14.69 \frac{\text{lbf}}{\text{in}^2} \right)$$

which yields $F = 10,190$ (momentum) + 0 (pressure)

or $F = 10,190 \text{ lbf (45,320 N)}$. All of the pressure thrust has now been converted to momentum thrust. Finally, $TSFC = \dot{m}_f/F$;

thus

$$TSFC = \frac{3.472 \frac{\text{lbm}}{\text{s}}}{10,190 \text{ lbf}} \times 3600 \frac{\text{s}}{\text{h}} = 1.227 \frac{\text{lbm}}{\text{h} \cdot \text{lbf}} \left(0.1251 \frac{\text{kg}}{\text{h} \cdot \text{N}} \right)$$

As one can see for this operating point, the results are only marginally better. The thrust is 1.8 percent higher than for the fixed converging nozzle, and the $TSFC$ is 1.7

percent lower. Consequently, for this particular design one would probably not add the complexity and cost of a variable converging–diverging nozzle for the small improvement that would result. However, as determined by the range of operating conditions or “flight envelope,” adding a variable converging–diverging nozzle could be advantageous. For example, if the engine were to be routinely used at different altitudes, nozzle inlet conditions, and thrust levels and speeds, a variable converging–diverging nozzle would probably be worth the extra engineering and cost.

Complementary Example 3.1.c: To isolate only the effects of variable specific heats and specific heat ratios for the different components, one can repeat the computations for the case of all ideal components but with variable specific heats. These calculations follow with all efficiencies and total pressure ratios of unity. Results are also compared with the results of Example 3.1 to show the effects of the losses.

DIFFUSER

First,

$$\begin{aligned} a_a &= \sqrt{\gamma_a \mathcal{R} T_a} \\ &= \sqrt{1.4029 \times 53.35 \frac{\text{ft}\cdot\text{lbf}}{\text{lbm}\cdot^\circ\text{R}} \times 32.17 \frac{\text{lbm}}{\text{slug}} \times 518.7^\circ\text{R} \times \frac{\text{slug}\cdot\text{ft}}{\text{lbf}\cdot\text{s}^2}} \\ &= 1,118 \text{ ft/s (340.6 m/s),} \end{aligned}$$

and thus the air speed is $u_a = M_a a_a = 0.75 \times 1118 \text{ ft/s} = 838.2 \text{ ft/s (255.5 m/s)}$,

$$\text{Next } \frac{T_{ta}}{T_a} = 1 + \frac{\gamma_d - 1}{2} M_a^2 = 1 + \frac{1.3997 - 1}{2} \times 0.75^2 = 1.1124$$

for $\gamma_d = 1.3997$ and $M_a = 0.75$;

thus $T_{t2} = T_{ta} = 1.1124 \times 518.7^\circ\text{R} = 577.0^\circ\text{R (320.6 K)}$ and

$$\frac{p_{ta}}{p_a} = \left[\frac{T_{ta}}{T_a} \right]^{\frac{\gamma_d}{\gamma_d - 1}} = [1.1124]^{\frac{1.3997}{1.3997 - 1}} = 1.4522.$$

$$\text{Next } \frac{p_{t2}}{p_a} = \pi_d \frac{p_{ta}}{p_a} = 1 \times 1.4522 = 1.4522,$$

and so $p_{t2} = 1.4522 \times 14.69 \text{ psia} = 21.33 \text{ psia (147.1 kPa)}$.

The total pressure into the compressor is thus 8.7 percent higher than for the nonideal case.

COMPRESSOR

The total pressure ratio of the compressor is again given as $\pi_c = 15$.

Therefore, $p_{t3} = \pi_c p_{t2} = 15 \times 21.33 \text{ psia} = 320.0 \text{ psia (2206 kPa)}$.

Ideally, $\tau'_c = [\pi_c]^{\frac{\gamma_c - 1}{\gamma_c}} = [15]^{\frac{1.3827 - 1}{1.3827}} = 2.116$ for $\gamma_c = 1.3827$ (iteration);

therefore, $T'_{t3} = \tau'_c T_{t2} = 2.116 \times 577.0^\circ\text{R} = 1221^\circ\text{R (678.3 K)}$,

but the compressor efficiency is unity for this case and

$$\eta_c = 1.00 = \frac{T'_{t3} - T_{t2}}{T_{t3} - T_{t2}}.$$

Thus, solving for T_{t3} , one finds $T_{t3} = 1221^\circ\text{R (678.3 K)}$.

This value compares with 1305°R for the nonideal case and indicates that considerably more power than ideal is being used to drive the compressor for the nonideal case.

PRIMARY COMBUSTOR

For this case, the total pressure ratio of the burner is unity.

Thus, $p_{t4} = \pi_b p_{t3} = 1.00 \times 320.0 \text{ psia} = 320.0 \text{ psia}$ (2206 kPa), which is 14.4 percent higher than in the nonideal case. This indicates that more high pressure air is available for the turbine to expand (and thus to derive more power) than in the nonideal case.

The energy analysis is

$$\Delta H \eta_b \dot{m}_f = \dot{m} c_{pb}(T_{t4} - T_{t3}) + \dot{m}_f c_{pb} T_{t4},$$

but for this case $\eta_b = 100$ percent and $\Delta H = 17,800 \text{ Btu/lbm}$ are given, thus, solving for the fuel mass flow rate yields

$$\begin{aligned} \dot{m}_f &= 165 \frac{\text{lbm}}{\text{s}} \times 0.2720 \frac{\text{Btu}}{\text{lbm} \cdot ^\circ\text{R}} \frac{2500^\circ\text{R} - 1221^\circ\text{R}}{1.00 \times 17,800 \frac{\text{Btu}}{\text{lbm}} - 0.2720 \frac{\text{Btu}}{\text{lbm} \cdot ^\circ\text{R}} \times 2500^\circ\text{R}} \\ &= 3.353 \text{ lbm/s} (1.521 \text{ kg/s}) \end{aligned}$$

again with the burner specific heat evaluated at the average burner temperature, which for this case is not an iteration. Since no afterburner is present, this is also the total fuel flow rate (\dot{m}_f). The fuel flow is 3.4 percent lower than for the nonideal case owing to the incomplete combustion for the latter.

Note also that $\dot{m}_f/\dot{m} = 0.02032$, which again is small.

TURBINE

The mechanical efficiency is given as unity, and so the shaft power balance

$$\dot{m} c_{pc}(T_{t3} - T_{t2}) = \eta_m \dot{m}_t c_{pt}(T_{t4} - T_{t5})$$

becomes

$$\begin{aligned} 165 \frac{\text{lbm}}{\text{s}} \times 0.2477 \frac{\text{Btu}}{\text{lbm} \cdot ^\circ\text{R}} (1221^\circ\text{R} - 577.0^\circ\text{R}) \\ = 1.000 \times \left(165 \frac{\text{lbm}}{\text{s}} + 3.353 \frac{\text{lbm}}{\text{s}} \right) \times 0.2817 \frac{\text{Btu}}{\text{lbm} \cdot ^\circ\text{R}} (2500^\circ\text{R} - T_{t5}); \end{aligned}$$

thus, the turbine exit total temperature $T_{t5} = 1945^\circ\text{R}$ (1081 K). Again, the specific heat of the turbine is iteratively found for the average turbine temperature.

The turbine efficiency is defined as $\eta_t = \frac{T_{t4} - T'_{t5}}{T_{t4} - T_{t5}}$ and is ideally unity for this case.

Thus, $T'_{t5} = T_{t5} = 1945^\circ\text{R}$ (1081 K),

and $\tau'_t = \frac{T'_{t5}}{T_{t4}} = \frac{1945}{2500} = 0.7781$;

ideally $\tau'_t = [\pi_t]^{\frac{\gamma-1}{\gamma}}$,

which results in a turbine total pressure ratio of

$\pi_t = 0.3565$ for $\gamma_t = 1.3216$ (evaluated at average turbine temperature).

Finally, the turbine exit total pressure is

$p_{t5} = \pi_t p_{t4} = 0.3365 \times 320.0 = 114.1 \text{ psia}$ (786.6 kPa),

and since no mixer is present $T_{t5.5} = T_{t5} = 1945^\circ\text{R}$ (1081 K)

and $p_{t5.5} = p_{t5} = 114.1 \text{ psia}$ (786.6 kPa), which is 74 percent higher than for the nonideal case. This indicates that much more high pressure air is available to the nozzle to expand to a high-velocity exit gas.

PRIMARY NOZZLE

Because no afterburner is present, the inlet total temperature for the nozzle is

$T_{t6} = T_{t5.5} = 1945^\circ\text{R}$ (1081 K),

and the inlet total pressure is $p_{t6} = p_{t5.5} = 114.1$ psia (786.6 kPa).

The nozzle is a variable converging–diverging nozzle, and so the exit pressure matches the ambient pressure and one does not need to check for choking; thus, $p_8 = 14.69$ psia (101.3 kPa).

Ideally,

$$T'_8 = T_{t6} \left[\frac{p_8}{p_{t6}} \right]^{\frac{\gamma_8 - 1}{\gamma_8}} = 1865 \left[\frac{14.69 \text{ psia}}{114.1 \text{ psia}} \right]^{\frac{1.3333 - 1}{1.3333}}$$

$$= 1165^\circ\text{R} (647.3 \text{ K}).$$

The nozzle efficiency is 100 percent; therefore, the nozzle exit temperature is $T_8 = T'_8 = 1165^\circ\text{R} (647.3 \text{ K})$.

Now $u_8 = \sqrt{2 c_{pn} (T_{t6} - T_8)}$,

and so

$$u_8 = \sqrt{2 \times 0.2742 \frac{\text{Btu}}{\text{lbm} \cdot ^\circ\text{R}} \times (1945^\circ\text{R} - 1165^\circ\text{R}) \times 32.17 \frac{\text{lbm}}{\text{slug}} \times 778.16 \frac{\text{ft} \cdot \text{lbf}}{\text{Btu}} \times \frac{\text{slug} \cdot \text{ft}}{\text{lbf} \cdot \text{s}^2}}$$

$$= 3272 \text{ ft/s} (997.4 \text{ m/s}),$$

which is 18.3 percent higher than the nonideal converging–diverging nozzle case in Example 3.1.b (2767 ft/s) and 71 percent higher than for the nonideal converging nozzle. These differences in exit velocity directly increase the momentum thrust.

The speed of sound at the exit is $a_8 = \sqrt{\gamma_8 \mathcal{R} T_8}$, and

$$\text{so } a_8 = \sqrt{1.3333 \times 53.35 \frac{\text{ft} \cdot \text{lbf}}{\text{lbm} \cdot ^\circ\text{R}} \times 32.17 \frac{\text{lbm}}{\text{slug}} \times 1165^\circ\text{R} \times \frac{\text{slug} \cdot \text{ft}}{\text{lbf} \cdot \text{s}^2}}$$

$$= 1632 \text{ ft/s} (497.7 \text{ m/s}).$$

thus, $M_8 = u_8/a_8 = 3273 \text{ ft/s}/1632 \text{ ft/s} = 2.004$, which is considerably higher than for the nonideal converging–diverging nozzle in Example 3.1b and obviously much higher than for the choked converging nozzle case.

The exit area is given by $A_8 = \frac{\dot{m}_8}{\rho_8 u_8}$,

where \dot{m}_8 is the total mass flow rate at 8 and is given by $\dot{m}_8 = \dot{m}_{a8} + \dot{m}_f$, and \dot{m}_{a8} is the air mass flow rate at 8 and is equal to \dot{m} ;

thus, $\dot{m}_{a8} = 165 \text{ lbm/s} (74.83 \text{ kg/s})$

and $\dot{m}_8 = 165 + 3.353 = 168.4 \text{ lbm/s} (76.35 \text{ kg/s})$.

Because both T_8 and p_8 are known, ρ_8 is again found from the ideal gas equation

$$\rho_8 = 0.001058 \text{ slug/ft}^3 (0.5452 \text{ kg/m}^3);$$

thus,

$$A_8 = \frac{168.4 \frac{\text{lbm}}{\text{s}} \times 144 \frac{\text{in.}^2}{\text{ft}^2}}{0.001058 \frac{\text{slug}}{\text{ft}^3} \times 3272 \frac{\text{ft}}{\text{s}} \times 32.17 \frac{\text{lbm}}{\text{slug}}} = 217.7 \text{ in.}^2 (0.1404 \text{ m}^2).$$

TOTAL THRUST AND TSFC

Finally, the thrust is given by

$$F = \dot{m}_8 u_8 - \dot{m}_{a8} u_a + A_8 (p_8 - p_a),$$

and so

$$F = \frac{168.4 \frac{\text{lbm}}{\text{s}} \times 3272 \frac{\text{ft}}{\text{s}} \text{ lbf-s}^2}{32.17 \frac{\text{lbm}}{\text{slug}} \text{ slug-ft}} - \frac{165 \frac{\text{lbm}}{\text{s}} \times 838.2 \frac{\text{ft}}{\text{s}} \text{ lbf-s}^2}{32.17 \frac{\text{lbm}}{\text{slug}} \text{ slug-ft}} + 217.7 \text{ in.}^2 \times \left(14.69 \frac{\text{lbf}}{\text{in.}^2} - 14.69 \frac{\text{lbf}}{\text{in.}^2} \right);$$

thus, $F = 12,830$ (momentum) + 0 (pressure)

or $F = 12,830$ lbf (57,050 N) and all of the thrust is momentum thrust.

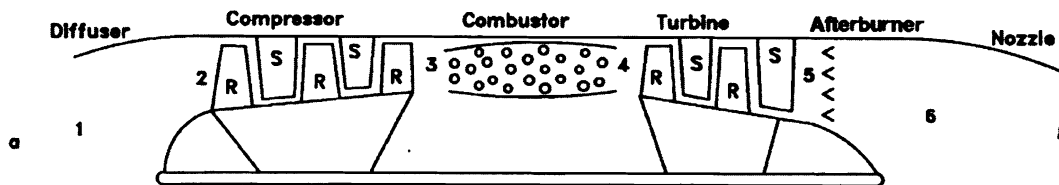
Finally, $TSFC = \dot{m}_f/F$,

and thus

$$TSFC = \frac{3.353 \frac{\text{lbm}}{\text{s}}}{12,830 \text{ lbf}} \times 3600 \frac{\text{s}}{\text{h}} = 0.9411 \frac{\text{lbm}}{\text{h-lbf}} \left(0.09597 \frac{\text{kg}}{\text{h-N}} \right).$$

As one can see, the thrust is 28.2 percent higher than for the nonideal components. The $TSFC$ is 24.6 percent lower for two reasons: the fuel flow rate is lower (by 3.4%) and the thrust is larger. Furthermore, by comparing these results with the ideal case having a constant specific heat throughout the engine (Example 2.2), one finds that the thrust, interestingly, is 11.5 percent higher (better) and the $TSFC$ is 8.2 percent higher (worse). The primary cause here is the effect of variable specific heats, although a small contribution is that, for the ideal case, the fuel mass flow is neglected in the calculations. Obviously, the effects of variable specific heats and specific heat ratios for the different components are very important and should be included.

Example 3.2: A turbojet with an afterburner flies at sea level at a Mach number of 0.75. It ingests 165 lbm/s (74.83 kg/s) of air. The compressor operates with a pressure ratio of 15 and an efficiency of 88 percent. The fuel has a heating value of 17,800 Btu/lbm (41,400 kJ/kg), and the burner total temperature is 2500 °R (1389 K). The burner has an efficiency of 91 percent and a total pressure ratio of 0.95, whereas the turbine has an efficiency of 85 percent. The afterburner exit total temperature is 3200 °R (1778 K). The afterburner has an efficiency of 89 percent and a total pressure ratio of 0.97. A converging nozzle is used, and the nozzle efficiency is 96 percent. The total pressure recovery for the diffuser is 0.92, and the shaft efficiency is 99.5 percent. Find the developed thrust and $TSFC$. Note that this is the same engine as in Example 2.3 with the exception of the nonideal effects. This is also the same engine as in Example 3.1 with the addition of an afterburner.



SOLUTION:

The solution up to the afterburner is the same as for Example 3.1. Thus, only the steps after the turbine will be shown.

AFTERBURNER

The total pressure ratio of the afterburner is given as 0.97;

thus, $p_{t6} = \pi_{ab} p_{t5.5} = 0.97 \times 65.46 \text{ psia} = 63.50 \text{ psia}$ (437.8 kPa),

and the energy analysis is $\Delta H \eta_{ab} \dot{m}_{fab} = (\dot{m} + \dot{m}_f) c_{pab} (T_{t6} - T_{t5.5}) + \dot{m}_{fab} c_{pab} T_{t6}$.

However, $\eta_{ab} = 0.89$ and $\Delta H = 17,800 \text{ Btu/lbm}$ are given, and

so solving for the afterburner fuel mass flow rate yields

$$\begin{aligned} \dot{m}_{fab} &= (165 + 3.472) \frac{\text{lbm}}{\text{s}} \\ &\quad \times 0.2904 \frac{\text{Btu}}{\text{lbm} \cdot ^\circ\text{R}} \frac{3200^\circ\text{R} - 1865^\circ\text{R}}{0.89 \times 17,800 \frac{\text{Btu}}{\text{lbm}} - 0.2904 \frac{\text{Btu}}{\text{lbm} \cdot ^\circ\text{R}} \times 3200^\circ\text{R}} \\ &= 4.378 \text{ lbm/s} (1.986 \text{ kg/s}), \end{aligned}$$

where the burner specific heat is evaluated at the average afterburner temperature, which is not an iteration.

The total fuel flow rate is therefore $\dot{m}_f = \dot{m}_f + \dot{m}_{fab}$

or $\dot{m}_f = 3.472 + 4.378 = 7.850 \text{ lbm/s}$ (3.560 kg/s).

PRIMARY NOZZLE

The inlet total pressure is $p_{t6} = 63.60 \text{ psia}$ (437.8 kPa).

Because the engine has a fixed converging nozzle, one must first check to see if the nozzle is choked.

If the nozzle is choked, its exit pressure is $p_8^* = p_{t6} \left[1 + \frac{1 - \gamma_n}{\gamma_n(1 + \gamma_n)} \right]^{\frac{\gamma_n}{\gamma_n - 1}}$;

thus, for $p_{t6} = 63.60 \text{ psia}$, $\eta_n = 0.96$ (given),

and $\gamma_n = 1.2841$ (iteratively found for the average nozzle temperature). Note that is lower than for the nonafterburning case (Example 3.1) owing to the significantly higher nozzle temperature:

$$p_8^* = 63.50 \text{ psia} \times \left[1 + \frac{1 - 1.2841}{0.96 \times (1 + 1.2841)} \right]^{\frac{1.2841}{1.2841 - 1}} = 33.91 \text{ psia} (233.8 \text{ kPa}),$$

but since $p_a = 14.69 \text{ psia}$ (101.3 kPa), which is well below the choking condition p_8^* , the nozzle is choked and the exit Mach number is identically unity as in Example 3.1

Therefore, the exit pressure is $p_8 = p_8^* = 33.91 \text{ psia}$ (233.8 kPa)

and $T_8 = \frac{2T_{t6}}{1 + \gamma_n}$ for $M_8 = 1$;

thus for $T_{t6} = 3200^\circ\text{R}$ (1778 K), $T_8 = \frac{2 \times 3200^\circ\text{R}}{1 + 1.2841} = 2802^\circ\text{R}$ (1557 K).

The nozzle exit velocity is given by $u_8 = \sqrt{2 c_{pn} (T_{t6} - T_8)}$;

thus,

$$\begin{aligned} u_8 &= \sqrt{2 \times 0.3098 \frac{\text{Btu}}{\text{lbm} \cdot ^\circ\text{R}} \times (3200^\circ\text{R} - 2802^\circ\text{R}) \times 32.17 \frac{\text{lbm}}{\text{slug}} \times 778.16 \frac{\text{ft} \cdot \text{lbf}}{\text{Btu}} \times \frac{\text{slug} \cdot \text{ft}}{\text{lbm} \cdot \text{s}^2}} \\ &= 2485 \text{ ft/s} (757.4 \text{ m/s}), \end{aligned}$$

which is 29.8 percent higher than for the nonafterburning case (Example 3.1) owing to the much higher temperatures.

From continuity the exit area is given by $A_8 = \frac{\dot{m}_8}{\rho_8 u_8}$,

where \dot{m}_8 is the total mass flow rate at 8 and is given by $\dot{m}_8 = \dot{m}_{a8} + \dot{m}_f$ and \dot{m}_{a8} is the air mass flow rate at 8 and is equal to \dot{m} , the ingested flow; thus, $\dot{m}_{a8} = 165 \text{ lbm/s}$ (74.83 kg/s).

The total mass flow rate at the exit is $\dot{m}_8 = 165 + 7.850 = 172.9 \text{ lbm/s}$ (78.39 kg/s). Since both T_8 and p_8 are known, ρ_8 is found from the ideal gas equation

$$\rho_8 = \frac{p_8}{R T_8} = \frac{33.91 \frac{\text{lbf}}{\text{in}^2} \times 144 \frac{\text{in}^2}{\text{ft}^2}}{53.35 \frac{\text{ft-lbf}}{\text{lbm-}^\circ\text{R}} \times 2802^\circ\text{R} \times 32.17 \frac{\text{lbm}}{\text{slug}}}$$

$$\rho_8 = 0.001016 \text{ slug/ft}^3 (0.5235 \text{ kg/m}^3);$$

thus, the nozzle exit area is

$$A_8 = \frac{172.9 \frac{\text{lbm}}{\text{s}} \times 144 \frac{\text{in}^2}{\text{ft}^2}}{0.001016 \frac{\text{slug}}{\text{ft}^3} \times 2485 \frac{\text{ft}}{\text{s}} \times 32.17 \frac{\text{lbm}}{\text{slug}}} = 306.6 \text{ in}^2 (0.1978 \text{ m}^2).$$

TOTAL THRUST AND *TSFC*

The thrust is given by

$$F = \dot{m}_8 u_8 - \dot{m}_{a8} u_a + A_8 (p_8 - p_a),$$

and so

$$F = \frac{172.9 \frac{\text{lbm}}{\text{s}} \times 2485 \frac{\text{ft}}{\text{s}}}{32.17 \frac{\text{lbm}}{\text{slug}}} \frac{\text{lbf-s}^2}{\text{slug-ft}} - \frac{165 \frac{\text{lbm}}{\text{s}} \times 838.2 \frac{\text{ft}}{\text{s}}}{32.17 \frac{\text{lbm}}{\text{slug}}} \frac{\text{lbf-s}^2}{\text{slug-ft}}$$

$$+ 306.6 \text{ in}^2 \times \left(33.91 \frac{\text{lbf}}{\text{in}^2} - 14.69 \frac{\text{lbf}}{\text{in}^2} \right);$$

thus, $F = 9053$ (momentum) + 5894 (pressure)

or $F = 14,950 \text{ lbf}$ (66,480 N).

Finally, $TSFC = \dot{m}_f / F$,

and so

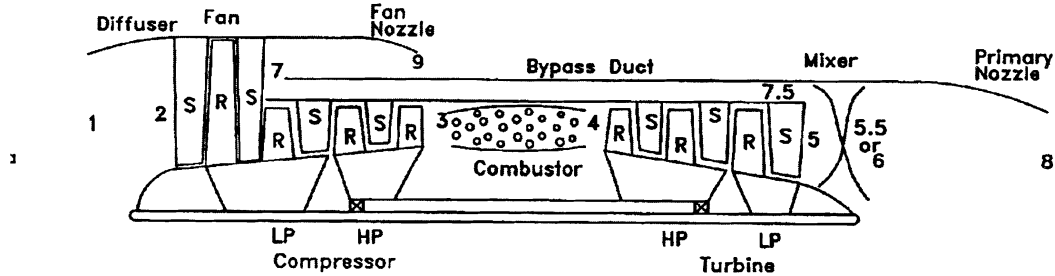
$$TSFC = \frac{7.850 \frac{\text{lbm}}{\text{s}}}{14,950 \text{ lbf}} \times 3600 \frac{\text{s}}{\text{h}}$$

$$= 1.891 \frac{\text{lbm}}{\text{h-lbf}} \left(0.1928 \frac{\text{kg}}{\text{h-N}} \right).$$

By comparing these results to the nonafterburning case, one can see that the thrust has been increased by 49.4 percent and the *TSFC* has been increased by 51.5 percent. Thus, although the thrust is greatly improved, the fuel economy is much worse. Also, by comparing these results with those of the ideal case (Example 2.3), one finds that the thrust is 10 percent lower but the *TSFC* is 50 percent higher owing to the losses.

Example 3.3: A turbofan flies at sea level at a Mach number of 0.75. It ingests 74.83 kg/s (165 lbm/s) of air to the core. The compressor operates with a pressure ratio of 15 and an efficiency of 88 percent. The engine has a bypass ratio of 3 and a split ratio of 0.25. The efficiency of the fan is 90 percent. The fuel has a heating value of 41,400 kJ/kg (17,800 Btu/lbm), and the burner total temperature is 1389 K (2500 °R). The burner has an efficiency of 91 percent and a total pressure ratio of 0.95, whereas the turbine has an efficiency of 85 percent. The duct has a total pressure ratio of 0.98, and the total pressure ratio of the mixer is 0.97. A variable

converging-diverging nozzle (to match the exit pressure to the ambient pressure) is used for the primary nozzle, and the efficiency is 96 percent. A converging nozzle is used for the fan nozzle, and the efficiency is 95 percent. The total pressure recovery for the diffuser is 0.92, and the shaft efficiency is 99.5 percent. The Mach numbers at the turbine and duct exits are nearly the same. Find the developed thrust and *TSFC*.



SOLUTION:

DIFFUSER

First, the speed of sound is

$$a_a = \sqrt{\gamma_a \mathcal{R} T_a} = \sqrt{1.403 \times 287.1 \frac{\text{J}}{\text{kg} \cdot \text{K}} \times 288.2 \text{ K} \times \frac{\text{N} \cdot \text{m}}{\text{J}} \times \frac{\text{kg} \cdot \text{m}}{\text{N} \cdot \text{s}^2}}$$

$$= 340.7 \text{ m/s (1118 ft/s),}$$

and so the engine airspeed is

$$u_a = M_a a_a = 0.75 \times 340.7 \text{ m/s} = 255.5 \text{ m/s (838.2 ft/s).}$$

$$\text{Next } \frac{T_{ta}}{T_a} = 1 + \frac{\gamma_d - 1}{2} M_a^2 = 1 + \frac{1.3997 - 1}{2} 0.75^2 = 1.1124$$

for $\gamma_d = 1.3997$ and $M_a = 0.75$;

$$\text{thus } T_{t2} = T_{ta} = 1.1124 \times 288.2 \text{ K} = 320.6 \text{ K (577.0 } ^\circ\text{R).}$$

$$\text{Also } \frac{p_{ta}}{p_a} = \left[\frac{T_{ta}}{T_a} \right]^{\frac{\gamma_d}{\gamma_d - 1}} = [1.1124]^{\frac{1.3997}{1.3997 - 1}} = 1.4522.$$

The pressure recovery factor for the diffuser is 0.92,

$$\text{and so } \frac{p_{t2}}{p_a} = \frac{p_{t2}}{p_{ta}} \frac{p_{ta}}{p_a} = \pi_d \frac{p_{ta}}{p_a} = 0.92 \times 1.4522 = 1.3360;$$

$$\text{thus } p_{t2} = 1.3360 \times 101.3 \text{ kPa} = 135.3 \text{ kPa (19.63 psia).}$$

COMPRESSOR

The compressor total pressure ratio is given as 15, and so

$$p_{t3} = \pi_c p_{t2} = 15 \times 135.3 \text{ kPa} = 2030 \text{ kPa (294.4 psia).}$$

One knows that, for a nonideal compressor,

$$\frac{p_{t3}}{p_{t2}} = \left\{ 1 + \eta_c \left[\frac{T_{t3}}{T_{t2}} - 1 \right] \right\}^{\frac{\gamma}{\gamma - 1}} = \pi_c = \{ 1 + \eta_c [\tau_c - 1] \}^{\frac{\gamma}{\gamma - 1}};$$

thus, solving for the total temperature ratio (the efficiency of the compressor is given as 88%) yields

$$\frac{T_{t3}}{T_{t2}} = \tau_c = \frac{\left[\frac{p_{t3}}{p_{t2}} \right]^{\frac{\gamma_c - 1}{\gamma_c}} - 1}{\eta_c} + 1 = \frac{[15]^{\frac{1.3805 - 1}{1.3805}} - 1}{0.88} + 1 = 2.2607$$

for $\gamma_c = 1.3805$ (iterative).

Therefore, the exit temperature of the compressor is
 $T_{13} = \tau_c T_{12} = 2.2607 \times 320.6 \text{ K} = 724.7 \text{ K} (1305 \text{ }^\circ\text{R})$.

FAN

For a mixed turbofan geometry, the fan total pressure ratio is unknown. Thus, one needs to find π_f by iteration. In effect, the duct exit pressure (which is the same as the turbine exit pressure) directly depends on the fan total pressure ratio. But this pressure ratio also affects the turbine power, which indirectly affects the turbine exit pressure. Thus, one can find the fan pressure ratio by a progressive iteration. Details of the Regula Falsi iteration are presented in Appendix G, Example G.2. Fortunately, the iteration process converges quickly (seven iterations for this case) and can easily be programmed with a commercial math solver. In actuality, four or five iterations could have been used with minimal effects on the net results. Also, note that, although precise values of the pressure ratio are desired for an engine design, it is not the dominant feature of examples or chapter problems.

For the purposes of this example, to demonstrate the thermodynamic calculations one can first try $\pi_f = 1.6305$, which will be checked later at the mixer:

$$p_{17} = \pi_f p_{12} = 1.6305 \times 135.3 \text{ kPa} = 220.6 \text{ kPa} (32.00 \text{ psia}).$$

It is known that

$$\frac{p_{17}}{p_{12}} = \left\{ 1 + \eta_f \left[\frac{T_{17}}{T_{12}} - 1 \right] \right\}^{\frac{\gamma_f}{\gamma_f - 1}} = \pi_f = \{ 1 + \eta_f [\tau_f - 1] \}^{\frac{\gamma_f}{\gamma_f - 1}},$$

and so solving for the total temperature ratio (the efficiency of the fan is given as 90%) yields

$$\frac{T_{17}}{T_{12}} = \tau_f = \frac{\left[\frac{p_{17}}{p_{12}} \right]^{\frac{\gamma_f - 1}{\gamma_f}} - 1}{\eta_f} + 1 = \frac{[1.6305]^{\frac{1.3971 - 1}{1.3971}} - 1}{0.88} + 1 = 1.1656$$

for $\gamma_f = 1.3971$ (iterative);

therefore, the exit temperature of the fan is

$$T_{17} = \tau_f T_{12} = 1.1656 \times 320.6 \text{ K} = 373.7 \text{ K} (672.6 \text{ }^\circ\text{R}).$$

BYPASS DUCT

The pressure ratio for the bypass duct is $\pi_u = \frac{p_{17.5}}{p_{17}} = 0.98$,

and so $p_{17.5} = 0.98 \times 220.6 \text{ kPa} = 216.2 \text{ kPa} (31.36 \text{ psia})$.

Also, since the duct is adiabatic, the total temperature is constant through the passage; thus,

$$T_{17.5} = T_{17} = 373.7 \text{ K} (672.6 \text{ }^\circ\text{R}).$$

PRIMARY COMBUSTOR

The total pressure ratio for the burner is 0.95, and so the burner exit total pressure is

$$p_{14} = \pi_b p_{13} = 0.95 \times 2030 \text{ kPa} = 1928 \text{ kPa} (279.7 \text{ psia}).$$

The energy balance yields $\Delta H \eta_b \dot{m}_f = \dot{m}_{c_{pb}} (T_{14} - T_{13}) + \dot{m}_f c_{pb} T_{14}$, where the burner efficiency is 91 percent and the heating value is 41,400 kJ/kg;

thus,

$$\begin{aligned} \dot{m}_f &= 74.83 \frac{\text{kg}}{\text{s}} \times 1.143 \frac{\text{kJ}}{\text{kg-K}} \times \frac{(1389 - 724.7) \text{ K}}{0.91 \times 41,400 \frac{\text{kJ}}{\text{kg}} - 1.143 \frac{\text{kJ}}{\text{kg-K}} \times 1389 \text{ K}} \\ &= 1.574 \text{ kg/s} (3.472 \text{ lbm/s}). \end{aligned}$$

The specific heat is evaluated at the average temperature (not an iteration) Since no afterburner is present, this is also the total fuel flow rate (\dot{m}_f).

Note that $f = \dot{m}_f/\dot{m} = 0.02104$, which is small.

TURBINE

The power balance for the shaft of the turbofan is

$\dot{m} c_{pc}(T_{13} - T_{12}) + \alpha \dot{m} c_{pt}(T_{17} - T_{12}) = \eta_m \dot{m}_t c_{pt}(T_{14} - T_{15})$, where the mechanical efficiency is 99.5 percent

or

$$\begin{aligned} & 74.83 \frac{\text{kg}}{\text{s}} \times 1.041 \frac{\text{kJ}}{\text{kg-K}} \times (724.7 \text{ K} - 320.6 \text{ K}) \\ & + 3 \times 74.83 \frac{\text{kg}}{\text{s}} \times 1.010 \frac{\text{kJ}}{\text{kg-K}} \times (373.7 \text{ K} - 320.6 \text{ K}) \\ & = 0.995 \times \left(74.83 \frac{\text{kg}}{\text{s}} + 1.574 \frac{\text{kg}}{\text{s}} \right) \times 1.160 \frac{\text{kJ}}{\text{kg-K}} \times (1389 \text{ K} - T_{15}); \end{aligned}$$

thus, the turbine exit temperature $T_{15} = 895.5 \text{ K}$ (1612 °R). The value of the turbine specific heat is found iteratively.

The turbine total temperature ratio is $\tau_t = \frac{T_{15}}{T_{14}} = \frac{895.5 \text{ K}}{1389 \text{ K}} = 0.6447$. One knows for a nonideal turbine that

$$\frac{p_{t5}}{p_{t4}} = \left\{ 1 - \frac{[1 - \frac{T_{15}}{T_{14}}]}{\eta_t} \right\}^{\frac{\gamma}{\gamma-1}} = \pi_t = \left\{ 1 - \frac{[1 - \tau_t]}{\eta_t} \right\}^{\frac{\gamma}{\gamma-1}},$$

but the turbine efficiency η_t is given as 85 percent; thus, the turbine total pressure ratio is

$$\pi_t = \left\{ 1 - \frac{[1 - 0.6447]}{0.85} \right\}^{\frac{1.3286}{1.3286-1}} = 0.1121 \text{ for } \gamma_t = 1.3286 \text{ (iterative with } c_{pt}).$$

Finally, the turbine exit total pressure is

$$p_{t5} = \pi_t p_{t4} = 0.1121 \times 1928 \text{ kPa} = 216.2 \text{ kPa} (31.36 \text{ psia}).$$

MIXER

Now one can now compare $p_{t7.5}$ from the duct and p_{t5} from the turbine and see that they are the same. Also, since the Mach numbers at stations 5 and 7.5 are given to be approximately the same ($M_5 \cong M_{7.5}$), and because the total pressures are identical, the static pressures will match. Thus, the initial guess of the fan pressure ratio, π_f , was excellent. If the two total pressures had been different, a new value of π_f would have had to be tried and all of the preceding work would have to be repeated as demonstrated in detail in Appendix G, Example G.2.

Next, one can find the temperature out of the mixer, $T_{15.5}$, by

$$\begin{aligned} T_{15.5} &= \frac{(1+f)c_{p_{mc}}T_{15} + \sigma\alpha c_{p_{mu}}T_{17.5}}{(1+f)c_{p_{mc}} + \sigma\alpha c_{p_{mu}}} \\ &= \frac{(1+0.02104) \times 1.091 \frac{\text{kJ}}{\text{kg-K}} \times 895.5 \text{ K} + 0.25 \times 3 \times 1.042 \frac{\text{kJ}}{\text{kg-K}} \times 373.7 \text{ K}}{(1+0.02104) \times 1.091 \frac{\text{kJ}}{\text{kg-K}} + 0.25 \times 3 \times 1.042 \frac{\text{kJ}}{\text{kg-K}}} \end{aligned}$$

where $c_{p_{mu}}$ is evaluated at the average temperature between stations 7.5 to 5.5, and $c_{p_{mc}}$ is from the average temperature between stations 5 to 5.5.

Thus, $T_{15.5} = 680.3 \text{ K}$ (1225 °R).

Also for this case, and with $M_5 = M_{7.5}$, $\pi_m = p_{15.5}/p_{15.2} = p_{15.5}/p_{15} = p_{15.5}/p_{17.5}$,

the total pressure ratio of the duct is 0.97; thus,
 $p_{15.5} = 0.97 \times 216.2 \text{ kPa} = 209.7 \text{ kPa} (30.42 \text{ psia})$.

PRIMARY NOZZLE

Because no afterburner is present, the inlet total temperature for the primary nozzle is

$$T_{16} = T_{15.5} = 680.3 \text{ K} (1225 \text{ }^\circ\text{R}),$$

and the inlet total pressure is $p_{16} = p_{15.5} = 209.7 \text{ kPa} (30.42 \text{ psia})$.

The nozzle is a variable converging-diverging nozzle, and so the exit pressure matches the ambient pressure and it is not necessary, to check for choking.

That is, $p_8 = 101.3 \text{ kPa} (14.69 \text{ psia})$.

Ideally

$$T'_8 = T_{16} \left[\frac{p_8}{p_{16}} \right]^{\frac{\gamma_n - 1}{\gamma_n}} = 680.3 \left[\frac{101.3 \text{ kPa}}{209.7 \text{ kPa}} \right]^{\frac{1.3664 - 1}{1.3664}} = 559.7 \text{ K} (1007^\circ\text{R}),$$

where $\gamma_n = 1.3664$ (iterative).

The nozzle efficiency is 96 percent;

thus, the nozzle exit temperature is

$$\begin{aligned} T_8 &= T_{16} - \eta_n (T_{16} - T'_8) \\ &= 680.3 \text{ K} - 0.96 \times (680.3 \text{ K} - 559.7 \text{ K}) = 564.5 \text{ K} (1016 \text{ }^\circ\text{R}). \end{aligned}$$

Now $u_8 = \sqrt{2 c_{pn} (T_{16} - T_8)}$,

and thus

$$\begin{aligned} u_8 &= \sqrt{2 \times 1.070 \frac{\text{kJ}}{\text{kg-K}} \times (680.3 \text{ K} - 564.5 \text{ K}) \times 1000 \frac{\text{J}}{\text{kJ}} \times \frac{\text{N-m kg-m}}{\text{J N-s}^2}} \\ &= 497.9 \text{ m/s} (1634 \text{ ft/s}). \end{aligned}$$

The speed of sound at the exit is $a_8 = \sqrt{\gamma_8 \mathcal{R} T_8}$,

and so

$$\begin{aligned} a_8 &= \sqrt{1.3664 \times 287.1 \frac{\text{J}}{\text{kg-K}} \times 564.5 \text{ K} \times \frac{\text{N-m}}{\text{J}} \times \frac{\text{kg-m}}{\text{N-s}^2}} \\ &= 470.5 \text{ m/s} (1544 \text{ ft/s}); \end{aligned}$$

thus, $M_8 = u_8/a_8 = 497.9 \text{ m/s}/470.5 \text{ m/s} = 1.058$.

The exit area is given by $A_8 = \frac{\dot{m}_8}{\rho_8 u_8}$,

where \dot{m}_8 is the total mass flow rate at 8 and is given by $\dot{m}_8 = \dot{m}_{a8} + \dot{m}_f$ (air flow and fuel flow), and \dot{m}_{a8} is the air mass flow rate at 8 and is given by $\dot{m}_{a8} = \dot{m} + \alpha \sigma \dot{m}$; that is, the core air and the air from the bypass duct. Thus

$$\dot{m}_{a8} = 74.83 \text{ kg/s} + 3 \times 0.25 \times 74.83 \text{ kg/s} = 131.0 \text{ kg/s} (288.8 \text{ lbm/s}),$$

and the total mass flow is $\dot{m}_8 = 131.0 \text{ kg/s} + 1.574 \text{ kg/s} = 132.6 \text{ kg/s} (292.2 \text{ lbm/s})$. Since both T_8 and p_8 are known, ρ_8 is found from the ideal gas equation:

$$\rho_8 = \frac{p_8}{\mathcal{R} T_8} = \frac{101.3 \text{ kPa} \times 1000 \frac{\text{Pa}}{\text{kPa}}}{287.1 \frac{\text{J}}{\text{kg-K}} \times 564.5 \text{ K}} \times \frac{\text{N}}{\text{Pa-m}^2} \times \frac{\text{J}}{\text{N-m}};$$

$$\rho_8 = 0.6252 \text{ kg/m}^3 (0.001213 \text{ slug/ft}^3);$$

thus, the exit area is

$$A_8 = \frac{132.6 \frac{\text{kg}}{\text{s}}}{0.6252 \frac{\text{kg}}{\text{m}^3} \times 497.9 \frac{\text{m}}{\text{s}}} = 0.4259 \text{ m}^2 (660.1 \text{ in.}^2).$$

FAN NOZZLE

Because the fan nozzle is a fixed converging device, one must first check to see if it is choked. For choking, the fan nozzle exit pressure is

$$p_9^* = p_{t7} \left[1 + \frac{1 - \gamma_{fn}}{\eta_{fn}(1 + \gamma_{fn})} \right]^{\frac{\gamma_{fn}}{\gamma_{fn} - 1}};$$

thus, for $p_{t7} = 220.6 \text{ kPa}$, $\eta_{fn} = 0.95$ (given), and $\gamma_{fn} = 1.3946$ (iterative),

$$p_9^* = 220.6 \text{ kPa} \times \left[1 + \frac{1 - 1.3946}{0.95 \times (1 + 1.3946)} \right]^{\frac{1.3946}{1.3946 - 1}} = 112.5 \text{ kPa (16.32 psia)},$$

but since $p_a = 101.3 \text{ kPa}$ (14.69 psia), which is well below the exit pressure for choking, the nozzle is choked and the exit Mach number is identically unity.

Therefore, $p_9 = p_9^* = 112.5 \text{ kPa}$ (16.32 psia)

and $T_9 = \frac{2T_{t7}}{1 + \gamma_{fn}}$ for $M_9 = 1.00$;

thus, for $T_{t7} = 373.7 \text{ K}$ (672.6 °R)

$$T_9 = \frac{2 \times 373.7 \text{ K}}{1 + 1.3946} = 312.1 \text{ K (561.8 °R)}.$$

Now $u_9 = \sqrt{2 c_{pfn} (T_{t7} - T_9)}$,

and so

$$\begin{aligned} u_9 &= \sqrt{2 \times 1.014 \frac{\text{kJ}}{\text{kg-K}} \times (373.7 \text{ K} - 312.1 \text{ K}) \times 1000 \frac{\text{J}}{\text{kJ}} \times \frac{\text{N-m kg-m}}{\text{J N-s}^2}} \\ &= 353.4 \text{ m/s (1160 ft/s)}. \end{aligned}$$

Alternatively, one could have found u_9 by first finding the speed of sound at the exit $a_9 = \sqrt{\gamma_9 \mathcal{R} T_9}$;

thus,

$$\begin{aligned} a_9 &= \sqrt{1.3946 \times 287.1 \frac{\text{J}}{\text{kg-K}} \times 312.1 \text{ K} \times \frac{\text{N-m}}{\text{J}} \times \frac{\text{kg-m}}{\text{N-s}^2}} \\ &= 353.4 \text{ m/s (1160 ft/s)}, \end{aligned}$$

but since the nozzle is choked $M_9 = 1 = u_9/a_9$. Thus, $u_9 = 353.4 \text{ m/s}$ (1160 ft/s), which is the same as since the nozzle is choked.

The exit area is given by $A_9 = \frac{\dot{m}_9}{\rho_9 u_9}$,

where \dot{m}_9 is the total mass flow rate at 9 and is given by

$$\begin{aligned} \dot{m}_9 &= \alpha(1 - \sigma)\dot{m} = 3 \times (1 - 0.25) \times 74.83 \text{ kg/s} \\ &= 168.4 \text{ kg/s (371.3 lbm/s)}. \end{aligned}$$

Since both T_9 and p_9 are known, ρ_9 is found from the ideal gas equation

$$\rho_9 = \frac{p_9}{\mathcal{R} T_9} = \frac{112.5 \text{ kPa} \times 1000 \frac{\text{Pa}}{\text{kPa}}}{287.1 \frac{\text{J}}{\text{kg-K}} \times 312.1 \text{ K}} \times \frac{\text{N}}{\text{Pa-m}^2} \times \frac{\text{J}}{\text{N-m}};$$

thus, $\rho_9 = 1.257 \text{ kg/m}^3$ (0.002438 slug/ft³).

Consequently, the fan nozzle exit area is

$$A_9 = \frac{168.4 \frac{\text{kg}}{\text{s}}}{1.257 \frac{\text{kg}}{\text{m}^3} \times 353.4 \frac{\text{m}}{\text{s}}} = 0.3793 \text{ m}^2 (587.9 \text{ in.}^2).$$

TOTAL THRUST AND *TSFC*

The thrust is given by

$$F = \dot{m}_8 u_8 - \dot{m}_{a8} u_a + A_8 (p_8 - p_a) + \dot{m}_9 u_9 - \dot{m}_9 u_a + A_9 (p_9 - p_a),$$

and so

$$\begin{aligned} F = & 132.6 \frac{\text{kg}}{\text{s}} \times 497.9 \frac{\text{m}}{\text{s}} \times \frac{\text{N}\cdot\text{s}^2}{\text{kg}\cdot\text{m}} - 131.0 \frac{\text{kg}}{\text{s}} \times 255.5 \frac{\text{m}}{\text{s}} \times \frac{\text{N}\cdot\text{s}^2}{\text{kg}\cdot\text{m}} \\ & + 0.4259 \text{ m}^2 \times (101.3 \text{ kPa} - 101.3 \text{ kPa}) \times \frac{\text{N}\cdot\text{m}^2}{\text{Pa}} \times \frac{1000 \text{ Pa}}{\text{kPa}} \\ & + 168.4 \frac{\text{kg}}{\text{s}} \times 353.4 \frac{\text{m}}{\text{s}} \times \frac{\text{N}\cdot\text{s}^2}{\text{kg}\cdot\text{m}} - 168.4 \frac{\text{kg}}{\text{s}} \times 255.5 \frac{\text{m}}{\text{s}} \times \frac{\text{N}\cdot\text{s}^2}{\text{kg}\cdot\text{m}} \\ & + 0.3793 \text{ m}^2 \times (112.5 \text{ kPa} - 101.3 \text{ kPa}) \times \frac{\text{N}\cdot\text{m}^2}{\text{Pa}} \times \frac{1000 \text{ Pa}}{\text{kPa}}; \end{aligned}$$

thus, $F = 32,540$ (momentum) + 0 (pressure) + 16,500 (fan momentum) + 4270 (fan pressure) or $F = 53,300$ N (11,980 lbf).

Therefore, the nondimensional thrust is

$$\bar{F} = \frac{F}{(1 + \alpha) \dot{m} a_a} = \frac{53,300 \text{ N}}{4 \times 74.83 \frac{\text{kg}}{\text{s}} \times 340.7 \frac{\text{m}}{\text{s}}} \times \frac{\frac{\text{kg}\cdot\text{m}}{\text{s}^2}}{\text{N}} = 0.5226.$$

Finally $TSFC = \dot{m}_f / F$,

and so

$$TSFC = \frac{1.574 \frac{\text{kg}}{\text{s}}}{53,300 \text{ N}} \times 3600 \frac{\text{s}}{\text{h}} = 0.1063 \frac{\text{kg}}{\text{h}\cdot\text{N}} \left(1.043 \frac{\text{lbm}}{\text{h}\cdot\text{lbf}} \right).$$

One can also compute the ideal performance for this engine. The ideal thrust is 77,930 N, and the *TSFC* is 0.05821 kg/h/N. Thus, for the real case the thrust is reduced by 32 percent, and the *TSFC* is increased by 83 percent because of the losses.

Complementary Example 3.3.a: With all other variables held constant in the Example 3.3, the effect of the bypass ratio is considered now in a complementary study. All of the preceding calculations are the same except for the parameter values. In Figure 3.19, the effects of changing the bypass ratio are shown. As the bypass ratio increases, the nondimensional thrust is continuously reduced, indicating that the thrust-to-weight ratio is decreasing. Also, as the bypass ratio increases, the nondimensional *TSFC* reaches a minimum and then increases. Both of these trends are shown in Chapter 2 for the ideal case. The optimum *TSFC* occurs at a bypass ratio value of approximately 3. This bypass ratio is lower than that for ideal conditions because, as the bypass ratio increases (more duct air flow) the duct and mixer losses have a greater impact.

Example 3.4: A turboprop flies at sea level at a Mach number of 0.70. It ingests 13.61 kg/s (30 lbf/s) of air. The compressor operates with a pressure ratio of 6.5 and an efficiency of 88 percent. The fuel has a heating value of 43,960 kJ/kg

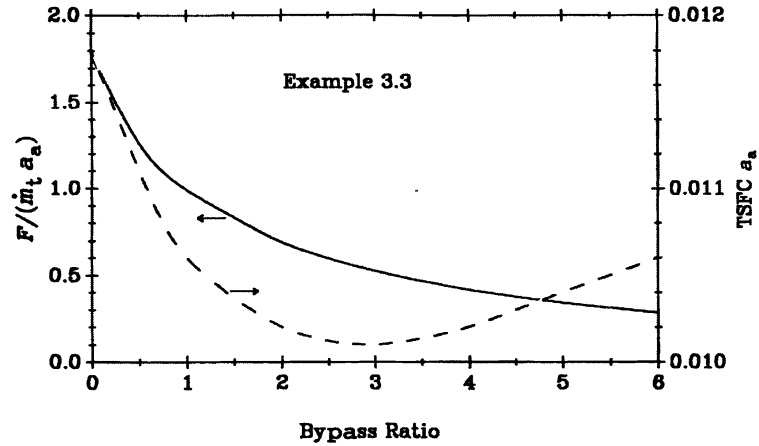
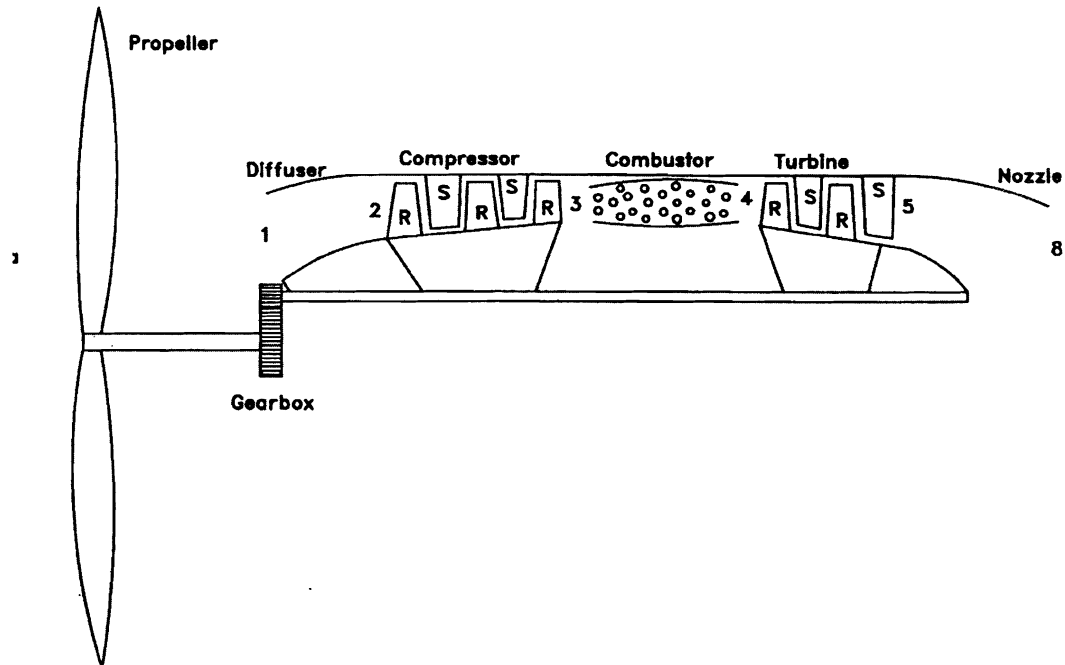


Figure 3.19 Dimensionless thrust (based on total flow) and dimensionless $TSFC$ versus bypass ratio for the nonideal turbofan in Example 3.3a.

(18,900 Btu/lbm), and the burner total temperature is 1389 K (2500 °R). The burner has an efficiency of 91 percent and a total pressure ratio of 0.95, whereas the turbine has an efficiency of 85 percent. A converging nozzle is used, and its efficiency is 96 percent. The total pressure recovery for the diffuser is 0.92, and the shaft efficiency is 99.5%. The work coefficient for the propeller is 1.0079, and the propeller efficiency is 70 percent. Find the developed thrust and $TSFC$. Note that this is the same engine as in Example 2.7 with the exception of the nonideal effects. The work coefficient for the propeller matches that for Example 2.7.



SOLUTION:

DIFFUSER

The standard conditions at sea level are $T_a = 518.7^\circ\text{R}$ and $p_a = 14.69$ psia.

The speed of sound is

$$\begin{aligned} a_a &= \sqrt{\gamma_a \mathcal{R} T_a} = \sqrt{1.403 \times 287.1 \frac{\text{J}}{\text{kg-K}} \times 288.2 \text{ K} \times \frac{\text{N-m}}{\text{J}} \times \frac{\text{kg-m}}{\text{N-s}^2}} \\ &= 340.7 \text{ m/s (1118 ft/s)}, \end{aligned}$$

and so the freestream airspeed is

$$u_a = M_a a_a = 0.70 \times 340.7 \text{ m/s} = 238.4 \text{ m/s (782.3 ft/s)}.$$

Next

$$\frac{T_{ta}}{T_a} = 1 + \frac{\gamma_d - 1}{2} M_a^2 = 1 + \frac{1.4001 - 1}{2} \times 0.70^2 = 1.0980$$

$$\text{for } \gamma_d = 1.4001 \text{ and } M_a = 0.70,$$

and so the exit temperature of the diffuser is

$$T_{t2} = T_{ta} = 1.0980 \times 288.2 \text{ K} = 316.4 \text{ K (569.5 }^\circ\text{R)}.$$

Also

$$\frac{p_{ta}}{p_a} = \left[\frac{T_{ta}}{T_a} \right]^{\frac{\gamma_d}{\gamma_d - 1}} = [1.0980]^{1.4001} = 1.3871.$$

The pressure recovery factor for the diffuser is 0.92,

$$\text{and so } \frac{p_{t2}}{p_a} = \frac{p_{t2}}{p_{ta}} \frac{p_{ta}}{p_a} = \pi_d \frac{p_{ta}}{p_a} = 0.92 \times 1.3871 = 1.2762;$$

therefore, the diffuser exit total pressure is

$$p_{t2} = 1.2762 \times 101.3 \text{ kPa} = 129.3 \text{ kPa (18.75 psia)}.$$

COMPRESSOR

Next the total pressure ratio of the compressor is given as $\pi_c = 6.5$.

Thus, the total pressure exiting the compressor is

$$p_{t3} = \pi_c p_{t2} = 6.5 \times 129.3 \text{ kPa} = 840.2 \text{ kPa (121.9 psia)}.$$

Ideally, $\tau'_c = [\pi_c]^{\frac{\gamma_c - 1}{\gamma_c}} = [6.5]^{\frac{1.3882 - 1}{1.3882}} = 1.6879$ for $\gamma_c = 1.3882$ (iterative);

therefore, $T'_{t3} = \tau'_c T_{t2} = 1.6879 \times 316.4 \text{ K} = 534.1 \text{ K (961.3 }^\circ\text{R)}$,

but the compressor efficiency is given as

$$\eta_c = 0.88 = \frac{T'_{t3} - T_{t2}}{T_{t3} - T_{t2}} = \frac{534.1 \text{ K} - 316.4 \text{ K}}{T_{t3} - 316.4 \text{ K}}.$$

Thus, solving for T_{t3} , one finds the compressor total exit temperature is

$$T_{t3} = 563.7 \text{ K (1015 }^\circ\text{R)}.$$

PRIMARY COMBUSTOR

The total pressure ratio of the burner is given as 0.95.

Thus, the burner exit total pressure is $p_{t4} = \pi_b p_{t3} = 0.95 \times 840.2 \text{ kPa} = 798.2 \text{ kPa (115.8 psia)}$, and the energy analysis is

$$\Delta H \eta_b \dot{m}_f = \dot{m} c_{pb} (T_{t4} - T_{t3}) + \dot{m}_f c_{pb} T_{t4}.$$

However, $\eta_b = 91$ percent and $\Delta H = 43,960$ kJ/kg are given, and thus solving for the fuel mass flow rate yields

$$\begin{aligned}\dot{m}_f &= 13.61 \frac{\text{kg}}{\text{s}} \times 1.127 \frac{\text{kJ}}{\text{kg}\cdot\text{K}} \times \frac{(1389 - 563.7) \text{ K}}{0.91 \times 43960 \frac{\text{kJ}}{\text{kg}} - 1.127 \frac{\text{kJ}}{\text{kg}\cdot\text{K}} \times 1389 \text{ K}} \\ &= 0.3293 \text{ kg/s} (0.7261 \text{ lbm/s})\end{aligned}$$

where the burner specific heat is evaluated at the average burner temperature, which for this case is not an iteration. Obviously, no afterburner is present, and so this is also the total fuel flow rate (\dot{m}_f). Note also that $\dot{m}_f/\dot{m} = 0.02420$, which, as for all previous examples, is small.

TURBINE

The mechanical efficiency is given as 0.995, and so the shaft power balance

$$\dot{m} c_{pc}(T_{t3} - T_{t2}) + C_{wp} \dot{m} c_{pa} T_a = \eta_m \dot{m}_t c_{pt}(T_{t4} - T_{t5})$$

becomes, given that the work coefficient for the propeller is 1.0079,

$$\begin{aligned}13.61 \frac{\text{kg}}{\text{s}} \times 1.026 \frac{\text{kJ}}{\text{kg}\cdot\text{K}} (563.7 \text{ K} - 316.4 \text{ K}) \\ + 1.0079 \times 13.61 \frac{\text{kg}}{\text{s}} \times 0.9992 \frac{\text{kJ}}{\text{kg}\cdot\text{K}} \times 288.2 \text{ K} \\ = 0.995 \times \left(13.61 \frac{\text{kg}}{\text{s}} + 0.3293 \frac{\text{kg}}{\text{s}} \right) \times 1.164 \frac{\text{kJ}}{\text{kg}\cdot\text{K}} (1389 \text{ K} - T_{t5});\end{aligned}$$

thus, the turbine exit total temperature $T_{t5} = 930.3$ K (1674 °R). Again, the specific heat of the turbine is iteratively found for the average turbine temperature, but the turbine efficiency is defined as $\eta_t = \frac{T_{t4} - T_{t5}}{T_{t4} - T'_{t5}}$ and given as 85 percent:

$$0.85 = \frac{1389 \text{ K} - 930.3 \text{ °R}}{1389 \text{ K} - T'_{t5}}.$$

Thus, the ideal exit total temperature $T'_{t5} = 849.3$ K (1529 °R), and ideally

$$\tau'_t = \frac{T'_{t5}}{T_{t4}} = \frac{849.3}{1389} = 0.6115.$$

$$\text{Also } \tau'_t = [\pi_t]^{n-1},$$

and thus the turbine total pressure ratio is $\pi_t = [\tau'_t]^{1/n-1} = (0.6115)^{1.3272-1}$ and $\pi_t = 0.1360$ for $\gamma_t = 1.3272$ (evaluated at average turbine temperature). Finally the turbine exit total pressure is $p_{t5} = \pi_t p_{t4} = 0.1360 \times 798.2$ kPa = 108.6 kPa (15.75 psia), and since no mixer is present $T_{t5.5} = T_{t5} = 930.3$ K (1674 °R) and $p_{t5.5} = p_{t5} = 108.6$ kPa (15.75 psia).

PRIMARY NOZZLE

Since no afterburner is present, the inlet total temperature for the nozzle is

$$T_{t6} = T_{t5.5} = 930.3 \text{ K} (1674 \text{ °R}), \text{ and the inlet total pressure is}$$

$$p_{t6} = p_{t5.5} = 108.6 \text{ kPa} (15.75 \text{ psia}).$$

Because the engine has a fixed converging nozzle, one must first check to see if the nozzle is choked. For choking, the nozzle exit pressure is

$$p_8^* = p_{t6} \left[1 + \frac{1 - \gamma_n}{\gamma_n(1 + \gamma_n)} \right]^{1/\gamma_n};$$

thus, for $p_{t6} = 108.6$ kPa, $\eta_n = 0.96$ (given),
and $\gamma_n = 1.3453$ (iteratively found),

$$p_8^* = 108.6 \text{ psia} \times \left[1 + \frac{1 - 1.3453}{0.96 \times (1 + 1.3453)} \right]^{\frac{1.3453}{1.3453-1}}$$

$$= 56.76 \text{ kPa (8.232 psia)}.$$

However, since $p_a = 101.3$ kPa (14.69 psia), which is well above the choking condition p_8^* , the nozzle is not choked, and so the exit pressure matches the ambient pressure.

Therefore $p_8 = p_a = 101.3$ kPa (14.69 psia).

Ideally

$$T_8' = T_{t6} \left[\frac{p_8}{p_{t6}} \right]^{\frac{\gamma_n - 1}{\gamma_n}} = 930.3 \text{ K} \left[\frac{101.3 \text{ kPa}}{108.6 \text{ kPa}} \right]^{\frac{1.3453 - 1}{1.3453}} = 913.8 \text{ K (1645 }^\circ\text{R)};$$

thus $T_8 = T_{t6} - \eta_n (T_{t6} - T_8') = 930.3 \text{ K} - 0.96 (930.3 \text{ K} - 913.8 \text{ K})$
 $= 914.5 \text{ K (1646 }^\circ\text{R)}$

The nozzle exit velocity is given by

$$u_8 = \sqrt{2 c_{pn} (T_{t6} - T_8)},$$

and so the exit velocity is

$$u_8 = \sqrt{2 \times 1.118 \frac{\text{kJ}}{\text{kg-K}} \times (930.3 \text{ K} - 914.5 \text{ K}) \times 1000 \frac{\text{J}}{\text{kJ}} \times \frac{\text{N-m kg-m}}{\text{J N-s}^2}}$$

$$= 188.0 \text{ m/s (616.7 ft/s)}.$$

The speed of sound at the exit is $a_8 = \sqrt{\gamma_8 \mathcal{R} T_8}$,

and so

$$a_8 = \sqrt{1.3453 \times 287.1 \frac{\text{J}}{\text{kg-K}} \times 914.5 \text{ K} \times \frac{\text{N-m}}{\text{J}} \times \frac{\text{kg-m}}{\text{N-s}^2}}$$

$$= 594.2 \text{ m/s (1949 ft/s)};$$

thus, $M_8 = u_8/a_8 = 188.0 \text{ m/s}/594.2 \text{ m/s} = 0.3163$, which is well into the subsonic range.

From the continuity equation, the exit area is given by $A_8 = \frac{\dot{m}_8}{\rho_8 u_8}$, where \dot{m}_8 is the total mass flow rate at 8 and is given by $\dot{m}_8 = \dot{m}_{a8} + \dot{m}_{ft}$, and \dot{m}_{a8} is the air mass flow rate at 8 and is equal to \dot{m} , the ingested flow.

Thus $\dot{m}_{a8} = 13.61$ kg/s (30 lbm/s),

and the total mass flow rate at the exit is $\dot{m}_8 = 13.61 + 0.3293 = 13.93$ kg/s (30.73 lbm/s).

Because both T_8 and p_8 are known, ρ_8 is found from the ideal gas equation

$$\rho_8 = \frac{p_8}{\mathcal{R} T_8} = \frac{101.3 \text{ kPa} \times 1000 \frac{\text{Pa}}{\text{kPa}}}{287.1 \frac{\text{J}}{\text{kg-K}} \times 914.5 \text{ K}} \times \frac{\text{N}}{\text{Pa-m}^2} \times \frac{\text{J}}{\text{N-m}}$$

$$= 0.3860 \text{ kg/m}^3 (0.0007488 \text{ slug/ft}^3);$$

thus, the nozzle exit area is

$$A_8 = \frac{13.93 \frac{\text{kg}}{\text{s}}}{0.3860 \frac{\text{kg}}{\text{m}^3} \times 188.0 \frac{\text{m}}{\text{s}}}$$

$$= 0.1921 \text{ m}^2 (297.8 \text{ in.}^2).$$

TOTAL THRUST AND *TSFC*

The thrust is given by

$$F = \dot{m}_8 u_8 - \dot{m}_{a8} u_a + A_8 (p_8 - p_a) + C_{wp} \eta_p c_{pa} T_a \dot{m} / u_a;$$

thus,

$$\begin{aligned} F &= 13.93 \frac{\text{kg}}{\text{s}} \times 188.0 \frac{\text{m}}{\text{s}} \times \frac{\text{N}\cdot\text{s}^2}{\text{kg}\cdot\text{m}} - 13.61 \frac{\text{kg}}{\text{s}} \times 238.4 \frac{\text{m}}{\text{s}} \times \frac{\text{N}\cdot\text{s}^2}{\text{kg}\cdot\text{m}} \\ &+ 0.1921 \text{ m}^2 \times (101.3 \text{ kPa} - 101.3 \text{ kPa}) \times \frac{\text{N}\cdot\text{m}^2}{\text{Pa}} \times \frac{1000 \text{ Pa}}{\text{kPa}} \\ &+ \frac{1.0079 \times 0.70 \times 0.9992 \frac{\text{kJ}}{\text{kg}\cdot\text{K}} \times 288.2 \text{ K} \times 13.61 \frac{\text{kg}}{\text{s}} \times 1000 \frac{\text{N}\cdot\text{m}}{\text{kJ}}}{238.3 \frac{\text{m}}{\text{s}}}, \end{aligned}$$

where the propeller efficiency is 70 percent.

Therefore, $F = -626 \text{ N}$ (momentum) + 0 N (pressure) + $11,600 \text{ N}$ (propeller),
or $F = 10,970 \text{ N}$ (2467 lbf).

Note that the momentum thrust is negative.

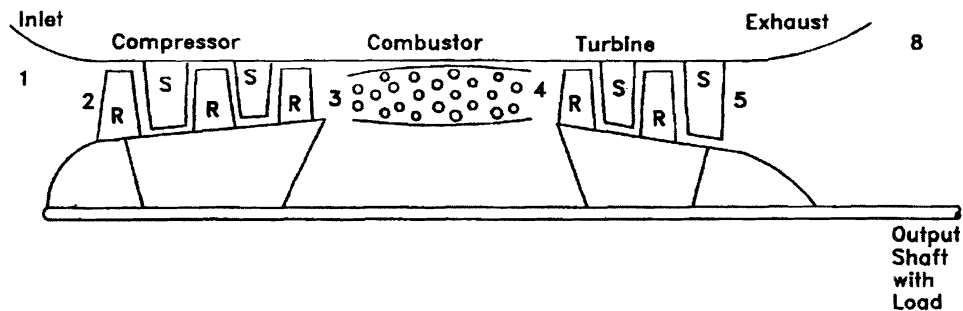
Finally, $TSFC = \dot{m}_f / F$;

thus

$$TSFC = \frac{0.3293 \frac{\text{kg}}{\text{s}}}{10,970 \text{ N}} \times 3600 \frac{\text{s}}{\text{h}} = 0.1081 \frac{\text{kg}}{\text{h}\cdot\text{N}} \left(1.060 \frac{\text{lbm}}{\text{h}\cdot\text{lbf}} \right)$$

By comparing these results with those of the ideal case (Example 2.7), one finds that the thrust is reduced by 46 percent and the *TSFC* is increased by 133 percent owing to the losses.

Example 3.5: A power-generation gas turbine approximating a modern moderate size unit operates at sea level. It ingests 66.67 kg/s (147 lbm/s) of air. The compressor operates with a pressure ratio of 18 and an efficiency of 88 percent. The fuel has a heating value of $42,800 \text{ kJ/kg}$ ($18,400 \text{ Btu/lbm}$), and the burner exit total temperature is 1456 K ($2620 \text{ }^\circ\text{R}$). The burner has an efficiency of 96 percent and a total pressure ratio of 0.96, whereas the turbine has an efficiency of 91.5 percent. The exhaust has a pressure ratio of 0.93. The total pressure recovery for the inlet is 0.98, and the shaft efficiency is 98 percent. Find the net output power, *SFC*, and net thermal efficiency.



SOLUTION:

INLET

First, flow is drawn into the gas turbine and accelerated to the inlet velocity from a stagnant condition far from the inlet. Because the velocity is zero far from the inlet, the ambient static and total pressures are equal ($p_{t_a} = p_a = 101.3 \text{ kPa}$), and the ambient static and total temperatures are equal ($T_{t_a} = T_a = 288.2 \text{ K}$). The process is also adiabatic;

thus, the exit total temperature is $T_{t_2} = T_{t_a} = 288.2 \text{ K}$ ($518.7 \text{ }^\circ\text{R}$).

Also, the inlet pressure recovery factor is 0.98,

and so the exit total pressure of the inlet is

$$p_{t_2} = \pi_1 p_{t_a} = 0.98 \times 101.3 \text{ kPa} = 99.27 \text{ kPa} (14.40 \text{ psia}).$$

COMPRESSOR

Next, the total pressure ratio of the compressor is given as $\pi_c = 18$.

Thus, the total pressure exiting the compressor is

$$p_{t_3} = \pi_c p_{t_2} = 18 \times 99.27 \text{ kPa} = 1787 \text{ kPa} (259.1 \text{ psia}).$$

Ideally, $\tau'_c = [\pi_c]^{1/\gamma_c} = [18]^{1/1.3836} = 2.2285$ for $\gamma_c = 1.3836$ (iteratively found); therefore, $T'_{t_3} = \tau'_c T_{t_2} = 2.2285 \times 288.2 \text{ K} = 642.2 \text{ K}$ ($1156 \text{ }^\circ\text{R}$),

but the compressor efficiency is given and

$$\eta_c = 0.88 = \frac{T'_{t_3} - T_{t_2}}{T_{t_3} - T_{t_2}} = \frac{642.2 \text{ K} - 288.2 \text{ K}}{T_{t_3} - 288.2 \text{ K}}.$$

Solving for T_{t_3} , one finds the compressor total exit temperature is

$$T_{t_3} = 690.5 \text{ K} (1243 \text{ }^\circ\text{R}).$$

COMBUSTOR

The total pressure ratio for the burner is 0.96.

Thus, the exit pressure is $p_{t_4} = \pi_b p_{t_3} = 0.96 \times 1787 = 1715 \text{ kPa}$ (248.8 psia), and the first law of thermodynamics yields

$$\Delta H \eta_b \dot{m}_f = \dot{m}_{c_{pb}} (T_{t_4} - T_{t_3}) + \dot{m}_f c_{pb} T_{t_4},$$

where the burner efficiency is 96% and the heating value is 42,800 kJ/kg. Solving for the fuel mass flow rate yields

$$\begin{aligned} \dot{m}_f &= 66.67 \frac{\text{kg}}{\text{s}} \times 1.147 \frac{\text{kJ}}{\text{kg-K}} \times \frac{(1456 - 690.5) \text{ K}}{0.96 \times 42800 \frac{\text{kJ}}{\text{kg}} - 1.147 \frac{\text{kJ}}{\text{kg-K}} \times 1456 \text{ K}} \\ &= 1.485 \text{ kg/s} (3.271 \text{ lbm/s}). \end{aligned}$$

No afterburner is present, and this is also the total fuel flow rate (\dot{m}_f).

Note that $\dot{m}_f/\dot{m} = 0.02227$, which is again small

EXHAUST

The gas velocity at the exhaust exit is very low, and thus the static and total pressures are equal ($p_{t_8} = p_8$).

Furthermore, since the velocity is small (subsonic), the exit and ambient pressures are the same ($p_8 = p_a$).

Thus, $p_{t_8} = p_a = 101.3 \text{ kPa}$.

Also, the pressure recovery for the exhaust is specified as 0.93

Thus, the inlet total pressure to the exhaust is

$$p_{t5} = p_{t8}/\pi_e = 101.3 \text{ kPa}/0.93 = 108.9 \text{ kPa (15.80 psia)}.$$

TURBINE

Because the inlet total pressure to the exhaust is the same as the exit total pressure for the turbine, the turbine total pressure ratio is

$$\pi_t = p_{t5}/p_{t4} = 108.9 \text{ kPa}/1715 \text{ kPa} = 0.06350.$$

Ideally the total temperature ratio is $\tau'_t = [\pi_t]^{n-1} = [0.06350]^{1.3297-1}$,

and thus $\tau'_t = 0.5047$ for $\gamma_t = 1.3298$ (iterative);

therefore, $T'_{t5} = \tau'_t T_{t4} = 0.5047 \times 1456 \text{ K} = 734.8 \text{ K (1322 }^\circ\text{R)}$,

but the turbine efficiency is $\eta_t = \frac{T_{t4} - T_{t5}}{T_{t4} - T'_{t5}}$ and is equal to 91.5 percent.

Thus,

$$0.915 = \frac{1456 \text{ K} - T_{t5}}{1456 \text{ K} - 734.8 \text{ K}}$$

The turbine exit total temperature $T_{t5} = 796.1 \text{ K (1433 }^\circ\text{R)}$.

NET POWER AND THERMAL EFFICIENCY

The power balance on the shaft is

$$\mathcal{P}_{\text{net}} = \eta_m \dot{m}_t c_{pt} (T_{t4} - T_{t5}) - \dot{m} c_{pc} (T_{t3} - T_{t2}),$$

or for a mechanical efficiency of 98 percent,

$$\begin{aligned} \mathcal{P}_{\text{net}} = & \left[0.98 \times (66.67 + 1.485) \frac{\text{kg}}{\text{s}} \times 1.157 \frac{\text{kJ}}{\text{kg-K}} \times (1456 - 796.1) \text{ K} \right. \\ & \left. - 66.67 \frac{\text{kg}}{\text{s}} \times 1.035 \frac{\text{kJ}}{\text{kg-K}} \times (690.5 - 288.2) \text{ K} \right] \times \frac{\text{kW}}{\text{kJ/s}}. \end{aligned}$$

The net power from the gas turbine that can be used for electric generation or other applications is

$$\mathcal{P}_{\text{net}} = 23,240 \text{ kW} = 23.24 \text{ MW (31,140 hp)}.$$

The overall thermal efficiency is $\eta_{\text{th}} = \frac{\mathcal{P}_{\text{net}}}{Q_{\text{in}}}$,

where the heat in is

$$\begin{aligned} Q_{\text{in}} = \dot{m}_f \Delta H &= 1.485 \frac{\text{kg}}{\text{s}} \times 42,800 \frac{\text{kJ}}{\text{kg}} \times \frac{\text{kW}}{\text{kJ/s}} \\ &= 63,560 \text{ kW} = 63.56 \text{ MW (85180 hp)} \end{aligned}$$

or $\eta_{\text{th}} = 23,240 \text{ kW}/63,560 \text{ kW} = 0.366$ or 36.6 percent.

Next, the heat rate is defined as $HR = \frac{\dot{m}_f \Delta H}{\mathcal{P}_{\text{net}}}$,

and so

$$HR = \frac{1.485 \frac{\text{kg}}{\text{s}} \times 42800 \frac{\text{kJ}}{\text{kg}} \times 3600 \frac{\text{s}}{\text{h}}}{23240 \text{ kW}} = 9845 \frac{\text{kJ}}{\text{kW-h}} \left(6959 \frac{\text{Btu}}{\text{hp-h}} \right).$$

Finally, the specific fuel consumption is defined as $SFC = \frac{\dot{m}_f}{\mathcal{P}_{\text{net}}}$,

and so

$$SFC = \frac{1.485 \frac{\text{kg}}{\text{s}}}{23,240 \text{ kW}} \times 3600 \frac{\text{s}}{\text{h}} = 0.2303 \frac{\text{kg}}{\text{kW-h}} \left(0.378 \frac{\text{lbm}}{\text{hp-h}} \right)$$

By comparing these results with those of the ideal case (Example 2.8), one can see that the net power is decreased by 22.7 percent and the SFC is increased by 53.7 percent. Furthermore, the overall thermal efficiency for the ideal case was 56.2 percent compared with the current value of 36.6 percent. Obviously, the losses have significantly reduced the effectiveness of the gas turbine.

3.4. Use of Cycle Analysis in Preliminary Design

Thus far in this chapter, the concept of cycle analysis has been presented and used in examples as a method of directly analyzing engines with given parameters. In fact, the method in practice can be used to perform a preliminary design analysis of an advanced engine (or gas turbine) or an engine that has just hit the drawing boards. For example, for a jet engine, a set of overall engine design conditions are first given to an engine manufacturer by a military group or commercial enterprise including, but not exclusively, thrusts and *TSCs* at different altitudes. A group of system design engineers then uses a cycle analysis to vary the engine types and component parameters parametrically to accomplish the overall design goals and to ensure that all of the components fit together. For example, the derived turbine power must match the compressor power requirements. The final sets of component parameters determined by this group then become the design goals of the more focused or specific component design groups – for example, compressor design or turbine design groups. To accomplish these component goals, detailed analyses and designs of the components are undertaken using methods presented in the next seven chapters. Such design methodology is a part of an “inverse” system design; that is, one starts with the overall design goals and works backward to determine the “inputs” or component characteristics that accomplish the goals. This is the first step in an industrial engine or gas turbine design. The software, “JETENGINECYCLE” or “POWERGTCYCLE”, are particularly useful in parametrically varying the design parameters.

3.5. Summary

In this chapter, nonideal effects have been included in the cycle analyses. First, the physical phenomena that contribute to the component losses were discussed. Next, one- and two-term specifiable losses and efficiencies were included in the operating equations and thermodynamic processes for all of the components in the different engine types: diffuser, compressor, fan, turbine, propeller, shaft, combustor, afterburner, primary nozzle, fan nozzle, bypass duct, bypass mixer, and power turbine exhaust. Enthalpy–entropy diagrams for the different components were presented showing the thermodynamic effects of losses. For the compressor and turbine, two different efficiencies were defined and discussed (conventional and polytropic). For the duct and mixer flow, stability was addressed. Simple models of losses for the components were chosen so that cycle analyses could be easily accomplished but would still enable the reader to make realistic predictions of engine performance. Also, the *h*–*s* diagrams were presented for the nonideal components. In addition, nonideal gas effects were included with the addition of variable specific heats for the different components. Next, components were assembled to determine the nonideal cycle performance of different gas turbine types. For nonideal cases, closed-form equations are not possible for the thrust and *TSC* as they are for the ideal cases. Four quantitative jet engine and one power gas turbine examples were presented in which the solutions were attained by stepping through the engines component by component. All cases were iterative in that specific heats were not known a priori. Also, one of the problems (mixed turbofan) was iterative

because the fan total pressure ratio was not known a priori. Although the examples required iteration methods, such iterations should not mask the purpose of the examples and should not dominate any problem solutions. Reasonable estimates can be made for any of the component properties for trend analyses and preliminary designs. Some trend studies were also presented, which resulted in the same tendencies as those found in the ideal cases (but quantitatively different). Also some component variations were performed to identify the corresponding effects on engine performance. For all four jet engine cases, the thrusts were significantly lower than for the corresponding ideal cases covered in Chapter 2. Inversely, the values of *TSFC* were significantly higher than in the ideal cases.

In this chapter, all of the component characteristics were considered to be known so that the overall engine parameters could be determined. This is not necessarily the case, however. Thus, in Chapters 4 through 10 tools will be developed to predict individual component characteristics.

Moreover, at this point the reader has a significant collection of analyses that can be used for the preliminary design of an engine as a system at selected operating points by using inverse design methodology. That is, one can parametrically study the effects of modifying components, component efficiencies, and engine types for different operating conditions until the engine design goals have been met. Thus, realistic comparisons can easily be accomplished for the engine as a system, and the desired operating conditions of the different components can be specified, which is the first step in industrial engine design.

List of Symbols

A	Area
a	Speed of sound
c_p	Specific heat at constant pressure
c_v	Specific heat at constant volume
C_{wp}	Propeller work coefficient
F	Force (thrust)
f	Fuel ratio
h	Specific enthalpy
ΔH	Heating value
HR	Heat rate
\dot{m}	Mass flow rate
M	Mach number
n	Number of stages
p	Pressure
\mathcal{P}	Power
\mathcal{R}	Ideal gas constant
s	Entropy
SFC	Specific fuel consumption
T	Temperature
$TSFC$	Thrust-specific fuel consumption
u	Specific internal energy
v	Specific volume
α	Bypass ratio
γ	Specific heat ratio
η	Efficiency

π	Total pressure ratio
ρ	Density
σ	Split ratio
τ	Total temperature ratio

Subscripts

a	Freestream
a	Due to air component only
ab	Afterburner
b	Primary burner
c	Compressor
d	Diffuser
e	Exit
f	Fan
f	Fuel
fn	Fan nozzle
m	Mechanical (shaft)
m	Mixer
mc	Mixer – core side
mu	Mixer – duct side
n	Nozzle
n	Net
o	Outside of diffuser
p	Propeller
p	Polytropic (small stage)
pc	Polytropic – compressor
pt	Polytropic – turbine
r	Recovery
ss	Single stage
t	Total (stagnation)
t	Total (summation)
t	Turbine
u	Duct
x	Inlet to single stage
y	Exit of single stage
1..9	Positions in engine

Superscripts

'	Ideal
*	Choked

Problems

- 3.1** The Mach number of a ramjet is 2.88, the external temperature is 400 °R, and the external pressure is 3.80 psia. The flow rate of air through the engine is 85 lbm/s. Because of the thermal limits of the materials, the burner exit total temperature is 3150 °R. The heating value of the fuel is 17,900 Btu/lbm. The efficiencies of the burner and converging nozzle are 89 and 93 percent, respectively. The total pressure ratios for the diffuser and burner are 0.94 and

- 0.93, respectively. What are the developed thrust, fuel ratio and *TSFC* for this engine?
- 3.2 A turbojet ingests 192 lbm/s of air at an altitude of 22,000 ft. It flies at a Mach number of 0.88, and the compressor pressure ratio is 17. The fuel has a heating value of 17,900 Btu/lbm, and the burner exit total temperature is 2350 °R. The efficiencies of the compressor, burner, turbine, shaft, and converging nozzle are 89, 95, 87, 99.7, and 97 percent, respectively. The total pressure ratios for the diffuser and burner are 0.93 and 0.93, respectively. Find the developed thrust and *TSFC*.
- 3.3 A turbojet with an afterburner flies at 22,000 ft with a Mach number of 0.88. It ingests 192 lbm/s of air, and the compressor pressure ratio is 17. The fuel has a heating value of 17,900 Btu/lbm. The primary burner and afterburner exit total temperatures are 2350 °R and 2980 °R, respectively. The efficiencies of the compressor, burner, turbine, shaft, and converging nozzle are 89, 95, 87, 99.7, and 97 percent, respectively. The total pressure ratios for the diffuser and burner are 0.93 and 0.93, respectively. The afterburner has an efficiency of 91% and a total pressure ratio of 0.97 (a) Find the developed thrust and *TSFC*. (b) Compare these values to those that would be obtained for the same engine without an afterburner.
- 3.4 A turbojet operates at 22,000 ft at Mach 0.89. The compressor pressure ratio is 13. The fuel has a heating value of 18,100 Btu/lbm, and the exit total temperature from the burner is 2475 °R. The airflow is 124 lbm/s. All of the aerodynamic efficiencies and recovery factors are 0.90 except for the shaft efficiency (99.4%). The nozzle is variable and converging–diverging (to match the exit pressure to the ambient pressure). Find the developed thrust and the *TSFC*.
- 3.5 Consider the turbojet above in Problem 3.4 and find what the performance would be if each component could be independently improved. That is, find the thrust and *TSFC* for the following independent conditions (where all other conditions are as in the previous problem): (a) compressor efficiency is 95 percent; (b) turbine efficiency is 95 percent; (c) burner efficiency is 95 percent; (d) burner total pressure ratio is 95 percent (e) diffuser recovery factor is 0.95 (f) nozzle efficiency is 95 percent. Where should the most money be spent in trying to improve the overall engine performance?
- 3.6 A turbofan with the fan fully exhausted operates at 20,000 ft at Mach 0.82. The compressor pressure ratio is 16, and the fan pressure ratio is 2.2. The fuel has a heating value of 17,700 Btu/lbm, and the exit total temperature from the burner is 2450 °R. The core airflow is 144 lbm/s, and the bypass ratio is 1.4. The compressor, burner, turbine, fan, shaft, primary variable converging–diverging nozzle (to match the exit pressure to the ambient pressure), and fan converging nozzle have efficiencies of 89, 94, 87, 88, 99.4, 97, and 95 percent, respectively. The diffuser and burner have total pressure ratios of 0.94 and 0.92, respectively. Find the developed thrust and the *TSFC*.
- 3.7 A turbofan with the fan fully exhausted operates at 15,000 ft at a Mach number of 0.93. The compressor and fan pressure ratios are 17 and 2.3, respectively. The core airflow rate is 143 lbm/s, and the bypass ratio is 1.1. The fuel has a heating value of 17,900 Btu/lbm, and the combustor exit total temperature

is 2550 °R. An afterburner is on the core and, when lit, results in a total temperature of 3200 °R in the nozzle. The compressor, burner, turbine, fan, shaft, converging primary nozzle, variable converging–diverging fan nozzle (to match the exit pressure to the ambient pressure), and afterburner have efficiencies of 90, 95, 84, 87, 99.2, 95, 97, and 90 percent, respectively. The diffuser, burner, and afterburner have total pressure ratios of 0.91, 0.94, and 0.97, respectively. Find the thrust and *TSFC* for both (a) nonafterburning and (b) afterburning conditions. (c) Compare the values found with those with the engine with no afterburner.

- 3.8** A turbofan with the fan fully mixed operates at 22,000 ft at Mach 0.89. The compressor pressure ratio is 13. The fuel has a heating value of 18,100 Btu/lbm, and the exit total temperature from the burner is 2475 °R. The core airflow is 124 lbm/s, and the bypass ratio is 1.15. All of the aerodynamic efficiencies and recovery factors are 0.90 except for the shaft efficiency (99.4%), and the duct and mixer total pressure ratios (0.985 and 0.975, respectively). The nozzle is variable and converging–diverging (to match the exit pressure to the ambient pressure). Find the developed thrust and the *TSFC*. What is the fan pressure ratio?
- 3.9** Consider the turbofan above in Problem 3.8 and find what the performance would be if each component could be independently improved. That is, find the thrust and *TSFC* for the following independent conditions (where all other conditions are as in the preceding problem): (a) compressor efficiency is 95 percent; (b) fan efficiency is 95 percent; (c) turbine efficiency is 95 percent; (d) burner efficiency is 95 percent; (e) burner total pressure ratio is 95 percent; (f) diffuser recovery factor is 0.95; (g) nozzle efficiency is 95%. Where should the most money be spent in trying to improve the overall engine performance?
- 3.10** A turbofan with the fan fully mixed operates at 22,000 ft at Mach 0.89. The compressor pressure ratio is 13. The fuel has a heating value of 18,100 Btu/lbm, and the exit total temperature from the burner is 2475 °R. The core airflow is 124 lbm/s, and the bypass ratio is 5.00. All of the aerodynamic efficiencies and recovery factors are 0.90 except for the shaft efficiency (99.4%), and the duct and mixer total pressure ratios (0.985 and 0.975, respectively). The nozzle is variable and converging–diverging (to match the exit pressure to the ambient pressure). Find the developed thrust and the *TSFC*. What is the fan pressure ratio?
- 3.11** Consider the turbofan above in Problem 3.10 and find what the performance would be if each component could be independently improved. That is, find the thrust and *TSFC* for the following independent conditions (where all other conditions are as in the preceding problem): (a) compressor efficiency is 95 percent; (b) fan efficiency is 95 percent; (c) turbine efficiency is 95 percent; (d) burner efficiency is 95 percent; (e) burner total pressure ratio is 95 percent; (f) diffuser recovery factor is 0.95; (g) nozzle efficiency is 95 percent. Where should the most money be spent in trying to improve the overall engine performance?
- 3.12** A turbofan with the fan fully mixed operates at 27,500 ft at Mach 0.93. The compressor pressure ratio is 17. The fuel has a heating value of 18,100

- Btu/lbm, and the exit total temperature from the burner is 2230 °R. The core airflow is 157 lbm/s, and the bypass ratio is 1.60. An afterburner is also used. When lit, the afterburner total exit temperature is 3300 °R. The compressor, burner, turbine, fan, shaft, variable converging–diverging primary nozzle (to match the exit pressure to the ambient pressure), and afterburner have efficiencies of 88, 95, 86, 91, 99.3, 94, and 90 percent, respectively. The diffuser, burner, and afterburner have total pressure ratios of 0.93, 0.91, and 0.96, respectively. Find the developed thrust and the *TSFC* for both when the afterburner is on and when it is off. What is the fan pressure ratio?
- 3.13** A turbofan with a split ratio of 0.5 operates at 27,500 ft at Mach 0.93. The compressor pressure ratio is 17. The fuel has a heating value of 18,100 Btu/lbm, and the exit total temperature from the burner is 2230 °R. The core airflow is 157 lbm/s, and the bypass ratio is 1.60. An afterburner is also used. When lit, the afterburner total exit temperature is 3300 °R. The compressor, burner, turbine, fan, shaft, variable converging–diverging primary nozzle, variable converging–diverging fan nozzle (both to match the exit pressure to the ambient pressure), and afterburner have efficiencies of 88, 95, 86, 91, 99.3, 94, 94, and 90 percent, respectively. The diffuser, burner, and afterburner have total pressure ratios of 0.93, 0.91, and 0.96, respectively. Find the developed thrust and the *TSFC* for when the afterburner is on and when it is off. What is the fan pressure ratio?
- 3.14** A turboprop is used to power an aircraft at 7000 ft. It flies at Mach 0.45, and the compressor pressure ratio is 5.4. The airflow rate is 19 lbm/s. The turbine inlet total temperature is 2278 °R, and the heating value of the fuel is 18,400 Btu/lbm. The work coefficient of the propeller is 0.85. The compressor, burner, turbine, shaft, converging primary nozzle, and propeller have efficiencies of 90, 95, 87, 99.6, 97, and 82 percent, respectively. The diffuser and burner have total pressure ratios of 0.93 and 0.93, respectively. Find the thrust, horsepower, exit Mach number, and *TSFC*.
- 3.15** A turbofan with the fan fully exhausted operates at 22,000 ft at Mach 0.89. The compressor pressure ratio is 13, and the fan pressure ratio is 1.6097. The fuel has a heating value of 18,100 Btu/lbm, and the exit total temperature from the burner is 2475 °R. The core airflow is 124 lbm/s, and the bypass ratio is 5.00. All of the aerodynamic efficiencies and recovery factors are 0.90 except for the shaft efficiency (99.4%). The nozzles are both variable and converging–diverging (to match the exit pressure to the ambient pressure). Find the developed thrust and the *TSFC*.
- 3.16** Consider the turbofan above in Problem 3.15 and find when the performance would be if each component could be independently improved. That is, find the thrust and *TSFC* for the following independent conditions (where all other conditions are as in the preceding problem): (a) compressor efficiency is 95%; (b) fan efficiency is 95%; (c) turbine efficiency is 95%; (d) burner efficiency is 95%; (e) burner total pressure ratio is 95%; (f) diffuser recovery factor is 0.95; (g) primary nozzle efficiency is 95%; (h) fan nozzle efficiency is 95%. Where should the most money be spent in trying to improve the overall engine performance?

- 3.17** A turboprop is used to power an aircraft at 3800 ft. It flies at Mach 0.38, and the compressor pressure ratio is 4.75. The airflow rate is 22 lbm/s. The turbine inlet total temperature is 2445 °R, and the heating value of the fuel is 17,850 Btu/lbm. The work coefficient of the propeller is 0.89. The compressor, burner, turbine, shaft, converging primary nozzle, and propeller have efficiencies of 89, 94, 91, 99.6, 96 and 78 percent, respectively. The diffuser and burner have total pressure ratios of 0.94 and 0.92, respectively. Find the thrust, horsepower, exit Mach number, and *TSFC*.
- 3.18** A turbofan with the fan fully mixed operates at an external pressure of 2.99 psia and a temperature of 383.2 °R at Mach 0.87. The compressor pressure ratio is 19.5. The fuel has a heating value of 17,900 Btu/lbm, and the exit total temperature from the burner is 2480 °R. The core airflow is 155 lbm/s, and the bypass ratio is 3.50. The aerodynamic efficiencies of the compressor, fan, turbine, burner, and nozzle are 88, 87, 91, 92, and 95 percent, respectively. The recovery factor for the diffuser is 0.93, and the burner has a total pressure ratio of 0.94. The shaft efficiency is 99.7 percent, and the duct and mixer total pressure ratios are 0.99 and 0.99, respectively. The nozzle is variable and converging–diverging (to match the exit pressure to the ambient pressure). Find the developed thrust and the *TSFC*. What is the fan total pressure ratio?
- 3.19** A turbofan with the fan fully exhausted operates at an external pressure of 2.99 psia and a temperature of 383.2 °R at Mach 0.87. The compressor pressure ratio is 19.5, and the fan pressure ratio is 2.14. The fuel has a heating value of 17,900 Btu/lbm, and the exit total temperature from the burner is 2480 °R. The core airflow is 155 lbm/s, and the bypass ratio is 3.50. The aerodynamic efficiencies of the compressor, fan, turbine, burner, primary nozzle, and fan nozzle are 88, 87, 91, 92, 95, and 95 percent, respectively. The recovery factor for the diffuser is 0.93 and the burner has a total pressure ratio of 0.94. The shaft efficiency is 99.7 percent. The nozzles are both variable and converging–diverging (to match the exit pressure to the ambient pressure). Find the developed thrust and the *TSFC*.
- 3.20** A turbofan with the fan fully exhausted operates at an external pressure of 2.99 psia and a temperature of 383.2 °R at Mach 0.87. The compressor pressure ratio is 19.5. The fuel has a heating value of 17,900 Btu/lbm, and the exit total temperature from the burner is 2480 °R. The core airflow is 155 lbm/s, and the bypass ratio is 3.50. The aerodynamic efficiencies of the compressor, fan, turbine, burner, primary nozzle, and fan nozzle are 88, 87, 91, 92, 95, and 95 percent, respectively. The recovery factor for the diffuser is 0.93, and the burner has a total pressure ratio of 0.94. The shaft efficiency is 99.7 percent. The nozzles are both variable and converging–diverging (to match the exit pressure to the ambient pressure). What is the optimal fan total pressure ratio to maximize the thrust? Find the optimum developed thrust and the *TSFC*.
- 3.21** For a turbojet, the compressor operates with a pressure ratio of 14 and an efficiency of 0.88, and the inlet total temperature to the compressor is 700 °R. The total airflow is 100 lbm/s. The burner has an efficiency of 0.85 and a pressure ratio of 0.93. The fuel has a heating value of 18,000 Btu/lbm and flows at 2.0 lbm/s. The turbine pressure ratio is 0.164, and it has an

efficiency of 0.83. The mechanical efficiency of the shaft system is 0.98. Assume $\gamma_c = 1.40$, $c_{pb} = 0.29$ Btu/lbm-°R, $\gamma_t = 1.33$.

- What is the exit total temperature of the compressor?
- What is the exit total temperature of the burner?
- What is the exit total temperature of the turbine?
- What is the power (hp) delivered to the compressor from the turbine?

3.22 A ramjet cruises at an external pressure of 0.895 psia and a temperature of 304.7 °R, and the Mach number is 5.0. The flow rate of air through the engine is 140 lbm/s. Because of the thermal limits of the materials, the burner exit total temperature is 3300 °R. The heating value of the fuel is 18,500 Btu/lbm. The efficiencies of the burner and converging nozzle are 94 and 96 percent, respectively. The total pressure ratios for the diffuser and burner are 0.90 and 0.92, respectively. The specific heat ratios for the ambient, diffuser, burner, and nozzle are 1.415, 1.347, 1.312, and 1.281, respectively. The specific heats at constant pressure are 0.234, 0.266, 0.288, and 0.313 Btu/lbm-°R, respectively.

- What are the developed thrust, fuel ratio, and *TSFC* for this engine?
- If the performance is poor, which component should be changed and how?

3.23 A high-bypass turbofan engine with the fan exhausted is to be analyzed. The core or primary flow has an afterburner. The fan does not have an afterburner. The fan has 2 stages and the compressor has 10; the turbine has 4 stages. The shaft operates at 10,500 rpm. The engine performance at 10,000 ft on a standard day is to be considered.

$\dot{m} = 75$ lbm/s (primary)	$\gamma_d = 1.40$
$\dot{m}_f = 1.74$ lbm/s	$\gamma_f = 1.40$
$\alpha = 3.2$	$\gamma_c = 1.38$
$\Delta H = 17,700$ Btu/lbm	$\gamma_b = 1.33$
$p_a = 10.11$ psia	$\gamma_t = 1.33$
$T_a = 483$ °R	$\gamma_{ab} = 1.32$
$\pi_f = 2.40$	$\gamma_n = 1.28$
$\pi_c = 22.0$ (includes fan)	$\eta_c = 0.89$
$T_{t6} = 3200$ °R	$\eta_b = 0.93$
$T_{t7} = 690$ °R	$\eta_t = 0.86$
$M_a = 0.66$	$\eta_{ab} = 0.88$
	$\eta_m = 0.995$
variable converging–diverging nozzle	$p_8/p_a = 1.00$
primary exhaust nozzle	$\eta_n = 0.97$
converging fan nozzle	$\eta_{fn} = 0.92$
engine mass = 2550 lbm	$\pi_{ab} = 0.98$
$N = 10,500$ rpm	$\pi_b = 0.95$
	$\pi_d = 0.92$

- Sketch the engine and clearly indicate the station numbers.
- What is the exit total temperature of the compressor?
- What is the exit total temperature of the primary burner if the total temperature at the exit of the compressor is 1322 °R?
- If the total temperature out of the primary combustor is 2650 °R and the total temperature at the exit of the compressor is 1322 °R, what is the total pressure out of the turbine?

- (e) If the total temperature into the afterburner is 1510 °R and the total pressure is 15.7 psia, what is the velocity exiting the primary nozzle?
- (f) What is the pressure at the exit of the fan nozzle?
- (g) What is the efficiency of the fan?
- 3.24** All of the following apply to the same turbojet.
- (a) A compressor operates with a pressure ratio of 14 and an efficiency of 0.88. The inlet total temperature is 700 °R. What is the exit total temperature? Assume $\gamma = 1.40$.
- (b) The airflow rate of a turbojet is 100 lbm/s. Air enters the burner at 1100 °R (total) temperature. The burner has an efficiency of 0.85 and a pressure ratio of 0.93. The fuel has a heating value of 18,000 B/lbm and flows at 2.0 lbm/s. Assume $c_p = 0.29$ Btu/lbm-°R. What is the exit total temperature?
- (c) The turbine pressure ratio is 0.30, and the turbine has an efficiency of 0.83. The incoming total temperature is 2100 °R, and the mechanical efficiency of the shaft system is 0.98. How much power is delivered to the compressor (hp) if the airflow rate of a turbojet is 100 lbm/s? Assume $c_p = 0.276$ Btu/lbm-°R and $\gamma = 1.33$.
- 3.25** You are to analyze the following engines for an aircraft flying at $M_a = 0.8$ at sea level on a standard day. The exit burner total temperature is 3000 °R, and the compressor pressure ratio is 16. Assume all aerodynamic efficiencies and recovery factors are 0.90 and that $\pi_b = 0.90$. Assume mechanical efficiencies of 1.00. For each engine, indicate clearly on a diagram where each of the different nonideal effects takes place. Consider thrust and *TSFC* for the following engines with converging nozzles and with compressor flow rates of 150 lbm/s and $\Delta H = 18,000$ Btu/lbm. Compute the overall performance by computing the performance of each component and compare with the performance for the ideal case.
- (a) Turbojet
- (b) Turbofan with mixed auxiliary flow, $\alpha = 1$. What is π_f ?
- (c) Turbofan with afterburner with mixed auxiliary flow, $\alpha = 1$, total afterburner temperature is 4200 °R, and $\pi_{ab} = 0.9$. What is π_f ?
- 3.26** Consider the turbojet above in Problem 3.25 and decide if the performances of different components could be independently improved. Again find the thrust and *TSFC* for the following independent conditions:
- (a) $\eta_c = 0.95$
- (b) $\eta_t = 0.95$
- (c) $\eta_b = 0.95$
- (d) $\pi_b = 0.95$
- (e) $\pi_d = 0.95$
- (f) $\eta_n = 0.95$
- Where should the most money be spent in trying to improve overall engine performance?
- 3.27** Consider the mixed turbofan with no afterburner above in Problem 3.25 and decide if the performances of different components could be independently improved. Again find the thrust and *TSFC* for the following independent conditions:
- (a) $\eta_c = 0.95$
- (b) $\eta_t = 0.95$

- (c) $\eta_f = 0.95$
- (d) $\eta_b = 0.95$
- (e) $\pi_b = 0.95$
- (f) $\pi_d = 0.95$
- (g) $\eta_n = 0.95$

Where should the most money be spent in trying to improve overall engine performance?

3.28 A turbofan with the fan fully mixed operates at 28,000 ft (4.77 psia and 418.9 °R) at Mach 0.79. The compressor pressure ratio is 19.5. The fuel has a heating value of 17,800 Btu/lbm, and the exit total temperature from the burner is 2750 °R. The core airflow is 152 lbm/s, and the bypass ratio is 3.4. The fuel flow to core airflow ratio is 0.0273. The compressor, burner, fan, shaft, and converging nozzle have efficiencies of 88, 94, 87, 99.6, and 95 percent, respectively. The diffuser, burner, duct, and mixer have total pressure ratios of 0.97, 0.93, 1.00, and 0.98, respectively. The specific heat ratios for the diffuser, compressor, fan, burner, turbine, mixer, and nozzle are 1.405, 1.387, 1.402, 1.333, 1.312, 1.384, and 1.383, respectively. The specific heats at constant pressure for the compressor, fan, turbine, burner, nozzle, and mixer are 0.246, 0.239, 0.283, 0.275, 0.248, and 0.247 Btu/lbm-°R, respectively. Solve the following five problems, which are independent of each other. Note that information given in each part does not necessarily apply to other parts.

- (a) If the inlet total temperature to the compressor is 471.8 °R and the inlet total pressure is 6.99 psia, what is the exit total temperature of the compressor?
- (b) If the inlet total pressure to the nozzle is 15.17 psia and the inlet total temperature is 892.0 °R, what is the thrust?
- (c) If the fan total pressure ratio is 2.21 and the turbine efficiency increases by 0.03 (3%), will the fan total pressure ratio increase, remain constant, or decrease? Why?
- (d) If the exit total temperature of the fan is 610.0 °R, the exit total pressure of the fan is 15.48 psia, and the exit total temperature of the turbine is 1772 °R, what are the total exit pressure and temperature from the mixer?
- (e) If the exit total pressures from the fan and compressor are 15.48 psia and 136.4 psia and the exit total temperatures from the fan and compressor are 610.0 °R and 1164 °R, what is the turbine efficiency?

3.29 You are to analyze a modern dual-spool turbofan engine with an afterburner. The fan has three stages, operates at 9600 rpm, and is driven by a two-stage low-pressure turbine. The high-pressure compressor has 10 stages, operates at 14,650 rpm, and is driven by a two-stage high-pressure turbine. You are to analyze its performance at 20,000 ft on a standard day. You may assume frictional losses exist in the bypass duct that reduce the fan exit total pressure to that equal to the low-pressure turbine exit pressure. The engine is shown below, and the following parameters are given:

$$\begin{aligned} \dot{m}_t &= 228 \text{ lbm/s} \\ \alpha &= 0.7 \text{ (bypass ratio)} \\ \Delta H &= 18,400 \text{ Btu/lbm} \\ p_a &= 6.76 \text{ psia} \\ T_a &= 447 \text{ °R} \end{aligned}$$

$$\begin{aligned} \gamma_d &= 1.40 \\ \gamma_s = \gamma_{c \text{ high}} &= 1.40 \\ \gamma_b = \gamma_{ab} &= 1.30 \\ \gamma_{t \text{ low}} = \gamma_{t \text{ high}} &= 1.30 \\ \gamma_n &= 1.30 \end{aligned}$$

$\pi_f = 2.10$	$\pi_d = 0.96$
$\pi_{c \text{ high}} = 11.2$	$\eta_b = 0.88$
$T_{t4} = 2300^\circ\text{R}$	$\pi_b = 0.93$
$T_{t3} = 1376^\circ\text{R}$	$\eta_{t \text{ high}} = 0.83$
$T_{t2.5} = 646^\circ\text{R} = T_{t7}$	$\eta_{t \text{ low}} = 0.78$
$M_a = 0.85$	$\eta_{ab} = 0.87$
	$\pi_{ab} = 0.92$
variable converging–diverging nozzle	$p_8/p_a = 1.00$
exhaust nozzle	$\eta_n = 0.97$
$N_{c \text{ high}} = 14,650 \text{ rpm}$	$N_{c \text{ low}} = 9600 \text{ rpm}$
Engine mass = 3000 lbm	

- If all stages in the high-pressure compressor have the same single-stage total pressure ratio, what is it?
- What is the efficiency of the high-pressure compressor?
- What is the primary fuel flow rate (lbm/s)?
- What is the high-pressure turbine exit total pressure? What is the low-pressure turbine exit total pressure?

Note: All four parts can be worked on independently.

- 3.30** An engine similar in size to an older nonafterburning turbojet ingests 120 lbm/s of air at sea level. When it flies at a Mach number of 0.00 (take-off, maximum power), the compressor pressure ratio is 14.6. The fuel has a heating value of 17,800 Btu/lbm, and the burner exit total temperature is 2580 °R. The efficiencies of the compressor, burner, turbine, shaft, and variable converging–diverging nozzle (to match the exit pressure to the ambient pressure) are 90, 95, 92, 100, and 96 percent, respectively. The total pressure ratios for the diffuser and burner are 0.97 and 0.95, respectively. The test stand thrust and *TSFC* were experimentally determined to be 11,200 lbf, and 0.89 lbm/h-lbf. Write a computer program to calculate the specific heat and specific heat ratio for each component at the average component temperature (iterative) and then predict the developed thrust and *TSFC*.
- 3.31** If all of the characteristics of the engine in Problem 3.30 at SLTO are held constant, except the compressor pressure ratio, vary this ratio to optimize the SLTO thrust.
- 3.32** A turbofan with the fan fully mixed operates at 32,000 ft (3.98 psia and 404.6 °R) at Mach 1.40. The compressor pressure ratio is 20.0. The fuel has a heating value of 17,800 Btu/lbm, the exit total temperature from the burner is 2850 °R, and the fuel flow ratio is 0.0257. The core airflow is 175 lbm/s, and the bypass ratio is 0.95. The turbine, burner, fan, shaft, and variable converging–diverging nozzle (to match the exit pressure to the ambient pressure) have efficiencies of 91, 93, 89, 100, and 95 percent, respectively. The diffuser, burner, duct, and mixer have total pressure ratios of 0.92, 0.90, 1.00, and 1.00, respectively. The specific heat ratios for the diffuser, compressor, fan, burner, turbine, mixer, and nozzle are 1.400, 1.378, 1.394, 1.326, 1.314, 1.384, and 1.357, respectively. The specific heats at constant pressure for the compressor, fan, turbine, burner, nozzle, and mixer are 0.250, 0.243, 0.287, 0.279, 0.260, and 0.247 Btu/lbm-°R, respectively. Solve the following six

parts, which are independent of each other. Note that information given in each part does not necessarily apply to other parts.

- (a) If the inlet total temperature to the compressor is 563.4 °R, the exit total temperature is 1399.4 °R, and the inlet total pressure is 11.64 psia, what is the efficiency of the compressor?
- (b) If the inlet total pressure to the nozzle is 35.72 psia and the inlet total temperature is 1416 °R, what is the thrust?
- (c) If the fan total pressure ratio is 3.07 and the compressor efficiency increases by 0.06 (6%), will the fan total pressure ratio increase, remain constant, or decrease? Why?
- (d) If the exit total temperature of the fan is 799.4 °R, the exit total pressure of the fan is 35.72 psia, and the exit total temperature of the turbine is 1955 °R, what is the total exit pressure from the mixer?
- (e) If the exit total temperature of the fan is 799.4 °R, the exit total pressure of the fan is 35.72 psia, and the exit total temperature of the turbine is 1955 °R, what is the total exit temperature from the mixer?
- (f) If the exit total pressure from the compressor is 232.8 psia, and the exit total temperatures from the fan and compressor are 799.4 °R and 1399 °R, respectively, what is the turbine exit total pressure?

- 3.33** You are to pick an engine for a transport aircraft flying at $M_a = 0.8$ at sea level on a standard day. The exit burner total temperature is 3000 °R, and $\Delta H = 18,000$ Btu/lbm. The air mass flow rate in the core is 180 lbm/s. Use a nonideal cycle analysis and compare the results with those obtained from the ideal analysis. Nonideal parameters for the different engine types are listed below.

$\pi_d = 0.92$	$\eta_c = 0.91$	$\pi_{ab} = 0.98$
$\eta_b = 0.93$	$\eta_f = 0.90$	$\eta_{ab} = 0.92$
$\pi_b = 0.96$	$\eta_t = 0.93$	$\pi_{duct} = 0.99$
nozzles all converging	$\eta_m = 0.996$	$\pi_{mixer} = 0.98$
$\eta_n = 0.97$	$\eta_{fn} = 0.96$	

- (a) Find the dimensionless quantity $F/\dot{m}_t a_{at}$ and the dimensional quantities F and $TSFC$ for the following engines:
 - (1) Ramjet
 - (2) Turbojet $\pi_c = 16$
 - (3) Turbojet with afterburner $\pi_c = 16$; total afterburner temperature is 4200 °R
 - (4) Turbofan with exhausted fan $\pi_c = 16$, $\pi_f = 4.0$, $\alpha = 1$
 - (5) Turbofan with mixed secondary flow and with afterburner $\pi_c = 16$, $\alpha = 1$; total afterburner temperature is 4200 °R. What is π_f ?
 - (b) Which engine will you choose and why?
- 3.34** A turbojet ingests 180 lbm/s of air at an altitude of 27,000 ft. It flies at Mach 0.85, and the compressor pressure ratio is 15.2. The fuel has a heating value of 17,800 Btu/lbm, and the fuel ratio is 0.026. The efficiencies of the compressor, burner, turbine, shaft, and converging nozzle are 89, 95, 91, 99.6, and 96 percent, respectively. The total pressure ratios for the diffuser and burner are 0.96 and 0.95, respectively. Find the developed thrust and $TSFC$.

- 3.35 Draw a general h - s diagram for a turbofan engine, which has an afterburner for the core flow, with a totally exhausted fan (see Fig. 2.46). Draw this to scales that show the correct relative magnitudes; that is, be careful to show reasonable relative pressures and enthalpies for the different components. Show all points (a, 1, 2, 3, 4, 5, 6, 7, 8, and 9) as well as static and total pressures. Show both the ideal and nonideal cases.
- 3.36 A ground-based gas turbine with characteristics approximating those of a modern moderate size unit and used for power generation ingests 147 lbm/s of air at standard sea level. The compressor pressure ratio is 18, whereas the fuel has a heating value of 18,400 Btu/lbm, and the burner exit total temperature is 2620 °R. The efficiencies of the compressor, burner, turbine, and shaft are 88, 96, 91.5, and 98 percent, respectively. The total pressure ratios for the inlet, burner, and exhaust are 0.98, 0.96 and 0.93, respectively. Find the overall thermal efficiency, developed net power output, heat rate (total input energy per unit time), and specific fuel consumption (SFC, fuel rate per unit net power output).
- 3.37 A turbofan with the fan fully mixed operates at sea level takeoff. The compressor pressure ratio is 18. The fuel has a heating value of 17,800 Btu/lbm, and the exit total temperature from the burner is 2850 °R. The core airflow is 150 lbm/s, and the bypass ratio is 0.80. The aerodynamic efficiencies of the compressor, fan, turbine, burner, and nozzle are 89, 90, 92, 95, and 96 percent, respectively. The recovery factor for the diffuser is 0.95, and the burner has a total pressure ratio of 0.94. The shaft efficiency is 99.8 percent, and the duct and mixer total pressure ratios are 0.99 and 0.99, respectively. The nozzle is variable and converging-diverging (to match the exit pressure to the ambient pressure). Find the developed thrust and the *TSFC*. What is the fan total pressure ratio?
- 3.38 A turbofan with the fan fully exhausted operates at sea level takeoff. The fan pressure ratio is 3.90. The fuel has a heating value of 17,800 Btu/lbm, and the exit total temperature from the burner is 2850 °R. The core airflow is 150 lbm/s, and the bypass ratio is 0.80. The aerodynamic efficiencies of the compressor, fan, turbine, burner, primary nozzle, and fan nozzle are 89, 90, 92, 95, 96, and 95 percent, respectively. The recovery factor for the diffuser is 0.95, and the burner has a total pressure ratio of 0.94. The shaft efficiency is 99.8 percent. The primary nozzle is variable and converging-diverging (to match the exit pressure to the ambient pressure), whereas the fan nozzle is fixed and converging. Vary the compressor pressure ratio and find the optimum developed thrust and the corresponding *TSFC*.
- 3.39 A turbofan with the fan fully exhausted operates at sea level takeoff. The compressor pressure ratio is 18. The fuel has a heating value of 17,800 Btu/lbm, and the exit total temperature from the burner is 2850 °R. The core airflow is 150 lbm/s, and the bypass ratio is 0.80. The aerodynamic efficiencies of the compressor, fan, turbine, burner, primary nozzle, and fan nozzle are 89, 90, 92, 95, 96, and 95 percent, respectively. The recovery factor for the diffuser is 0.95, and the burner has a total pressure ratio of 0.94. The shaft efficiency is 99.8 percent. The primary nozzle is variable and converging-diverging (to match the exit pressure to the ambient pressure), whereas the fan nozzle is fixed and converging.

- (a) Vary the fan pressure ratio and find the optimum developed thrust and the corresponding *TSFC*.
- (b) For a fan pressure ratio equal to that in Problem 3.37, what are the thrust and *TSFC*? Why are these different from those found in Problem 3.37?
- 3.40** A turbofan with the fan fully exhausted operates at sea level takeoff. The compressor pressure ratio is 18, and the fan pressure ratio is 3.90. The fuel has a heating value of 17,800 Btu/lbm, and the exit total temperature from the burner is 2850 °R. The core airflow is 150 lbm/s. The aerodynamic efficiencies of the compressor, fan, turbine, burner, primary nozzle, and fan nozzle are 89, 90, 92, 95, 96, and 95 percent, respectively. The recovery factor for the diffuser is 0.95 and the burner has a total pressure ratio of 0.94. The shaft efficiency is 99.8 percent. The primary nozzle is variable and converging–diverging (to match the exit pressure to the ambient pressure), whereas the fan nozzle is fixed and converging. Vary the bypass ratio and find the optimum *TSFC* and corresponding thrust.
- 3.41** A turbojet flies at sea level at a Mach number of 0.75. It ingests 165 lbm/s (74.83 kg/s) of air. The compressor operates with an efficiency of 88 percent. The fuel has a heating value of 17,800 Btu/lbm (41,400 kJ/kg), and the burner total temperature is 2500 °R (1389 K). The burner has an efficiency of 91 percent and a total pressure ratio of 0.95, whereas the turbine has an efficiency of 85 percent. A converging nozzle is used, and the nozzle efficiency is 96 percent. The total pressure recovery for the diffuser is 0.92, and the shaft efficiency is 99.5 percent. Find and plot the developed nondimensional thrust and *TSFC* for compressor pressure ratios of 10 to 20. Note that this is the same engine as in Example 3.1 with the exception of the compressor pressure ratio.
- 3.42** A turbofan flies at sea level at Mach 0.75. It ingests 74.83 kg/s (165 lbm/s) of air to the core. The compressor operates with a pressure ratio of 15 and an efficiency of 88 percent. The engine has a split ratio of 0.25. The efficiency of the fan is 90 percent. The fuel has a heating value of 41,400 kJ/kg (17,800 Btu/lbm), and the burner total temperature is 1389 K (2500 °R). The burner has an efficiency of 91 percent and a total pressure ratio of 0.95, whereas the turbine has an efficiency of 85 percent. The duct has a total pressure ratio of 0.98, and the total pressure ratio of the mixer is 0.97. A variable converging–diverging nozzle (to match the exit pressure to the ambient pressure) is used for the primary nozzle, and the efficiency is 96 percent. A converging nozzle is used for the fan nozzle, and the efficiency is 95 percent. The total pressure recovery for the diffuser is 0.92, and the shaft efficiency is 99.5 percent. The Mach numbers at the turbine and duct exits are nearly the same. Find and plot the developed nondimensional thrust and *TSFC* for bypass ratios of 1 to 6. Note that this is the same engine as in Example 3.3 with the exception of the bypass ratio.
- 3.43** Draw a general *h*–*s* diagram for an afterburner-equipped turbofan engine with a totally mixed fan (see Fig. 2.55). Draw this to scales that show the correct relative magnitudes; that is, be careful to show reasonable relative pressures and enthalpies for the different components. Show all points (a, 1, 2, 3, 4, 5, 5.5, 6, 7, 7.5, and 8) and show both static and total pressures. Show both ideal and nonideal cases.

- 3.44 A low-bypass afterburning turbofan engine with the fan mixed is to be analyzed. The fan has 2 stages, and the compressor has 12; the turbine has 5 stages. The engine mass is 2950 lbm. The shafts operate at 8500 and 11,500 rpm. The engine performance at 37,000 ft on a standard day is to be considered. The following details are known:

$\dot{m} = 140$ lbm/s (core)	$\gamma_d = 1.40$
$\dot{m}_{fab} = 9.121$ lbm/s	$\gamma_s = 1.39$
$\alpha = 0.7$	$\gamma_c = 1.38$
$\Delta H = 17,800$ Btu/lbm	$\gamma_b = 1.33$
$p_a = 3.14$ psia	$\gamma_t = 1.31$
$T_a = 387$ °R	$\gamma_{ab} = 1.31$
$a_a = 968$ ft/s	$\gamma_n = 1.27$
$M_a = 1.40$	$\eta_c = 0.90$
$T_{16} = 3500$ °R	$\eta_b = 0.95$
$T_{17} = 817$ °R	$\eta_t = 0.93$
$T_{14} = 2800$ °R	$\eta_{ab} = 0.90$
$T_{13} = 1272$ °R	$\eta_m = 0.995$
$p_{12} = 9.19$ psia	$p_8/p_a = 5.61$
$p_{17} = 34.92$ psia	$\eta_n = 0.96$ (fixed converging)
Thrust (afterburner on) = 23,250 lbf	$\pi_d = 0.92$
Thrust (afterburner off) = 11,120 lbf	$\pi_{ab} = 0.96$
	$\pi_b = 0.93$

- What is the exit total pressure of the compressor?
 - What is the fuel flow rate of the primary burner?
What is the *TSFC* with the afterburner on?
What is the *TSFC* with the afterburner off?
 - What is the dimensionless thrust with the afterburner on?
 - What is the exit total temperature of the turbine if the fuel flow rate is negligible?
 - What is the efficiency of the fan?
 - What type of application do you expect this engine to have? Why (list specific reasons)?
- 3.45 A ramjet cruises at 251 °R and 0.324 psia at a Mach number of 4.0. The flow rate of air through the engine is 190 lbm/s. The fuel ratio is 0.0457 and is used because of the thermal limits of the nozzle materials. The heating value of the fuel is 18,000 Btu/lbm. The efficiencies of the burner and converging nozzle are 91 and 95 percent, respectively. The total pressure ratios for the diffuser and burner are 0.92 and 0.88, respectively. The specific heat ratios for the ambient, diffuser, burner, and nozzle are 1.418, 1.377, 1.320, and 1.274, respectively. The specific heats at constant pressure are 0.233, 0.250, 0.283, and 0.319 Btu/lbm-°R, respectively. Find the burner exit total temperature, developed thrust, and *TSFC*.
- 3.46 A turbojet flies at sea level at Mach 0.75. It ingests 165 lbm/s (74.83 kg/s) of air. The compressor operates with a compressor pressure ratio of 15 and an efficiency of 88 percent. The fuel has a heating value of 17,800 Btu/lbm (41,400 kJ/kg), and the burner total temperature is 2500 °R (1389 K). The burner has an efficiency of 91 percent and a total pressure ratio

of 0.95, whereas the turbine has an efficiency of 85 percent. A converging nozzle is used, and the nozzle efficiency is 96 percent. The total pressure recovery for the diffuser is 0.92, and the shaft efficiency is 99.5 percent. Find the developed nondimensional thrust and *TSFC* for two independent conditions: (a) the compressor efficiency is increased by three points, and (b) the turbine efficiency is increased by three points. Which is more effective in improving performance? One should note that this is the same engine as in Example 3.1 with the exception of the compressor and turbine efficiencies.

- 3.47** A turbofan flies at sea level at a Mach number of 0.75. It ingests 74.83 kg/s (165 lbm/s) of air to the core. The compressor operates with a pressure ratio of 15 and an efficiency of 88 percent. The engine has a bypass ratio of 3 and a split ratio of 0.25. The efficiency of the fan is 90 percent. The fuel has a heating value of 41,400 kJ/kg (17,800 Btu/lbm), and the burner total temperature is 1389 K (2500 °R). The burner has an efficiency of 91 percent and a total pressure ratio of 0.95, whereas the turbine has an efficiency of 85 percent. The duct has a total pressure ratio of 0.98, and the total pressure ratio of the mixer is 0.97. A variable converging–diverging nozzle (to match the exit pressure to the ambient pressure) is used for the primary nozzle, and the efficiency is 96 percent. A converging nozzle is used for the fan nozzle, and the efficiency is 95 percent. The total pressure recovery for the diffuser is 0.92, and the shaft efficiency is 99.5 percent. The Mach numbers at the turbine and duct exits are nearly the same. Find the developed nondimensional thrust and *TSFC* for two independent conditions: (1) the compressor efficiency is increased by three points and (2) the turbine efficiency is increased by three points. Which is more effective in improving performance? One should note that this is the same engine as in Example 3.3 with the exception of the compressor and turbine efficiencies.
- 3.48** You are to choose an engine for takeoff from an aircraft carrier on a standard day. The exit burner total temperature is 2600 °R, and $\Delta H = 17,900$ Btu/lbm. The air mass flow rate in the core is 230 lbm/s. Use a nonideal cycle analysis and compare the results with those from the ideal analysis. Nonideal parameters for the different engine types are listed below.

$$\begin{array}{lll} \pi_d = 0.94 & \eta_c = 0.92 & \pi_{ab} = 0.98 \\ \eta_b = 0.93 & \eta_f = 0.91 & \eta_{ab} = 0.92 \\ \pi_b = 0.96 & \eta_t = 0.94 & \pi_u = 0.99 \\ \text{nozzles all converging} & \eta_m = 0.995 & \pi_m = 0.98 \\ \eta_n = 0.96 & \eta_{fn} = 0.97 & \end{array}$$

- (a) Find the dimensionless quantity $F/\dot{m}_t a_a$ and the dimensional quantities F and *TSFC* for the following engines:
- (1) Ramjet
 - (2) Turbojet $\pi_c = 23.5$
 - (3) Turbojet with afterburner $\pi_c = 23.5$;
total afterburner temperature is 3900 °R
 - (4) Turbofan with exhausted fan $\pi_c = 23.5$, $\pi_f = 1.98$, $\alpha = 5.0$
 - (5) Turbofan with mixed secondary flow and with afterburner
 $\pi_c = 23.5$, $\alpha = 0.7$; total afterburner temperature is 3900 °R.

What is π_f ?

(b) Which engine will you choose and why?

- 3.49** A high-bypass afterburning turbofan engine with the fan exhausted is to be analyzed. The fan has one stage and the compressor has 14; the turbine has 4 stages. The primary airflow is 144 lbm/s, and the bypass ratio is 4.40. The engine mass is 4540 lbm. The primary burner fuel mass flow rate is 3.62 lbm/s. The inlet and exit total temperatures for the compressor are 529 and 1268 °R, respectively. The inlet total temperature for the fan is 529 °R. The exit total temperatures for the primary burner and turbine are 2770 and 1783 °R, respectively. The thrust without the afterburner is 15,760 lbf, and the total temperature into the primary nozzle is 1783 °R. The thrust with the afterburner is 22,110 lbf, and the total temperature into the primary nozzle is 3850 °R. The total pressure ratio for the primary burner and afterburners are 0.95 and 0.97, respectively. The efficiencies for the primary burner and afterburners are 97 and 90 percent, respectively. The heat of reaction of the fuel is 17,800 Btu/lbm. Both nozzles are converging; the primary and fan nozzles have efficiencies of 97 and 96 percent, respectively. The inlet and exit total pressures to the turbine are 215.0 and 28.4 psia, respectively. The efficiencies of the fan and compressor are 89 and 90 percent, respectively. The recovery factor for the diffuser is 0.96, and the shaft mechanical efficiency is 99.7 percent. The shafts operate at 7400 and 10,900 rpm. The engine performance at a Mach number of 0.90 at 18,000 ft on a standard day ($p_a = 7.33$ psia, $T_a = 455$ °R, $a_a = 1047$ ft/s) is to be considered. The following specific heat ratios are known:

$\gamma_d = 1.40$	$c_{pd} = 0.2390$ Btu/lbm-°R
$\gamma_s = 1.40$	$c_{ps} = 0.2401$ Btu/lbm-°R
$\gamma_c = 1.38$	$c_{pc} = 0.2477$ Btu/lbm-°R
$\gamma_b = 1.33$	$c_{pb} = 0.2762$ Btu/lbm-°R
$\gamma_t = 1.32$	$c_{pt} = 0.2832$ Btu/lbm-°R
$\gamma_{ab} = 1.30$	$c_{pab} = 0.2985$ Btu/lbm-°R
$\gamma_n = 1.26$	$c_{pn} = 0.3301$ Btu/lbm-°R
$\gamma_{fn} = 1.40$	$c_{pfn} = 0.2412$ Btu/lbm-°R

- What is the total pressure ratio of the fan (afterburner on)?
 - What is the fuel flow rate of the afterburner when lit?
What is the *TSFC* with the afterburner on?
 - What is the dimensionless thrust with the afterburner off?
 - What is the efficiency of the turbine (afterburner on)?
 - What is the exit velocity from the primary nozzle (afterburner on)?
- 3.50** Draw a general h - s diagram for a turbojet engine that has a lit afterburner (see Fig. 2.38). Draw this to scales that show the correct relative magnitudes; that is, be careful to show reasonable relative pressures and enthalpies for the different components. Show all points (a, 1, 2, 3, 4, 5, 6, and 8) as well as static and total pressures. Show only the nonideal case.
- 3.51** A high-bypass turbofan engine with the fan exhausted is to be analyzed. The core or primary flow has an afterburner. The fan does not have an afterburner. The fan has 2 stages, and the compressor has 10; the turbine has 4 stages. The single-shaft operates at 10,500 rpm. The engine performance at 10,000 ft on a standard day is to be considered.

Overall

$\dot{m} = 75 \text{ lbm/s (core)}$	$T_a = 483 \text{ }^\circ\text{R}$	$p_a = 10.10 \text{ psia}$
$M_a = 0.66$	$\eta_m = 0.995$	Thrust = 8894 lbf
engine mass = 2550 lbm	$N = 10,500 \text{ rpm}$	

Diffuser

$\pi_d = 0.92$	$\gamma_d = 1.40$	$c_{pd} = 0.240 \text{ Btu/lbm-}^\circ\text{R}$
----------------	-------------------	---

Compressor

$\pi_c = 22.0 \text{ (includes fan)}$	$\gamma_c = 1.38$	$c_{pc} = 0.248 \text{ Btu/lbm-}^\circ\text{R}$
---------------------------------------	-------------------	---

 $\eta_c = 0.89$ *Fan*

$\pi_f = 2.40$	$\gamma_f = 1.40$	$c_{pf} = 0.240 \text{ Btu/lbm-}^\circ\text{R}$
----------------	-------------------	---

 $\alpha = 3.2$ $T_{t7} = 687 \text{ }^\circ\text{R}$ *Burner*

$\dot{m}_f = 1.74 \text{ lbm/s}$	$\gamma_b = 1.33$	$c_{pb} = 0.275 \text{ Btu/lbm-}^\circ\text{R}$
----------------------------------	-------------------	---

 $\Delta_H = 17,700 \text{ Btu/lbm}$ $\eta_b = 0.93$ $\pi_b = 0.95$ *Turbine*

$\eta_t = 0.86$	$\gamma_t = 1.33$	$c_{pt} = 0.278 \text{ Btu/lbm-}^\circ\text{R}$
-----------------	-------------------	---

Afterburner

$\dot{m}_{fab} = 2.52 \text{ lbm/s}$	$\gamma_{ab} = 1.32$	$c_{pab} = 0.285 \text{ Btu/lbm-}^\circ\text{R}$
--------------------------------------	----------------------	--

 $T_{t6} = 3200 \text{ }^\circ\text{R}$ $\eta_{ab} = 0.88$ $\pi_{ab} = 0.98$ *Primary Nozzle*

variable converging-diverging

 $p_8/p_a = 1.00$ $\eta_n = 0.97$ $\eta_n = 1.28$ $c_{pn} = 0.310 \text{ Btu/lbm-}^\circ\text{R}$ *Fan Nozzle*

converging

 $\eta_{fn} = 0.92$ $\gamma_{fn} = 1.39$ $c_{pfn} = 0.243 \text{ Btu/lbm-}^\circ\text{R}$

- What is the exit total temperature of the compressor?
- What is the exit total temperature of the primary burner if the total temperature at the exit of the compressor is 1321 °R?
- If the total temperature out of the primary combustor is 2650 °R and the total temperature at the exit of the compressor is 1321 °R, what is the total pressure out of the turbine?
- What is the *TSFC*?
- What is the pressure at the exit of the fan nozzle?
- What is the efficiency of the fan?

All parts can be worked independently.

- 3.52 A transport craft with a nonideal engine is to fly at Mach 0.80 at sea level on a standard day. The burner exit total temperature is 2400 °R, and the core airflow rate is 180 lbm/s. The fuel has a heating value of 17,900 Btu/lbm. Nonideal parameters for the different engine types are listed below.

$\pi_d = 0.94$	$\eta_c = 0.90$	$\pi_{ab} = 0.98$
$\eta_b = 0.93$	$\eta_f = 0.89$	$\eta_{ab} = 0.91$
$\pi_b = 0.95$	$\eta_t = 0.92$	$\pi_u = 0.99$
$\eta_m = 0.997$		$\pi_m = 0.98$
fan nozzle converging		primary nozzle converging-diverging
$\eta_{fn} = 0.96$		$\eta_n = 0.98$

- (a) Find the thrust, dimensionless thrust, and *TSFC* for the following engines:
- (1) Ramjet
 - (2) Turbojet $\pi_c = 13$
 - (3) Turbojet with afterburner $\pi_c = 13$;
total afterburner exit temperature is 3800 °R
 - (4) Turbofan with mixed auxiliary air $\pi_c = 13$, $\alpha = 1.4$;
What is π_f ?
 - (5) Turbofan with the fan all exhausted $\pi_c = 13$, $\alpha = 1.4$;
 π_f is the same as for the mixed case
 - (6) Turbofan with an afterburner and mixed auxiliary air
 $\pi_c = 13$, $\alpha = 1.4$;
total afterburner exit temperature is 3800 °R.
- (b) Which engine would you choose and why?
- 3.53** The following are from a mixed turbofan with a bypass ratio of 0.55:
- (a) A compressor operates with an inlet total temperature of 518 °R and an exit total temperature of 1252 °R. The inlet total pressure is 12.5 psia, and the exit total pressure is 237.5 psia. The specific heat ratio is 1.3834.
 - (1) What is the compressor efficiency?
 - (2) If the input power remains constant, the inlet total conditions remain constant, and the efficiency is raised to 100 percent, what is the exit total pressure of the compressor?
 - (b) A turbine operates with an inlet total temperature of 2860 °R and an inlet total pressure of 230.4 psia. The compressor and fan have inlet total temperatures of 518 °R. The compressor and fan have exit total temperatures of 1252 and 815 °R, respectively. The core mass flow rate is 190 lbm/s, and the fuel flow rate is 5.4 lbm/s. The turbine efficiency is 90 percent, and the shaft mechanical efficiency is 99.9 percent. The specific heat ratio of the compressor, fan, and turbine are 1.3834, 1.3949, and 1.3109, respectively. The specific heats at constant pressure for the compressor, fan, and turbine are 0.2474, 0.2422, and 0.2891 Btu/lbm-°R, respectively.
 - (1) Find the exit total pressure of the turbine.
 - (c) At 10,000 ft, the net thrust with an afterburner lit is 34,240 lbf. The primary burner fuel flow rate is 5.4 lbm/s, and the afterburner fuel flow is 13.1 lbm/s. The core flow rate is 190 lbm/s. The inlet total temperature to the nozzle is 3860 °R, and the inlet total pressure to the nozzle is 54.0 psia.
 - (1) Find the nondimensional thrust.
 - (2) Find the *TSFC*.
- 3.54** An exhausted turbofan with a bypass ratio of 0.80 at SLTO has the following components. The core mass flow rate is 150 lbm/s.
- (a) The compressor operates with an inlet total temperature of 519 °R and an exit total temperature of 1235 °R. The inlet total pressure is 13.96 psia, and the efficiency is 89 percent. The specific heat ratio is 1.3838. What is the total exit total pressure from the compressor? If the input power remains constant, the inlet total conditions remain constant, and the efficiency is raised to 100 percent, what is the exit total pressure of the compressor?

- (b) The turbine operates with an inlet total temperature of 2850 °R and an inlet total pressure of 236.1 psia. The compressor and fan have inlet total temperatures of 519 °R. The compressor and fan have exit total temperatures of 1235 and 790 °R, respectively. The fuel flow rate is 4.2 lbm/s. The turbine exit total pressure is 53.9 psia, and the shaft mechanical efficiency is 99.8 percent. The specific heat ratio of the compressor, fan, and turbine are 1.3838, 1.3955, and 1.3119, respectively. The specific heats at constant pressure for the compressor, fan, and turbine are 0.2472, 0.2419, and 0.2884 Btu/lbm-°R, respectively. Find the efficiency of the turbine. If the turbine efficiency is raised to 100 percent, what percent increase of power to the fan and compressor will result for the same turbine inlet total pressure and temperature and the same turbine exit total pressure?
- (c) The thrust from the primary nozzle of an exhausted turbofan (with an afterburner off) is 13,212 lbf. The primary burner fuel flow rate is 4.16 lbm/s. The core flow rate is 150 lbm/s. The inlet total temperature to the variable converging-diverging primary nozzle is 2074 °R, and the inlet total pressure to the primary nozzle is 53.9 psia; the efficiency is 96 percent, the specific heat ratio is 1.3278, and the exit velocity is 2757 ft/s. The inlet total temperature to the converging fan nozzle is 790 °R, and the inlet total pressure to the fan nozzle is 54.4 psia; the efficiency is 95 percent and the specific heat ratio is 1.3883. Find the nondimensional thrust. Find the *TSFC*.
- 3.55** An aircraft with an afterburning turbojet engine cruises at 866 ft/s with the ambient pressure at 5.45 psia and ambient temperature at 429.6 °R. The engine has the components listed below. The core mass flow rate is 210 lbm/s.
- (a) The compressor operates with an inlet total temperature of 492.3 °R and an exit total temperature of 1187 °R. The inlet total pressure is 8.22 psia, and the total pressure ratio is 19.0. The specific heat ratio is 1.3857. What is the efficiency of the compressor?
- (b) The afterburner operates with an inlet total temperature of 2171 °R, an inlet total pressure of 50.95 psia, an efficiency of 92 percent, and a total pressure ratio of 0.99. The primary burner fuel flow rate is 5.59 lbm/s, and the afterburner fuel flow rate is 6.29 lbm/s. The specific heat at constant pressure for the afterburner is 0.3012 Btu/lbm-°R, and the heating value of the fuel is 17,800 Btu/lbm. Find the exit total temperature of the afterburner.
- (c) The turbine operates with an inlet total temperature of 2750 °R and an inlet total pressure of 150.0 psia. The compressor has an inlet total temperature of 492.3 °R and an exit total temperature of 1187 °R. The core mass flow rate is 210 lbm/s, and the fuel flow rate is 5.59 lbm/s. The turbine exit total pressure is 51.0 psia, and the shaft mechanical efficiency is 99.8 percent. The specific heat ratios of the compressor, and turbine are 1.3857 and 1.3119, respectively. The specific heats at constant pressure for the compressor, and turbine are 0.2463 and 0.2883 Btu/lbm-°R, respectively. Find the efficiency of the turbine.
- 3.56** An aircraft powered by a turbofan with the fan exhausted cruises at 993 ft/s with the ambient pressure at 10.10 psia and ambient temperature at 483 °R.

The engine has the components listed below. The core mass flow rate is 255 lbm/s, and the primary burner fuel flow rate is 6.64 lbm/s.

- (a) The turbine operates with an inlet total temperature of 2950 °R and an exit total temperature of 2094 °R. The inlet total pressure is 411, psia, and the total pressure ratio is 0.205. The specific heat ratio is 1.310. What is the efficiency of the turbine?
 - (b) The primary combustor operates with an inlet total temperature of 1434 °R, an inlet total pressure of 419 psia, an efficiency of 96 percent, and a total pressure ratio of 0.98. The specific heat at constant pressure is 0.281 Btu/lbm-°R, and the heating value of the fuel is 17,900 Btu/lbm. Find the exit total temperature of the combustor.
 - (c) The turbine operates with an inlet total temperature of 2950 °R and an exit total temperature of 2094 °R; the inlet total pressure is 411 psia. The compressor has an inlet total temperature of 565 °R and an exit total temperature of 1434 °R; the inlet total pressure is 16.8 psia. The fan has an inlet total temperature of 565 °R, an inlet total pressure of 16.8 psia, and an exit total pressure of 37.7 psia. The bypass ratio is 0.95, and the shaft mechanical efficiency is 99.8%. The specific heat ratios of the fan, compressor, and turbine are 1.396, 1.378, and 1.310, respectively. The specific heats at constant pressure for the fan, compressor, and turbine are 0.242, 0.250, and 0.290 Btu/lbm-°R, respectively. Find the efficiency of the fan.
- 3.57** A new commercial aircraft is to be designed to fly routinely at 36,000 ft at an air speed of 826 ft/s. Owing to expected drag characteristics of the airframe, two engines are needed, and the required thrust is 42,500 lbf per engine. Fuel economy considerations dictate that the engines need to operate with *TSFC* values of 0.62 lbm/h-lbf. The limit on the exit temperature of the burner is 2950 °R. Design an engine for this application.
- 3.58** A new military fighter aircraft is to be designed to fly routinely at a variety of altitudes. One particular condition is at 20,000 ft at an air speed of 935 ft/s. Owing to expected drag characteristics of the airframe, two engines are needed, and the required thrust is 16,500 lbf per engine. Engine weight considerations dictate that the engines need to operate with nondimensional thrusts of 1.90 and with a *TSFC* value of 0.92 lbm/h-lbf. Moreover, since the aircraft is a fighter craft, short increases in thrust for rapid acceleration to supersonic speeds are required to a total of 31,500 lbf per engine. The limits on the exit temperatures of the primary burner and afterburner are 3000 and 3600 °R, respectively. Design an engine for this application and these conditions.
- 3.59** A ground-based gas turbine with regeneration (Fig. 1.13.a), which is used for electric power generation, ingests 132 lbm/s of air at standard sea level. The compressor pressure ratio is 15.6, the fuel has a heating value of 18,000 Btu/lbm, and the burner exit total temperature is 2477 °R. The efficiencies of the compressor, burner, turbine, and shaft are 87.7, 91, 92, and 99.5 percent, respectively. The total pressure ratios for the inlet, burner, and exhaust are 0.983, 0.967 and 0.979, respectively. The total pressure ratios for both paths (3–3x, and 5–5x) of the regenerator are 0.991 (owing to total pressure losses from friction), and the regenerator effectiveness is 0.75. The specific heat

ratios for the compressor, burner, turbine, inlet, and exhaust are 1.385, 1.335, 1.334, 1.400, and 1.366, respectively. The specific heats for paths (3-3x, and 5-5x) of the regenerator are 0.257 and 0.258 Btu/lbm-°R, respectively. Find

- (a) overall thermal efficiency
- (b) developed net power output
- (c) specific fuel consumption (SFC, fuel rate per unit net power output).

For reference, if all component efficiencies and their effectiveness are unity and no irreversible pressure losses occur, the results are 56.1 percent, 36,660 hp, and 0.252 lbm/hp-h.

3.60 Before reaching altitude, an aircraft powered by a turbofan with the fan totally mixed flies at 540 ft/s with the ambient pressure at 10.10 psia and ambient temperature at 483 °R. The core mass flow rate is 195 lbm/s, and the primary burner fuel flow rate is 5.18 lbm/s. The bypass ratio is 0.75.

- (a) The turbine operates with an inlet total temperature of 2850 °R and an efficiency of 93 percent. The turbine inlet total pressure is 281.9 psia. The turbine specific heat ratio is 1.314, and the specific heat at constant pressure is 0.287 Btu/lbm-°R. The compressor has inlet and exit total temperatures of 507 and 1308 °R, an efficiency of 91 percent, a specific heat ratio of 1.382, and the $c_p = 0.248$ Btu/lbm-°R. The fan has inlet and exit total temperatures of 507 and 815 °R, a total pressure ratio of 4.66, a specific heat ratio of 1.395, and the $c_p = 0.242$ Btu/lbm-°R. The shaft mechanical efficiency is 100 percent. What is the exit total temperature of the turbine?
- (b) The afterburner operates with an inlet total temperature of 1509 °R, an inlet total pressure of 419 psia, an efficiency of 88 percent, and a total pressure ratio of 0.99. The afterburner fuel flow rate is 17.48 lbm/s. The specific heat at constant pressure is 0.296 Btu/lbm-°R, and the heating value of the fuel is 17,800 Btu/lbm. Find the exit total temperature of the afterburner.
- (c) The fan has inlet and exit total temperatures of 507 and 815 °R, a total pressure ratio of 4.66, a specific heat ratio of 1.395, and the $c_p = 0.242$ Btu/lbm-°R. Find the efficiency of the fan.
- (d) Analyze the fixed converging nozzle of the engine with the afterburner off. The inlet total temperature to the nozzle is 1509 °R, the inlet total pressure is 52.6 psia, the efficiency is 97 percent, the specific heat ratio is 1.353, and the specific heat at constant pressure is 0.263 Btu/lbm-°R. The nozzle exit area is 498 in.². Find the exit Mach number of the nozzle, engine thrust, and *TSFC*.

3.61 A compressor is composed of N stages, each with a total pressure ratio of 1.25 and an efficiency of 90 percent. Plot the compressor efficiency and total pressure ratio for N from 1 to 16.

3.62 A ground-based gas turbine (Fig. 1.11.a) used for electric power generation ingests 132 lbm/s of air at standard sea level. The compressor pressure ratio is 15.6, the fuel has a heating value of 18,000 Btu/lbm, and the burner exit total temperature is 2477 °R. The efficiencies of the compressor, burner, turbine, and shaft are 87.7, 91, 92, and 99.5 percent, respectively. The total pressure ratios for the inlet, burner, and exhaust are 0.983, 0.967 and 0.979, respectively. The specific heat ratios for the compressor,

burner, turbine, inlet, and exhaust are 1.385, 1.338, 1.334, 1.403, and 1.366, respectively.

- (a) Find the overall thermal efficiency, developed net power output, and specific fuel consumption (*SFC*, fuel rate per unit of net power output).
 - (b) If the inlet air is precooled so that the inlet static temperature is dropped by 50°R , find the overall thermal efficiency, developed net power output, and specific fuel consumption.
- 3.63** A fully mixed afterburning turbofan flies at 35,000 ft at Mach 0.93. It ingests 95 lbm/s of air to the core. The compressor operates with a pressure ratio of 24 and an efficiency of 91 percent. The engine has a bypass ratio of 0.66. The efficiency of the fan is 92 percent. The fuel has a heating value of 17,800 Btu/lbm, and the burner total temperature is 2870°R . The burner has an efficiency of 97 percent and a total pressure ratio of 0.96, whereas the turbine has an efficiency of 93 percent. The duct has a total pressure ratio of 1.00, and the total pressure ratio of the mixer is 0.99. A variable converging–diverging nozzle (to match the exit pressure to the ambient pressure) is used, and its efficiency is 96 percent. The total pressure recovery for the diffuser is 0.96, and the shaft efficiency is 99.5 percent. The Mach numbers at the turbine and duct exits are nearly the same. The efficiency of the afterburner is 92 percent, and the total pressure ratio is 0.98. The exit total temperature from the afterburner is 3940°R . Find the developed thrust, nondimensional thrust, and *TSFC*.
- 3.64** A high-bypass turbofan engine with the fan exhausted is to be analyzed. The primary airflow is 200 lbm/s, and the bypass ratio is 6. The total pressure ratios for the fan and compressor are 2.2 and 36, respectively. The exit total temperature for the primary burner is 3020°R , and the total pressure ratio for the burner is 0.95. The efficiency for the burner is 95 percent, and the heat of reaction of the fuel is 17,800 Btu/lbm. Both nozzles are converging; the primary and fan nozzles have efficiencies of 96 and 96 percent, respectively. The efficiencies of the fan, compressor, and turbine are 92, 90, and 91 percent, respectively. The recovery factor for the diffuser is 0.97, and the shaft mechanical efficiency is 99.3 percent. The engine performance at Mach 0.30 at 0 ft on a standard day is to be considered (just after takeoff). Find the developed thrust, nondimensional thrust, and *TSFC*.
- 3.65** The turbine of a turbofan with the fan mixed operates with an inlet total temperature of 2880°R and an efficiency of 93 percent. The turbine inlet total pressure is 147.0 psia. The turbine specific heat ratio is 1.313, and the specific heat at constant pressure is 0.288 Btu/lbm- $^\circ\text{R}$. The core mass flow rate is 177 lbm/s, the bypass ratio is 0.90, and the primary burner fuel flow rate is 5.00 lbm/s. The aircraft flies at 919 ft/s with the ambient pressure at 3.14 psia and ambient temperature at 387°R . The compressor has inlet and exit total temperatures of 458 and 1238°R , a total pressure ratio of 29, a specific heat ratio of 1.385, and the $c_p = 0.246$ Btu/lbm- $^\circ\text{R}$. The fan has inlet and exit total temperatures of 458 and 761°R , a total pressure ratio of 5.328, a specific heat ratio of 1.398, and the $c_p = 0.241$ Btu/lbm- $^\circ\text{R}$. The primary burner operates with an inlet total temperature of 1238°R , an inlet total pressure of 153 psia, an efficiency of 95 percent, and a total pressure ratio of 0.96. The primary burner fuel flow rate is 5.00 lbm/s, and the afterburner fuel

flow rate is 16.78 lbm/s. The burner-specific heat at constant pressure is 0.277 Btu/lbm-°R, and the heating value of the fuel is 17,800 Btu/lbm. The inlet total temperature to the fixed converging nozzle is 3975 °R, the inlet total pressure is 27.85 psia, the nozzle efficiency is 97 percent, the nozzle specific heat ratio is 1.258, the specific heat at constant pressure is 0.334 Btu/lbm-°R, and the nozzle exit area is 1614 in.². The shaft mechanical efficiency is 100 percent.

- (a) What is the exit total pressure of the turbine?
- (b) Find the efficiency of the compressor.
- (c) If the compressor has 14 stages, what is the average total pressure ratio for each stage?
- (d) Find the exit total temperature of the burner.
- (e) Find the exit Mach number of the nozzle.
- (f) Find the thrust.
- (g) Find the *TSFC*.

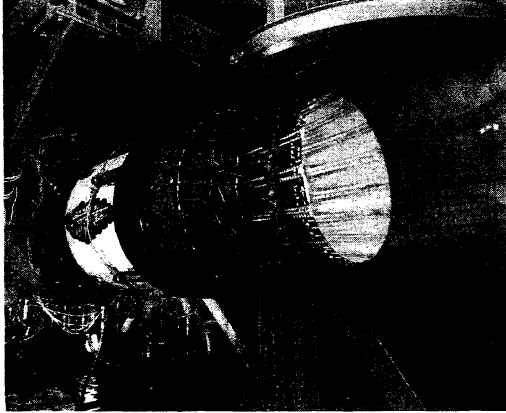
For comparison, if a converging–diverging nozzle were used matching the exit pressure to the ambient pressure, the thrust would be 44113 lbf and the *TSFC* would have a value of 1.778 lbm/h-lbf.

- 3.66** An air standard power-generation Brayton cycle operates with a maximum temperature of 1606 K. The inlet air temperature and pressure to the compressor are 0 °C and 102 kPa, respectively, and the compressor pressure ratio is 21. The compressor, turbine, and burner have efficiencies of 91, 93, and 100 percent, respectively. The total pressure ratios for the inlet, burner, and exhaust are all unity. The airflow rate is 25 kg/s. The heating value of the fuel is 42,000 kJ/kg. Assume constant specific heats and $\gamma = 1.36$. Draw the T-s diagram and find
- (a) net power output
 - (b) system thermal efficiency
 - (c) the fuel flow rate.
- 3.67** A new advanced commercial aircraft is to be designed to routinely fly at 39,000 ft at an air speed of 845 ft/s. Due to expected drag characteristics of the airframe, three engines are required and the required thrust is 16,000 lbf per engine and fuel economies dictate that the engines are to operate with *TSFC* values of 0.59 lbm/h-lbf. The material limit on the exit temperature of the burner is 2975 °R. Design an engine for this application.
- 3.68** A new advanced military fighter aircraft is to be designed to routinely fly at a variety of altitudes. One particular condition is at 24,000 ft at an air speed of 992 ft/s. Due to expected drag characteristics of the airframe, two engines are required and the required thrust is 14,500 lbf per engine and engine weight considerations dictate that the engines are to operate with non-dimensional thrusts of 2.00 and with a *TSFC* value of 0.92 lbm/h-lbf. Furthermore, since the aircraft is a fighter aircraft, short increases in thrust for rapid acceleration to supersonic speeds are required for a total of 28,100 lbf per engine. The material limits on the exit temperatures of the primary burner and afterburner are 3000 °R and 3700 °R, respectively. Design an engine for this application and conditions.
- 3.69** You are to analyze parts of a turbofan engine (with the fan fully exhausted). The aircraft cruises at 818 ft/s with the ambient pressure at 4.36 psia and

ambient temperature at 412 °R. The core air mass flow rate is 200 lbm/s. The turbine operates with an inlet total temperature of 2870 °R and an exit total temperature of 1561 °R. The inlet total pressure is 158 psia and the exit total pressure is 8.66 psia. The compressor has an inlet total temperature of 468 °R and an exit total temperature of 1237 °R; the inlet total pressure is 6.58 psia. The fan has an inlet total temperature of 468 °R, an inlet total pressure of 6.58 psia, an exit total pressure of 14.5 psia, and an efficiency of 91 percent. The primary combustor operates with an inlet total temperature of 1237 °R, an inlet total pressure of 165 psia, an efficiency of 95 %, and a total pressure ratio of 0.96. The primary burner fuel flow rate is 5.58 lbm/s. The heating value of the fuel is 17,900 Btu/lbm. The inlet total temperature to the fan nozzle is 600 °R, the inlet total pressure is 14.5 psia. The exit area is 3930 in.². The shaft mechanical efficiency is 100 %. The specific heat ratios of the fan, compressor, turbine, and nozzle are 1.400, 1.385, 1.322, and 1.398, respectively. The specific heats at constant pressure for the fan, compressor, burner, turbine, and nozzle are 0.240, 0.247, 0.277, 0.281, and 0.241 Btu/lbm-°R, respectively. Using inter-component data:

- (a) Calculate the efficiency of the turbine.
- (b) Calculate the exit total temperature of the combustor.
- (c) Calculate the exit total pressure of the combustor.
- (d) Calculate the exit Mach number of the fan nozzle.
- (e) Calculate the total mass flow rate through the fan nozzle.
- (f) Calculate the bypass ratio.

Component Analysis



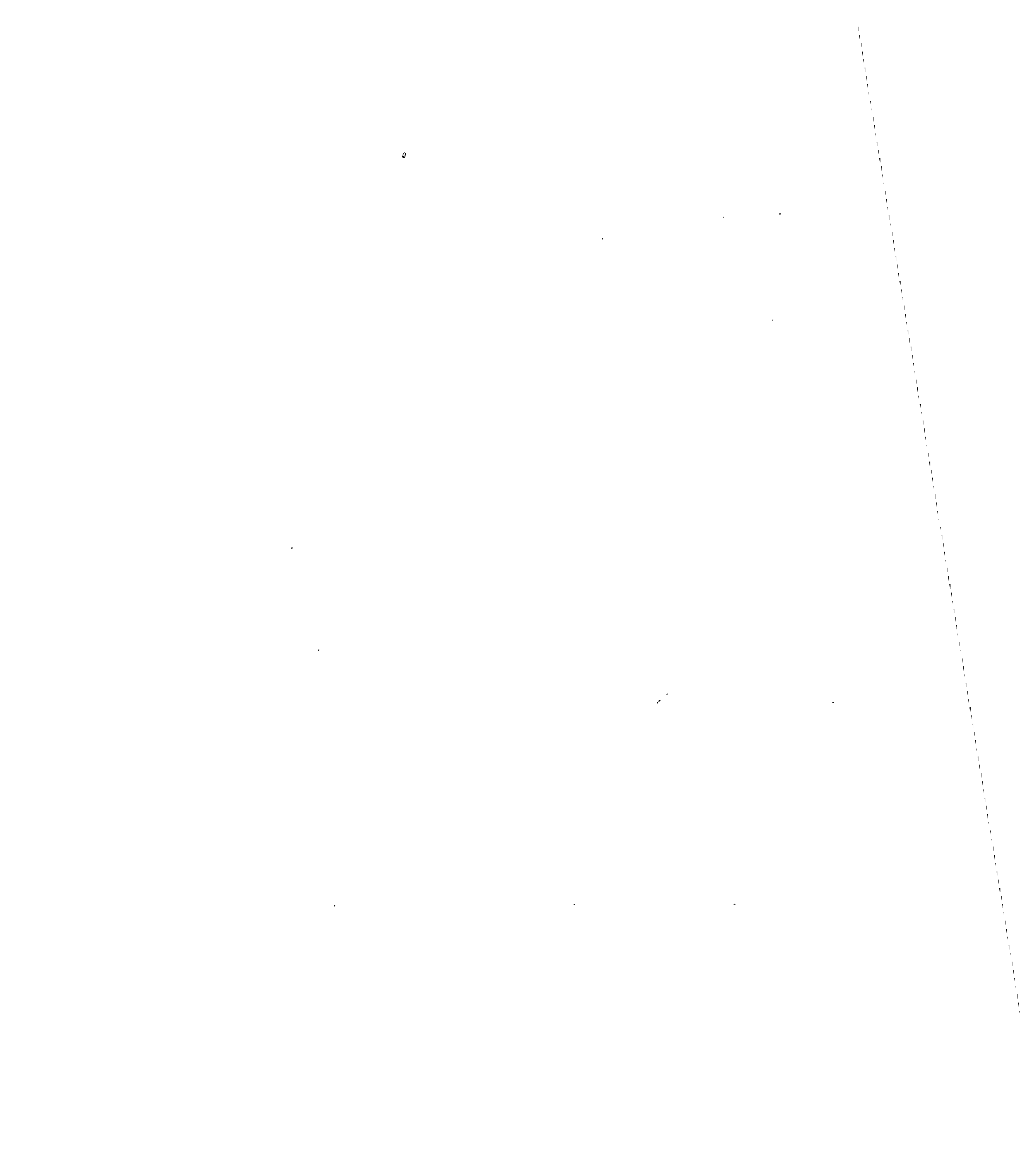
F100-PW-229A Nozzle
(courtesy of Pratt & Whitney)



RB211 Compressor Blades
(courtesy of Rolls-Royce)



RB211-524 Inlet
(courtesy of Rolls-Royce)



Diffusers

4.1. Introduction

The purposes of the diffuser or inlet are first to bring air smoothly into the engine, second to slow the fluid and to increase the pressure, and third to deliver a uniform flow to the compressor. As indicated by studies for cycle analyses in Chapters 2 and 3, engine performance improves with increasing pressure to the burner. The first component the air encounters is the diffuser, and the second component is the compressor. Thus, if the diffuser incurs a large total pressure loss, the total pressure into the burner will be reduced by the compressor total pressure ratio times this loss. For example, if 2 psia are lost in the diffuser, for a large engine this can result in 50 psia less in the burner.

The losses result from several processes and affect engine performance in several ways. First, losses in total pressure occur outside of the diffuser primarily as the result of shock interactions. The flow outside the diffuser can also actually affect the flow around the entire engine and add a drag to the aircraft. Second, ideally the flow inside the diffuser is uniform and the streamlines are smooth. However, because of the unfavorable pressure gradient, the boundary layer on the walls tends to grow and separate. This has three subeffects. First, as the result of the wall shear, the flow is not isentropic; thus, the total pressure is further reduced. Second, because of the separation, the flow area is decreased. The flow velocity therefore remains high and the static pressure is not increased as much as in the ideal situation. Lastly, because of the separation, the flow is highly nonuniform as it enters the compressor. This, as a result, reduces the compressor efficiency and stability. Thus, it is very important for the diffuser to operate efficiently both internally and externally.

Computational fluid dynamic (CFD) three-dimensional (3-D) and unsteady methods have been developed extensively over the past decade and are used in the design of all gas turbine components. However, they are not exclusively used because they are not yet totally reliable. As a result, empiricism and experimental testing are used to complement CFD. Furthermore, the use of CFD is beyond the scope of this book. Thus, empiricism and one-dimensional (1-D) and two-dimensional (2-D) models will be presented instead to demonstrate trends as well as a first-pass (but reasonable) calculation method consistent with the effort required by the included problems.

Initially, the diffuser or inlet was assumed to operate isentropically both internally and externally. As discussed in Chapter 3, this is not the case. Losses can occur both before the air reaches the diffuser and also once it enters the diffuser. The diffuser essentially operates adiabatically. The losses inside and outside the diffuser will be discussed separately.

The concept of total pressure recovery is introduced to quantify these losses. This is defined as

$$\pi_d = \frac{P_{t2}}{P_{t1}} \quad 4.1.1$$

Note that this recovery factor represents the loss from the freestream to the diffuser exit.

A second loss is often defined to identify internal diffuser losses. This is the diffuser pressure recovery factor and is defined as

$$\pi_r = \frac{p_{t2}}{p_{t1}} \quad 4.1.2$$

This represents the losses only within the diffuser due to boundary layers and separation.

Losses can also occur before the flow enters the diffuser. They are usually due to shocks outside of, or in the plane of, the diffuser inlet. This loss is defined by

$$\pi_o = \frac{p_{t1}}{p_{ta}} \quad 4.1.3$$

and is the loss from the freestream to the diffuser inlet. For subsonic flow, this quantity is usually unity or very close to unity. As the freestream Mach number increases past unity, this loss can increase quickly as the result of shocks, as is discussed in Section 4.3. Thus, from Eqs. 4.1.1, 4.1.2, and 4.1.3, one finds that

$$\pi_d = \pi_r \pi_o \quad 4.1.4$$

Thus, by either specifying π_d or both π_o and π_r , the losses associated with the diffuser can be included in a cycle analysis. One objective of this chapter is to develop a method whereby both π_o and π_r can be estimated for a given diffuser.

4.2. Subsonic

4.2.1. External Flow Patterns

A diffuser must be designed for a variety of flight conditions. That is, it must be able to collect the needed airflow and ready the flow for the compressor for different Mach numbers, altitudes, engine mass flows, and so on. For a subsonic diffuser, the design is not nearly as critical as for a supersonic diffuser. This is because the governing equations of the flow are elliptic, and small pressure fluctuations are signaled upstream of the diffuser to adjust flow patterns into the diffuser as the needs change.

For example, streamlines for two flow conditions are shown in Figure 4.1. First, the streamline for high aircraft speed, or low ingested air flow rate, or both is shown. Far away from the inlet, the encompassed area of the airflow is smaller than the diffuser inlet area. Thus, as it approaches the inlet, the flow decelerates and the pressure increases. To allow

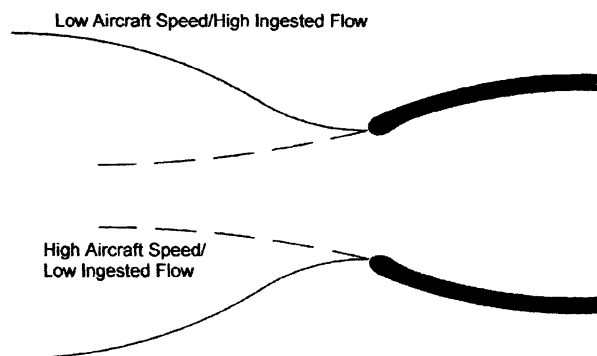


Figure 4.1 Inlet flow pattern for two conditions.

for streamline curvature at the intersection of the inlet and for crossflows, the inlet is well rounded at the leading edge so that air enters with minimal separation.

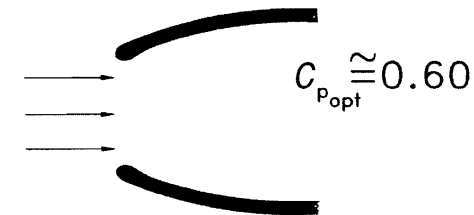
Next the streamline for low aircraft speed, high airflow rate, or both is shown. This condition would occur for an aircraft on the runway or an engine on the test stand. Far away from the inlet, the encompassed area of the airflow is now larger than the diffuser inlet area. Thus, as the flow approaches the inlet, the flow accelerates and the pressure decreases. A well-rounded inlet at the leading edge is even more important for this condition as the streamlines change direction (converging to diverging) at the front of the diffuser. CFD predictions aid significantly in the design of the lip of the cowl.

4.2.2. Limits on Pressure Rise

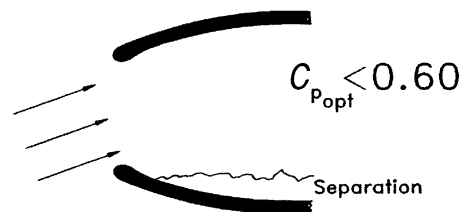
As indicated in Chapters 1 through 3, the developed thrust of the engine will be increased if the pressure into the nozzle is increased. Thus, it is desirable to increase the pressure out of the diffuser as much as possible as well as to reduce the velocities into the compressor. As a result, an adverse pressure gradient is present that tends to cause separation of the boundary layer. It is this separation that is one of the limits of diffuser operation. To estimate the limit, Hill and Peterson (1992) considered the general pressure coefficient defined by

$$C_p \equiv \frac{\Delta p}{\frac{1}{2}\rho u^2}, \quad 4.2.1$$

where u is the inlet relative velocity to the component. Typically, for a simple diffuser having walls with limited curvature and ideal inlet conditions (Fig. 4.2.a), C_p is less than or approximately equal to 0.6 for flow without separation. If the pressure coefficient becomes greater than about 0.6, the flow separates. If the walls have a pronounced curvature, or if the flow enters the diffuser in a skewed direction (Fig. 4.2.b) or the flow direction fluctuates,



(a) Flow enters aligned with diffuser



(b) Flow enters mis-aligned with diffuser

Figure 4.2 Separation in diffuser.

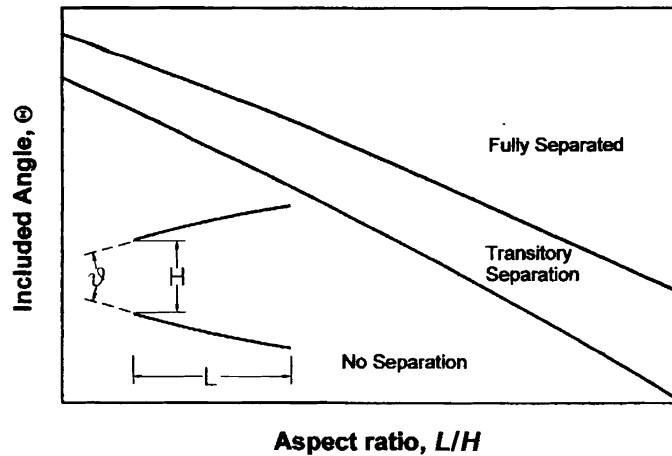


Figure 4.3 General empirical data trends for separation in a simple diffuser.

this upper limit on the pressure coefficient will be reduced appreciably to perhaps 0.1 to 0.2. Again, a well-rounded leading edge improves performance. A second empirical method of predicting separation (which complements the preceding results) is shown in Figure 4.3. Here the limiting expansion angle of a general simple diffuser is shown as a function of diffuser length-to-width ratio. Such data can be achieved for planar, axisymmetric, or other elliptical diffusers with a variety of wall shapes (straight, curved, etc.). The particular empiricism will depend on the diffuser of interest and is usually found with a well-controlled flow into the diffuser. For a given aspect ratio (L/H), if the included angle is too large, the diffuser area is enlarging too quickly and separation will occur. On the other hand, for a given expansion angle ϑ , if the aspect ratio is too large, separation will occur. In general, a region exists for which separation can be transitory – that is, the size of the separated region fluctuates.

Fox and Kline (1962) present data such for a simple 2-D planar diffuser with straight walls. Curve fitting their data yields two equations that approximate the two curves:

$$\ln \vartheta_{\min} = 3.28 - 0.46 \ln(L/H) - 0.031(\ln(L/H))^2 \quad 4.2.2.a$$

$$\ln \vartheta_{\max} = 3.39 - 0.38 \ln(L/H) - 0.020(\ln(L/H))^2, \quad 4.2.2.b$$

where ϑ is in degrees. For example if $L/H = 4$, separation will be expected to initiate for an included angle between about 13° and 17° for a simple straight-walled planar diffuser with a well-controlled inlet.

Next, a pressure coefficient can be defined specifically for a diffuser as

$$C_p = \frac{p_2 - p_1}{\frac{1}{2} \rho_1 u_1^2}. \quad 4.2.3$$

For the diffuser, one can consider the square of the inlet Mach number as

$$M_1^2 = \frac{u_1^2}{a_1^2} = \frac{\rho_1 u_1^2}{\gamma p_1} \quad 4.2.4$$

Thus, from Eq. 4.2.3, one finds

$$\frac{p_2}{p_1} = \frac{1}{2} \frac{\rho_1 u_1^2 C_p}{p_1} + 1, \quad 4.2.5$$

and from Eq. 4.2.4 the following expression results:

$$\frac{p_2}{p_1} = 1 + \frac{1}{2}\gamma C_p M_1^2. \quad 4.2.6$$

Namely, as the Mach number increases a larger pressure rise can be expected, without an increasing concern for separation, due to the added momentum of the fluid.

To appreciate the order of magnitude of the area ratios at hand, note that, for *ideal incompressible* flow, Eq. 4.2.3 will yield

$$C_p = 1 - \left[\frac{A_1}{A_2} \right]^2; \quad 4.2.7$$

thus, for a pressure coefficient limit of 0.6 the exit to inlet area ratio becomes 1.581 which is much larger than would be present on an engine inlet. Note in particular that Eq. 4.2.7 does not apply to compressible flow.

Example 4.1: Flow enters an ideal diffuser with a Mach number of 0.8, an inlet pressure of 13.12 psia, and an inlet diameter of 40 in. If the diffuser operates with the optimum (or maximum or limiting pressure) coefficient of 0.6, what is the resulting exit Mach number and diffuser area ratio? Assume isentropic flow and $\gamma = 1.40$.

SOLUTION:

For the given inlet Mach number, general one-dimensional isentropic flow (Appendix H) and the tables of Appendix B reveal that the static-to-total pressure ratio is

$$p_1/p_{t1} = 0.6560$$

and $A_1/A^* = 1.0382$;

thus, the total pressure at the inlet is $p_{t1} = 13.12/0.6560 = 20.00$ psia, which for the case of isentropic flow is also the pressure at the exit, p_{t2} . From Eq. 4.2.6, one finds that

$$\frac{p_2}{p_1} = 1 + \frac{1}{2}\gamma C_p M_1^2,$$

and so for $C_p = 0.60$ the ratio of static pressures is

$$\frac{p_2}{p_1} = 1 + \frac{1}{2} \times 1.40 \times 0.60 \times 0.80^2 = 1.2688;$$

thus, the exit static pressure is $p_2 = 1.2688 \times 13.12 = 16.65$ psia. The static-to-total pressure ratio at the exit is $p_2/p_{t2} = 16.65/20.00 = 0.8323$. From the isentropic flow tables for this pressure ratio, the exit Mach number is

$$M_2 = 0.5188$$

and $A_2/A^* = 1.3055$.

Thus, the area ratio is $A_2/A_1 = 1.3055/1.0382 = 1.257$, which is different than it would be if incompressible flow were assumed. Note that if $L/H = 2$, this leads to an included angle of 6.9° , which, if one can use data from Fox and Kline (1962) (developed for planar flow), is well below the separation limit.

4.2.3. Fanno Line Flow

Boundary layers and other viscous flows are the primary means by which total pressure losses occur within diffusers. This will be analyzed based on Fanno line flow, which is flow with friction but no heat addition or loss. Fanno line flow is a constant area process that does not exactly represent a diffuser. However, when the exit-to-inlet area ratio is near unity and the flow consequently does not separate, the Fanno line analysis can be used to make a reasonable prediction of the total pressure losses. The flow is analyzed in Appendix H with a control volume approach. The analysis results in 11 equations. Seventeen variables are present, and so six must be specified. For example, if inlet conditions M_1 , T_1 , and p_{t1} , and geometry parameters L , D , and f (Fanning friction factor) are specified, exit conditions, including the total pressure p_{t2} , can be found.

Example 4.2: Flow with an incoming Mach number of 0.8 and an inlet total pressure of 20 psia enters a diffuser 24 in. long with a 40 in. average diameter and a Fanning friction factor of 0.020. What is the total pressure ratio if the specific heat ratio is 1.40?

SOLUTION:

From the tables for a Mach number of 0.80 it is possible to find the following nondimensional length-to-diameter and pressure parameters:

$$\left. \frac{4fL^*}{D} \right]_1 = 0.0723$$

and

$$\frac{p_{t1}}{p_t^*} = 1.0382;$$

thus, one can find the total pressure at the sonic condition, which is a *reference* condition (which means it usually does not occur in the actual conditions), as follows:

$$p_t^* = 20/1.0382 = 19.26 \text{ psia.}$$

From the duct geometry, it is possible to find the parameter

$$\left. \frac{4fL}{D} \right]_{1-2} = \frac{4 \times 0.020 \times 24}{40} = 0.048;$$

thus, the corresponding length-to-diameter parameter at the exit can be found as follows:

$$\left. \frac{4fL^*}{D} \right]_2 = \left. \frac{4fL^*}{D} \right]_1 - \left. \frac{4fL}{D} \right]_{1-2} = 0.0723 - 0.048 = 0.0243.$$

The exit Mach number can then be found from the tables; namely,

$$M_2 = 0.874.$$

Thus, as a result of friction the Mach number increased about 9 percent. From the tables, at this Mach number

$$\frac{p_{t2}}{p_t^*} = 1.0143,$$

and so the exit total pressure can be found: $p_{t2} = 1.0143 \times 19.26 = 19.54$ psia. The pressure ratio for the inlet for Fanno line flow is therefore

$$\pi_r = \frac{p_{t2}}{p_{t1}} = \frac{19.54}{20} = 0.977.$$

4.2.4. Combined Area Changes and Friction

In the preceding two sections, area changes and friction were treated separately. However, in a diffuser the two effects occur simultaneously. Thus, an analysis is needed in which both are included. The technique that will be used here is the so-called generalized one-dimensional flow method; it is described in Appendix H and is a differential equation analysis from which influence coefficients are derived. These influence coefficients relate changes of one variable on another. Applying the method entails numerically integrating the differential equations along the length of the diffuser, which incorporate both friction and area changes.

Example 4.3: Flow with an incoming Mach number of 0.8 and an inlet total pressure of 15 psia enters a diffuser channel 36 in. long and with a 36 in. diameter (with an inlet area of 1018 in.²). The flow has a Fanning friction factor of 0.020 and an exit-to-inlet area ratio of 1.50. The total temperature remains constant at 500 °R. What is the total pressure ratio if the specific heat ratio is 1.40?

SOLUTION:

This problem will be solved by numerically integrating Eqs. H.12.3 and H.12.4. One hundred steps will be used, and area change and friction will be assumed to be uniform along the length of the diffuser. The exit area is 1527 in.²; thus, the area increases by 509 in.². Therefore, $\Delta A = 5.09$ in.², and $\Delta x = 0.36$ in. for each step. A forward difference method is used. Thus, for the first step from Eq. H.12.1 (the first term is due to area changes, and the second term results from friction),

$$\Delta(M^2) = -2M^2 \left[\frac{\left(1 + \frac{\gamma-1}{2}M^2\right)}{1 - M^2} \right] \left[\frac{\Delta A}{A} \right] + 4f\gamma M^4 \left[\frac{\left(1 + \frac{\gamma-1}{2}M^2\right)}{1 - M^2} \right] \left[\frac{\Delta x}{D} \right]$$

$$\text{so } M_i^2 = M_{i-1}^2 + \Delta(M^2)$$

$$\begin{aligned} M^2 &= 0.8^2 - 2 \times 0.8^2 \left[\frac{\left(1 + \frac{1.40-1}{2}0.8^2\right)}{1 - 0.8^2} \right] \left[\frac{5.09}{1018} \right] \\ &\quad + 4 \times 0.020 \times 1.40 \times 0.8^4 \left[\frac{\left(1 + \frac{1.40-1}{2}0.8^2\right)}{1 - 0.8^2} \right] \left[\frac{0.36}{36} \right] = 0.6214, \end{aligned}$$

$$\text{or } M = 0.7883.$$

From Eq. H.12.2, the total pressure loss is only due to friction:

$$\Delta p_t = -\frac{1}{2}p_t 4f\gamma M^2 \left[\frac{\Delta x}{D} \right] = -2p_t f\gamma M^2 \left[\frac{\Delta x}{D} \right],$$

$$\text{and so } p_{ti} = p_{t(i-1)} + \Delta(p_t)$$

$$p_t = 15 - 2 \times 15 \times 0.020 \times 1.40 \times 0.8^2 \times \frac{0.36}{36} = 14.995.$$

This is repeated for all 100 steps, where the previous step is used for the initial conditions for the following step. The area and diameter are of course updated from step to step. Thus, one finds after 100 steps that

$$M_2 = 0.4160$$

$$p_{t2} = 14.76 \text{ psia,}$$

and thus

$$\pi = \frac{p_{t2}}{p_{t1}} = \frac{14.76}{15} = 0.984.$$

For comparison one can approximate the flow by separately analyzing the flow with area change (isentropic flow) and Fanno line flow and superimposing the two results. For example, when the simple area change is considered for the preceding area ratio, the exit Mach number is found to be 0.4105 and the total pressure does not change. Thus, the average Mach number is 0.6053 and the average diameter is 40 in. Consequently, $\frac{4fL}{D} \Big|_{1-2} = \frac{4 \times 0.020 \times 36}{40} = 0.072$. Using this in an analysis similar to that of Example 4.2 and the average Mach number as the inlet condition, one finds an exit Mach number due to only friction of 0.6257, and, most importantly,

$$\pi = \frac{p_{t2}}{p_{t1}} = 0.981.$$

Thus, for this case the approximate superposition analysis is quite close to the more accurate method. In practice, a CFD method is used to calculate the total pressure loss and resulting exiting 2-D or 3-D velocity profile. As already noted, however, using CFD is beyond the scope of this book.

4.3. Supersonic

4.3.1. Shocks

a. Normal Shocks

When an aircraft flies supersonically, shocks will usually occur exterior to, or near, the inlet plane of the diffuser. The strongest possible shock is the normal shock. This type of shock is covered extensively in fluid mechanics and gas dynamics texts; because of this, the development of the analysis is reviewed in Appendix H. In Figure 4.4, a standing normal shock is shown. The inlet conditions to the shock are subscripted with *i*, whereas the exit conditions are noted with *j*.

For an inlet Mach number M_i , the exit Mach number is determined by

$$M_j^2 = \frac{M_i^2 + \frac{2}{\gamma-1}}{\frac{2\gamma}{\gamma-1} M_i^2 - 1}, \quad 4.3.1$$

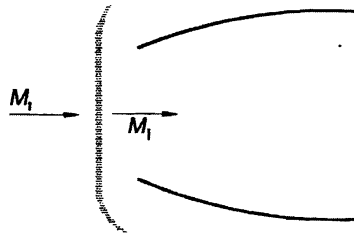


Figure 4.4 Standing normal shock at diffuser inlet.

and the total properties are related by

$$T_{tj} = T_{ti} \quad 4.3.2$$

$$\frac{p_{tj}}{p_{ti}} = \frac{\left[\frac{\frac{\gamma+1}{2} M_i^2}{1 + \frac{\gamma-1}{2} M_i^2} \right]^{\frac{\gamma}{\gamma-1}}}{\left[\frac{2\gamma}{\gamma+1} M_i^2 - \frac{\gamma-1}{\gamma+1} \right]^{\frac{1}{\gamma-1}}}. \quad 4.3.3$$

As an aid in problem solving, these and other quantities are presented in tables in Appendix E for three values of γ . Note that the exit Mach number is always less than unity. Also, several equations are listed in Appendix H to relate exit and inlet conditions to the Mach numbers.

Example 4.4: A diffuser on a Mach 2 aircraft operates with a standing normal shock outside of the inlet at STP. If the internal diffuser recovery factor is 0.90, what is the diffuser exit total pressure and the total pressure recovery from the freestream to the diffuser exit?

SOLUTION:

From the tables for $\gamma = 1.40$ and $M_i = 2.00$, or from the equations one finds that the exit Mach number from the normal shock is

$$M_j^2 = \frac{M_i^2 + \frac{2}{\gamma-1}}{\frac{2\gamma}{\gamma-1} M_i^2 - 1} = 0.3333$$

$$M_j = 0.5774.$$

It can be found from the tables or equations that the total pressure ratio is

$$\frac{p_{tj}}{p_{ti}} = \frac{\left[\frac{\frac{\gamma+1}{2} M_i^2}{1 + \frac{\gamma-1}{2} M_i^2} \right]^{\frac{\gamma}{\gamma-1}}}{\left[\frac{2\gamma}{\gamma+1} M_i^2 - \frac{\gamma-1}{\gamma+1} \right]^{\frac{1}{\gamma-1}}} = 0.7209,$$

which is also $\pi_o = \frac{p_{t1}}{p_{ta}}$, and the static pressure ratio is

$$\frac{p_j}{p_i} = \frac{2\gamma}{\gamma+1} M_i^2 - \frac{\gamma-1}{\gamma+1} = 4.500.$$

Next, from Eq. 2.1.9 one finds for $p_a = 101.3$ kPa (14.69 psia) that

$$p_{ta} = p_a \left[1 + \frac{\gamma-1}{2} M_a^2 \right]^{\frac{\gamma}{\gamma-1}} = 11.3 \text{ kPa} \left[1 + \frac{1.40-1}{2} 2^2 \right]^{\frac{1.40}{1.40-1}}$$

$$p_{ta} = 792.6 \text{ kPa} \quad (115.0 \text{ psia}).$$

Thus, the total pressure at the entrance to the diffuser is

$$p_{t1} = 0.7209 \times 792.6 = 571.3 \text{ kPa} \quad (82.86 \text{ psia}).$$

Therefore, a loss of 221.3 kPa (32.09 psi) in total pressure is realized as a result of the normal shock.

The exit total pressure from the diffuser is

$$p_{t2} = \pi_d p_{t1} \times 0.90 \times 571.3 = 514.2 \text{ kPa} \quad (74.57 \text{ psia}). \quad <\text{ANS}$$

Therefore, the overall recovery factor is

$$\pi_d = \frac{p_{t2}}{p_{ta}} = \frac{514.2}{792.6} = 0.649. \quad <\text{ANS}$$

Thus, the loss is very high and methods should be found to reduce it.

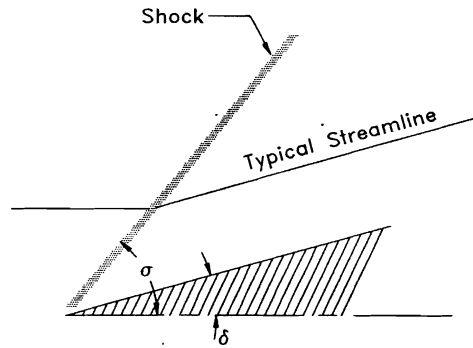


Figure 4.5 Oblique shock.

b. Oblique Planar Shocks

To reduce the losses encountered with normal shocks, supersonic diffusers are designed so that oblique shocks occur. Figure 4.5 shows an oblique shock. The losses that are encountered with oblique shocks are significantly less than with normal shocks, and the losses in total pressure are much lower. In actuality, many oblique shocks in aircraft applications are conical. However, planar 2-D shocks are first considered for two reasons. First, the required mathematics is much simpler for planar than for conical shapes, and thus the fundamentals can be better understood. Flow behind the planar shock is uniformly parallel to the wedge. Second, some applications exist in which oblique planar shocks are present; for example, when an inlet is attached to the fuselage of the aircraft, the inlet is more or less rectangular, resulting in a planar shock. Results for conical shocks are covered in the next section. Further details can be found in several gas dynamics texts, including Shapiro (1953), and the mathematics are reviewed in Appendix H. The five resulting important equations are repeated here:

$$\frac{p_j}{p_i} = \frac{\left[\frac{\gamma+1}{\gamma-1} \right] \frac{\rho_j}{\rho_i} - 1}{\left[\frac{\gamma+1}{\gamma-1} \right] - \frac{\rho_j}{\rho_i}} \quad 4.3.4$$

$$\frac{\rho_j}{\rho_i} = \frac{\tan \sigma}{\tan(\sigma - \delta)} \quad 4.3.5$$

$$\frac{p_j}{p_i} = 1 + \gamma M_i^2 \sin^2 \sigma \left[1 - \frac{\rho_i}{\rho_j} \right] \quad 4.3.6$$

$$\frac{p_i}{p_j} = 1 + \gamma M_j^2 \sin^2(\sigma - \delta) \left[1 - \frac{\rho_j}{\rho_i} \right] \quad 4.3.7$$

$$\frac{p_{tj}}{p_{ti}} = \frac{p_j}{p_i} \left[\frac{1 + \frac{\gamma-1}{2} M_j^2}{1 + \frac{\gamma-1}{2} M_i^2} \right]^{\frac{\gamma}{\gamma-1}} \quad 4.3.8$$

Equations 4.3.4 to 4.3.8 contain seven independent variables: σ , δ , M_i , M_j , p_j/p_i , p_{tj}/p_{ti} , and ρ_j/ρ_i . Therefore, if two are specified, the remaining five can be determined. For example, for a given incoming Mach number (M_i) and a given turning angle (δ), one can find the shock angle, exit Mach number, total pressure ratio, and all of the other variables. These equations can easily be programmed in a commercial math solver. Figure 4.6 presents graphs

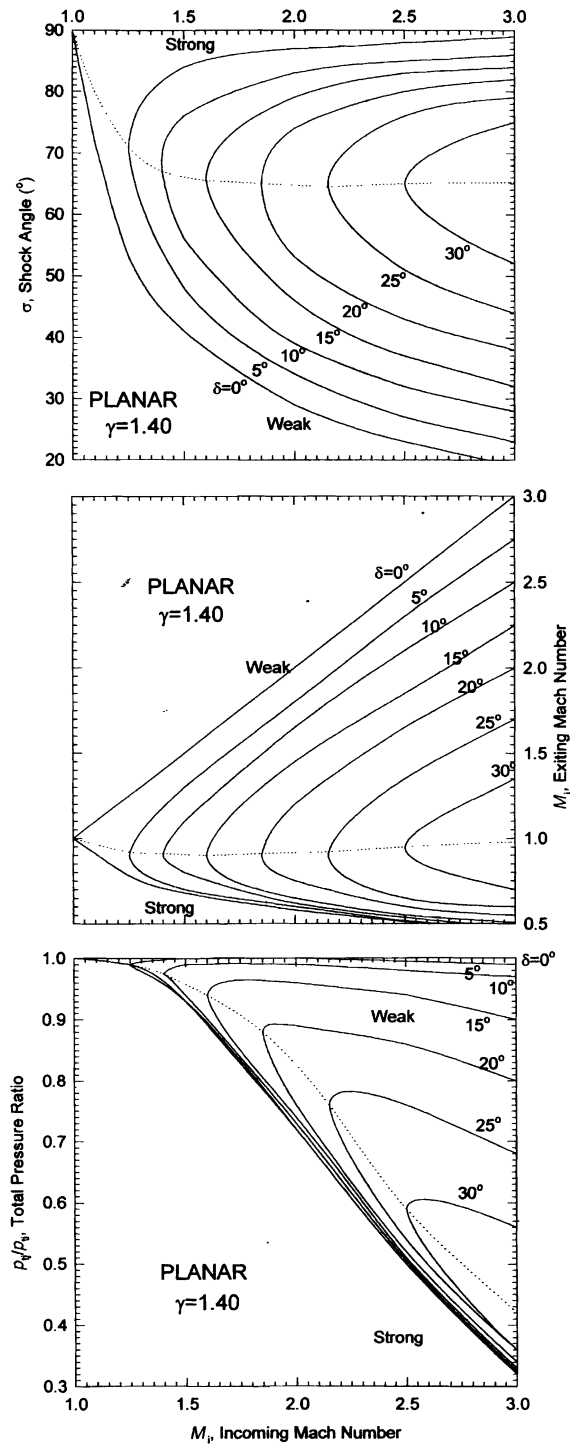


Figure 4.6 Oblique planar shocks – shock angle, exit Mach number, and total pressure ratio as functions of incoming Mach number.

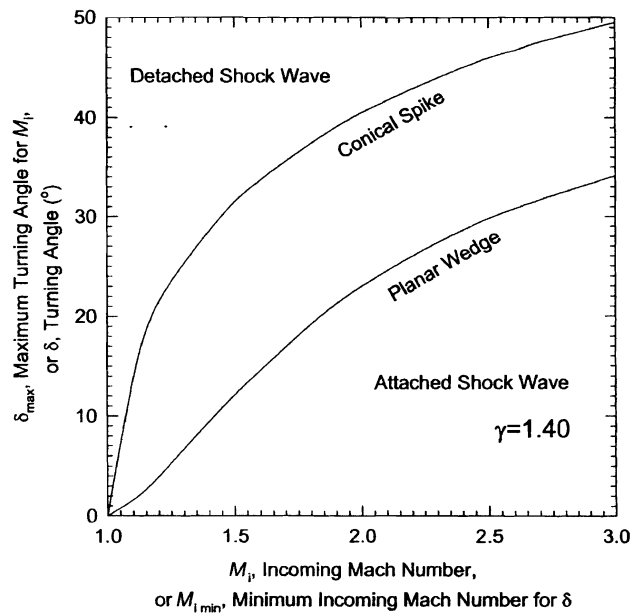


Figure 4.7 Oblique planar and conical shocks: conditions for shock detachment.

for $\gamma = 1.40$ to aid in the theoretical solution. This figure is in a sense a large number of general solutions to the five equations of interest. It is important to note that, for every set of conditions, two solutions exist. The first is the “strong” shock in which the exit Mach number is subsonic and that results in a large loss in stagnation pressure. The second is the “weak” shock in which the exit Mach number is supersonic or high subsonic for a few cases. The weak shock occurs when a low pressure is incurred downstream of the shock and results in a smaller total pressure loss. For most jet engine applications, weak oblique shocks occur. One limit is for $\delta = 0^\circ$ for which the solutions reduce to the normal shock solutions. Another important limit is reached when the turning is too large for a given Mach number (or the Mach number is too small for a given turning angle). When this limit is exceeded, an oblique shock solution is not possible. Physically, the oblique shock is no longer attached and “pops” off of the wedge, resulting in a standing normal shock in front of the inlet. These limiting lines are shown in Figure 4.6 and are also summarized in Figure 4.7.

c. Oblique Conical Shocks

In Figure 4.8.a, a typical simple oblique shock system in the design condition is shown for a supersonic inlet. First, a conical (axisymmetric) ramp is used to generate an oblique shock, which decelerates the flow to a less supersonic condition. An example is the spike on the Blackbird shown in Figure 4.8.b. Next, a normal shock further decelerates the flow to a subsonic condition for the internal flow in the diffuser. For the case of axisymmetric oblique shocks, the flow is not uniformly parallel to the spike and streamlines curve toward the cone. One can develop the equations for oblique conical shocks in much the same way as those for oblique planar shocks. However, this is a more complicated procedure and requires numerical integration of some equations owing to the coordinate system. It

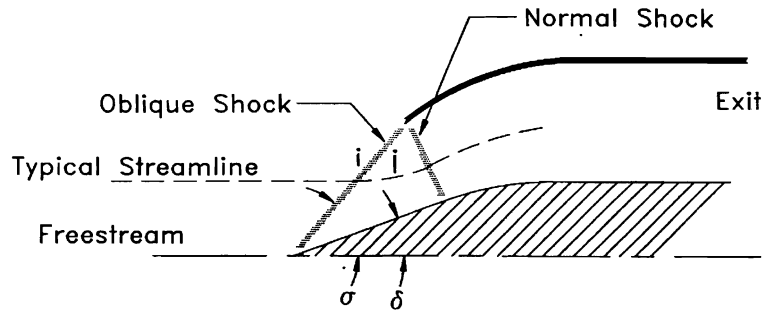


Figure 4.8a Diffuser inlet with one conical oblique shock and one normal shock.

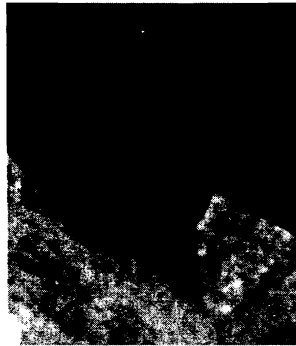


Figure 4.8b Spike on Blackbird (courtesy of NASA).

suffices to say that the number of variables and equations remains the same. Details can be found in several gas dynamics texts, including Zucrow and Hoffman (1976). Again, the equations can be programmed, and theoretical solutions to these equations are presented for $\gamma = 1.40$ in the form of graphs in Figure 4.9. Note however, that, unlike oblique planar shocks, oblique conical shocks only have one solution (weak). Also, the flowfield is two-dimensional and the pressure and Mach number are not uniform behind the shock as in the case of a planar oblique shock, but they are functions of radius because the differential flow area changes with radius. Solutions for only the spike surface are presented here. As for planar shocks, when the turning is too large for a given Mach number (or the Mach number is too small for a given turning angle), an oblique shock solution is not possible and a standing normal shock in front of the inlet results. These limiting lines are shown in Figure 4.9 and are also summarized in Figure 4.7. As can be seen, more turning is allowed for the conical shock than for the oblique shock before detachment. Solutions for normal, planar oblique, and conical oblique shocks can also be obtained using the software, "SHOCK".

Example 4.5: A diffuser on a Mach 2 aircraft operates with one oblique conical and one normal shock outside of the inlet at STP. If the turning angle is 20° and the internal diffuser recovery factor is 0.90, what is the diffuser exit total pressure and the total pressure recovery from the freestream to the diffuser exit on the spike?

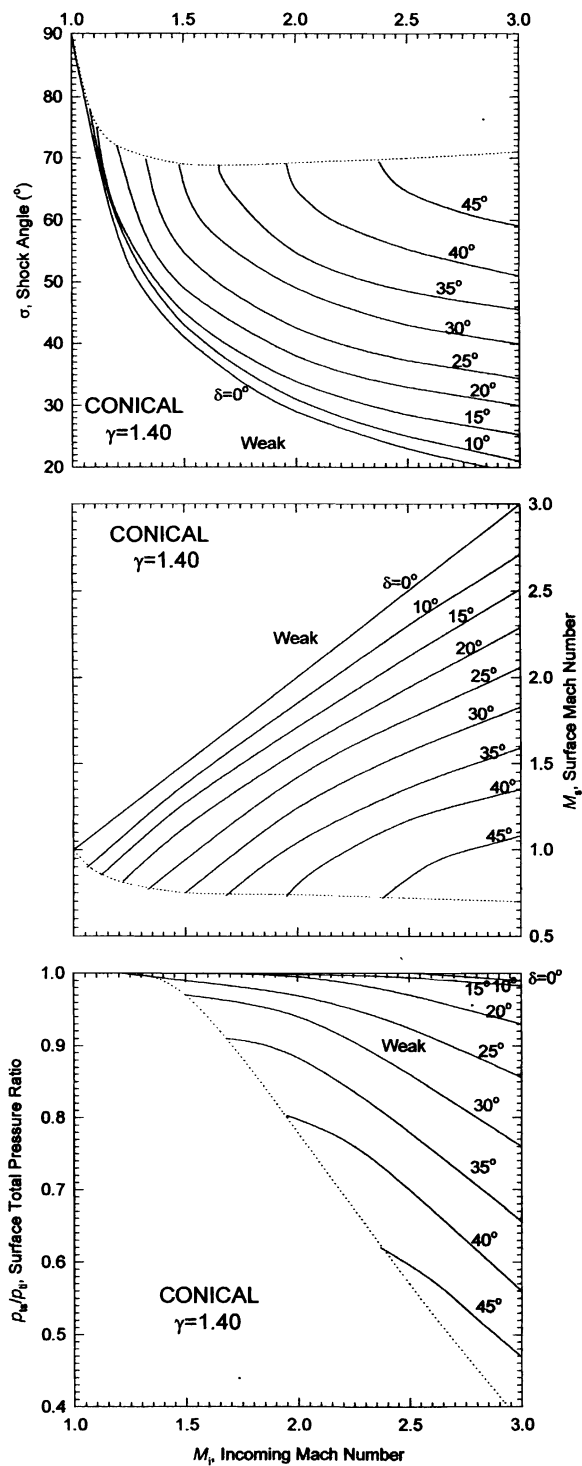
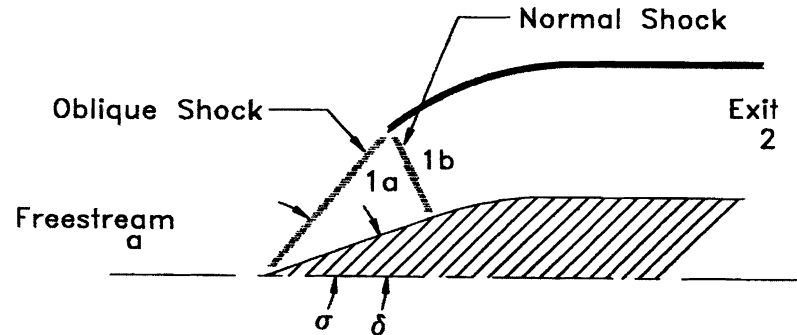


Figure 4.9 Oblique conical shocks – shock angle, exit Mach number, and total pressure ratio as functions of incoming Mach number.

Note that this is the same problem as found in Example 4.3 with the addition of the oblique shock.



SOLUTION:

Referring to the figure above, one finds for the notation that for a freestream Mach number of $M_a = 2.00$ and a turning angle of $\delta = 20^\circ$ from Figure 4.9.b, the Mach number behind the oblique shock and on the spike surface is

$$M_{1a} = 1.568,$$

and from Figure 4.9.c the total pressure ratio for the oblique shock is

$$p_{t1a}/p_{ta} = 0.9901.$$

Also, from Figure 4.9.a the shock angle is

$$\sigma = 37.80^\circ.$$

Although the latter quantity is not used in the solution, the diffuser should be designed for this shock angle so that the diffuser cowl intersects the shock as shown. If it does not, "spillage" and additional drag can occur, which will be covered in Section 4.3.2. Next, to analyze the normal shock for an incoming Mach number of $M_{1a} = 1.568$, one finds from Appendix E that the Mach number behind the normal shock is

$$M_{1b} = 0.6784,$$

and the total pressure ratio for the normal shock is $p_{t1b}/p_{t1a} = 0.9070$; thus, combining results yields

$$p_{t1b}/p_{ta} = p_{t1a}/p_{ta} \times p_{t1b}/p_{t1a} = 0.9901 \times 0.9070 = 0.8980,$$

which is the same as π_o .

Therefore, from Example 4.4, the freestream total pressure is $p_{ta} = 792.6$ kPa (115.0 psia), and thus the total pressure at the inlet plane of the diffuser is

$$p_{t1b} = 0.8980 \times 792.6 = 711.7 \text{ kPa} \quad (103.2 \text{ psia}).$$

Because $p_{t2} = \pi_r p_{t1b}$, the total pressure at the exit of the diffuser is

$$p_{t2} = 0.90 \times 711.7 = 640.5 \text{ kPa} \quad (92.89 \text{ psia}). \quad < \text{ANS}$$

Finally, the total recovery of the diffuser is

$$\pi_d = \frac{p_{t2}}{p_{ta}} = \frac{640.5}{792.6} = 0.808. \quad < \text{ANS}$$

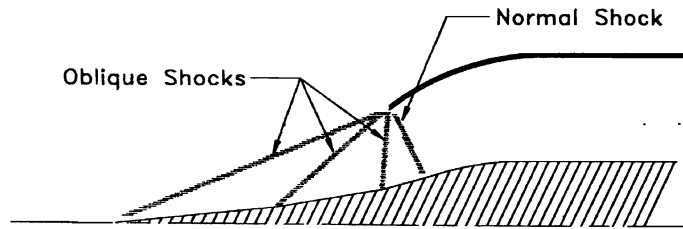


Figure 4.10 Diffuser inlet with three oblique shocks and one planar normal shock.

Although still low, which indicates a significant total pressure loss, this value is much higher than for a single standing normal shock, as calculated in Example 4.4 ($\pi_d = 0.649$). It is easy to understand why conical ramps are used to reduce the severity of the shock structure.

To reduce the losses even further, one can use a series of oblique shocks, as indicated in Figure 4.10. This has the effect of decreasing the incoming Mach number to the normal shock and thus reducing the losses. Unfortunately, this also has the effect of adding to the complexity of the geometric design, increasing the total turning angle and length (and weight). Optimally designing such an inlet so that the total pressure ratio of the unit is minimized requires that each of the losses across the individual shocks be the same. For example, if two oblique and one normal shock are used, they all should have the same total pressure ratio. Figure 4.11 summarizes the typical effects. In this figure, the value of π_o and total turning angle are presented as a function of the freestream Mach number for four different designs ranging from a single normal shock to three oblique shocks with a normal shock. One can also take advantage of oblique shocks that result in high but subsonic exit Mach numbers. As can be seen, as more oblique shocks are used, the loss diminishes – particularly for large Mach numbers. It is important to realize that the optimized spike shape will be different for different Mach numbers.

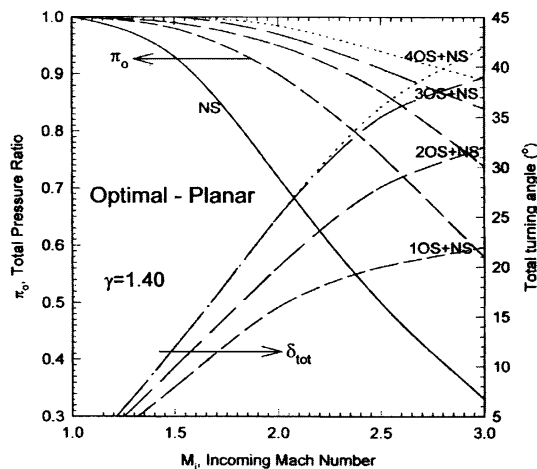


Figure 4.11 External total pressure ratio as a function of Mach number for different optimal diffuser planar shock designs.

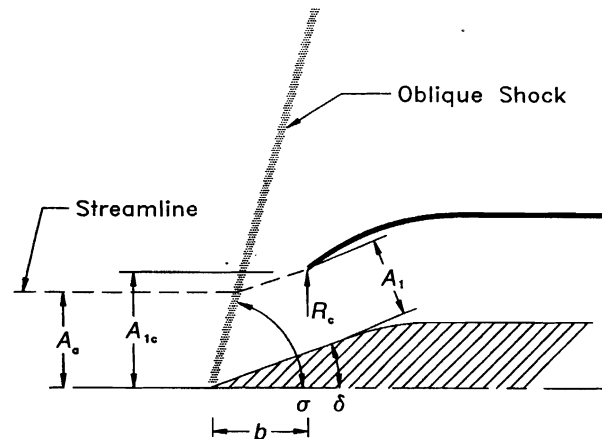


Figure 4.12 Definition of areas for mass flow ratio.

4.3.2. Internal Area Considerations

a. Mass Flow or Area Ratio

A fixed area diffuser will only operate at peak efficiency at one condition. However, it will usually be run at many different conditions. As an aid to the understanding of off-design performance and a help in determining the required area variation to extend the design range, the so-called mass flow or area ratio is used. This parameter will assist in defining the different off-design regimes in which a diffuser may operate.

At the design condition, a supersonic diffuser will operate as shown in Figure 4.8.a. As depicted, the oblique shock intersects the diffuser cowl and does not extend any farther. For this condition, all of the air that crosses the oblique shock enters the engine. One off-design condition is shown in Figure 4.12. As can be seen, for this condition the oblique shock extends outside the diffuser. Several definitions are made in this figure. For example, the area A_{1c} is the projected area based on the outside diameter of the cowl, area A_a is defined by the streamline that intersects the cowl, and area A_1 is the cross-sectional area normal to the flow at the inlet plane of the diffuser.

A reference parameter with the dimensions of mass flow rate is defined as

$$\dot{m}_i = \rho_a u_a A_{1c}, \quad 4.3.9$$

and the true ingested mass flow rate is of course

$$\dot{m}_1 = \rho_1 u_1 A_1; \quad 4.3.10$$

thus, the mass flow ratio is defined as

$$MFR \equiv \frac{\dot{m}_1}{\dot{m}_i}, \quad 4.3.11$$

and so

$$MFR = \frac{\rho_1 u_1 A_1}{\rho_a u_a A_{1c}}. \quad 4.3.12$$

The mass flow that enters the engine is, however, also given by (from Fig. 4.12):

$$\dot{m}_a = \rho_a u_a A_a, \quad 4.3.13$$

which is also \dot{m}_1 . So from Eqs. 4.3.11 and 4.3.13 one finds

$$\frac{\dot{m}_1}{\dot{m}_i} = MFR = \frac{A_a}{A_{ic}}, \quad 4.3.14$$

thus giving rise to the other name, area ratio. Note that the quantity A_a will not always be easy to define for a diffuser because it is a function of the operating and flight conditions. The mass flow ratio represents the inlet flow rate normalized to the maximum inlet flow rate. The value of MFR is thus between zero and unity.

b. Modes of Operation

As indicated in the last section, a fixed area diffuser operates most effectively for any given condition at only one flow rate. Three modes of operation exist: the flow rate is at the design rate, the flow rate is too small, and the flow rate is too great. The first to be discussed is the critical condition, which is by definition the same as the design condition. This is shown in Figure 4.8 and duplicated in Figure 4.13.a. For this case the mass flow rates \dot{m}_1 and \dot{m}_i are the same and the terminal shock occurs just inside the cowl lip; moreover, no “spillage” occurs. For this case internal shocks may not be present (not shown) or a single normal shock may sit in the inlet plane as shown. For the latter case the Mach number at the diffuser inlet plane is defined as unity, because the Mach number is ill-defined at exactly the inlet plane (i.e., a normal shock stands in the inlet).

If the flow rate is decreased, the pressure in the diffuser will be increased owing to the decreased Mach number in the diffuser. As a result, the normal shock will be pushed outside of the inlet plane. It will be stronger and will result in a larger total pressure loss. The normal shock will also join with the oblique shock to form a “ λ -shock.” Note that, ideally (i.e., at design), air encompassed by A_{ic} (far from the inlet) enters the diffuser. However, for this condition some of the air within A_{ic} (far from the diffuser, Fig. 4.12) will be “spilled.” The axial position of the spike can affect the resulting area ratio. This condition is undesirable for a variety of reasons. One reason is that the engine is compressing air using the shock (and thus working on the fluid) outside of the diffuser that is not being used, thereby wasting



Figure 4.13a Critical supersonic operation.

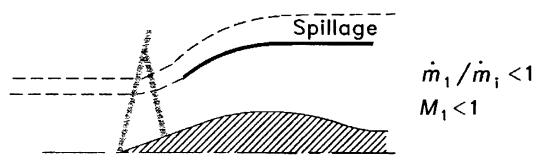


Figure 4.13b Subcritical supersonic operation.



Figure 4.13c Supercritical supersonic operation.

power. As discussed in the next section, this spillage of high-pressure air results in additive drag. For this condition, the Mach number in the inlet plane is less than unity. This overall condition is called the subcritical condition, as shown in Figure 4.13.b. Hill and Peterson (1992) further subcategorize the condition into high and low subcritical.

As the flow increases beyond the critical condition, the pressure in the diffuser decreases. Thus, the normal shock moves into the diffuser. The diffuser is now at least in part acting like a supersonic nozzle. Shocks occur in the diverging section of the diffuser at high Mach numbers, and, as a result, more total pressure is lost. This condition is the supercritical condition and is shown in Figure 4.13.c. Now the Mach number in the inlet plane is greater than unity. However, because the external flow is supersonic, the mass flows \dot{m}_1 and \dot{m}_i are still the same. No spillage occurs for this condition.

c. Off-Design Operation of the Diffuser

When a diffuser is operated at off-design conditions (i.e., at conditions different than those for which it was designed), the areas should be varied so that it operates efficiently. This is often accomplished by the axial location of the wedge or spike. The objective of this section is to develop a method by which the inlet area can be determined for given conditions and a given spike (or wedge).

First, one can examine Figure 4.12 and see immediately that, for the case of a single planar oblique shock,

$$\frac{A_a}{A_1} = \frac{\sin \sigma}{\sin(\sigma - \delta)}. \quad 4.3.15.a$$

Note that this ratio of areas is greater than unity. For a conical shock, this ratio can be found by CFD or by the numerical solution to the “Taylor–Maccoll” flow around a cone as described by Maccoll (1937) and Zucrow and Hoffman (1976):

$$\frac{A_a}{A_1} = f\left(\sigma, \delta, \frac{b}{R_c}\right). \quad 4.3.15.b$$

Note that the ratio of b/R_c (spike position to cowl radius) affects this ratio for a conical shock because of the streamline curvature but does not for the planar shock.

The engine mass flow rate is given by

$$\dot{m}_1 = \rho_1 u_1 A_1. \quad 4.3.16$$

or by

$$\dot{m}_1 = \rho_a u_a A_a. \quad 4.3.17$$

As indicated earlier, in Section 4.3.2(a) the quantity A_a is difficult to determine for conditions other than design conditions. Similarly, ρ_1 and u_1 are difficult to determine because they vary with flight and engine conditions. However, from Eq. 4.3.17, one finds

$$\dot{m}_1 = \rho_a u_a A_1 \left[\frac{A_a}{A_1} \right]. \quad 4.3.18$$

Similarly,

$$\dot{m}_1 = \rho_a u_a A_{1c} \left[\frac{A_a}{A_{1c}} \right] = MFR \dot{m}_i. \quad 4.3.19$$

One can now see more usefulness to the reference mass flow rate \dot{m}_i , for it is an easily definable quantity. The problem of finding the area variation has not been solved yet,

however. First, from solution of the oblique shock equations one can find the variation of shock angle σ with the Mach number for a given turning angle. Next a curve of the required variation of the area ratio A_a/A_1 with Mach number can be generated from the shock angle variation and Eq. 4.3.15. Next, other information on the engine performance must be used. For the operation of the engine as a system, as is covered in Chapter 11 (i.e., the matching of the inlet, compressor, burner, turbine, nozzle, etc.), one finds an engine and aircraft specification that results in the proper thrust for given conditions. These specifications result in the specification of engine mass flow rate as a function of the freestream Mach number. Lastly, one finds from Eq. 4.3.18 that

$$A_1 = \frac{\dot{m}_1}{\rho_a u_a \left[\frac{A_a}{A_1} \right]}, \quad 4.3.20$$

and so for any given freestream Mach number one can find \dot{m}_1 from the specifications, A_a/A_1 from the shock angle and Eq. 4.3.15, and ρ_a and u_a for a given altitude to generate the relation of required inlet area as a function of Mach number. Thus, it is now possible to define how the inlet area of the diffuser must vary with Mach number – that is, how the axial wedge or spike position varies with Mach number. For the case of a planar shock, the process is straightforward. For the case of the conical shock, however, an iteration loop is needed because Eq. 4.3.15.b is a function of spike position, which is also the desired end result.

Example 4.6: An engine is used on a Mach 2.5 aircraft at sea level and STP ($T_a = 288.2 \text{ K}$ or $518.7 \text{ }^\circ\text{R}$ and $p_a = 101.3 \text{ kPa}$ or 14.69 psia). The craft routinely flies between Mach numbers of 1.5 and 2.5 and at Mach numbers of 1.5, 2.0, and 2.5. At this altitude the required mass flow rate of the engine resulting from a component matching analysis is 36.28, 54.42, and 64.40 kg/s (80, 120, and 142 lbf/s), respectively. A planar wedge with an angle of 10.0° is used. What is the required inlet area variation? Assume $\gamma = 1.40$.

SOLUTION:

First, from Figure 4.7 one finds, for an incoming Mach number of $M_1 = 2.00$ and a turning angle of $\delta = 10.00^\circ$, that the shock angle is

$$\sigma = 39.31^\circ;$$

thus,

$$\frac{A_a}{A_1} = \frac{\sin \sigma}{\sin(\sigma - \delta)} = \frac{\sin 39.31^\circ}{\sin(39.31^\circ - 10.00^\circ)} = 1.294.$$

Next,

$a_a = \sqrt{\gamma \mathcal{R} T_a}$, and so at this altitude at STP

$$\begin{aligned} a_2 &= \sqrt{1.4 \times 287.1 \frac{\text{J}}{\text{kg-K}} \times 288.2 \text{ K} \times \frac{\text{N-m}}{\text{J}} \times \frac{\text{kg-m}}{\text{N-s}^2}} \\ &= 340.3 \text{ m/s (1116.4 ft/s)} \end{aligned}$$

and

$$\begin{aligned} \rho_a &= \frac{p_a}{\mathcal{R} T_a} = \frac{101.3 \text{ kPa} \times 1000 \frac{\text{N/m}^2}{\text{kPa}}}{287.1 \frac{\text{J}}{\text{kg-K}} \times 288.2 \text{ K} \times \frac{\text{N-m}}{\text{J}}} \\ &= 1.225 \text{ kg/m}^3 \text{ (0.00238 slug/ft}^3\text{)}; \end{aligned}$$

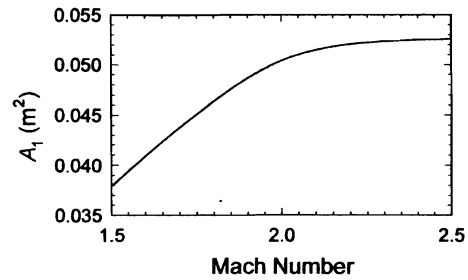


Figure 4.14 Required area variation of inlet for Example 4.6.

thus,

$$u_a = M_a a_a = 2.00 \times 340.3 = 680.6 \text{ m/s} \quad (2232.8 \text{ ft/s}).$$

Finally, from Eq. 4.3.45, one obtains

$$\begin{aligned} A_1 &= \frac{\dot{m}_1}{\rho_a u_a \left[\frac{A_a}{A_1} \right]} = \frac{54.42 \frac{\text{kg}}{\text{s}}}{1.225 \frac{\text{kg}}{\text{m}^3} \times 680.6 \frac{\text{m}}{\text{s}} \times 1.294} \\ &= 0.0504 \text{ m}^2 (0.543 \text{ ft}^2 \text{ or } 78.2 \text{ in.}^2). \end{aligned}$$

Repeating the calculations for the other two Mach numbers yields the area variation shown in Figure 4.14.

4.3.3. Additive Drag

Figure 4.15 displays a general turbojet. In the earlier analysis in Chapter 1, the flows both inside and outside the engine inlet and exit planes were assumed to be uniform.

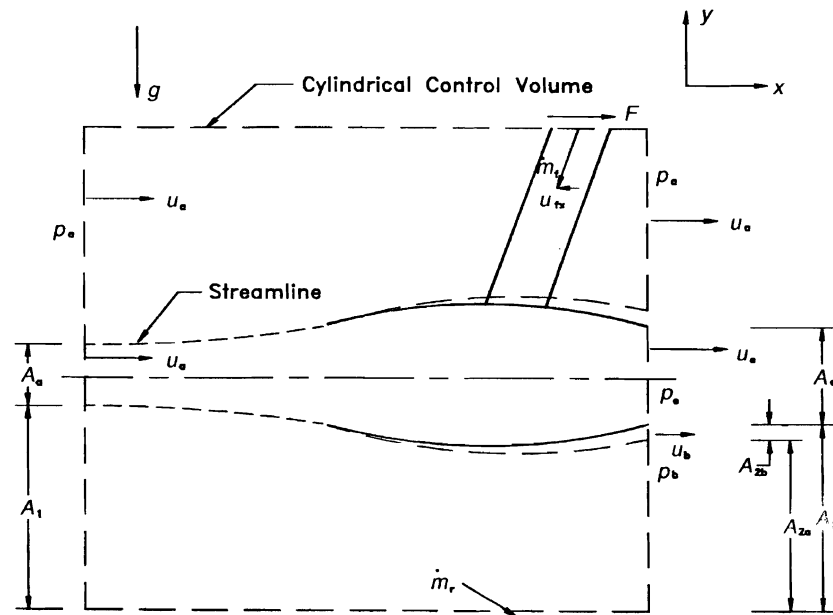


Figure 4.15 Control volume definition for a turbojet with additive drag.

However, owing to diffuser spillage and boundary layers on the exterior of the engine this is not true. These interactions lead to a reduction of thrust called additive drag. At this point, calculation of engine internal processes are not undertaken, although the results are important. A control volume, which is affixed to the engine, is drawn around the engine as shown. As before, the engine moves in air to the left with velocity u_a . The cylindrical control volume cuts through the engine strut. Fuel is also injected into the engine. One surface is at the exit plane of the engine, and the front plane is far from the inlet.

Writing the general momentum equation in rectangular coordinates yields

$$\sum \mathbf{F}_s + \sum \mathbf{F}_b = \frac{\partial}{\partial t} \int_{CV} \mathbf{V} \rho d\mathcal{V} + \int_{CS} \mathbf{V} \rho \mathbf{V} \cdot d\mathbf{A}. \quad 4.3.21$$

However, if the flow is considered to be steady, the first term on the right-hand side ($\frac{\partial}{\partial t}$ or unsteady term) disappears. Next, the thrust (x) direction should be considered. The surface forces are due to pressures on the control volume and to the cutting of the strut F , which is the force holding the engine in place. Thus, the force F represents the thrust. Because the front surface is far from the engine, the pressure is uniform and at atmospheric conditions, p_a , at this surface. At the front surface, the air flows at velocity u_a across the area $A_a + A_1$. Also, at the engine exit, the pressure in the engine is p_e , the pressure in the boundary layer is p_b , and the pressure far outside the engine is atmospheric pressure p_a . The velocity of the engine exhaust is u_e . The area of the engine exhaust is A_e , and the area of the boundary layer at the exit plane is A_{2b} . Air crosses the exit areas A_{2b} and A_{2a} with velocities u_b and u_a , respectively. The fuel is injected at a mass flow rate of \dot{m}_f with velocity $-u_{fx}$ in the x direction, but the fuel flow does not significantly contribute to the flux portion of the momentum equation. A mass flow term \dot{m}_r exits from the sides of the control volume. Thus, evaluating each of the terms and rewriting the momentum equation yield

$$\begin{aligned} F + p_a A_a + p_a A_1 - p_e A_e - p_a A_{2a} - p_b A_{2b} + F_{bx} \\ = -u_a \rho_a A_a u_a + u_e \rho_e A_e u_e - u_a \rho_a A_1 u_a + u_a \rho_a A_{2a} u_a \\ + u_b \rho_b A_{2b} u_b + \dot{m}_r u_a - \dot{m}_f u_{fx} \end{aligned} \quad 4.3.22$$

Next, one should realize that no body forces exist in the x direction ($F_{bx} = 0$). Also, uniform flow is assumed across areas A_e , A_{2b} , A_{2a} , A_1 , and A_a . The mass fluxes across these inlet and exit surfaces, which are the gas flows into and out of the engine, respectively, are once again

$$\dot{m}_a = \rho_a u_a A_a \quad 4.3.23$$

and

$$\dot{m}_e = \rho_e u_e A_e. \quad 4.3.24$$

one can also define

$$\dot{m}_b = \rho_b u_b A_{2b}. \quad 4.3.25$$

Next, by inspecting the control volume, one can see the areas are related by

$$A_1 + A_a = A_2 + A_e \quad 4.3.26$$

and

$$A_2 = A_{2a} + A_{2b}. \quad 4.3.27$$

Because the flow is steady, the continuity equation yields

$$\dot{m}_e = \dot{m}_a + \dot{m}_r \quad 4.3.28$$

and

$$\dot{m}_e + \rho_a u_a A_{2a} + \rho_b u_b A_{2b} + \dot{m}_r = \dot{m}_a + \rho_a u_a A_1 + \dot{m}_r; \quad 4.3.29$$

thus, using Eq. 4.3.28 yields

$$\rho_a u_a A_{2a} + \rho_b u_b A_{2b} + \dot{m}_r = \rho_a u_a A_1, \quad 4.3.30$$

and therefore

$$\dot{m}_r = \rho_a u_a (A_1 - A_{2a}) - \dot{m}_b. \quad 4.3.31$$

Now, using Eqs. 4.3.22 and 4.3.31, one finds

$$\begin{aligned} F + p_a A_a + p_a A_1 - p_e A_e - p_a A_{2a} - p_b A_{2b} \\ = u_e \rho_e A_e u_e - u_a \rho_a A_a u_a - u_a \rho_a A_1 u_a + u_a \rho_a A_{2a} u_a \\ + u_b \rho_b A_{2b} u_b + \rho_a u_a^2 (A_1 - A_{2a}) - \dot{m}_b u_a - \dot{m}_r u_{fx}, \end{aligned} \quad 4.3.32$$

or, using Eq. 4.3.25 and adding and subtracting like terms yield

$$\begin{aligned} F = -p_a A_a - p_a A_1 + p_e A_e + p_a A_{2a} + p_b A_{2b} + p_a A_{2b} - p_a A_{2b} \\ + \dot{m}_e u_e - \dot{m}_a u_a + \dot{m}_b (u_b - u_a) - \dot{m}_r u_{fx}. \end{aligned} \quad 4.3.33$$

Thus, using Eq. 4.3.27 results in

$$\begin{aligned} F = -p_a A_a - p_a A_1 + p_e A_e + p_a A_{2a} + A_{2b} (p_b - p_a) \\ + \dot{m}_e u_e - \dot{m}_a u_a + \dot{m}_b (u_b - u_a) - \dot{m}_r u_{fx}, \end{aligned} \quad 4.3.34$$

and so using Eq. 4.3.26 yields

$$F = (p_e - p_a) A_e + A_{2b} (p_b - p_a) + \dot{m}_e u_e - \dot{m}_a u_a + \dot{m}_b (u_b - u_a) - \dot{m}_r u_{fx}. \quad 4.3.35$$

One can next reexamine Eq. 1.4.10 for the ideal case with no additive drag and recognize that the thrust is

$$F' = (\dot{m}_e u_e - \dot{m}_a u_a) + A_e (p_e - p_a) - \dot{m}_r u_{fx}. \quad 1.4.10$$

From Eq. 4.3.35, it is possible to see that, for the current case,

$$F = F' + A_{2b} (p_b - p_a) + \dot{m}_b (u_b - u_a), \quad 4.3.36$$

or by defining an additive drag as

$$D_a = A_{2b} (p_a - p_b) + \dot{m}_b (u_a - u_b), \quad 4.3.37$$

one finds

$$F = F' - D_a. \quad 4.3.38$$

Thus, the current analysis yields the same thrust as in the ideal case considered in Chapter 1 with the exception of a thrust reduction due to the additive drag. Unfortunately, evaluating the additive drag is difficult. Obtaining the data required to evaluate the drag is a time-consuming process. Estimating these pressures and velocities for an engine on the drawing board can be accomplished by CFD. Thus, for the sake of practicality, dimensionless wind

tunnel studies have been performed, correlated, and published for a variety of engines with different diffusers. The drags are then presented as drag coefficients; that is,

$$C_{da} = \frac{D_a}{\frac{1}{2} \gamma M_a^2 p_a A_{in}}, \quad 4.3.39$$

where A_{in} is the frontal area of the inlet.

Note that the preceding analysis was performed for a turbojet engine. However, if one were to repeat the analysis for any type of engine, the thrust would be found equal to that for the ideal case with a reduction due to additive drag. For any type of engine, the actual drag will be evaluated based on CFD predictions in conjunction with wind tunnel testing of that particular geometry.

In general the additive drag coefficient for a given inlet and cowl will be the function:

$$C_{da} = f\left(\frac{\dot{m}_1}{\dot{m}_i}, M_a, \delta\right) \quad 4.3.40$$

For an inlet with a spike or wedge, M_a and δ predetermine the shock structure. In general the drag coefficient decreases with increasing mass flow ratio because of reduced spillage. At a mass flow ratio of unity, spillage does not occur and the drag coefficient is near zero. Also, as would be expected, the drag is less for a diffuser with an oblique shock than for a diffuser with a normal shock. For a normal shock, the drag coefficient increases with increasing Mach number.

4.3.4. “Starting” an Inlet

A few supersonic engines are designed to operate at least part of the time with an inlet without shocks – that is, a monotonically decelerating inlet using “internal compression” from supersonic flow to sonic to subsonic due to the converging–diverging geometry. Such an inlet has the advantage of minimal total pressure losses due to the lack of shocks. However, the idea of “starting” the diffuser becomes a problem. “Starting” can also be a problem for inlets designed to operate with oblique shocks to ensure proper sizing of the inlet and location of the shocks. For either case, the aircraft must accelerate from takeoff to the nominal flight Mach number with the inlet operating efficiently. Starting is simply defined as having the aircraft reach the desired speed and having the inlet operate at the desired design condition, including proper location of or lack of any shocks. The problem encountered is similar to starting a supersonic wind tunnel. Two methods can be used to start an inlet as described in the following paragraphs.

For this concept, refer to Figure 4.16. For the following scenario the aircraft is considered to have a fixed-area diffuser and is eventually to operate supersonically at Mach number M_d and without any shocks, but initially it will be at rest. The diffuser has fixed inlet, minimum, and exit areas, which are designed for one particular freestream Mach number M_d so that the flow enters supersonically, decelerates to the sonic condition at the throat using internal compression, and then decelerates further in the diverging section. Hill and Peterson (1992) and Zucrow and Hoffman (1976) discuss the procedure in greater detail and with analyses.

First, however, consider the aircraft to be moving very slowly (for example at takeoff) – that is, well into the subsonic regime. For this condition, the flow enters the diffuser and accelerates into the minimum area and decelerates in the diverging area, but the flow remains subsonic throughout. Next, as the aircraft speed increases but remains subsonic,

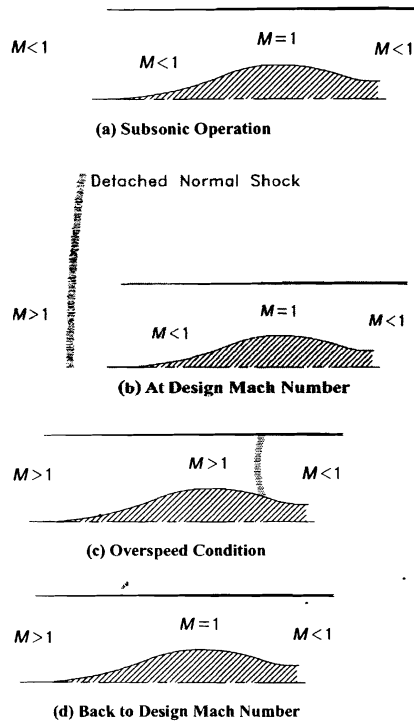


Figure 4.16 Transient shock development for an accelerating supersonic aircraft with a fixed-geometry diffuser.

the Mach number increases in the minimum area until it eventually chokes at the condition shown in Figure 4.16.a. In the diverging region, the flow decelerates subsonically. For this condition, the diffuser is actually acting like a choked nozzle, which is the opposite of the desired effect. Then, as the aircraft speed increases further, a standing normal shock develops outside of the diffuser. Initially, this shock is weak because of a low supersonic Mach number but eventually becomes strong with further increases in aircraft speed until the design speed M_d is attained (Fig. 4.16.b). The diffuser continues to operate like a choked nozzle with the strong standing shock, and the inlet is not yet operating efficiently. Next, the aircraft must be oversped to a Mach number M_s so that the shock moves toward the inlet and is suddenly swallowed (M_s is significantly greater than M_d) into the diverging part of the diffuser (Fig. 4.16.c). At this condition the flow is supersonic in the diffuser inlet, decelerates to the minimum area but remains supersonic, and accelerates supersonically up to the normal shock, where it decelerates to a subsonic condition. The standing shock is still undesirable because it results in large losses in the diffuser. As a final step, the aircraft Mach number is reduced back to M_d , where the flow is supersonic in the converging section, sonic at the throat (i.e., it is an infinitely weak shock), and subsonic in the diverging section (Fig. 4.16.d). At this point the diffuser is operating at maximum efficiency. It is important to note that the area ratio was selected for the given nominal flight Mach number M_d and does not apply to other Mach numbers.

A second, more mechanically complex method can be used to start a shockless inlet, but it does not require overspeeding. For example, consider an aircraft at operating speed

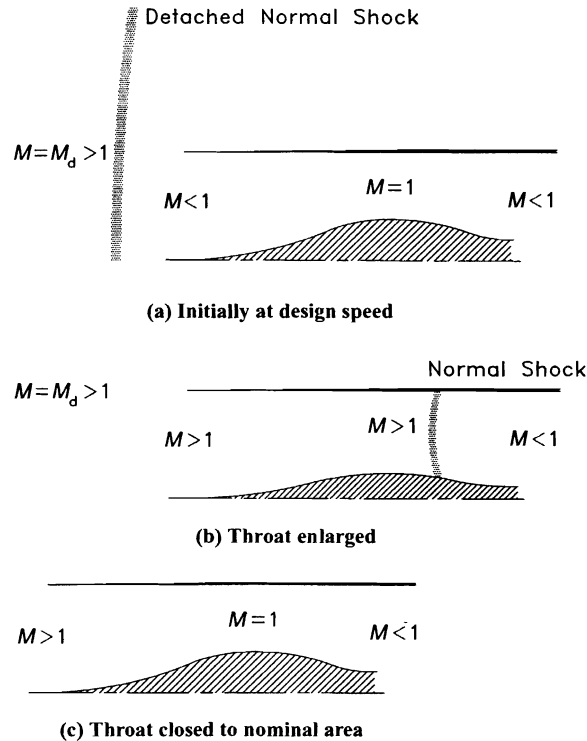


Figure 4.17 Transient shock development for a supersonic aircraft at the design Mach number with a variable geometry diffuser.

for which the geometry is held constant (Fig. 4.16.b). This condition is also shown in Figure 4.17.a. Note that for this condition the diffuser is acting like a choked nozzle, and thus the Mach number in the minimum area is unity. Next, if the minimum area is increased, the shock will be swallowed or move into the diverging region, as shown in Figure 4.17.b. Now the Mach number in the minimum area is supersonic but less so than in the inlet plane. Finally, if the minimum area is decreased to the proper value, the shock will move back to the throat and become infinitely weak – that is, the Mach number is unity (Fig. 4.17.c). Thus, now the Mach number in the inlet plane is supersonic and the flow decelerates monotonically through the diffuser. Such a method of “starting” is also used for supersonic wind tunnels. The RR/Snecma Olympus 593 (Concorde) uses a variation of this approach. For an aircraft, another method of changing the areas is by an axially moving plug, as shown in Figure 4.18. By proper design of the plug and internal cowl shapes and by controlling the axial placement of the plug, the minimum and inlet areas are varied. In Figure 4.18 two plug placements are shown depicting how the inlet and minimum areas change with axial plug position. In general, the position and area can be changed during acceleration at different altitudes and Mach numbers, increasing the envelope of efficient operation over a fixed geometry inlet.

Furthermore, a plug has the added advantage of affecting the shock positions and thus the mass flow ratio for inlets designed to operate with shocks. For example, if an aircraft has attained the design speed and if a detached normal shock is present instead of the desired

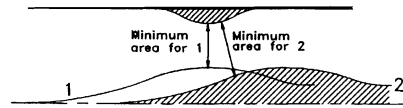


Figure 4.18 Variable diffuser geometry using a plug.

oblique shock, the plug can be moved so that the area changes, thus swallowing the normal shock and setting up the oblique shock to intersect the cowl. In Figure 4.19, a supersonic inlet designed to operate with one oblique shock and internal deceleration is shown. First, the figure presents unstarted case, which includes a detached normal shock. Second, the started inlet is shown.

4.4. Performance Map

Performance curves or “maps,” which will be developed for all of the components, are usually used to provide a working medium or methodology. These maps are used to condense a wealth of data and information as much as possible and to make the data more versatile so it can be used over a wide range of operating conditions. These maps provide a quick and accurate view of the conditions at which the inlet is operating and of what can be expected of the diffuser (and what goes to the compressor) if the flow conditions are changed. As has been seen for subsonic flow, the recovery is a function of the inlet Mach number due to friction, which is in turn a function of the freestream Mach number. For supersonic operation, the recovery factor is a strong function of the freestream Mach number due to shocks and to the inlet Mach number due to friction. Thus, the total pressure ratio for a diffuser can be written in the general form

$$\pi_d = f(M_a), \quad 4.4.1$$

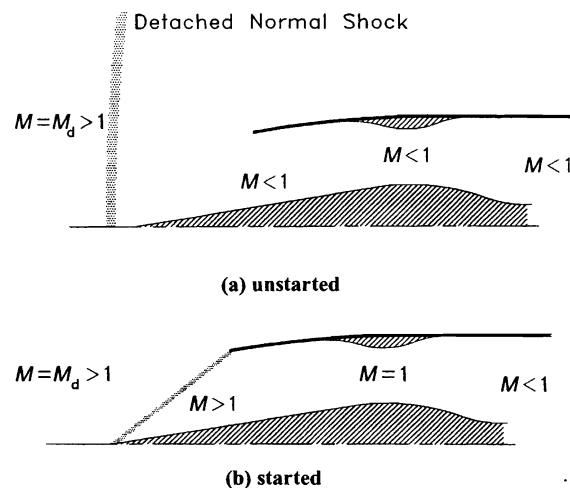


Figure 4.19 Inlet with an oblique shock.

where f can be determined from shock and Fanno line analyses, generalized one dimensional flow analysis, CFD analysis, or experimental data and can be found based on geometrical considerations. For example, for supersonic conditions for a given Mach number, the shock pattern can be found and the value of π_d can be calculated. This will not necessarily be done through a closed-form equation, for graphical or tabular means can be used as well. As has been seen through analyses for either sub- or supersonic operation, as the Mach number increases, the recovery factor decreases.

More simply, diffuser designers have found an approximate and simple (but moderately accurate) empirical correlation for well-designed diffusers. The recovery factor can be modeled as

$$\pi_d = \pi_{d_0}[1 - d(M_a - 1)^{1.35}], \quad 4.4.2$$

where π_{d_0} is the maximum pressure recovery and the constant d is 0.0 for subsonic operation and is typically 0.075 for supersonic operation. Of course, if data or analyses are available, they should be used in lieu of Eq. 4.4.2.

4.5. Summary

In this chapter the basic operating characteristics of diffusers or inlets were covered. The basic goal of the inlet is to bring the flow of air smoothly into the engine, slow the flow and increase the pressure, and deliver the air to the compressor uniformly. Two losses were found to exist. The first is due to the flow up to the inlet plane of the diffuser. This loss is greatest for a supersonic diffuser as a result of shocks and is minimal for subsonic aircraft. The second loss occurs in the internal flow in the diffuser between the diffuser inlet and inlet to the compressor. This loss is primarily caused by friction resulting from the boundary layer, turbulence, and associated separation zones. Limitations on the attainable pressure rise were addressed, and guidelines for minimizing separation areas were given. The frictional losses can first be approximated by Fanno line flow; more advanced predictions can be made using generalized 1-D frictional flow with area changes. Normal, planar oblique, and conical oblique shocks were all discussed and were seen to be functions of the Mach number and inlet geometry, which makes it possible for external loss predictions to be made. Oblique shocks or a series of gradual oblique shocks can be used to minimize losses below the level that result from normal shocks. Limits on flow turning and attached oblique shocks were discussed; if the Mach number is too low or the turning is too large, a standing normal shock (with large losses) was seen to result. For supersonic aircraft, the mass flow ratio was defined for use in developing a method to predict the off-design geometry requirements. Two distinct modes of off-design operation, which change with aircraft speed and engine mass flow rates, were discussed for supersonic diffusers. For subcritical operation, mass flow spillage occurs – that is, a portion of the airflow that ideally enters the engine spills around the inlet. For supercritical operation, the flow is supersonic in the diffuser and the resulting shocks cause a higher level of internal losses than would be experienced during subsonic operation. Additive drag on the engine cowl was found to detract directly from engine thrust because of mass flow spillage. Lastly, the concept of “starting” a supersonic inlet was discussed. Starting implies that incoming supersonic flow gradually decreases to subsonic flow without strong shocks. To start a diffuser properly one must either overspeed the aircraft until the shocks are “swallowed” or vary the inlet geometry to swallow the shocks.

 List of Symbols

A	Area
a	Speed of sound
b	Spike or wedge position
C_d	Drag coefficient
C_p	Pressure coefficient
D	Diameter
D_a	Additive drag
F	Force
f	Fanning friction factor
h	Specific enthalpy
H	Height
L	Length
M	Mach number
MFR	Mass flow ratio
R	Radius
p	Pressure
\mathcal{R}	Ideal gas constant
s	Entropy
T	Temperature
u	Specific internal energy
u	Velocity
V	Velocity
γ	Specific heat ratio
δ	Flow turning angle
π	Total pressure ratio
ρ	Density
σ	Shock angle

 Subscripts

a	Axial
a	Additive drag
b	Boundary layer
c	Cowl
d	Diffuser
d	Design
e	Exit
f	Fuel
i	Counter
i	Before shock
in	Inlet or diffuser
j	After shock
max	Maximum before detachment
n	Normal to
o	Outside of diffuser
r	Recovery
r	Rejected
s	Surface

s	Overspeed
t	Total (stagnation)
t	Tangent to
x	x direction
1	Inlet to diffuser
2	Exit of diffuser
1,2	Areas of control volume

Superscripts

'	Ideal
*	Choked

Problems

- 4.1** A supersonic inlet is designed with a two-dimensional conical spike (with a half-cone angle of 25°) to operate at a flight Mach number of 2.6. The standing oblique shock is attached to the spike and cowl, and a converging inlet section with a throat of area A_m is used to decelerate the flow using internal compression. Assume $\gamma = 1.4$ and $\pi_r = 1.0$.
- Estimate π_d on the assumption that the inlet starts (i.e., the normal shock is swallowed; see Fig. 4.19.b). Also, find the required A_m/A_1 and sketch the geometry to scale.
 - Find π_d on the assumption the inlet does not start and has a standing normal shock located in front of the spike (Fig. 4.19.a).
- 4.2** A supersonic inlet is designed with a two-dimensional conical spike (with two half-cone angles of 12° and 25° relative to the axial centerline, respectively; i.e., the turning angles are 12° and 13° , respectively). The inlet is to operate at a flight Mach number of 2.6. The two standing oblique shocks are attached to the spike and cowl, and a converging inlet section with a throat of area A_m is used to decelerate the flow using internal compression. Assume $\gamma = 1.4$ and $\pi_r = 1.0$.
- Estimate π_d on the assumption the inlet starts (i.e., the normal shock is swallowed; see Fig. 4.19.b). Also, find the required A_m/A_1 and sketch the geometry to scale.
 - Find π_d on the assumption the inlet does not start and has a standing normal shock located in front of the spike (Fig. 4.19.a).
- 4.3** Analyze a turbojet engine for an aircraft flying at $M_a = 2.6$ at sea level on a standard day. The exit burner total temperature is 3200°R , and the compressor pressure ratio is 16. Assume all aerodynamic coefficients and recovery factors are 0.90 and that $\pi_b = 0.90$ except for the diffuser, which has an internal recovery factor of 0.97. Assume a mechanical efficiency of 1.00. Consider thrust and $TSFC$ for the engine with the following three inlets having a converging-diverging nozzle, a compressor flow rate of 150 lbm/s, and $\Delta H = 18,000$ Btu/lbm.
- Inlet has a standing normal shock.
 - Inlet has a conical cone with one ramp at 25° to the centerline.
 - Inlet has a cone with two ramps. The first is 12° to the centerline and the second is 13° to the first (25° to the centerline).

- (d) Compare the results with those that would be obtained in a subsonic case with $M_a = 0.8$ and a converging–diverging nozzle.
- 4.4 Find the external recovery factor and the Mach number after the shock of a supersonic diffuser as functions of the freestream Mach number for a normal shock if $\gamma = 1.40$. Plot the results.
- 4.5 Find the external recovery factor and the Mach number after the shock of a supersonic diffuser having a spike with a cone half-angle of 15° as functions of freestream Mach number if $\gamma = 1.40$. Plot the results.
- 4.6 Flow with an incoming Mach number of 0.72 and an inlet total pressure of 12 psia enters a duct 45 in. long and 45 in. in diameter with a Fanning friction factor of 0.015. What is the total pressure ratio if the specific heat ratio is 1.40?
- 4.7 Flow with an incoming Mach number of 0.85 and an inlet total pressure of 12 psia enters a diffuser channel 45 in. long and 36 in. in diameter with an inlet area of 1018 in.². The flow has an area ratio of 1.60. The total temperature remains constant at 480 °R. What is the exit Mach number if there are no frictional losses and if the specific heat ratio is 1.40? What is the exit pressure and pressure coefficient? Comment.
- 4.8 Flow with an incoming Mach number of 0.85 and an inlet total pressure of 12 psia enters a diffuser channel 45 in. long and 36 in. in diameter with an inlet area of 1018 in.². The flow has a Fanning friction factor of 0.015 and an area ratio of 1.60. The total temperature remains constant at 480 °R. What is the total pressure ratio if the specific heat ratio is 1.40?
- 4.9 A supersonic inlet is designed with a two-dimensional conical spike (with a half-cone angle of 20°) to operate at a flight Mach number of 1.9. The standing oblique shock is attached to the spike and cowl, and a converging inlet section with a throat of area A_m is used to decelerate the flow using internal compression. Assume $\gamma = 1.4$ and $\pi_r = 0.97$.
- (a) Estimate π_d on the assumption the inlet starts (i.e., the normal shock is swallowed; see Fig. 4.19.b). Also, find the required A_m/A_1 and sketch the geometry to scale.
- (b) Find π_d on the assumption the inlet does not start and has a standing normal shock located in front of the spike (Fig. 4.19a).
- 4.10 A supersonic inlet is designed with a two-dimensional conical spike (with two half-cone angles 10° and 20° relative to the axial centerline, respectively; i.e., the turning angles are 10° and 10° , respectively). The inlet is to operate at a flight Mach number of 1.9. The two standing oblique shocks are attached to the spike and cowl, and a converging inlet section with a throat of area A_m is used to decelerate the flow through internal compression. Assume $\gamma = 1.4$ and $\pi_r = 0.97$.
- (a) Estimate π_d on the assumption the inlet starts (i.e., the normal shock is swallowed). Also, find the required A_m/A_1 and sketch the geometry to scale.
- (b) Find π_d on the assumption the inlet does not start and has a standing normal shock located in front of the spike.
- 4.11 Analyze a turbofan engine (fully mixed) with a bypass ratio of 2.2 for an aircraft flying at $M_a = 1.9$ at 22,000 ft on a standard day. The burner exit

total temperature is 2800 °R, and the compressor pressure ratio is 19. Assume all aerodynamic coefficients and recovery factors are 0.90 and $\pi_b = 0.90$ except for the diffuser, which has an internal recovery factor of 0.97. Assume a mechanical efficiency of 0.998, a mixer total pressure ratio of 0.99, and a duct total pressure ratio of 0.99. Find the thrust and *TSFC* for the engine with a converging nozzle, a compressor flow rate of 140 lbm/s, and $\Delta H = 17,800$ Btu/lbm for the following three inlets.

- (a) Inlet has a standing normal shock.
- (b) Inlet has a conical cone with one ramp at 20° to the centerline.
- (c) Inlet has a cone with two ramps. The first is 10° to the centerline, and the second is 10° to the first (20° to the centerline).

4.12 Analyze a turbofan engine (fully exhausted) with a bypass ratio of 2.2 for an aircraft flying at $M_a = 1.9$ at 22,000 ft on a standard day. The burner exit total temperature is 2800 °R, and the compressor pressure ratio is 19. Assume all aerodynamic coefficients and recovery factors are 0.90 and $\pi_b = 0.90$ except for the diffuser, which has an internal recovery factor of 0.97. Assume a mechanical efficiency of 0.998 and a fan total pressure ratio of 1.90. Find the thrust and *TSFC* for the engine with converging nozzles, a compressor flow rate of 140 lbm/s, and $\Delta H = 17,800$ Btu/lbm for the following three inlets.

- (a) Inlet has a standing normal shock.
- (b) Inlet has a conical cone with one ramp at 20° to the centerline.
- (c) Inlet has a cone with two ramps. The first is 10° to the centerline and the second is 10° to the first (20° to the centerline).

4.13 A diffuser with a spike is used on a supersonic aircraft. The freestream Mach number is 2.0, and the cone half-angle is 25°. Inside the diffuser (which is designed to be shockless), there is a recovery factor of 0.95. What is the total recovery factor (freestream to diffuser exit) of the diffuser? Assume the diffuser has started.

4.14 A standing normal shock occurs on an aircraft flying at Mach 1.50. The internal recovery factor of the diffuser is 0.98, and the specific heat ratio is 1.40. Find the total recovery factor for the diffuser.

4.15 An aircraft moves at Mach 1.6 and has a diffuser with a conical spike. The cone has an angle of 15° relative to the centerline. You can assume that the diffuser has started (swallows the shock and is shockless inside the diffuser). If the internal total pressure ratio is 0.98, what is the overall pressure recovery factor? What is the inlet Mach number at the diffuser inlet? Assume a specific heat ratio of 1.40.

4.16 A supersonic inlet is designed with a two-dimensional conical spike (with a half-cone angle of 24°) to operate at a flight Mach number of 2.2. The standing oblique shock is attached to the spike and cowl, and a converging inlet section with a throat of area A_m is used to decelerate the flow through internal compression. Assume $\gamma = 1.4$ and $\pi_r = 0.98$.

- (a) Estimate π_d on the assumption the inlet starts (i.e., the normal shock is swallowed; see Fig. 4.19.b). Also, find the required A_m/A_1 and sketch the geometry to scale.
- (b) Find π_d on the assumption the inlet does not start and has a standing normal shock located in front of the spike (Fig. 4.19.a).

- 4.17** A supersonic inlet is designed with a two-dimensional conical spike (with two half-cone angles 12° and 24° relative to the axial centerline, respectively; i.e., the turning angles are 12° and 12° , respectively). The inlet is to operate at a flight Mach number of 2.2. The two standing oblique shocks are attached to the spike and cowl, and a converging inlet section with a throat of area A_m is used to decelerate the flow using internal compression. Assume $\gamma = 1.4$ and $\pi_r = 0.98$.
- Estimate π_d on the assumption the inlet starts (i.e., the normal shock is swallowed; see Fig. 4.19.b). Also, find the required A_m/A_1 and sketch the geometry to scale.
 - Find π_d on the assumption the inlet does not start and has a standing normal shock located in front of the spike (Fig. 4.19.a).
- 4.18** An engine similar in size to an older military nonafterburning turbojet ingests 120 lbm/s of air at sea level. When it flies at a Mach number of 2.2, the compressor pressure ratio is 14.6. The fuel has a heating value of 17,800 Btu/lbm, and the burner exit total temperature is 2580°R . The efficiencies of the compressor, burner, turbine, shaft, and converging–diverging nozzle are 90, 95, 92, 100, and 96 percent, respectively. The total pressure ratio for the burner is 0.95. The diffuser has an internal pressure recovery factor of 0.98. Find the thrust and *TSFC* for the engine for the following three inlets:
- Inlet has a standing normal shock.
 - Inlet has a conical cone with one ramp at 24° to the centerline.
 - Inlet has a cone with two ramps. The first is 12° to the centerline, and the second is 12° to the first (24° to the centerline).
- 4.19** Design a diffuser to attain the maximum pressure rise if the incoming Mach number is 0.80. That is, find the aspect ratio (L/D_1), area ratio (A_2/A_1), pressure ratio, and exit Mach number.
- 4.20** An aircraft moves at Mach 2.5 and has a diffuser with a conical spike. The cone has an angle of 50° relative to the centerline. If the internal total pressure ratio is 0.97, what is the overall pressure recovery factor? What is the inlet Mach number at the diffuser inlet? Assume a specific heat ratio of 1.40.
- 4.21** Flow enters a long converging inlet for a gas turbine at Mach 0.30. The mass flow rate is 100 lbm/s, and the inlet total pressure and temperature are 14 psia and 500°R , respectively. The L/D ratio is 20, and the area ratio is 0.70. The Fanning friction coefficient is 0.015, and the specific heat ratio is 1.40. The air warms slightly to a total temperature of 530°R . Use a generalized 1-D analysis and find the internal recovery factor of the inlet.
- 4.22** An aircraft moves over a range of Mach numbers and has a diffuser with a movable conical spike. The cone has a fixed angle of 20° relative to the centerline. What is the minimum flight Mach number that will allow the diffuser to operate efficiently? If the internal total pressure ratio is 0.98, what is the overall pressure recovery factor? Accurately sketch the diffuser. Should the diffuser have a minimum area for this minimum flight condition? Assume a specific heat ratio of 1.40.
- 4.23** A rectangular supersonic inlet is constructed with a two-dimensional planar ramp. Following the oblique shock, the inlet is designed to be shockless at

the design Mach number of 2.00. The engine mass flow rate is 100 lbm/s at sea level. Assume $\gamma = 1.40$ and an internal recovery coefficient of 0.97.

- (a) What is the maximum deflection angle before the shock detaches?
- (b) Obtain the total recovery coefficient for the diffuser for the maximum deflection angle.
- (c) Sketch the inlet.
- (d) What is the required inlet area of the diffuser for the maximum deflection angle?

4.24 An annular supersonic inlet is constructed with a two-dimensional cone. Following the oblique shock, the inlet is designed to operate without any shocks at a design freestream Mach number of 2.00. The engine mass flow rate is 145 lbm/s at sea level. Assume $\gamma = 1.40$ and an internal recovery coefficient of 0.96.

- (a) What is the maximum deflection (half-cone) angle before the oblique shock detaches?
- (b) Obtain the total recovery coefficient for the diffuser for the maximum deflection angle.
- (c) Sketch the inlet showing important angles.

4.25 A planar two-dimensional ramp is used with a rectangular supersonic inlet. The aircraft flies at a Mach number of 1.70 ($\gamma = 1.40$). A shock angle of 40° results.

- (a) What is the ramp angle, exit Mach number, and total pressure ratio of the shock?
- (b) To what angle could the ramp be increased and still maintain an attached shock? For this condition, what is the exit Mach number and total pressure ratio of the shock?

4.26 A conical two-dimensional spike is used with a supersonic inlet. The aircraft flies at a Mach number of 2.60 ($\gamma = 1.40$). A shock angle of 35° results.

- (a) What is the ramp angle, exit Mach number, and total pressure ratio of the shock?
- (b) To what angle could the ramp be increased and still maintain an attached shock? For this condition, what is the exit Mach number and total pressure ratio of the shock?

4.27 Find the external recovery factor and the Mach number after the shock of a supersonic diffuser with a wedge having a wedge angle of 15° as functions of freestream Mach number if $\gamma = 1.40$. Plot the results.

4.28 A conical two-dimensional spike is used with an inlet for an aircraft that flies at a Mach number of 1.60 ($\gamma = 1.40$) at an altitude with a static pressure of 5 psia. A half-cone angle of 36° is used. The internal pressure recovery is 0.98.

- (a) What are the Mach number and total pressure behind the shock?
- (b) What is the overall pressure recovery of the inlet?

4.29 Find the external recovery factor and the Mach number after a single oblique shock and normal shock of a supersonic diffuser with a spike having a cone half-angle of 25° as functions of freestream Mach number if $\gamma = 1.40$. Plot the results.

- 4.30** A planar two-dimensional wedge is used with an inlet for an aircraft that flies at a Mach number of 2.00 ($\gamma = 1.40$) at an altitude with a static pressure of 7 psia. A half-wedge angle of 21° is used. The internal pressure recovery is 0.975.
- What is the Mach number behind the shock?
 - What is the shock angle?
 - What is the total pressure at the exit of the diffuser?
 - For this wedge angle, what is the minimum freestream Mach number before the shock detaches?
- 4.31** A planar two-dimensional wedge and resulting oblique shock is used with a normal shock in an inlet for an aircraft that flies at a Mach number of 2.50 ($\gamma = 1.40$) at an altitude with a static pressure of 5 psia. A half-wedge angle of 17° is used. The internal pressure recovery is 0.980.
- What is the Mach number behind the normal shock?
 - What is the oblique shock angle?
 - What is the total pressure at the exit of the diffuser?
 - For this wedge angle, what is the minimum freestream Mach number before the shock detaches?
- 4.32** A planar two-dimensional wedge with a half-wedge angle of 18° is used in an inlet for an aircraft. When a resulting oblique shock occurs, a normal shock follows, which reduces the Mach number below unity. Plot the external recovery factor for a Mach number range of 1.0 to 3.0
- 4.33** Flow with an incoming Mach number of 0.80 and an inlet total pressure of 12 psia enters a diffuser channel 45 in. long having a 36 in. diameter. The diffuser has an area ratio of 1.20. The total temperature remains constant at 480°R . The flow has a Fanning friction factor of 0.015 and the specific heat ratio is 1.40.
- What is the total pressure ratio?
 - What is the pressure coefficient? Comment.
- 4.34** A solid cone and resulting conical oblique shock are used in an inlet of an aircraft that flies at Mach 2.00 ($\gamma = 1.40$) at an altitude of 30,000 ft.
- What cone angle will yield the smallest Mach number behind the oblique shock?
 - What is the resulting Mach number behind the shock on the cone surface?
 - What is the oblique shock angle?
 - What is the total pressure ratio?
 - For this cone angle, what is the minimum freestream Mach number before the oblique shock detaches?
- 4.35** A planar two-dimensional wedge is used for an inlet of an aircraft that flies at a Mach number of 2.00 ($\gamma = 1.40$) at an altitude with a static pressure of 7 psia. A half wedge angle of 28° is used. The internal pressure recovery is 0.980. What is the total pressure at the exit of the diffuser?
- 4.36** A conical two-dimensional spike is used for an inlet of an aircraft that flies at a Mach number of 2.00 ($\gamma = 1.40$) at an altitude with a static pressure of 7 psia. A half cone angle of 45° is used. The internal pressure recovery is 0.980. What is the total pressure at the exit of the diffuser?

Nozzles

5.1. Introduction

A nozzle is sometimes called the exhaust duct or tail pipe and is the last component of a jet engine through which the air passes. Up to two parallel nozzles are present on an engine: primary and fan (or secondary). In this chapter, both converging and converging–diverging nozzle types are discussed, and the two nozzles can be any combination of the two types (i.e., converging and converging–diverging, converging and converging, etc.). Recall that the functions of the nozzles are to convert high-pressure, high-temperature energy (enthalpy) to kinetic energy and to straighten the flow so that it exits in the axial direction. It is from this conversion process that the thrust is derived. Because of the high temperatures that a nozzle experiences, materials used in nozzle construction are usually a nickel-based alloy, titanium alloy, or ceramic composite. In Chapter 3, the nonideal effects of nozzles are discussed. In this chapter, these effects are covered in more detail along with other design considerations.

5.2. Nonideal Equations

The governing equations for one-dimensional flow in nonideal nozzles are presented in Chapter 3. For the sake of convenience they are repeated in this chapter.

5.2.1. Primary Nozzle

$$\eta_n = \frac{h_{t6} - h_8}{h_{t6} - h'_8} \quad 5.2.1$$

$$u_8 = \sqrt{2(h_{t6} - h_8)} \quad 5.2.2$$

$$u_8 = \sqrt{2 c_p \eta_n (T_{t6} - T'_8)} \quad 5.2.3$$

$$\frac{T_8}{T_{t6}} = \frac{1}{1 + \frac{\gamma-1}{2} M_8^2} \quad 5.2.4$$

$$\frac{p_8}{p_{t6}} = \left[\frac{T'_8}{T_{t6}} \right]^{\frac{\gamma}{\gamma-1}} \quad 5.2.5$$

$$\frac{p_8}{p_{t6}} = \left[\frac{\frac{1}{1 + \frac{\gamma-1}{2} M_8^2} - 1 + \eta_n}{\eta_n} \right]^{\frac{\gamma}{\gamma-1}} \quad 5.2.6$$

$$\frac{p^*}{p_{t6}} = \left[1 + \frac{1 - \gamma}{\eta_n (1 + \gamma)} \right]^{\frac{\gamma}{\gamma-1}} \quad 5.2.7$$

$$\frac{A_8}{A^*} = \frac{1}{M_8} \sqrt{\frac{\gamma + 1}{2 + (\gamma - 1)M_8^2}} \left[\eta_n \frac{1 + \frac{1-\gamma}{\eta_n(1+\gamma)}}{\frac{1}{1 + \frac{\gamma-1}{2}M_8^2} - 1 + \eta_n} \right]^{\frac{\gamma}{\gamma-1}} \quad 5.2.8$$

5.2.2. Fan Nozzle

$$\eta_f = \frac{h_{t7} - h_9}{h_{t7} - h_9'} \quad 5.2.9$$

$$u_9 = \sqrt{2(h_{t7} - h_9)} \quad 5.2.10$$

$$u_9 = \sqrt{2c_p \eta_{fn}(T_{t7} - T_9')} \quad 5.2.11$$

$$\frac{T_9}{T_{t7}} = \frac{1}{1 + \frac{\gamma-1}{2}M_9^2} \quad 5.2.12$$

$$\frac{p_9}{p_{t7}} = \left[\frac{T_9'}{T_{t7}} \right]^{\frac{\gamma}{\gamma-1}} \quad 5.2.13$$

$$\frac{p_9}{p_{t7}} = \left[\frac{\frac{1}{1 + \frac{\gamma-1}{2}M_9^2} - 1 + \eta_{fn}}{\eta_{fn}} \right]^{\frac{\gamma}{\gamma-1}} \quad 5.2.14$$

$$\frac{p^*}{p_{t7}} = \left[1 + \frac{1-\gamma}{\eta_{fn}(1+\gamma)} \right]^{\frac{\gamma}{\gamma-1}} \quad 5.2.15$$

$$\frac{A_9}{A^*} = \frac{1}{M_9} \sqrt{\frac{\gamma + 1}{2 + (\gamma - 1)M_9^2}} \left[\eta_{fn} \frac{1 + \frac{1-\gamma}{\eta_{fn}(1+\gamma)}}{\frac{1}{1 + \frac{\gamma-1}{2}M_9^2} - 1 + \eta_{fn}} \right]^{\frac{\gamma}{\gamma-1}} \quad 5.2.16$$

5.2.3. Effects of Efficiency on Nozzle Performance

Before the details of nozzle operation and design are addressed, it behooves the reader to better understand the effect of efficiency on nozzle performance. Figures 5.1 and 5.2 serve this purpose. In Figure 5.1, the nozzle pressure ratio is presented as a function of the Mach number for three different efficiencies for $\gamma = 1.35$ and only the ideal case for $\gamma = 1.30$. As can be seen, lowering the nozzle efficiency tends to reduce this ratio. This can be interpreted in two ways. For example, for a nozzle with a given total inlet pressure and an area ratio designated so that the nozzle exit pressure matches the ambient pressure, as the efficiency is decreased the exit Mach number declines as well. As a result, the developed thrust also decreases. From another perspective, for a nozzle with an area ratio again designated so that the nozzle exit pressure matches the ambient pressure, if a particular exit Mach number is desired, the inlet total pressure is larger for the nonideal case than for the ideal one, thus requiring a higher pressure from the turbine.

In Figure 5.2, the area ratio (A/A^*) is plotted versus the Mach number for three efficiencies for $\gamma = 1.35$ and only the ideal case for $\gamma = 1.30$. For subsonic flow, the ratio decreases with decreasing efficiency. However, for supersonic flow, the ratio increases with decreasing efficiency. Therefore, achieving a given supersonic Mach number requires a larger nozzle (larger exit area) for the nonideal case than for the ideal one. Also, with a choked converging

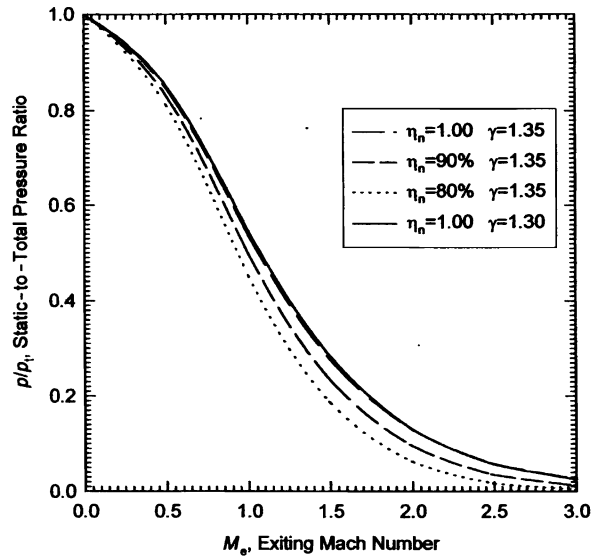


Figure 5.1 Variation of Mach number with nozzle pressure ratio.

nozzle, more convergence is necessary for a nozzle with losses than for an ideal nozzle. Also note that the Mach number is slightly less than one at the minimum area and that the minimum area is slightly less than the sonic area for efficiencies less than one. The specific heat ratio has minimal effects for both plots – especially for low Mach numbers.

5.3. Converging Nozzle

The simplest type of nozzle is the ideal converging nozzle. As the name implies, the exit cross-sectional flow area is smaller than the inlet area. This type of nozzle can be found on the primary and/or fan nozzle, or both. This nozzle can operate under two different

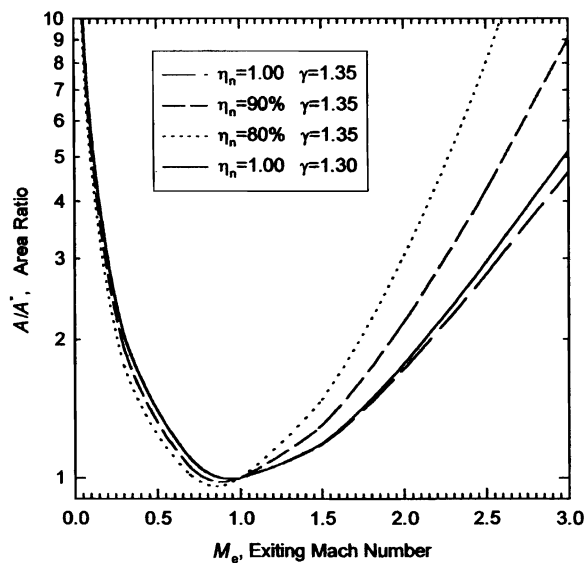


Figure 5.2 Variation of area ratio with Mach number.

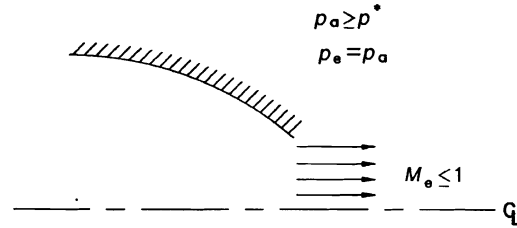


Figure 5.3a Exhaust of converging nozzle with matching exhaust and ambient pressures.

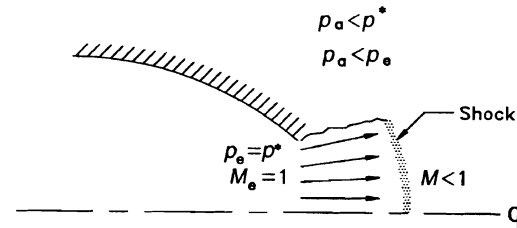


Figure 5.3b Exhaust of underexpanded converging nozzle.

conditions. First, the exit pressure can match the ambient condition. For this case, the exit Mach number is equal to or less than unity and the exit pressure is greater than or equal to the reference pressure at the sonic condition p^* , as determined from Eq. 5.2.7 or 5.2.15. This condition is shown in Figure 5.3.a.

For the second condition, the ambient pressure is less than the value of p^* . Inside the nozzle the flow accelerates up to the exit, and in the plane of the exit the Mach number is unity. However, after the gas exits from the nozzle, it continues to expand in a two-dimensional manner and accelerate for a short distance in an effort to match the back pressure (Fig. 5.3.b). In this small region the Mach number is greater than 1. Eventually, a near-normal shock or series of oblique shocks occur downstream of the nozzle, which decelerates the flow to a subsonic condition. The flow remains subsonic after these shocks. This condition is called the supercritical or underexpanded condition.

For a choked converging nozzle with an efficiency less than unity, the nozzle exit Mach number is actually slightly less than one. However, as indicated in Chapter 3 to simplify the analyses in this book, the sonic condition will be used for the choked case because the difference has minimal effect on the engine thrust and *TSFC*.

5.4. Converging–Diverging Nozzle

As the name implies, the cross-sectional area decreases and then increases along the nozzle centerline. This nozzle type is often called a de Laval or Laval nozzle. This is a more complex geometry, and seven different conditions can be experienced with this type of nozzle. The seven conditions are compared in Figure 5.4 and discussed below. This type of nozzle can be found for the primary nozzle but is used less often as a fan nozzle. For the following discussions, a fixed nozzle geometry with an efficiency of unity will be assumed so that the areas do not change as a function of operating condition. Variable nozzles are discussed in the following section.

The first condition to be considered is operation of the nozzle with the nozzle exit pressure equal to the ambient conditions and with the flow subsonic throughout (case 1, Fig. 5.4). The maximum Mach number is at the minimum area. This nozzle type typically is not operated in this regime.

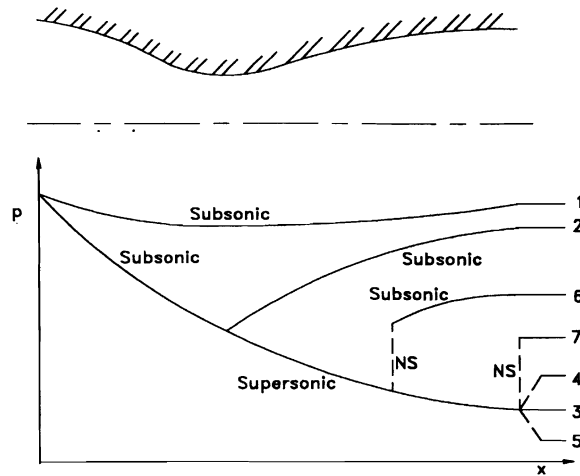


Figure 5.4 Seven conditions of a converging-diverging nozzle.

The second condition is shown as case 2 and is similar to case 1, but now the Mach number at the minimum area is unity. Again, this nozzle type is usually not operated in this regime.

The third case to be considered is case 3, which is characterized by smooth and shockless flow throughout the nozzle, and the exit pressure matches the ambient pressure. In the converging section the flow is subsonic, and in the diverging area the flow is supersonic. For the ideal case, this would represent the design condition of the nozzle because it would result in the maximum thrust.

For the fourth case the ambient pressure is slightly above the design exit pressure. This results in a complex two-dimensional flow pattern outside the nozzle, as shown in Figure 5.5. This is considered to be an overexpanded case, and the flow suddenly is compressed and decelerates outside of the nozzle. A series of compression waves and expansion waves are generated that can be calculated based on two-dimensional compressible flow – for example,

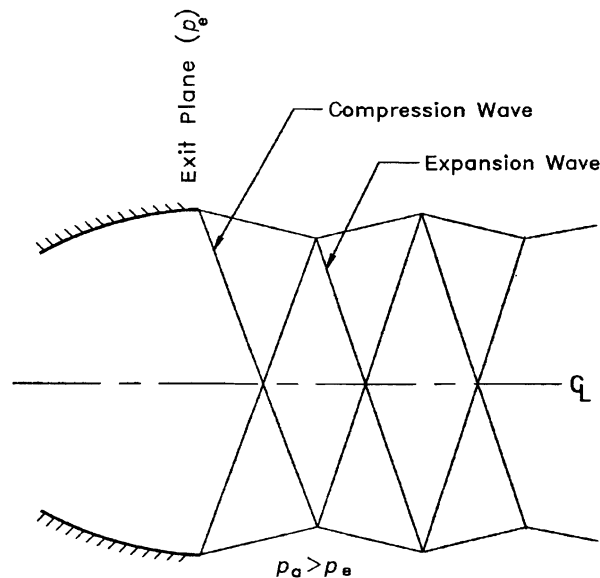


Figure 5.5 Exhaust of overexpanded converging-diverging nozzle (Case 4).

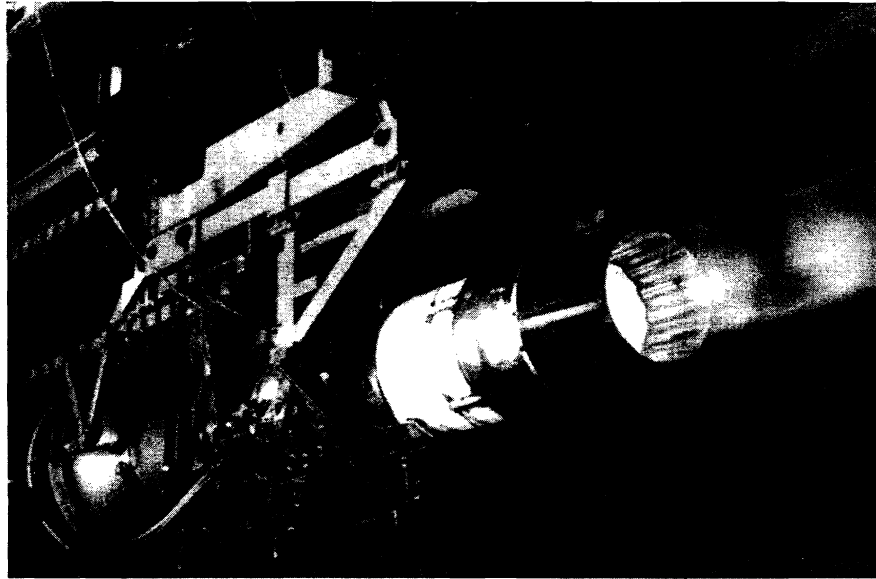


Figure 5.6 Pratt & Whitney F100 engine on test stand – overexpanded exit (courtesy of Pratt & Whitney).

with the method of characteristics described by Zucrow and Hoffman (1976). The net result is a series of “shock diamonds,” which are shown in Figure 5.6 in a photograph of a test on a Pratt & Whitney F100 afterburning turbofan (mixed fan, Fig. 1.33). A Schlieren photograph of this condition is shown in Figure 5.7.a. A schlieren is an optical technique that can be used to visualize a flowfield with large density gradients (Merzkirch 1974).

For the fifth case the ambient pressure is below the design exit pressure. This again results in a complex two-dimensional flow pattern outside the nozzle, as shown in Figure 5.8. This is considered to be an underexpanded or supercritical case, and the flow continues to expand and accelerate outside the nozzle. A series of expansion waves and compression waves are generated that can be calculated based on two-dimensional compressible flow. The net result is again a series of “shock diamonds,” which are opposite in order to those found for the overexpanded case. A Schlieren photograph of this condition is presented in Figure 5.7.b, and a shadowgraph photograph is presented in Figure 5.9. A shadowgraph is an optical technique that can be used to visualize flowfields with large values of $\nabla^2 \rho$ (Merzkirch 1974).

For the sixth case the ambient pressure is significantly above the nozzle design exit pressure but below the pressure covered in case 2. This condition results in a single normal shock in the nozzle diverging region or a series of oblique and normal shocks called λ shocks. This is also an overexpanded case and is shown in Figure 5.10. This case results in a subsonic exit Mach number, which is undesirable from the standpoint of thrust.

A limiting condition of case 6 is an exit pressure that causes a normal shock to occur exactly in the exit plane. This is considered to be case 7. Note that case 4 falls between this limiting case and case 3.

Although one-dimensional flow is assumed for the working equations presented, the flow can be two- or three-dimensional. As the flow deviates from the one-dimensional case, the axial component of velocity decreases because the flow has a radial component. The radial component does not contribute to the thrust as dictated by the momentum equation. The two-dimensional nature is best demonstrated by observations of the sonic line near the

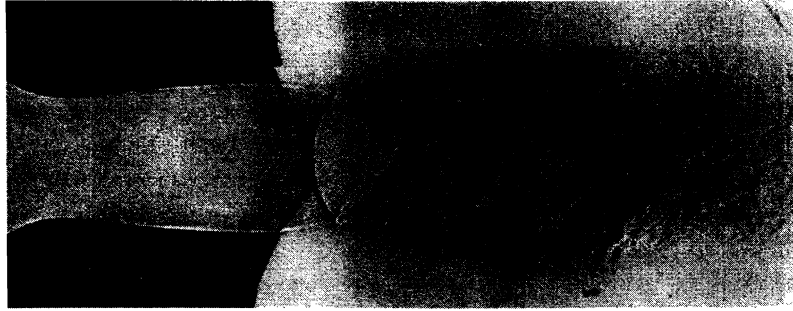


Figure 5.7a Schlieren photograph of overexpanded jet.

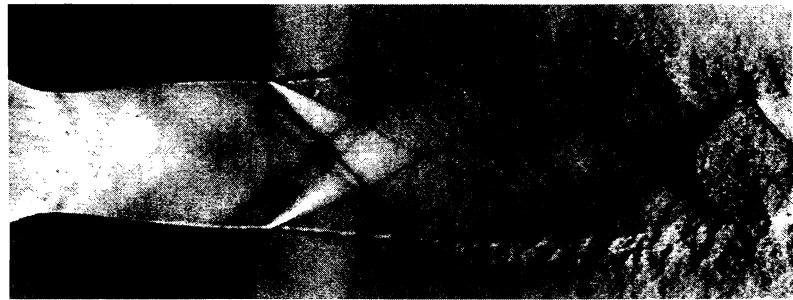


Figure 5.7b Schlieren photograph of underexpanded jet (from Howarth (1953)) (© Crown copyright 1953 reproduced by permission of the Controller of HMSO).

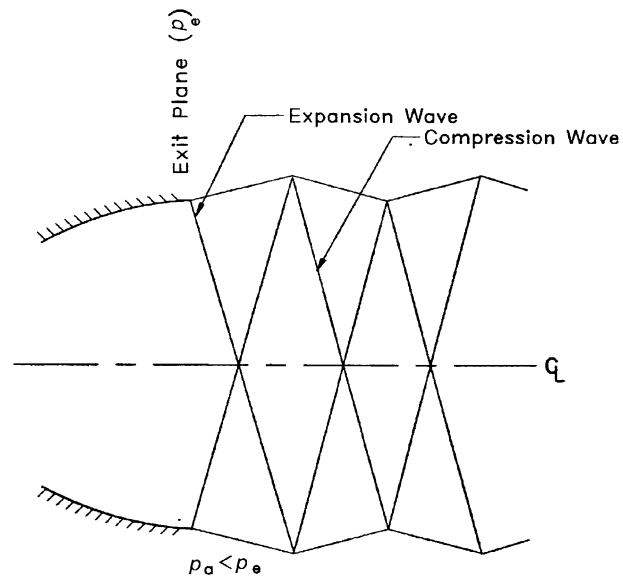


Figure 5.8 Exhaust of underexpanded converging-diverging nozzle (Case 5).

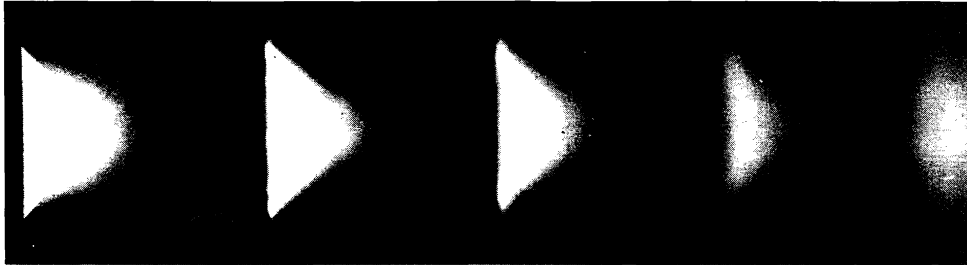


Figure 5.9 Shadowgraph of underexpanded jet (courtesy of Goldstein Lab., University of Manchester).

throat of a converging–diverging nozzle. Ideally, the sonic line is a straight line between the surfaces at the minimum area. However, Flack and Thompson (1975) measured the sonic line position for a series of symmetric and nonsymmetric planar geometries, and a typical result is shown in Figure 5.11. The sonic line is in fact curved, indicating the nature of the two-dimensionality.

When addressing a problem or design of a converging–diverging nozzle, the general operating regime must be determined before details of the flow can be established. For example, if the back pressure is known for a given nozzle geometry, only one of the seven preceding conditions will hold. To determine which case applies, one must establish the brackets; that is, one must determine what back pressures will result in limiting cases 2, 3, and 7. Once the brackets are determined, the flow regime in which the nozzle is operating for a given back pressure can be found, which will make it possible to proceed with the analysis of the details. Solutions can also be obtained for a shockless converging or converging–diverging nozzle using the software, “NOZZLE” and can be combined with results from “SHOCK” to accommodate all of the various regimes. Also, note that property variations in both nozzle types can be predicted using the generalized one-dimensional flow model from Appendix H (as done in Chapter 4), which can, in fact, be used to predict nozzle efficiency (Problems 5.20 and 5.31).

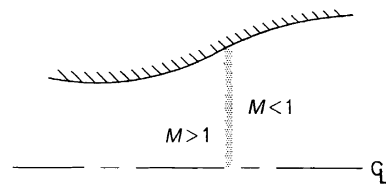


Figure 5.10a Exhaust of overexpanded converging–diverging nozzle with single normal shock in diverging area (Case 6).

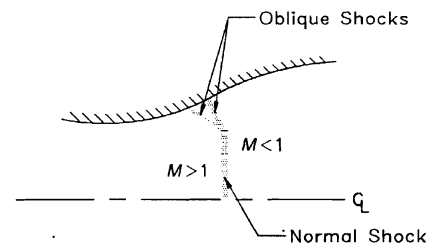


Figure 5.10b Exhaust of overexpanded converging–diverging nozzle with several oblique (λ) shocks in diverging area.

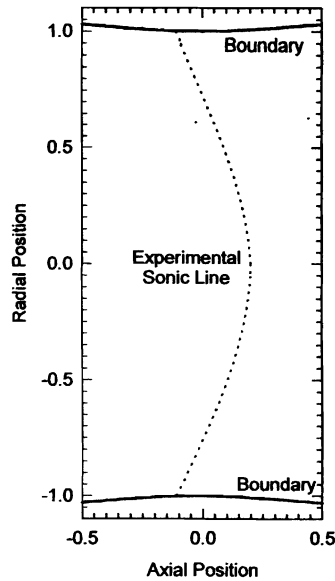


Figure 5.11 Typical sonic line.

Example 5.1: A converging–diverging nozzle operates at an atmospheric pressure of 68.95 kPa (10 psia). It has a minimum area of 0.1393 m² (1.5 ft²) and an exit area of 0.2786 m² (3.0 ft²). The inlet total pressure and temperature are 241.3 kPa (35 psia) and 611.1K (1100 °R), respectively. The effective specific heat ratio is 1.340, and the nozzle efficiency is 98 percent. Find the overall general operating condition and mass flow rate.

SOLUTION:

Before proceeding, it is necessary to determine under what general conditions the nozzle is operating. For example, if the nozzle were choked, the problem would be solved differently than if it were not choked. Thus, to proceed, one must determine for which of the seven conditions in Figure 5.4 the nozzle is operating. To determine this, one must find what back pressure will cause conditions 2, 3, and 7. Once these brackets are found, the remainder of the problem can be solved or more internal details can be determined if desired.

Case 2

For this case, the nozzle is shockless and choked but subsonic at the exit. One must find the exit Mach number and then the exit pressure. First, from Eq. 5.2.8,

$$\frac{A_8}{A^*} = \frac{1}{M_8} \sqrt{\frac{\gamma + 1}{2 + (\gamma - 1)M_8^2}} \left[\eta_n \frac{1 + \frac{1-\gamma}{\eta_n(1+\gamma)}}{\frac{1}{1 + \frac{\gamma-1}{2}M_8^2} - 1 + \eta_n} \right]^{\frac{\gamma}{\gamma-1}}$$

Thus, (A^* is approximately 0.1393 m²)

$$\frac{0.2786}{0.1393} = 2.0 = \frac{1}{M_8} \sqrt{\frac{2.34}{2 + 0.34M_8^2}} \left[0.98 \frac{1 + \frac{-0.34}{0.98 \times 2.34}}{\frac{1}{1 + \frac{0.34}{2}M_8^2} - 1 + 0.98} \right]^{\frac{1.34}{0.34}}$$

Solving for M_8 (iteratively), one finds $M_8 = 0.3035$.

Next, from Eq. 5.2.6, one finds that

$$\frac{p_8}{p_{t6}} = \left[\frac{\frac{1}{1 + \frac{\gamma-1}{2} M_8^2} - 1 + \eta_n}{\eta_n} \right]^{\frac{\gamma}{\gamma-1}},$$

and

$$\frac{p_8}{p_{t6}} = \left[\frac{\frac{1}{1 + \frac{0.34}{2} 0.3035^2} - 1 + 0.98}{0.98} \right]^{\frac{1.34}{0.34}} = 0.9394.$$

Thus, for this case the back pressure that would cause this condition is

$$p_8 = 0.9394 \times 241.3 \text{ kPa} = 226.7 \text{ kPa} \quad (32.88 \text{ psia}).$$

Case 3

For this case the nozzle is shockless and choked but now supersonic at the exit. One must again find the exit Mach number and then the exit pressure. From Eq. 5.2.8,

$$2.0 = \frac{1}{M_8} \sqrt{\frac{2.34}{2 + 0.34 M_8^2}} \left[0.98 \frac{1 + \frac{-0.34}{0.98 \times 2.34}}{\frac{1}{1 + \frac{0.34}{2} M_8^2} - 1 + 0.98} \right]^{\frac{1.34}{0.34}}.$$

This is exactly the same equation as above for case 2 (there are two roots to the equation). Solving for M_8 (iteratively, for conditions are now supersonic), one finds $M_8 = 2.103$. Next, Eq. 5.2.6 yields

$$\frac{p_8}{p_{t6}} = \left[\frac{\frac{1}{1 + \frac{0.34}{2} 2.103^2} - 1 + 0.98}{0.98} \right]^{\frac{1.34}{0.34}} = 0.1032.$$

Thus, for case 3 the back pressure is

$$p_8 = 0.1032 \times 241.35 \text{ kPa} = 24.91 \text{ kPa} \quad (3.613 \text{ psia}).$$

Also, for this case, the static temperature in the exit plane is found by

$$\frac{T_8}{T_{t6}} = \frac{1}{1 + \frac{\gamma-1}{2} M_8^2}.$$

Thus,

$$\frac{T_8}{T_{t6}} = \frac{1}{1 + \frac{0.34}{2} 2.103^2} = 0.5708.$$

Therefore, $T_8 = 0.5708 \times 611.1 \text{ K} = 348.8 \text{ K} (627.9^\circ \text{R})$. Note that the calculation of the temperature in the exit plane is independent of the ambient temperature.

Case 7

For this case the nozzle is shockless and choked and is supersonic just in front of the exit. A normal shock is in the exit plane. Once again, the exit Mach number and then the exit pressure must be found.

Just upstream of the exit, the Mach number and pressure are exactly the same as for case 3. Using normal shock equations (i.e., Eqs. 4.3.1 and 4.3.3), one obtains

$$M_3^2 = \frac{M_i^2 + \frac{2}{\gamma-1}}{\frac{2\gamma}{\gamma-1} M_i^2 - 1}.$$

Thus,

$$M_{8j}^2 = \frac{2.103^2 + \frac{2}{0.34}}{\frac{2 \times 1.34}{0.34} 2.103^2 - 1}$$

Therefore, just beyond the nozzle exit plane the Mach number is

$$M_{8j} = 0.5516 \quad (\text{obviously subsonic}).$$

Also, across the normal shock the pressure ratio is

$$\frac{p_j}{p_i} = \frac{2\gamma}{\gamma + 1} M_i^2 - \frac{\gamma - 1}{\gamma + 1}$$

Thus,

$$\frac{p_{8j}}{p_{8i}} = \frac{2 \times 1.34}{2.34} 2.103^2 - \frac{0.34}{2.34} = 4.921.$$

Therefore, for case 7 the back pressure is

$$p_{8j} = 4.921 \times 24.91 \text{ kPa} = 122.6 \text{ kPa} (17.78 \text{ psia}).$$

Clearly, the imposed condition (68.95 kPa ambient conditions) falls between cases 3 and 7. Thus, by examining Figure 5.4 one can quickly see that the imposed condition corresponds to condition 4 and nonisentropic shocks and compressions outside the nozzle. Up to the nozzle exit, the flow behaves as for case 3.

Had the back pressure been greater than 226.7 kPa (32.88 psia), the flow would have been subsonic throughout the nozzle. If the back pressure had been between 122.6 and 226.7 kPa, a standing normal shock would have been present in the diverging section of the nozzle. The axial position of the shock would have had to be found by iteration, as discussed in the next example. Had the back pressure been less than 24.91 kPa, the flow within the nozzle would have been exactly as it is for case 3; however, a series of nonisentropic 2-D expansions would have occurred outside the nozzle.

Since the flow is choked for the case of interest, one can simply use the conditions from case 3 to calculate the mass flow rate. That is,

$$\dot{m} = \rho_8 u_8 A_8,$$

but $u_8 = M_8 a_8$ and

$$\begin{aligned} a_8 &= \sqrt{\gamma \mathcal{R} T_8} \\ &= \sqrt{1.34 \times 287.1 \frac{\text{J}}{\text{kg-K}} \times 348.8 \text{ K} \times \frac{\text{N-m}}{\text{J}} \times \frac{\text{kg-m}}{\text{N-s}^2}} \\ &= 366.4 \text{ m/s} (1202 \text{ ft/s}) \end{aligned}$$

Thus $u_8 = 2.103 \times 366.4 = 770.2 \text{ m/s} (2527 \text{ ft/s})$.

Also, from the ideal gas law, for $T_8 = 348.8 \text{ K}$ and $p_8 = 24.91 \text{ kPa}$,

$$\rho_8 = 0.2489 \text{ kg/m}^3 (0.0004828 \text{ slug/ft}^3).$$

Lastly, for the mass flow rate,

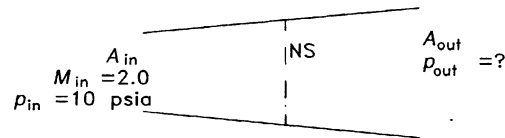
$$\begin{aligned} \dot{m} &= 0.2489 \frac{\text{kg}}{\text{m}^3} \times 770.2 \frac{\text{m}}{\text{s}} \times 0.2786 \text{ m}^2 \\ &= 53.42 \text{ kg/s} (117.8 \text{ lbm/s}). \end{aligned}$$

Example 5.2: An exhaust air stream at Mach 2.0, pressure 10 psia, and temperature 1400 °R enters a frictionless diverging nozzle with a ratio of exit area to inlet area

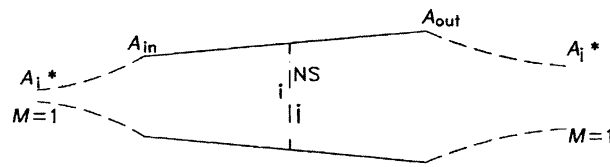
of 3.0. Determine the back pressure necessary to produce a normal shock in the channel at an area equal to twice the inlet area. Assume one-dimensional steady flow with the air behaving as a perfect gas with constant specific heats and a specific heat ratio of 1.36; assume isentropic flow except for the normal shock.

SOLUTION:

For isentropic flow, the area at which Mach number is equal to 1 is defined as A^* , and, this area is used as a reference. In this problem, the flow is not isentropic from cross section “i” to cross section “j” because of the normal shock. Therefore, the reference area A_i^* for the flow from A_{in} to A_i is not equal to the reference area A_j^* for the isentropic flow from A_j to A_{out} . Determining the flow conditions after the shock requires a relationship between A_i^* and A_j^* .



NOTE: Section “i” is immediately before the shock, and section “j” is immediately after the shock.



The flow from “in” to “i” is isentropic and accelerating because of the divergence; thus,

$$p_{in} = p_{ti}$$

But for $M_{in} = 2.0$, one finds $A_{in}/A_i^* = 1.719$ (from isentropic flow tables or equations); thus,

$$p_{in}/p_{ti} = 0.1289$$

$$\text{or } p_{ti} = 10/0.1289 = 77.58 \text{ psia.}$$

$$\text{Also } \frac{A_i}{A_i^*} = \frac{A_i}{A_{in}} \frac{A_{in}}{A_i^*},$$

$$\text{thus, } A_i/A_i^* = 2 \times 1.719 = 3.439$$

$$\text{and } M_i = 2.723 \text{ (from isentropic flow tables)}$$

$$\text{and } p_i/p_{ti} = 0.0406$$

$$\text{or } p_i = 0.0406 \times 77.58 = 3.15 \text{ psia.}$$

By knowing the incoming Mach number for a normal shock, one can find the exiting Mach number (e.g., by normal shock tables):

$$M_j = 0.4855$$

$$p_{tj}/p_{ti} = 0.3991$$

$$p_j/p_i = 8.393.$$

$$\text{Thus, } p_j = 8.393 \times 3.15 = 26.75 \text{ psia}$$

$$\text{and } p_{tj} = 0.3991 \times 77.58 = 30.96 \text{ psia.}$$

Now, since the decelerating flow due to divergence from “j” to “out” is isentropic for $M_j = 0.4855$, one finds $A_j/A_j^* = 1.372$ (by isentropic flow tables or equations)

$$\text{and } \frac{A_{\text{out}}}{A_j^*} = \frac{A_{\text{out}}}{A_{\text{in}}} \frac{A_{\text{in}}}{A_j} \frac{A_j}{A_j^*} = 3 \times \frac{1}{2} \times 1.372 = 2.058.$$

Note again that the reference area A_j^* is not the same as A_i^* . Therefore, by isentropic flow tables or calculations,

$$M_{\text{out}} = 0.2975$$

$$\text{and } p_{\text{out}}/p_{ij} = 0.942$$

$$\text{or finally } p_{\text{out}} = 29.16 \text{ psia.}$$

Had the exit pressure been specified (p_{out}), the location (or area A_i) at which the shock was located would not have been known and would have been found by iteration. For example, one would assume a value of A_i , go through the preceding procedure, and calculate p_{out} . If the calculated value of p_{out} did not match the specified exit pressure, a new value of A_i would be guessed and iterated upon until the calculated and specified exit pressures matched. The iteration is quick to converge if, for example, the Reguli Falsi method is used (Appendix G).

5.5. Effects of Pressure Ratios on Engine Performance

As indicated in Chapters 1, 2, and 3 in the book, if the nozzle exit pressure exactly matches the ambient pressure, the only thrust component is due to the momentum flux. If the nozzle exit pressure is less than the ambient condition (overexpanded), a negative thrust due to the pressures results. However, a larger-than-ideal thrust from the momentum flux occurs because the exit velocity is larger than for the ideally expanded case. On the other hand, if the nozzle pressure is higher than the ambient pressure (underexpanded), a positive thrust results from the pressure terms. However, a lower-than-ideal thrust results from the momentum flux because a lower-than-ideal exit velocity occurs. Since, for both cases for which the exit pressure, fails to match the ambient pressure, the two thrust components have opposite trends, one may wish to know for what conditions the optimum (or maximum) thrust occurs. This question is best answered with examples.

Example 5.3: An ideal turbojet flies at sea level ($p_a = 14.69$ psia) at Mach 0.75. It ingests 165 lbm/s of air, and the compressor operates with a pressure ratio of 15. The fuel has a heating value of 17,800 Btu/lbm, and the burner exit total temperature is 2500 °R. Find the developed thrust for a nozzle exit pressure from 12.69 to 16.69 psia that is controlled by the exit area. This is similar to Example 2.2 with the exception of the difference between the exit and ambient pressures.

SOLUTION:

Because this is nearly identical to Example 2.2, details of the computations are not shown. However, bear in mind that the exit pressures are specified for this problem and are not set equal to the ambient pressure.

Basically, results are presented graphically in Figure 5.12. Shown here are the net thrust, exit area, and exit jet velocity as functions of the exit pressure. As can be seen, the maximum thrust occurs when the exit pressure (p_8) exactly matches the ambient pressure (p_a). Although this fact was shown numerically here, it can also

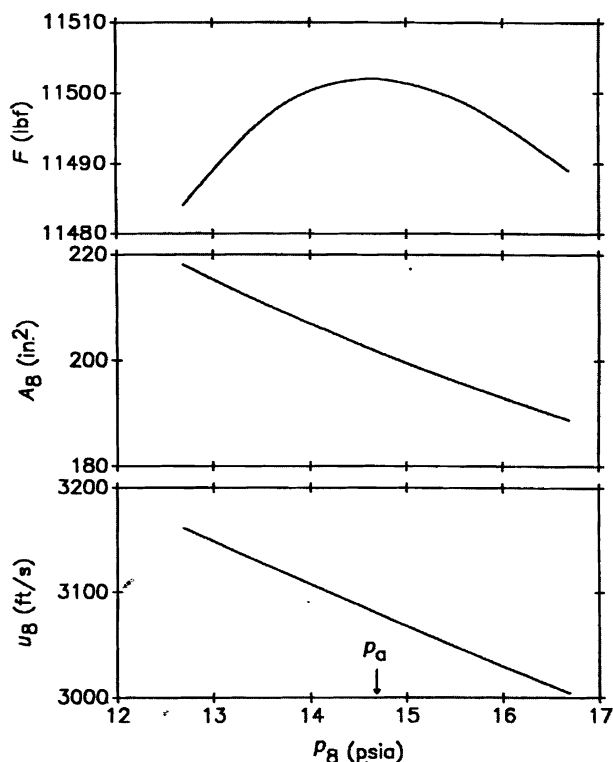


Figure 5.12 Variation of net thrust, exit area, and exit velocity with exit pressure for an ideal turbojet.

be shown analytically by differentiating the net thrust equation, setting the term to zero, and solving for p_8 (Problem 5.17). From Figure 5.12, one should note that, although the maximum thrust occurs when $p_8 = p_a$, under off-design conditions the net thrust does not deteriorate quickly.

Also shown is that the required exit area decreases with increasing exit pressure and that the exit velocity follows the same trend. Thus, at low pressures, the thrust due to the momentum flux is greater than for the case in which the exit pressure matches the ambient pressure; however, at this condition the pressure-generated thrust is negative and more than offsets the increase due to momentum flux. Similarly, at high pressures, although the pressure generates a positive thrust, the reduced momentum flux more than offsets this increase.

Example 5.4: A turbojet flies at sea level ($p_a = 14.69$ psia) at a Mach number of 0.75. It ingests 165 lbm/s of air. The compressor operates with a pressure ratio of 15 and an efficiency of 88 percent. The fuel has a heating value of 17,800 Btu/lbm, and the burner total temperature is 2500 °R. The burner has an efficiency of 91 percent and a total pressure ratio of 0.95, whereas the turbine has an efficiency of 85 percent. A converging-diverging nozzle is used, and total pressure recovery for the diffuser is 0.92. The shaft efficiency is 99.5 percent. Find the developed thrust as a function of nozzle efficiency and exit pressure. This is similar to the preceding example with the exception of the nonideal effects.

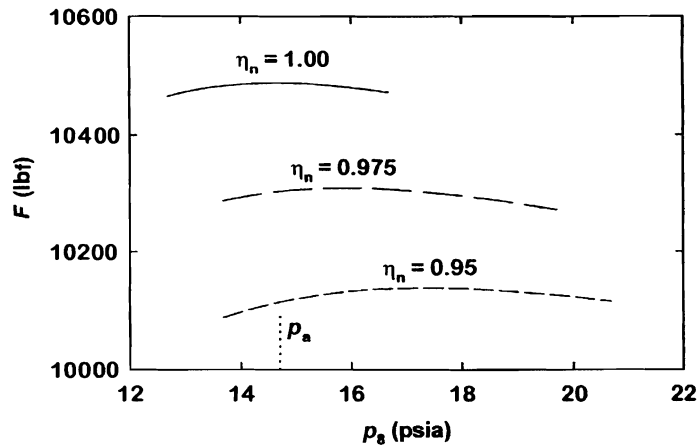


Figure 5.13 Variation of net thrust with exit pressure for three nozzle efficiencies for a nonideal turbojet.

SOLUTION:

With the exception of the nozzle efficiency and exit pressure, this is identical to Example 3.1.b, and details of the computations will not be shown. Keep in mind, however, that the exit pressures are specified for this problem and are not set equal to the ambient pressure but are varied by changing the exit area. Results are presented graphically in Figure 5.13. The net thrust is shown here as a function of the exit pressure for three values of nozzle efficiency: 1.00, 0.975, and 0.95.

As can be seen from Figure 5.13, for $\eta_n = 1.00$ the maximum thrust is once again obtained (and the maximum occurs for $p_e = p_a$). However, for $\eta_n = 0.975$ the maximum thrust occurs at an exit pressure of approximately 15.9 psia. Finally, for $\eta_n = 0.95$, the maximum thrust is realized at an exit pressure of about 17.3 psia. Thus, as the nozzle efficiency is decreased, more thrust is obtained if the exit pressure is above the ambient conditions. This indicates that, for these conditions, less of the enthalpy is converted to the momentum flux and that more additional thrust is obtained from the pressure generator term. This conclusion is also implied by the definition of the nozzle efficiency. Note also that the maximum of the thrust–exit pressure curve is less “peaked” for lower efficiencies, and thus when there is a deviation from the optimum exit pressure, the thrust does not deteriorate significantly.

5.6. Variable Nozzle

One means by which a nozzle can be forced to operate at maximum thrust or “on design” under many different flight conditions is through a variable geometry. For such a nozzle, the area of the exit, throat, or both is varied so that the optimum exit pressure can be obtained. Two nozzle shapes are usually used: a simple circular (iris) nozzle or a plug nozzle. Note that variable nozzles are typically not used on commercial aircraft because of the limited flight envelope – that is, the craft and engine basically are optimally designed for one altitude and flight condition. Military fighters, on the other hand, must be designed to operate under a variety of conditions, including aircraft carrier takeoff. As a result, most of these engines have variable nozzles.

In Figure 5.14, the Pratt & Whitney TF30 afterburning turbofan (fan mixed) is shown. This engine is equipped with a variable iris nozzle. In Figure 5.14.a, a photograph is shown, and Figure 5.14.b presents a schematic. Two nozzle orientations are shown in the schematic: the fully open position with the largest exit area and the fully closed position with the smallest exit area. The open position would be used for high altitudes (low ambient pressure), and the closed position would be used for low altitudes. The nozzle assembly is essentially a series of curved “flaps,” each of which is a four-bar linkage system driven by a hydraulic piston (Fig. 5.14.c). By moving the identical flaps fore-to-aft by identical amounts, the areas are changed by prescribed amounts based on the movement amplitude and flap shapes. Both the exit and throat areas are controlled for the P&W TF30. Positions between the two extremes can also be used to optimize the performance. Many modern engines, especially in military applications, use such an arrangement. For example, the F100 (Fig. 5.6) also has a variable iris nozzle. With the proper flap geometry or shape, the nozzle can be operated as either a converging nozzle or a converging–diverging nozzle. Furthermore, with the proper shape, the minimum and exit areas can both be varied.

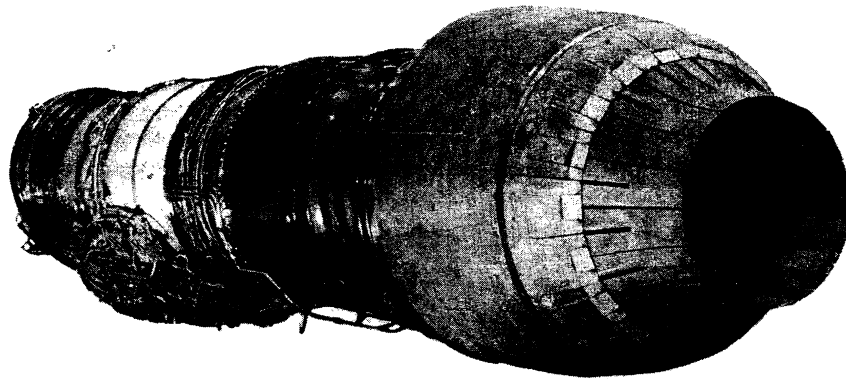


Figure 5.14a Photograph of Pratt & Whitney TF30 with variable exhaust nozzle (courtesy of Pratt & Whitney).

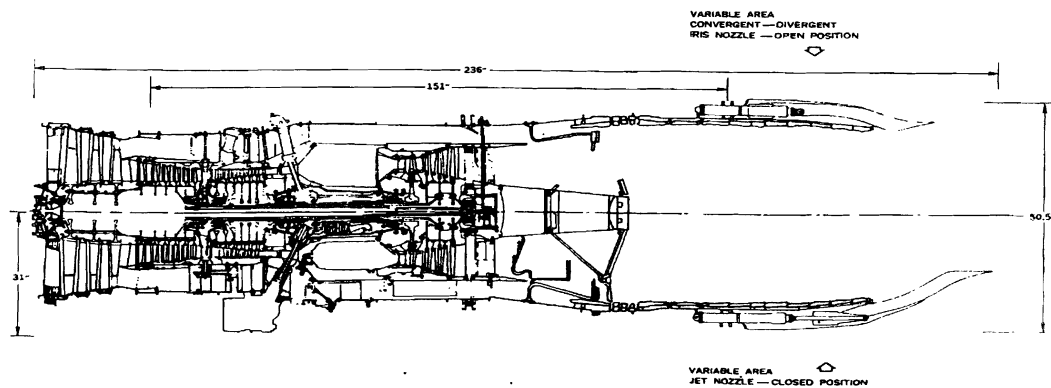


Figure 5.14b Schematic of Pratt & Whitney TF30 showing two nozzle positions (courtesy of Pratt & Whitney).

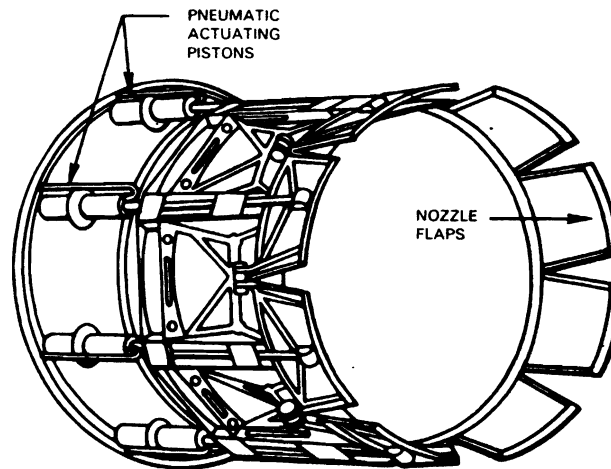


Figure 5.14c Schematic of iris nozzle with flaps (courtesy of Pratt & Whitney).

A second geometry that is sometimes used is the plug nozzle shown in Figure 5.15. For this geometry, the exit area is not only varied but the throat area is controlled. Thus, varying the axial location of the plug changes the area ratio to adjust the exit pressure. Two such positions of the plug are shown in Figure 5.15. The major problem with this geometry is that the plug and the positioning mechanism are subjected to the extreme freestream temperatures.

5.7. Performance Maps

5.7.1. Dimensional Analysis

Performance “maps” are usually used, as for a diffuser, to provide a working medium or methodology for a nozzle engineer. Again, these maps are used to simplify a substantial amount of data and make these data most versatile for use over a wide range of operation. These maps provide a quick and accurate view of the conditions at which the nozzle is operating and what can be expected of the nozzle if the flow conditions are changed. Of primary concern is the mass flow rate of a nozzle – that is \dot{m}_6 for a primary nozzle or \dot{m}_7 for a fan nozzle – and the exit Mach number (M_8 and M_9 for the primary and fan nozzles, respectively). The mass flow rate is a function of many variables, and the

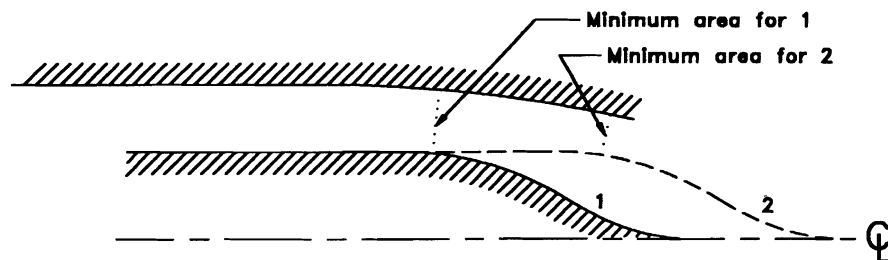


Figure 5.15 Plug nozzle.

functional relationship for a primary nozzle can be written as

$$\dot{m}_6 = \mathcal{f}\{T_{t6}, A_8, p_{t6}, p_a, \gamma, \mathcal{R}\}. \quad 5.7.1$$

One can use dimensionless parameters to reduce the number of independent variables. Using the Buckingham Pi theorem, one finds for a given value of γ that

$$\dot{m}_6 \frac{\sqrt{\mathcal{R} T_{t6}}}{A_8 p_{t6}} = \mathcal{f} \left\{ \frac{p_{t6}}{p_a} \right\}. \quad 5.7.2$$

This form is rarely used to document the performance of a nozzle, however. Usually, one finds a modification of this; that is,

$$\dot{m}_6 \frac{\sqrt{\theta_{t6}}}{\delta_{t6}} = \dot{m}_{c6} = \mathcal{f} \left\{ \frac{p_{t6}}{p_a} \right\}, \quad 5.7.3$$

where

$$\delta_{t6} = \frac{p_{t6}}{p_{stp}} \quad 5.7.4$$

and

$$\theta_{t6} = \frac{T_{t6}}{T_{stp}} \quad 5.7.5$$

and where stp refers to the standard conditions. For reference and from Appendix A, p_{stp} is equal to 14.69 psia or 101.33 kPa, and T_{stp} is equal to 518.7 °R or 288.2 K. Note that the two parameters in Eq. 5.7.3 are not truly dimensionless but are prudently chosen so that the function \mathcal{f} retains the important characteristics of nondimensionalization. The first parameter (left-hand side) is called the “corrected” mass flow and has dimensions of mass flow, whereas the pressure ratio (inside the brackets) is dimensionless. Thus, since they both are not dimensionless and, in particular, since the parameter A_8 has been eliminated, the resulting function cannot be used to correlate or compare different nozzles. The function can be used to characterize the data over a range of conditions, altitudes, and so on for one particular nozzle, however, as is the usual case. Thus, a nozzle can be tested under one set of conditions, and the results can be “corrected” so that *results are applicable to other conditions so long as the parameter $\frac{p_{t6}}{p_a}$ is matched*. Similarly, for the exit Mach number, one finds

$$M_8 = \mathcal{g} \left\{ \frac{p_{t6}}{p_a} \right\}, \quad 5.7.6$$

where the function \mathcal{g} is different from that of \mathcal{f} . One can develop similar relationships for a secondary nozzle. The functions \mathcal{g} and \mathcal{f} can be derived from experimental data, modeling, or a combination of empiricism and modeling.

5.7.2. Trends

a. Fixed Converging Nozzle

Typical trends of \dot{m}_{c6} and M_8 are shown in Figures 5.16 through 5.18 for three particular nozzle types. In Figure 5.16, typical trends for a fixed converging nozzle are shown. As can be seen, the corrected mass flow rate increases as the pressure ratio rises – until the nozzle chokes – and then remains constant as the pressure ratio increases further.

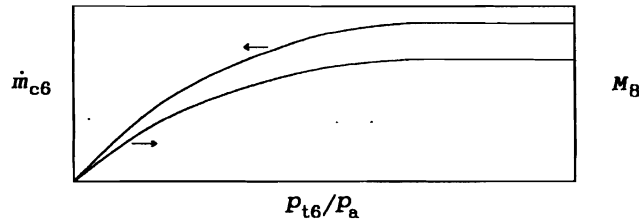


Figure 5.16 Typical nozzle performance map for a fixed converging nozzle.

For this case, one can show that

$$\dot{m}_{c6} = \rho_{\text{stp}} a_{\text{stp}} A_e \frac{p_8}{p_{t6}} M_8 \sqrt{\frac{\gamma}{\gamma_{\text{stp}}}} \sqrt{\frac{\mathcal{R}_{\text{stp}}}{\mathcal{R}}} \sqrt{1 + \frac{\gamma - 1}{2} M_8^2}, \quad 5.7.7$$

which includes variations in the specific heat ratio and ideal gas constant. Next, by grouping some constants and defining a reference mass flow rate \dot{m}_n as $\rho_{\text{stp}} a_{\text{stp}} A_e$, one finds

$$\dot{m}_{c6} = \dot{m}_n \frac{p_8}{p_{t6}} M_8 \sqrt{\frac{\gamma}{\gamma_{\text{stp}}}} \sqrt{\frac{\mathcal{R}_{\text{stp}}}{\mathcal{R}}} \sqrt{1 + \frac{\gamma - 1}{2} M_8^2}. \quad 5.7.8$$

For this case, if p_a is less than p^* given by Eq. 5.2.7, then p_8 is about equal to p^* and the exit Mach number is about unity. Note that, if the nozzle is choked and if p_{t6} is increased, the corrected mass flow rate \dot{m}_{c6} remains constant whereas the true flow rate \dot{m}_6 increases. However, if p_a is greater than or equal to p^* , then p_8 is equal to p_a and the exit Mach number is equal to

$$M_8 = \sqrt{\frac{2}{\gamma - 1} \left[\frac{1}{\eta_n \left[\frac{p_8}{p_{t6}} \right]^{\frac{\gamma - 1}{\gamma}} + 1} - 1 \right]}. \quad 5.7.9$$

b. Variable Converging–Diverging Nozzle – Fixed Exit Area

Figure 5.17 shows typical trends for a variable converging–diverging nozzle with a fixed exit area and a “schedule” so that the exit pressure matches the ambient pressure. A “schedule” is a prescribed and predetermined specific variation of the minimum area that is a function of altitude and other local conditions. For this case, the exit Mach number can be subsonic or supersonic and the corrected mass flow increases until the nozzle chokes at

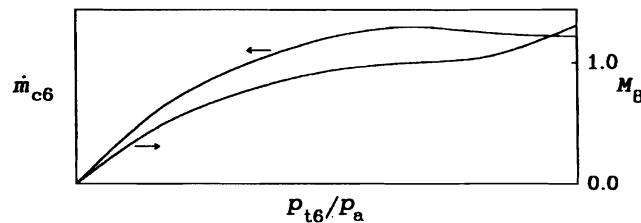


Figure 5.17 Typical nozzle performance map for a variable converging–diverging nozzle with a fixed exit area.

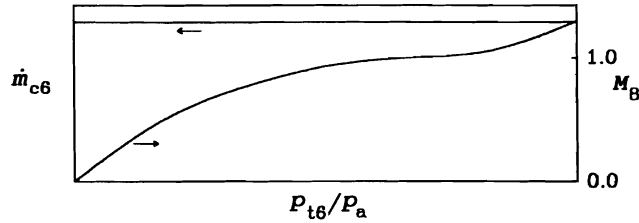


Figure 5.18 Typical nozzle performance map for a variable converging–diverging nozzle with a fixed minimum area.

the exit and then decreases. For this case, one again finds, as for the converging nozzle, that

$$\dot{m}_{c6} = \rho_{\text{stp}} a_{\text{stp}} A_e \frac{p_8}{p_{t6}} M_8 \sqrt{\frac{\gamma}{\gamma_{\text{stp}}}} \sqrt{\frac{\mathcal{R}_{\text{stp}}}{\mathcal{R}}} \sqrt{1 + \frac{\gamma - 1}{2} M_8^2}. \quad 5.7.10$$

Once again, by grouping some constants and defining \dot{m}_n as for the converging nozzle, one finds

$$\dot{m}_{c6} = \dot{m}_n \frac{p_8}{p_{t6}} M_8 \sqrt{\frac{\gamma}{\gamma_{\text{stp}}}} \sqrt{\frac{\mathcal{R}_{\text{stp}}}{\mathcal{R}}} \sqrt{1 + \frac{\gamma - 1}{2} M_8^2}, \quad 5.7.11$$

where the exit Mach number is always given by

$$M_8 = \sqrt{\frac{2}{\gamma - 1} \left[\frac{1}{\eta_n \left[\frac{p_8}{p_{t6}} \right]^{\frac{\gamma-1}{\gamma}} + 1} - 1 \right]}. \quad 5.7.12$$

c. Variable Converging–Diverging Nozzle – Fixed Minimum Area

Finally, in Figure 5.18 typical trends are shown for a variable converging–diverging nozzle with a choked and fixed minimum area and again a “schedule” to match the exit pressure to the ambient pressure by varying the exit area. As can be seen, the corrected mass flow is constant regardless of the pressure ratio; however, the exit Mach number may again be subsonic or supersonic. For this case, once again

$$\dot{m}_{c6} = \rho_{\text{stp}} a_{\text{stp}} A_e \frac{p_8}{p_{t6}} M_8 \sqrt{\frac{\gamma}{\gamma_{\text{stp}}}} \sqrt{\frac{\mathcal{R}_{\text{stp}}}{\mathcal{R}}} \sqrt{1 + \frac{\gamma - 1}{2} M_8^2}, \quad 5.7.13$$

which can be put in the form

$$\dot{m}_{c6} = \rho_{\text{stp}} a_{\text{stp}} A^* \frac{A_e p_8}{A^* p_{t6}} M_8 \sqrt{\frac{\gamma}{\gamma_{\text{stp}}}} \sqrt{\frac{\mathcal{R}_{\text{stp}}}{\mathcal{R}}} \sqrt{1 + \frac{\gamma - 1}{2} M_8^2}, \quad 5.7.14$$

where Eq. 5.7.9 still applies. By equating the mass flows at the minimum area (which is sonic) and exit ($\dot{m} = \rho V A = \rho M A \sqrt{\gamma \mathcal{R} T} / (\mathcal{R} T)$), one finds

$$\frac{A_8}{A^*} = \frac{\sqrt{\frac{\gamma + 1}{2 + (\gamma - 1) M_8^2}}}{M_8 \frac{p_8}{p^*}}. \quad 5.7.15$$

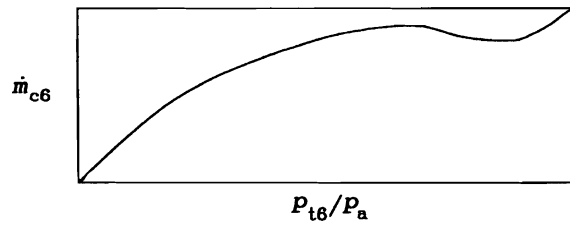


Figure 5.19 General nozzle map.

From Eqs. 5.2.6 and 5.2.7,

$$\frac{p_8}{p^*} = \left[\frac{1}{\eta_n} \left[\frac{\eta_n}{\frac{2}{\gamma+1} - 1 + \eta_n} \right] \left[\frac{1}{1 + \frac{\gamma-1}{2} M_8^2} - 1 + \eta_n \right] \right]^{\frac{\gamma}{\gamma-1}} \quad 5.7.16$$

It can be shown that the three preceding equations reduce to

$$\dot{m}_{c6} = \rho_{\text{stp}} a_{\text{stp}} A^* \sqrt{\frac{\gamma}{\gamma_{\text{stp}}}} \sqrt{\frac{\mathcal{R}_{\text{stp}}}{\mathcal{R}}} \sqrt{\frac{\gamma+1}{2}} \left[\frac{\eta_n(\gamma+1) + 1 - \gamma}{\eta_n(\gamma+1)} \right]^{\frac{\gamma}{\gamma-1}}, \quad 5.7.17$$

or, by defining \dot{m}_n as $\rho_{\text{stp}} a_{\text{stp}} A^*$, which is different than for the converging nozzle, one obtains

$$\dot{m}_{c6} = \dot{m}_n \sqrt{\frac{\gamma}{\gamma_{\text{stp}}}} \sqrt{\frac{\mathcal{R}_{\text{stp}}}{\mathcal{R}}} \sqrt{\frac{\gamma+1}{2}} \left[\frac{\eta_n(\gamma+1) + 1 - \gamma}{\eta_n(\gamma+1)} \right]^{\frac{\gamma}{\gamma-1}} \quad 5.7.18$$

It is important (and interesting) to note that, for this type of nozzle, \dot{m}_{c6} is constant for all conditions.

d. Other Nozzle Geometries

The preceding nozzle geometries and figures are intended to show typical trends for three limiting nozzle cases. Typically, variable nozzles do not have constant exit or minimum areas and both may change; a general map is shown in Figure 5.19. Thus, actual maps will combine the trends for the two types covered above. The actual maps (and functions f and \mathcal{P}) will depend on the precise “schedules” of the two area variations of the nozzles, which will be functions of the pressure ratio and altitude.

Example 5.5: Find the corrected mass flow rate for a fixed converging primary nozzle for a total inlet pressure of 344.8 kPa (50 psia), a total inlet temperature of 944.4 K (1700 °R), an exit area of 0.1613 m² (250 in.²), an efficiency of 0.97, and $\gamma = 1.36$. The atmospheric pressure is 68.95 kPa (10 psia).

SOLUTION:

First, one must determine if the nozzle is choked under these conditions. Thus, from Eq. 5.2.7,

$$\frac{p^*}{p_{t6}} = \left[1 + \frac{1 - \gamma}{\eta_n(1 + \gamma)} \right]^{\frac{\gamma}{\gamma-1}} = \left[1 + \frac{-0.36}{0.97 \times 2.36} \right]^{\frac{1.36}{0.36}} = 0.5239,$$

and so $p^* = 0.5239 \times 344.8 \text{ kPa} = 180.6 \text{ kPa}$ (26.20 psia).

Since p_a is less than p^* , the flow is choked ($M_8 = 1.00$),

and thus $p_8 = p^* = 180.6 \text{ kPa}$ (26.20 psia).

Note also that, $p_{t6}/p_a = 5$.

Next, from Eq. 5.2.4,

$$\frac{T_8}{T_{t6}} = \frac{1}{1 + \frac{\gamma-1}{2} M_8^2} = \frac{1}{1 + \frac{0.36}{2}} = 0.8475,$$

and thus $T_8 = 0.8475 \times 944.4 \text{ K} = 800.6 \text{ K} (1441 \text{ }^\circ\text{R})$.

From the ideal gas law, for p_8 and T_8 , one finds

$$\rho_8 = 0.7866 \text{ kg/m}^3 (0.001526 \text{ slug/ft}^3).$$

Also, for an ideal gas

$$\begin{aligned} a_8 &= \sqrt{\gamma \mathcal{R} T_8} = \sqrt{1.36 \times 287.1 \frac{\text{J}}{\text{kg}\cdot\text{K}} \times 800.6 \text{ K} \times \frac{\text{N}\cdot\text{m}}{\text{J}} \times \frac{\text{kg}\cdot\text{m}}{\text{N}\cdot\text{s}^2}} \\ &= 559.0 \text{ m/s} (1834 \text{ ft/s}). \end{aligned}$$

Therefore, the mass flow rate at the exit (which is the same as the inlet) is

$$\begin{aligned} \dot{m}_6 = \dot{m}_8 &= \rho_8 u_8 A_8 = 0.7866 \frac{\text{kg}}{\text{m}^3} \times 559.9 \frac{\text{m}}{\text{s}} \times 0.1613 \text{ m}^2 \\ &= 70.86 \text{ kg/s} (4.857 \text{ slugs/s}). \end{aligned}$$

Finally,

$$\dot{m}_{c6} = \dot{m}_6 \frac{\sqrt{\theta_{t6}}}{\delta_{t6}} = \dot{m}_6 \frac{\sqrt{\frac{T_{t6}}{T_{stp}}}}{\frac{p_{t6}}{p_{stp}}} = 70.86 \frac{\sqrt{\frac{944.4}{288.2}}}{\frac{344.8}{101.3}} = 37.69 \text{ kg/s} (83.11 \text{ lbm/s}).$$

Note that one would have obtained the same results for any value of atmospheric pressure below the choking condition (180.6 kPa).

Also, if nozzle conditions had changed but the pressure ratio had remained constant ($p_{t6}/p_a = 5$), for different values of p_{t6} the mass flow rate would change but the corrected mass flow rate would remain the same. On the other hand, had p_{t6}/p_a increased for a constant value of p_{t6} (decreased p_a), the mass flow rate would remain unchanged, and the corrected mass flow rate would again remain the same. Regardless, the nondimensional dependence (Eq. 5.7.3) is preserved. These calculations are left as an exercise for the reader.

5.8. Thrust Reversers and Vectoring

5.8.1. Reversers

The difficult problem of stopping an aircraft after landing has become more pronounced with modern aircraft because of the large aircraft weights, high speeds, and existing runways. Wheel brakes alone are not an effective means to stop such an aircraft owing to brake pad and tire thermal limitations. A reversible pitch propeller is used for turboprops to reverse the thrust direction upon landing. Turbojet and turbofans do not have such an option, however. To provide a “brake” for such aircraft, a thrust reverser is usually used.

For this, the turbine exhaust, fan air, or both are diverted at a suitable angle in the reverse direction by the means of an inverted cone, half-sphere, turning vanes, or other shape introduced in the exhaust flow upon landing. Because the exhaust flow is turned by almost 180° , the linear momentum equation can be used to show that the thrust is nearly reversed. The clamshell and cascade reversers are two of the most common of these devices.

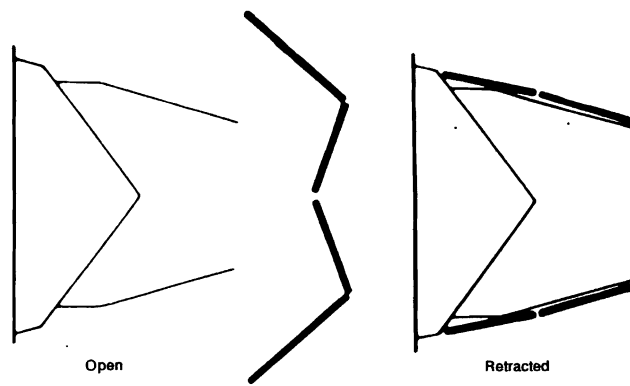


Figure 5.20a Clamshell thrust reverser.

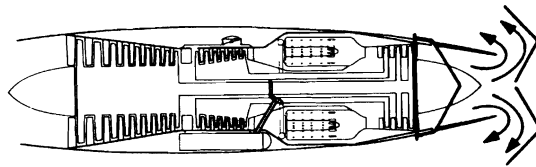


Figure 5.20b Clamshell thrust reverser in operation (courtesy of Pratt & Whitney).

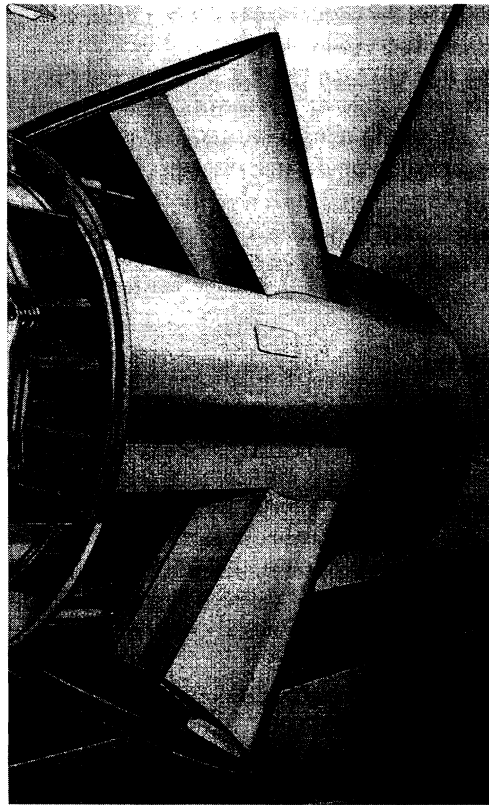


Figure 5.20c Rolls-Royce BR710 clamshell (courtesy of Rolls-Royce).

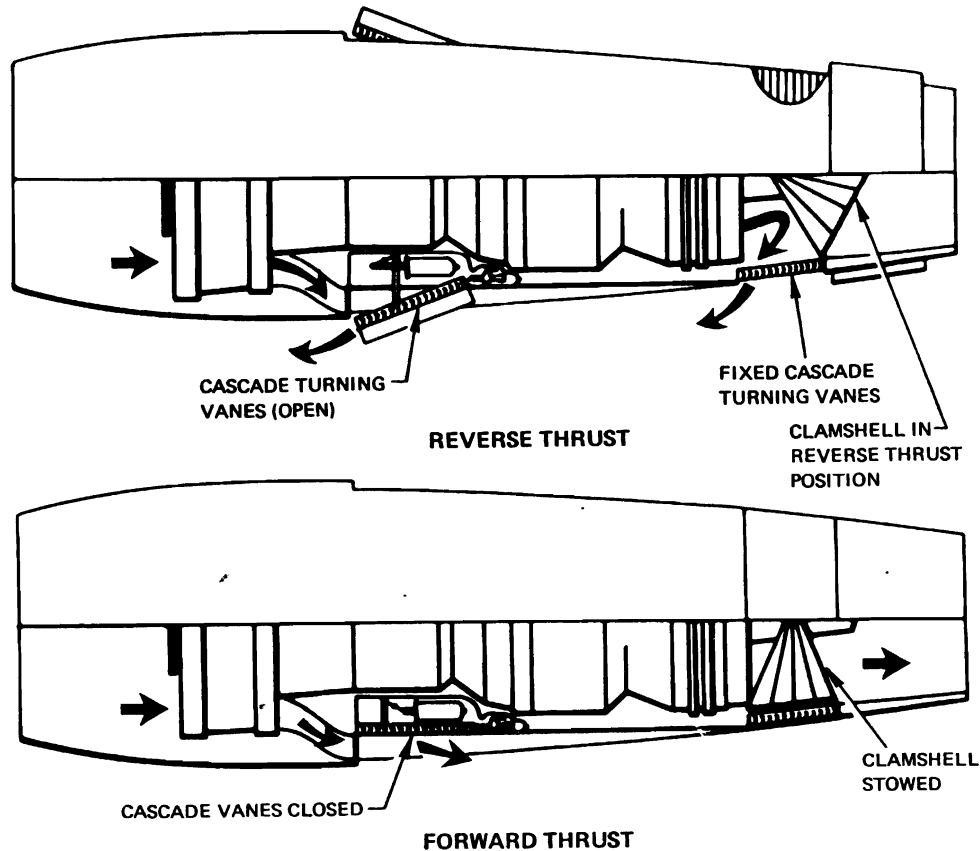


Figure 5.21 Thrust reversers for turbofan engine – exhausted fan (courtesy of Pratt & Whitney).

In Figure 5.20, the clamshell type is shown. For this geometry, the clamshell is opened upon landing and the shell is approximately one diameter downstream of the exhaust. When the reverser is not in use, the shell is retracted and stowed around the nozzle. Sometimes the retracted shell forms a part of the rear section of the nozzle nacelle.

A cascade-type reverser employs numerous vanes in the gas path to reverse the gas flow. Reversers for turbofans are often of this type. In Figures 5.21 and 5.22, the reversers for an exhausted turbofan are shown. For the fan (“cold air”) itself, only turning vanes are used, as shown for the two positions. For forward thrust, the vanes are out of the gas path; however, for reverse thrust, they are moved into the flow path. For the primary flow (hot gas), a combination of clamshell and cascade reversers are used. For this geometry, the clamshell is directly downstream of the turbine and, when activated, diverts the flow to the fixed cascade of vanes. Hydraulic pistons move both the movable vanes and clamshell. It is interesting to note that the engine manufacturer is usually not totally responsible for the design of thrust reversers but that this is left to the airframe manufacturer or a joint effort between the airframe and engine manufacturer.

5.8.2. *Vectoring*

To gain more control of aircraft maneuverability in military fighter applications, manufacturers have begun to develop thrust vectoring (thrust direction control) as a part of the exhaust of the engine. Thus, instead of the thrust being along the engine centerline,

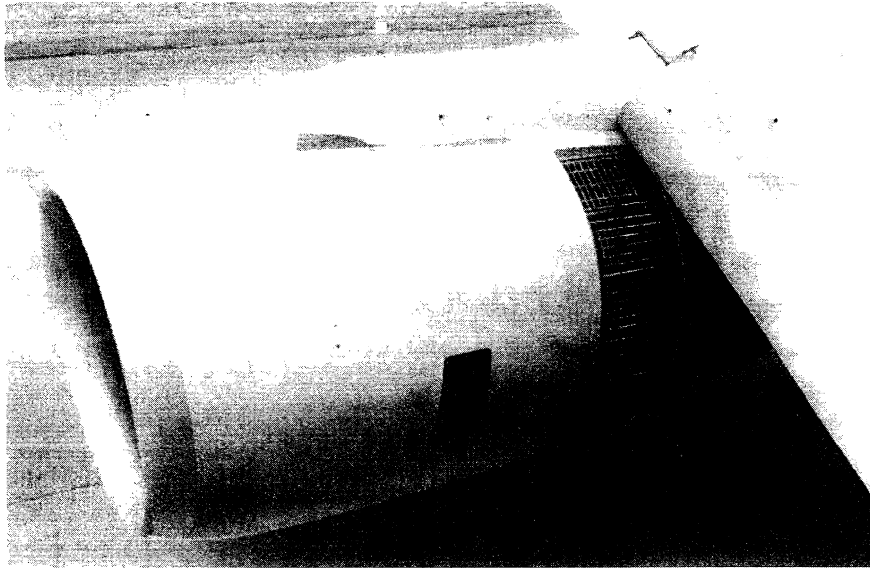


Figure 5.22 “Cold air” thrust reverser on a Rolls-Royce engine (courtesy of Rolls-Royce).

the thrust can be along another vector. Vectoring the thrust reduces response times. Such designs also allow for more rapid takeoffs. Applications include two-directional vectoring and multidirection vectoring. Thrust vectors can typically be varied from up to 20° from the nominal direction. Although the design is somewhat more complicated, weight and complexity of vectoring thrust nozzles are not much greater than for nozzles with variable areas. In fact, the all-directional vectoring nozzles use the iris variable area design as a basis for the vectoring. That is, the “flaps” are independently controlled and moved by independent amounts, thus allowing the thrust direction to be changed.

Two examples of vectoring are shown in Figures 5.23 and 5.24. In Figure 5.23, a two-directional thrust-vectoring engine is shown (Pratt & Whitney F119-PW-100). Figure 5.24

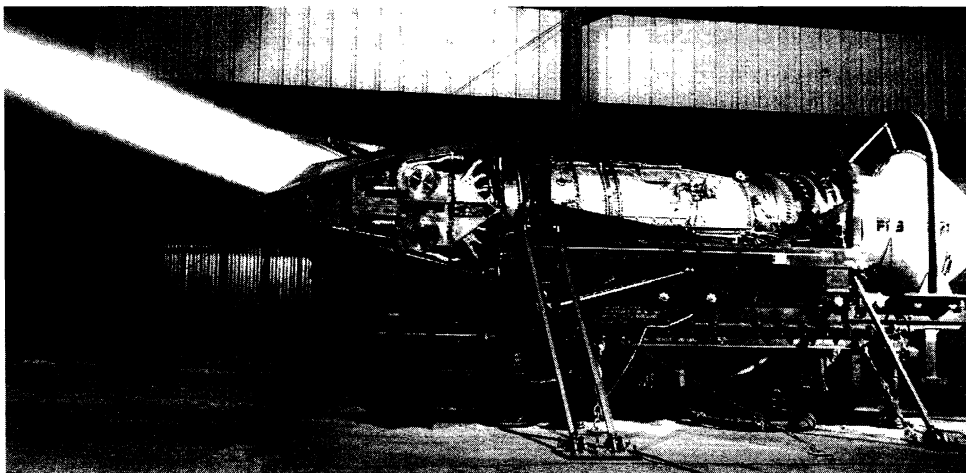


Figure 5.23 Two-directional thrust vectoring for Pratt & Whitney F119-PW-100 (courtesy of Pratt & Whitney).



Figure 5.24 Multidirectional thrust vectoring for Pratt & Whitney PYBBN (courtesy of Pratt & Whitney).

shows a double-exposed photograph for the Pratt & Whitney “Pitch-Yaw Balanced Beam Nozzle” (PYBBM). This is a multidirection iris design that can be used on the P&W F100 engine. Two different exhaust streams can easily be seen on this photograph resulting from two nozzle settings. This allows the reader to experience the visual effect of changing the thrust direction.

5.9. Summary

This chapter discussed exit nozzles. The primary functions of nozzles are to convert high-pressure, high-temperature energies (enthalpies) to kinetic energies (high velocities) and to straighten the flow so that the flow exits in the axial direction develop high thrust levels. The basic concepts apply to both fan and primary nozzles. Both converging and converging–diverging nozzles were covered. Methods were developed by which 1-D flow can be predicted in the different nozzles. Internal friction, defined as a part of a nozzle efficiency, was studied and was seen to affect the thrust. Basically, two distinct operating conditions (choked and nonchoked) can occur for a converging nozzle, whereas seven conditions can occur in a converging–diverging nozzle. Choking was seen to be a potential problem for all fixed-geometry nozzles and was seen to limit the exit velocity and thus to detract from the ideal developed thrust. Shocks in the diverging sections of converging–diverging nozzles were shown to increase nozzle losses. For an ideal nozzle, the maximum thrust is obtained when the nozzle exit pressure matches the ambient pressure. However, for a nonideal nozzle, slightly more thrust is obtained when the nozzle exit pressure is somewhat above the ambient pressure. Some flexibility in operating conditions is often provided by using variable nozzles so that an engine can operate with maximum thrust at a variety of altitudes and flight conditions – usually for military fighters but not for commercial aircraft. Next, performance curves or “maps” based on similarity parameters were presented as a method of summarizing the characteristics of a nozzle for both for on- and off-design conditions. Maps for three specific nozzle types (limiting cases) were covered in detail, and maps for a general nozzle type were discussed. Finally, different geometries of thrust reversers, which are a means by which negative thrust is developed so that aircraft can be quickly and safely decelerated upon landing were discussed. Thrust vectoring, which is a means of changing the direction of developed thrust for better (primarily military fighters) aircraft performance, was also considered.

List of Symbols

A	Area
a	Speed of sound
c_p	Specific heat at constant pressure
h	Specific enthalpy
\dot{m}	Mass flow rate
M	Mach number
p	Pressure
\mathcal{R}	Ideal gas constant
T	Temperature
γ	Specific heat ratio
δ	Ratio of pressure to standard pressure
η	Efficiency
θ	Ratio of temperature to standard temperature
ρ	Density

Subscripts

a	Ambient
c	Corrected
e	Exit
fn	Fan nozzle
i	Before shock

j	After shock
n	Nozzle
stp	Standard temperature and pressure
t	Total (stagnation)
6	Inlet to primary nozzle
7	Inlet to fan nozzle
8	Exit from primary nozzle
9	Exit from fan nozzle

Superscripts

'	Ideal
*	Choked

Problems

- 5.1 Find the variation of the corrected mass flow rate for a fixed primary converging nozzle as a function of p_{t6}/p_a for a specific heat ratio of 1.337, a total inlet pressure of 65.5 psia, a total inlet temperature of 1865 °R, an exit area of 218 in.², and a constant efficiency of 0.96. Plot the results as well as the variation in the exit Mach number versus the pressure ratio p_{t6}/p_a .
- 5.2 Find the variation of the corrected mass flow rate for a variable primary converging–diverging nozzle with a fixed exit area as a function of p_{t6}/p_a for a specific heat ratio of 1.337, a total inlet pressure of 65.5 psia, a total inlet temperature of 1865 °R, an exit area of 288 in.², and a constant efficiency of 0.96. The exit pressure matches the ambient pressure. Plot the results as well as the variation in the exit Mach number versus the pressure ratio p_{t6}/p_a . Also plot A_e/A_{\min} versus p_{t6}/p_a .
- 5.3 Find the variation of the corrected mass flow rate for a variable primary converging–diverging nozzle with a sonic and fixed minimum area as a function of p_{t6}/p_a for a specific heat ratio of 1.337, a total inlet pressure of 65.5 psia, a total inlet temperature of 1865 °R, a minimum area of 218 in.², and a constant efficiency of 0.96. The exit pressure matches the ambient pressure. Plot the results as well as the variation in the exit Mach number versus the pressure ratio p_{t6}/p_a .
- 5.4 Find the variation of the corrected mass flow rate for a fixed primary converging–diverging nozzle as a function of p_{t6}/p_a for a specific heat ratio of 1.337, a total inlet pressure of 65.5 psia, a total inlet temperature of 1865 °R, an exit area of 288 in.², a minimum area of 218 in.², and a constant efficiency of 0.96. Plot the results as well as the variation in the exit Mach number versus the pressure ratio p_{t6}/p_a .
- 5.5 A converging–diverging nozzle with an exit area of 350 in.² and a minimum area of 275 in.² has an upstream total pressure of 20 psia. The nozzle efficiency is 0.965, and the specific heat ratio is 1.35.
- At what atmospheric pressure and altitude will the nozzle flow be shockless?
 - At what atmospheric pressure and altitude will a normal shock stand in the exit plane?
- 5.6 Derive Eq. 5.7.7

- 5.7 Derive Eq. 5.7.10
- 5.8 Derive Eq. 5.7.17
- 5.9 A converging–diverging nozzle has an inlet total pressure of 25 psia and an inlet total temperature of 1400 °R. The ambient pressure is 4.2 psia, and the nozzle has an efficiency of 94.5 percent and a minimum area of 100 in.². What exit area is required for the flow to be shockless? Assume $\gamma = 1.35$.
- 5.10 An ideal fixed converging–diverging nozzle has an inlet total pressure of 19 psia. The inlet, minimum, and exit radii are 27, 22, and 25 in., respectively. These radii occur at axial locations of 0, 12, and 21 in., respectively. The walls of the nozzle are linear cones. The specific heat ratio is 1.30
- Find the altitude at which the flow is shockless and plot the internal pressure distribution axially down the nozzle.
 - If the engine is operated at sea level, plot the internal pressure distribution axially down the nozzle.
- 5.11 A fixed converging–diverging nozzle with a nozzle efficiency of 95 percent has an inlet total pressure of 19 psia. The inlet, minimum, and exit radii are 27, 22, and 25 in., respectively. These radii occur at axial locations of 0, 12, and 21 in., respectively. The walls of the nozzle are linear cones. The specific heat ratio is 1.30.
- Find the altitude at which the flow is shockless and plot the internal pressure distribution axially down the nozzle.
 - If the engine is operated at sea level, plot the internal pressure distribution axially down the nozzle.
- 5.12 At what atmospheric pressure and altitude will the following conditions occur for a converging–diverging nozzle with an exit area of 4500 in.², a minimum area of 4000 in.², and an upstream total pressure of 10 psia. The nozzle efficiency is 0.97 and the specific heat ratio is 1.35.
- The flow is shockless and the nozzle exit Mach number is supersonic.
 - A normal shock stands in the exit plane of the nozzle.
- 5.13 The total inlet pressure to a converging nozzle is 12 psia, and the inlet total temperature is 1200 °R. The specific heat ratio is 1.36, and the efficiency is 96.4 percent. The exit area is 120 in.², the ambient pressure is 8.2 psia, and the ambient temperature is 400 °R. Find the exit Mach number and mass flow rate.
- 5.14 The total inlet pressure to a converging nozzle is 20 psia, and the inlet total temperature is 1500 °R. The specific heat ratio is 1.365 and the efficiency is 97.4 percent. The exit area is 100 in.². The ambient pressure is 8.0 psia, and the ambient temperature is 380 °R. Find the exit Mach number and the mass flow rate.
- 5.15 Find the corrected mass flow rate for a fixed converging primary nozzle for a total inlet pressure of 20 psia, a total inlet temperature of 1400 °R, an exit area of 250 in.², an efficiency of 0.97, and $\gamma = 1.36$.
- The atmospheric pressure is 4 psia. Compare the results to those of Example 5.5. Comment.
 - The atmospheric pressure is 15 psia. Compare the results to those of part (a) above. Comment.
- 5.16 Find the corrected mass flow rate for a variable primary converging–diverging nozzle having a fixed exit area with $p_{t6}/p_a = 2.5$ for a specific heat ratio of

- 1.337, a total inlet pressure of 65.5 psia, a total inlet temperature of 1865 °R, an exit area of 288 in.², and an efficiency of 0.96. The exit pressure matches the ambient pressure.
- 5.17** For an ideal turbojet (all efficiencies are unity, total pressure losses are zero, properties are constant throughout, and the fuel ratio is negligible), analytically show that the maximum thrust is obtained when the exit pressure of the nozzle matches the ambient pressure. Consider the flight Mach number, altitude, core mass flow rate, compressor total pressure ratio, burner exit total temperature, and fuel properties to be known.
- 5.18** (a) Find the mass flow rate and the corrected mass flow rate for a fixed primary converging nozzle at standard sea level, a specific heat ratio of 1.35, a total inlet pressure of 40.0 psia, a total inlet temperature of 1700 °R, an exit area of 160 in.², and an efficiency of 0.97. (b) Also, sketch the general map for this nozzle type and indicate the relative location for the single data point from part (a).
- 5.19** A converging nozzle operates with a specific heat ratio of 1.33. The inlet Mach number is 0.10. The inlet total temperature is 1700 °R, and the exit total temperature is 1820 °R. The inlet total pressure is 60 psia. The Fanning friction factor is 0.015, and the length-to-diameter ratio is 4. What area ratio will cause the exit Mach number to be 1.00? What is the resulting total pressure at the exit? What is the ideal (frictionless and adiabatic) area ratio?
- 5.20** An adiabatic converging nozzle operates with a specific heat ratio of 1.33. The inlet Mach number is 0.10. The inlet total temperature is 1700 °R, and the inlet total pressure is 60 psia. The Fanning friction factor is 0.015, and the length-to-diameter ratio is 4. What area ratio will cause the exit Mach number to be 1.00? What is the resulting total pressure at the exit? What is the nozzle efficiency?
- 5.21** Find the mass flow rate and the corrected mass flow rate for a fixed primary converging–diverging nozzle at 40,000 ft with a specific heat ratio of 1.35, a total inlet pressure of 40.0 psia, a total inlet temperature of 1800 °R, an exit-to-minimum area ratio of 1.55, an exit area of 260 in.², and an efficiency of 96 percent. The exit Mach number is 1.80, the speed of sound at the exit is 1633 ft/s, and the exit static temperature is 1151 °R.
- 5.22** Find the mass flow rate and the corrected mass flow rate for a fixed primary converging nozzle at 20,000 ft (447.5 °R and 6.76 psia) with a specific heat ratio of 1.36, a total inlet pressure of 28.0 psia, a static inlet pressure of 27.25 psia, a total inlet temperature of 1650 °R, a static inlet temperature of 1638 °R, an exit area of 500 in.², and an efficiency of 95 percent.
- 5.23** At 18,380 ft, will a shock occur (and if so where) in a fixed converging–diverging nozzle with an exit area of 4500 in.², a minimum area of 4000 in.², an upstream total pressure of 10 psia, and an upstream total temperature of 1600 °R? The nozzle efficiency is 0.97, and the specific heat ratio is 1.35. Also, find the mass flow rate and corrected mass flow rate.
- 5.24** Find the exit Mach number, mass flow rate, and the corrected mass flow rate for a fixed primary converging nozzle at an ambient pressure of 12 psia and ambient temperature of 400 °R. The nozzle has a specific heat ratio of 1.34, a total inlet pressure of 30.0 psia, a total inlet temperature of 1600 °R, an exit area of 200 in.², and an efficiency of 96.5 percent.

- 5.25 A fixed-fan converging nozzle operates with an inlet total pressure of 18 psia and an inlet total temperature of 750 °R. The nozzle has an exit area of 224 in.² and an efficiency of 96.6 percent. The specific heat ratio is 1.385. Ambient conditions are 10.8 psia and 400 °R.
- Find the mass flow rate, corrected mass flow rate, and exit Mach number.
 - If the inlet total temperature is increased by 20 percent, what are the new mass flow rate and corrected mass flow rate?
- 5.26 Analyze the fixed converging–diverging nozzle of an afterburning turbojet (with the afterburner on). The total fuel flow rate is 11.87 lbm/s. The inlet total temperature to the nozzle is 3650 °R, the inlet total pressure is 50.44 psia, the efficiency is 97 percent, and the specific heat ratio is 1.2687. The minimum area is 527.7 in.², and the exit Mach number is 2.191. The aircraft cruises at 866 ft/s with the ambient pressure at 5.45 psia and ambient temperature at 429.6 °R.
- Find the total mass flow rate.
 - Find the corrected mass flow rate.
 - Find the thrust.
 - Find the *TSFC*.
- 5.27 Analyze the variable converging–diverging nozzle of the exhausted fan of a turbofan engine. The aircraft cruises at 993 ft/s with the ambient pressure at 10.10 psia and ambient temperature at 483 °R. The nozzle areas vary such that the exit pressure matches the ambient pressure. The inlet total temperature to the nozzle is 725 °R, the inlet total pressure is 37.7 psia, the efficiency is 97 percent, the specific heat ratio is 1.392, and the specific heat at constant pressure is 0.244 Btu/lbm-°R. The exit area is 398 in.².
- Find the exit Mach number of the nozzle.
 - Find the total mass flow rate through the nozzle.
 - Find the corrected mass flow rate.
- 5.28 A fixed-fan converging nozzle operates with an inlet total pressure of 16 psia and an inlet total temperature of 650 °R. The nozzle has an exit area of 950 in.² and an efficiency of 97.4 percent. The specific heat ratio is 1.390. Ambient conditions are 12.6 psia and 420 °R.
- Find the mass flow rate, corrected mass flow rate, and exit Mach number.
 - If the inlet total temperature is increased to 700 °R (nothing else changes), what are the new mass flow rate and corrected mass flow rate?
- 5.29 A fixed-fan converging nozzle operates with an inlet total pressure of 15 psia and an inlet total temperature of 625 °R. The nozzle has an exit area of 1000 in.² and an efficiency of 98.0 percent. The specific heat ratio is 1.390. Ambient conditions are 12.0 psia and 400 °R.
- Find the mass flow rate, corrected mass flow rate and exit Mach number.
 - If the inlet total temperature is increased to 700 °R (nothing else changes), what are the new mass flow rate and corrected mass flow rate?
- 5.30 An ideal adiabatic converging nozzle operates with a specific heat ratio of 1.35. The inlet total temperature is 1500 °R and the inlet total pressure is 100 psia. The length-to-diameter ratio is 4, and the area ratio is 0.30. The nozzle is choked. Find the exit pressure, temperature, and velocity.
- 5.31 An adiabatic converging nozzle operates with a specific heat ratio of 1.35. The inlet total temperature is 1500 °R, and the inlet total pressure is 100 psia.

The Fanning friction factor is 0.010, the length-to-diameter ratio is 4, and the area ratio is 0.30. The nozzle is choked. Find the exit pressure, temperature, efficiency, and velocity.

- 5.32** A converging nozzle operates with a specific heat ratio of 1.35. The inlet total temperature is 1500 °R, and the inlet total pressure is 100 psia. The Fanning friction factor is 0.010, the length-to-diameter ratio is 4, and the area ratio is 0.30. Owing to heat transfer, the exit total temperature is 1400 °R. The nozzle is choked. Find the exit pressure, temperature, and velocity. Does the conventional definition of efficiency make sense?
- 5.33** A converging nozzle (fixed) for a fan exhaust operates with an inlet total pressure of 14 psia and an inlet total temperature of 620 °R. The nozzle has an exit area of 700 in.² and an efficiency of 98 percent. The specific heat ratio is 1.3920. Ambient conditions are 5 psia and 400 °R.
- Find the mass flow rate, corrected mass flow rate and exit Mach number.
 - If the inlet total temperature is increased to 690 °R, and the inlet total pressure is increased to 15 psia (nothing else changes), what are the new mass flow rate and corrected mass flow rate?
- 5.34** A fixed converging–diverging nozzle operates with an inlet total pressure of 30 psia and an inlet total temperature of 1450 °R. The nozzle has an exit area of 195 in.² and an efficiency of 96 percent. The specific heat ratio is 1.340. Ambient conditions are 10.0 psia and 425 °R.
- Find the area ratio ($A_{\text{exit}}/A_{\text{min}}$) if the exit pressure matches the ambient pressure
 - Find the exit Mach number if the exit pressure matches the ambient pressure
 - Find the mass flow rate and corrected mass flow rate.
- 5.35** A fixed primary converging–diverging nozzle operates with an inlet total pressure of 23 psia and an inlet total temperature of 1300 °R. The nozzle has an exit area of 400 in.² and an efficiency of 98.4 percent. The specific heat ratio is 1.370. The nozzle is designed to operate with an exit Mach number of 1.422 so that the exit pressure matches the ambient pressure. The nozzle is operating off-design with ambient conditions of 11.0 psia and 430 °R.
- Find the mass flow rate and corrected mass flow rate for the off design conditions.
 - If the inlet total temperature is increased to 1400 °R (nothing else changes), what are the new mass flow rate and corrected mass flow rate?
- 5.36** A fixed converging–diverging nozzle operates with an inlet total pressure of 32 psia and an inlet total temperature of 1700 °R. The nozzle has an exit area of 800 in.², a minimum area of 579 in.², and an efficiency of 97.0 percent. The exit pressure matches the ambient pressure. The specific heat ratio is 1.360. Ambient conditions are 6.4 psia and 400 °R.
- Find the mass flow rate, corrected mass flow rate and exit Mach number.
 - If the inlet total temperature is increased to 1900 °R (nothing else changes), what are the new mass flow rate and corrected mass flow rate?

Axial Flow Compressors and Fans

6.1. Introduction

As discussed in previous chapters, a fan or compressor is the first rotating component that the fluid encounters. A cross-sectional view of a compressor for a simple, single-shaft turbojet is shown in Figure 6.1. The basic function of a compressor is to impart kinetic energy to the working fluid (air) by means of some rotating blades and then to convert the increase in energy to an increase in total pressure, which is needed by the combustor. The limits of operation of an engine are often dictated by a compressor, as is discussed in this chapter. Furthermore, the design of an efficient axial flow fan or compressor remains such a complex process that the success or failure of an engine often revolves around the design of a compressor. Many fundamental and advanced design details are available in Cumpsty (1988), Hawthorne (1964), Horlock (1958), Howell (1945a, 1945b) and Johnsen and Bullock (1965). Rhie et al. (1998), LeJambre et al. (1998), Adamczyk (2000), and Elmendorf et al. (1998) demonstrate how modern computational fluid dynamic (CFD) tools can effectively be used for the complex three-dimensional analysis and design of compressors.

Compressors were the main stumbling block of the early engines and the primary cause of the delays in the development of jet engines for World War II. Dunham (2000) and Meher-Homji (1996, 1997a, 1999) present interesting historical perspectives and technical information on early compressor development. The Germans were the first to apply axial flow compressors successfully. The first British engine incorporated a centrifugal compressor, which is the topic of Chapter 7. Centrifugal compressors are comparatively inefficient with some room for improvement. Because of this, it became apparent during the War that any large-thrust engine would require an efficient compressor. Since that time, considerable research and development have occurred, and thus current axial flow compressors are reliable and efficient components.

The compressor is vital to the operation of the engine because it readies the air for the combustor. Work is done on the fluid by the compressor, which is derived from the turbine. The total pressure is thus increased across the compressor, which is necessary for the combustion process, as is discussed in Chapter 9, and the production of thrust. Typically, the total pressure ratio across the compressor is from 5 to 35 as determined by the particular engine. As indicated in Chapter 1, by examining Eq. 1.2.4, one can see that, as the compressor pressure ratio increases, the thermodynamic efficiency increases for a closed cycle. Also, in general, the *TSFC* of an engine decreases with increasing compressor pressure ratio. In short, as the pressure ratio increases, the required fuel flow decreases and the extracted power increases.

In addition to the function just described in the previous paragraph, the compressor delivers high-pressure air to serve other functions. For example, a small portion of the air is bled to provide some cockpit and electronics environmental control. Also, a small portion is bled to provide pressurized air for inlet anti-icing. Finally, some of the high-pressure “cool”

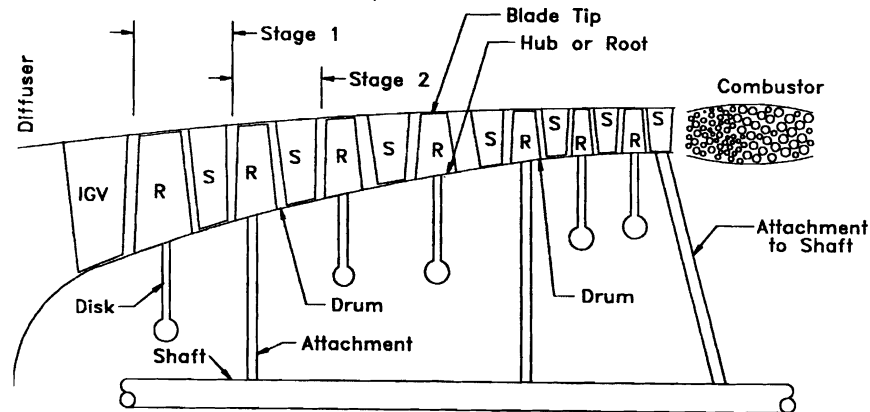


Figure 6.1 Single-shaft compressor.

air is directed to the turbine and used to reduce the temperature of the hot turbine blades, as is discussed in Chapter 8.

6.2. Geometry

A compressor comprises a series of stages that all share the work load. The total pressure ratio across a single stage is typically from 1.15 to 1.28. The typical number of stages in an axial compressor is from 5 to 20. A stage is composed of two blade components (Fig. 6.1). A set (or cascade) of rotating blades are attached to a “disk” at the “hub” or “root.” The region of the blade with the largest radius is called the “tip.” The tip diameter and housing diameter are approximately constant through a compressor. This first blade component is called the set of rotor blades. These blades do the work on the fluid. The second blade component is a set of stationary blades, which are attached to the case at the tips of the blades. These are termed stator blades or, more commonly, vanes. These vanes take the fluid from the previous set of rotor blades and ready the fluid velocity and direction for incidence-free entrance into the next or following set of rotor blades. Thus, the stator vanes do not input any energy into the fluid but are necessary for the operation of the compressor. A three-dimensional view of the rotor and stator blades is shown in Figure 6.2; the blades, vanes, and disks are clearly visible. Fan blades are constructed from

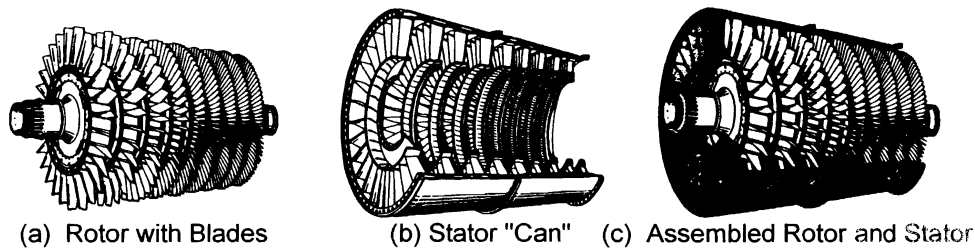


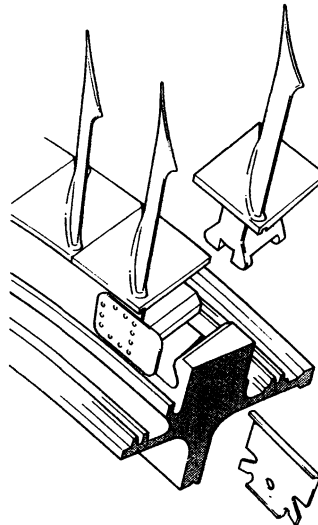
Figure 6.2 Three-dimensional view of rotor and stator blades and disks (courtesy of Pratt & Whitney Aircraft).



(a) Fir Tree
(courtesy of Rolls-Royce)



(b) Bulb of Westinghouse J30
(photo by R. Flack)



(c) "Loose"
(courtesy of Rolls-Royce)

Figure 6.3 Attachment of a rotor blade to disk.

titanium alloys, whereas the compressor blades operating in the “cool” region are made from titanium alloys and the compressor blades operating in the “warm” region are constructed from nickel alloys. Also see Figures 2.7 and 2.10 for views of the compressor and fan blading.

As noted, the blades are attached to a “disk,” which is sometimes attached directly to the shaft. Disks are used for structural and dynamic stabilizing integrity. Each cascade of blades is attached to a different disk. Disk diameters range from 6 in. for small engines to over 40 in. for large turbofans with fan diameters over 90 in. Several blade attachment methods are used. Three such arrangements are shown in Figure 6.3. The first two are older methods using tight fits into the disk and are called a “fir tree” and a bulb. The third method (Fig. 6.3.c) is currently used on many compressors. In this case the blades are loose fits into the disk and held in place axially with a cover plate. Upon installation the blades are still loose (a few hundredths of a mm or less). However, during compressor operation, the blades are held tightly in place as the result of thermal growth and centrifugal forces. This attachment method allows the blades to be removed easily for replacement in case of blade damage. Figure 6.4 is a photograph of the Rolls-Royce RB211 high-pressure (HP) compressor.

As will be discussed in Section 6.11.2.b, tip losses can considerably compromise compressor efficiency as a result of flow moving from the pressure sides of the vanes or blades to the suction sides. Thus, some of the high-pressure fluid is lost. For the case of the rotor blades, narrowing the gap between the blade tip and housing reduces the flow (and associated losses). Of course any shaft vibrations will require the tip clearance to be finite, or the blade can rub the housing and fail. Two methods are used to minimize the gap. First, the blade tips are sometimes made of an ablating material that conforms to the housing.

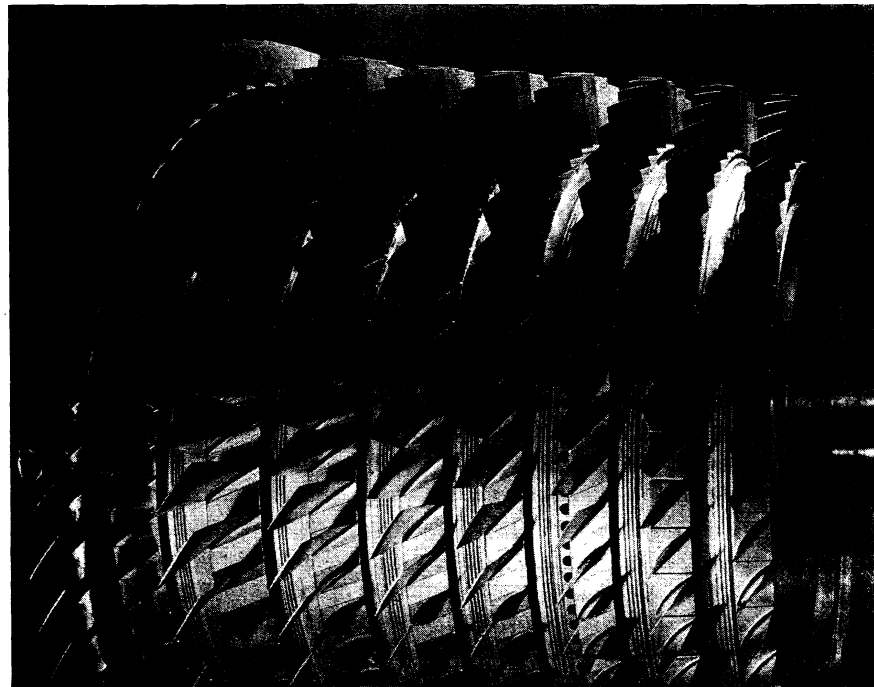


Figure 6.4 Rolls-Royce RB 211 high-pressure compressor (courtesy of Rolls-Royce).

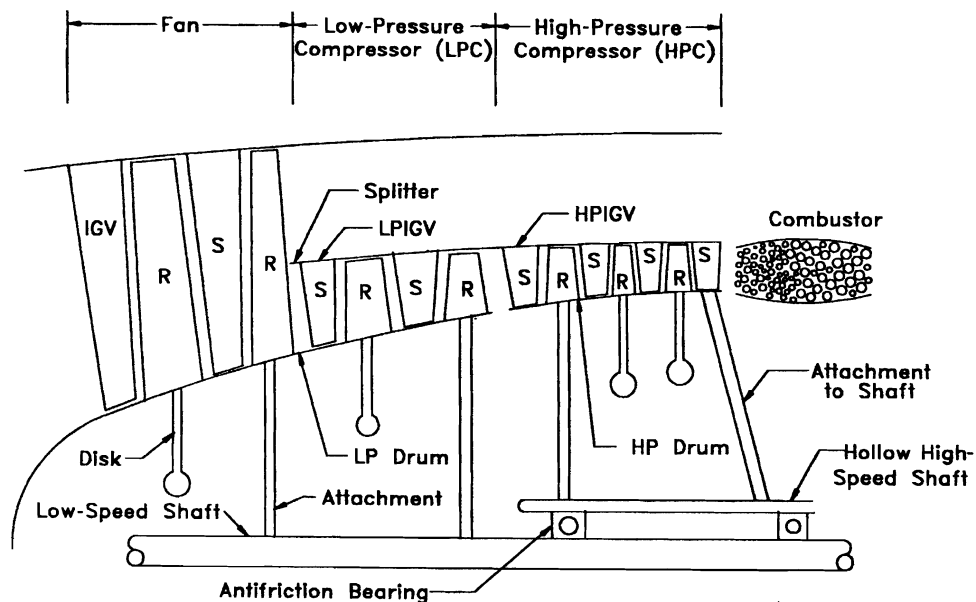


Figure 6.5 Twin-spool turbofan.

Consequently, as the compressor rotates the blades “wear in” their own required clearances. Second, the housing temperature is sensed, and cooling can be controlled automatically to change the housing temperature and thus the housing diameter due to thermal growth of the housing. As a result, the rotor-blade-tip-to-housing clearance is dynamically changed.

At the point before the fluid enters the first stage, many engines have another set of nonrotating blades, which are a set of airfoils termed the inlet guide vanes (IGV). These are similar in operation to the stator vanes, because this set of vanes readies the fluid direction and velocity for the first set of rotor blades. However, the design of such vanes is quite different from that of the stator vanes. These vanes turn the incoming air, which is predominately in the axial direction, in a direction that makes the flow into the first rotor blades incident free. Also, sometimes an engine have a set of stator vanes after the last stage that readies the flow for entrance to the combustor. These vanes are termed the exit guide vanes (EGV). The geometry for this set of vanes is also different from that of a normal set of stator vanes and is typically designed to add swirl to the flow, which aids in mixing within the combustor. Also, a set of exit guide vanes is often used for a turbofan at the exit of the fan to ready the flow either for the fan nozzle or bypass duct. These exit guide vanes straighten the flow and reduce the absolute velocity.

As discussed in Chapters 1, 2 and 3, many modern engines operate with two shafts and a fan. Such a design is shown in Figure 6.5. As illustrated, the fluid first enters the fan and then the low-pressure (LP) compressor, which is usually on the same shaft as the fan. The air next enters the high-pressure (HP) compressor, which is on a higher speed shaft. One set of inlet guide vanes is used for the fan or low-pressure compressor, and a second set is used for the high-pressure compressor. The blades of a fan are usually quite large, and blade heights decrease in size as the pressure increases down the engine. The actual blade shapes and designs are somewhat different for a fan, low-pressure compressor, and high-pressure compressor. In particular, fan blades are quite long with a large tip-to-hub radius ratio and, as will be discussed later, this results in blades having more curvature at the hub and less at

the tip and with significant blade twist from hub to tip. Typical total pressure ratios for fans are 1.3 to 1.5 per stage. However, the fundamental thermodynamics, fluid mechanics, and design methodology are the same for the fan and two compressors. Thus, for the remainder of this chapter no distinctions are made in the analysis of the three stage types.

If one were to unwrap the blades around the periphery of the compressor and consider its geometry to be planar two-dimensional when viewed from the top, a series of “cascades” would be seen as shown in Figure 6.6.a. The fluid first enters the inlet guide vanes. Next, it enters the first rotating passage. In Figure 6.6.a, the rotor blades are shown to be moving with linear velocity U , which is found from $R\omega$, where ω is the angular speed and R is the mean radius of the passage. The blades and vanes are in fact airfoils, and the pressure (+ +) and suction surfaces (— —) can be defined as shown in the figure. After passing through the cascade of rotor blades, the fluid enters the cascade of stator vanes. The fluid is turned by these stationary vanes and readied to enter the second stage, beginning with the second rotor blades, ideally incidence free. In general, the second stage has a slightly different design than the first stage (all of the stages are different). The process is repeated for each stage. In Figure 6.6.a, compressor component stations 0 through 3 are defined. It is very important not to confuse these with engine station designations.

An important parameter in compressor design is the solidity, which is defined as C/s , where s is the blade spacing, or pitch, and C is the chord. The solidity is the inverse of the pitch-to-chord ratio s/C . Both parameters are defined in Figure 6.6.a. If the solidity becomes too large, frictional effects, which decrease the efficiency and total pressure ratio, become large because the boundary layers dominate the passage flow. However, if the solidity becomes too small, sufficient flow guidance is not attained (this phenomenon is termed “slip”) and the flow thus does not adequately follow the blade shape. Separation can also become a major problem. For the low-solidity case due to slip, less power is added to the flow than desired; as a result, the compressor does not operate at the necessary pressure ratio. Because of accompanying separation (and losses), the maximum efficiency is not realized. Thus, a compromise is needed. In Section 6.11 a method is presented to optimize the single-stage aerodynamic performance or maximize the efficiency. Typical values of solidity for a compressor are approximately 1. The selection of solidity is partially responsible for the resulting number of blades in a cascade. For example, for the Pratt & Whitney JT9D turbofan, 46 blades are used on the fan rotor stage, and the number of blades on the compressor stages ranges from 60 to 154. For comparison, the exit guide vanes for the fan (which has an extremely large chord) have only nine blades.

It is very important that the number of stator vanes and rotor blades for a stage or nearby stages be different. If they were equal, a resonance due to fluid dynamic blade interactions could be generated, resulting in large blade, disk, and shaft vibrations accompanied by noise. This would reduce the life of the blades and compromise engine safety. Often, and if possible, blade or vane numbers are selected as prime numbers, but they are always chosen such that common multiple resonances are not excited. Cumpsty (1977) reviews this topic in detail.

Another important parameter for blade performance is the ratio of the distance to the maximum camber to the chord length of the blade a . This distance is also shown in Figure 6.6.a. This parameter strongly influences the lift and drag characteristics of blades, which in turn have marked effects on the efficiency and pressure ratio of a stage.

If one examines the cross-sectional flow areas in the passages between the blades (area normal to the mean flow direction), it will be seen that the areas increase from the inlet to the exit of the rotor, as shown in Fig 6.6.b, and also increase from the inlet to the exit of the stator. Thus, both the rotor and stator blade rows act like diffuser sections.

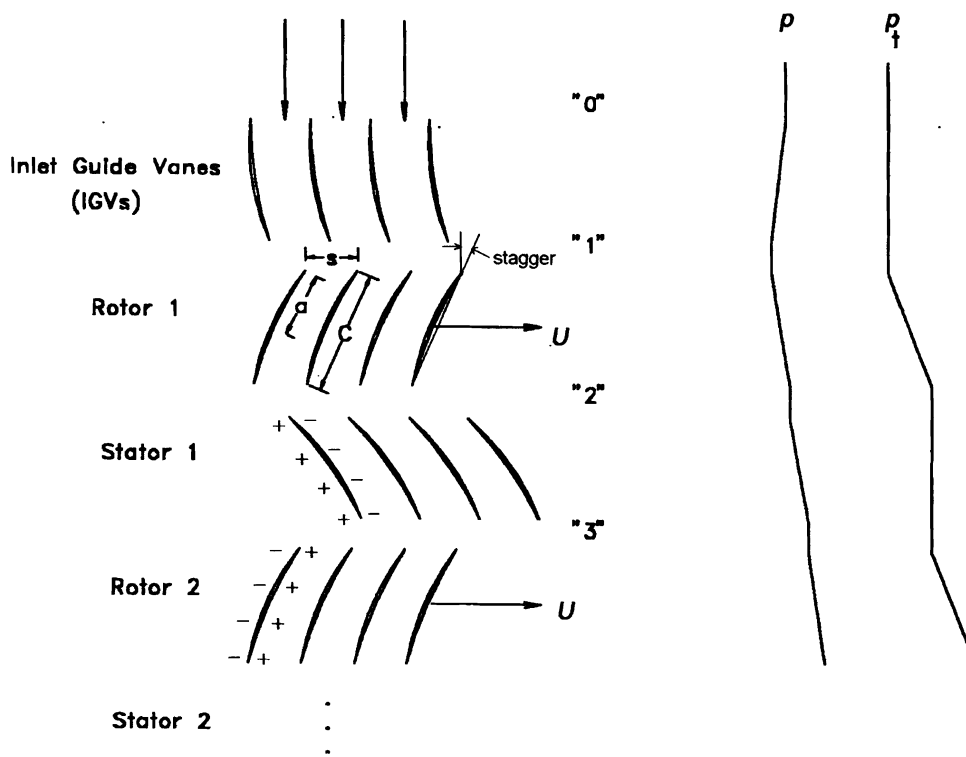


Figure 6.6a Cascade view of blades and vanes with pressure profiles.

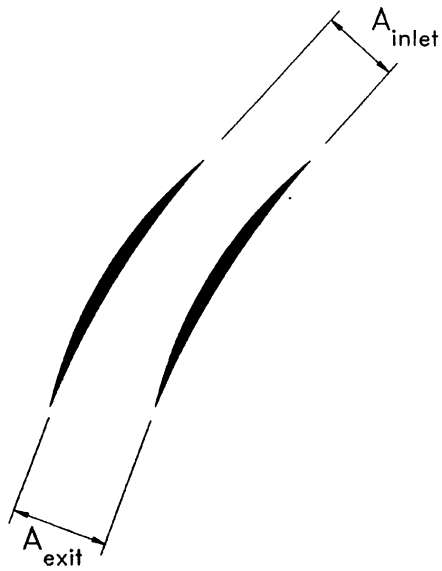


Figure 6.6b Areas in a blade passage.

Also shown in Figure 6.6.a are axial pressure profiles down the compressor. Both the total and static pressures are indicated. As can be seen, the static pressure decreases across the inlet guide vanes but increases across all of the rotor and stator blades, which is consistent with the observation that rotor and stator blade rows act like diffusers. The total pressure remains approximately constant across the inlet guide vanes and stator vanes but increases across the rotor blades, where energy is put into the flow and the enthalpy increases. For the remainder of this chapter, pressure changes are related to the geometry of the compressor. That is, for a given geometry of blades and rotational speed, what are the static and total pressure rises and ratios?

A few design concerns should be identified at this point. First, as a fluid particle traverses a compressor, the pressure increases. As a result, the density increases. A common design practice is to keep the axial velocity component approximately constant through a compressor. Therefore, to compensate for the increase in fluid density, the blade heights must decrease through a compressor. Next, a compressor stage cannot be expected to increase the pressure without limits. When pressure increases in a stage, it acts like a diffuser. If the pressure rise becomes too large, the flow in the stage separates, causing a gross reduction in efficiency and a phenomenon called surge. Such a condition reduces the thrust to zero and also causes large oscillatory pressure fluctuations in the compressor, which can cause case mechanical failure. Finally, flow compressibility induces limits. For example, supersonic flow over the blade surfaces generates shock waves. Such a formation both reduces the total pressure of the gas (thus reducing the compressor efficiency) and also leads to flow separation, which also reduces the efficiency. These concerns are addressed more throughout the chapter.

6.3. Velocity Polygons or Triangles

Because energy is being added to the flow (which results in a pressure rise) and a part of the compressor is moving, one must be able to understand the complex flow patterns in a compressor. As the theoretical analysis in the next section demonstrates, the pressure rise is directly dependent on the fluid velocity magnitudes and directions in a compressor. The purpose of this section is to introduce a means of interpreting the fluid velocities for use with the governing equations. That is, since one component rotates (rotor) and one component is stationary (stator), an analyst must be able to relate the velocities between the two so that the components are compatible. The rotor blades have a set of coordinates that move with the blades, and the stator vanes have a set of coordinates that are stationary with the blades. Converting velocities from one frame to the other is accomplished through a vector analysis termed velocity polygons or sometimes velocity triangles.

First consider the inlet guide vanes, as shown in Figure 6.7.a. The inlet flow to the inlet guide vanes is typically aligned with the axis of the engine. The axial flow velocity relative to the engine frame (referred to as absolute velocity for the remainder of the book) at the IGV inlet is c_0 . The blade inlet angle is usually aligned with the axis. As the fluid passes through the IGV, it is turned; thus, the absolute flow velocity (or velocity in the nonrotating frame) at the IGV exit (and the rotor inlet) is c_1 , and it has a flow angle α_1 relative to the axis of the engine. The IGV exit blade angle is α'_1 . If the flow is exactly parallel to the blade at the exit, α_1 and α'_1 are identical. This is usually not true in an actual design, however, because of slip.

The inlet to the rotor stage, as shown in Figure 6.7.b, can be considered next. However, the rotor blades are rotating around the engine centerline or are moving in the planar two-dimensional plane with absolute velocity U_1 in the tangential direction. The objective is

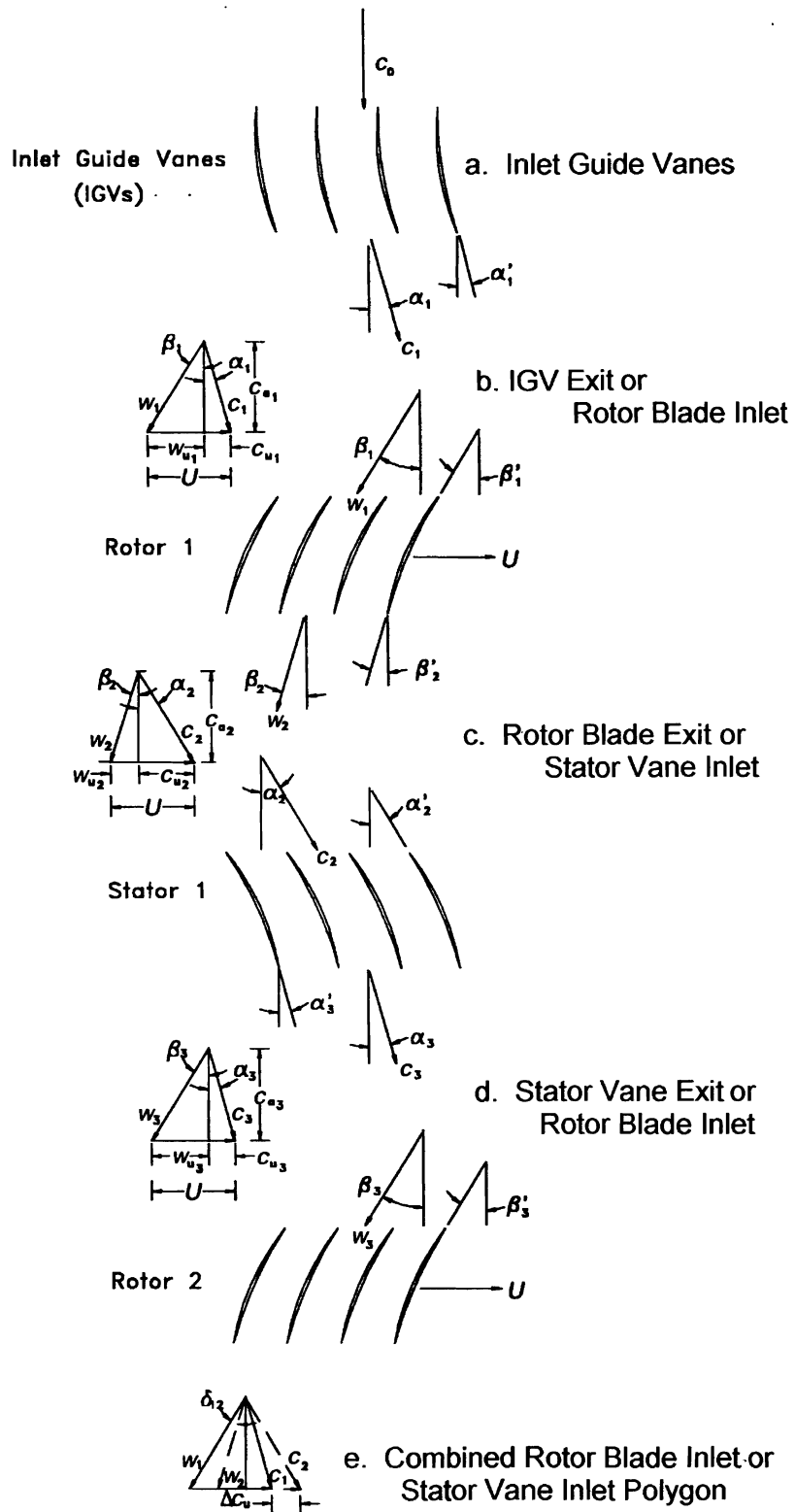


Figure 6.7 Definitions of blade geometries and velocity polygons for compressors.

therefore to relate the velocities in the stationary frame to those in the rotating frame and vice versa. Thus, to find the velocity of the fluid relative to the rotating blades, one must subtract the blade velocity vector from the absolute flow vector ($\mathbf{V}_{\text{abs}} = \mathbf{V}_{\text{rel}} + \mathbf{V}_{\text{ref frame}}$) or ($\mathbf{c} = \mathbf{w} + \mathbf{U}$). This is graphically performed in Figure 6.7.b. The resulting velocity vector in the rotating frame is \mathbf{w}_1 and has a flow angle β_1 relative to the axial direction. It is important to note that the rotor blades have inlet and exit angles (relative to the axial direction) of β'_1 and β'_2 , respectively. Once again, if the relative flow direction matches the blade angles exactly, the values β'_1 and β_1 are the same, and the *incidence* angle (the difference between β'_1 and β_1 at the leading edge) is zero. However, this usually does not occur in practice – especially at off-design conditions. The difference at the trailing edge β'_2 and β_2 , is called the *deviation*.

When drawing the polygons, one should always draw the triangles exactly to scale. This not only allows “rough” checking of algebraic computations but also allows makes it possible to observe the relative magnitudes of the different velocity vectors and the “health” of a compressor stage, as is discussed in Sections 6.4.2 and 6.4.3 with the percent reaction. When an undesirable situation is observed, it is much easier to see how to correct the condition by changing geometric parameters and visualizing them with a scale diagram than by means of equations.

Next, one can break the vectors into components, as indicated in Figure 6.7.b. As shown, the absolute velocity \mathbf{c}_1 has a component in the tangential direction that is equal to c_{u1} and a component in the axial direction that is c_{a1} . Also, the relative velocity \mathbf{w}_1 has components w_{u1} and w_{a1} in the tangential and axial directions, respectively.

Figure 6.7.c shows the velocity polygon for the rotor exit and stator inlet. The exit relative velocity (to the rotor blades) is \mathbf{w}_2 , and this velocity is at an angle of β_2 relative to the axial direction. The blade velocity is \mathbf{U}_2 and can be vectorially added to \mathbf{w}_2 to find the absolute exit velocity \mathbf{c}_2 . Note that \mathbf{U}_2 and \mathbf{U}_1 may be slightly different because the radii at the rotor inlet and exit may be slightly different. The absolute flow angle of \mathbf{c}_2 is α_2 relative to the engine axis. Once again, the rotor blade exit angle is β'_2 , which may be different from the flow angle β_2 . Furthermore, the stator vane inlet angle is α'_2 and will in general be different from α_2 . Also shown in Figure 6.7.c are the components of both \mathbf{w}_2 and \mathbf{c}_2 in the tangential and axial directions.

Finally, in Figure 6.7.d the stator exit triangle is shown (which is also the inlet velocity polygon to the next set of rotor blades). The absolute velocity is \mathbf{c}_3 , which makes an angle of α_3 to the axial direction. Once again, the absolute flow angle α_3 will in general be different from the absolute stator vane angle α'_3 . The next rotor blade velocity at the inlet is \mathbf{U}_3 , and the relative velocity (to the next rotor blades) is \mathbf{w}_3 , which makes an angle of β_3 to the axis. The method just described can be used for all of the downstream stages.

Next, as shown in Figure 6.7.e, the velocity polygons for the rotor entrance and exit are often combined to form one polygon. As is shown in the next section, the power and pressure ratio of the stage are directly related to the change in absolute tangential velocity across a set of rotor blades if the radius is approximately constant ($\Delta c_u = c_{u1} - c_{u2}$). Thus, combining the two triangles makes the change easy to observe graphically. Furthermore, by examining the difference of the two vectors \mathbf{w}_1 and \mathbf{w}_2 , one can see that the rotor flow turning angle or *deflection* is $\beta_2 - \beta_1$ or δ_{12} . Once again, if the vectors are to scale, it is relatively easy to see how to alter the performance of a stage by changing geometric parameters.

Finally, in Figure 6.8 a side view of the first stage of a typical compressor is shown. Defined are the blade heights (t) and the average radii of the blades (R).

Before one proceeds, a consistent sign notation is needed. First, all positive tangential velocities are defined to the right. Thus, rotor blades always move to the right with positive

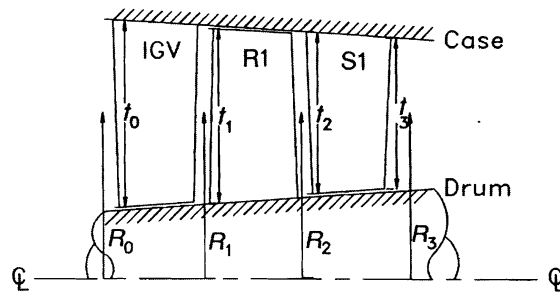


Figure 6.8 Side view of first stage.

velocity U . Second, all angles are measured relative to the axial direction and positive angles are considered to be counterclockwise.

Note that the velocity polygons are similar for an incompressible axial turbomachine, (i.e., pumps). Thus, the same type of analysis is used to understand the flow velocities and relate them to power requirements, pressure rises, and so on. One basic difference, however, is that pump manufacturers typically do not measure the flow angles relative to the axial direction. They instead use the tangential direction as a reference. Both reference conditions lead to identical velocity polygons and other results. One needs to be aware of the different conventions and angle definitions when using other reference material, however.

In Table 6.1, the trends of the velocity magnitudes, flow passage areas or cross-sectional areas normal to the mean flow, and pressures across the different components are shown. As can be seen, the static pressure increases across both the stator and rotor blades because the relative velocities across both decrease. On the other hand, as the absolute and relative velocities across the IGVs increase, the static pressure decreases. Details of, and reasons for, these trends are covered in the next section.

6.4. Single-Stage Energy Analysis

In this section, the equations used in single-stage energy analysis are summarized so that the velocities from polygons can be related to the pressure rise and other important compressor characteristics. In Appendix I, this derivation was performed for a single-stage (rotor and stator) using a two-dimensional planar “mean line” control volume approach. That is, for an axial flow compressor, a point located midway between the hub and tip is used to evaluate the radii, fluid properties, and velocities. Figure 6.9 illustrates a single stage. The objective of this section is to relate the inlet and exit conditions to the property changes.

Table 6.1. *Axial Flow Compressor Component Trends*

	Absolute Velocity	Relative Velocity	Area	p	p_t
IGV	Increases	Increases	Decreases	Decreases	Constant
Rotor	Increases	Decreases	Increases	Increases	Increases
Stator	Decreases	Decreases	Increases	Increases	Constant

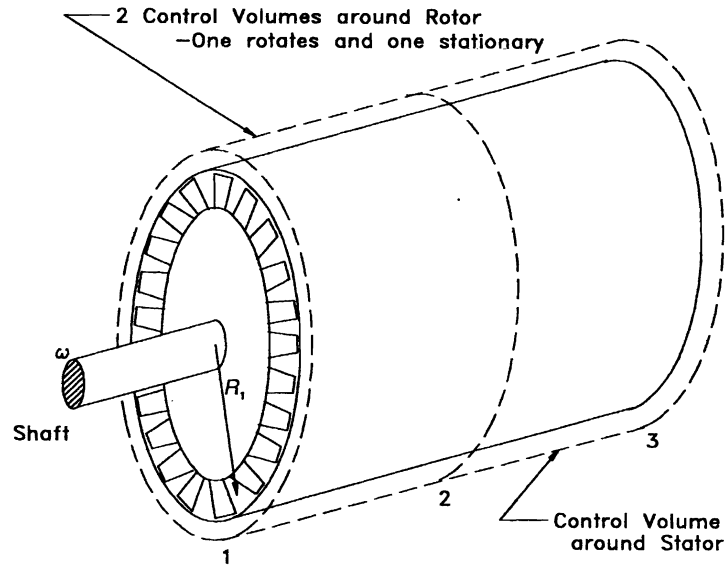


Figure 6.9 Control volume definition for compressor stage.

6.4.1. Total Pressure Ratio

The three basic equations used in Appendix I are those for continuity, moment of momentum, and energy equations. For the power input to the shaft, one finds (Eq. 1.2.17).

$$\dot{W}_{sh} = \dot{m}[U_2 c_{u2} - U_1 c_{u1}] \quad 6.4.1$$

Next, one can solve for the total pressure ratio of the stage and find (Eq. 1.2.26)

$$\frac{p_{t2}}{p_{t1}} = \left[\eta_{12} \frac{U_2 c_{u2} - U_1 c_{u1}}{c_p T_{t1}} + 1 \right]^{\frac{\gamma}{\gamma-1}}, \quad 6.4.2$$

which is greater than unity. Note that if $R_2 = R_1 = R$ ($U_2 = U_1 = U$), p_{t2}/p_{t1} is proportional to $U \Delta c_u$ to a power. Furthermore, by referring to Figure 6.7.e, one can see that, as the rotor flow turning angle δ_{12} increases, so does Δc_u . Therefore, increasing the pressure ratio of a stage is accomplished by increasing the rotor turning angle. Note also that U is proportional to R and, as U increases, the total pressure ratio increases. Thus, as the radius becomes larger, so does the total pressure ratio. Therefore, once the velocity information of a rotor is known from the velocity polygons and the efficiency, it is possible to find the total pressure rise.

6.4.2. Percent Reaction

An important characteristic for a compressor is termed the percent reaction. This is a relation that approximates the relative loading of the rotor and stator based on the enthalpy

rise. From Appendix I (Eq. I.2.32),

$$\%R = \frac{1}{1 + \left[\frac{c_2^2 - c_1^2}{w_1^2 - w_2^2} \right]}. \quad 6.4.3$$

Therefore, for compressible flow the percent reaction of the stage can be related to the absolute and relative velocities at the inlet and exit of the rotor. Implications and physical insight of the percent reaction are discussed later.

6.4.3. Incompressible Flow

For comparison, one may wish to find the pressure rise and percent reaction of a turbomachine with an incompressible fluid (i.e., an axial flow pump). More pump information can be found in Stepanoff (1957) and Brennen (1994), who give great details on axial flow pump performance. However, Appendix I presents Eqs. I.2.34, I.2.37, and I.2.39:

$$\dot{W}_{sh} = \dot{m}[U_2 c_{u2} - U_1 c_{u1}] \quad 6.4.4$$

$$p_{t2} - p_{t1} = \rho \eta_{12} [U_2 c_{u2} - U_1 c_{u1}] \quad 6.4.5$$

$$\%R = \frac{1}{1 + \left[\frac{c_2^2 - c_1^2}{w_1^2 - w_2^2} \right]}. \quad 6.4.6$$

Comparing this equation with that for compressible flow reveals that they are identical. Also, the percent reaction for incompressible and ideal flow reduces to Eq. I.2.41, an equation with a practical implication:

$$\%R = \frac{p_2 - p_1}{p_{t3} - p_{t1}}. \quad 6.4.7$$

For example, typical incompressible turbomachine stages with short blades have percent reactions of 0.50 to 0.55. For a nonideal pump, this dictates that approximately half of the enthalpy increase occurs in the rotor and half in the stator. For an ideal pump, this also means that half of the static pressure increase occurs in the rotor and half in the stator. This implies that the force or “load” distributions on the rotor and stator blades are about the same, and thus neither the stator vanes nor rotor blades are subjected to higher-than-needed stresses, which can lead to catastrophic failures. If, however, the percent reaction differs greatly from 0.5, a large pressure rise occurs in either the stator (<0.5) or the rotor (>0.5). If this occurs, separation or partial separation of the cascade is likely. As a result of the associated losses, the efficiency will be less than optimum. Such an optimization is covered in Section 6.11 in detail. However, in summary, for an axial flow pump the percent reaction should be close to 0.50 for two reasons: (1) the efficiency will be maximized and (2) force loads will be distributed so that blades and vanes are less susceptible to material failure.

Owing to compressibility of the gas in a compressor, the percent reaction tends to be higher than 0.5 in modern compressors. That is, as the stage total pressure rise increases to maintain an even pressure rise in the rotor and stator, the percent reaction tends to be greater than 0.5. So although the convenient incompressible analysis presented in Section 6.11 can be used as a starting point, one should keep in mind that the overriding idea is

to control the separation and maximize the efficiency. Also, as the flow becomes more three-dimensional (e.g., as the tip-to-hub diameter increases for front stages), maintaining a constant percent reaction in the radial direction becomes more difficult, as discussed in Section 6.10. Even worse, if a stage were designed with a mean line reaction of 50 percent, some hub regions would experience negative values of reaction due to radial flow, which is obviously unacceptable. As a result, some stages are designed so that the mean line reaction is significantly above 50 percent; this results in tip regions well above 50 percent with the hub regions above 0 percent. Fortunately, as will be shown, the efficiency does not decrease rapidly as one deviates from the optimal 50 percent reaction.

6.4.4. Relationships of Velocity Polygons to Percent Reaction and Pressure Ratio

As indicated by Eqs. 6.4.3 and 6.4.6, the velocities dictate the percent reaction. In Figure 6.10, three special cases are shown. In particular, sets of velocity polygons (rotor inlet and exit) for 50, 0, and 100-percent reaction compressor stages are shown for a constant axial velocity. Of particular interest is the set of polygons for a 50-percent stage. As can be seen, for this case the inlet and exit polygons are similar triangles but reversed. Once again, if the polygons are drawn to scale, one can easily observe if the percent reaction is close to 50 percent simply by examining the symmetry of the triangles. Also, one can use polygons to make preliminary predictions on performance trends due to geometry changes. For example, for a compressor stage that originally operates close to a 50-percent reaction, if δ_{12} is increased the percent reaction is decreased if other parameters are constant (Fig. 6.10.b). Similarly, if the absolute inlet angle is decreased while holding other parameters constant, the percent reaction increases (Fig. 6.10.c).

Moreover, for general trends, one can examine both the governing equations and velocity polygons for individual variations in the absolute inlet angle α_1 , the rotor flow turning angle

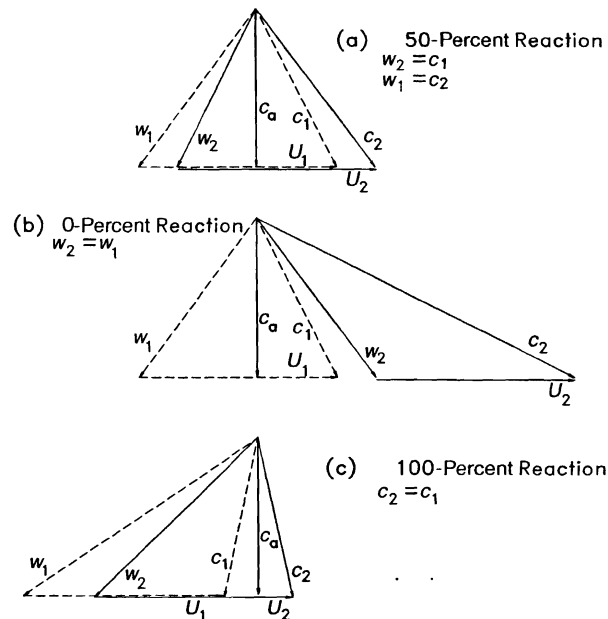


Figure 6.10 Three special cases of velocity polygons.

Table 6.2. Geometric and Operating Condition Effects on Compressor Parameters

Decrease in	Percent Reaction, %R	Total Pressure Ratio, p_3/p_1
Absolute inlet angle, α_1	Increase	Increase
Rotor flow turning angle, δ_{12}	Increase	Decrease
Rotational speed, N	Decrease	Decrease
Axial velocity component, c_a	Increase	Increase

δ_{12} , the rotational speed N , and mass flow rate (or axial velocity component) \dot{m} (or c_a). The resulting effects on the stage total pressure ratio and percent reaction can be determined. A matrix of general trends is presented in Table 6.2.

Example 6.1: A stage approximating the size one of the last stages (rotor and stator) of a high-pressure compressor is to be analyzed. It rotates at 8000 rpm and compresses 280 lbm/s (8.704 slugs/s) of air. The inlet pressure and temperature are 272 psia and 850 °F, respectively. The average radius of the blades is 13.2 in., and the inlet blade height is 1.24 in. The absolute inlet flow angle to the rotor is the same as the stator exit flow angle (15°), and the rotor flow turning angle (δ_{12}) is 25°. The stage has been designed so that the blade height varies and the axial velocity remains constant through it. The efficiency of the stage is 90%. The values of c_p and γ are 0.2587 Btu/lbm-°R and 1.361, respectively, which are based on the resulting value of T_2 or average static temperature of the stage. The following details are to be found: blade heights at the rotor and stator exits, the static and total pressures at the rotor and stator exits, the stator turning angle, the Mach numbers at the rotor and stator exits, the required power for the stage, and the percent reaction for the stage.

SOLUTION:

To obtain the solution, velocity polygons will be used. Before proceeding, a few preliminary calculations are needed.

$$U = R\omega = \frac{13.2 \text{ in.}}{12 \frac{\text{in.}}{\text{ft}}} \frac{8000 \text{ rev}}{\text{min}} \frac{2\pi \text{ rad}}{\text{rev}} \frac{1}{60 \frac{\text{s}}{\text{min}}} = 921.5 \text{ ft/s}$$

$$A_1 = \pi D_1 t_1 = \pi \frac{2 \times 13.2 \text{ in.}}{12 \frac{\text{in.}}{\text{ft}}} \frac{1.24 \text{ in.}}{12 \frac{\text{in.}}{\text{ft}}} = 0.7142 \text{ ft}^2$$

For $p_1 = 272$ psia and $T_1 = 850$ °F = 1310 °R, the ideal gas equation yields

$$\rho_1 = \frac{p_1}{\mathcal{R}T_1} = \frac{272 \frac{\text{lbf}}{\text{in.}^2} \times 144 \frac{\text{in.}^2}{\text{ft}^2}}{53.35 \frac{\text{ft-lbf}}{\text{lbm-}^\circ\text{R}} \times 1310^\circ\text{R} \times 32.17 \frac{\text{lbm}}{\text{slug}}} = 0.01742 \frac{\text{slug}}{\text{ft}^3}$$

Next,

$$c_{a1} = \frac{\dot{m}}{\rho_1 A_1} = \frac{8.704 \frac{\text{slugs}}{\text{s}}}{0.01742 \frac{\text{slug}}{\text{ft}^3} \times 0.7142 \text{ ft}^2} = 699.6 \text{ ft/s}$$

Finally,

$$a_1 = \sqrt{\gamma \mathcal{R}T_1} = \sqrt{1.361 \times 53.35 \frac{\text{ft lbf}}{\text{lbm-}^\circ\text{R}} \times 32.17 \frac{\text{lbm}}{\text{slug}} \times 1310^\circ\text{R} \times \frac{\text{slug-ft}}{\text{s}^2 \text{lbf}}} = 1749 \text{ ft/s.}$$

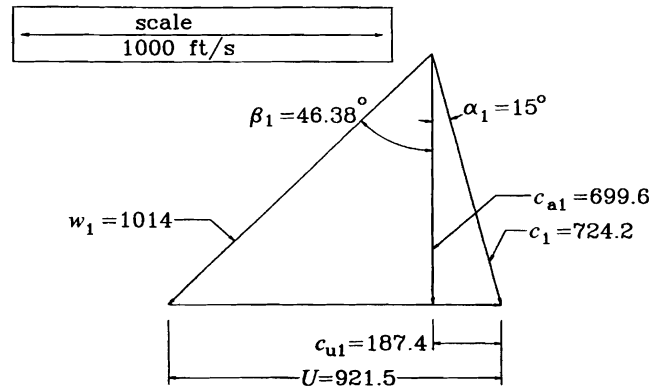


Figure 6.11a Velocity polygon at rotor inlet.

Rotor Inlet

Next, one must refer to Figure 6.11.a, which is the velocity polygon (to scale) for the rotor inlet.

First,

$$c_1 = \frac{c_{a1}}{\cos \alpha_1} = \frac{699.6}{\cos(15^\circ)} = 724.2 \text{ ft/s.}$$

Also,

$$c_{u1} = c_1 \sin \alpha_1 = 724.2 \sin(15^\circ) = 187.4 \text{ ft/s,}$$

and thus

$$w_{u1} = c_{u1} - U = 187.4 - 921.5 = -734.1 \text{ ft/s}$$

and

$$\beta_1 = \cot^{-1} \left[\frac{c_{a1}}{c_{u1} - U_1} \right] = \cot^{-1} \left[\frac{c_{a1}}{w_{u1}} \right] = \cot^{-1} \left[\frac{699.6}{-734.1} \right] = -46.38^\circ$$

Moreover,

$$w_1 = \frac{c_{a1}}{\cos \beta_1} = \frac{699.6}{\cos(-46.38^\circ)} = 1014 \text{ ft/s.}$$

At this point the reader is reminded that this is a mean line analysis and that flow is assumed to be uniform from hub to tip. However, as a quick calculation, if the absolute flow angle is radially constant, the preceding calculations can be repeated for the hub ($R_h = 12.58$ in.) and tip ($R_t = 13.82$ in.) which yields that the relative flow angle varies from -44.6° to -48.0° .

Returning to the mean line analysis, one finds that the Mach number in the rotating frame is

$$M_{1\text{rel}} = \frac{w_1}{a_1} = \frac{1014}{1749} = 0.5798. \quad < \text{ANS}$$

It is important to note that the flow is subsonic in the rotating frame; thus, shocks cannot occur in the inlet plane of the rotor blades. Next, in the absolute or nonrotating frame,

$$M_{1\text{abs}} = \frac{c_1}{a_1} = \frac{724.2}{1749} = 0.4141.$$

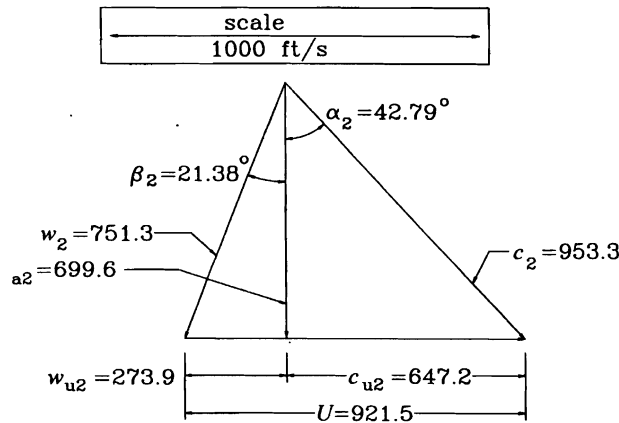


Figure 6.11b Velocity polygon at rotor exit and stator inlet.

Thus flow is also subsonic in the stationary frame and shock formation in the exit of the previous stator vanes should also not be a problem. Also,

$$\frac{T_{t1}}{T_1} = 1 + \frac{\gamma-1}{2} M_{1\text{abs}}^2 = 1 + \frac{0.361}{2} 0.4141^2 = 1.031$$

and

$$T_{t1} = 1.031 \times 1310 = 1350^\circ\text{R} = 890^\circ\text{F}.$$

$$\text{Moreover, } \frac{p_{t1}}{p_1} = \left[\frac{T_{t1}}{T_1} \right]^{\frac{\gamma}{\gamma-1}} = [1.031]^{\frac{1.361}{0.361}} = 1.122$$

$$p_{t1} = 1.122 \times 272 = 305.1 \text{ psia.}$$

Rotor Exit–Stator Inlet

For the rotor exit and stator inlet velocity polygon, refer to Figure 6.11.b. Since the rotor flow turning angle is known, it is possible to find the relative exit angle by

$$\beta_2 = \beta_1 + \delta_{12} = -46.38^\circ + 25^\circ = -21.38^\circ.$$

Also, because the axial velocity is constant through the stage,

$$c_{a2} = c_{a1} = 699.6 \text{ ft/s.}$$

$$\text{Next, } w_2 = \frac{c_{a2}}{\cos \beta_2} = \frac{699.6}{\cos(-21.38^\circ)} = 751.3 \text{ ft/s.}$$

$$\text{Also, } w_{u2} = c_{a2} \tan \beta_2 = 699.6 \tan(-21.38^\circ) = -273.9 \text{ ft/s}$$

$$\text{and } c_{u2} = U + w_{u2} = 921.5 - 273.9 = 647.7 \text{ ft/s;}$$

thus,

$$\alpha_2 = \cot^{-1} \left[\frac{c_{a2}}{U + w_{u2}} \right] = \cot^{-1} \left[\frac{c_{a2}}{c_{u2}} \right] = \cot^{-1} \left[\frac{699.6}{647.7} \right] = 42.79^\circ$$

$$\text{and } c_2 = \frac{c_{a2}}{\cos \alpha_2} = \frac{699.6}{\cos(42.79^\circ)} = 953.3 \text{ ft/s.}$$

Next, the moment of momentum equation can be used with results from the velocity polygons to yield

$$h_{t2} - h_{t1} = U(c_{u2} - c_{u1}) = 921.5 \times (647.7 - 187.4) = 424,107 \text{ ft}^2/\text{s}^2.$$

From the energy equation, one can find

$$\frac{p_{t2}}{p_{t1}} = \left[\frac{\eta_{12}(h_{t2} - h_{t1})}{c_p T_{t1}} + 1 \right]^{\frac{\gamma}{\gamma-1}}.$$

Thus,

$$\frac{p_{t2}}{p_{t1}} = \left[\frac{0.90 \times 424107 \frac{\text{ft}^2}{\text{s}^2}}{0.2587 \frac{\text{Btu}}{\text{lbm} \cdot ^\circ\text{R}} \times 1350^\circ\text{R} \times 778.16 \frac{\text{ft} \cdot \text{lbf}}{\text{Btu}} \times 32.17 \frac{\text{lbm}}{\text{slug}} \text{ slug} \cdot \text{ft}} + 1 \right]^{\frac{1.361}{0.361}},$$

$$= 1.175 \quad < \text{ANS}$$

and so $p_{t2} = 1.175 \times 305.1 = 358.5$ psia.

Also,

$$T_{t2} - T_{t1} = \frac{h_{t2} - h_{t1}}{c_p}$$

$$= \frac{424,107 \frac{\text{ft}^2}{\text{s}^2}}{0.2587 \frac{\text{Btu}}{\text{lbm} \cdot ^\circ\text{R}} \times 778.16 \frac{\text{ft} \cdot \text{lbf}}{\text{Btu}} \times 32.17 \frac{\text{lbm}}{\text{slug}} \text{ slug} \cdot \text{ft}},$$

$$= 65.5^\circ\text{R}$$

thus, $T_{t2} = 1416^\circ\text{R} = 956^\circ\text{F}$.

Moreover,

$$T_2 = T_{t2} - \frac{c_2^2}{2c_p}$$

$$= 1416^\circ\text{R} - \frac{953.2^2 \frac{\text{ft}^2}{\text{s}^2}}{2 \times 0.2587 \frac{\text{Btu}}{\text{lbm} \cdot ^\circ\text{R}} \times 778.16 \frac{\text{ft} \cdot \text{lbf}}{\text{Btu}} \times 32.17 \frac{\text{lbm}}{\text{slug}} \text{ slug} \cdot \text{ft}}$$

$$= 1346^\circ\text{R} = 886^\circ\text{F}.$$

Next

$$a_2 = \sqrt{\gamma \mathcal{R} T_2} = \sqrt{1.361 \times 53.35 \frac{\text{ft} \cdot \text{lbf}}{\text{lbm} \cdot ^\circ\text{R}} \times 32.17 \frac{\text{lbm}}{\text{slug}} \times 1346^\circ\text{R} \times \frac{\text{slug} \cdot \text{ft}}{\text{s}^2 \cdot \text{lbf}}}$$

$$= 1773 \text{ ft/s}.$$

Thus, the Mach number in the rotating frame is

$$M_{2\text{rel}} = \frac{w_2}{a_2} = \frac{751.3}{1773} = 0.4237. \quad < \text{ANS}$$

It is once again important to note that the flow is thus subsonic in the rotating frame, and shock formation in the exit of the rotor should not be a problem. Next, in the absolute frame,

$$M_{2\text{abs}} = \frac{c_2}{a_2} = \frac{953.3}{1773} = 0.5378. \quad < \text{ANS}$$

Thus, the flow is also subsonic in the stationary frame, and so shocks cannot occur in the inlet plane of the following stator blades. Using the absolute Mach number yields

$$\frac{p_{t2}}{p_2} = \left[1 + \frac{\gamma - 1}{2} M_{2\text{abs}}^2 \right]^{\frac{\gamma}{\gamma - 1}} = \left[1 + \frac{0.361}{2} 0.5378^2 \right]^{\frac{1.361}{0.361}} = 1.211,$$

and thus

$$p_2 = \frac{358.5}{1.211} = 295.9 \text{ psia}. \quad < \text{ANS}$$

Next, from the ideal gas law for $p_2 = 295.9$ psia and $T_2 = 1346^\circ\text{R}$ one obtains

$$\rho_2 = \frac{p_2}{\mathcal{R} T_2} = \frac{295.9 \frac{\text{lbf}}{\text{in}^2} \times 144 \frac{\text{in}^2}{\text{ft}^2}}{53.35 \frac{\text{ft} \cdot \text{lbf}}{\text{lbm} \cdot ^\circ\text{R}} \times 1346^\circ\text{R} \times 32.17 \frac{\text{lbm}}{\text{slug}}} = 0.01845 \frac{\text{slug}}{\text{ft}^3},$$

and because $\dot{m} = \rho_2 c_{a2} A_2$,

$$A_2 = \frac{\dot{m}}{\rho_2 c_{a2}} = \frac{8.704 \frac{\text{slugs}}{\text{s}}}{0.01845 \frac{\text{slug}}{\text{ft}^3} \times 699.6 \frac{\text{ft}}{\text{s}}} = 0.6744 \text{ ft}^2.$$

Also $A_2 = \pi D_2 t_2$;
thus,

$$t_2 = \frac{A_2}{\pi D_2} = \frac{0.6744 \text{ ft}^2 \times 144 \frac{\text{in}^2}{\text{ft}^2}}{\pi \times 2 \times 13.2 \text{ in.}} = 1.171 \text{ in.} \quad < \text{ANS}$$

Note that this is smaller than the rotor inlet height because of the compressibility of the fluid.

One can define a pressure coefficient for the rotor (which is covered in detail in Section 6.6) as

$$C_{\text{pr}} = \frac{p_2 - p_1}{\frac{1}{2} \rho_1 w_1^2}$$

$$C_{\text{pr}} = \frac{(295.9 - 272.0) \frac{\text{lbf}}{\text{in}^2} \times \frac{\text{slug-ft}}{\text{s}^2 \text{-lbf}} \times \frac{144 \text{ in}^2}{\text{ft}^2}}{\frac{1}{2} \times 0.01742 \frac{\text{slug}}{\text{ft}^3} \times 1014^2 \frac{\text{ft}^2}{\text{s}^2}} = 0.384.$$

Implications of this parameter are discussed in Section 6.6. Next, one can find the input stage power by

$$\dot{W}_{\text{sh}} = \dot{m}(h_{t2} - h_{t1}) = \frac{8.704 \frac{\text{slugs}}{\text{s}} \times \left(424,107 \frac{\text{ft}^2}{\text{s}^2}\right)}{550 \frac{\text{ft-lbf}}{\text{s-hp}}} \left(\frac{\text{s}^2 \text{-lbf}}{\text{slug-ft}}\right)$$

$$= 6712 \text{ hp} \quad < \text{ANS}$$

And the percent reaction can be found by

$$\%R = \frac{1}{1 + \left[\frac{c_2^2 - c_1^2}{w_1^2 - w_2^2}\right]} = \frac{1}{1 + \left[\frac{953.3^2 - 724.2^2}{1014^2 - 751.3^2}\right]} = 0.5469.$$

On initial inspection, this is a reasonable value for the percent reaction, for it is slightly above 0.5. One can also combine the polygons for the rotor inlet and exit as shown in Figure 6.11.c. The rotor turning angle is easily seen as well as the change in absolute tangential velocity (Δc_u). As indicated in Section 6.4.1 and Table 6.2, if

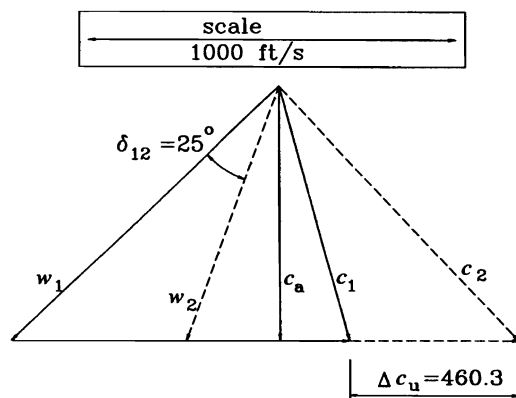


Figure 6.11c Combined rotor inlet-stator inlet polygon.

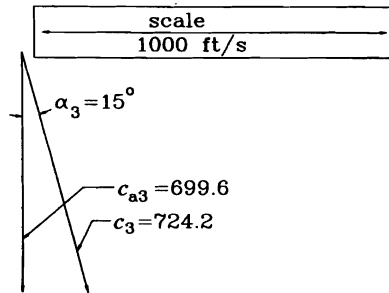


Figure 6.11d Velocity polygon at stator exit.

the rotor turning is increased, so is the change in absolute tangential velocity. Also, it is apparent that the two polygons in Figure 6.11.c are approximately symmetric, indicating that the percent reaction should be about 0.5, which it is. One should, however, compare the pressure rises for the rotor and stator later.

Stator Exit

Next, refer to Figure 6.11.d for the stator exit velocity polygon. Once again, the axial velocity is constant through the stage, and so

$$c_{a3} = c_{a2} = c_{a1} = 699.6 \text{ ft/s.}$$

Also the absolute exit angle is given, $\alpha_3 = 15^\circ$; thus,

$$c_3 = \frac{c_{a3}}{\cos \alpha_3} = \frac{699.6}{\cos(15^\circ)} = 724.2 \text{ ft/s.}$$

The turning angle of the stator can be found by

$$\delta_{23} = \alpha_3 = \alpha_2 = 15 - 42.79 = -27.79^\circ.$$

Thus, the magnitude of the turning angle for the stator vane is approximately that of the rotor blade. Next, for the stator,

$$T_{13} = T_{12} = 1416^\circ\text{R,}$$

and

$$\begin{aligned} T_3 &= T_{13} - \frac{c_3^2}{2c_p} \\ &= 1416^\circ\text{R} - \frac{724.2^2 \frac{\text{ft}^2}{\text{s}^2}}{2 \times 0.2587 \frac{\text{Btu}}{\text{lbm}\cdot^\circ\text{R}} \times 778.16 \frac{\text{ft}\cdot\text{lbf}}{\text{Btu}} \times 32.17 \frac{\text{lbm}}{\text{slug}} \text{ slug}\cdot\text{ft}} \\ &= 1375^\circ\text{R} \end{aligned}$$

Next,

$$\begin{aligned} a_3 &= \sqrt{\gamma \mathcal{R} T_3} = \sqrt{1.361 \times 53.35 \frac{\text{ft}\cdot\text{lbf}}{\text{lbm}\cdot^\circ\text{R}} \times 32.17 \frac{\text{lbm}}{\text{slug}} \times 1375^\circ\text{R} \times \frac{\text{slug}\cdot\text{ft}}{\text{s}^2\cdot\text{lbf}}} \\ &= 1792 \text{ ft/s,} \end{aligned}$$

and so

$$M_{3\text{abs}} = \frac{c_3}{a_3} = \frac{724.2}{1792} = 0.4041. \quad < \text{ANS}$$

Therefore, the flow is once again subsonic in the stationary frame, and so shocks cannot occur in the exit plane of the stator blades.

In addition,

$$\frac{p_{t3}}{p_3} = \left[1 + \frac{\gamma-1}{2} M_{3\text{abs}}^2 \right]^{\frac{\gamma}{\gamma-1}} = \left[1 + \frac{0.361}{2} 0.4041^2 \right]^{\frac{1.361}{0.361}} = 1.116.$$

Also, for the stator $p_{t3} = p_{t2} = 358.5$ psia;

thus,

$$p_3 = \frac{358.5}{1.116} = 321.3 \text{ psia.} \quad < \text{ANS}$$

From the ideal gas law, for $T_3 = 1375^\circ\text{R}$ and $p_3 = 321.3$ psia,

$$\rho_3 = \frac{p_3}{\mathcal{R}T_3} = \frac{321.3 \frac{\text{lbf}}{\text{in}^2} \times 144 \frac{\text{in}^2}{\text{ft}^2}}{53.35 \frac{\text{ft-lbf}}{\text{lbm-}^\circ\text{R}} \times 1375^\circ\text{R} \times 32.17 \frac{\text{lbm}}{\text{slug}}} = 0.01960 \frac{\text{slug}}{\text{ft}^3}.$$

One can define a pressure coefficient for the stator (which is covered in detail in Section 6.6) as

$$C_{\text{ps}} = \frac{p_3 - p_2}{\frac{1}{2} \rho_2 c_2^2}$$

$$C_{\text{ps}} = \frac{(321.3 - 295.9) \frac{\text{lbf}}{\text{in}^2} \times \frac{\text{slug-ft}}{\text{s}^2\text{-lbf}} \times \frac{144 \text{ in}^2}{\text{ft}^2}}{\frac{1}{2} \times 0.01845 \frac{\text{slug}}{\text{ft}^3} \times 953.3^2 \frac{\text{ft}^2}{\text{s}^2}} = 0.436.$$

As for the rotor, implications of this parameter are discussed in Section 6.6. Also, since $\dot{m} = \rho_3 c_{a3} A_3$,

$$A_3 = \frac{\dot{m}}{\rho_3 c_{a3}} = \frac{8.704 \frac{\text{slugs}}{\text{s}}}{0.01960 \frac{\text{slug}}{\text{ft}^3} \times 699.6 \frac{\text{ft}}{\text{s}}} = 0.6348 \text{ ft}^2.$$

In addition, $A_3 = \pi D_3 t_3$,

and so

$$t_3 = \frac{A_3}{\pi D_3} = \frac{0.6348 \text{ ft}^2 \times 144 \frac{\text{in}^2}{\text{ft}^2}}{\pi \times 2 \times 13.2 \text{ in.}} = 1.102 \text{ in.} \quad < \text{ANS}$$

Once again, note that this is smaller than the stator inlet height because of the compressibility of the fluid. Note also that the static pressure rises across the rotor and stator are 23.9 and 25.4 psia, respectively. Thus, they are approximately the same. One should remember that the calculated percent reaction was 0.547, which is in keeping with the pressure distribution.

Thus, all of the variables of interest have been found. For the sake of comparison, one can find similar parameters for an approximation to the fifth engine stage or first high-pressure stage, of the same engine. For this stage, the radius is 14.9 in. and the inlet blade height is 4.70 in. (much larger than the last stage). Also, the inlet pressure is 32 psia, whereas the inlet temperature is 220 °F. The stage efficiency is again 0.90. The inlet absolute flow angle to the rotor is 23° and the rotor blade turning angle is 15°, which is lower than that of the last stage. The resulting values of c_p and γ are 0.2432 Btu/lbm-°R and 1.393, respectively. The resulting axial velocity is 721.4 ft/s, which is close to that of the last stage. The relative inlet angle to the rotor blade is 45.49°, and the absolute inlet angle to the stator is 40.46°. The percent reaction is 0.5570, which is again reasonable, and the total pressure ratio is 1.251, which is higher than that of the last stage. Details of the calculations are left as an exercise to the reader.

Also, in this example the axial component of velocity was given as being constant with axial position, and the blade heights were calculated. However, if the

blade heights would have been given, the axial component of velocity would have needed to be determined. The solution would have been iterative, using the same procedure as given.

Example 6.2: Solve example 6.1 if an incompressible flow with a density of that at the inlet ($\rho = 0.01742 \text{ slug/ft}^3$) is assumed.

SOLUTION:

Many of the results can be used from Example 6.1. That is,

$$U = R\omega = \frac{13.2 \text{ in.}}{12 \frac{\text{in.}}{\text{ft}}} \frac{8000 \text{ rev}}{\text{min}} \frac{2\pi \text{ rad}}{\text{rev}} \frac{1}{60 \frac{\text{s}}{\text{min}}} = 921.5 \text{ ft/s,}$$

$$A_1 = \pi D_1 t_1 = \pi \frac{2 \times 13.2 \text{ in.}}{12 \frac{\text{in.}}{\text{ft}}} \frac{1.24 \text{ in.}}{12 \frac{\text{in.}}{\text{ft}}} = 0.7142 \text{ ft}^2,$$

and

$$c_{a1} = \frac{\dot{m}}{\rho_1 A_1} = \frac{8.704 \frac{\text{slugs}}{\text{s}}}{0.01742 \frac{\text{slug}}{\text{ft}^3} \times 0.7142 \text{ ft}^2} = 699.6 \text{ ft/s.}$$

Thus, since the axial and rotational velocities and the angles are the same as for the compressible case, the velocity polygons are the same.

Rotor Inlet

Refer to Figure 6.10.a, which is the velocity polygon for the rotor inlet.

First,

$$c_1 = \frac{c_{a1}}{\cos \alpha_1} = \frac{699.6}{\cos(15^\circ)} = 724.2 \text{ ft/s.}$$

Also,

$$c_{u1} = c_1 \sin \alpha_1 = 724.2 \sin(15^\circ) = 187.4 \text{ ft/s;}$$

thus,

$$w_{u1} = c_{u1} - U = 187.4 - 921.5 = -734.1 \text{ ft/s}$$

and

$$\beta_1 = \cot^{-1} \left[\frac{c_{a1}}{c_{u1} - U_1} \right] = \cot^{-1} \left[\frac{c_{a1}}{w_{u1}} \right] = \cot^{-1} \left[\frac{699.6}{-734.1} \right] = -46.38^\circ.$$

Moreover,

$$w_1 = \frac{c_{a1}}{\cos \beta_1} = \frac{699.6}{\cos(-46.38^\circ)} = 1014 \text{ ft/s.}$$

Also, for the incompressible case the total pressure is

$$p_{t1} = p_1 + \frac{\rho c_1^2}{2} = 272 \text{ psia} + \frac{0.01742 \frac{\text{slug}}{\text{ft}^3} \times 724.2^2 \frac{\text{ft}^2}{\text{s}^2}}{2 \times 12 \frac{\text{in.}}{\text{ft}} \times 12 \frac{\text{in.}}{\text{ft}}} = 303.7 \text{ psia.}$$

Rotor Exit and Stator Inlet

For the rotor exit and stator inlet velocity polygon, refer to Figure 6.11.b. Because the rotor flow turning angle is known, one can find the relative exit angle by

$$\beta_2 = \beta_1 + \delta_{12} = -46.38 + 25 = -21.38^\circ.$$

Also, since the axial velocity is constant through the stage,

$$c_{a2} = c_{a1} = 699.6 \text{ ft/s.}$$

Next,

$$w_2 = \frac{c_{a2}}{\cos \beta_2} = \frac{699.6}{\cos(-21.38^\circ)} = 751.3 \text{ ft/s.}$$

Also, $w_{u2} = c_{a2} \tan \beta_2 = 699.6 \tan(-21.38^\circ) = -273.9 \text{ ft/s}$

and $c_{u2} = U + w_{u2} = 921.5 - 273.9 = 647.7 \text{ ft/s}$;

thus,

$$\alpha_2 = \cot^{-1} \left[\frac{c_{a2}}{U + w_{u2}} \right] = \cot^{-1} \left[\frac{c_{a2}}{c_{u2}} \right] = \cot^{-1} \left[\frac{699.6}{647.7} \right] = 42.79^\circ$$

and

$$c_2 = \frac{c_{a2}}{\cos \alpha_2} = \frac{699.6}{\cos(42.79^\circ)} = 953.3 \text{ ft/s.}$$

Next, for the incompressible case, $p_{t2} - p_{t1} = \rho \eta_{12} U [c_{u2} - c_{u1}]$

$$\begin{aligned} p_{t2} - p_{t1} &= 0.01742 \frac{\text{slug}}{\text{ft}^3} \times 0.90 \times 921.5 \frac{\text{ft}}{\text{s}} \times [647.7 - 187.4] \frac{\text{ft}}{\text{s}} \times \frac{1}{144 \frac{\text{in}^2}{\text{ft}^2}} \\ &= 46.2 \text{ psia,} \end{aligned}$$

and so $p_{t2} = 303.72 + 46.18 = 349.9 \text{ psia}$.

Therefore, $\frac{p_{t2}}{p_{t1}} = \frac{349.9}{303.7} = 1.152$,

which is 1.96 percent lower than found in Example 6.1 owing to the incompressibility of the fluid.

Next,

$$p_2 = p_{t2} - \frac{\rho c_2^2}{2} = 349.9 \text{ psia} - \frac{0.01742 \frac{\text{slug}}{\text{ft}^3} \times 953.3^2 \frac{\text{ft}^2}{\text{s}^2}}{2 \times 12 \frac{\text{in}}{\text{ft}} \times 12 \frac{\text{in}}{\text{ft}}} = 294.9 \text{ psia}$$

Also, the required power is

$$\dot{W}_{\text{sh}} = \dot{m} U (c_{u2} - c_{u1}) = \frac{8.704 \frac{\text{slugs}}{\text{s}} \times 921.5 \frac{\text{ft}}{\text{s}} \times (647.7 - 187.4) \frac{\text{ft}}{\text{s}}}{550 \frac{\text{ft-lbf}}{\text{s-hp}}} = 6712 \text{ hp,}$$

which is identical to that in Example 6.1.

Finally,

$$\%R = \frac{1}{1 + \left[\frac{c_2^2 - c_1^2}{w_1^2 - w_2^2} \right]} = \frac{1}{1 + \left[\frac{953.3^2 - 724.2^2}{1014^2 - 751.3^2} \right]} = 0.5469,$$

which is also identical to the percent reaction in Example 6.1.

Also, since the flow is incompressible, the blade heights remain constant through the stage; thus, $t_2 = 1.24 \text{ in}$.

Stator Exit

Refer to Figure 6.11.c for the stator exit velocity polygon.

Once again, the axial velocity is constant through the stage, and thus

$$c_{a3} = c_{a2} = c_{a1} = 699.6 \text{ ft/s.}$$

Also the absolute exit angle is given, $\alpha_3 = 15^\circ$, and so

$$c_3 = \frac{c_{a3}}{\cos \alpha_3} = \frac{699.6}{\cos(15^\circ)} = 724.2 \text{ ft/s.}$$

Since $p_{t3} = p_{t2}$, the exit static pressure is

$$p_3 = p_{t2} - \frac{\rho c_3^2}{2} = 349.9 \text{ psia} - \frac{0.01742 \frac{\text{slug}}{\text{ft}^3} \times 724.2^2 \frac{\text{ft}^2}{\text{s}^2}}{2 \times 12 \frac{\text{in}}{\text{ft}} \times 12 \frac{\text{in}}{\text{ft}}} = 318.2 \text{ psia.}$$

The turning angle of the stator can be found by

$$\delta_{23} = \alpha_3 - \alpha_2 = 15 - 42.79 = -27.29^\circ.$$

Thus, the turning angle for the stator vane is approximately that of the rotor blade. Again, because the flow is incompressible, the blade height remains constant throughout the stage; thus, $t_3 = 1.24$ in.

6.5. Performance Maps

6.5.1. Dimensional Analysis

As a working medium for a compressor engineer, performance curves or “maps” are usually used to present experimental data. These enable an engineer to make a quick, comprehensive, and accurate assessment of the general conditions at which the turbomachine is operating and to understand what can be expected of the machine if the flow conditions are changed. In Appendix I, a dimensional analysis of the different parameters is performed, and similitude is shown. Of primary concern is the total pressure ratio of a compressor, namely, p_{t3}/p_{t2} . From Appendix I (Eqs. I.3.3, I.3.7, and I.3.8),

$$\pi_c = p_{t3}/p_{t2} = \mathcal{f} \left\{ \dot{m} \frac{\sqrt{\theta_{t1}}}{\delta_{t1}}, \frac{N}{\sqrt{\theta_{t1}}} \right\} = f \{ \dot{m}_{c2}, N_{c2} \}, \quad 6.5.1$$

where

$$\delta_{t2} = p_{t2}/p_{stp} \quad 6.5.2$$

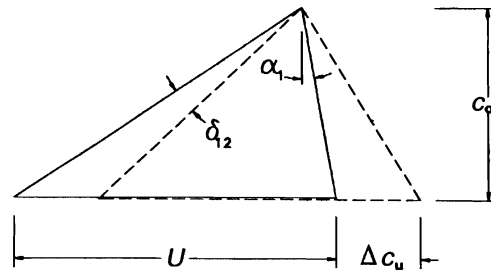
and

$$\theta_{t2} = T_{t2}/T_{stp}, \quad 6.5.3$$

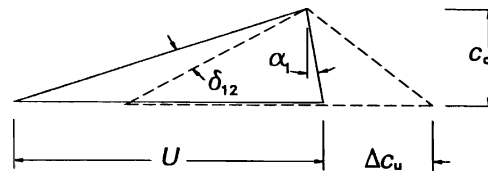
where the subscript *stp* refers to standard conditions, the subscript *t2* denotes the inlet total condition to the compressor (not to be confused with the exit total condition of a rotor cascade), and the subscript *t3* signifies the exit total condition out of the compressor. Similarly, for the efficiency, one finds (Eqs. I.3.6, I.3.7, and I.3.8):

$$\eta_c = \mathcal{g} \left\{ \dot{m} \frac{\sqrt{\theta_{t1}}}{\delta_{t1}}, \frac{N}{\sqrt{\theta_{t1}}} \right\} = \mathcal{g} \{ \dot{m}_{c2}, N_{c2} \}. \quad 6.5.4$$

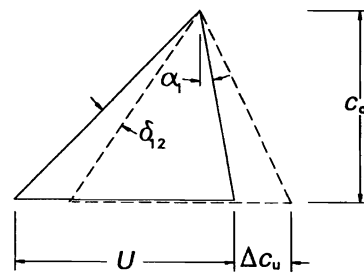
The two functions \mathcal{f} and \mathcal{g} are empirically determined from experimental data. These functions are not necessarily analytical (closed form algebraic expressions) (and in fact rarely are) but are most commonly graphical presentations or tabular data. The two independent parameters (\dot{m}_{c2} and N_{c2}) are not truly dimensionless. The first is called the “corrected” mass flow and has dimensions of mass flow, whereas the second is called the “corrected” speed and has dimensions of rotational speed. Thus, because they are not dimensionless, the resulting function cannot be used to correlate or compare different engines. The function for one particular engine can be used under different operating conditions, however, as is the usual case. That is, the compressor can be tested under one set of conditions but applied to markedly different conditions so long as the corrected speed and mass flow rates are identically matched. For example, the map is applicable regardless of altitude, aircraft speed, atmospheric conditions, and so on.



(a) On-design Flow and Rotational Speed



(b) Low Flow Rate



(c) Low Rotational Speed

Figure 6.12 Trends of compressor velocity polygons.

6.5.2. Trends

One should also know how the developed pressure ratio varies with the two independent variables – namely, the trends. First, consider how p_3/p_2 varies with \dot{m} if all other parameters are held constant. Figure 6.12 is applicable to this study. In Figure 6.12.a, the inlet and exit velocity polygons for one stage are shown for the design condition. If the mass flow is decreased, the axial component of velocity is decreased, as shown in Figure 6.12.b. However, for the same inlet flow angle and rotor turning angle, the difference $\Delta c_u = c_{u2} - c_{u1}$ is increased. Thus, from Eq. 6.4.2 it can be seen that, as the flow rate decreases, the pressure ratio increases.

The next consideration is how the pressure ratio will change as the rotational speed is changed with all other parameters are held constant. For example, in Figure 6.12.a, the inlet and exit velocity polygons are presented for the design condition. In Figure 6.12.c, the velocity polygons are presented for a decreased rotational speed with the inlet angle and rotor turning angle the same as for the design condition. Now, $\Delta c_u = c_{u2} - c_{u1}$ has been decreased. Also, U has been decreased. Thus, one can examine Eq. 6.4.2 again and see that the pressure ratio decreases with decreasing rotational speed.

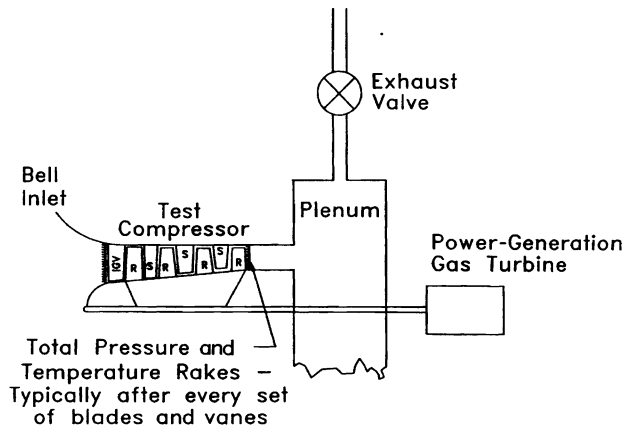


Figure 6.13 Compressor rig test facility.

6.5.3. Experimental Data

As indicated in Section 6.5.1, the two compressor parameters that are most important are the total pressure ratio and the efficiency. To determine these parameters, the compressor must be tested independently of the other engine components in a compressor test facility (Fig. 6.13). In such a facility, the compressor is usually driven by an auxiliary gas turbine. The rotational speed is independently controlled through a gearbox, and the flow rate is independently controlled by a large valve system. Typically, the test rig is run at a series of constant rotational speeds. At each speed the flow rate is incrementally decreased, the system is allowed to reach steady state, and pressure and temperature measurements are taken at every mass flow rate until the compressor pressure ratio becomes so large that the compressor has massive flow reversal or “surges.” This unstable flow reversal is accompanied by tremendous vibration forces on the blades and disks as well as a burner “flameout” in an engine. Surge results when one or more rows of blades or vanes stall, namely flow separates. The unstable behavior in one stage expands to other stages until all or most of the stages have separated.

The compressor stages are all instrumented with a series of total and static pressure probes and total and static temperature thermocouples. At the inlet and exit of each stage, a pressure and temperature “rake” (a series of radially located probes) is installed. Thus, for the inlet and exit of each stage, a total pressure and temperature profile from hub to tip is measured, giving the design engineer great detail about the internal performance. By averaging (weighted by mass flow rate) the total pressures at the inlet to, and exit of, the compressor, the total pressure ratio of the compressor can be found for each speed and flow rate condition. Next, by averaging (again weighted by mass flow rate) the total temperature at the inlet to, and exit of, the compressor, the total temperature ratio of the compressor can be determined. Finally, from the experimental data the overall compressor efficiency can be found by using Eq. 3.2.8 as follows:

$$\eta_c = \frac{\left[\frac{p_{t3}}{p_{t2}} \right]^{\frac{\gamma-1}{\gamma}} - 1}{\left[\frac{T_{t3}}{T_{t2}} \right] - 1} \quad 6.5.5$$

While a constant speed line is traversed, as the mass flow decreases, the efficiency increases to a maximum and then decreases as the compressor nears surge. The maximum efficiency on this line becomes a part of the desired operating line.

All of the preceding discussions in this section have been confined to analysis of the overall compressor data. Note that the interstage total pressure and temperature profile data are also used to find the efficiency and total pressure ratio for only the fan and the low- and high-pressure compressors. Furthermore, data from individual stages are examined using an equation similar to Eq. 6.5.5 and reduced to give total pressure ratios and efficiencies of individual stages. Furthermore, data from the hub, midstream, and tip regions of stages are analyzed so that performance of the radial regions of stages can be investigated. Thus, not only are the overall conditions of the compressor found, but the efficiency and total pressure ratio of the subcomponents, each stage, and radial regions of all stages are determined. These specific and local details obviously allow an engineer to determine the inefficient regions of a compressor so that local blade shape changes can be made and, thus, improvements to the overall improvement of the whole compressor can be achieved.

6.5.4. Mapping Conventions

Finally, in Figure 6.14 a typical compressor map, which is generated from the data taken during compressor stand tests, is presented. The pressure ratio is plotted versus the corrected mass flow, and the corrected speed is a second parameter. Thus, a series of corrected speed lines are also included in the figure, and these are often presented as a percentage of the nominal or design rotational speed. Also shown in this figure is the so-called surge line. Surge arises when the pressure gradient overwhelms the flow momentum and causes massive flow reversal in the engine. Locally, massive flow separation occurs on the different blades in the engine at this condition, and the performance goes to zero. This is a very dangerous condition for the engine to operate in because of excessive vibrations and the zero overall engine thrust.

A second set of complementary compressor data are plotted so that curves are fitted between points of constant efficiency on the different speed lines. Lines on which the efficiency is constant are shown (dotted) in this figure and are called efficiency "islands."

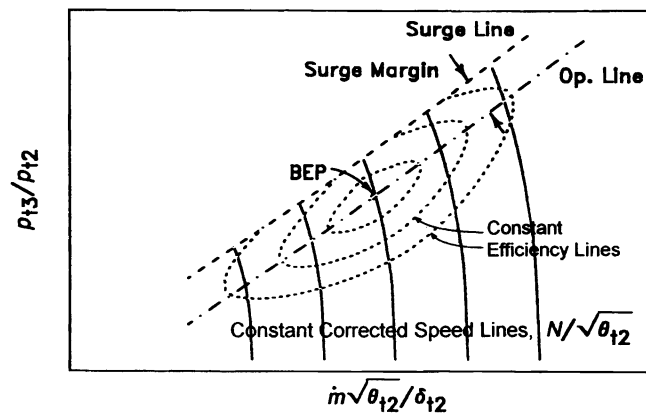


Figure 6.14 Typical compressor map.

The typical design point of an engine is near the peak or best efficiency point (BEP). Thus, as one changes conditions from the design point, the efficiency decreases. Also shown in Figure 6.14 is the operating line. This line passes through the design point and represents the different conditions at which an engine typically operates. In this figure, one can easily see that, along a constant speed line, as the mass flow decreases, the efficiency increases to a maximum on the operating line and then decreases as the compressor nears surge. The surge margin is the remaining performance information presented shown in this figure. This is the margin between the operating line and the surge line and is regarded a safety margin. In designing a compressor, one encounters a trade-off because the objective is usually to design for a large pressure ratio at the operating condition. On the other hand, a small surge margin is undesirable because the compressor could surge as the result of a small perturbation – for example, a wind gust or sudden yaw or acceleration. Typical surge margins for modern engines range from 15 to 20 percent. Overall, once a compressor map is found, if the corrected mass flow and corrected speed are known, the total pressure ratio and efficiency can be found regardless of other conditions.

As discussed in this section, maps are considered for the entire compressor as well as individual maps for the fan and low- and high-pressure compressors. There will be a map for each stage of the engine and, in most instances, for the hub, pitch, and tip regions of each stage. In Table 6.3, some characteristic fan, compressor, and turbine parameters are shown for selected modern engines. The reader should be attentive to the pressure ratios, bypass ratios, and number of stages. Table 6.3 was integrated from engine data in *Aviation Week & Space Technology*; *Flight International*; information from manufacturers, users, and the military; brochures; and Web pages. Although every effort has been made to ensure maintain accuracy by cross-checking, the information is for reference and is not intended for technical applications. Also, many of the engines have different “builds” for different applications and for those cases typical characteristics are presented.

6.5.5. Surge Control

Because surge is a dangerous condition and the operating lines for most compressors are near surge, active control is often used to ensure safe operation. Such automatic control is usually in two forms and both rely on an early detection system that monitors the pressure profiles on vanes in selected stages to detect any flow separation. First, if a detection system senses preliminary stall for a stage, air can be bled from the compressor to increase the mass flow rate. Thus, on the map, as the mass flow increases, the compressor moves along a constant speed line away from the surge line. The second form of active control used if a detection system senses preliminary stall for a stage “entails using variable” stators, which are discussed in Section 6.7, that can be turned so that the incidence angles are decreased, thus reducing stall. Usually a combination of the two methods is used.

6.6. Limits on Stage Pressure Ratio

As indicated in Chapter 1, the overall thermodynamic efficiency of a machine is improved if the compressor pressure ratio is increased. Thus, it is desirable to have as high a pressure ratio as possible across each stage without separation, which leads to lower efficiencies and stall. In Section 6.4, equations were derived whereby the pressure ratio can be found for given blade and flow geometries. If one examines these equations, it becomes apparent that there are essentially no limits on the possible developed pressure ratios. Yet,

Table 6.3. Typical Axial Flow Engine Compressor and Turbine Characteristics at Maximum Power

Engine	Manufacturer	Type and No. of Compressive Stages	Overall Total Pressure Ratio	Bypass Ratio	LP+(IP)+HP Turbine Stages
CF6-50C2B	GE	1F, 3A, 14A	31.1	4.6	4+2
CF6-80C2A5	GE	1F, 4A, 14A	31.5	5.3	5+2
F101-102	GE	2F, 9A	26.8	1.9	1+2
F110-100	GE	3F, 9A	30.4	0.8	1+2
CF34-3A	GE	1F, 14A	21	6.2	4+2
F404	GE	3F, 7A	26	0.33	1+1
GE90-115B	GE	1F, 4A, 9A*	42	9.0	6+2
J79-8	GE	17A	12.9	NA	3
J85-17AB	GE	8A	6.9	NA	2
CFM56-5B1	CFM	1F, 4A, 9A	32	5.5	4+1
GP 7200	EA	1F, 4A, 9A	43.9	8.7	5+2
TF30-P-100	PWA	3F, 13A	21.8	0.7	3+1
F100-PW-232	PWA	3F, 10A	35	0.34	2+2
JT8D	PWA	2F, 11A	18.2	1.7	3+1
JT9D	PWA	1F, 15A	26.7	4.8	4+2
PW2037	PWA	1F, 5A, 11A	27.4	6	5+2
PW4056	PWA	1F, 4A, 11A	30.0	4.9	4+2
PW4098	PWA	1F, 6A, 12A	42.8	6.4	7+2
F117	PWA	1F, 5A, 11A	30.8	5.9	5+2
J52	PWA	12A	13.6	NA	2
J58	PWA	9A	8.8	NA	2
J75	PWA	8A, 7A	12.0	NA	2+1
Spey-101	RR	4F, 12A	16.5	0.7	2+2
RB211-535C	RR	1F, 7A, 6A	34.5	4.3	3+1+1
Trent 895	RR	1F, 8A, 6A	41.6	6.5	5+1+1
Tyne	RR	6A, 9A	13.5	NA	3+1
Viper 522	RR	8A	5.6	NA	1
T56A-15	RR	14A	9.5	NA	4
ALF502	Honeywell	3F, 7A, 1R	13.8	5.6	2+2
TFE731-2	Honeywell	1F, 4A, 1R	13	2.7	3+1

F = Fan stages

A = Axial Compressor stages

*1F, 4A, 9A = 1 Fan + 4 Axial stages on low speed shaft 9 Axial stages on high speed shaft etc

R = Radial stages

modern compressors have maximum stage total pressure ratios of about 1.25 to 1.30. In this section, the practical *stage* limits are examined.

First, keep in mind that both a rotor and stator blade passage are essentially diffusers. Both have flow passage areas that increase as the flow passes through, and the static pressures increase. Thus, in both cases an adverse pressure gradient is present that tends to cause separation of the boundary layer. It is this separation that limits the operation of a compressor through surge or stall. One can use a relatively simple model postulated by Hill and Peterson (1992) using pressure coefficients. The pressure coefficient is defined by

$$C_p = \frac{\Delta p}{\frac{1}{2} \rho_i w_i^2}, \quad 6.6.1$$

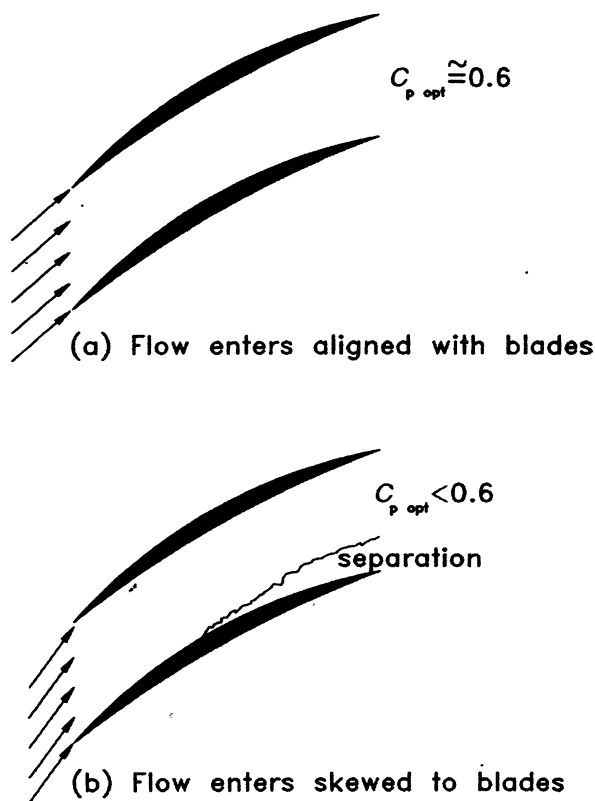


Figure 6.15 Simple blade passage.

where w_1 is the inlet relative velocity to the diffuser. Typically, for a simple diffuser having walls with limited curvature and ideal incidence-free inlet conditions (Fig. 6.15.a), C_p is less than or approximately equal to 0.6 for flow without separation. If the pressure coefficient becomes greater than about 0.6, the flow separates. Once the flow separates, the effective area ratio is not very large, and thus the pressure ratio of the stage is minimal. Also, the efficiency of the stage is greatly reduced. And finally, a stage separation can lead to compressor surge. If the walls have significant curvature or if the flow enters the diffuser in a skewed direction, or with incidence (Fig. 6.15.a), this upper limit on the pressure coefficient will be reduced significantly to perhaps 0.1 to 0.4. Now, referring to Figure 6.6, one can apply Eq. 6.6.1 and define a pressure coefficient for the rotor. Because the rotor is moving, the relative velocity must be used; thus,

$$C_{pr} = \frac{p_2 - p_1}{\frac{1}{2} \rho_1 w_1^2} \quad 6.6.2$$

For the stator, which is stationary, the absolute velocity is used; thus,

$$C_{ps} = \frac{p_3 - p_2}{\frac{1}{2} \rho_2 c_2^2} \quad 6.6.3$$

where the subscripts 1 and 2 refer to the stage inlet and midstage properties, respectively. Next, for the rotor one can consider the square of the relative inlet Mach number as

$$M_{1 \text{ rel}}^2 = \frac{w_1^2}{a_1^2} = \frac{\rho_1 w_1^2}{\gamma p_1} \quad 6.6.4$$

Therefore, from Eq. 6.6.2, one finds

$$\frac{p_2}{p_1} = \frac{1}{2} \frac{\rho_1 w_1^2 C_{pr}}{p_1} + 1, \quad 6.6.5$$

and from Eq. 6.6.4,

$$\frac{p_2}{p_1} = 1 + \frac{1}{2} C_{pr} \gamma M_{1rel}^2. \quad 6.6.6$$

Next, the square of the inlet Mach number as experienced by the stator is

$$M_{2abs}^2 = \frac{c_2^2}{a_2^2} = \frac{\rho_2 c_2^2}{\gamma p_2}. \quad 6.6.7$$

Finally, from Eqs. 6.6.3 and 6.6.7 one finds

$$\frac{p_3}{p_2} = 1 + \frac{1}{2} C_{ps} \gamma M_{2abs}^2. \quad 6.6.8$$

One very important fact is obvious. Since the maximum allowable C_p is approximately fixed, if a designer wants to increase the pressure ratio limit of a rotor, stator passage, or both for a given pressure coefficient (without stall), it is necessary to increase the inlet Mach number.

Example 6.3: For the stage geometry in Example 6.1, find the approximate optimum limit on p_3/p_1 . The pressure coefficients can be assumed to be 0.6 (the upper limit) for both the rotor and stator. Note that, in Example 6.1, the rotor and stator pressure coefficients were found to be 0.384 and 0.436, respectively. Thus, as compared with the maximum or optimum limit of approximately 0.6, a reasonable safety margin was used, which in turn yields the surge margin.

SOLUTION:

The specific heat ratio is $\gamma = 1.361$, and the relative inlet Mach number to the rotor is

$$M_{1rel} = \frac{w_1}{a_1} = \frac{1014}{1749} = 0.5798.$$

The inlet Mach number to the stator was already found and is as follows:

$$M_{2abs} = 0.5378.$$

Thus, for the maximum pressure coefficient,

$$\left. \frac{p_2}{p_1} \right|_{\text{limit}} = 1 + \frac{1}{2} C_{pr} \gamma M_{1rel}^2 = 1 + \frac{1}{2} \times 0.6 \times 1.361 \times 0.5798^2 = 1.137.$$

Also

$$\left. \frac{p_3}{p_2} \right|_{\text{limit}} = 1 + \frac{1}{2} C_{ps} \gamma M_{2abs}^2 = 1 + \frac{1}{2} \times 0.6 \times 1.361 \times 0.5378^2 = 1.118,$$

and so

$$\left. \frac{p_3}{p_1} \right|_{\text{limit}} = \left. \frac{p_2}{p_1} \right|_{\text{limit}} \times \left. \frac{p_3}{p_2} \right|_{\text{limit}} = 1.137 \times 1.118 = 1.271.$$

The true pressure ratio from Example 6.1 is

$$\frac{p_3}{p_1} = \frac{321.3}{272} = 1.181.$$

Thus, the stage is not running at the maximum limit. It likely is running at the limit with a reasonable surge margin for the particular geometry determined from tests, however.

For comparison one can consider the effect if the inlet relative Mach numbers were increased to 0.8. Repeating the preceding calculations, one finds that

$$\left. \frac{p_3}{p_1} \right|_{\text{limit}} = 1.591.$$

Thus, the limit is much higher for the higher Mach numbers. However, other losses that accompany higher Mach numbers in a design must be considered.

Therefore, as shown in the previous example, increasing the inlet Mach numbers to the transonic regime greatly increases the potential pressure ratio. However, increasing the Mach number into the transonic regime also decreases the efficiency of the stage. Typically, when a stage is operating transonically, several localized supersonic regions occur. These regions are accompanied by shocks, which decrease the total pressure and thus reduce the efficiency. Also, shocks can lead to separation. Therefore, a trade-off is realized. If the Mach number is high, a large pressure ratio can be attained; however, usually the efficiency is low. As a result, although a few modern compressors operate near the transonic regime, most operate with inlet Mach numbers of approximately 0.6 to 0.9. Also, most compressors do not operate with the optimum value of C_p . One must remember that separation occurs at a pressure coefficient of 0.6 for only very well controlled conditions. When time-varying or periodic inlet conditions (especially velocities and velocity directions) are present at a compressor stage as the result of the blade jet and wakes of the previous stage, the critical pressure coefficient is reduced considerably from 0.6 because the incidence angle will be periodic as well.

6.7. Variable Stators

6.7.1. Theoretical Reasons

Currently, most modern jet engines and gas turbines have at least some stages with variable stators. This means that the stator vanes are turned or rotated about the blade radial axis as determined by the operating conditions. Basically, the idea is to change the vane angles so that the leading blade angles match the flow angles, thus providing a flow with minimal incidence to both the rotor blades and stator vanes. This is done to improve off-design performance and stall control. Stator vanes are chosen because they are not moving and can be rotated relatively easily. Rotating the rotor blades on the shaft would be a difficult task to accomplish mechanically. The concept is best demonstrated with an example.

Example 6.4: The same stage geometry as in Example 6.1 is to be studied for an operating flow rate of 50 percent of the design condition (140 lbm/s). One can assume that all conditions are the same for the purpose of demonstration and that, in the previous example, the blade angles exactly matched the flow angles and that all stages have similar geometries. Through what angle will the stator have to be turned so that the blades best match the flow? As will be seen, the incidence angle

cannot be forced to zero for both the rotor and stator, and so a trade-off will be necessary as determined through a design process.

SOLUTION:

Once again, velocity polygons will be necessary for the solutions, and one can refer to Figure 6.16, which is again to scale. First, recall that, at design, the flow angle is,

$$\beta_1 = -46.38^\circ;$$

thus, the blade angle is $\beta'_1 = -46.38^\circ$.

Now, if $\alpha_1 = 15^\circ$, one can draw a new velocity polygon (Fig. 6.16.a) and find that the new flow angle is

$$\beta_1 = -67.09^\circ.$$

Thus, the rotor blade inlet incidence angle (ι_{β_1}) is shown in Figure 6.16.b and is

$$\iota_{\beta_1} = \beta_1 - \beta'_1 = -67.09^\circ - (-46.38^\circ) = -20.71^\circ.$$

This angle is very large and would lead to a premature flow separation from the rotor blade suction surface and result in very poor performance (pressure rise and efficiency). Next, one can consider changing the upstream stator exit angle so that the flow angle matches the blade angle. For this case (Fig. 6.16.c), one has

$$\beta_1 = -46.38^\circ,$$

but now, working backward on the velocity polygon, one finds the flow angle is

$$\alpha_1 = 57.76^\circ \text{ (as against } 15^\circ \text{ previously).}$$

Thus, if one were to rotate the previous stator by $57.76^\circ - 15^\circ = 42.76^\circ$, the rotor blade inlet would be matched if all conditions remained constant and the stator vane exit flow angle matched the stator vane exit angle. Now the rotor blade exit and stator vane inlet angles (Fig. 6.16.d) should be considered.

As for the design case, $\beta_2 = -21.38^\circ$, which now leads to $\alpha_2 = 65.97^\circ$.

Thus, the downstream stator vane inlet incidence angle without stator turning is shown in Figure 6.16.e and is

$$\iota_{\alpha_2} = \alpha_2 - \alpha'_2 = 65.97^\circ - 42.79^\circ = 23.18^\circ.$$

Once again, the incidence angle is large and would lead to reduced performance. If one were to rotate the downstream stator by 23.18° , the flow angle would match the blade angle ($\alpha_2 = \alpha'_2$). Since the stage inlet and stage exit design absolute flow angles are the same, it can be assumed that the upstream and downstream stators are approximately the same designs. Therefore, the current analysis indicates that the upstream stator should be rotated by 42.76° so that the rotor blade inlet angle is matched; however, the analysis also indicates that the downstream stator should be rotated by 23.18° so that the stator vane inlet angle is matched. Therefore, if the downstream stator is rotated by 23.18° , the next downstream rotor blade will be mismatched because, to match this rotor blade, the stator will have to be rotated by approximately 42.76° . Thus, it will unfortunately be impossible to match both the rotor and stator inlet angles by simply rotating the stator vanes. At this point some engineering judgment must be exercised to decide if the off-design condition with fixed stators can at least be improved upon. One can consider rotating the stators by an average of the two specified rotations; that is, $(23.18^\circ + 42.76^\circ)/2 = 32.97^\circ$.

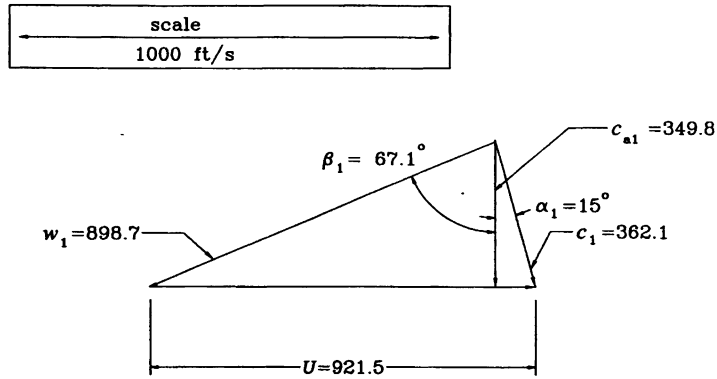


Figure 6.16a Rotor inlet polygon – No stator turning.

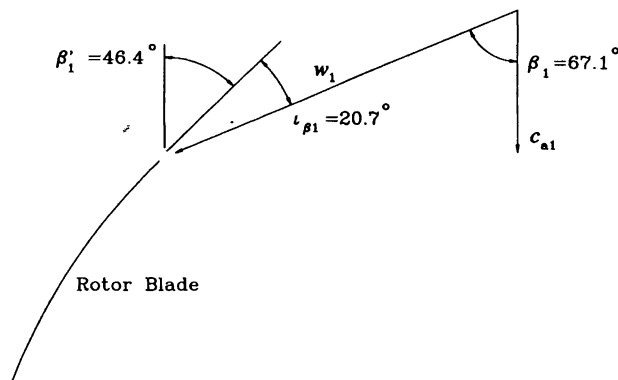


Figure 6.16b Rotor inlet incidence – No stator turning.

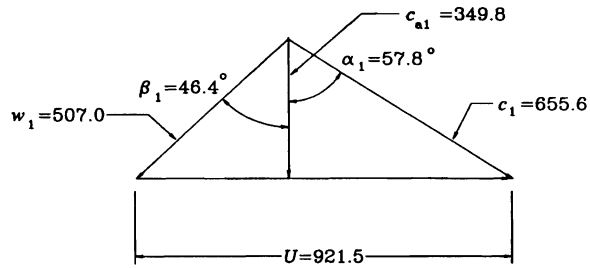


Figure 6.16c Rotor inlet polygon – Stator turned by 42.76° .

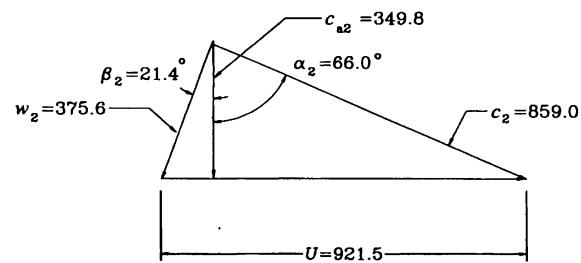


Figure 6.16d Rotor exit or stator inlet polygon – No stator turning.

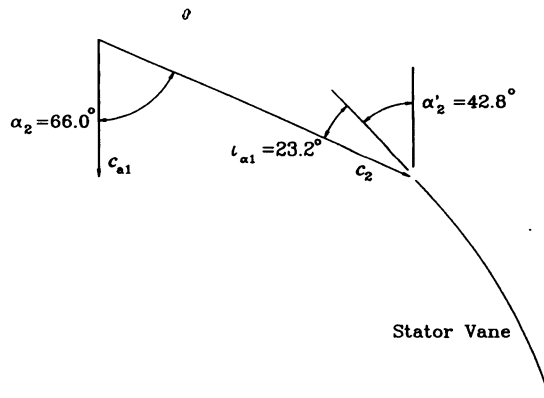


Figure 6.16e Stator inlet incidence – No stator turning.

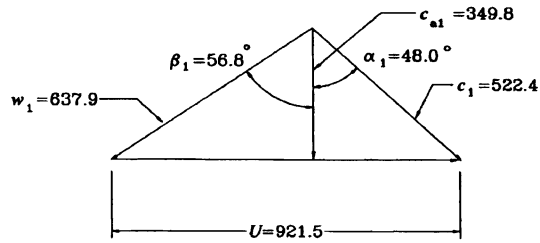


Figure 6.16f Rotor inlet polygon – Stator turned by 32.97°.

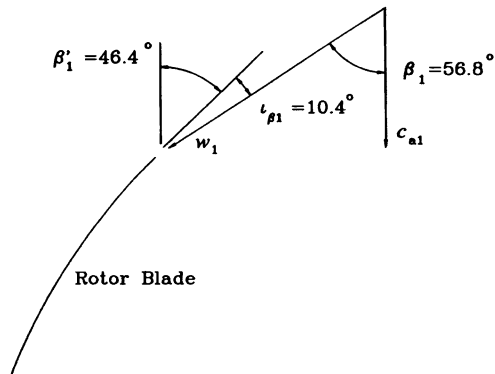


Figure 6.16g Rotor inlet incidence – Stator turned by 32.97°.

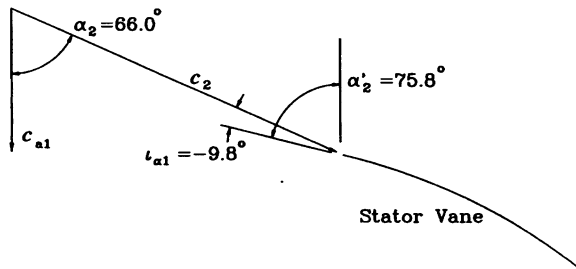


Figure 6.16h Stator inlet incidence – Stator turned by 32.97°.

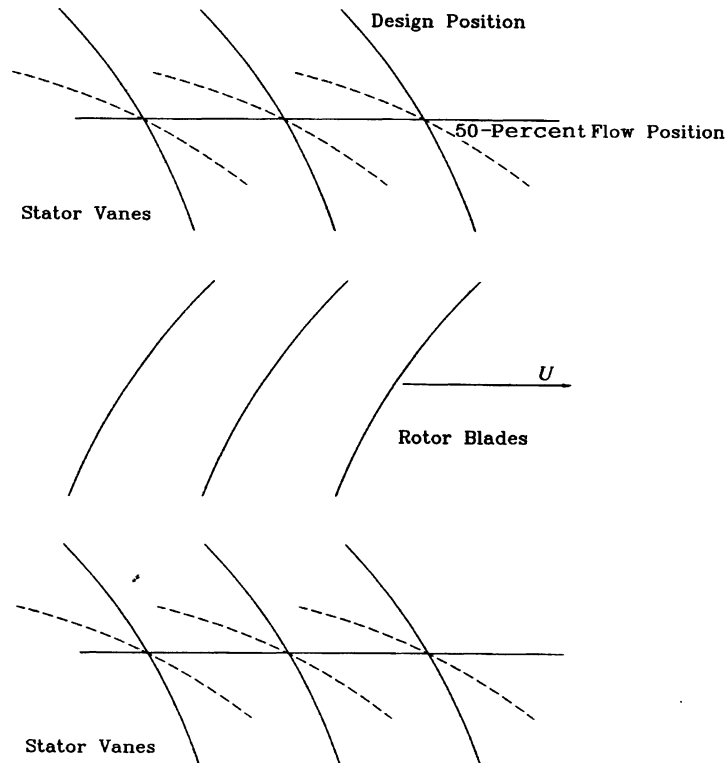


Figure 6.16i Vane positions for both 100- and 50-percent flow rates.

In Figure 6.16.f, one can see that now

$$\alpha_1 = 15^\circ + 32.97^\circ = 47.97^\circ,$$

and thus the flow angle is $\beta_1 = -56.75^\circ$;
however the blade angle is $\beta'_1 = -46.38^\circ$.

The inlet incidence angle is thus

$$\iota_{\beta_1} = -56.75^\circ - (-46.38^\circ) = -10.37^\circ,$$

as shown in Figure 6.16.g.

This is better than the incidence angle without stator turning that was found above (-20.71°). Consequently, the new inlet stator vane angle is $\alpha'_2 = 42.79^\circ + 32.97^\circ = 75.76^\circ$.

If the exit absolute angle from the rotor remains the same ($\alpha_2 = 65.97^\circ$), the incidence angle of the stator inlet is $\iota_{\alpha_2} = 65.97^\circ - 75.76^\circ = -9.79^\circ$, as shown in Figure 6.16.h. This is also better than the incidence angle without stator turning (23.18°) that was found earlier in this section.

Thus, as a result of the stator turning, the incidence angles to both the rotor and stator inlets have been reduced by more than a factor of 2. In Figure 6.16.i, the resulting schematic of the stage, including the previous stator, is shown indicating the variable stator locations.

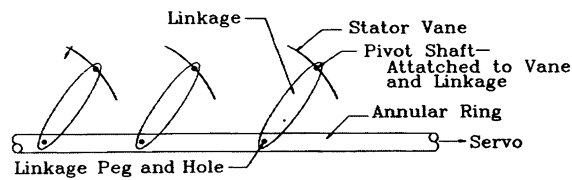


Figure 6.17a Linkage system.

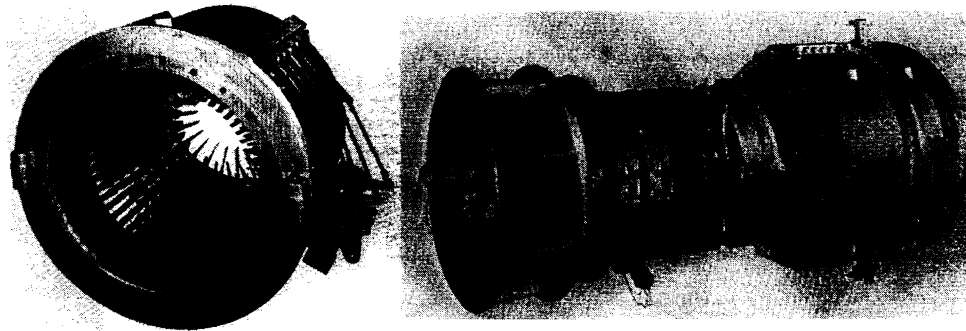


Figure 6.17b Front and side views of Ruston Tornado gas turbine showing servos (Photos courtesy of Alstom).

6.7.2. Turning Mechanism

Turning of the stator vanes is essentially accomplished through a mechanical linkage. A schematic of the mechanism is shown in Figure 6.17.a, and photographs of an application are shown in Figure 6.17.b for a Ruston power-generation gas turbine. Basically, each vane is rigidly attached to a linkage and pivot but is free to pivot around a point. The linkages of a given row of vanes are attached to an annular ring by pegs and holes. Thus, as the ring rotates, the vanes of the row are turned by equal amounts. The rings of the different stator rows are attached to a servo system, or, for some cases, a separate servo system is used for each row. Thus, as the servo is activated as shown, all of the vanes of all of the variable stages are rotated. By making the linkage lengths different for the different stator rows or by having a separate servo system for each ring, the stators of the different rows can be rotated by different amounts. Thus, each stator row can be rotated by a different angle as determined by the particular design and conditions.

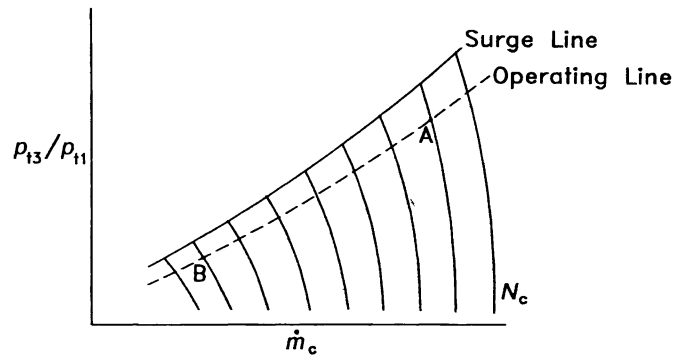
6.8. Twin Spools

6.8.1. Theoretical Reasons

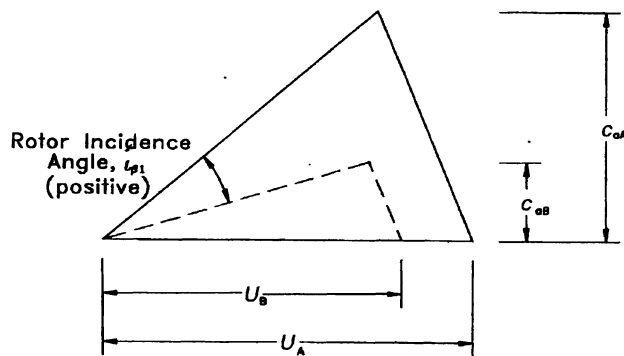
All turbfans and most modern turbojets operate with at least two shafts. Such a design has previously been defined as a twin-spool engine. The low-pressure section runs at a markedly lower rotational speed than does the high-pressure section. The purpose of this section is to demonstrate that two or more shafts are used in modern engines for two basic reasons: off-design operation and power distribution.

a. Off-Design Operation

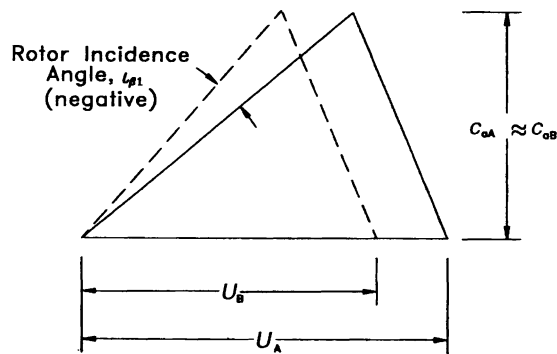
Like variable stators, one basic purpose of twin spools is to improve off-design performance. If an engine were to operate at one flow rate, one speed, and so on, it would



(a) Performance Map



(b) First Stage Velocity Polygons



(c) Last Stage Velocity Polygons

Figure 6.18 Velocity polygons for off-design operation.

be possible to design all of the blade angles so that the flow matched every stage without any incidence. However, engines must be able to operate over a range of flow rates and speeds efficiently (takeoff, cruise, dog fight, landing, etc.). Thus, the incidence angles on the different stages will change with operating conditions.

Consider a typical map for a single-spool engine, as shown in Figure 6.18.a. In this figure, the design point is designated as point A. If the speed of the engine were reduced,

its operation would be at some point B. Typically, the air mass flow rate experimentally decreases faster than the rotational speed of the engine.

Consider now the two rotor inlet velocity polygons for the first stage of the engine, as shown in Figure 6.18.b. First, one should examine the design polygon (solid line). Next, as the rotational speed is decreased, so is the mass flow rate and thus so is the inlet axial velocity component (c_a). The absolute flow angle is the same for both cases. Because c_a is reduced faster than U , the polygons are not similar. Thus, a positive incidence angle arises for the rotor inlet. Thus, for this flow rate it would be desirable to reduce U (and thus N) to force the incidence to zero for an early stage.

Next, the two velocity polygons for one of the last stages as shown in Figure 6.18.c (solid line is the design case) should be examined. For the latter stages, the pressure is not as great for the off-design condition as for the design case. Thus, the density is also lower for the off-design condition. As a result, although the mass flow rate may be significantly lower, the axial component of velocity remains approximately constant (in fact it can increase slightly). Again, the absolute flow angle is the same for both cases. Now the velocity polygons indicate that a negative incidence angle results for the rotor inlet. Thus, to force this incidence angle to zero, it would be desirable to increase the rotational speed for the latter stage – this is opposite to the effect from the early stage.

Therefore, to operate at off-design conditions, one must be able to change the rotational speed of the compressor with opposite trends from the front to the rear. Ideally, one would like to operate each stage with a different rotational speed because, for this situation, the incidence angle for each stage would be reduced to zero. However, the mechanical complexities would outweigh the aerodynamic gains. Thus, as a trade-off for modern engines, two shafts are typically used. Incidence angles are still realized by some stages at off-design conditions; however, they are much smaller than would be seen with a single shaft.

b. Power

Power considerations constitute a second reason for using twin shafts. That is, if one recalls Eq., I.2.24,

$$\dot{W}_{sh} = \frac{\dot{m} c_p T_1}{\eta_{12}} \left[\left[\frac{p_{t2}}{p_{t1}} \right]^{\frac{\gamma-1}{\gamma}} - 1 \right]. \quad 6.8.1$$

Inasmuch as the total pressure ratios are approximately the same for all stages of a compressor, the required power to be delivered to the last or high-pressure stages must be higher because the total temperature is higher for these stages. Next, recalling Eq. 6.4.1, one obtains

$$\dot{W}_{sh} = \dot{m} [U_2 c_{u2} - U_1 c_{u1}]. \quad 6.8.2$$

Now given that $c_{u2} - c_{u1}$ is limited by the turning angle of the rotor blades and that all stages have approximately the same turning angles, the only practical means to increase the input power is to increase the rotational speed U . Thus, once again, the high-pressure sections must rotate at a higher speed than the low-pressure stages.

6.8.2. Mechanical Implementation

In Figure 6.5, the geometry for a twin-spool compressor is shown. The high-pressure shaft is hollow. A set of antifriction or rolling element bearings separates the high- and low-speed shafts. The gain in aerodynamic performance is not without difficulties, however. For example, with the addition of more bearings, the mechanical or shaft efficiency

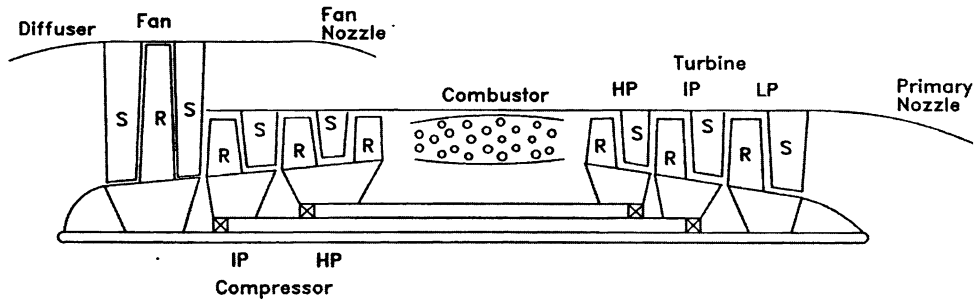


Figure 6.19 Three-spool turbofan.

is reduced. Also, because the high-speed shaft is hollow, it is more flexible. Thus, the shaft may demonstrate several resonances or critical speeds in the operating range. Care must be taken in the design so that the resonances do not occur at design points and enough damping is in the engine so that the resonances are not excited upon engine transients.

6.8.3. Three Spools

Although most modern engines operate with two spools, a few successful engines have three shafts, as shown in Figure 6.19. In such an engine, three compressors and turbines are used (low-, intermediate-, and high-pressure). Two examples are the Rolls-Royce Trent (Fig. 1.10) and the Rolls-Royce RB 211, as shown in Figures 1.26 and 6.20. The RB 211 is used to power the Lockheed L 1011. For this engine, a single-stage fan operates at 3530 rpm, an intermediate pressure compressor operates at 5100 rpm, and the high-pressure stages run at 9390 rpm. Such an engine is aerodynamically superior to twin-spool engines but

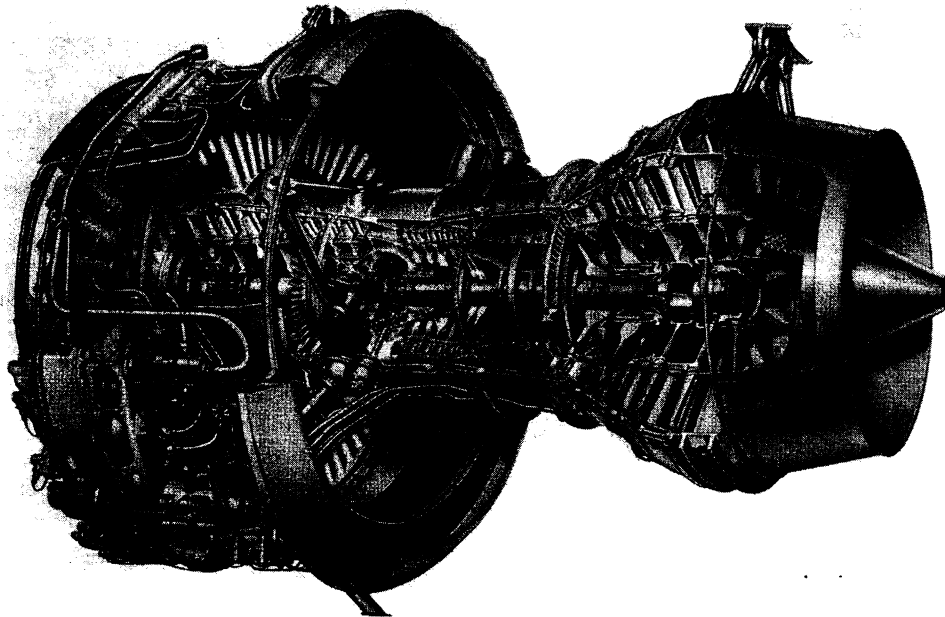


Figure 6.20 Rolls-Royce RB211 three-spool turbofan (courtesy of Rolls-Royce).

is relatively complex because of the increased number of bearings and resonances in the operating speed range. As a result, only a few such designs have been used successfully.

6.9. Radial Equilibrium

So far in this chapter, only a mean line analysis of the flow has been considered. In this section, three-dimensionality will be addressed – that is, hub-to-tip variations. A possible phenomenon occurs at the interface between each rotor and stator that is often considered in the design of stages. At these interblade stations, an equilibrium condition is often assumed for which the flow is to be only in the axial and tangential directions (no radial flow). That is, at the interfaces the sum of the surface forces on each fluid element is assumed to be equal to the centrifugal force. Between the interfaces, such conditions are not imposed, and thus radial flow does exist within the blade rows. It is this so-called radial equilibrium condition that allows an analysis of the three-dimensionality of the flow.

6.9.1. Differential Analysis

First, consider Figure 6.21. Here an incremental element of a thin radial wedge is shown. The wedge has an inner radius of r and an outer radius of $r + dr$. The wedge subtends an angle of $d\theta$. The pressures on the inner and outer surfaces are p and $p + dp$, respectively. On the side surfaces, the pressures are $p + dp/2$. For radial equilibrium the sum of the forces must equal zero, or the sum of all the pressure forces must equal the centrifugal force. All of the tangential forces resulting from the pressures cancel. One therefore only has to be concerned with the radial forces. Thus,

$$(p + dp)(r + dr) d\theta - prd\theta - 2 \left(p + \frac{dp}{2} \right) dr \frac{d\theta}{2} = \frac{dm}{2} c_u^2. \quad 6.9.1$$

Now the mass of the wedge is

$$dm = \rho r d\theta dr. \quad 6.9.2$$

Thus, using Eqs. 6.9.13 and 6.9.14 and neglecting all of the higher-order terms, one obtains

$$\frac{dp}{dr} = \frac{\rho}{r} c_u^2. \quad 6.9.3$$

This is the requirement for radial equilibrium. The radial pressure gradient is shown to be a function of both tangential velocity and radius. Several different velocity profiles can be

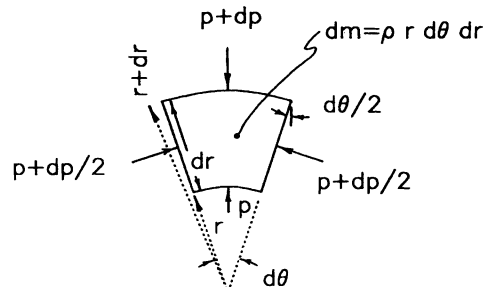


Figure 6.21 Force balance on incremental radial fluid wedge.

fitted to this condition, and the implications can be studied. Two such considerations are presented in the next two sections.

6.9.2. Free Vortex

One goal of a design may be to keep the total pressure constant with radius:

$$\frac{\partial p_t}{\partial r} = 0. \quad 6.9.4$$

From the two-dimensional analysis already presented, recall that

$$\dot{m}[U_2 c_{u2} - U_1 c_{u1}] = \dot{m} [h_{t2} - h_{t1}], \quad 6.9.5$$

and so, if R_2 is equal to R_1 ,

$$\Delta h_t = r \omega \Delta c_u. \quad 6.9.6$$

Thus, a constant flux of power to the fluid in the radial direction is necessary so that Eq. 6.9.4 is maintained:

$$\frac{\partial \Delta h_t}{\partial r} = \frac{\partial (r \omega \Delta c_u)}{\partial r} = 0; \quad 6.9.7$$

thus, $r \Delta c_u$ is constant with radius. One method to ensure this condition is to keep $r \Delta c_u$ constant with radius. This consideration is the so-called free vortex. For this condition,

$$c_u r = \kappa \quad 6.9.8$$

or

$$c_u = \frac{\kappa}{r}, \quad 6.9.9$$

where κ is a constant.

If the Bernoulli equation is used (incompressible flow) to identify the total pressure,

$$p_t = p + \frac{1}{2} \rho c^2, \quad 6.9.10$$

along with Eq. 6.9.4,

$$\frac{\partial p}{\partial r} + \rho \frac{1}{2} \frac{\partial c^2}{\partial r} = \frac{\partial p_t}{\partial r} = 0, \quad 6.9.11$$

and along with Eq. 6.9.3,

$$\frac{\rho}{r} c_u^2 + \frac{1}{2} \rho \frac{\partial c^2}{\partial r} = \frac{\partial p_t}{\partial r} = 0. \quad 6.9.12$$

From the velocity polygon, however,

$$c^2 = c_u^2 + c_a^2; \quad 6.9.13$$

thus,

$$\frac{\rho}{r} c_u^2 + \rho \left[c_u \frac{\partial c_u}{\partial r} + c_a \frac{\partial c_a}{\partial r} \right] = 0, \quad 6.9.14$$

and, for c_u , from the free vortex condition, Eq. 6.9.9,

$$\rho c_a \frac{\partial c_a}{\partial r} = 0. \quad 6.9.15$$

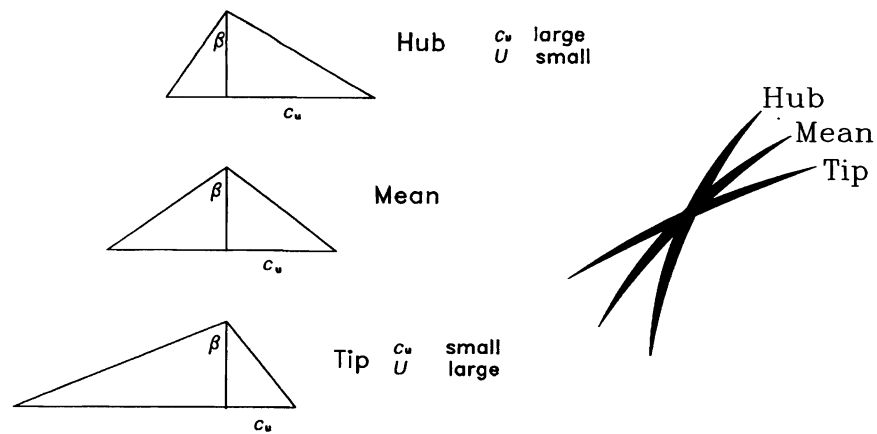


Figure 6.22 Velocity polygons and blade shapes for free vortex specification.

Consequently, either c_a is zero (no mass flow, which is not a very interesting or practical case) or the axial component of velocity is not a function of radius; hence, c_a is exactly constant with radius.

Finally, some of the implications of this condition need to be addressed. If the radius is nearly constant from blade hub to tip, the tangential component of velocity will not change significantly. However, if the radius change is large for (e.g., a fan blade), significant variations in c_u can occur. Furthermore the axial component has been shown to be constant with radius. Thus, if c_u varies significantly, so will blade angles. As an example, Figure 6.22, which represents three velocity polygons for a rotor blade, is presented. At the blade hub, the blade speed U is relatively small, but c_u is relatively large. At the tip, the blade speed is relatively large, but now c_u is relatively small. From the diagrams one can easily see that the blade angle β changes markedly from hub to tip. Thus, radial equilibrium results in highly twisted blades as well as large changes in the blade curvature (most curved at the hub and flatter at the tip). Furthermore, the condition can lead to large (and undesirable) variations in the percent reaction from hub to tip.

6.9.3. Constant Reaction

As implied in the previous section, another consideration may be to force the reaction to be constant from hub to tip (or approximately so). With this idea in mind, one can propose radial variations for the tangential velocity such as

$$c_{u1} = ar - b/r \quad 6.9.16$$

for the velocity after the stator and

$$c_{u2} = ar + b/r \quad 6.9.17$$

for the velocity after the rotor where a and b are constants. Next, it can be demonstrated that, for incompressible flow without losses, if the axial velocity is approximately constant across the rotor ($c_{a1} \cong c_{a2}$),

$$\%R \cong 1 - \frac{a}{\omega} \quad 6.9.18$$

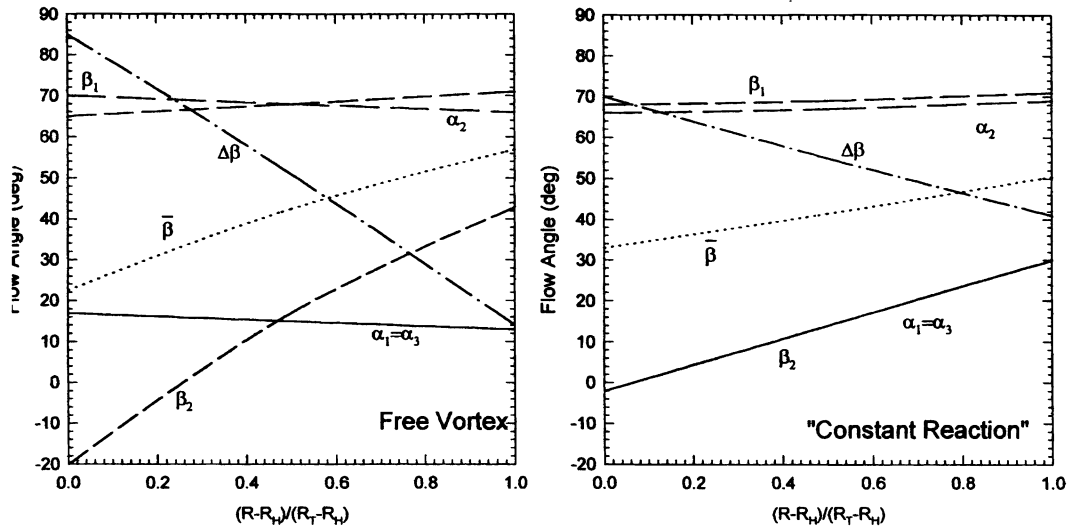


Figure 6.23 Typical flow angle distributions for free vortex and "constant reaction" specifications.

That is, the percent reaction is not a (strong) function of radius. One can also show that the input power per unit mass flow across the rotor blade is

$$\frac{\mathcal{P}}{\dot{m}} = 2b\omega. \quad 6.9.19$$

Note that this is not approximate but identically true. An implication of this is that the rise in total pressure is constant with radius (because the net specific power into the fluid is constant with radius), as shown in Eq. 6.9.4. Thus, using the definition of total pressure,

$$p_t = p + \frac{1}{2}\rho [c_u^2 + c_a^2], \quad 6.9.20$$

one can show that, behind the rotor

$$c_{a2}^2 = \text{constant} - 2a^2 \left[r^2 + 2\frac{b}{a} \ln(r) \right], \quad 6.9.21$$

and behind the stator

$$c_{a1}^2 = \text{constant} - 2a^2 \left[r^2 - 2\frac{b}{a} \ln(r) \right]. \quad 6.9.22$$

It can therefore be seen that, at any value of r , c_{a1} does not exactly equal c_{a2} , as assumed earlier in this section. As a result, the percent reaction is not exactly constant with radius. However, for many cases of interest, the approximation is close and allows for the a priori specification of a velocity profile.

Once again, if the implications of this condition are examined, one finds that the blades are moderately twisted. The geometries are not as awkward as for a free-vortex distribution but yet are not as simple as one would have hoped. Two typical sets of angle profiles are presented in Figure 6.23 for designs based on the free vortex and constant reaction specifications; for these geometries the tip-to-hub diameter ratio is 1.28. In these figures, the variation of different angles from hub, $(R - R_H)/(R_T - R_H) = 0$, to tip, $(R - R_H)/(R_T - R_H) = 1$, are presented. As can be seen, the rotor blade angles change significantly from hub to tip for the

free vortex case; in fact β_2 changes sign. Also note that much more rotor flow turning ($\Delta\beta$) is near the hub than near the tip. The average rotor flow angle ($\bar{\beta}$) changes markedly from hub to tip, indicating severe blade twist. The stator angles are somewhat better behaved, but the stator turning ($\Delta\alpha$ – not shown) is much different than the rotor turning. Because of the different rotor and stator flow turning angles, the percent reaction changes from 36 to 61 percent from hub to tip for the free vortex. For the constant reaction case, the rotor blade angles do not change as drastically from blade hub to tip (i.e., the blades are not as twisted), but the stator vanes change more. Significant changes in rotor flow turning are still present from hub to tip, but there is less variation than in the free vortex case. As one might conclude from these two cases, in reality no one such simple postulation is used in blade designs. By examining Figures 6.3.a, 6.3.b, and 6.22, one can easily see the relative changes in blade curvature and twist. The two specifications in this section are intended as starting profiles that may be attempted before refinements are made to an iterative design.

6.10. Streamline Analysis Method

Up to this point in the chapter, the analyses of flows in the compressor have been assumed to be two-dimensional and any radial distributions or velocity components have been assumed to be negligible in calculations, although Section 6.9.3 indicates that three-dimensionality is indeed present. In Section 6.9, radial equilibrium was covered and the implications for three-dimensionality were discussed. As implied, because the ratios of blade height to hub diameter for many modern machines are not small and centrifugal forces are large, three-dimensional flows result. As is demonstrated in this section, significant radial variations in parameter profiles will result when the tip radius is approximately 1.1 times the hub radius or greater. The variations become more pronounced as the rotational speed increases, and the absolute flow angles increase as implied by Eq. 6.9.1. For example, in Figure 6.3.a significant blade twist is evident; that is, the average blade angle varies from hub to tip.

Several numerical “throughflow” techniques have been developed that can be used to predict the flow’s three-dimensionality. Furthermore, CFD is certainly an important tool used in the design of compressors and fans, as discussed early in this chapter and considered by Rhie et al. (1998), LeJambre et al. (1998), Adamczyk (2000), and Elmendorf et al. (1998). All of these approaches are for compressible flow and are robust methods intended for sophisticated predictions. Unfortunately, these methods require significant background and have a learning curve. They are thus not appropriate to learning the fundamentals of three-dimensional flows in turbomachines.

This section presents a streamline analysis method. Basically, different streamline paths are analyzed by a control volume approach through a compressor passage. The method is for flow in axial flow fans or compressors and is primarily intended for educational purposes; however, it can also be used for preliminary designs and applied in the inverse mode for the analysis of experimental pressure data. Streamline analysis can be used to predict three-dimensional trends resulting from blade curvatures and twists and centrifugal forces, thus contributing valuable insight into the flow’s three-dimensionality. This method provides a tool through which a “feel” for the magnitudes of the resulting three-dimensionality of the flow fields can easily be developed as blade configurations are varied. The technique converges relatively quickly and can be written with commercial math solvers. The software, “SLA” was developed to accommodate a few select boundary condition types.

The flow passage is divided into a finite number of annuli, and the equations are solved for each blade row independently. As is demonstrated, different conditions can be considered

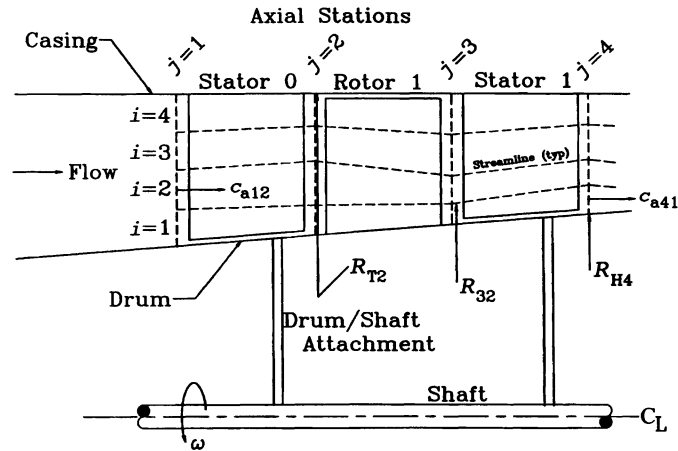


Figure 6.24 Axial flow turbomachine for streamline analysis.

with the method. For example, free vortex or irrotational flow can be assumed throughout, and the flow angles are then calculated. As discussed in the previous section, this condition does not result in radial flow and therefore does not require an iterative solution. Also, the flow angles can be specified. This case has an iterative solution whereby radial migration of the flow is predicted. Radial efficiency distributions for each blade row can also be specified for the second condition. Other conditions are discussed.

Steady incompressible adiabatic flow is assumed to simplify the analysis and to accelerate the numerical convergence of the solution. Moderate accuracy can be obtained using an average density – particularly for one- or two-stage analyses. Moreover, the incompressible assumption does not mask the fundamental three-dimensional trends predicted from the method, which can also be extended to include compressibility effects. Flack (1987) gives more details and other applications.

6.10.1. Flow Geometry

In Figure 6.24 a stage in an axial flow turbomachine is shown with varying cross-sectional area, although more stages can be stacked behind. The analysis begins at the inlet to the previous stator (which can be an inlet guide vane). Each stage is divided into N annuli. In Figure 6.24, the annuli number (i) and the axial position number (j) are defined. For the sake of simplicity, only four annuli are shown. Each annulus represents a bundle of streamlines, and a different control volume is applied to each annulus. In general, the annuli will not be constant in area between axial stations. This is due to the resulting radial flow and changing cross section of the stage. For the control volume analysis, the flow is assumed to be uniform, both radially and circumferentially, within each annulus, and the velocities are evaluated at the radial center of the annulus. Thus, blade-to-blade variations are not predicted as is the case in a CFD analysis. The exiting conditions for Stator 0 are used as the inlet conditions for Rotor 1, and so on. The radii of all of the axial and radial stations can in general be different. The radius R_{32} (typical) represents the outer radius of the first streamline bundle and the inner radius of the second streamline bundle at the third axial station. Also, the axial component of velocity at axial station 4 and annulus 1 is shown, c_{a41} .

6.10.2. Working Equations

The equations for each annulus are described in this section. The equations are *independently derived* for each annulus by a control volume analysis similar to the mean line flow analysis for incompressible flow described in Section 6.4. However, equations for all of the annuli must be *solved simultaneously*. It is important to note that the control volumes can be drawn in general. However, the exact positions and sizes (radii) of the control volumes are actually found as a part of the solution.

a. Geometric Equations

The velocity of the blades at the radial center of the element is U_{ji} . Shown in Figure 6.7 are the absolute flow velocity (c) and the flow velocity relative to the blades (w). Also shown is the normal component c_a . Velocity polygons, as in Figure 6.7, are constructed for each annulus and axial position. As in previous sections, α and β are the absolute and relative flow angles, respectively. Important relationships that result from the velocity polygons for each annulus are as follows:

$$c_{a_{ji}} = c_{ji} \cos \alpha_{ji} \quad 6.10.1$$

$$c_{u_{ji}} = c_{ji} \sin \alpha_{ji} \quad 6.10.2$$

$$\tan \beta_{ji} = \frac{c_{u_{ji}} - U_{ji}}{c_{a_{ji}}}, \quad 6.10.3$$

where

$$U_{ji} = \bar{R}_{ji} \omega \quad 6.10.4$$

and

$$\bar{R}_{ji} = \frac{1}{2}(R_{ji} + R_{j+1}). \quad 6.10.5$$

The value of \bar{R}_{ji} represents the radius at the center of the i th element at the j th station.

b. Control Volume Equations

Next, the conservation of mass equation is considered. Because each control volume follows the streamlines, *no flow crosses the annuli*, which accounts for the name of the method. As a result, the only mass flux occurs at the axial planes. The volumetric flow rate given by the continuity equation (Eq. I.2.1) thus becomes

$$Q_i = c_{a_{ji}} \pi (R_{j+1}^2 - R_{ji}^2). \quad 6.10.6$$

Note that this is constant for all axial locations within the stream tube. The moment of momentum equation (Eq. I.2.2) becomes

$$T_{ji} = \rho Q_i (\bar{R}_{j+1} c_{u_{j+1}} - \bar{R}_{ji} c_{u_{ji}}), \quad 6.10.7$$

where T_{ji} is the torque on the shaft for that annulus. Thus, summing all annular torques yields the total torque. The energy equation (Eq. I.2.3) becomes

$$\dot{W}_{ji} = \frac{Q_i}{\eta_{ji}} \left[(p_{j+1} - p_{ji}) + \frac{1}{2} \rho (c_{j+1}^2 - c_{ji}^2) \right], \quad 6.10.8$$

where \dot{W}_{ji} and η_{ji} are, respectively, the shaft power and efficiency for the single annulus. Thus, summing all annular powers yields the total power. Furthermore, the torque and rotor power for each annulus are related by

$$\dot{W}_{ji} = T_{ji}\omega, \quad 6.10.9$$

where ω is the rotational speed of the rotor. When stator blades are analyzed for the power, ω is of course zero. The last consideration occurs at the interface between each rotor and stator. At these stations, radial equilibrium which is covered in Section 6.9 is assumed. The resulting equation is Eq. 6.9.3. Writing this equation in difference form for each station, one obtains

$$\frac{P_{j+1} - P_{ji}}{R_{j+1} - R_{ji}} = \rho \frac{\bar{c}_{u_{ji}}^2}{R_{j+1}}, \quad 6.10.10$$

where

$$\bar{c}_{u_{ji}} = \frac{1}{2} (c_{u_{j+1}} + c_{u_{ji}}). \quad 6.10.11$$

c. Closure Equations

Before one attempts a solution, counting of the variables is appropriate. For N annuli, N values of c , c_a , c_u , α , β , η , T , Q , p , p_t , \dot{W}_{sh} , U , and \bar{R} will result as will $N + 1$ values of R , $N - 1$ values of \bar{c}_u , one value of ω , and one value of ρ . On the other hand, there are N Eqs. 6.10.1 through 6.10.9 and 6.9.10, $N - 1$ Eqs. 6.10.10 and 6.10.11, two values of R (hub and tip), one value of ω , and one value of ρ . Thus, there are $15N + 2$ variables and $12N + 2$ equations. Clearly, to obtain a solution, one must specify $3N$ variables or $3N$ more equations are needed.

Three separate conditions are considered in detail in the following sections. In all cases, all flow conditions into the inlet of the previous stator are specified. The annuli locations at $j = 1$ are specified and can be specified to be equally spaced, but this is not necessary if strong velocity gradients are present. Thus, Q_i for each annulus is found because the flow into the previous stator is specified. Thus, N more variables are specified for these cases for a total of $13N + 2$ equations, leaving the need for $2N$ more specifications. Some different cases are discussed in detail in the following sections. Other cases can certainly be used to specify the fourth set of conditions.

Potential Flow or Free Vortex Flow. The flow is assumed to be irrotational as well as inviscid ($\eta_{ji} = 1.0$). Next, from Eq. 6.9.9,

$$c_{u_{ji}} \bar{R}_{ji} = c_{u_{j+1}} \bar{R}_{j+1}, \quad 6.10.12$$

which adds $N - 1$ equations. Also, as shown in Section 6.9.2, this condition, along with radial equilibrium, results in a constant axial velocity at each axial plane and no radial flow between the axial stations. That is, $c_{a_{ji}}$ is not a function of R (or i). Lastly, for this condition the absolute flow angle at some radius (usually at the center of each axial plane) is usually specified, which adds the last needed variable. For example, if $N = 7$, values of α_{i4} are specified. As an equally valid alternative specification for this case, the relative flow angle at some radius could be specified; if $N = 7$, values of β_{j4} could be specified. This case is relatively simple and does not require an iteration technique.

Specified Flow Angle Distribution. For this case, the second set of boundary conditions is for specified flow angle variations (hub to tip). Absolute flow angles (α_{ji}) and efficiencies

(η_{ji}) are chosen to be input at all axial stations and at specified radial positions. Thus, $2N$ variables (α and η) are specified, and a solution is possible. Although flow angles and efficiencies are specified at certain radii, these do not necessarily correspond to annuli centroids and can be a curve fit to a radial distribution or table for interpolation at different radii. Alternatively, and equally valid, the relative flow angles (β_{ji}) and efficiencies (η_{ji}) could be chosen to be input at all axial stations and at specified radial positions. The solution to this case requires a 2-nested loop iterative solution.

Specified Pressure Distribution. If limited experimental data are available, radial profiles of static and total pressure (p and p_t) may be known. Thus, for this case, the second set of boundary conditions is for specified static and total pressure variations (hub to tip) and a solution is possible providing angle, efficiency, and other parameter radial distributions to complement the data. Therefore, p_{ij} and p_{tj} are input at all axial stations and at specified radial positions. Again, $2N$ variables (p and p_t) are specified and a solution is possible. As in the previous section, the radii do not necessarily correspond to annuli centroids. The solution to this case also requires a 2-nested loop iterative solution.

Other Specified Conditions. As indicated in Section 6.10.2.3, in general there are $15N + 2$ variables and $12N + 2$ equations. One can designate conditions other than specified angles or pressures that would allow a solution. Many other possibilities could be used to specify closure equations.

Solution Method. The equations discussed in Section 6.10.2 and its subsections can be solved using any of the commercial math solvers. To find a solution, one starts at $j = 2$ (if conditions at $j = 1$ are known) and analyzes each axial station separately, repeatedly marching in the axial direction.

For known flow angle and efficiency distributions, the solution requires a two-nested loop iterative solution. One approach is presented in the steps below.

- (1) A value for $c_{a_{j+1}}$ is first estimated.
- (2) The inner annulus ($i = 1$) is analyzed, and R_{j+1i+1} is found (Eq. 6.10.6).
- (3) α_{j+1i} and η_{j+1i} are found from the known radial distributions.
- (4) The values of c_{j+1i} , $c_{u_{j+1i}}$, and β_{j+1i} are found (Eqs. 6.10.1, 6.10.2, and 6.10.3).
- (5) The torque and power are found (Eqs. 6.10.7 and 6.10.9).
- (6) p_{j+1i} is found (Eq. 6.10.8).
- (7) The next annulus is analyzed. A value of $c_{a_{j+1i+1}}$ is estimated, and the same procedure as immediately above is used to find p_{j+1i+1} .
- (8) Radial equilibrium (Eq. 6.10.10) is now also used to find a second value of p_{j+1i+1} .
- (9) If the two independent values of p_{j+1i+1} are the same within a set tolerance, i is incremented and the next annulus analyzed, and so on, until the last annulus. If the two are different, a new value of $c_{a_{j+1i+1}}$ is used and the process starting at (7) is repeated.
- (10) For the last annulus, R_{j+1N} is known, and thus $c_{a_{j+1N}}$ is found (Eq. 6.10.6). The same procedure as immediately above is used to find p_{j+1N} and radial equilibrium (Eq. 6.10.10) is now used also to find a second value of p_{j+1N} .
- (11) The two values of p_{j+1N} are again compared. If these two values are different, a new $c_{a_{j+1}}$ is used, and the entire procedure, starting at (1), is repeated until convergence.

Thus, this case has two nested iteration loops. The Regula Falsi method (Appendix G) can be used to accelerate the converging iteration for both loops. As discussed at the beginning of this section, the radial size and position of the control volumes are found as a part of the solution. Also, initial estimates can have a strong influence on convergence of such schemes.

For known total and static pressures, a similar two-nested loop iterative solution is needed:

- (1) A value for $c_{a_{j+1i}}$ is first estimated.
- (2) The inner annulus ($i = 1$) is then analyzed and R_{j+1i+1} is found from Eq. 6.10.6. Next, $p_{t_{ji}}$ and $p_{s_{ji}}$ are found from the known radial distribution of pressures.
- (3) The value of $c_{j_{ji}}$ is next found (Eq. 6.9.10).
- (4) Then α_{j+1i} , $c_{u_{j+1i}}$, and β_{j+1i} are found (Eqs. 6.10.1, 6.10.2, and 6.10.3).
- (5) The torque and power are found (Eqs. 6.10.7 and 6.10.9).
- (6) The efficiency at $(j + 1, i)$ is found from Eq. 6.10.8.
- (7) The next annulus is analyzed. A value of $c_{a_{j+1i+1}}$ is estimated, and the same procedure as immediately above is used to find all parameters, including p_{j+1i+1} and η_{j+1i+1} .
- (8) Radial equilibrium (Eq. 6.10.10) is now also used to find a second value of p_{j+1i+1} .
- (9) If the two values of p_{j+1i+1} are the same within a set tolerance, the next annulus is analyzed, and so on, until the last annulus. If the two are different, a new value of $c_{a_{j+1i+1}}$ is used and the process is repeated starting at (7).
- (10) For the last annulus, R_{j+1N} is known and $c_{a_{j+1N}}$ is found from Eq. 6.10.6. Two values of p_{j+1N} are found.
- (11) The two independent values of p_{j+1N} are compared. If these two values of p_{j+1N} are different, a new $c_{a_{j+1}}$ is used and the entire procedure repeated starting at (1) until convergence.

Example 6.5: A single stage of a compressor with an IGV and free vortex or potential flow is analyzed ($\eta = 1$). The compressor geometry and operating conditions approximate those on the first low-pressure compressor stage on a small engine. The tip and hub diameters, which are axially constant, are 0.391 and 0.320 m (1.283 and 1.050 ft), respectively, and the compressor operates at 12,000 rpm. The resulting tip-to-hub diameter ratio is 1.222, which indicates that predictable radial flow and variations should exist. Air enters at 97.9 kPa (14.2 psia), the density is 1.21 kg/m^3 ($0.00235 \text{ slug/ft}^3$), and the flow rate is 11.3 kg/s (25 lbm/s). The mid-stream absolute flow angles at the exit of the IGV, rotor blades and stator blades are

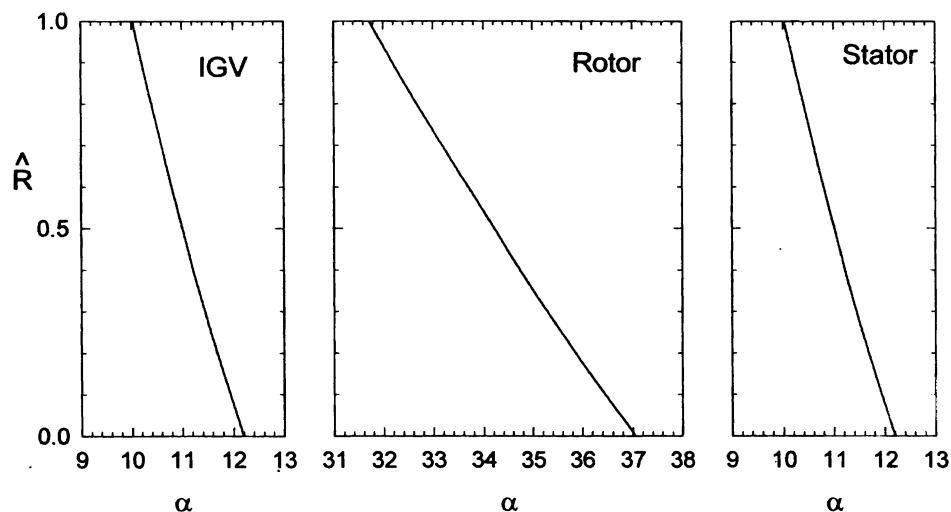


Figure 6.25 Exit absolute flow angles – Example 6.5.

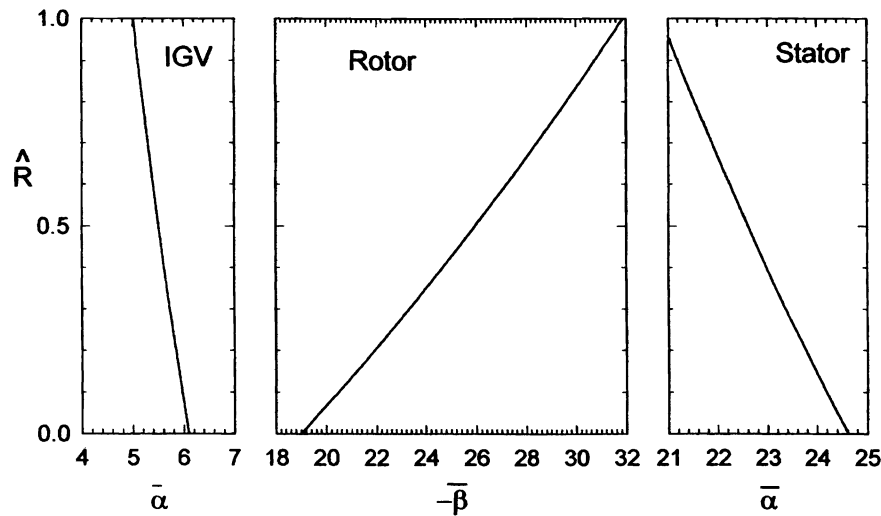


Figure 6.26 Average flow angles – Example 6.5.

11°, 34.2°, and 11°, respectively. The flow angles, blade curvatures, blade twists, percent reaction, and pressure profiles at the exit of the rotor and stator are to be found for nine annuli.

Results:

Results for this case are shown in Figures 6.25 through 6.28 in which characteristics are plotted from hub to tip (as a function of the dimensionless radial position $\hat{R} = (R - R_H) / (R_T - R_H)$). Because the flow is irrotational, the axial component of velocity is constant at all radial and axial positions and equal to 236.1 m/s (774.6 ft/s), and the streamlines are all axial and parallel.

In Figure 6.25, the absolute flow angles at the exits of the IGV, rotor, and stator are shown. As can be seen, the angles vary by approximately 2° across each passage for the IGV and stator and approximately 5° for the rotor.

The average flow angle (i.e., $\bar{\beta}_{ji} = [\beta_{ji} + \beta_{j+1i}]/2$) is shown in Figure 6.26. This angle varies by only 1° for the IGV. However, the rotor flow angle varies by approximately 13° across the passage. This indicates that the blade is moderately twisted. The stator vane is less twisted, and the average flow angle varies by approximately 4°.

The turning angles of the blades are presented in Figure 6.27 (i.e., $\Delta\beta_{ji} = \beta_{j+1i} - \beta_{ji}$). The IGV turning angle varies by approximately 2° from hub to tip. The rotor turning angle varies by 9° across the passage. This figure indicates that, at the hub, the blade is moderately curved, whereas at the tip the blade is relatively flat. Also, the turning angle for the stator vane varies by only 3°.

The performance of this geometry is shown in Figure 6.28. The static and total pressure profiles at the exits of the rotor and stator are presented along with the rotor reaction profile. The static pressure varies by 3 percent across the exit of the rotor blades. However, at the exit of the stator the pressure varies by only 0.3 percent. The exit total pressure profile is exactly constant across the passage, as it should be for free vortex flow. The rotor reaction varies from 0.43 to 0.62 from hub to tip. Thus, this design is least efficient near the hub owing to the low reaction. The total power required is 290 kW (389 hp).

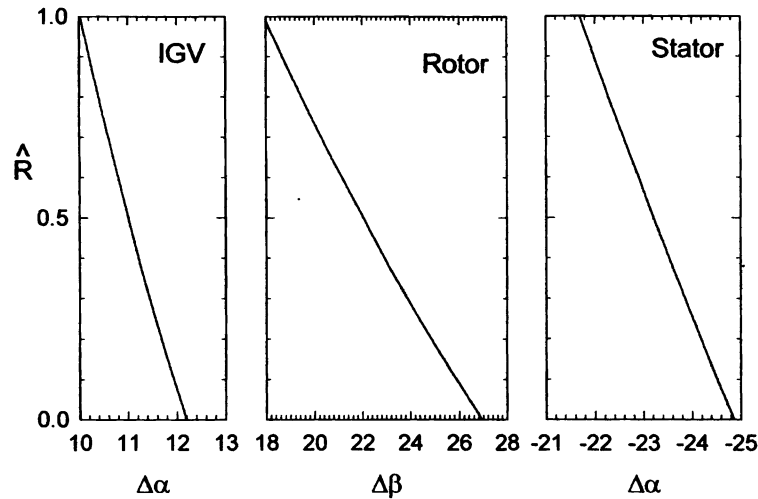


Figure 6.27 Flow turning angles – Example 6.5.

The three-dimensionality of the flow is obvious from this example. The absolute flow angles are mild functions of the radius, whereas the rotor blade angles, pressure profiles, and reaction profiles are stronger functions of the radius.

For comparison with the nine-annuli case, this geometry was also solved for one annulus and also with an isentropic, two-dimensional, mean line compressible flow analysis. For the three methods, the total power and the meanline pressures were exactly the same. The total pressure from streamline analysis at the exit of the stage was found to be within 1 percent of the value calculated using the compressible meanline flow analysis.

Example 6.5a: The next cases to be considered are also single-stage compressors with potential flow and are extensions of Example 6.5. The mean diameter is 0.356 for all four cases, and the compressor again operates at 12,000 rpm. The hub and

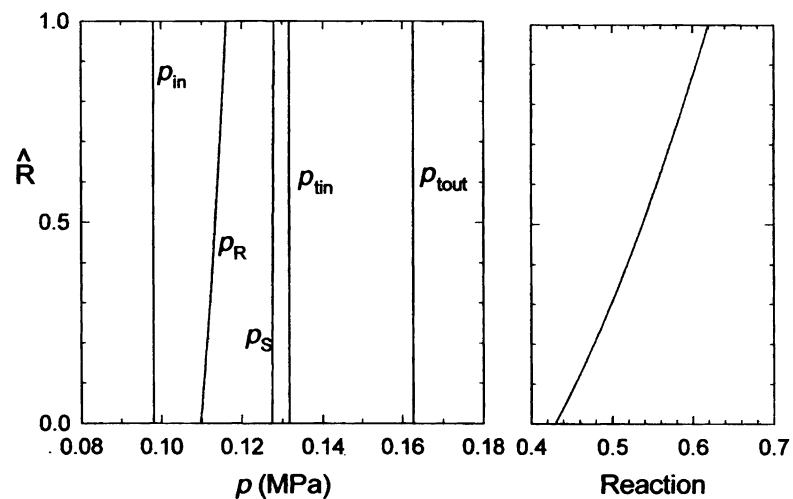


Figure 6.28 Exit pressure and rotor reaction profiles – Example 6.5.

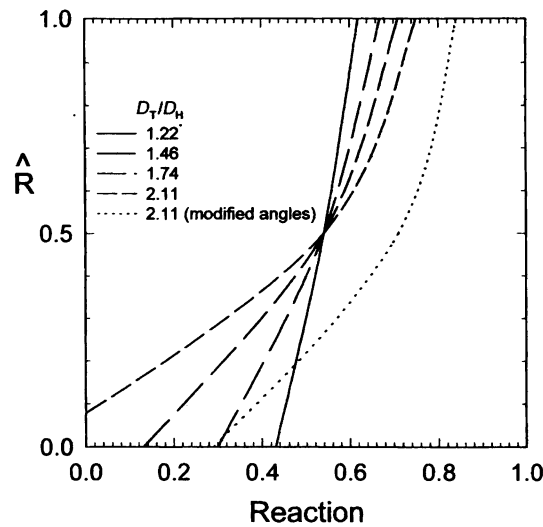


Figure 6.29 Reaction profiles for Example 6.5.a – Effect of diameter ratio.

tip diameters are parametrically varied so that the tip-to-hub diameter increases from 1.22 to 2.11. The axial velocity is the same as in Example 6.5; as a result, the mass flow rate increases as the tip-to-hub diameter increases. The average density is 1.21 kg/m^3 ($0.00235 \text{ slug/ft}^3$). An inlet guide vane is used, and the mean line flow angles at the exit of the IGW, rotor blades, and stator blades are 11° , 34.2° , and 11° , respectively. Of particular interest is the percent reaction profile.

Results:

The results are shown in Figure 6.29. As can be seen, all of the geometries operate with a mean line value of reaction of 54 percent. Near the tip, the reaction increases as the diameter ratio increases. Most importantly, near the hub, as the diameter ratio increases, the reaction rapidly decreases. In fact, for $D_T/D_H = 2.11$, the reaction is negative at the hub. This is obviously unacceptable for a compressor because it implies a pressure drop.

As a result, for cases with low or negative values of reaction, the compressor must be designed so that the mean line reaction will be large enough that such problems are not encountered at the hub. If this example is extended one step further, it can be noted that, for the highest diameter ratio case, the flow angles were adjusted so that the reaction increased but the total pressure rise remained constant. The mean line flow angles at the exit of the IGW, rotor blades, and stator blades are 2° , 27.5° , and 2° , respectively. Reactions at the mean and tip are significantly larger than 50 percent for this case, and tip reactions may approach unity for some cases. This is a significant observation – particularly for front stages of a compressor or fans, where the diameter ratio is much larger than 1.

Example 6.6: In Example 6.5, a compressor with irrotational flow was studied. The second case is the same turbomachine, but now the absolute flow angles across the exit of each blade row are specified and are constant from hub to tip. The same flow rate and speed are studied, and the flow angles are presented in Figure 6.30. Also in Figure 6.30 is the specified stage efficiency. Efficiencies of 87 percent are

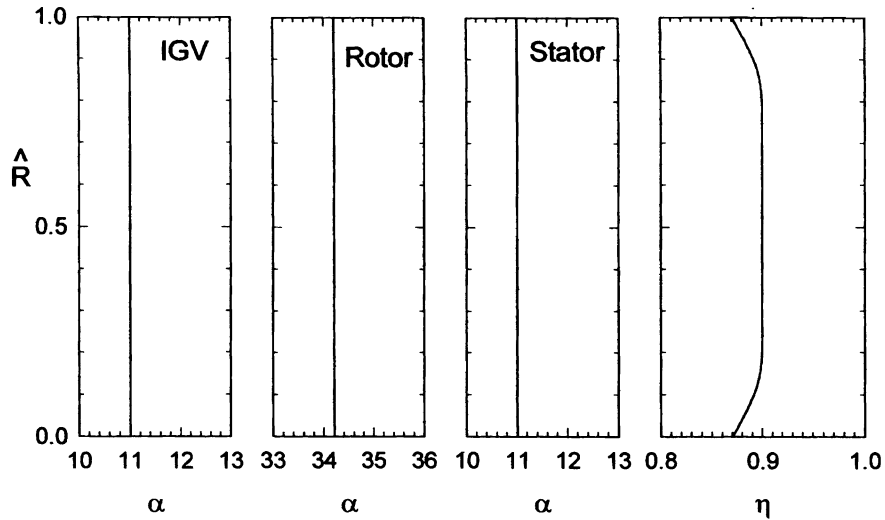


Figure 6.30 Specified exit absolute flow angles and stage efficiency – Example 6.6.

used at the hub and tip and 90 percent at the midstream. This is a limiting case to demonstrate the changes in profiles from the free vortex case.

Results:

Results are presented in Figures 6.31 through 6.34. Figure 6.31 presents nine streamlines. As can be seen in the rotor cascades, a slight, net inward radial flow results from the radial equilibrium condition. In the stator cascades, a net outward radial flow results. For the first case (Example 6.5), one should remember that no radial flow existed. Thus, the present case exemplifies the types of radial flows that can result. Note that, owing to the radial equilibrium condition, either a net inward or outward flow can be realized as determined by the specified flow angles.

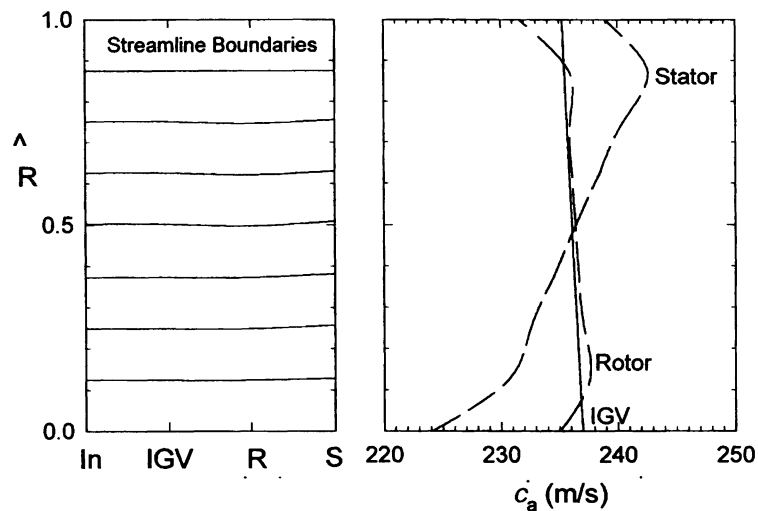


Figure 6.31 Streamlines through stage and exit velocity profiles – Example 6.6.

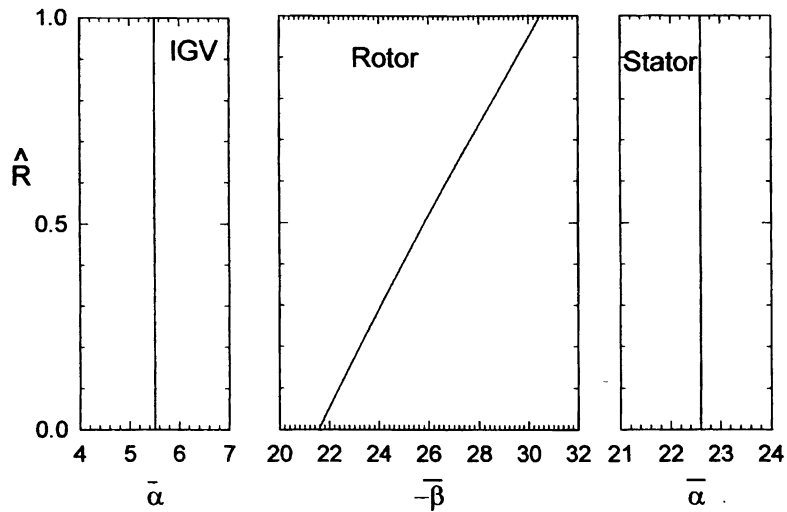


Figure 6.32 Average flow angles – Example 6.6.

Axial velocity profiles are also presented in Figure 6.31. The profile for the IGV exit varies by 0.4 percent from the mean, whereas the rotor exit profile varies by 2 percent. The stator exit profile varies by 5 percent from the mean. As can be seen for the stator, the highest velocities are near the tip, which also indicates a net flow outward.

Average and turning flow angles are presented in Figures 6.32 and 6.33. The blade shapes are different from those in the preceding case, and the magnitude of the twists for this case is slightly smaller. For the IGV, rotor, and stator blades, twists (radial change in $\bar{\alpha}$ or $\bar{\beta}$) of 0° , 9° , and 0° from hub to tip are present. Similarly, the amount of change in the blade curvatures from hub to tip is slightly

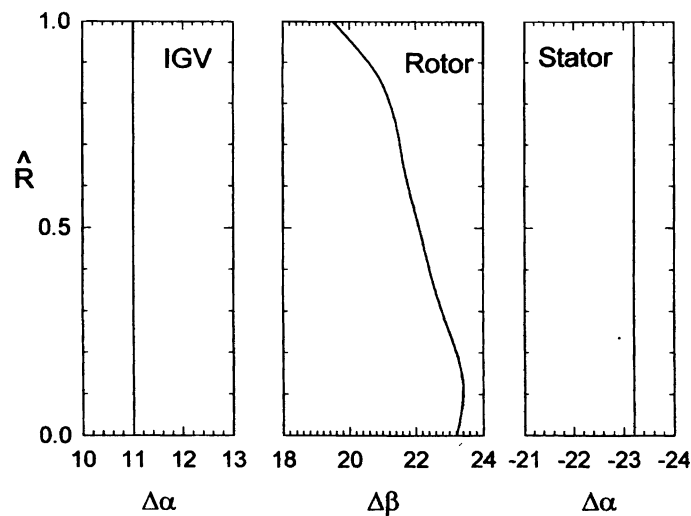


Figure 6.33 Flow turning angles – Example 6.6.

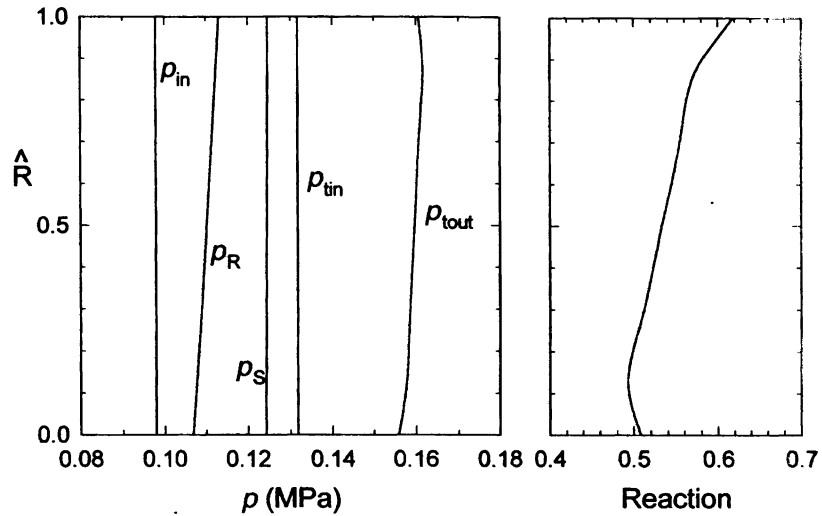


Figure 6.34 Exit pressure and rotor reaction profiles – Example 6.6.

less. For the IGV, rotor, and stator cascades the turning angles ($\Delta\alpha$ or $\Delta\beta$) vary by 0° , 4° , and 0° across the passages.

Lastly, the performance for this case is illustrated in Figure 6.34. Once again, the static pressure profile from the rotor stage is skewed, whereas the profile from the stator stage is flat within 1 percent. The total pressure profile varies by 3 percent from the mean and is lowest near the hub. This low total pressure area is the result of the low efficiency in this region. The rotor reaction varies from 0.51 to 0.62. The reaction is between 0.50 and 0.60 for over 90 percent of blade span, however, which indicates that this blade row is operating relatively efficiently.

For this case, 291 kW (390 hp) is required to power the compressor. This power is minimally higher than for the free vortex (potential) flow case.

For comparison, this case was also run for three annuli (hub, midstream, and tip). The axial pressure profiles and other results were found to vary from the nine-annuli case at most by 0.3 percent.

This last example was obtained by varying the flow angles and observing how the performance of the machine varied. It is not meant to represent an optimized geometry but is merely intended to illustrate the type of study that can be performed. It demonstrates how one can iterate on geometries to improve the performance characteristics. As indicated earlier, the three-dimensional effects increase as the tip-to-hub diameter ratio, rotational speed, and absolute flow angle increase.

6.11. Performance of a Compressor Stage

Thus far, predictions of stage performance (primarily efficiency) for given geometries have not been addressed. That is, methods of relating changes in operating conditions (e.g., flow rate) to changes in efficiency have not been covered. One should remember that a compressor stage or cascade is made up of a series of airfoils. Like wings, airfoils have lift and drag characteristics. For the case of a cascade, a large lift implies a large torque, which has been shown to result in a large pressure ratio. On the other hand, drag implies

frictional losses, which result in a loss in total pressure. Furthermore, both the lift and drag are (strong) functions of leading-edge incidence angle. Sizable amounts of detailed cascade and blade data are available for the varied series of NACA and NASA blade shapes. Abbott and von Doenhoff (1959) present a considerable amount of pressure, lift, and drag data for many blades shapes, but this still is only a small proportion of the data available in many sources. These data are in terms of lift and drag coefficients rather than efficiency information. A compressor designer is interested in efficiency, however. Thus, the purpose of this section is to develop a method to relate the lift and drag characteristics directly to efficiency. The method presented in this section is a combination of theoretical considerations and empiricism. Incompressible flow is assumed to simplify the mathematics. The method can be used to select the blade characteristics – for example, angles, solidity, pitch, chord, and so on – to maximize the efficiency. This general approach was used in early compressor design and was developed by Vavra (1974) in 1960, Logan (1993) and several others; the author does not want to imply it is a modern technology. As indicated earlier, CFD is certainly an important tool in the design of modern compressors and fans. These CFD codes are robust methods and are thus not appropriate for teaching the fundamental characteristics of efficiency variations in turbomachines. Therefore, most importantly, the method in this section gives great insight into how the stage performance and blade characteristics are fundamentally related – for example, how the efficiency will vary for part flow conditions (with increasing incidence angle) – which are fundamentals that engineers often lose sight of in CFD analyses. The analysis is included herein and expanded upon, including application examples.

6.11.1. Velocity Polygons

Although velocity polygons have been covered already, they are discussed again in this section. For the rotor, the relevant velocities for a blade are shown in Figure 6.35.a. For the stator, the relevant velocities for a vane are shown in Figure 6.35.b. Both figures illustrate the lift and drag forces acting on the blades (F_l and F_d , respectively). As usual, the inlet and exit flow angles to the rotor blade are β_1 and β_2 respectively, and the flow deflection is δ_{12} . The average flow angle is defined as β_m , which is *approximately* the stagger, and the forces are relative to this angle. Inlet and exit flow angles for the stator are α_2 and α_3 , respectively. Once again, a consistent sign notation is needed, and the same notation as described in Section 6.3 is used. That is, all positive tangential velocities are to the right. Thus, rotor blades move to the right with positive velocity U . Also, all positive flow and force angles are considered to be counterclockwise. Positive lift and drag loads are assumed to be opposite to the direction of flow turning or deflection and in the direction of flow, respectively.

Next, recall the definition of percent reaction results in

$$\%R = \frac{1}{1 + \left[\frac{c_2^2 - c_1^2}{w_1^2 - w_2^2} \right]} \quad 6.11.1$$

One can use

$$c^2 = c_u^2 + c_a^2 \quad 6.11.2$$

and

$$w^2 = w_u^2 + w_a^2 \quad 6.11.3$$

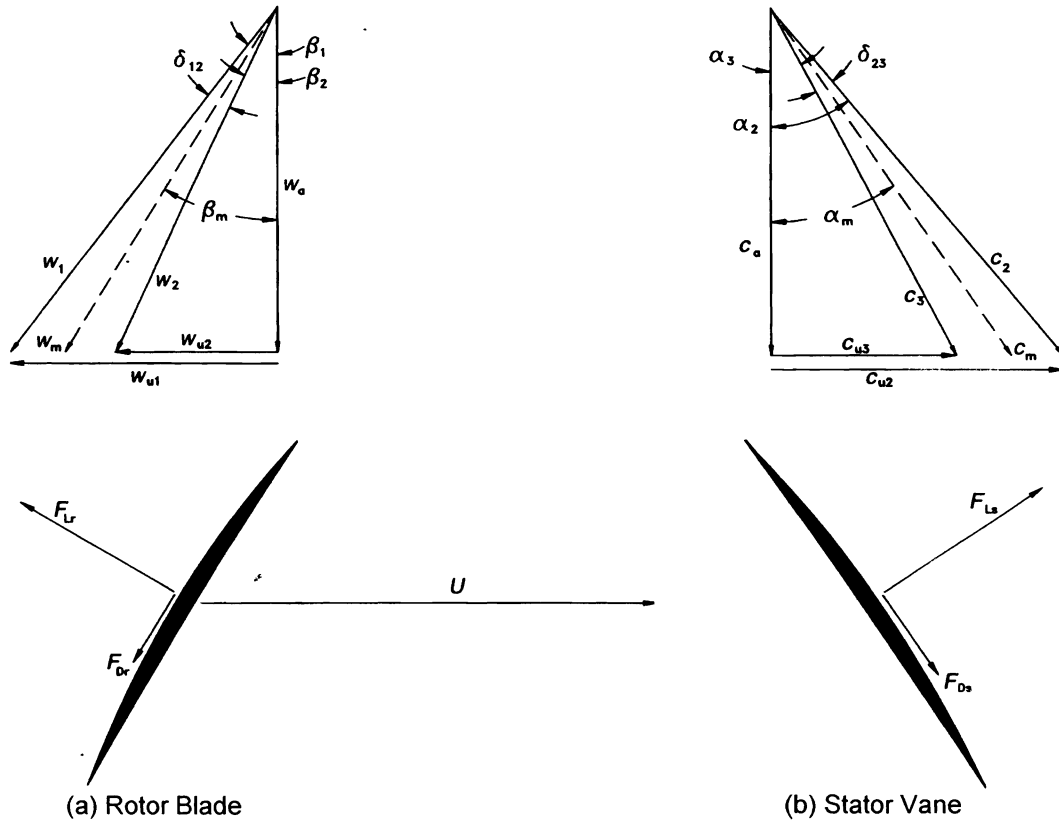


Figure 6.35 Velocity polygons and forces.

with the assumption that the axial component of velocity remains constant through a stage to find that

$$\%R = \frac{1}{1 + \left[\frac{c_{u2}^2 - c_{u1}^2}{w_{u1}^2 - w_{u2}^2} \right]}, \quad 6.11.4$$

or, by grouping and expanding, that

$$\%R = \frac{(w_{u1} + w_{u2})(w_{u1} - w_{u2})}{(w_{u1} + c_{u1})(w_{u1} - c_{u1}) - (w_{u2} + c_{u2})(w_{u2} - c_{u2})}. \quad 6.11.5$$

It is apparent from Figures 6.7 and 6.35 if $\alpha_1 = \alpha_3$ (used hereafter) that

$$U = c_{u1} - w_{u1} = c_{u2} - w_{u2}; \quad 6.11.6$$

thus, using Eq. 6.11.5 and rearranging yield

$$\%R = -\frac{(w_{u1} + w_{u2})(w_{u1} - w_{u2})}{U\{(w_{u1} - w_{u2}) - (c_{u2} + c_{u1})\}}, \quad 6.11.7$$

and using Eq. 6.11.6 results in

$$c_{u2} - c_{u1} = w_{u2} - w_{u1}. \quad 6.11.8$$

Thus, from Eq. 6.11.7,

$$\%R = -\frac{(w_{u1} + w_{u2})}{2U}. \quad 6.11.9$$

Therefore, the reaction is the average tangential component of relative velocity (to the blade) divided by the rotational velocity. Finally, two new definitions can be introduced. The first is the conventional flow coefficient, which is a nondimensional velocity based on the axial component and thus represents the total flow rate as follows:

$$\phi = \frac{c_a}{U} = \frac{w_a}{U} \quad 6.11.10$$

The blade velocity, U , is conventionally used to nondimensionalize velocities. The second is the deflection coefficient (nondimensional deflection), which represents the blade turning. For a rotor blade,

$$\tau_r = \frac{w_{u2} - w_{u1}}{U}, \quad 6.11.11$$

and, for a stator vane,

$$\tau_s = \frac{c_{u2} - c_{u3}}{U}; \quad 6.11.12$$

thus, for the case of $\alpha_3 = \alpha_1$,

$$\tau_s = \frac{c_{u2} - c_{u1}}{U}. \quad 6.11.13$$

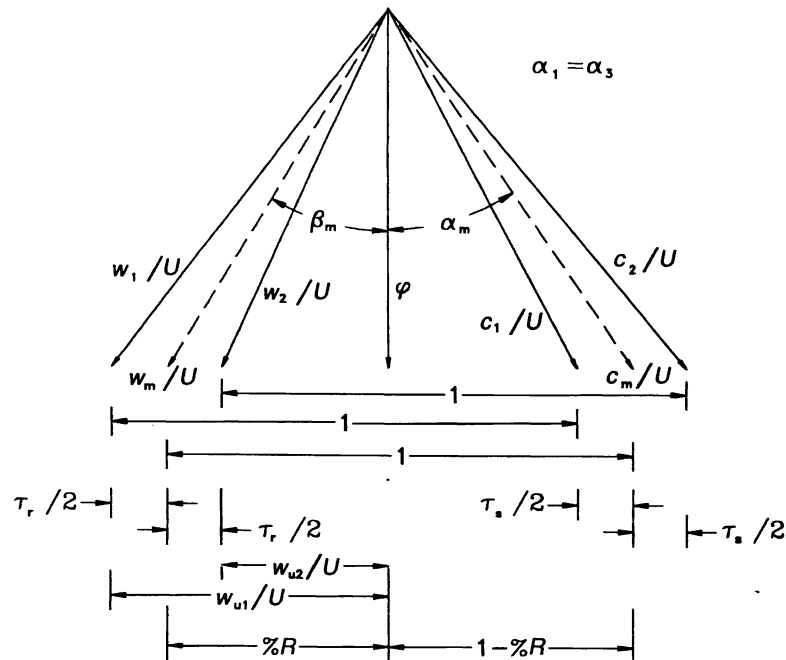


Figure 6.36 Nondimensional velocity polygons for a single stage.

One can now nondimensionalize the entire set of velocity polygons in Figure 6.35 by U to generate Figure 6.36. In Figure 6.36, one can see the different physical quantities – $\%R$, ϕ , and τ – and thus gain an understanding of the relevance of velocity polygons to compressor stage performance. For example, if α_1 is equal to α_3 and $\%R = 0.50$, then τ_r is equal to τ_s and once again the polygon is symmetric as discussed in Section 6.4.4. Also shown on Figure 6.36 are the average angles β_m (defined as $\tan^{-1}\{\frac{1}{2}[\tan \beta_1 + \tan \beta_2]\}$) and α_m (defined as $\tan^{-1}\{\frac{1}{2}[\tan \alpha_2 + \tan \alpha_3]\}$). One can readily see, for example, that

$$\tan \beta_m = -\frac{\%R}{\phi} \quad 6.11.14$$

and that

$$\tan \alpha_m = \frac{1 - \%R}{\phi}. \quad 6.11.15$$

Using the preceding two equations yields

$$\tan \alpha_m = \frac{1 + \phi \tan \beta_m}{\phi}. \quad 6.11.16$$

Also, using the geometry of Figure 6.36, one sees that

$$\tau_r = \phi(\tan \beta_2 - \tan \beta_1) \quad 6.11.17$$

and that

$$\tau_r = \phi(\tan \alpha_2 - \tan \alpha_1). \quad 6.11.18$$

Finally, it can also be demonstrated from Figure 6.36 that

$$\tau_r/2 = \phi(\tan \beta_m - \tan \beta_1) = \phi(\tan \beta_2 - \tan \beta_m) \quad 6.11.19$$

and

$$\tau_r/2 = \phi(\tan \alpha_2 - \tan \alpha_m) = \phi(\tan \alpha_m - \tan \alpha_1). \quad 6.11.20$$

6.11.2. Lift and Drag Coefficients

Next, the forces acting on the blades can be considered and related to lift and drag coefficients. First, by examining the forces in Figures 6.35.a and 6.35.b, one can break the forces into different components as shown in Figures 6.37.a and 6.37.b. Shown in these figures are the forces in the axial and tangential directions F_a and F_u , respectively. Thus, for the rotor, the forces can be related by

$$F_{lr} = F_{ur} \cos \beta_m - F_{ar} \cos \beta_m \quad 6.11.21$$

and

$$F_{dr} = -F_{ur} \sin \beta_m - F_{ar} \cos \beta_m, \quad 6.11.22$$

and the angle between the drag and lift forces is found from

$$\tan \varepsilon_r = \frac{F_{dr}}{F_{lr}}. \quad 6.11.23$$

For the stator,

$$F_{ls} = F_{us} \cos \alpha_m - F_{as} \sin \alpha_m \quad 6.11.24$$

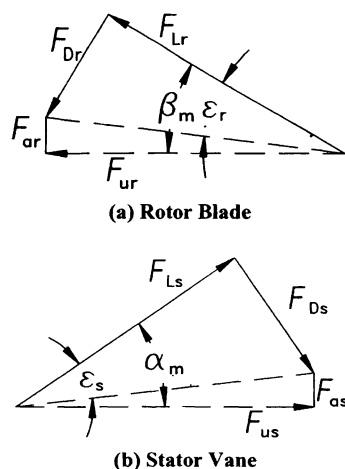


Figure 6.37 Force polygons.

and

$$F_{ds} = F_{us} \sin \alpha_m - F_{as} \cos \alpha_m, \quad 6.11.25$$

and the angle between the two forces for the stator is found from

$$\tan \varepsilon_s = -\frac{F_{ds}}{F_{ls}}. \quad 6.11.26$$

Also, the lift and drag coefficients are defined as

$$C_l \equiv \frac{F_l}{\frac{1}{2} \rho v_m^2 C} \quad 6.11.27$$

and

$$C_d \equiv \frac{F_d}{\frac{1}{2} \rho v_m^2 C}, \quad 6.11.28$$

where C is the chord length, and v_m is a representative velocity and is equal to w_m for a rotor and c_m for a stator; thus with Eqs. 6.11.23 and 6.11.26,

$$\tan \varepsilon_r = \frac{C_{dr}}{C_{lr}} \quad 6.11.29$$

and

$$\tan \varepsilon_s = -\frac{C_{ds}}{C_{ls}}. \quad 6.11.30$$

a. Infinitely Long Blades

Blades are obviously of finite length. However, the first blades that will be considered are of infinite length because they are more ideal. In the next sub-section, correction factors are applied to account for deviations from the finite length assumption. If a control volume is drawn on the rotor blades, as shown in Figure 6.38, the linear momentum

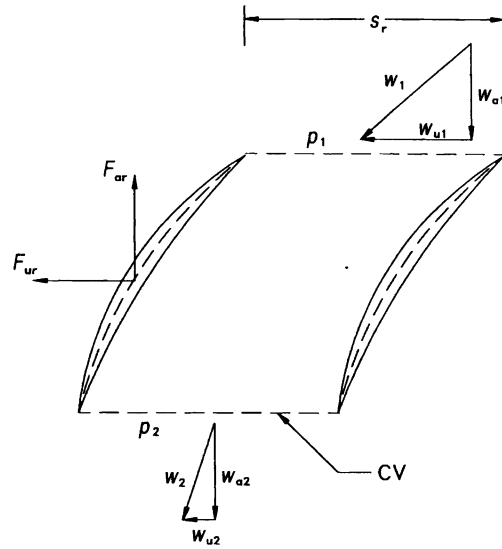


Figure 6.38, Control volume on rotor cascade.

equation can be used to show that, for the tangential force of the fluid on a blade, if one remembers remembering that the force on the blade is equal and opposite to the force on the fluid,

$$F_{ur} = \dot{m} (w_{u2} - w_{u1}). \quad 6.11.31$$

Also, for an axial force on a rotor blade,

$$F_{ar} = \dot{m} (w_{a1} - w_{a2}) + (p_2 - p_1) s_r. \quad 6.11.32$$

As discussed earlier, however, one usually tries to hold the axial velocity constant in an axial compressor ($c_{a2} = c_{a1}$ or $w_{a2} = w_{a1}$), and thus

$$F_{ar} = (p_2 - p_1) s_r. \quad 6.11.33$$

Thus, from Eq. 6.11.29, one can multiply and divide by U^2 (noting that, if the flow is incompressible, the mass flow rate is $\rho s_r w_a$) to find

$$F_{ur} = \rho s_r U^2 \left[\frac{w_a}{U} \right] \left[\frac{(w_{u2} - w_{u1})}{U} \right]. \quad 6.11.34$$

First, if the drag is considered, using Eqs. 6.11.22, 6.11.33 and 6.11.34 yields

$$F_{dr} = -\rho s_r U^2 \left[\frac{w_a}{U} \right] \left[\frac{(w_{u2} - w_{u1})}{U} \right] \sin \beta_m - (p_2 - p_1) s_r \cos \beta_m, \quad 6.11.35$$

or trigonometry results in

$$F_{dr} = -\rho s_r w_a^2 [\tan \beta_2 - \tan \beta_1] \sin \beta_m - (p_2 - p_1) s_r \cos \beta_m. \quad 6.11.36$$

The pressure difference $p_2 - p_1$ is defined as

$$p_2 - p_1 = p_2 - \frac{1}{2} \rho w_2^2 - p_1 + \frac{1}{2} \rho w_1^2 \quad 6.11.37$$

or

$$p_2 - p_1 = \frac{1}{2} \rho (w_1^2 - w_2^2) - \zeta_r, \quad 6.11.38$$

where ζ_r is the total pressure loss ($p_{t2} - p_{t1}$) due to friction. This can be related to the flow angles by

$$p_2 - p_1 = \rho c_a^2 (\tan \beta_1 - \tan \beta_2) \tan \beta_m - \zeta_r. \quad 6.11.39$$

Using this with Eq. 6.11.36, one finds

$$F_{dr} = s_r \zeta_r \cos \beta_m. \quad 6.11.40$$

Using the definition of the drag coefficient (Eq. 6.11.28) yields

$$C_{drp} = \frac{s_r \zeta_r \cos \beta_m}{C \frac{1}{2} \rho w_m^2}. \quad 6.11.41$$

The sub-subscript p is used to remind the reader that all of the drag arises from the pressure loss.

To calculate the lift, one can use Eqs. 6.11.21, 6.11.33, and 6.11.34 to find

$$F_{lr} = \rho s_r U^2 \left[\frac{w_a}{U} \right] \left[\frac{(w_{u2} - w_{u1})}{U} \right] \cos \beta_m - (p_2 - p_1) s_r \sin \beta_m, \quad 6.11.42$$

or using trigonometry Eq. 6.11.42 becomes:

$$F_{lr} = \rho s_r w_a^2 [\tan \beta_2 - \tan \beta_1] \cos \beta_m - (p_2 - p_1) s_r \sin \beta_m. \quad 6.11.43$$

Finally, using Eq. 6.11.39 results in

$$F_{lr} = \rho s_r w_a^2 [\tan \beta_2 - \tan \beta_1] \cos \beta_m - \rho s_r c_a^2 [\tan \beta_1 - \tan \beta_2] \tan \beta_m \sin \beta_m + s_r \zeta_r \sin \beta_m \quad 6.11.44$$

Using the definition of the lift coefficient (Eq. 6.11.27), one finds with some rearrangement that

$$C_{lr} = 2 \frac{s_r}{C} \cos^2 \beta_m [\tan \beta_2 - \tan \beta_1] [\cos \beta_m + \tan \beta_m \sin \beta_m] + \frac{s_r \zeta_r}{C \frac{1}{2} \rho w_m^2} \cos \beta_m \tan \beta_m. \quad 6.11.45$$

Using some trigonometric identities and Eq. 6.11.41 yields

$$C_{lr} = 2 \frac{s_r}{C} \cos \beta_m [\tan \beta_2 - \tan \beta_1] + C_{drp} \tan \beta_m. \quad 6.11.46$$

Interestingly, the lift coefficient is directly related to the drag coefficient. Expressions similar to those used above apply to a stator blade row as follows:

$$F_{us} = \dot{m} (c_{u2} - c_{u1}) \quad 6.11.47$$

$$F_{us} = (p_3 - p_2) s_s \quad 6.11.48$$

$$p_3 - p_2 = \rho c_a^2 [\tan \alpha_2 - \tan \alpha_1] \tan \alpha_m - \zeta_s \quad 6.11.49$$

$$F_{ds} = s_s \zeta_s \cos \alpha_m \quad 6.11.50$$

$$C_{d_{sp}} = \frac{s_s \zeta_s \cos \alpha_m}{C \frac{1}{2} \rho c_m^2} \quad 6.11.51$$

$$F_{ls} = \rho s_s c_a^2 [\tan \alpha_2 - \tan \alpha_1] \cos \alpha_m - \rho s_s c_a^2 [\tan \alpha_1 - \tan \alpha_2] \tan \alpha_m \sin \alpha_m - s_s \zeta_s \sin \alpha_m \quad 6.11.52$$

$$C_{ls} = 2 \frac{s_s}{C} \cos \alpha_m [\tan \alpha_2 - \tan \alpha_1] - C_{d_{sp}} \tan \alpha_m \quad 6.11.53$$

b. Finite Length Blades

In the preceding section, the lift and drag coefficients were identified for very long blades. Drag was determined to arise from pressure losses alone. However, when blades are not infinitely long but are of length h , other mechanisms add to the drag. For example, for finite length blades, tip leakages are encountered. That is, flows migrate from the high-pressure surface to the low-pressure or suction surface. This leakage, when coupled with the flow turning, can produce transverse or secondary flows, as shown in Figure 6.39. The losses result in shear losses and added drag; the additional coefficient will be identified as C_{dr_s} . Correlations from Howell (1945a) indicate that, for a rotor blade row, the drag can be approximately

$$C_{dr_s} = 0.018 C_{lr}^2 \quad 6.11.54$$

Shear losses on the hub and case due to the boundary layers also occur. That is, the added surface areas at the outer and inner radii increase the drag. The added loss is called annular drag and is represented by C_{dr_a} . Previous correlations from Howell (1945a) indicate that the drag may be approximated as

$$C_{dr_a} = 0.020 \left[\frac{s}{h} \right]_r, \quad 6.11.55$$

where s/h is the pitch-to-blade height ratio.

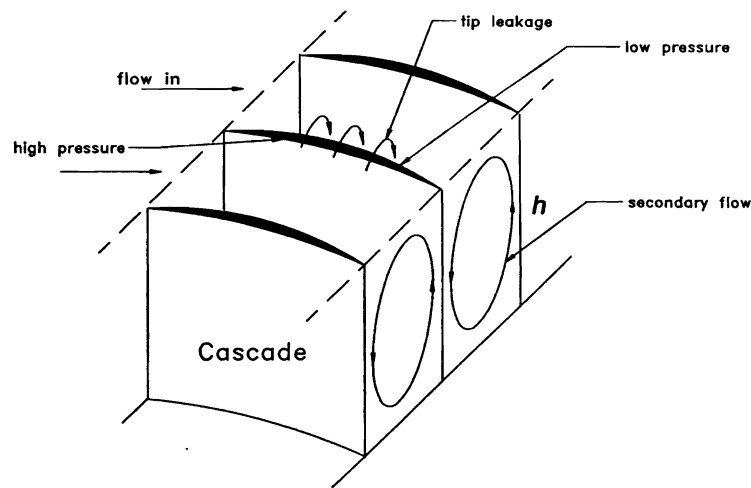


Figure 6.39 Complex viscous flows in a cascade with finite-length blades.

Lastly, to find the drag on the blade row, one can approximate the total as the linear sum of the three drags discussed above. That is,

$$C_{dr_t} = C_{dr_p} + C_{dr_s} + C_{dr_a}. \quad 6.11.56$$

Although the preceding equations are written for a rotor blade row, similar expressions apply for stator blade rows because the same correlations apply. Thus, for the stator,

$$C_{ds_s} = 0.018C_{ls}^2 \quad 6.11.57$$

$$C_{ds_a} = 0.020 \left[\frac{s}{h} \right]_s \quad 6.11.58$$

$$C_{ds_t} = C_{ds_p} + C_{ds_s} + C_{ds_a}. \quad 6.11.59$$

6.11.3. Forces

One can find the actual forces on the blades in terms of the lift and drag coefficients, percent reaction, and flow coefficient. Thus, using Eqs. 6.11.10, 6.11.11 and 6.11.34 yields

$$F_{ur} = \rho s_r \phi \tau_r U^2. \quad 6.11.60$$

Similarly, for the stator,

$$F_{us} = \rho s_s \phi \tau_s U^2 \quad 6.11.61$$

From the force triangles, one can see that

$$F_{ar} = -F_{ur} \tan(\beta_m + \varepsilon_r). \quad 6.11.62$$

However, by a trigonometric rule,

$$\tan(\beta_m + \varepsilon_r) = \frac{\tan \beta_m + \tan \varepsilon_r}{1 - \tan \beta_m \tan \varepsilon_r}. \quad 6.11.63$$

If the drag force is low, implying that ε_r is small, which is the usual case,

$$\tan(\beta_m + \varepsilon_r) = \frac{\tan \beta_m + \varepsilon_r}{1 - \varepsilon_r \tan \beta_m}; \quad 6.11.64$$

thus, from Eq. 6.11.62,

$$F_{ar} = -F_{ur} \frac{\tan \beta_m + \varepsilon_r}{1 - \varepsilon_r \tan \beta_m}, \quad 6.11.65$$

and so from Eq. 6.11.14,

$$F_{ar} = F_{ur} \left[\frac{\frac{\%R}{\phi} - \varepsilon_r}{1 + \varepsilon_r \frac{\%R}{\phi}} \right]. \quad 6.11.66$$

Similarly, for the stator

$$F_{as} = F_{us} \frac{\tan \alpha_m + \varepsilon_s}{1 - \varepsilon_s \tan \alpha_m}. \quad 6.11.67$$

Thus, using Eq. 6.11.15 with Eq. 6.11.67 as was done for the rotor yields

$$F_{as} = F_{us} \left[\frac{\left(\frac{1-\%R}{\phi} \right) + \varepsilon_s}{1 - \varepsilon_s \left(\frac{1-\%R}{\phi} \right)} \right]. \quad 6.11.68$$

6.11.4. Relationship of Blade Loading and Performance

The preceding forces need to be related to the efficiencies and reactions of the stage. For a rotor blade, from Eqs. 6.11.33 and 6.11.66 one obtains

$$\Delta p_r = p_2 - p_1 = \frac{F_{ur}}{s_r} \left[\frac{\frac{\%R}{\phi} - \varepsilon_r}{1 + \varepsilon_r \frac{\%R}{\phi}} \right], \quad 6.11.69$$

or using Eq. 6.11.64 and rearranging yields

$$\Delta p_r = \rho \phi \tau_r U^2 \left[\frac{\%R - \phi \varepsilon_r}{\phi + \varepsilon_r \%R} \right]. \quad 6.11.70$$

Similarly, for a stator, from Eqs. 6.11.48, 6.11.61, and 6.11.68,

$$\Delta p_s = p_3 - p_2 = \rho \phi \tau_s U^2 \left[\frac{1 - \%R + \phi \varepsilon_s}{\phi - \varepsilon_s (1 - \%R)} \right]; \quad 6.11.71$$

thus, if $\alpha_3 = \alpha_1$ (so that $\tau_r = \tau_s = \tau$), the pressure rise across the complete stage is

$$\Delta p = p_3 - p_1 = \Delta p_r + \Delta p_s = \rho \phi \tau U^2 \left\{ \left[\frac{\%R - \phi \varepsilon_r}{\phi + \varepsilon_r \%R} \right] + \left[\frac{1 - \%R + \phi \varepsilon_s}{\phi - \varepsilon_s (1 - \%R)} \right] \right\}. \quad 6.11.72$$

If one considers the case of frictionless flow (no drag) so that ε_r and ε_s are both zero, the ideal pressure rises are

$$\Delta p'_r = \rho \tau U^2 \%R \quad 6.11.73$$

and

$$\Delta p'_s = \rho \tau U^2 (1 - \%R); \quad 6.11.74$$

thus, for the stage,

$$\Delta p' = \rho \tau U^2. \quad 6.11.75$$

Therefore, for ideal flow, from Eqs. 6.11.73 and 6.11.75, one obtains

$$\%R = \frac{\Delta p'_r}{\Delta p'}, \quad 6.11.76$$

which is consistent with Eq. 6.4.7.

From the energy equation (Eq. I.2.33), one finds for the power that

$$\dot{W}_{sh} = \frac{\dot{m}}{\eta_{12}} \left[\frac{p_2 - p_1}{\rho} + \frac{c_2^2 - c_1^2}{2} \right] = \frac{\dot{m}}{\rho \eta_{12}} [p_{t2} - p_{t1}], \quad 6.11.77$$

where

$$\dot{W}_{sh} = \frac{\dot{W}'_{sh}}{\eta_{12}}; \quad 6.11.78$$

thus, further,

$$\dot{W}_{sh} = \frac{\dot{m}}{\rho\eta} [p_{t3} - p_{t1}] \quad 6.11.79$$

where, as before, the efficiency is defined as the ratio of actual to ideal power required for a given pressure rise. Now the ideal pressure rise for the given power is defined as

$$\dot{W}'_{sh} = \frac{\dot{m}}{\rho} [p'_{t3} - p'_{t1}], \quad 6.11.80$$

and thus the efficiency is also

$$\eta = \frac{\Delta p_t}{\Delta p'_t}. \quad 6.11.81$$

Finally, recall that the case of $\alpha_3 = \alpha_1$ and constant axial velocity is being considered, which implies $c_3 = c_1$. This in turn implies that the rise in total and static pressures is identical across the stage, and thus from Eqs. 6.11.75 and 6.11.81

$$\eta = \frac{\Delta p}{\rho\tau U^2}. \quad 6.11.82$$

Therefore, using Eqs. 6.11.72 and 6.11.82 yields

$$\eta = \phi \left\{ \left[\frac{\%R - \phi\varepsilon_r}{\phi + \varepsilon_r\%R} \right] + \left[\frac{1 - \%R + \phi\varepsilon_s}{\phi - \varepsilon_s(1 - \%R)} \right] \right\}. \quad 6.11.83$$

The stage efficiency is consequently a function of four variables: percent reaction, flow coefficient, the angle between the drag and lift for the rotor, and the angle between the drag and lift for the stator. Thus, if it is possible to evaluate the lift and drag for a given condition, the efficiency can be estimated. One observation is that, as the drag on blades and vanes increases, the stage efficiency decreases. Furthermore, velocity polygons for different operating conditions can be used to evaluate the flow angles (and thus yield the vane and blade incidence angles), and if information or data for the lift and drag on a cascade (as a function of incoming incidence angle) are available, the efficiency can be estimated.

6.11.5. Effects of Parameters

One may wish to see the effects of the different parameters on the overall performance. It is desirable for the efficiency to be as high as possible. Thus, from Eq. 6.11.83, Vavra (1974) showed that one can differentiate η with respect to $\%R$ (for given values of ε_r and ε_s) and set to zero; that is,

$$\frac{\partial \eta}{\partial \%R} = 0, \quad 6.11.84$$

which yields

$$\%R_{opt} = \frac{1 - \frac{\phi}{\varepsilon_s} \left[1 - \sqrt{\frac{1 + \varepsilon_s^2}{1 + \varepsilon_r^2}} \right]}{1 - \frac{\varepsilon_r}{\varepsilon_s} \sqrt{\frac{1 + \varepsilon_s^2}{1 + \varepsilon_r^2}}}. \quad 6.11.85$$

If both ε_r and ε_s are small,

$$\%R_{opt} \cong \frac{1}{1 - \frac{\varepsilon_r}{\varepsilon_s}}, \quad 6.11.86$$

and if ε_r and ε_s are the same magnitude ($\varepsilon_r = -\varepsilon_s = \varepsilon$),

$$\%R_{\text{opt}} = 0.50. \quad 6.11.87$$

This is an extremely important finding. *When the percent reaction is 50 percent not only are the forces equal on the rotor and stator blades, but the efficiency is at a maximum!* Thus, most axial flow pumps are designed with percent reactions of approximately 50 percent. Note that incompressible flow was assumed for this analysis. For the same performance phenomena to be realized in compressors, compressor stages tend to have percent reactions somewhat higher than 0.5 (especially for highly loaded stages) due to flow compressibility and long blades. The efficiency at this value of $\%R$ is

$$\eta_{\%R=0.50} = 2\phi \left[\frac{1 - 2\varepsilon\phi}{\varepsilon + 2\phi} \right]. \quad 6.11.88$$

The optimum value of flow coefficient (maximum efficiency) can be found by differentiating Eq. 6.11.92 with respect to ϕ and setting to zero:

$$\frac{\partial \eta_{\%R=0.50}}{\partial \phi} = 0; \quad 6.11.89$$

thus,

$$\phi_{\text{opt}\%R=0.50} = \frac{1}{2} \left[\sqrt{1 + \varepsilon^2} - \varepsilon \right], \quad 6.11.90$$

and if ε is small, using a Taylor series expansion yields

$$\phi_{\text{opt}\%R=0.50} \cong \frac{1}{2} [1 - \varepsilon]. \quad 6.11.91$$

From the optimized values of $\%R$ and ϕ one can find the optimum flow angles by using Eqs. 6.11.14 and 6.11.15. As a limiting case, note that, as the drag approaches zero, the optimum value of ϕ approaches 0.50. Thus, the flow angles β_m and α_m approach 45° . Finally, the maximum value of efficiency under the general conditions is

$$\eta_{\text{max}\%R=0.50} = 1 + 2\varepsilon^2 - 2\varepsilon\sqrt{1 + \varepsilon^2}, \quad 6.11.92$$

which, for small ε , becomes

$$\eta_{\text{max}\%R=0.50} \cong 1 - 2\varepsilon [1 - \varepsilon]. \quad 6.11.93$$

Obviously, as the drag approaches zero, the efficiency approaches unity. Figure 6.40 indicates the order of magnitudes and trends one can expect. For this figure, percent reactions of 50 percent and 60 percent (done numerically) are used with ε varying from 0.0 to 0.10. Both the optimum flow coefficient and resulting efficiency are shown. As can be seen, the optimum flow coefficient decreases with ε and increases with $\%R$. The efficiency decreases with increasing ε (or drag), as expected. However, for the optimum flow coefficient, the efficiency has minimal dependence on $\%R$, which is an important finding. Thus, although the optimum reaction is 50 percent, the value can be increased without major penalties on efficiency.

It is also possible to acquire a better overall understanding of the influences of the different parameters through the following analysis. By using Eq. 6.11.83, which is the most general form of the equation, one can combine terms and ignore second-order terms (i.e., terms of ε_r and ε_s), which are very small. This results in

$$\eta = \frac{\phi + (\varepsilon_r - \varepsilon_s)(\%R - \%R^2 - \phi^2)}{\phi + \varepsilon_r \%R - \varepsilon_s(1 - \%R)}. \quad 6.11.94$$

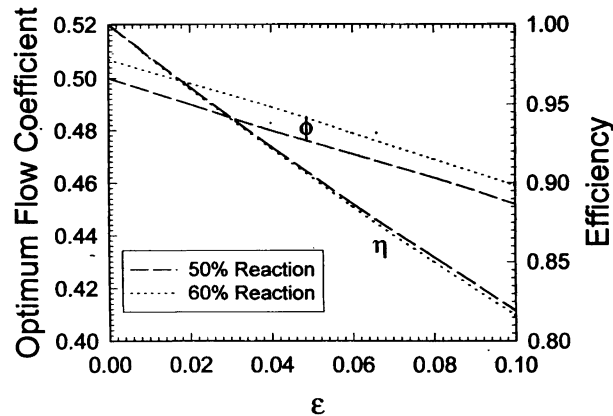


Figure 6.40 Dependence of optimum flow coefficient and efficiency on ε .

Next, if one assumes that $\varepsilon_r = -\varepsilon_s = \varepsilon$,

$$\eta = \frac{\phi + 2\varepsilon(\%R - \%R^2 - \phi^2)}{\phi + \varepsilon} \quad 6.11.95$$

A general three-dimensional depiction of the dependence of the efficiency on the flow coefficient, reaction, and drag to lift angle is presented in Figure 6.41. For clarity, only one value of efficiency (90%) is depicted. A series of conoids result – one for each value of η . Vavra (1974) has shown that the loci of constant efficiency are indeed circles. As has been shown in Section 6.7 as the flow rate deviates from the design value, the flow angle does not match the blade angle (incidence). Thus, as the flow rate deviates from the design value, the drag increases, thus possibly increasing ε (lift may increase also). As a result, as one deviates from the design point, the efficiency changes because of two different effects. That is, as the flow rate is changed from the design value, movement is in both the ϕ and

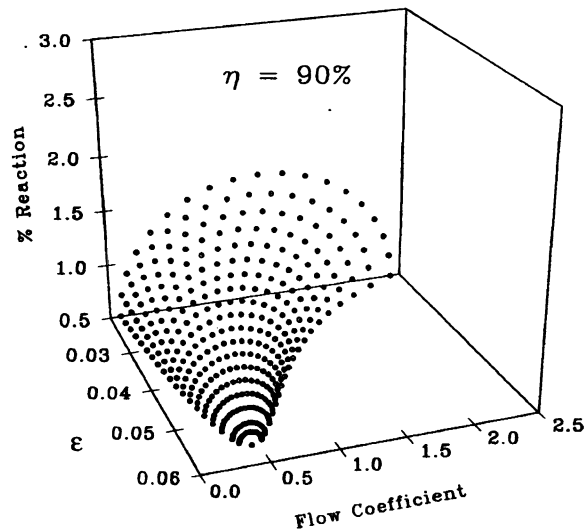


Figure 6.41 Constant single-stage efficiency conoid for $\eta = 90$ percent.

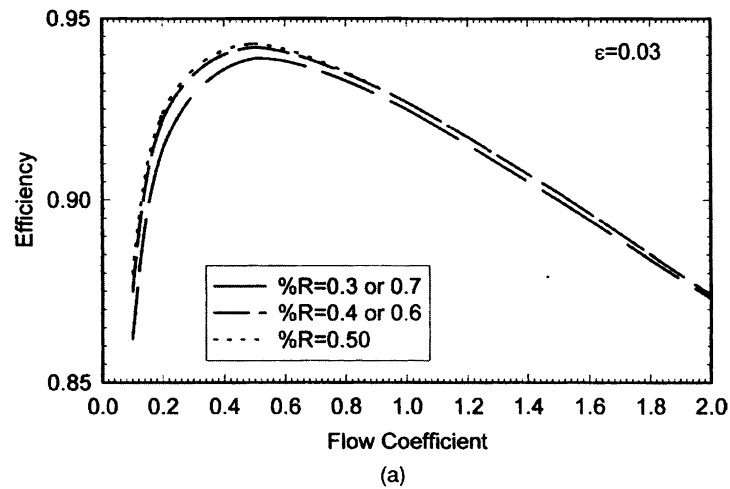


Figure 6.42a Dependence of the single-stage efficiency on flow coefficient for $\varepsilon_r = -\varepsilon_s = 0.03$.

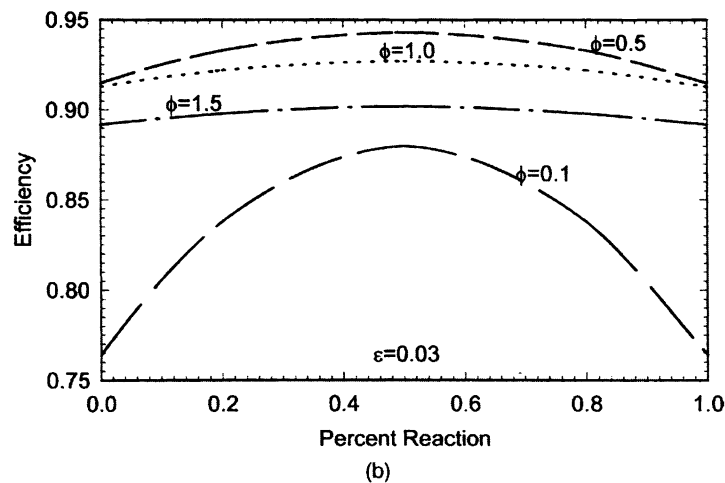


Figure 6.42b Dependence of the single-stage efficiency on percent reaction for $\varepsilon_r = -\varepsilon_s = 0.03$.

ε directions. Furthermore, with each parameter treated separately, if $\%R$ and ϕ are held constant, as ε decreases, the efficiency *always* increases.

Taking a slice of this figure and similar conoids for other values of efficiency at a particular value of ε (0.03 shown here) yields Figure 6.42. As can be seen, the maximum efficiency for $\varepsilon = 0.03$ is 0.942, and as the flow coefficient or percent reaction deviates from the optimum values the efficiency drops off. Note particularly that, for low flow rates, as the flow rate drops the efficiency drops very quickly – especially for a 50 percent reaction. However, for large flow rates, as the flow rate increases the efficiency again drops – but not rapidly. For small values of flow coefficient, as the reaction increases from 0, the efficiency rapidly increases and then decreases. For large flow rates, however, as the reaction increases, changes in efficiency are not large.

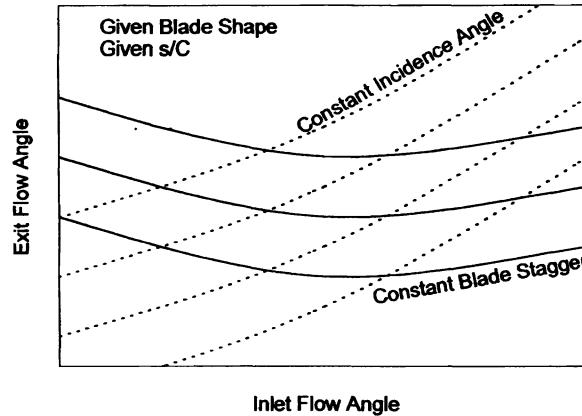


Figure 6.43 Dependence of the exit flow angle on inlet flow angle, incidence angle, and stagger angle (given blade shapes and pitch-to-chord ratio).

6.11.6. Empiricism Using Cascade Data

Next, two-dimensional cascade data is discussed as an empirical method that integrates the previous analyses to predict the efficiency performance of a compressor stage. For example, for a given cascade of stator vanes, as in Figure 6.7.c, if the flow enters at angle α_2 , the flow will exit at angle α_3 . The exit angle will be determined by several variables, including the vane shapes, pitch-to-chord ratio (s/C), incidence angle ($\alpha_2 - \alpha'_2$), and stagger angle (Fig. 6.6.a). For a given set of vanes (fixed shape and fixed s/C), one can experimentally generate a figure showing the functional relationship of α_2 – namely, Figure 6.43. A similar figure could be generated for a cascade of rotor blades. Note that the difference in the inlet and exit flow angles is the flow deflection – that is, how much the flow is turned. Horlock (1958) presents a large amount of such detailed data.

These data and similar data for other values of solidity can then be correlated with generate deflection data as in Figure 6.44. The deflection, δ , has previously been defined as the flow turning angle ($[\alpha_3 - \alpha_2]$ for a stator and $[\beta_2 - \beta_1]$ for a rotor). In this figure, the

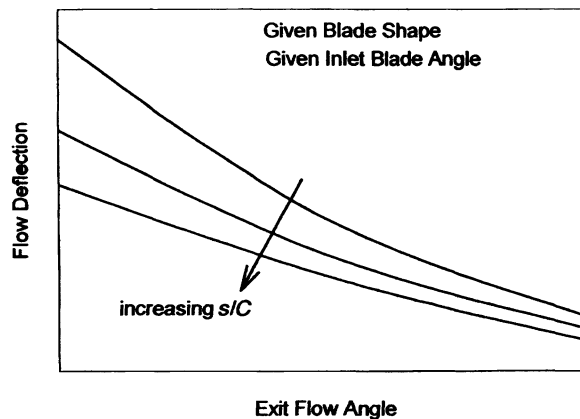


Figure 6.44 Dependence of the generalized flow deflection angle on exit flow angle and pitch-to-chord ratio (given inlet blade or vane angle and shape).

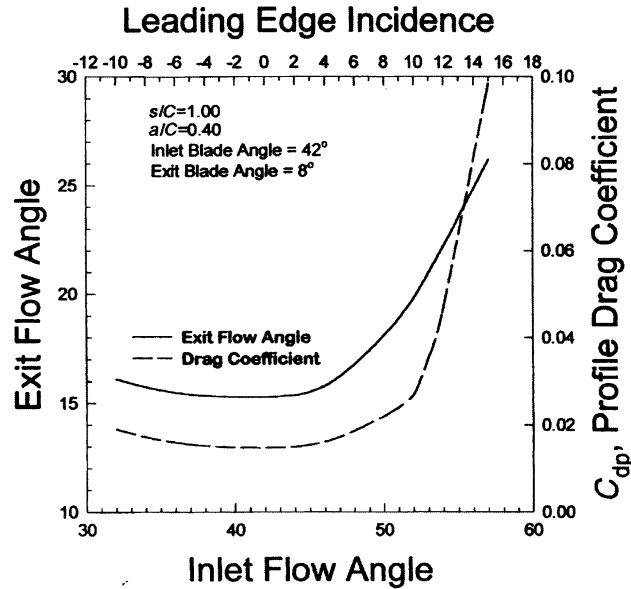


Figure 6.45 Cascade data for Example 6.7.

flow deflection is shown as a general function of exit angle for a given family of blades and given stagger. Such a figure can be used, for example, to determine the necessary solidity for a given deflection and exit flow angle.

Example 6.7: A stage with a relative rotor inlet blade angle of -42° and a relative rotor exit blade angle of -8° is to be analyzed. The stator inlet blade angle is 42° and the stator exit blade angle is 8° . Cascade data are presented in Figure 6.45 for this particular stagger. On the basis of the sign definitions adopted in this book, for the rotor blades the inlet and exit flow angles are $-\beta_1$ and $-\beta_2$ and for the stator they are α_2 and α_3 , respectively. The maximum camber is at 40 percent of the chord, the pitch-to-chord ratio is 1.0, and the pitch-to-blade height is 0.75. The percent reaction is 50 percent, and the incidence to the rotor is $+2.3^\circ$. Find the flow coefficient and predict the flow angles and efficiency. As the flow coefficient changes, consider other incidence angles and for a constant percent reaction predict efficiency as a function of flow coefficient.

SOLUTION:

First, one can determine the blade deflection angles or ideal deflections:

$$\delta'_{12} = \beta'_2 - \beta'_1 = 34^\circ$$

$$\delta'_{23} = \alpha'_3 - \alpha'_2 = -34^\circ.$$

Second, the flow deflection is determined. One must consider the incidence and inlet flow angles. For the rotor,

$$\iota_1 = 2.3^\circ.$$

Therefore,

$$\beta_1 = \beta'_1 - \iota_1 = -44.3^\circ,$$

and thus from Figure 6.45 the rotor exit flow angle is

$$\beta_2 = -15.8^\circ.$$

Ideally, the exit angle is -8° , the difference being the deviation. Also, for reference,

$$\beta_2 = \beta_1 + \delta_{12},$$

and so the actual deflection is

$$\delta_{12} = 28.5^\circ \text{ (less than ideal).}$$

Next,

$$\tan \beta_m = \frac{1}{2} [\tan \beta_1 + \tan \beta_2],$$

and so $\beta_m = -32.2^\circ$.

Finally,

$$-\tan \beta_m = 0.6294 = \frac{\%R}{\phi};$$

thus,

$$\phi = \frac{\%R}{-\tan \beta_m} = \frac{0.50}{0.6294} = 0.794.$$

For the stator, one can examine the polygons in Figure 6.36 and see that

$$\tan \alpha_2 = \frac{1 + \phi \tan \beta_2}{\phi}.$$

Therefore, solving for α_2 yields

$$\alpha_2 = 44.3^\circ,$$

but

$$\alpha_2 = \alpha'_2 - \iota_2;$$

thus,

$$\iota_2 = -2.3^\circ.$$

Note also that the absolute values of β_1 and α_2 are exactly the same, as well as the incidences, which is a result of the percent reaction's being 50%. For other cases of $\%R$, the angles and incidences will in general be different. From Figure 6.45, the stator exit flow angle is

$$\alpha_3 = 15.8^\circ,$$

which is again larger than ideal. As reference,

$$\alpha_3 = \alpha_2 + \delta_{23};$$

thus,

$$\delta_{23} = -28.5^\circ \text{ (again less than ideal).}$$

Next,

$$\tan \alpha_m = \frac{1}{2} [\tan \alpha_2 + \tan \alpha_3],$$

and so $\alpha_m = 32.2^\circ$.

The lift and drag coefficients must also be considered. For the profile drag of the rotor blades, using Figure 6.45 yields

$$C_{drp} = 0.015.$$

Next, the lift data are needed. Because it was not given, it can be estimated using

$$C_{lr} = 2 \frac{S_r}{C} \cos \beta_m [\tan \beta_2 - \tan \beta_1] + C_{drp} \tan \beta_m$$

$$C_{lr} = 2 \times 1.0 \times \cos(-32.2^\circ) \times [\tan(-15.8^\circ) - \tan(-44.3^\circ)] \\ + 0.015 \times \tan(-32.2^\circ)$$

$$C_{lr} = 1.164.$$

Secondary flow losses can be estimated using

$$C_{drs} = 0.018 C_{lr}^2 = 0.025,$$

and annulus flow losses can be obtained from

$$C_{dra} = 0.020 \frac{S_r}{h} = 0.015;$$

thus, the total drag is

$$C_{drt} = C_{drp} + C_{drs} + C_{dra} = 0.055.$$

Finally, the angle between drag and lift is defined by

$$\tan \varepsilon_r = \frac{C_{drt}}{C_{lr}} = 0.0473 \text{ and is positive because of the definition of angles}$$

and since ε_r is small, $\varepsilon_r = 0.0473$ radians.

Similarly, for the profile drag of the stator, using Figure 6.45

$$C_{dsp} = 0.015.$$

Thus, using

$$C_{ls} = 2 \frac{S_s}{C} \cos \alpha_m [\tan \alpha_2 - \tan \alpha_3] - C_{dsp} \tan \alpha_m$$

results in

$$C_{ls} = 1.164.$$

Secondary flow losses can be estimated using

$$C_{dss} = 0.018 C_{ls}^2 = 0.025,$$

and annulus flow losses can be obtained from

$$C_{dsa} = 0.020 \frac{S_s}{h} = 0.015;$$

thus, the total drag is

$$C_{dst} = C_{dsp} + C_{dss} + C_{dsa} = 0.055.$$

Finally, the angle between drag and lift is defined by

$$\tan \varepsilon_s = \frac{C_{dst}}{C_{ls}} = -0.0473 \text{ and is negative because of the definition of angles}$$

and since ε_s is small, $\varepsilon_s = -0.0473$ radians.

Finally, the efficiency is predicted by

$$\eta = \phi \left\{ \left[\frac{\%R - \phi \varepsilon_r}{\phi + \varepsilon_r \%R} \right] + \left[\frac{1 - \%R + \phi \varepsilon_s}{\phi - \varepsilon_s (1 - \%R)} \right] \right\}$$

$$\eta = 0.794 \left\{ \left[\frac{0.50 - 0.794 \times 0.0473}{0.794 + 0.0473 \times 0.50} \right] + \left[\frac{1 - 0.50 - 0.794 \times 0.0473}{0.794 + 0.0473 (1 - 0.50)} \right] \right\}$$

$$\eta = 0.898.$$

Thus, for the given blades and vanes and the given incidence angle, the flow coefficient is 0.794 and the efficiency is 89.8 percent.

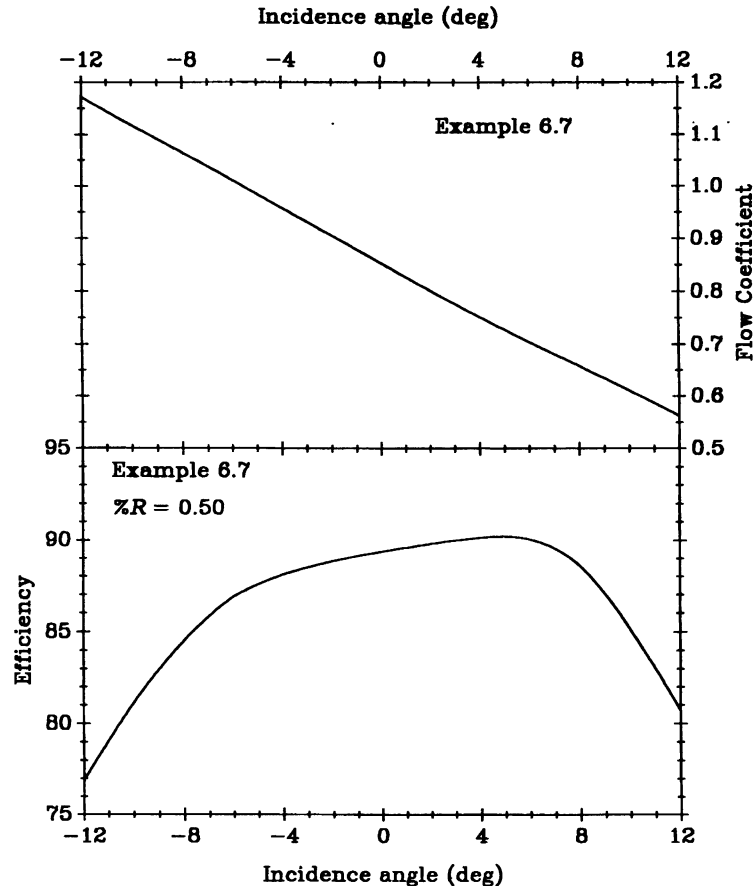


Figure 6.46 Dependence of the flow coefficient and stage efficiency on incidence angle (Example 6.7).

Next, the process is repeated for a range of incidence angles from -12° to $+12^\circ$. Because the calculation procedure is exactly the same, details will not be repeated. Only the final results are shown. In Figure 6.46 the efficiency and flow coefficient are plotted versus the incidence angle. As can be seen, the maximum efficiency occurs at an incidence angle of 5.5° – not zero. Although the minimum drag is at zero incidence, the lift increases significantly as the incidence increases, thus reducing ε – at least for small positive incidence angles. The efficiency and angle between the lift and drag (ε) are plotted in Figure 6.47. The optimum flow coefficient is 0.72. The minimum value of ε is 0.046, which corresponds to the maximum efficiency. However, from Figures 6.39 and 6.40 one can see that the optimum value of ϕ is considerably below 0.5 for a constant value of ε between 0.04 and 0.05. From Figure 6.47, it is apparent that, as the flow coefficient decreases below the optimum, the value of ε increases sharply, implying a reduction in efficiency. Thus, as observed in Section 6.11.4, the efficiency is really a function of independent variations of both ϕ and ε . For this particular case, reducing ϕ (independent of ε) from 0.794 would increase the efficiency. However, because this change also increases ε , the efficiency decreases. Also for this example, two-dimensional cascade data for the given blade shapes for deflection and drag were used and lift was calculated. However, for an accurate prediction of stage performance, including efficiency, CFD would certainly be the best method.

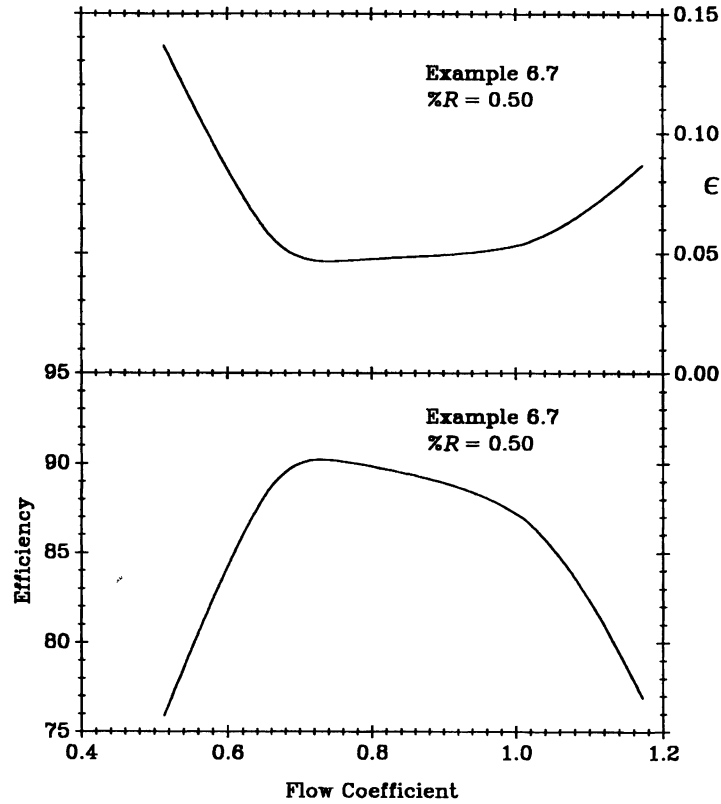


Figure 6.47 Dependence of the lift to drag angle and stage efficiency on flow coefficient (Example 6.7).

6.11.7. Further Empiricism

Empiricism has shown that much of the data for different blade or vane shapes and conditions can be correlated with a single figure. Thus, if particular data are not available, general correlated data can be used to make predictions. For example, if the exit area to inlet area ratio of the cascade is too large (Δp is too large), separation will occur. Because this area ratio is directly related to the deflection angle, one can define the stall deflection angle for a given cascade as the value of deflection at which separation occurs. By definition, the *nominal* deflection angle is

$$\hat{\delta} = 0.80 \delta_{\text{stall}}. \quad 6.11.101$$

Using this definition and extended data, which include the stall condition, results in the data from Figure 6.44 and similar figures empirically (and conveniently) reducing to Figure 6.48, in which the nominal deflection angle is a function of the nominal exit angle for both rotor blades and stator vanes. On the basis of the sign definitions adopted in this text, for the rotor blades the nominal exit flow angle is $-\hat{\beta}_2$ and for the stator it is $\hat{\alpha}_3$. Also, for the rotor blades the nominal deflection angle is $\hat{\delta}_{12}$, and for the stator it is $-\hat{\delta}_{23}$. Data in this figure are conveniently not functions of the inlet angle or blade shapes. All of the following calculations use this nominal deflection angle and other nominal conditions (flow angles, incidence angles, etc.), as a reference at this point.

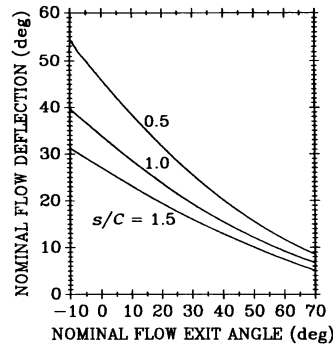


Figure 6.48 Dependence of the empirical nominal flow deflection on nominal exit flow angle and pitch-to-chord ratio (general case) (from Fig. 68, Howell 1945a with permission of the Council of the Institution of Mechanical Engineers).

Next, the nominal deviation of the flow from the blade angle at the exit is given by the following empirical relationship from Howell (1945a):

$$\hat{\xi} = m\delta' \sqrt{\frac{s}{C}}. \quad 6.11.102$$

Thus, for a stator, the value of $\hat{\xi}$ is equal to $\alpha'_3 - \hat{\alpha}_3$, and for a rotor cascade it is $\beta'_2 - \hat{\beta}_2$. The value of δ' is the deflection angle of the blades; that is, for a stator cascade the value of δ' is equal to $\alpha'_3 - \alpha'_2$, and for a rotor cascade it is $\beta'_2 - \beta'_1$. The value of m has been correlated by Howell (1945a) to be

$$m = 0.23 \left[\frac{2a}{C} \right] + 0.1 \left[\frac{\hat{\chi}_{\alpha\beta}}{50} \right], \quad 6.11.103$$

where a is the distance from the leading edge of a blade to the point of maximum camber, as shown in Figure 6.6.a. Also, the quantity $\hat{\chi}_{\alpha\beta}$ is equal to the absolute magnitude of $\hat{\alpha}_3$ for a stator cascade and the absolute magnitude of $\hat{\beta}_2$ for a rotor cascade. For a quick calculation, or if the value of a is unknown, a value of $m \cong 0.26$ can be used.

Lastly, Figure 6.49 presents a correlation for the nondimensionalized deflection $\delta/\hat{\delta}$ as a function of the nondimensionalized difference in actual and nominal incidence angle, $(\iota - \hat{\iota})/\hat{\delta}$. As indicated in Figure 6.49, this is independent of s/C and is valid for a wide range of geometries. Note that, for the case of zero incidence and zero nominal incidence, the deflection is equal to the nominal value, $\delta/\hat{\delta} = 1$. Also shown in Figure 6.49 is a generalized profile drag coefficient, C_{Dp} , as a function of $(\iota - \hat{\iota})/\hat{\delta}$.

The calculations are being facilitated by fitting the curves in Figures 6.48 and 6.49 with the polynomials below. Values for the parameters are listed in Table 6.4.

$$\hat{\delta} = a_1 + a_2\hat{\alpha} + a_3\hat{\alpha}^2 \quad 6.11.104$$

$$\delta/\hat{\delta} = b_1 + b_2 \left[\frac{\iota - \hat{\iota}}{\hat{\delta}} \right] + b_3 \left[\frac{\iota - \hat{\iota}}{\hat{\delta}} \right]^2 + b_4 \left[\frac{\iota - \hat{\iota}}{\hat{\delta}} \right]^3 + b_5 \left[\frac{\iota - \hat{\iota}}{\hat{\delta}} \right]^4 \quad 6.11.105$$

$$C_D = c_1 + c_2 \left[\frac{\iota - \hat{\iota}}{\hat{\delta}} \right] + c_3 \left[\frac{\iota - \hat{\iota}}{\hat{\delta}} \right]^2 + c_4 \left[\frac{\iota - \hat{\iota}}{\hat{\delta}} \right]^3 \quad \text{for} \quad \left[\frac{\iota - \hat{\iota}}{\hat{\delta}} \right] \leq 0.4 \quad 6.11.106$$

$$C_D = d_1 + d_2 \left[\frac{\iota - \hat{\iota}}{\hat{\delta}} \right] + d_3 \left[\frac{\iota - \hat{\iota}}{\hat{\delta}} \right]^2 \quad \text{for} \quad \left[\frac{\iota - \hat{\iota}}{\hat{\delta}} \right] \geq 0.4 \quad 6.11.107$$

Table 6.4. Polynomial Parameters

s/C	a_1	a_2	a_3	b_1	b_2	b_3	b_4	b_5
0.5	46.4	-0.819	0.0041	1.009	0.971	-0.727	-0.860	0.281
1.0	34.1	-0.553	0.0025	1.009	0.971	-0.727	-0.860	0.281
1.5	26.9	-0.400	0.00125	1.009	0.971	-0.727	-0.860	0.281

s/C	c_1	c_2	c_3	c_4	d_1	d_2	d_3
0.5	0.0185	-0.0118	0.0606	0.0389	0.118	0.063	1.00
1.0	0.0143	0.00076	0.0538	0.0429	0.118	0.063	1.00
1.5	0.0117	0.00736	0.0535	0.0440	0.118	0.063	1.00

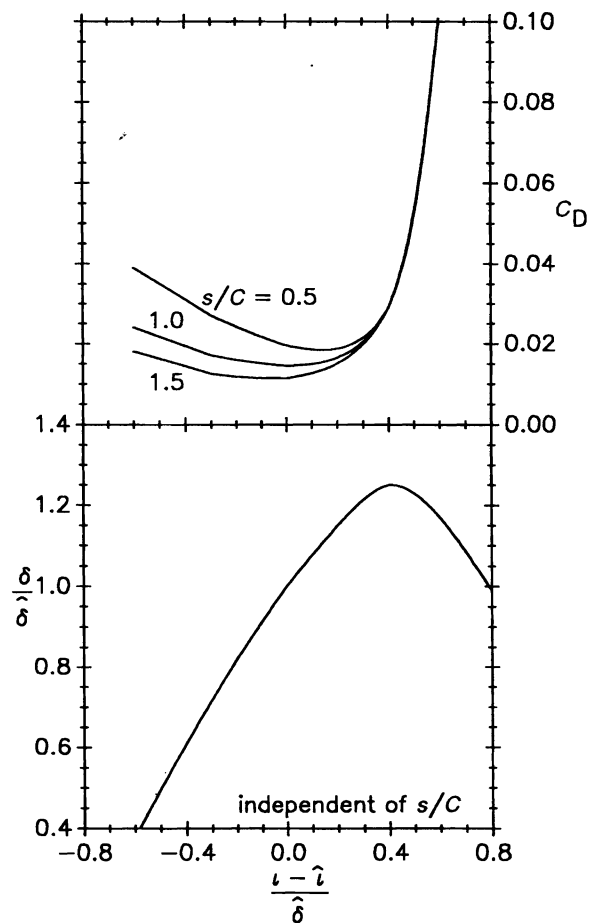


Figure 6.49 Dependence of the normalized flow deflection and generalized drag coefficient on normalized inlet flow angle and pitch-to-chord ratio (from Howell 1942).

The generalized correlations presented in Figure 6.49 give reasonable to very good results. It goes without saying, however, that if deflection data are available for specific blades and vanes – for example, specific data as in Figure 6.43 and as used in Example 6.7, experimental drag and lift data for a specific blade row, or all of these data – such data should be used in lieu of general correlations.

6.11.8. Implementation of General Method

The previous seven sections are integrated, in this section, and the implementation of the method to predict the performance of a single stage using these results is discussed. For the purposes of discussion, the blade angles are assumed to be known as a part of the design process or because the stage has already been built. Blade shapes, heights, chord lengths, pitch, distance to maximum camber, and flow coefficient are also assumed to be known.

Howell (1942, 1945a) developed and demonstrated the overall technique. The method starts with determining the nominal deflection angle $\hat{\delta}$ and nominal deviation $\hat{\xi}$ by using the blade geometry. Next, the nominal flow angles $\hat{\beta}_1, \hat{\beta}_2, \hat{\alpha}_2, \hat{\alpha}_3$, and so on are determined using the nominal deflections and deviations. The nominal incidences \hat{i}_1 and \hat{i}_2 can be found from

$$\hat{\beta}_1 = \beta'_1 - \hat{i}_1 \quad 6.11.108$$

and

$$\hat{\alpha}_2 = \alpha'_2 - \hat{i}_2. \quad 6.11.109$$

The flow coefficient is also known, however, and thus the flow angles can be determined and the blade to flow incidence angles can be found from

$$\beta_1 = \beta'_1 - \iota_1 \quad 6.11.110$$

and

$$\alpha_2 = \alpha'_2 - \iota_2. \quad 6.11.111$$

One can also find ι_1 and ι_2 from

$$\beta_1 = \hat{\beta}_1 - (\iota_1 - \hat{i}_1) \quad 6.11.112$$

$$\alpha_2 = \hat{\alpha}_2 - (\iota_2 - \hat{i}_2). \quad 6.11.113$$

Although the nominal deflection is known, the actual deflection is not. Using Figure 6.49, one can determine the actual deflection and use this to identify the actual flow angles β_2 and α_3 . Thus, all of the flow angles are known, and the flow coefficient and percent reaction can be found. Also, the lift coefficients can be found. Next, the sum of the different drag coefficients can be determined. The ratio of drag to lift can be found, and thus the angle between the drag and lift is known. Finally, the efficiency of the stage can be found from these angles as well as the percent reaction and flow coefficient. Solutions can also be obtained using the software, “COMPRESSORPERF”, which incorporates all of the concepts in this section.

6.12. Summary

The thermodynamics of strictly axial flow compressors and fans was considered in this chapter. The basic operating principle of a compressor or fan is to impart kinetic energy to the incoming air by means of rotating blades and then convert the increase in energy to an increase in total pressure. For a compressor, this high-pressure air enters the combustor, which requires such conditions. For an exhausted fan, this air enters a fan nozzle, which generates thrust. The basic geometries were discussed and hardware parts were identified; the important geometric parameters that affect performance were also defined. The air was seen to flow alternately between rows of rotating rotor blades and stationary stator vanes. Velocity triangles or polygons, which are a means of changing from a rotating to a stationary reference frame and vice versa, were used to analyze such turbomachines. Although the geometries (especially blade shape) and operating performance can be quite different for fans and compressors, the fundamental thermodynamics and fluid mechanics are the same. First, for analysis of the compressors, two-dimensional flow was assumed and the radial components of velocity were assumed to be small. On the basis of these geometric parameters, tools were developed using a control volume approach through which the resulting performance of a stage can be predicted. Continuity, momentum, and energy equations were used to derive equations from which the total pressure ratio, percent reaction, and other parameters could be determined. Incompressible cases were also considered. Rotational speed and blade and vane turning were seen to have strong influences on performance. Although the total pressure ratio of a stage is very important, percent reaction, which usually be somewhat above 50 percent owing to radial variations and compressibility, was identified as a measure of the relative loading of the rotor and stator blade rows. Also, the limiting factors on stage pressure ratio before flow separation from the blades and vanes occurs (which leads to surge) were discussed. These can usually be controlled by prudent designs in which the operating Mach number and the pressure coefficients based on geometry of the blade and vane rows are carefully considered. Also, performance maps were described by which the important operating characteristics of a compressor can accurately and concisely be presented. Although the maps are dimensional they are based on a dimensional analysis of the turbomachine characteristics. Methods of experimentally deriving stage, compressor, and fan maps were discussed. Four of the most important output characteristics on a map are the pressure ratio, efficiency, surge line, and operating line. From a map, for example, if the corrected speed and flow rates are known, the efficiency and pressure ratio can be found. Methods of improving off-design performance were covered such as variable stators and multispool machines. These more complex geometries basically allow the blade rows to operate with low incidence angles over a wide range of conditions, which directly improves the efficiency over the range. A more complex (advanced) streamline analysis method was also used to predict and account for the three-dimensional flows resulting from radial equilibrium. Such an analysis becomes more important as longer blades and vanes are considered. Significant hub-to-tip blade twist and turning variations were seen to be required for longer blades. Finally, because a cascade is made up of a series of airfoils, a method of using lift and drag coefficients of blade cascades and other empirical data was demonstrated for incompressible flow to predict and optimize stage efficiency, including such effects as blade incidence angles. A percent reaction of approximately 50 percent was shown to optimize the efficiency of a stage, although the efficiency does not rapidly deteriorate as the reaction deviates from this value. For incompressible flow, the method gives great insight into how the stage performance and fundamental airfoil (vane or blade) characteristics are related and can be used to maximize the efficiency, for example, with

the proper choice of blade shapes and solidity or as the leading edge incidence increases. Throughout the chapter, design guidelines were presented to make it possible to predict or determine if a stage is operating reasonably.

List of Symbols

A	Area
a	Speed of sound
a	Leading edge to maximum camber length
a	“Constant reaction” coefficient
b	“Constant reaction” coefficient
c	Absolute velocity
c_p	Specific heat at constant pressure
C	Chord length
C_d	Drag coefficient
C_l	Lift coefficient
C_p	Pressure coefficient
D	Diameter
F	Force
g	Gravitational constant
h	Specific enthalpy
i	Radial counter (streamline analysis)
j	Axial counter (streamline analysis)
\dot{m}	Mass flow rate
m	Empirical constant, Eq. 6.11.109
M	Mach number
N	Rotational speed
p	Pressure
\mathcal{P}	Power
\dot{Q}	Heat transfer rate
\dot{Q}	Volumetric flow rate
\mathcal{R}	Ideal gas constant
R	Radius
$\%R$	Percent reaction
r	Radius of circle
s	Blade spacing or pitch
T	Torque
T	Temperature
t	Blade height
u	Specific internal energy
U	Blade velocity
v	Specific volume
w	Relative velocity
\dot{W}	Power
α	Absolute (stator) angle
β	Relative (rotor) angle
$\hat{\chi}_{\alpha\beta}$	Parameter in Eq. 6.11.109
γ	Specific heat ratio
δ	Flow turning angle, deflection
δ	Ratio of pressure to standard pressure

ε	Angle between lift and drag forces
κ	Free vortex constant
ζ	Total pressure loss
η	Efficiency
θ	Ratio of temperature to standard temperature
ι	Incidence angle
ξ	Deviation
ρ	Density
τ	Deflection coefficient
ϕ	Flow coefficient
ω	Rotational speed

Subscripts

a	Axial
abs	In absolute frame (stator)
c	Center of circle
c	Corrected
d	Drag
H	Hub
i	Radial counter (streamline analysis)
j	Axial counter (streamline analysis)
l	Lift
loss	Loss in shaft
m	Mean or average
r	Rotor
rel	In rotating frame (rotor)
s	Stator
sh	Applied to shaft
stall	Separation
stp	Standard conditions
t	Total (stagnation)
T	Tip
u	Tangential
z	Along shaft
0	Upstream of IGV
1,2,3	Positions in stage
2	Inlet to compressor
3	Exit of compressor

Superscripts

'	For the blade
'	Ideal
^	Nominal
^	Normalized radius

Problems

- 6.1** A single stage of a compressor is to be analyzed. It rotates at 12,400 rpm and compresses 120 lbm/s of air. The inlet pressure and temperature are 140

psia and 900 °R, respectively. The average radius of the blades is 8.0 in., and the inlet blade height is 1.15 in. The absolute inlet angle to the rotor is the same as the stator exit angle (18°), and the rotor flow turning angle (δ_{12}) is 17°. The compressor stage has been designed so that the blade height varies and the axial velocity remains constant through the stage. The efficiency of the stage is 88%. The values of c_p and γ are 0.2483 Btu/lbm-°R and 1.381, respectively.

Find the following:

- (a) blade heights at the rotor and stator exits,
- (b) the static pressure at the rotor and stator exits,
- (c) the total pressure ratio for the stage,
- (d) the stator turning angle,
- (e) the required power for the stage,
- (f) the percent reaction for the stage.

- 6.2** A single stage of a compressor is to be analyzed. It rotates at 12,400 rpm and compresses 120 lbm/s of air. The inlet pressure and temperature are 140 psia and 900 °R, respectively. The average radius of the blades is 8.0 in., and the inlet blade height is 1.15 in. The absolute inlet angle to the rotor is the same as the stator exit angle (18°), and the percent reaction is 0.500. The compressor stage has been designed so that the blade height varies and the axial velocity remains constant through the stage. The efficiency of the stage is 88 percent. The values of c_p and γ are 0.2484 Btu/lbm-°R and 1.381, respectively.

Find the following:

- (a) blade heights at the rotor and stator exits,
- (b) the static pressure at the rotor and stator exits,
- (c) the total pressure ratio for the stage,
- (d) the stator turning angle,
- (e) the rotor turning angle,
- (f) the required power for the stage.

- 6.3** A single stage of a compressor is to be analyzed. It rotates at 12,400 rpm and compresses 120 lbm/s of air. The inlet pressure and temperature are 140 psia and 900 °R, respectively. The average radius of the blades is 8.0 in. and the inlet blade height is 1.15 in. The absolute inlet angle to the rotor is the same as the stator exit angle (18°), and the total pressure ratio is 1.200. The compressor stage has been designed so that the blade height varies and the axial velocity remains constant through the stage. The efficiency of the stage is 88 percent. The values of c_p and γ are 0.2484 Btu/lbm-°R and 1.381, respectively.

Find the following:

- (a) blade heights at the rotor and stator exits,
- (b) the static pressure at the rotor and stator exits,
- (c) the stator turning angle,
- (d) the rotor turning angle,
- (e) the required power for the stage.

- 6.4** A stage approximating the size the first stage (rotor and stator) of an older low-pressure compressor operating at Standard temperature and pressure is to be analyzed. It rotates at 7,500 rpm and compresses 153 lbm/s of air. The inlet pressure and temperature are 31.4 psia and 655 °R, respectively. The

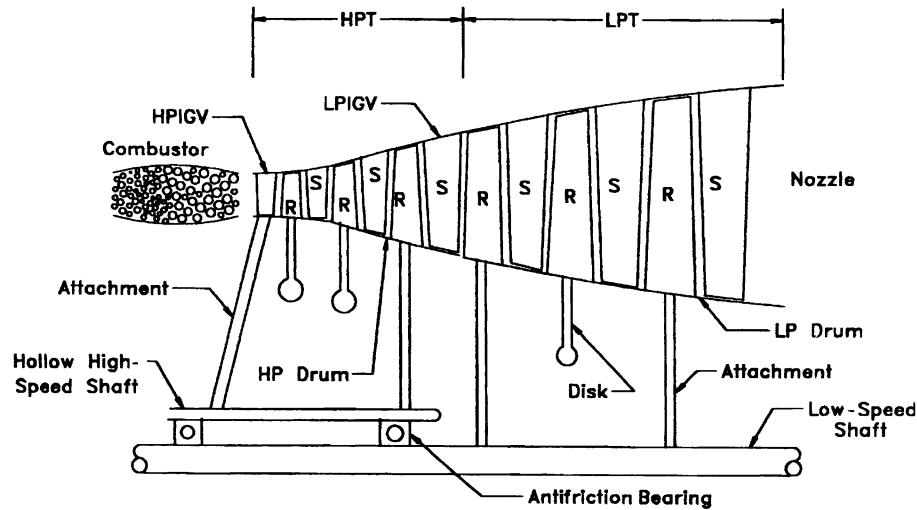


Figure 8.1 Twin-spool turbine.

8.2. Geometry

8.2.1. Configuration

Like a compressor, a turbine comprises a series of stages, all of which derive energy from the fluid. A stage again has two components: a set of rotor blades, which are attached to the disks and shaft, and the stator vanes, which are attached to the engine case. The rotor blades extract energy from the fluid, and the stator vanes ready the flow for the following set of rotor blades.

Many modern engines operate with two spools. Such a design is shown in Figure 8.1. The high-temperature gas leaves the combustor and enters the high-pressure turbine. This component is on the high-speed shaft. A set of inlet guide vanes is sometimes used to ready the flow for the first set of rotor blades. After exiting the high-pressure turbine, the gas enters the low-pressure turbine. This component is on the low-speed shaft. The energy from the low-pressure turbine drives the low-pressure compressor (and fan if present). The high-pressure turbine drives the high-pressure compressor. Because the gas pressure is dropping down the turbine, the gas density decreases down the turbine axis. Thus, the flow areas and blade heights increase down the turbine. Often a set of nonrotating blades is used at the exit of the turbine to ready the flow for the afterburner (if present) or the nozzle. The blades are termed the exit guide vanes (EGV) and differ in design from normal stator vanes. If an afterburner is present, the vanes impart swirl to the flow to encourage mixing. If an afterburner is not present, the vanes straighten the flow for entrance into the nozzle. Finally, although the actual designs for high- and low-pressure stages are different, the same basic thermodynamics, gas dynamics, and design methodology apply to both. For example, larger variations in blade angle and twist are found for a low-pressure turbine than for a high-pressure turbine owing to the larger radius ratio (similar to that for an axial flow compressor) Thus, for the remainder of this chapter, distinctions are not made between the two components.

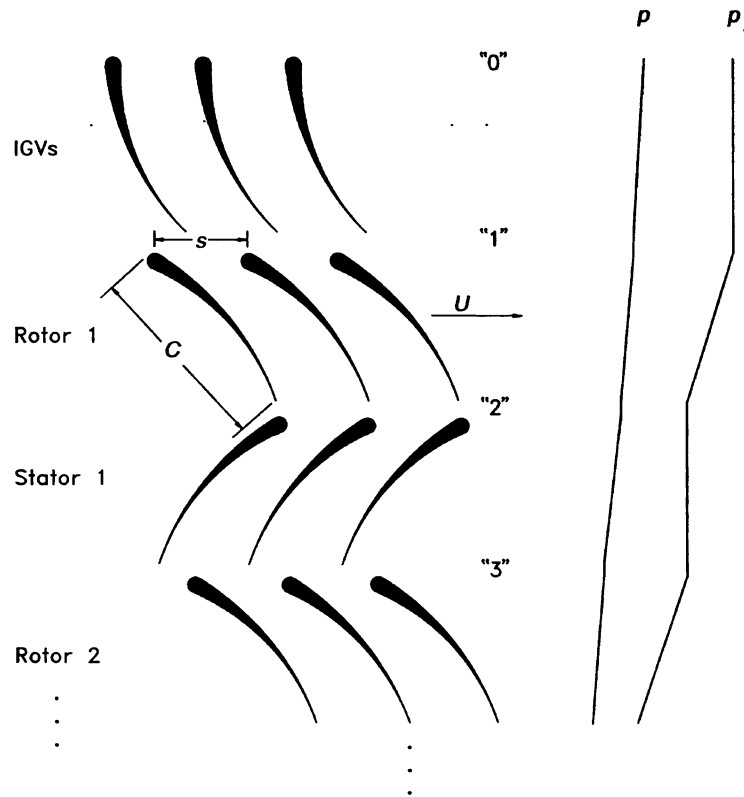


Figure 8.2 Cascade view of blades.

If one were to look at a turbine from the top and consider the geometry to be planar two-dimensional by unwrapping the geometry, a series of cascades would be seen as shown in Figure 8.2. The fluid first enters the inlet guide vanes (if used). Next, it enters the first rotating passage. In Figure 8.2, the rotor blades are shown to be moving with linear velocity U , which is found from $R\omega$, where ω is the angular speed and R is the mean radius of the passage. After passing through the rotor blades, the fluid enters the stator vanes. The fluid is turned by these stationary vanes and readied to enter the second stage beginning with the second rotor blades. In general, the second stage is slightly different in design than the first stage (all of the stages are different). The process is repeated for each stage. In Figure 8.2, turbine component stations 0 through 3 are defined. It is very important not to confuse these with engine station numbers.

As is the case for compressors, an important parameter is the solidity (C/s), which is the inverse of the pitch-to-chord ratio s/C . Again, if the solidity is too large, the frictional losses will be too large. If the solidity is too small, the flow will not follow the blades (slip), and less than ideal power will be derived from the hot gas. Again, for a turbine, typical solidities are unity. For example, for the Pratt & Whitney JT9D, the number of turbine blades on the stages ranges from 66 to 138. For comparison, the turbine exit guide vane (which has a very long chord) has 15 blades.

Also shown in Figure 8.2 are axial pressure profiles down the turbine. Both the total and static pressures are shown. As can be seen, the static pressure decreases across the inlet

guide vanes and also decreases across all of the rotor and stator blades. The total pressure remains approximately constant across the inlet guide vanes and stator vanes but decreases across the rotor blades. Consistent with the approach to compressors, it is the objective for the remainder of this chapter to relate the pressure changes to the geometry of the turbine, that is, to relate the static and total pressure rises and ratios to a given geometry of blades and rotational speed.

Next, a few of the design considerations are discussed. First, as indicated, the temperature is of great concern. Such high temperatures coupled with high rotational speeds lead to high centrifugal stresses in the blades. Thus, not only are the aerodynamics important in the design of blade shapes but so are the developed stresses. As is discussed in this chapter, blade cooling is often used to combat this problem. Second, high efficiencies are of course desirable. However, airflow leakage around the blade tips becomes more important than is the case for a compressor because of the higher pressure drops across the stages and higher temperatures. The clearance between the blade tip and case varies with operating conditions because of the thermal growth of the blades. A large clearance is not desirable because the turbine efficiency drops about 1 percent with each 1 percent of flow across the tip. That is, expanding gas bypasses the turbine stage by flowing from the rotor blade pressure surface to the suction surface in the tip clearance, but no useful work is derived from the flow. However, if the clearance is too small, thermal growth or vibrations can cause a blade rub, which can result in total destruction of the engine. Third, losses also occur owing to viscous shear and shocks. For example, high blade loading produces high velocities on the suction surfaces of the blades; with high velocities, flows can become locally supersonic and form shocks. These shocks drop the total pressure nonisentropically as well as set up separation regions, which further decrease the total pressure. The end result is to reduce the stage efficiency. Finally, flow must be properly directed into the turbine. A uniform flow (velocities, pressures, and temperatures) of gas is desired. For example, if more flow is directed near the blade root, the amount of torque (and thus power) derived from the fluid will be reduced. Also, if hot areas of flow exist at the turbine inlet, early blade failure can result; again such failures can be catastrophic. These and other concerns are discussed further in the chapter. More details can be found in Fielding (2000), Glassman (1972a, 1972b, 1973, 1975), Hawthorne (1964), Horlock (1966), Adamczyk (2000), Kercher (1998, 2000), Han, Dutta, and Ekkad (2000), Dunn (2001), and Shih and Sultanian (2001).

8.2.2. Comparison with Axial Flow Compressors

a. Passage Areas between Blades

Figure 8.3 illustrates the passage shapes of a turbine and compressor. For a turbine cascade, the exit area is less than the inlet area ($A_{\text{exit}} < A_{\text{inlet}}$). Consequently, the passage acts like a nozzle. For comparison, however, the exit area for a compressor cascade is greater than that of the inlet. Thus, the passage acts like a diffuser as previously discussed in Chapter 6.

b. Pressures

The purpose of a turbine is to extract energy from the flow. As a result, the total and static pressures drop through a turbine; that is, the flows are expanding. For comparison, the pressures increase in a compressor. Also, the flows in turbines are usually subsonic. Thus, the trends agree with those for the areas as discussed in the paragraph above. Typical pressure ratios across (inlet to exit) a turbine stage are two.

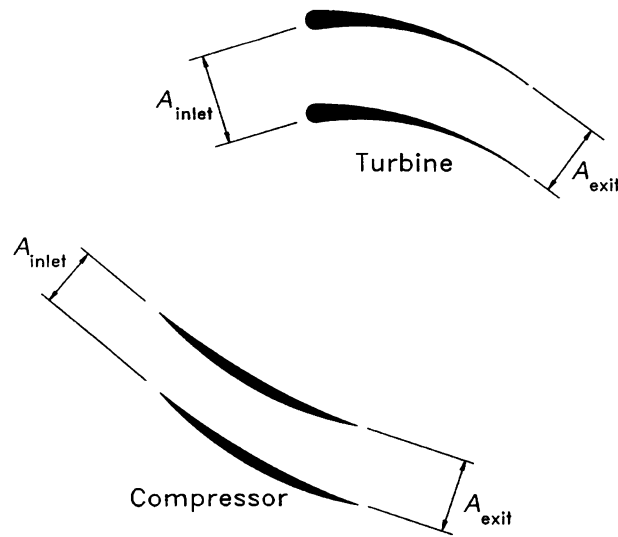


Figure 8.3 Comparison of turbine and compressor passage shapes.

c. Turning Angles

For a turbine the inlet pressure to a stage is greater than the exit pressure. Thus, separation will not occur on the blades because of an adverse pressure gradient. As a result, more expansion can be accomplished by a turbine than compression can be accomplished by a compressor. This means that $(A_{inlet}/A_{exit})_{turbine} > (A_{exit}/A_{inlet})_{compressor}$. Thus, on the basis of Figure 8.3, the turning angle is greater for a turbine cascade than for a compressor cascade. Because each turbine stage has more flow turning than a compressor stage, more energy is extracted per stage than in a compressor.

d. Number of Stages

As just noted, more energy is extracted per stage than in a compressor. Since all of the turbine power is used to drive the compressive devices for a jet engine, the number of turbine stages is less than the number of compressor stages. Power-generation gas turbines have additional stages for the external load, but still the total number of stages is less than for the compressor. The typical ratio of the number of compressor stages to turbine stages is from 2 to 6.

e. Temperatures

The typical inlet temperature to a turbine is currently around 3000 °R, which is now limited from a practical standpoint by the materials properties. For comparison, the hottest temperature realized by a compressor is at the exit and is typically 1400 °R. As discussed in Section 8.4, considerable efforts have been undertaken to increase the turbine inlet temperature limit. One method entails using better materials. A second method involves blade cooling as shown in a typical arrangement depicted in Figure 8.4. Cool air is pumped through a hollow core in the turbine blades to cool them. Sometimes small holes are machined into the blade so that the cool air forms a protective boundary layer between the blade and the hot gas exiting from the combustor. Because of the cooler operating temperatures, compressors do not need such complex geometries.

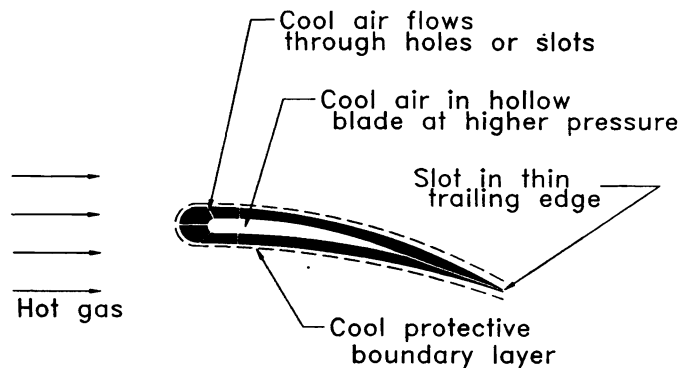


Figure 8.4 Blade cooling.

f. Radii and Blade Height

The air temperature is much higher in a turbine than in a compressor. However, the pressures are comparable. Thus, the density in a turbine is lower than the density in a compressor. The turbine area must be larger than the compressor area to pass the same flow rate.

In estimating the relative sizes, the compressor air flow rate is given by $\dot{m}_c = \rho_c c_a A_c$, whereas that for the turbine is $\dot{m}_t = \rho_t c_a A_t$, which is approximately equal to \dot{m}_c . The density can be found from the ideal gas equation $\rho = \frac{p}{\mathcal{R}T}$. One can now consider the axial Mach number, $M_a = \frac{c_a}{a}$ and realize that $a = \sqrt{\gamma \mathcal{R}T}$. Thus, if γ_c is approximately equal to γ_t , ρ_c is approximately equal to ρ_t and the turbine and compressor Mach numbers are about the same (which is typical). The turbine cross-sectional area is $A_t \approx A_c \sqrt{\frac{T_t}{T_c}}$. Thus, turbine passage areas are typically larger than compressor passage areas by 30 to 50 percent. This is accomplished by making the blade heights larger for a turbine than for a compressor. Typically, owing to the increased blade heights, the hub radius is smaller for the turbine than for a compressor, but not always.

g. Blade Thickness

The thickness of a turbine blade is typically greater than the thickness of a compressor blade. This is the result of three factors. First, the inlet or exit area ratio is larger for a turbine cascade. Second, blade cooling is often used, which, because of the hollow region, requires a thicker blade. And third, to improve the structural soundness or reliability of the blade, the blade must be thicker. Care must be taken in the design of such blades to minimize the “profile” losses and to avoid blocking the flow too much.

h. Shrouding

Unlike compressors, some turbines have “shrouds.” These are circumferential bands that wrap around the outside diameter of the blade tips and lock them together, as shown in Figure 8.5 (turbine blades are often attached to the disk using “fir trees,” as was discussed for some axial flow compressors). Shrouds are used on turbines for four reasons. First, because of the high operating temperatures, the blades are weakened and thus need additional support so they do not fail in the presence of the steady-state forces (or loads) resulting from flow turning. Second, similarly, they need extra support to control blade vibrations, which can lead to blade failure. Third, because more flow turning is used in turbines than in compressors, larger loads occur on a turbine blade than on a compressor

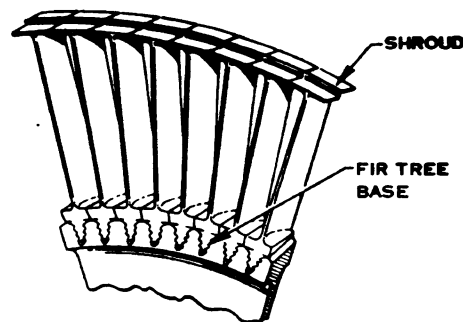


Figure 8.5 Shrouded turbine rotor blades (courtesy of Pratt & Whitney).

blade; once again more structural support is needed. Fourth, again because more flow turning is used, larger pressure changes occur in a turbine stage than in a compressor stage. As a result, flow tends to “leak” around the tip of a turbine blade from the pressure surface to the suction surface, which is similar to the wing-tip vortices on an aircraft wing. These secondary flows reduce the aerodynamic efficiency of a turbine stage; shrouds block these leakages and thus improve the efficiency. Shrouds are used less in modern turbines than in the past.

i. Number of Blades per Stage

Although the blades of a turbine are typically thicker and longer, the solidity of both compressors and turbines is about the same. Thus, the blade spacing is larger for a turbine than for a compressor. However, the hub radius of the blades is typically larger. As a result, approximately the same number of blades is used on a turbine or compressor cascade. As is the case for a compressor, enough blades are needed to minimize separation and direct the flow in the desired direction, but not so many blades should be used that frictional losses become intolerable. Thus, efficiency is maximized by selecting the optimum number of blades. Ainley and Mathieson (1951) and Traupel (1958) postulated the optimum pitch-to-chord ratio correlations that are still often used today. The recommended values are correlated in Figure 8.6 in a format similar to that used for presenting compressor values and are dependent on the exit and deflection flow angles as is true for the compressor.

As is the case for an axial compressor, choosing different numbers of stator vanes and rotor blades for a stage or nearby stages is very important. If the numbers of vanes and blades are equal, a resonance due to fluid dynamic blade interactions can be generated and large blade, disk, and shaft vibrations and noise can result. This reduces the life of the blades and safety of the engine. Blade or vane numbers are often selected as prime numbers (but less so than in the past), but they are always chosen so that common multiple resonances are not excited. Dring et al. (1982) review details of this topic.

j. Efficiency

Overall, the efficiency is slightly larger for a turbine than for a compressor. This results from two opposite effects. Because of the favorable pressure gradient, one would expect the efficiency to be improved more than would be the case for a compressor. However, as a result of the blade cooling and injected cool air (including added turbulence, frictional losses, pressure drops, and enthalpy reduction), a decrease in efficiency would be anticipated. The net effect of the conditions is to improve the efficiency slightly as compared with a compressor.

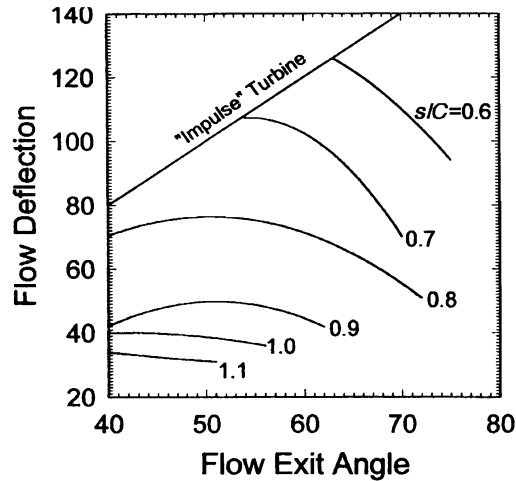


Figure 8.6 Optimum pitch-to-chord ratio (correlated from data of Ainley and Mathleson 1951 and Traupel 1958).

8.3. Velocity Polygons or Triangles

Because energy is being derived from the flow (which results in a pressure drop) and part of the turbine is moving, it is important to be able to understand the complex flow patterns in a turbine. As is the case for a compressor and as is shown in the next section, the pressure drop is directly dependent on the velocity magnitudes and directions in a turbine. The purpose of this section is to present a means for interpreting fluid velocities. That is, since one component rotates and one component is stationary, the velocities must again be related so that the components are compatible.

First consider the inlet guide vanes shown in Figure 8.7.a. The exit flow from the combustor or the inlet flow to the inlet guide vanes is typically aligned with the axis of the engine. The flow velocity relative to the stationary frame (referred to as absolute velocity for the remainder of the book) at the IGV inlet is c_0 . The blade inlet angle is usually aligned with the axis. As the fluid passes through the IGV, it is turned so that the absolute flow velocity at the IGV exit (and the rotor inlet) is c_1 , and it has a flow angle α_1 relative to the axis of the engine. The IGV exit blade angle is α'_1 . If the flow is exactly parallel to the blade at the exit, α_1 and α'_1 are identical. This is usually not true in an actual design, however, owing to slip.

Next consider the inlet to the rotor stage as shown in Figure 8.7.b. However, the rotor blades are rotating around the engine centerline or are moving in the planar two-dimensional plane with absolute velocity U_1 in the tangential direction. Thus, to find the velocity of the fluid relative to the rotating blades, one must subtract the blade velocity vector from the absolute flow vector. This is performed in Figure 8.7.b. The resulting vector is w_1 , and it has a flow angle β_1 relative to the axial direction. It is important to note that the rotor blades have inlet and exit angles (relative to the axial direction) of β'_1 and β'_2 , respectively. Once again, if the relative flow direction matches the blade angles exactly, the values β'_1 and β_1 are the same and the incidence angle is zero. However, this usually does not occur in practice — especially at off-design conditions.

When drawing the polygons, one should always draw the triangles to scale. This not only allows “rough” checking of algebraic computations but provides the capability of

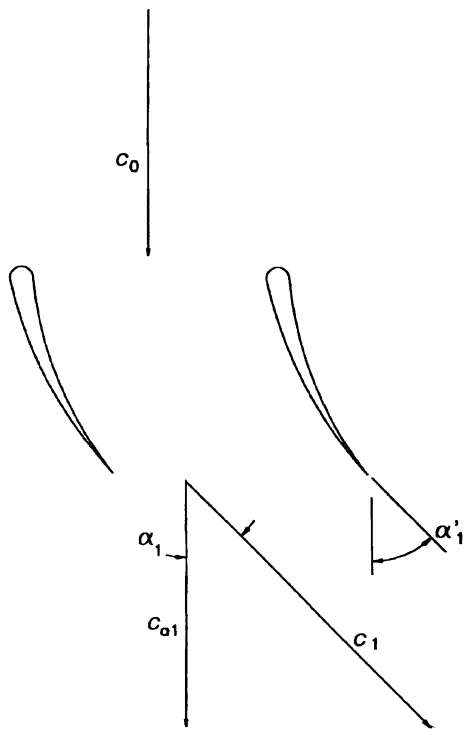


Figure 8.7a Definition of IGV geometry and velocities.

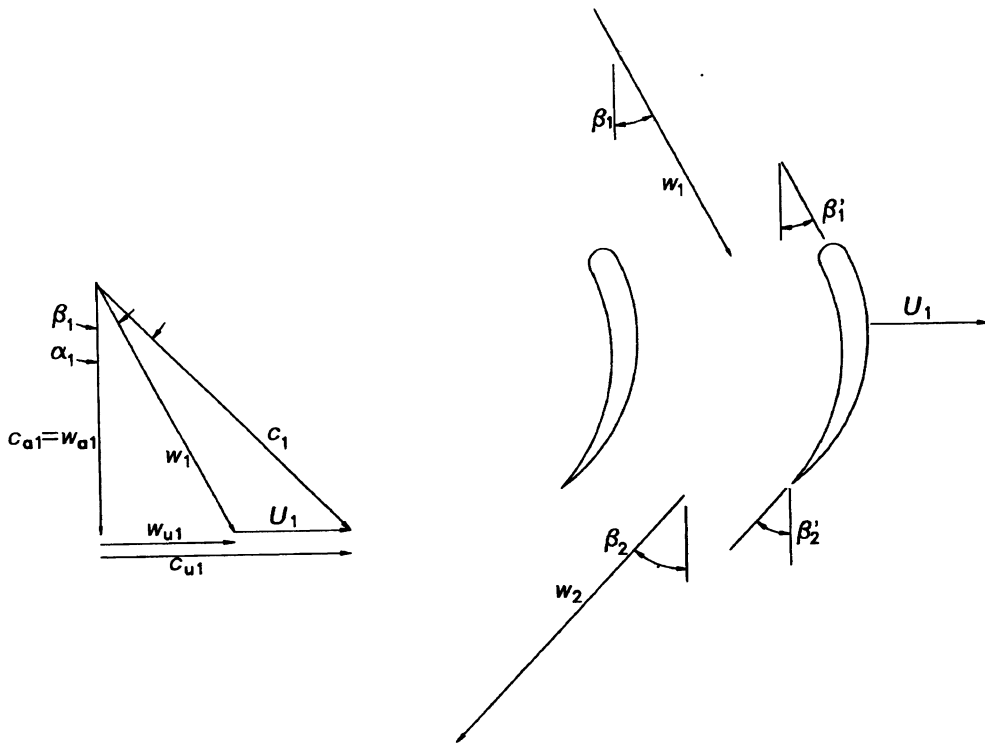


Figure 8.7b Definition of IGV exit and rotor blade inlet and velocity polygons.

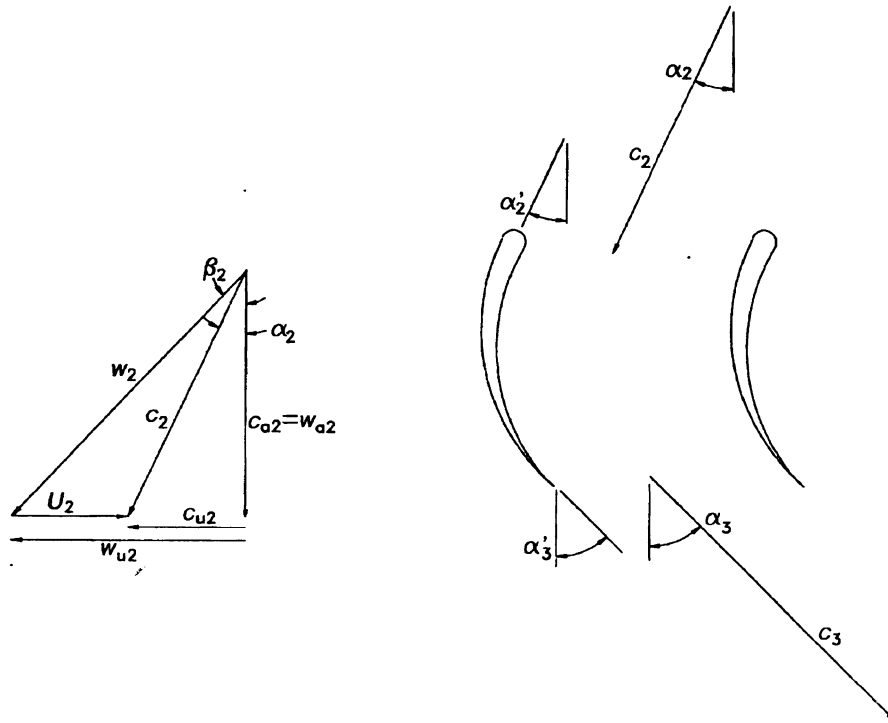


Figure 8.7c Definition of rotor blade exit and stator vane inlet and velocity polygons.

observing the relative magnitudes of the different velocity vectors and the viability of a turbine stage design, as will be discussed in the next section, for example, with the percent reaction. When a compromising situation is observed, it is easier to see how to change the condition by altering geometric parameters by using a scale diagram rather than equations.

One can break the vectors into components as indicated in Figure 8.7.b. As shown, the absolute velocity c_1 has a component in the tangential direction that is equal to c_{u1} and a component in the axial direction that is c_{a1} . Also, the relative velocity, w_1 has components w_{u1} and w_{a1} in the tangential and axial directions, respectively.

Figure 8.7.c shows the velocity polygon for the rotor exit and stator inlet. The exit relative velocity (to the rotor blades) is w_2 , and this velocity is at an angle of β_2 relative to the axial direction. The blade velocity is U_2 and can be vectorially added to w_2 to find the absolute exit velocity c_2 . Note that U_2 and U_1 may be slightly different because the radii at the rotor inlet and exit may be slightly different. The absolute flow angle of c_2 is α_2 relative to the engine axis. Once again, the rotor blade exit angle is β_2' , which may be different from the relative flow angle β_2 owing to slip. Furthermore, the stator vane inlet angle is α_2' and will in general be different from α_2 , indicating nonzero incidence. Also shown in Figure 8.7.c are the components of both w_2 and c_2 in the tangential and axial directions.

The stator exit triangle, which is also the inlet velocity polygon to the next rotor blades, is shown in Figure 8.7.d. The absolute velocity is c_3 , which makes an angle of α_3 to the axial direction. Once again, the flow absolute flow angle α_3 will in general be different from the absolute stator vane angle α_3' . The next rotor blade velocity at the inlet is U_3 , and the

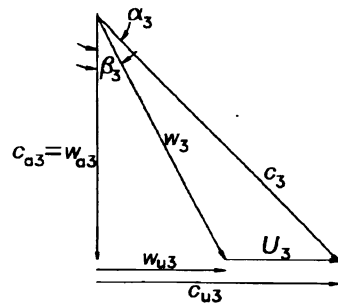


Figure 8.7d Definition of stator vane exit and rotor blade inlet and velocity polygons.

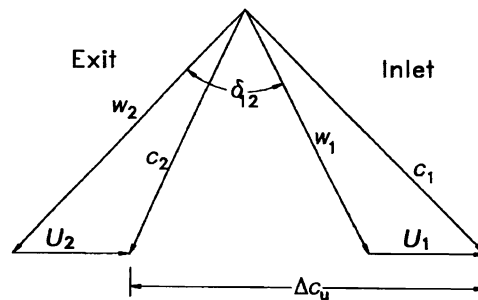


Figure 8.7e Combined rotor blade polygon.

relative velocity (to the next rotor blades) is w_3 , which makes a relative angle of β_3 to the axis. The methodology described here can be used for all of the downstream stages.

As shown in Figure 8.7.e, the polygons for the rotor entrance and exit are often combined to form one polygon. As is true for a compressor and demonstrated in the next section, the power of the stage is directly related to the change in absolute tangential velocity if the radius is approximately constant ($\Delta c_u = c_{u1} - c_{u2}$). Thus, by combining the two triangles, one can easily observe the change graphically.

Finally, a side view of a turbine first stage is presented in Figure 8.8. In this figure, the average blade radii (R) and blade heights (t) are defined.

Once again, a consistent sign notation is needed, and this notation will be the same as that used for axial flow and centrifugal compressors. First, all positive tangential velocities are to the right. Thus, rotor blades always move to the right with positive velocity U . Second, all angles are measured relative to the axial direction, and positive angles are considered to be counterclockwise.

In Table 8.1, the trends of the velocity magnitudes, flow cross-sectional areas, and pressures across the different components are shown. As can be seen, the static pressure decreases across both the stator and rotor blades because the relative velocities across both increase. Also, as the absolute and relative velocities across the IGVs increase, the static pressure decreases. Details of these trends are discussed in the next section.

8.4. Single-Stage Energy Analysis

This section summarizes the equations so that the velocities can be related to the derived power, pressure drop, and other important turbine characteristics. The derivation is performed using a “mean-line” control volume approach described in detail in Appendix I

Table 8.1. Axial Flow Turbine Component Trends

	Absolute Velocity	Relative Velocity	Area	p	p_t
IGV	increases	increases	decreases	decreases	constant
Rotor	decreases	increases	decreases	decreases	decreases
Stator	increases	increases	decreases	decreases	constant

for a single stage (rotor and stator). Figure 8.9 shows a single stage. The objective is to relate the inlet and exit conditions to the property changes.

8.4.1. Total Pressure Ratio

In Appendix I, the continuity, moment of momentum, and energy equations are used. For the delivered shaft power, they result in (Eq. I.2.17)

$$\dot{W}_{sh} = \dot{m}[U_2 c_{u2} - U_1 c_{u1}], \quad 8.4.1$$

and for the total pressure drop they result in (Eq. I.2.26)

$$\frac{p_{t2}}{p_{t1}} = \left[\frac{[U_2 c_{u2} - U_1 c_{u1}]}{\eta_{12} c_p T_{t1}} + 1 \right]^{\frac{\gamma}{\gamma-1}}. \quad 8.4.2$$

Thus, knowing the velocity information of a rotor from polygons and the efficiency, one can find the total pressure drop. A few subtle differences exist between the equations for the compressor and turbine. For example, the power or work output from the turbine stage is less than the ideal value, but it is more for a compressor. Also, the pressure ratio (p_{t2}/p_{t1}) is less than unity but is greater than 1 for a compressor.

8.4.2. Percent Reaction

An important characteristic for an axial flow turbine is the percent reaction. This relation again approximates the relative loading of the rotor and stator and is given by (Eq. I.2.32)

$$\% R = \frac{1}{1 + \left[\frac{c_2^2 - c_1^2}{w_1^2 - w_2^2} \right]}. \quad 8.4.3$$

Thus, for compressible flow the percent reaction of the stage can be related to the absolute and relative velocities at the inlet and exit of the rotor.

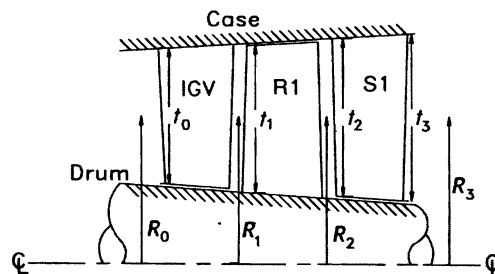


Figure 8.8 Side view of first stage.

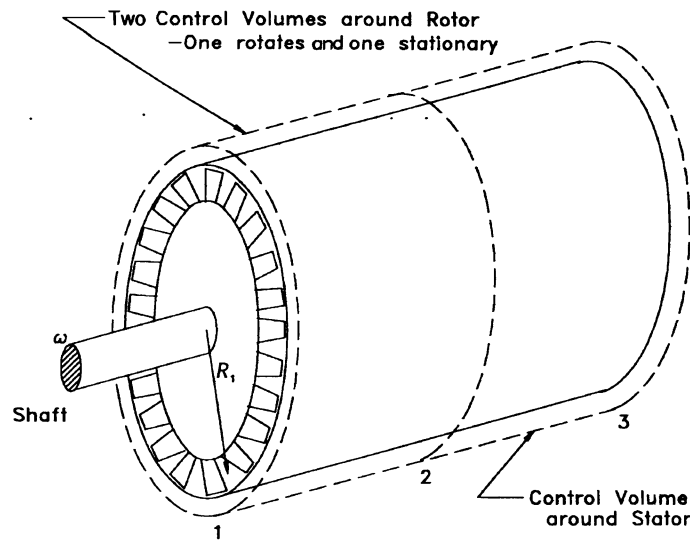


Figure 8.9 Control volume definition for turbine stage.

8.4.3. Incompressible Flow (Hydraulic Turbine)

For comparison, one may wish to find the delivered power, pressure drop, and percent reaction of a turbine with an incompressible fluid. This condition would apply to a hydraulic turbine. From Appendix I (Eqs. I.2.34, I.2.37, I.2.39),

$$\dot{W}_{sh} = \dot{m}[U_2 c_{u2} - U_1 c_{u1}] \quad 8.4.4$$

$$p_{t2} - p_{t1} = \frac{\rho}{\eta_{12}} [U_2 c_{u2} - U_1 c_{u1}] \quad 8.4.5$$

$$\%R = \frac{1}{1 + \left[\frac{c_2^2 - c_1^2}{w_1^2 - w_2^2} \right]} \quad 8.4.6$$

The percent reaction for incompressible and ideal flow is given by (Eq. I.2.41)

$$\%R = \frac{p_2 - p_1}{p_{t3} - p_{t1}} \quad 8.4.7$$

For example, typical axial flow turbine stages have percent reactions of about 0.50. For a nonideal hydraulic turbine, the percent reaction dictates that approximately half of the enthalpy drop occurs in the rotor and half in the stator. For an ideal hydraulic turbine, this also means that half of the pressure drop occurs in the rotor and half in the stator. This implies that the force “loads” on the rotor and stator blades are about the same. For a compressible flow turbine, however, it merely means that half of the enthalpy increase occurs in the rotor and half in the stator. The pressure drops may not be exactly the same – even for the ideal case – but they are approximately the same. Regardless, if the percent reaction differs greatly from 0.5, a large pressure drop occurs in either the stator ($\%R < 0.5$) or the rotor ($\%R > 0.5$). For a turbine, if a large pressure drop occurs, choking or partial choking of the cascade is likely. The resulting efficiency will be less than optimum because of the associated losses. Furthermore, as is observed for a compressor, when the blade heights

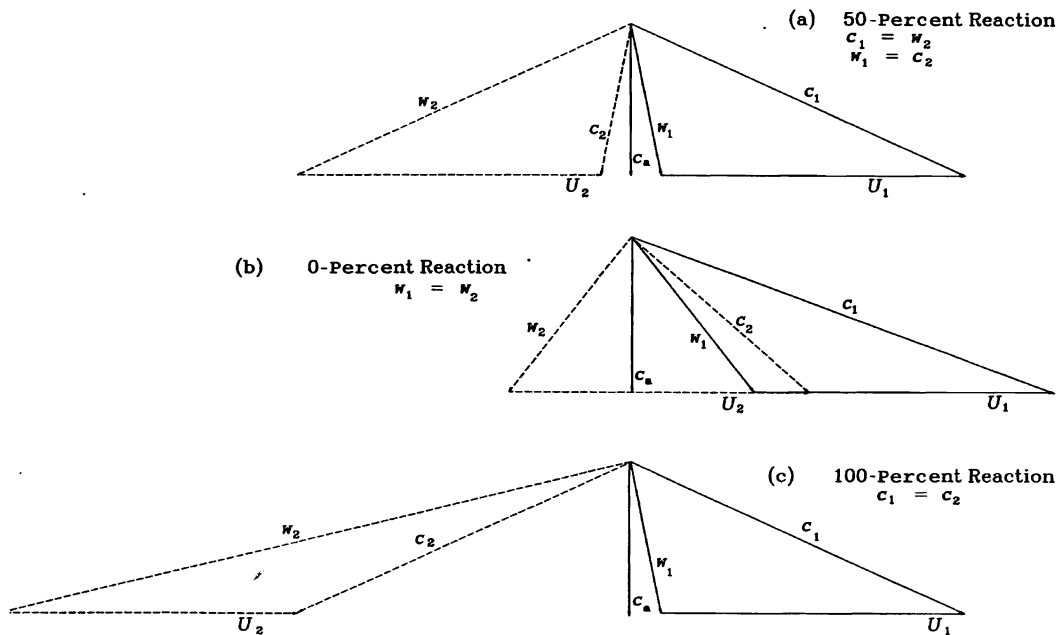


Figure 8.10 Three special cases of velocity polygons.

are significant relative to the radius, the reaction increases from hub to tip. For a turbine, if the percent reaction is less than zero, the stage operates as a compressor. Thus, the mean line reaction must be chosen such that the reaction at the hub is greater than zero.

8.4.4. Relationships of Velocity Polygons to Percent Reaction and Performance

As occurs for a compressor stage, the velocities dictate the percent reaction. Three special cases are shown in Figure 8.10. In particular, sets of velocity polygons (rotor inlet and exit) for 100-, 0-, and 50-percent reaction turbine stages are shown for the same axial velocity. Of particular interest is the set of polygons for a 50-percent reaction (Fig. 8.10.a). For this case, the inlet and exit polygons are similar triangles but reversed. If the polygons are drawn to scale, one can easily observe if the percent reaction is close to 50-percent simply by examining the symmetry of the triangles. Also, the polygons can be used to make preliminary predictions on performance trends due to geometry changes. For example, one can see from Figure 8.10.c that, for a turbine stage that originally operated close to a 50-percent reaction, if $|\delta_{12}|$ is increased and other parameters are constant, the percent reaction increases – eventually going to 100 percent. Such a 100-percent reaction turbine is often called a “reaction turbine,” and all of the pressure drop occurs in the rotor. Also, one can see that, if α_1 is increased (with other parameters held constant), the percent reaction decreases – eventually going to 0 percent (Fig. 8.10.b). This is often called an “impulse turbine,” and all of the static pressure drop takes place in the stator.

Moreover, for general trends, one can examine both the governing equations and velocity polygons for variations in the absolute inlet angle α_1 , the rotor flow turning angle δ_{12} , the rotational speed N , and the mass flow rate (or axial velocity component) \dot{m} (or c_a). The

Table 8.2. Geometric and Operating Condition Effects on Turbine Parameters

Decrease in	Percent Reaction, %R	Total Pressure Ratio, p_{t3}/p_{t1}	Power Output
Absolute inlet angle, α_1	increase	decrease	increase
Rotor flow turning angle, $ \delta_{12} $	decrease	increase	decrease
Rotational speed, N	decrease	increase	decrease
Axial velocity component, c_a	increase	decrease	increase

resulting effects on the stage total pressure ratio and percent reaction can be determined. A matrix of general trends is presented in Table 8.2.

Example 8.1: A stage of approximately the same size as one of the first stages (rotor and stator) of a high-pressure turbine is to be analyzed. It rotates at 8000 rpm and expands 280 lbm/s (8.704 slugs/s) of air. The inlet pressure and temperature are 276 psia and 2240 °F, respectively. The average radius of the blades is 17.5 in., and the inlet blade height is 2.12 in. The absolute inlet flow angle to the rotor is the same as the stator exit flow angle (65°), and the rotor flow turning angle (δ_{12}) is 75°. The stage has been designed so that the blade height varies and the axial velocity remains constant through the stage. The efficiency of the stage is 85 percent. The values of c_p and γ are 0.2920 btu/lbm-°R and 1.307, respectively, which are based on the resulting value of T_2 . The following details are to be found: blade heights at the rotor and stator exits, the static and total pressures at the rotor and stator exits, the stator turning angle, the Mach numbers at the rotor and stator exits, the derived power from the stage, and the percent reaction for the stage. Note that this turbine can be compared with the compressor in Example 6.1. Both turbomachines are from the same engine and are operating at about the same pressure.

SOLUTION:

Velocity polygons will be used to obtain the solution. Before proceeding, a few preliminary calculations are needed.

$$U = R\omega = (17.5/12)(8000 \times 2\pi/60) = 1222 \text{ ft/s.}$$

$$A_1 = \pi D_1 t_1 = \pi(2 \times 17.5)(2.12)/144 = 1.619 \text{ ft}^2$$

For $p_1 = 276$ psia and $T_1 = 2240$ °F = 2700 °R the ideal gas equation yields

$$\rho_1 = 0.008577 \text{ slug/ft}^3.$$

$$\text{Next, } c_{a1} = \frac{\dot{m}}{\rho_1 A_1} = \frac{8.704}{0.008577 \times 1.619} = 626.9 \text{ ft/s.}$$

$$\text{Finally, } a_1 = \sqrt{\gamma \mathcal{R} T_1} = \sqrt{1.307 \times 53.35 \times 2700 \times 32.17} = 2461 \text{ ft/s}$$

Rotor Inlet

Next, refer to Figure 8.11.a, which is the velocity polygon for the rotor inlet.

$$\text{First } c_1 = \frac{c_{a1}}{\cos \alpha_1} = \frac{626.9}{\cos(65^\circ)} = 1483 \text{ ft/s.}$$

$$\text{Also } c_{u1} = c_1 \sin \alpha_1 = 1483 \sin(65^\circ) = 1344 \text{ ft/s;}$$

thus,

$$\beta_1 = \cot^{-1} \left[\frac{c_{a1}}{c_{u1} - U_1} \right] = \cot^{-1} \left[\frac{626.9}{1344 - 1222} \right] = 11.07^\circ,$$

$$\text{And } w_1 = \frac{c_{a1}}{\cos \beta_1} = \frac{626.9}{\cos(11.07^\circ)} = 638.8 \text{ ft/s.}$$

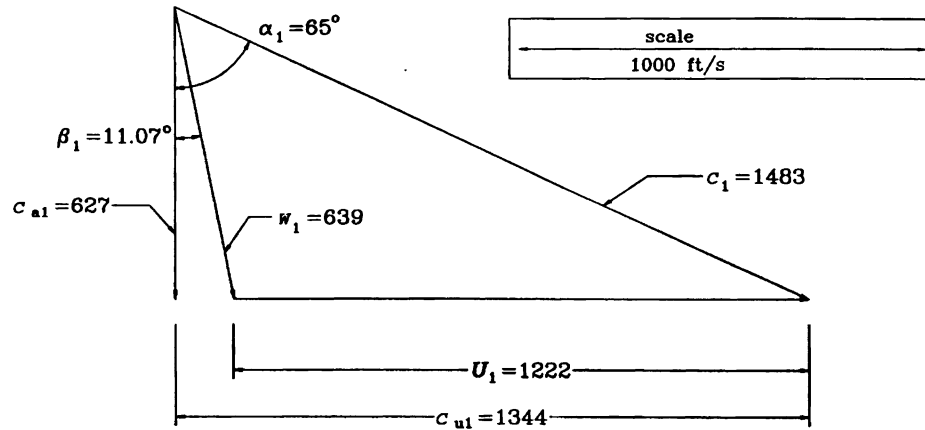


Figure 8.11a Velocity polygon for rotor inlet for Example 8.1.

Thus, the Mach number in the rotating frame is

$$M_{1\text{rel}} = \frac{w_1}{a_1} = \frac{638.8}{2461} = 0.2596.$$

Flow is thus subsonic in the rotating frame, and shock formation in the inlet of the rotor should not be a problem. Next, in the absolute frame,

$$M_{1\text{abs}} = \frac{c_1}{a_1} = \frac{1483}{2461} = 0.6028.$$

Flow therefore is also subsonic in the stationary frame, and shock formation in the exit of the previous stator should also not be a problem. Additionally,

$$\frac{T_{t1}}{T_1} = 1 + \frac{\gamma - 1}{2} M_{1\text{abs}}^2 = 1 + \frac{0.307}{2} 0.6028^2 = 1.056$$

$$T_{t1} = 1.056 \times 2700 = 2851 \text{ }^\circ\text{R} = 2391 \text{ }^\circ\text{F}$$

$$\text{Finally } \frac{p_{t1}}{p_1} = \left[\frac{T_{t1}}{T_1} \right]^{\frac{\gamma}{\gamma-1}} = [1.056]^{\frac{1.307}{0.307}} = 1.260$$

$$p_{t1} = 1.260 \times 276 = 347.7 \text{ psia.}$$

Rotor Exit and Stator Inlet

For the rotor exit or stator inlet velocity polygon, refer to Figure 8.11.b. Because the rotor flow turning angle is known (and for a turbine rotor blade it will be negative), one can find the relative exit angle from:

$$\beta_2 = \beta_1 + \delta_{12} = 11.07 - 75.00 = -63.93^\circ.$$

Also, because the axial velocity is constant through the stage,

$$c_{a2} = c_{a1} = 626.9 \text{ ft/s.}$$

$$\text{Next, } w_2 = \frac{c_{a2}}{\cos \beta_2} = \frac{626.9}{\cos(-63.93^\circ)} = 1427 \text{ ft/s}$$

$$\text{and } w_{u2} = c_{a2} \tan \beta_2 = 626.9 \tan(-63.93^\circ) = -1281 \text{ ft/s;}$$

thus,

$$\alpha_2 = \cot^{-1} \left[\frac{c_{a2}}{U + w_{u2}} \right] = \cot^{-1} \left[\frac{626.9}{1222 - 1281} \right] = -5.43^\circ,$$

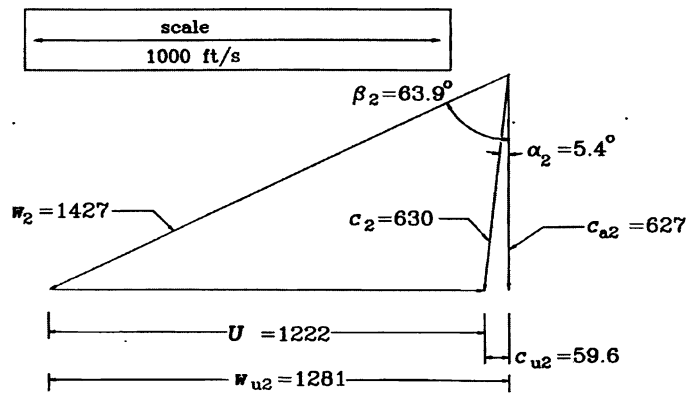


Figure 8.11b Velocity polygon for rotor exit and stator inlet for Example 8.1.

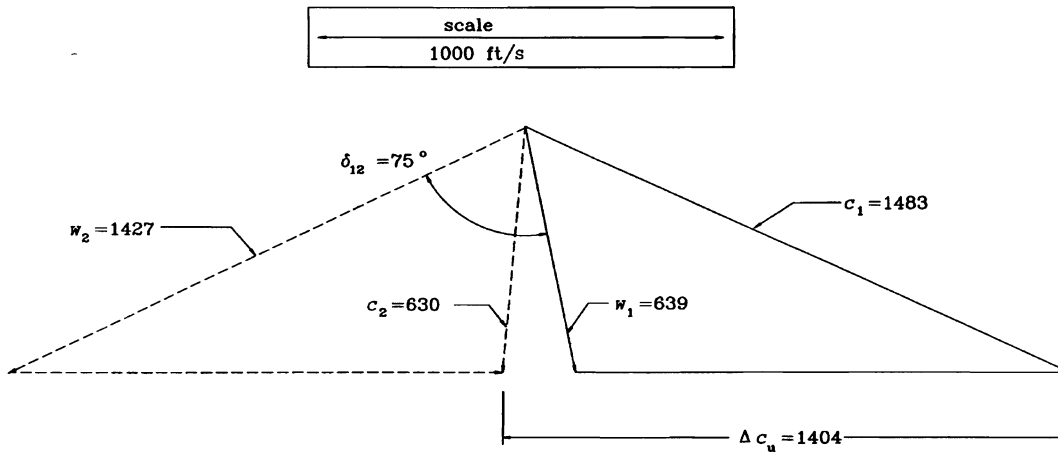


Figure 8.11c Combined rotor velocity polygons for Example 8.1.

$$c_2 = \frac{c_{a2}}{\cos \alpha_2} = \frac{626.9}{\cos(-5.43^\circ)} = 629.7 \text{ ft/s,}$$

$$\text{and } c_{u2} = U + w_{u2} = 1222 - 1281 = -59.6 \text{ ft/s.}$$

Next, the moment of momentum equation can be used to yield

$$\begin{aligned} h_{t2} - h_{t1} &= U(c_{u2} - c_{u1}) = 1222(-1404) \\ &= -1,715,329 \text{ ft}^2/\text{s}^2. \end{aligned}$$

The quantity $\Delta c_u = (c_{u2} - c_{u1}) = -1404 \text{ ft/s}$ is shown in Figure 8.11.c. Also, note the negative sign for Δh_t indicating that power is derived from the fluid. From the energy equation, one can find

$$\begin{aligned} \frac{p_{t2}}{p_{t1}} &= \left[\frac{(h_{t2} - h_{t1})}{\eta_{12} c_p T_{t1}} + 1 \right]^{\frac{\gamma}{\gamma-1}} \\ &= \left[\frac{-1,715,329}{0.85 \times 0.2920 \times 2851 \times 778.16 \times 32.17} + 1 \right]^{\frac{1.307}{0.307}} = 0.6480, \end{aligned}$$

$$\text{and thus } p_{t2} = 0.6480 \times 347.7 = 225.3 \text{ psia.}$$

<ANS.

Note that the total pressure change in this turbine is much larger than the change in total pressure in the compressor in Example 6.1.

$$\text{Also, } T_{t2} - T_{t1} = \frac{h_{t2} - h_{t1}}{c_p} = \frac{-1,715,329}{0.2920 \times 778.16 \times 32.17} = -234.7^\circ\text{R},$$

and so $T_{t2} = 2616^\circ\text{R} = 2156^\circ\text{F}$.

$$\text{Now } T_2 = T_{t2} - \frac{c_2^2}{2c_p} = 2616 - \frac{629.7^2}{2 \times 0.2920 \times 778.16 \times 32.17} = 2589^\circ\text{R} = 2129^\circ\text{F}.$$

$$\text{Next } a_2 = \sqrt{\gamma \mathcal{R} T_2} = \sqrt{1.307 \times 53.35 \times 2589 \times 32.17} = 2410 \text{ ft/s}.$$

Thus, the Mach number in the rotating frame is

$$M_{2\text{rel}} = \frac{w_2}{a_2} = \frac{1427}{2410} = 0.5921. \quad < \text{ANS}$$

Flow is thus subsonic in the rotating frame, and shock formation in the exit of the rotor should not be a problem. Next, in the absolute frame,

$$M_{2\text{abs}} = \frac{c_2}{a_2} = \frac{629.7}{2410} = 0.2613. \quad < \text{ANS}$$

Flow is therefore also subsonic in the stationary frame, and shock formation in the inlet of the stator should not be a problem either. Using the absolute Mach number yields

$$\frac{p_{t2}}{p_2} = \left[1 + \frac{\gamma - 1}{2} M_{2\text{abs}}^2 \right]^{\frac{\gamma}{\gamma - 1}} = \left[1 + \frac{0.307}{2} 0.2613^2 \right]^{\frac{1.307}{0.307}} = 1.045,$$

and so $p_2 = 225.3/1.045 = 215.5 \text{ psia}$. < ANS

Next, from the ideal gas law for $p_2 = 215.5 \text{ psia}$ and $T_2 = 2589^\circ\text{R}$,

$$\rho_2 = 0.006986 \text{ slug/ft}^3,$$

and since $\dot{m} = \rho_2 c_{a2} A_2$,

$$A_2 = \frac{\dot{m}}{\rho_2 c_{a2}} = \frac{8.704}{0.006986 \times 626.9} = 1.987 \text{ ft}^2.$$

Also $A_2 = \pi D_2 t_2$,

$$\text{and so } t_2 = \frac{A_2}{\pi D_2} = \frac{1.987 \times 144}{\pi \times 2 \times 17.5} = 2.603 \text{ in}. \quad < \text{ANS}$$

Note that this is larger than the rotor inlet height because of the compressibility of the fluid. Next, the input stage power can be found from

$$\dot{W}_{\text{sh}} = \dot{m}(h_{t2} - h_{t1}) = 8.704 \times (-1,715,329)/550 = -27145 \text{ hp}. \quad < \text{ANS}$$

For comparison, the power for one of the last stages of the high-pressure compressor (Example 6.1) is only 6712 hp. The percent reaction can be found from

$$\%R = \frac{1}{1 + \left[\frac{c_2^2 - c_1^2}{w_1^2 - w_2^2} \right]} = \frac{1}{1 + \left[\frac{629.7^2 - 1483^2}{638.9^2 - 1427^2} \right]} = 0.4742. \quad < \text{ANS}$$

This is a reasonable value for the percent reaction.

Stator Exit

Refer to Figure 8.11.d for the stator exit velocity polygon. Once again, the axial velocity is constant through the stage, and so

$$c_{a3} = c_{a2} = c_{a1} = 626.9 \text{ ft/s}.$$

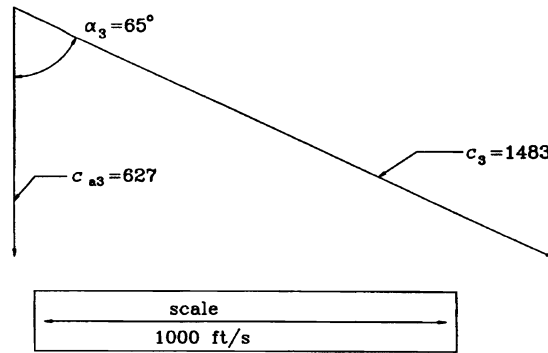


Figure 8.11d Velocity polygon for stator exit for Example 8.1.

Also, the absolute exit angle is given, $\alpha_3 = 65^\circ$, and thus

$$c_3 = \frac{c_{a3}}{\cos \alpha_3} = \frac{626.9}{\cos(65^\circ)} = 1483 \text{ ft/s.}$$

The turning angle of the stator can be found from

$$\delta_{23} = \alpha_3 - \alpha_2 = 65 + 5.43 = 70.43^\circ.$$

Thus, the turning angle for the stator vane is approximately that of the rotor blade as one would expect for a percent reaction of about 0.50. For the stator,

$$T_{13} = T_{12} = 2616^\circ\text{R.}$$

$$T_3 = T_{13} - \frac{c_3^2}{2c_p} = 2616 - \frac{1483^2}{2 \times 0.2920 \times 778.16 \times 32.17} = 2465^\circ\text{R.}$$

Furthermore $a_3 = \sqrt{\gamma \mathcal{R} T_3} = \sqrt{1.307 \times 53.35 \times 2465 \times 32.17} = 2352 \text{ ft/s.}$

Thus, the Mach number in the absolute frame is

$$M_{3\text{abs}} = \frac{c_3}{a_3} = \frac{1483}{2352} = 0.6308. \quad <\text{ANS}$$

Flow is therefore also subsonic in the stationary frame, and shock formation in the exit of the stator should not be a problem. Since the absolute Mach number is known,

$$\frac{p_{13}}{p_3} = \left[1 + \frac{\gamma - 1}{2} M_{3\text{abs}}^2 \right]^{\frac{\gamma}{\gamma - 1}} = \left[1 + \frac{0.307}{2} 0.6308^2 \right]^{\frac{1.307}{0.307}} = 1.287.$$

Also, for the stator, $p_{13} = p_{12} = 225.3 \text{ psia,}$

and so $p_3 = 225.3/1.287 = 175.1 \text{ psia.}$

<ANS

From the ideal gas law, for $T_3 = 2465^\circ\text{R}$ and $p_3 = 175.1 \text{ psia,}$

$$\rho_3 = 0.005958 \text{ slug/ft}^3,$$

and so $\dot{m} = \rho_3 c_{a3} A_3$

$$A_3 = \frac{\dot{m}}{\rho_3 c_{a3}} = \frac{8.704}{0.005958 \times 626.9} = 2.330 \text{ ft}^2.$$

Moreover, $A_3 = \pi D_3 t_3,$

$$\text{and so } t_3 = \frac{A_3}{\pi D_3} = \frac{2.330 \times 144}{\pi \times 2 \times 17.5} = 3.052 \text{ in.}$$

<ANS

Once again, note that this is larger than the stator inlet height because of the compressibility of the fluid. Also observe that all of the blade height changes are

much larger for this turbine than for the compressor in Example 6.1. Thus, all of the variables of interest have been found.

8.5. Performance Maps

8.5.1. Dimensional Analysis

Experimental performance curves or “maps” are usually used that are similar to those for a compressor to provide a working medium for a turbine engineer. These provide an engineer with a quick and accurate view of the conditions at which the machine is operating and what can be expected of the turbine if the flow conditions are changed. Similitude is derived in Appendix I for turbines, and results are presented in this section. Of primary concern is the total pressure ratio of a turbine; namely, p_{t5}/p_{t4} or p_{t4}/p_{t5} (Eqs. I.3.3, I.3.7., I.3.8.):

$$p_{t4}/p_{t5} = \mathcal{f} \left\{ \frac{\dot{m}\sqrt{\theta_{t4}}}{\delta_{t4}}, \frac{N}{\sqrt{\theta_{t4}}} \right\} = \mathcal{f} \{ \dot{m}_{c4}, N_{c4} \}, \quad 8.5.1$$

where

$$\delta_{t4} = p_{t4}/p_{stp} \quad 8.5.2$$

and

$$\theta_{t4} = T_{t4}/T_{stp} \quad 8.5.3$$

and the subscript stp refers to the standard conditions and t4 refers to the inlet total conditions. Similarly, for the efficiency, one finds (Eqs. I.3.6, I.3.7, I.3.8)

$$\eta = \mathcal{g} \left\{ \frac{\dot{m}\sqrt{\theta_{t4}}}{\delta_{t4}}, \frac{N}{\sqrt{\theta_{t4}}} \right\} = \mathcal{g} \{ \dot{m}_{c4}, N_{c4} \}. \quad 8.5.4$$

Again, note that the two independent parameters (\dot{m}_{c4} and N_{c4}) are not truly dimensionless. The first is called the “corrected” mass flow and has dimensions of mass flow, whereas the second is called the “corrected” speed and has dimensions of rotational speed. Note that for a given engine at a given operating condition, the “corrected” values for a turbine and compressor are markedly different because of the significantly different reference or inlet conditions.

8.5.2. Mapping Conventions

Figure 8.12.a presents a typical turbine map. Data are taken in a dedicated turbine test facility similar to a compressor facility. However, for the case of a turbine, high-pressure (“blowdown”) air is expanded through the turbine and energy is derived from the turbine. Thus, a load is placed on the shaft. Static and total pressures and temperatures are measured between stages as well as the flow rate and derived power. The pressure and temperature ratios are found and the efficiency is calculated as follows:

$$\eta_t = \frac{1 - \left[\frac{T_{t5}}{T_{t4}} \right]}{1 - \left[\frac{p_{t5}}{p_{t4}} \right]^{\frac{\gamma-1}{\gamma}}}. \quad 8.5.5$$

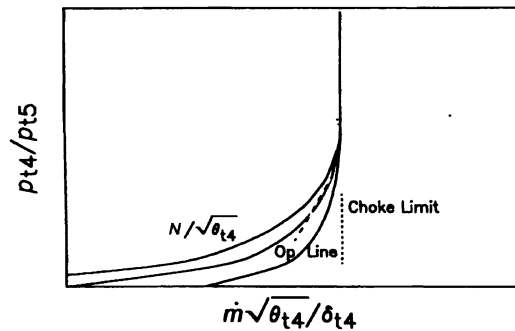


Figure 8.12a Typical turbine map – primary form.

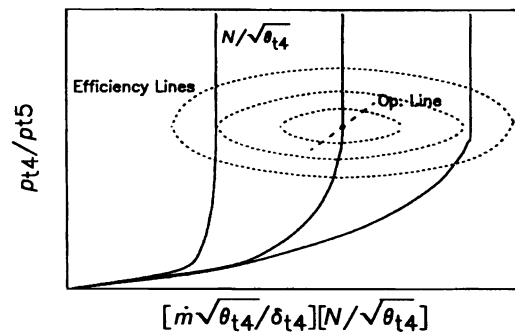


Figure 8.12b Typical turbine map – alternative form.

The pressure ratio is plotted versus the corrected mass flow with the corrected speed as a second parameter. Also shown in this figure is the so-called choke line. This condition occurs when the pressure ratio grows so large across the turbine that the flow becomes sonic at one or more of the stage exits and the flow is thus choked. This condition basically limits the airflow rate through the entire engine. Note that, because of the favorable pressure gradient in a turbine, massive stall, and, therefore surge, are not present.

One problem with the presentation in Figure 8.12.a is the congestion of data near the choke line (and this is where most turbines operate). An alternative form of presentation is given in Figure 8.12.b. Here the corrected mass flow is multiplied by the corrected speed so that each speed line has a different choke line. Also shown in this figure are lines of constant efficiency. The typical design point of an engine is near the peak efficiency point. Thus, as one changes conditions from the design point, the efficiency decreases. Finally, shown in Figures 8.12.a and 8.12.b is the operating line. This line passes through the design point and represents the different conditions at which an engine typically operates.

Lastly, up to this point maps have been considered for the entire turbine. Typically, as is the case for a compressor, the same techniques are applied to a variety of combinations during the development stage. For example, one would have a map for only the low-pressure turbine and another for only the high-pressure turbine. Each stage of the engine will also have a map as well as the hub, pitch, and tip regions of each stage to enable the design of particular regions of a turbine to be improved. The maximum efficiencies are typically 88 percent to 90 percent for modern engines. Tables 6.3 and 7.3 list characteristics of some turbines from modern engines that complement the compressor information. One



Figure 8.13 Turbine rotor blade failure due to excessive temperatures (courtesy of Rolls-Royce).

interesting note from these tables is that, for high by pass turbofans (large mass flow rates), many low-pressure turbine stages are required to deliver the needed power to the fan even though the pressure ratios for the fans are relatively low.

8.6. Thermal Limits of Blades and Vanes

As indicated in Chapters 2 and 3, the thermodynamic efficiency and net power output of the overall engine can be improved by increasing the turbine operating temperature. However, the material composition of the turbine limits the safe operation of the engine. Excessive temperatures can lead to catastrophic blade failures, as shown in Figure 8.13 (also note the fir tree attachment to the disk). With failures such as these, blades can be thrown through the engine case and into the aircraft.

An historical view of the maximum turbine temperature limit is shown in Figure 8.14. As can be seen, the limit has steadily increased over the years. Until about 1960, increases in the temperature limit were due strictly to enhancements in material characteristics. However, around 1960 the slope of the line in the figure increases significantly. At that time, air cooling of the blades came into more widespread use. Since the early 1960s, improvements have been realized owing both to advances in heat transfer enhancement and material characteristics. However, the current limit is still well below the typical stoichiometric temperature of modern fuels. Currently, considerable research is being conducted in materials, including ceramics and composites, and better heat transfer mechanisms to increase the limit further.

“Blade cooling” is often used to reduce the temperature of the blades. Three different types of cooling are used. All three bleed “cool,” high-pressure air from the compressor. This air is directed into both stator vanes and rotor blades, as shown in Figure 8.15. More

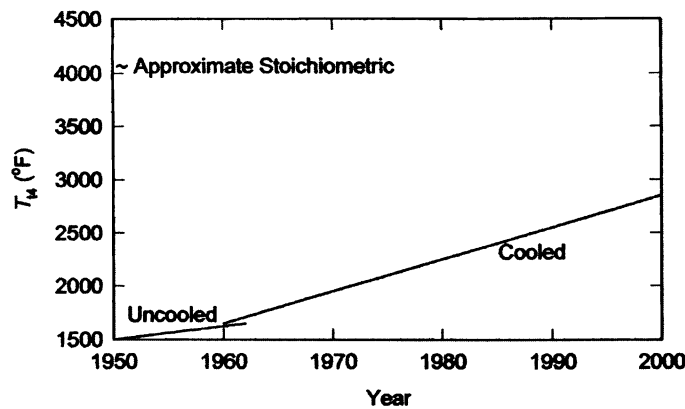


Figure 8.14 History of Turbine inlet temperature history.

details about the prediction and measurement of these effects can be found in Kercher (1998, 2000), Han et al. (2000), Dunn (2001), and Shih and Sultanian (2001).

8.6.1. Blade Cooling

The first type of blade cooling to be discussed is internal or convection cooling. For this type of cooling, cool air is pumped through the inside of the blades and the material is cooled by forced convection on the inside surface and by conduction through the blade. A schematic for this method is shown in Figure 8.16.a. Overall, for this type of cooling, high-velocity cool air scrubbing the inside surface is desirable. Also, a large surface area on the inside is preferable; thus, for many designs, roughened internal “microfins” are utilized, as can be seen in Figure 8.16.b. The internal flow paths are also shown in Figure 8.16.b. For this blade, cool air is pumped into the blade at the root and makes multiple passes before exiting.

The second type of cooling is termed film cooling. In this method, air is pumped out of the blade (Fig. 8.4 and 8.17) at different locations along the blade – but particularly at the leading edge. This cool air provides a cool protective boundary layer along the blade so that the high-temperature gas does not come in contact with the blade. Many arrangements have been chosen for the injection holes. Overall, for this type of cooling enough air is needed to cool the blades; however, the turbine efficiency decreases significantly with increasing bleed air. Thus, bleeding too much air is detrimental.

The third type of blade cooling is transpiration cooling. In this approach, a wire cloth or wire mesh is used for the exterior of the blade and air is leaked uniformly through it

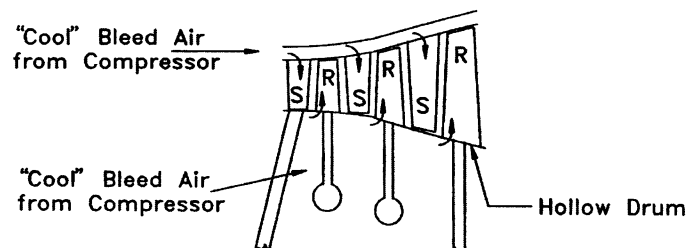


Figure 8.15 Cooling of turbine components using “cool” air from compressor.

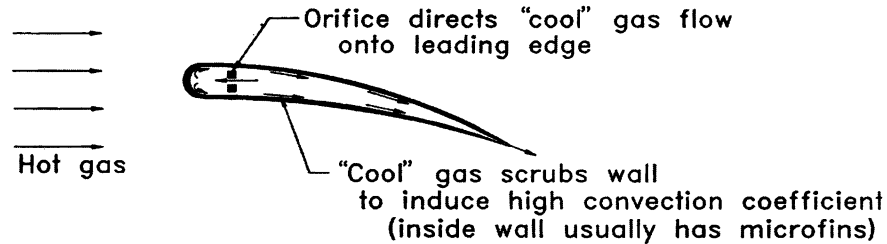


Figure 8.16a Impingement-cooled leading edge; convection-cooled pressure and suction surfaces; chordwise fins in midchord region.

as shown in Figure 8.18. This type tends both to cool the surface and provide a protective layer. However, once again, too much cooling will tend to decrease the turbine efficiency markedly.

Also, combinations of these three types of cooling are often used. For example, in Figure 8.19 a combination of internal and film cooling is used. Convection cooling is used near the leading edge (called impingement cooling), and air is injected into the freestream at a few locations along the blade. One can also note the shrouding and fir tree on this blade.

Overall, blade cooling is a very complex and expensive solution to increasing the turbine inlet temperature. Manufacturing of blades with internal passages is not an easy or inexpensive process. Also, the hollow blades are weaker than their solid counterparts. Furthermore, ducting the cool air from the compressor to the turbine without losses is a complicated design problem. For these reasons, any large improvements in the future in turbine operating temperature will probably result from advances in blade material.

8.6.2. Blade and Vane Materials

Although blade cooling can be used to reduce the temperatures, heat transfer mechanisms limit the blade temperatures that can be obtained in such hostile environments. Thus, considerable effort has been made to improve the material characteristics. Nickel-based alloys containing chromium-cobalt are common materials for modern turbine blades. Turbine disks are typically made from a nickel-based alloy.

Two types of blades are usually used. First, a conventionally cast blade is a myriad of crystals. Such a blade has multidirectional mechanical properties – that is, the blades are strong in all directions. However, because of the boundaries between the crystals, the strength is compromised and blade failures usually occur at these boundaries. Such failures are typically due to long-term high stress levels accompanied by creep caused by the centrifugal and fluid forces, fatigue due to the high-frequency blade-pass frequencies, or corrosion resulting from the high temperatures and combustion products. Yet, these blades are relatively inexpensive (compared with the process described in Section 8.6.3) and find applications in sections in which the temperatures are not high.

A second type that is used is the directionally solidified blade. During the manufacturing process, the blade is cooled so that it comprises many long or columnar crystals. The blade has a dominant axis along which the blade demonstrates excellent strength properties. For rotating blades, this axis is chosen along the blade length owing to the high tensile stresses that result from the centrifugal forces. This type of blade is usually used in the first stages of a turbine because of the extreme temperatures. A photograph of such a blade is presented in Figure 8.20



Figure 8.16b Split Pratt & Whitney rotor blade showing cooling passages and flow paths (photo by R. Flack; Split blade courtesy of Pratt & Whitney).

A third type that is under development is the “single crystal” blade, which, as its name implies, is a blade that, during the manufacturing process, cools as a single crystal. This blade type does not have any crystal boundaries and has multidirectional mechanical properties, making it ideal for turbine applications. As noted in Section 8.6, ceramics and composites are also currently being developed for turbine applications.

8.6.3. *Blade and Vane Manufacture*

The manufacture of intricate turbine blades, as shown in Figure 8.16.b, is a very complex process. It is accomplished by the practice known as the investment or lost-wax process. It is about a fourteen-step process as follows:



Figure 8.17 Film Cooling on a Rolls-Royce nozzle inlet guide (courtesy of Rolls-Royce).

1. A two-piece die is made that is an exact (very accurate) “negative” of the eventual blade shape. This die will be used thousands of times.
2. If the eventual blade is hollow, a ceramic core in the exact shape of the internal passages is precisely placed in the die. The ceramic core is of course a “negative” of the passages.
3. The die is filled with a hot paraffin-based wax (liquid), and the wax is allowed to cool and harden. Waxes are chosen so that they do not shrink upon cooling.
4. The die is separated and the wax piece is removed. The wax is now an exact replica of the eventual metal blade. If the eventual blade is hollow, the ceramic core is still in the wax replica.

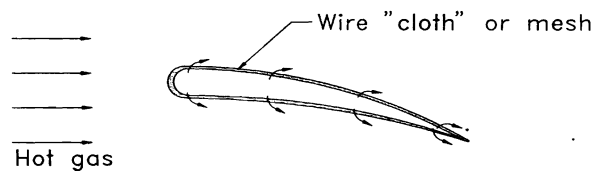


Figure 8.18 Transpiration cooling.

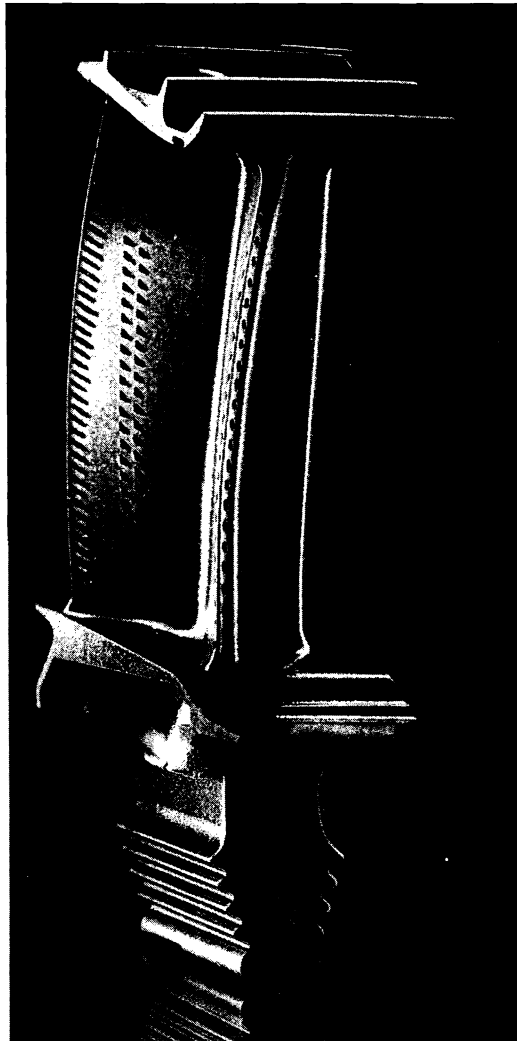


Figure 8.19 Combined film and convection cooling on a Rolls-Royce turbine rotor blade (courtesy of Rolls-Royce).

5. The wax blade is coated (by dipping, spraying, or both) with a slurry and then stucco with multilayers. A silica, alumina, or other ceramic “flour,” or a combination of these are typically used to create the hard stucco shell.
6. The wax inside of the stucco shell is melted and escapes through an exit hole. If the blade is to be hollow, the ceramic core remains accurately in place in the stucco shell.
7. The stucco shell, which is heat resistant, is filled with the blade material and the blade material is allowed to cool.
8. The stucco shell is removed from the blade by air or sand blasted.
9. If a hollow core is present, the ceramic core is removed by immersion in a caustic solution that dissolves the internal ceramic core.

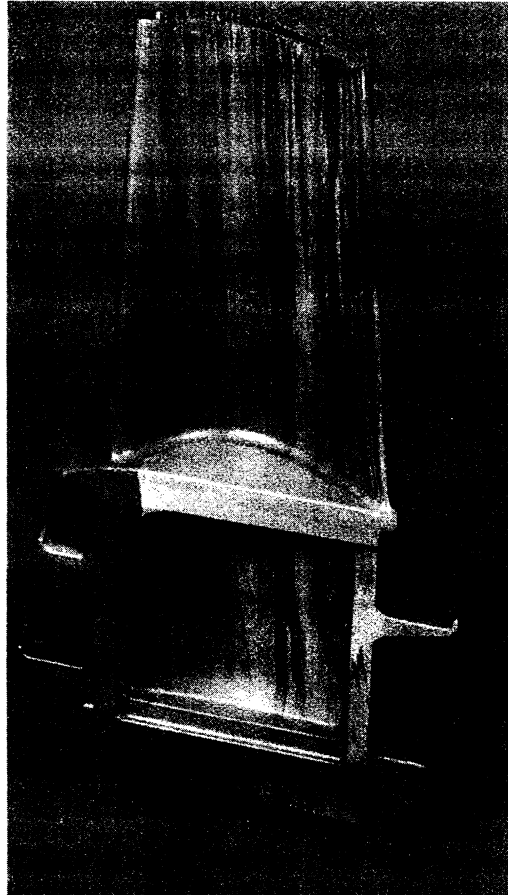


Figure 8.20 Howmet directionally solidified blade for a General Electric gas turbine (courtesy GE Power Systems).

10. Finishing or trimming is accomplished by removing any metal used for holding the blades in place.
11. The blades are inspected by X ray and fluorescing surface die for internal and surface defects. If minor imperfections are found, they are repaired. If major imperfections are found, the blade is discarded.
12. Some blades are coated with a very thin film of a poor heat conductor.
13. Any surface holes for film cooling are “drilled” using precise, electrochemical, electrodischarge, waterjet, or laser machining.
14. Some machining may be needed on the root (e.g., a fir tree) for placement on the wheel or drum. After this expensive and long multistep process, the blades are ready for installation.

8.7. Streamline Analysis Method

In the thermodynamic and gas dynamic analyses in Section 8.4 the flows in the turbine are assumed to be two-dimensional (axial and tangential), and any radial distributions

or velocity components are ignored. However, because the ratios of blade height to hub diameter for most of these machines are not small and centrifugal forces are large, three-dimensional flows result; that is, radial flows can result. As is the case for axial compressors, significant radial variations in parameter profiles will result when the tip radius is approximately 1.1 times the hub radius or greater.

As done for axial compressors, a streamline analysis method can be used to predict the three-dimensional behavior of the flow due to the centrifugal forces acting on the fluid elements. The control volume forms of the continuity, moment of momentum, and energy equations are again applied to streamline bundles, and radial equilibrium is used along with the appropriate boundary conditions.

The incompressible method is nearly identical to that covered in detail in Chapter 6 and, as a result, will not be considered in detail in this chapter. One difference is in the energy equation and the definition of efficiency. For example, Eq. 6.I.11 does not apply to a turbine and should be replaced by

$$\dot{W}_{ji} = Q_i \eta_{ji} \left[p_{j+1i} - p_{ji} + \frac{1}{2} \rho (c_{j+1i}^2 - c_{ji}^2) \right]. \quad 8.7.1$$

The remainder of the equations are identical for axial flow turbines and compressors. The application of the equations and solution methods is the same as before.

8.8. Summary

The thermodynamics of a strictly axial flow turbine were considered in this chapter. The purpose of the turbine is to extract energy (enthalpy) from the fluid to drive the compressive devices; thus, the actual operation of a turbine is the opposite of that of a compressor. The remaining enthalpy is used to generate thrust in the nozzle. As in an axial flow compressor, the air was seen to flow alternately between rows of rotating rotor blades and stationary stator vanes. Geometries and hardware were discussed, and the important geometric parameters were defined. Comparisons were made with axial compressors, and several major differences in blade and other designs and operating conditions were discussed, most of which result from the pressure drop through the turbine (as compared with a pressure rise for a compressor) and the high inlet temperatures. Velocity triangles or polygons were once again used to analyze the turbomachines. In the initial analysis of turbines, two-dimensional flow was postulated and the radial components of velocity were assumed to be small. From the known geometric parameters, working equations were derived through which to predict the resulting derived power, pressure ratios, and percent reactions using a control volume approach (continuity, momentum, and energy equations). The fundamental equations are very similar to those for an axial flow compressor, but their application to turbines is significantly different. Rotational speed and blade and vane turning were seen to be very important to the overall performance. The total power of a stage is a major consideration since this is used to drive the compressive devices, and percent reaction was identified as a measure of relative loading of the rotor and stator blade rows, which should be about 50 percent. Because of the favorable pressure gradient (pressure drop), separation does not pose the same problem for a turbine that it does for a compressor. Axial flow turbine stages were found to operate with much larger blade turning and pressure differences than axial flow compressors; thus, fewer turbine stages are needed in an engine. However, because of the pressure drop, a turbine stage can choke. Performance maps (derived from dimensional analysis) were also described by which the important operating characteristics of a turbine

can accurately and concisely be presented using similarity parameters. The data for a turbine map are best presented in a slightly different format than for a compressor. Four of the most important output characteristics are the pressure ratio, efficiency, operating line, and choke line. From a map, for example, if the speed and flow rates are known, the efficiency and pressure ratio can be found. From these maps, choking was seen to be a serious problem in turbines and needs to be carefully addressed in stage design. Next, over the past decades turbine inlet temperatures have increased markedly, thus potentially reducing the integrity of the turbine blades. Developments in new materials and methods of cooling the turbine blades were covered: convection, film, and transpiration cooling. Blade materials and material structures have also improved over the past decades, allowing higher burner exit temperatures. The manufacturing of turbine blades is complex and costly, particularly for hollow blades, and was discussed. Lastly, more complex streamline analysis methods for single stages were discussed to account for the three-dimensional flows resulting from radial equilibrium. These analysis approaches disclose that radial variations result, as they do for axial flow compressors, when the blade heights are significant. Throughout the chapter, turbine design guidelines were presented to facilitate prediction or determination of the reasonable stage operation.

List of Symbols

A	Area
a	Speed of sound
c	Absolute velocity
c_p	Specific heat at constant pressure
C	Chord length
D	Diameter
g	Gravitational constant
h	Specific enthalpy
\dot{m}	Mass flow rate
M	Mach number
N	Rotational speed
p	Pressure
Q	Volumetric flow rate
\mathcal{R}	Ideal gas constant
R	Radius
$\%R$	Percent reaction
s	Blade spacing
T	Temperature
t	Blade height
U	Blade velocity
w	Relative velocity
\dot{W}	Power
α	Absolute (stator) angle
β	Relative (rotor) angle
γ	Specific heat ratio
δ	Flow turning angle
δ	Ratio of pressure to standard pressure
η	Efficiency
θ	Ratio of temperature to standard temperature

ρ	Density
ω	Rotational speed

Subscripts

a	Axial
abs	In absolute frame (stator)
c	Compressor
c	Corrected
i	Radial counter (streamline analysis)
j	Axial counter (streamline analysis)
rel	In rotating frame (rotor)
sh	Applied to shaft
stp	Standard conditions
t	Total (stagnation)
t	Turbine
u	Tangential
0	Upstream of IGV
1,2,3	Positions
4	Inlet to turbine
5	Exit of turbine

Subscripts

'	For the blade
---	---------------

Problems

- 8.1** A single stage (rotor and stator) of a high-pressure turbine is to be analyzed. It rotates at 11,000 rpm and expands 105 lbm/s of air. The inlet pressure and temperature are 207 psia and 1700 °R, respectively. The average radius of the blades is 10.0 in., and the inlet blade height is 1.25 in. The absolute inlet flow angle to the rotor is the same as the stator exit flow angle (55°), and the rotor flow turning angle (δ_{12}) is 45°. The stage has been designed so that the blade height varies and the axial velocity remains constant through the stage. The efficiency of the stage is 83 percent. The values of c_p and γ are 0.2662 Btu/lbm-°R and 1.347, respectively. Find the following:
- blade heights at the rotor and stator exits,
 - the static pressure at the rotor and stator exits,
 - total pressure ratio across the stage,
 - the stator flow turning angle,
 - the derived power from the stage,
 - the percent reaction for the stage.
- 8.2** A single stage (rotor and stator) of a high-pressure turbine is to be analyzed. It rotates at 13,200 rpm and expands 100 lbm/s of air. The inlet pressure and temperature are 256 psia and 2100 °R, respectively. The average radius of the blades is 11.0 in., and the inlet blade height is 1.10 in. The absolute inlet flow angle to the rotor is the same as the stator exit flow angle (65°), and the total pressure ratio is 0.65. The stage has been designed so that the blade height varies and the axial velocity remains constant through the stage.

The efficiency of the stage is 87 percent. The values of c_p and γ are 0.2761 Btu/lbm-°R and 1.330, respectively.

Find the following:

- (a) blade heights at the rotor and stator exits,
- (b) the static pressure at the rotor and stator exits,
- (c) rotor flow and stator flow turning angles,
- (d) the derived power from the stage,
- (e) the percent reaction for the stage.

8.3 A single stage (rotor and stator) of a high-pressure turbine is to be analyzed. It rotates at 10,000 rpm and expands 100 lbm/s of air. The inlet pressure and temperature are 256 psia and 2100 °R, respectively. The average radius of the blades is 11.0 in., and the inlet blade height is 1.10 in. The absolute inlet flow angle to the rotor is the same as the stator exit flow angle (50°), and percent reaction is 0.50. The stage has been designed so that the blade height varies and the axial velocity remains constant through the stage. The efficiency of the stage is 87 percent. The values of c_p and γ are 0.2776 Btu/lbm-°R and 1.328, respectively. Find the following:

- (a) blade heights at the rotor and stator exits,
- (b) the static pressure at the rotor and stator exits,
- (c) rotor flow and stator flow turning angles,
- (d) the derived power from the stage,
- (e) the total pressure ratio across the stage:

8.4 An axial flow turbine stage rotates at 10,000 rpm with a mean radius of 11 in. and a blade height of 1.10 in. The efficiency of the stage is 87 percent, and 100 lbm/s of air pass through the stage. The absolute flow angle into the rotor is 50°, which is the same as the absolute flow angle out of the stator. The rotor turning angle is 25°. Assume $\gamma = 1.30$. The inlet static pressure is 256 psia, and the inlet static temperature is 2100 °R.

- (a) What is the percent reaction?
- (b) What is the total pressure ratio?
- (c) What is the power derived from the fluid (hp)?
- (d) What is the stator blade turning angle?

8.5 A single stage of an axial flow turbine is to be analyzed. The shaft rotates at 11,000 rpm, and the average radius is 10 in. The inlet blade height is 1.25 in., and the inlet pressure and temperature are 207 psia and 1700 °R, respectively. The specific heat at constant pressure is 0.266 Btu/lbm-°R, and the specific heat ratio is 1.347. The absolute angle at the rotor inlet is 55° (relative to the axial direction), and the rotor turning angle is 45°. The mass flow rate through the stage is 105 lbm/s. The axial velocity remains constant at 586 ft/s. The total pressure ratio of the stage is 0.737, and the percent reaction is 0.532.

- (a) Find the stage efficiency.
- (b) Is this a good design? Why or why not? Be specific.
- (c) If the design is not good, what would you do to improve it? Be specific.

8.6 A single stage (rotor and stator) of a high-pressure turbine is to be analyzed. It rotates at 8000 rpm and expands 200 lbm/s of air. The inlet pressure and temperature are 222 psia and 1800 °R, respectively. The average radius of

the blades is 13.0 in., and the inlet blade height is 1.20 in. The absolute inlet flow angle to the rotor is the same as the stator exit flow angle (50°), and the rotor flow turning angle (δ_{12}) is 58° . The stage has been designed so that the blade height varies and the axial velocity changes by +3.0 percent across each blade row (not stage). The total pressure ratio of the stage is 0.688. The values of c_p and γ are 0.268 Btu/lbm- $^\circ$ R and 1.343, respectively. Find the following:

- (a) blade heights at the rotor and stator exits,
- (b) the static pressure at the rotor and stator exits,
- (c) efficiency of the stage,
- (d) the stator flow turning angle,
- (e) the derived power from the stage,
- (f) the percent reaction for the stage.

- 8.7** Initially an axial flow turbine stage operates with a 50-percent reaction. However, in a later test the mass flow rate decreases. If the absolute inlet angle to the rotor and the absolute exit angle from the stator remain constant, the relative rotor turning angle remains the same, the inlet conditions remain constant, and the rotational speed remains the same, what happens to the reaction? Explain with polygons.
- 8.8** Initially, an axial flow turbine stage operates with a 50-percent reaction. However, in a later test the rotational speed decreases. If the absolute inlet angle to the rotor and the absolute exit angle from the stator remain constant, the relative rotor turning angle remains the same, and the inlet axial velocity component remains the same, what happens to the reaction? Explain with polygons.
- 8.9** A single stage (rotor and stator) of a low-pressure turbine is to be analyzed. It rotates at 7000 rpm and expands 250 lbm/s of air. The inlet pressure, temperature, and density are 120 psia, 1200 $^\circ$ R, and 0.00839 slug/ft³, respectively. The inlet total pressure and total temperature are 179.3 psia and 1338 $^\circ$ R, respectively. The resulting axial velocity at the inlet is 758.1 ft/s; the speed of sound at the inlet is 1681 ft/s. The average radius of the blades is 14.0 in., and the inlet blade height is 2.00 in. The resulting tangential blade velocities are 855.2 ft/s. The absolute inlet flow angle to the rotor is the same as the stator exit flow angle ($+55^\circ$), and the rotor flow turning angle ($|\delta_{12}|$) is 73° . The stage has been designed so that the blade height varies and the axial velocity decreases by 2.5 percent across each blade row (not stage). The total pressure ratio of the stage is 0.5573. The values of c_p and γ are 0.2528 Btu/lbm- $^\circ$ R and 1.372, respectively. Find the following:
- (a) the sign of δ_{12} ,
 - (b) the velocity polygons,
 - (c) the efficiency of the stage,
 - (d) the stator flow turning angle,
 - (e) the percent reaction for the stage,
 - (f) the derived power from the stage.
- 8.10** Initially an axial flow turbine stage operates with a 50-percent reaction. However, in a later test the rotor blades are replaced so that the relative flow turning in the rotor is less. If the absolute inlet angle to the rotor, the absolute exit

angle from the stator, the mass flow rate, and the rotational speed remain the same, what happens to (explain with polygons and equations)

- (a) the total pressure ratio of the exit to inlet (increases, decreases, or remains the same)
- (b) percent reaction (increases, decreases, or remains the same).

8.11 The shaft of a single stage (rotor and stator) of a low-pressure turbine rotates at 7600 rpm. The turbine expands 195 lbm/s of air. The average radius of the blades is 12.0 in., and the inlet blade height is 1.60 in. The resulting tangential blade velocities are 795.9 ft/s. The inlet total pressure and total temperature are 217.2 psia and 1327 °R, respectively. The inlet static pressure, temperature, and density are 150 psia, 1200 °R, and 0.01049 slug/ft³, respectively. The speed of sound at the inlet is 1681 ft/s. The resulting axial velocity at the inlet is 689.9 ft/s; the turbine has been designed so that the axial velocity remains constant across each blade row. The absolute inlet flow angle to the rotor is the same as the stator exit flow angle (+57°), and the rotor flow turning angle ($|\delta_{12}|$) is 80°. The total pressure ratio of the stage is 0.5645. The values of c_{ab} and γ are 0.2527 Btu/lbm-°R and 1.372, respectively. Find the following:

- (a) the velocity polygons (to scale),
- (b) the sign of δ_{12} ,
- (c) the efficiency of the stage,
- (d) the stator flow turning angle,
- (e) the percent reaction for the stage.

8.12. The shaft of a single stage (rotor and stator) of a low-pressure turbine rotates at 9200 rpm. The turbine expands 177 lbm/s of air. The average radius of the blades is 9.0 in., and the inlet blade height is 1.10 in. The resulting tangential blade velocities are 722.6 ft/s. The inlet static pressure, temperature, and density are 240 psia, 1200 °R, and 0.0168 slug/ft³, respectively. The speed of sound at the inlet is 1680 ft/s. The inlet total pressure and total temperature are 314.3 psia and 1291 °R, respectively. The resulting axial velocity at the inlet is 759.0 ft/s; the turbine has been designed so that the axial velocity remains constant across each blade row. The absolute inlet flow angle to the rotor is the same as the stator exit flow angle (+45°), and the rotor flow turning angle ($|\delta_{12}|$) is 50°. The efficiency of the stage is 93 percent. The values of c_p and γ are 0.2538 Btu/lbm-°R and 1.370, respectively. Find the following:

- (a) accurate velocity polygons (to scale),
- (b) the sign of δ_{12} ,
- (c) the total pressure ratio of the stage,
- (d) the percent reaction for the stage,
- (e) the optimum pitch-to-chord ratio for the stator vanes (estimate).

8.13 Find the corrected mass flow rate and corrected speed for the stage in Problem 8.1. If the stage is run at 9000 rpm and the flow rate is 90 lbm/s, find the inlet pressure and inlet temperature so that the corrected parameters are matched. Use these conditions to find the resulting flow angles and total pressure ratio and compare them with those from Problem 8.1. Comment.

Combustors and Afterburners

9.1. Introduction

The burner and afterburner are the only components through which energy is added to the engine. That is, in these two components the total temperature of the gas increases. For the primary burner, a part of this energy is used by the turbine to drive the compressor, and the other part is left to generate a high-velocity gas from the nozzle, generating thrust. For the afterburner, all of this energy increase is used to generate an increase of the fluid enthalpy and consequently a higher velocity gas from the nozzle, generating more thrust. As a result of these direct impacts, efficient operation of these components is necessary for the overall efficiency of the engine. However, several complex considerations must be realized in the design of either of these components, and some of the more advanced topics are summarized by Lefebvre (1983) and Peters (1988). Furthermore, Malecki et al. (2001) demonstrate the application of CFD predictions to modern combustor design.

The following are essential considerations in the design of a burner:

1. A major objective is complete combustion or fuel will be wasted.
2. Minimal total pressure loss is another important design goal. As discussed in Section 9.2, these first two objectives are in direct conflict.
3. All of the combustion must take place in the combustor and not the turbine, or the turbine life will be reduced.
4. Minimal deposits are desired because large deposits indicate burning inefficiencies and further compromise the burning efficiency, reduce the pressure, and cause hot spots.
5. For obvious reasons, one wants easy ignition and relighting of the fuel as well as a high entrance pressure (exit of the high-pressure compressor).
6. Burners and afterburners should have long lives and should not fail because burner failure can lead to an engine explosion.
7. The exit temperature should be uniform both in space and time because extremes should not be introduced to the turbine in the case of a primary combustor or to the nozzle in the case of an afterburner.
8. No internal hot spots should be present because these can lead to burner failure.
9. The flame should be stable over a range of mass flows, speeds, and other operating conditions. An unstable flame can lead to fluctuating exit conditions, which can adversely affect thrusts and loading of the other components and ultimately lead to their failure.
10. The flame should not be prone to “flame out” because this can result in total loss of thrust.
11. The burner or afterburner should have minimal volume because weight is of primary concern – especially with military craft. Overall, the design of a combustor is not as straightforward as the design of a compressor or turbine and requires more empiricism and testing.

9.2. Geometries

Several design criteria need to be considered as follows:

1. A good mixture ratio of fuel to air is required along the burner axis. Although the stoichiometric ratio for most fuels is typically 0.06 to 0.07 and the fuel-to-air ratio for the engine is typically 0.015 to 0.03, in the primary burning zone the mixture is fuel rich and this ratio is typically 0.08.
2. The temperature of the reactants should be warmed to above the ignition temperature of the fuel before entering the burner.
3. The proper temperature in the burner must be achieved to sustain the burn.
4. Good turbulence is required so that the fuel will be well mixed into the air.
5. A low pressure loss is desired so the gas will enter the turbine with a high pressure. However, high turbulence results in a large pressure loss. Thus, although a high turbulence level is desired, it should not be any higher than necessary to ensure a good mix.
6. Time is needed for each fuel particle to burn completely. If the gas velocity is higher than the flame speed, the burner will “flame out.” The flame speed is the velocity at which the flame will move in a quiescent and uniform mixture of fuel and air. Typically, laminar flame speeds are 1 to 5 ft/s and turbulent flame speeds are 60 to 100 ft/s. Therefore, the size of the burner should be large enough so that the velocities will remain low. If large sizes cannot be maintained, flameholders (flame stabilizers) are often used to set up standing recirculation wakes. Thus, low-velocity zones are realized; however, they are at the expense of increased pressure losses.
7. The exit temperatures of a primary burner and afterburner are significantly different. The allowable turbine inlet temperature limits the exit temperature of the primary burner. On the other hand, the allowable nozzle inlet temperature limits the exit temperature of the afterburner. Because the turbine blades are rotating, the stress levels are much higher than the nozzle stress levels. As a result, the turbine inlet temperatures must be much lower than the nozzle temperatures.

9.2.1. Primary Combustors

Three types of main burners are used: can (or tubular), annular, and cannular (or can-annular). The three general geometries are compared in Figure 9.1. Typically, cans were used on early engines and annular and cannular burners are used on modern engines. Each will be discussed separately.

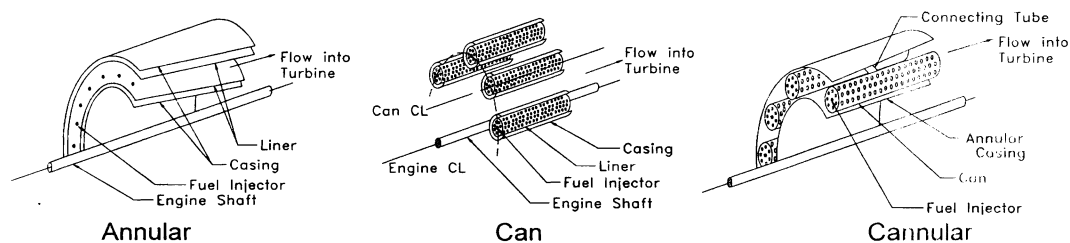


Figure 9.1 Three basic types of primary burners.

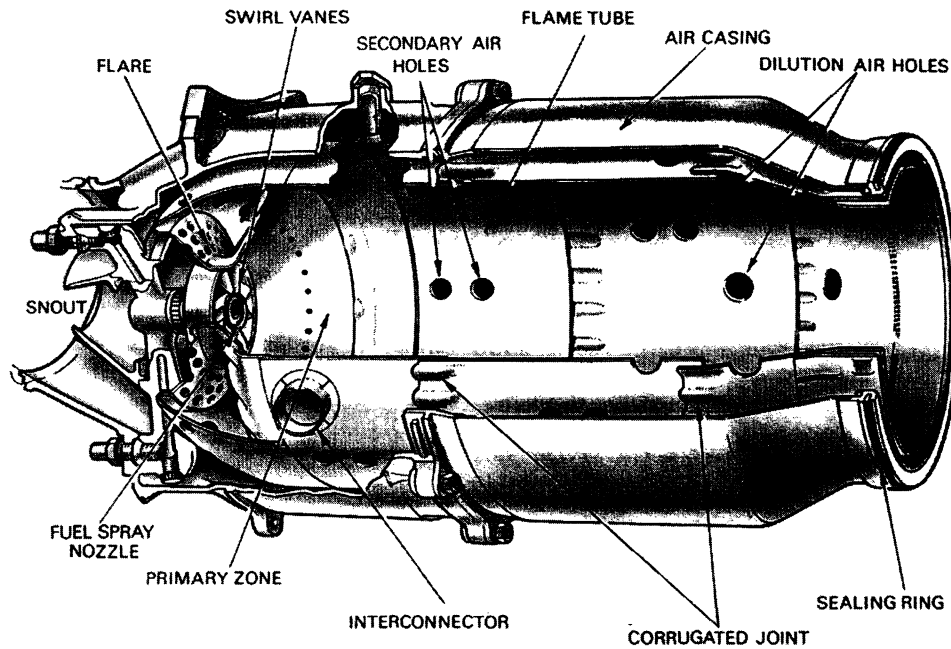


Figure 9.2 An older model can burner (courtesy of Rolls-Royce).

In Figures 9.2 and 9.3, cross sections of a can burner are shown, and in Figure 9.4 a schematic is presented. Several of these self-contained cans are evenly spaced and situated circumferentially around the engine. Typically, 7 to 14 cans are used. As can be seen from Figure 9.4, “primary” air first enters from the compressor and is decelerated to decrease the velocity and then swirled to increase the turbulence level of the flow, which enhances the mixing. Fuel is injected at a relatively low velocity. “Secondary” air is bounded by the outer liner (which also acts as a heat shield) and gradually fed into the combustion zone through holes or slits in the inner liner. Slits are used to form a cool boundary layer on the liner to maintain a tolerable liner temperature; holes are used to force air to the center of the burner so that the combustion will occur away from the walls. Usually, a combination of holes and slits is used. Typically, smaller holes are used near the front of the inner liner and larger holes at the rear of the liner so that air will be uniformly fed into the burning zone along the axis of the burner. Air finally exits at a relatively high velocity into the turbine.

Figure 9.5 shows a cutaway of an annular burner. Air enters the burning zone both from the inner and outer diameters, and hole sizes are again used to control the relative air flow rates along the axis.

As implied in the name, a cannular burner is a combined version of the can and annular geometries. Such a geometry is shown in Figure 9.6. Basically, a series of cans are circumferentially connected so that they interact more so than a series of cans. For example, any circumferential pressure variations are minimized. Connecting tubes, which directly connect the cans and allow for flow between cans, are often used. Furthermore, as shown in Figures 9.1 and 9.6, the can casings have holes that allow moderate circumferential flow.

One can compare the relative advantages of the three types of burners. With a can burner, the fuel-to-air ratio can easily be controlled circumferentially. If a particular burner can is suspected of failing during use, one can economically inspect and replace only that

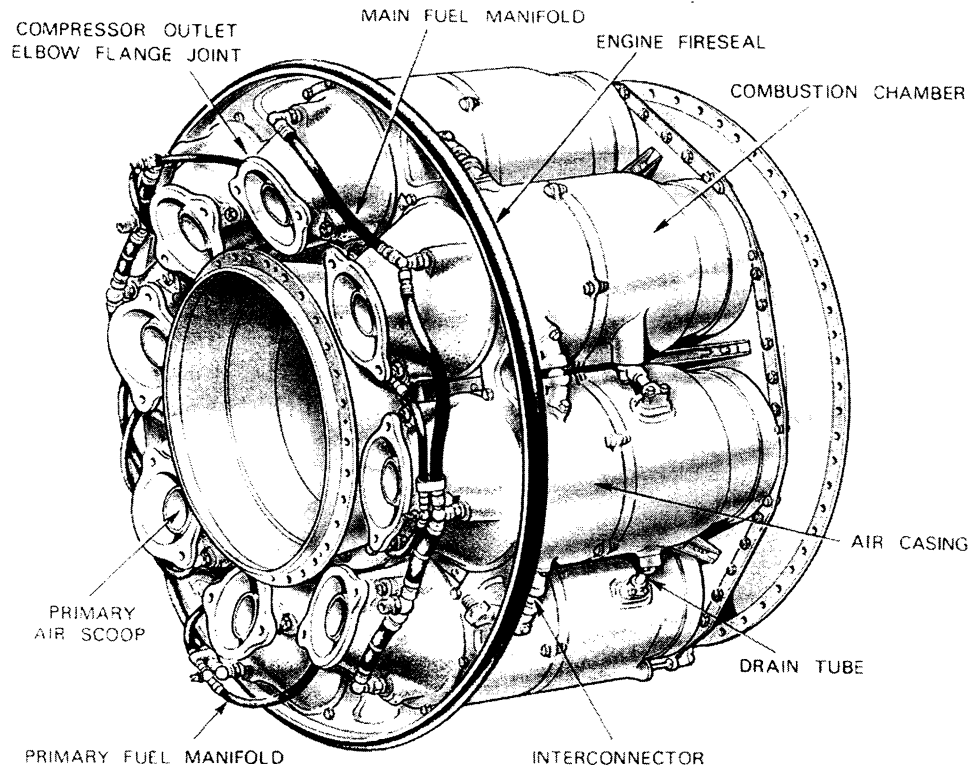


Figure 9.3 Three-dimensional view of an assembled set of can burners (courtesy of Rolls-Royce).

component. During testing, only one can needs to be tested, thus reducing the required flow rates and therefore test chamber size and cost. However, when fully assembled, can burners tend to be larger and heavier than the other types. Also, pressure drops are higher (about 7%), and each can must contain its own igniter; moreover, the flow into the turbine tends to be less uniform in temperature than for the other two geometries. As a result of these disadvantages, can burners are rarely used on modern large engines. They are of small diameter and have relatively long lengths and good survivability characteristics. They are used extensively in small turboshaft engines with centrifugal compressors.

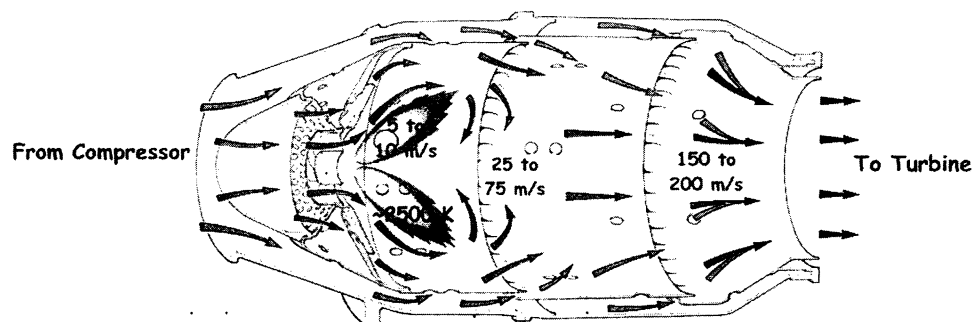


Figure 9.4 Flow patterns in a can burner (adapted from Rolls-Royce).

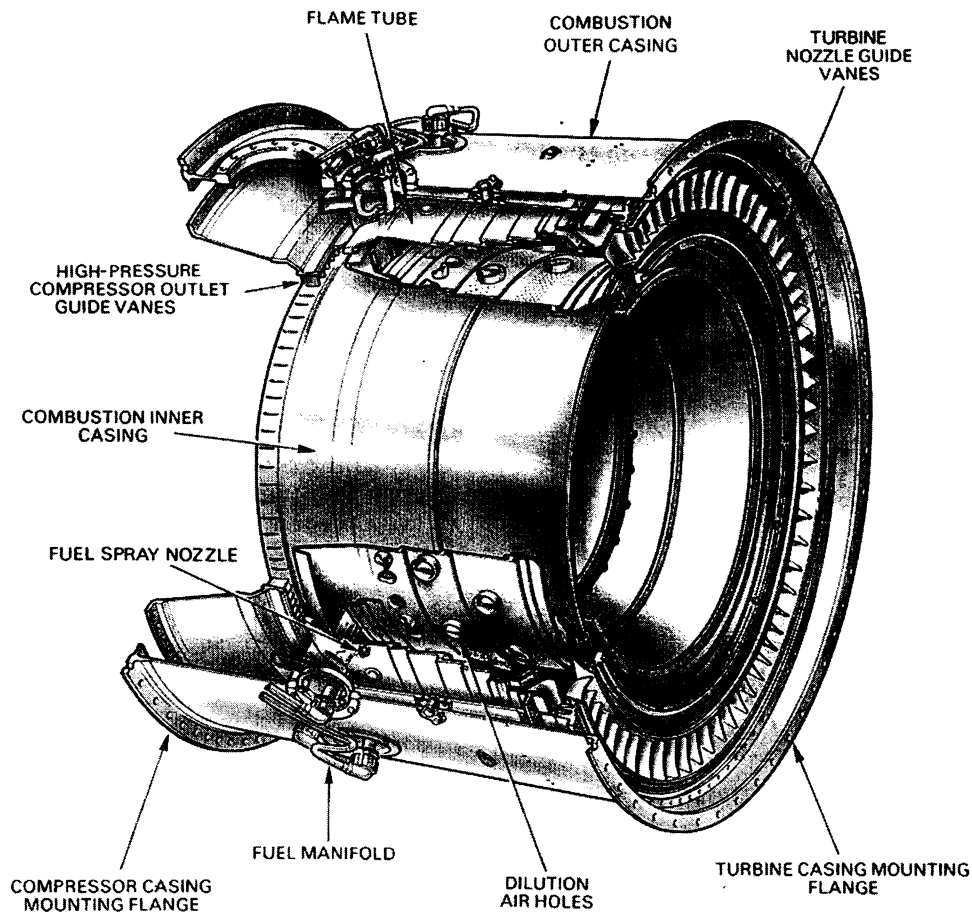


Figure 9.5 Three-dimensional view of an annular burner (courtesy of Rolls-Royce).

Cannular burners tend to have smaller cross-sectional areas and thus weigh less. Fewer ignition systems are required because flow can propagate circumferentially. Circumferentially controlling the temperatures is more difficult with cannular burners, but they tend naturally to produce uniform exit temperatures. Also, if one component fails, replacing only that component can be more expensive than for a can burner. Finally, owing to the method by which the burn areas are connected, thermal growth can cause thermal stresses to be generated. Pressure drops are lower than for can burners (approximately 6%). In general however, cannular burners capture the advantages of the other two types and are used on both turbojets and turbopumps.

Annular burners are the simplest, the most compact, and the lightest. They demonstrate the lowest pressure drop (about 5%) and feature good mixing and high efficiencies. Controlling the circumferential variation of temperature is most difficult with annular burners, but they also tend naturally to produce uniform exit temperatures. Mechanically, they also are not quite as rugged as the other types but have improved dramatically over the past few years as the result of improved materials. These burners are the hardest to service; often if an annular burner needs to be replaced, the entire engine must be removed from an aircraft and disassembled.

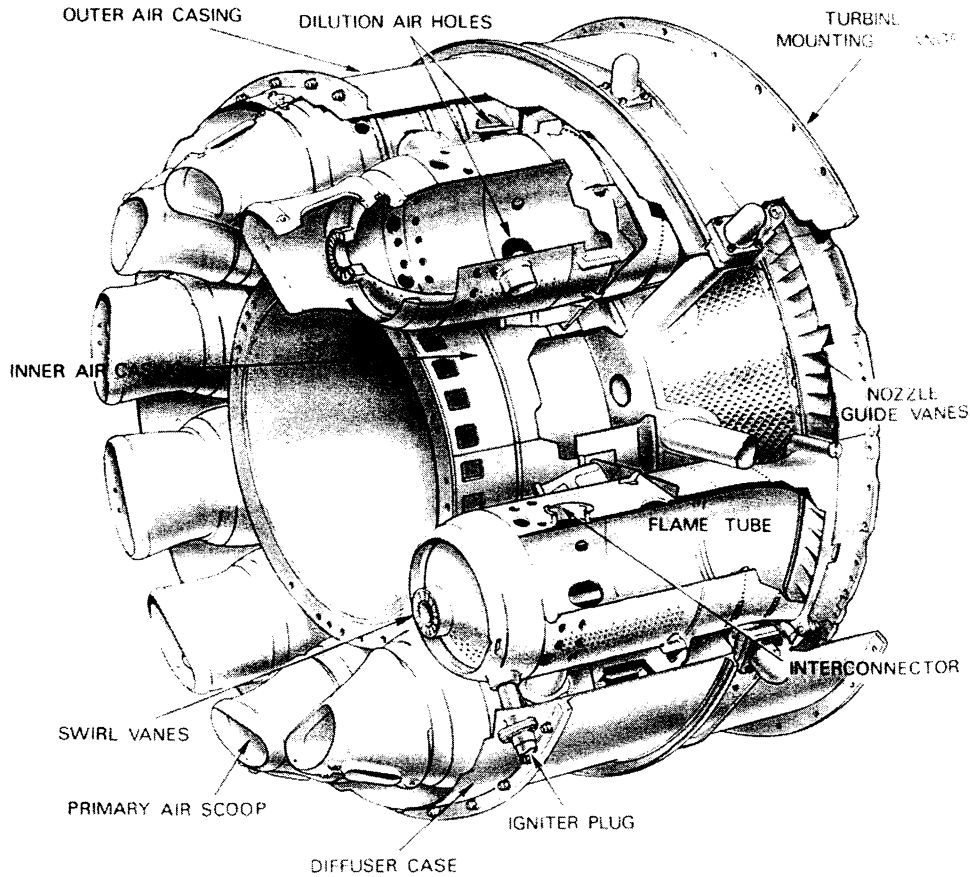


Figure 9.6 Three-dimensional view of a cannular (can-annular) burner (courtesy of Rolls-Royce).

Most primary burners are constructed of nickel-based alloys; ceramic composites are good candidates for future materials. Most modern combustors are of the annular design, including the GE CF6, GE90, P&W F100, P&W PW4098, RR RB211, and RR Trent. Burner exit temperatures range from 2200 to 3100 °R. Total pressure ratios are typically 0.94 to 0.96.

9.2.2. Afterburners

As covered in Chapters 2 and 3, the objective of an afterburner (or thrust augmentor) is to increase the thrust by about a factor of 1.5 to 2.0 for short periods. The *TSFC* also significantly increases (by about a factor of 2.0) during these times. The primary combustors only burn about 25 percent of the air (they operate well below the stoichiometric condition). Thus, the afterburners can burn up to the remaining 75 percent of the initial air. Because afterburners are rarely used (carrier takeoff, emergencies, etc.), the design of such a component is relatively simple. That is, they are only lit for takeoff, climb, sudden accelerations, and maximum speed bursts. However, because they are permanently installed they will impart total pressure losses to the flow even when not in use (called the dry condition) and thus will decrease the thrust and increase the *TSFC* of an engine. Afterburners

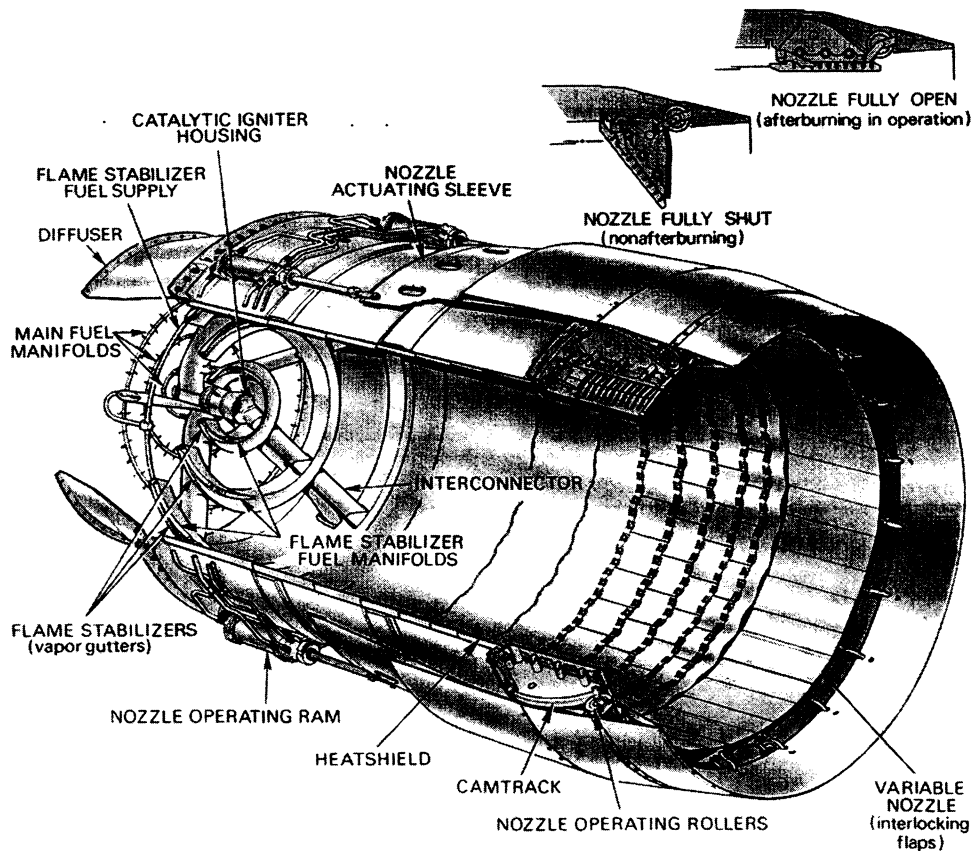


Figure 9.7 Three-dimensional view of a Rolls-Royce afterburner with nozzle (courtesy of Rolls-Royce).

consequently are not designed to be high-turbulence generators. As a result, they do not mix the fuel with the air as well as a primary burner and demonstrate lower burn efficiencies than do primary burners. In fact, when afterburners are in use, a large percentage of the fuel is often burned in or after the nozzle (see Fig. 1.22). However, they do not demonstrate pressure drops as large as those encountered in primary burners. Such a configuration is shown in Figure 9.7. Fuel is injected into the flow with a series of radial spray bars, circumferential (annular) spray rings, or both. Fuel is usually transversely injected (namely at 90° to the flow) to enhance atomization and mixing through the shearing action of the freestream gas. Small flameholders are often used. The design of an afterburner is similar to that of a simple ramjet. A cooling liner is used to feed cool air gradually along the boundary so the case does not overheat. In Figure 9.7, a variable nozzle with flaps, which is integral with the afterburner, is also shown with two nozzle positions.

Some of the particular design concerns are as follows. The flame can not be too hot or the nozzle (or liner) will be burned. The afterburner should be designed to operate for a relatively wide range of temperatures. This is accomplished by using augmented stages for the fuel injection. Combustion instability (called screech) should be minimized. Screech is periodic high-pressure fluctuations caused by an unsteady release of enthalpy during the combustion process. The intense noise levels are not just undesirable audible signals but

can lead to mechanical fatigue of the flameholders, afterburner duct, and nozzle. Usually, a screech liner is used to subdue the fluctuations. Lastly, visual cues such as external flames and excessive smoke should be minimized for military and environmental reasons. Most afterburners are constructed of nickel-based alloys or ceramic composites. Typical afterburner exit temperatures are 3000 to 3700 °R.

9.3. Flame Stability, Ignition, and Engine Starting

9.3.1. Flame Stability

As discussed in Section 9.1, a flame must be stable for combustion to be efficient and thrust to be continuous. Specific guidelines, which are somewhat fuel-type dependent, can be used to ensure that the flame will remain in the burner and that combustion can take place stably in the *local burn zone* in the burner. Two general important and typical graphs that represent guidelines are presented in Figures 9.8 and 9.9.

In Figure 9.8, a generalized “flammability” plot is presented, and Olson et al. (1955) present such data for a gasoline or “wide cut” fuel. This cross-plot shows a region of pressure and fuel-to-air ratio in which combustion is possible. Note and remember that the typical overall fuel-to-air ratio for an engine is 0.02. Thus, as indicated on this diagram, if the local fuel-to-air ratio in the burner was the same, the overall engine fuel-to-air ratio, combustion would not be possible. From the diagram, it can be seen that the pressure must be high in the burn zone in the combustor which indicates why high pressure is needed from the compressor, and that the fuel-to-air ratio should be high enough so that the condition falls in the stable region; as is shown in Section 9.4, the stoichiometric value is approximately 0.067. As a result, in the center of the burn zone the fuel-to-air mixture is usually stoichiometric or slightly fuel rich (slightly higher than the stoichiometric ratio).

The flame speed is also very important to a stable combustor. If the gas mixture is moving opposite to the direction of the flame and at the flame velocity, the flame will be stationary. If the gas mixture moves faster than the flame speed, the flame will be carried out of the

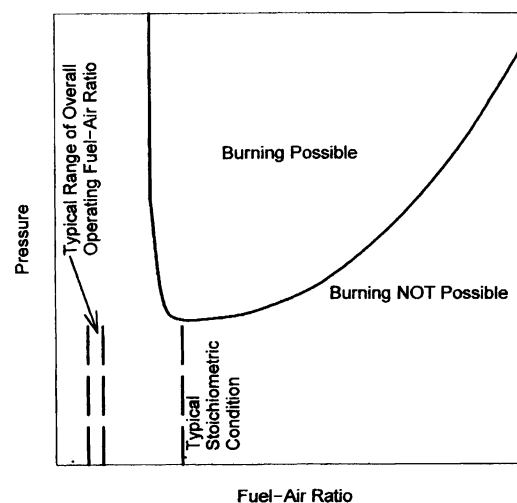


Figure 9.8 Generalized “flammability” map.

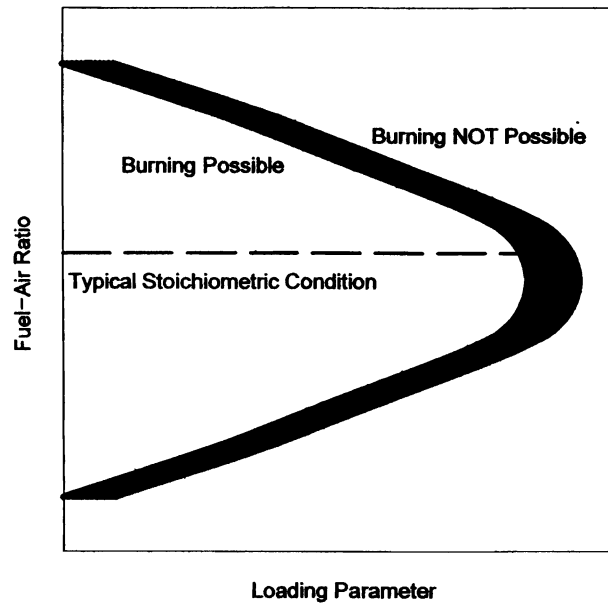


Figure 9.9 Combined flammability and flame speed information.

burner; that is, the engine will experience flameout. Thus, flow velocities in the burner must be less than the flame speed. Flameholders are used in burners to ensure that velocities in local regions will be less than the flame speed. Note also that, for a mixture that is nearly stoichiometric, the flame speed is almost the highest, and thus again conditions are nearly stoichiometric in the center of the burn zone. At pressures of 1 atm, typical turbulent flame speeds are up to 40 m/s (but the speed depends on the fuel, fuel-to-air ratio, the mixing process, and the turbulence parameters), whereas laminar flame speeds are much lower. Again, Olson et al. (1955) present such data for a “wide cut” fuel.

Lastly, these data sets can be prudently combined to give a generalized set of data for which flame stability can be expected (Oates 1989). A generalized trend is presented in Figure 8.9 in which the region of possible burning is shown for a cross-plot of the fuel-to-air ratio and the loading parameter $\frac{\dot{m}}{\mathcal{V} p^n}$, where \mathcal{V} is the effective volume of the combustion region and n is empirically determined. For example, if the mass flow rate is too large or the burner size is too small, the velocity will be greater than the flame speed and the loading parameter will be large; thus, the operating condition will fall outside of the stable region. Similarly, if the pressure is too low, the loading parameter will be large and the operating condition again will fall outside of the stable region. The peak loading parameter for stable operation typically occurs for a slightly fuel lean mixture.

9.3.2. Ignition and Engine Starting

Igniting a burner is directly tied to starting the engine. That is, if the compressor is not operating, the high-pressure air required by the combustor is not present. The first step in igniting the burner is thus, in actuality, rotating the compressor. For two-spool engines, only the high-pressure compressor is normally driven. Six basic and different techniques

are used initially to rotate the compressor and all require high torque levels. They are as follows:

1. For small engines (turboprops, etc.), a high-torque DC electric starter motor is usually used to spin the shaft with a clutch.
2. For most larger engines (turbofans, etc.), stored compressed air or high-pressure air from another source is used to drive an air turbine (air motor), which in turn drives the engine shaft with a clutch.
3. For a few of the larger engines, a small auxiliary gas turbine is used. Such a turbine must also be started, and this is done by using either a pressurized fuel cartridge, which when used expands and burns the gas and thus drives the turbine, or from an electric motor. The Pratt & Whitney Canada PW901A is one such auxiliary gas turbine.
4. Hydraulic motors driven by a high-pressure hydraulic fluid from a ground source drive the shaft; these are often used on turboshaft engines or power-generation gas turbines.
5. For small engines, a pressurized fuel cartridge, as described above in entry 3, directly drives the turbine.
6. For a few of the older turbojets, auxiliary compressed air is injected into the high-pressure turbine to impinge on the blades and drive the shaft.

After the shaft is first rotated and after the compressor reaches partial speed through an auxiliary motor system, enough high pressure is generated for combustion. Usually, a high-energy spark technique is then utilized in the primary combustion chamber. Fuel is sprayed into the chamber, and a spark is generated by a high-voltage igniter plug to ignite the fuel. Thus, a high-temperature and low-density gas enters the turbine, which is then able to drive the compressor, and the shaft ramps up to full rotational speed.

Ignition of an afterburner is usually quite different because it is not linked to engine starting. One method that is often used is the “hot streak” technique. For this method, extra fuel is *briefly* injected into one of the primary burner fuel nozzles. The extra fuel burns as it passes through the turbine and into the afterburner region, where it ignites the afterburner fuel. After afterburner ignition, the primary fuel flow is reduced to the normal flow rate. The second method is the torch technique. For this method a pilot light is mounted in one of the spray bars. As the name implies, the torch is constantly burning, and when afterburner fuel is injected the torch ignites the fuel. A third method is the spark method, which is similar to that used on primary burners. A fourth method that is sometimes used is a platinum-based element that is catalytic with the fuel and is located downstream of the fuel and mounted on the spray bar.

9.4. Adiabatic Flame Temperature

Because the overall performance of an engine and the life of a turbine are strongly dependent on the burner exit temperature, predicting this temperature is extremely important. Previously (in the cycle analyses), a relatively simple method was used to predict the burner performance. For this technique, the fuel heating value was used, and one value was assumed to be valid for all conditions. Furthermore, one specific heat was used for the fuel and air, and the air and fuel were assumed to be at approximately the same temperature. However, this is not true. Also, the air specific heat was previously assumed to be constant

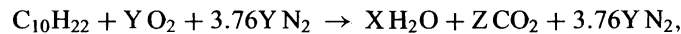
in the combustor, which is also not true because of the extreme temperatures. In this section these assumptions are relaxed and the adiabatic flame temperature is found.

9.4.1. Chemistry

First, a review of burner chemistry is in order. This is best accomplished with an example that entails balancing the chemical equation of the burner. All jet fuels are hydrocarbons, and most have characteristics similar to those of kerosene. *N*-decane ($C_{10}H_{22}$) is a hydrocarbon that accurately represents kerosene. Balancing the stoichiometric chemical equation is necessary before one can proceed to the thermodynamics of the burning process. The stoichiometric condition is often called 100-percent air. The stoichiometric condition has exactly the correct proportions of oxygen and fuel such that all of the oxygen and fuel are consumed and no oxygen or fuel remains in the products. For other conditions, the definition of percent air is the ratio of the mass of air provided to that required at the stoichiometric condition.

Example 9.1: If kerosene can be approximated by *n*-decane, balance the chemical equation for the stoichiometric combustion of this fuel in air and find the stoichiometric fuel-to-air ratio.

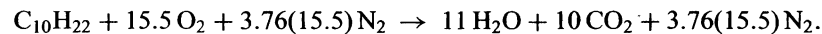
Thus, the first step in solving the problem is to balance the stoichiometric equation for the fuel. That is, all of the oxygen and fuel are burned so that they do not remain in products. Thus,



where air is Y parts oxygen and $3.76Y$ parts nitrogen. Thus, one must find Y , X , and Z to balance the equation. Note that the nitrogen does not actively participate in the reaction. It does, however, enter into the thermodynamics. If each element is considered, one finds

$$\begin{aligned} C : 10 &= Z && \text{thus } Z = 10 \\ H : 22 &= 2X && \text{thus } X = 11 \\ O : 2Y &= X + 2Z && \text{thus } Y = Z + X/2 \text{ or } Y = 15.5 \end{aligned}$$

The balanced equation is therefore



One must remember that the molecular weights \mathcal{M} of C, H, O, and of N are 12, 1, 16, and 14, respectively. This results in a molecular weight for *n*-decane of 142. Also, note that, for a jet engine, the combustor exhaust is all gas; therefore H_2O is not a liquid. Thus, for the stoichiometric condition (100% air), one can find the fuel ratio from:

$$\begin{aligned} f &= \frac{\dot{m}_f}{\dot{m}_{\text{air}}} = \frac{1(10\mathcal{M}_C + 22\mathcal{M}_H)}{15.5 \times 2\mathcal{M}_O + 3.76 \times 15.5 \times 2\mathcal{M}_N} \\ &= \frac{1(10 \times 12 + 22 \times 1)}{15.5(2 \times 16 + 3.76 \times 2 \times 14)} = \frac{142}{2127.8} = 0.0667. \end{aligned}$$

This value is much higher than that for overall engine operation. In fact, if this ratio were burned in the primary combustor, the exit temperature would be far too hot and the turbine would be rapidly destroyed. Thus, most engines run fuel lean (i.e., more than 100% air) to reduce the turbine temperatures, although as discussed earlier, in local burn zones the combustors are fuel rich.

9.4.2. Thermodynamics

Now that the chemistry of the problem has been reviewed, one can use thermodynamics to analyze the burner. For the analysis herein, disassociation of any of the products and resulting equilibrium will be ignored. Although, at high temperatures, these effects are measurable on temperatures and products, including these effects would create undue complication. Furthermore, these effects are secondary as compared with the effects of using adiabatic flame temperature and as compared with the simple heating value analysis. The reaction will be assumed to go to completion without any equilibrium considerations. Equilibrium effects can be included using the analysis of Reynolds (1986). Thus, applying the first law of thermodynamics to a burner yields

$$\dot{Q} + \dot{W} = \Delta\dot{h} + \Delta\dot{KE} + \Delta\dot{PE}. \quad 9.4.1$$

In the absence of work, heat transfer, and potential energy changes, this becomes

$$\Delta h_t = 0 \quad 9.4.2$$

or

$$\sum (N_i h_{ti})_{\text{products}} = \sum (N_i h_{ti})_{\text{reactants}}, \quad 9.4.3$$

where h_{ti} is the total enthalpy of a constituent i , and N_i is the number of moles of constituent i . Now for a given substance at any temperature T , the specific static enthalpy is

$$h_{iT} = \Delta h_{if}^\circ + (h_T - h_{298})_i, \quad 9.4.4$$

where Δh_{if}° is the enthalpy of formation of the substance at the standard state (298 K), h_T is the enthalpy at temperature T , and h_{298} is the enthalpy at 298 K. For a substance from which heat is released upon formation, the enthalpy of formation is negative. The enthalpy of formation is based on the fact that both the substance and its constituents are in given states during the formation of the substance. The enthalpy of formation is fixed for a given substance and state and is not the same as the heat of combustion. One can obtain $(h_T - h_{298})_i$ either by real gas tables (preferred) or approximately by

$$(h_T - h_{298})_i = \int_{298}^T c_{pi} dT. \quad 9.4.5$$

Sometimes the specific heat can be approximated over a given (but relatively small) temperature range by

$$c_{pi} = a_i + b_i T. \quad 9.4.6$$

The method can be used to find the heating value or heat of combustion, which was used in Chapters 2 and 3 for a combustion analysis. If both the products and reactants are gases, as in a jet engine, the value is called the lower heating value. Thus, the heat released is termed the heating value (at any temperature T); it is defined and found by

$$\begin{aligned} \Delta H_T = & - \sum (N_i (\Delta h_{if}^\circ + (h_T - h_{298})_i))_{\text{products}} \\ & + \sum (N_i (\Delta h_{if}^\circ + (h_T - h_{298})_i))_{\text{reactants}}. \end{aligned} \quad 9.4.7$$

For example, if both the products and reactants are at the standard temperature, the heating

Table 9.1. Thermodynamic Parameters for Selected Compounds

Compound	Δh_f° (kJ/kg-mole)	c_p (298 K) (kJ/kg-mole-K)	a	b
			(kJ/kg-mole-K)	(kJ/kg-mole-K ²)
CO	-110,530	29.1	27.4	0.0058
CO ₂	-393,520	37.1	28.8	0.0280
H ₂ O	-241,820	33.6	30.5	0.0103
H ₂	0	28.9	28.3	0.0019
N ₂	0	29.1	27.6	0.0051
O ₂	0	29.4	27.0	0.0079
C ₄ H ₁₀ (g)	-126,150	98.0	35.6	0.2077
C ₈ H ₁₈ (l)	-249,950	254	254	0
C ₁₀ H ₂₂ (l)	-294,366	296	296	0

value at the standard conditions is found by

$$\Delta H_{298} = - \sum (N_i \Delta h_{if}^\circ)_{\text{products}} + \sum (N_i \Delta h_{if}^\circ)_{\text{reactants}} \quad 9.4.8$$

These computations can be performed for any compound, and fortunately the heating value does not change greatly with temperature. One needs to know the standard enthalpies of formation for the different constituents for such computations. These are usually found in JANAF (Chase (1998)) or equivalent tables. In Table 9.1, a few important thermodynamic parameters for some selected compounds are presented. The values of a and b have been evaluated over typical temperature ranges.

Example 9.2: Find the heating value of liquid *n*-decane at 298 K based on the enthalpies of formation.

First, one needs the enthalpies of formation of all of the reactants and products:

$$\text{H}_2\text{O}(\text{g}): \Delta h_{if}^\circ = -241,820 \text{ kJ/kg-mole}$$

$$\text{O}_2(\text{g}): \Delta h_{if}^\circ = 0$$

$$\text{N}_2(\text{g}): \Delta h_{if}^\circ = 0$$

$$\text{CO}_2(\text{g}): \Delta h_{if}^\circ = -393,520 \text{ kJ/kg-mole}$$

$$\text{C}_{10}\text{H}_{22}(\text{l}): \Delta h_{if}^\circ = -294,366 \text{ kJ/kg-mole.}$$

Thus, recalling that the molecular weight is 142, one can find the heating value of *n*-decane at 298 K through the following calculation:

$$\Delta H_{298} = -N_{\text{H}_2\text{O}} \Delta h_{\text{H}_2\text{O}f}^\circ - N_{\text{CO}_2} \Delta h_{\text{CO}_2f}^\circ + N_{\text{C}_{10}\text{H}_{22}} \Delta h_{\text{C}_{10}\text{H}_{22}f}^\circ$$

$$\Delta H_{298} = -11(-241,820) - 10(-393,520) + 1(-294,366)$$

$$= 6,300,854 \text{ kJ/kg-mole}$$

$$= 6,300,854 \text{ kJ/kg-mole} / (4.186 \text{ J/cal} \times 142 \text{ kg/kg-mole})$$

$$= 10,600 \text{ cal/g}$$

$$= 19,080 \text{ Btu/lbm.}$$

Heating values are used to approximate the real combustion process, as is done in the earlier chapters of this book. However, it is best to use the adiabatic flame temperature to better predict the operating temperature of a combustor. An example is presented to demonstrate the method. In Table 9.2, a listing of the lower heating values of some

Table 9.2. Heating Values of a Few Selected Fuels

Name	Formula	Lower Heating Value (cal/g)
isobutane(g)	C ₄ H ₁₀	10,897
n-octane(l)	C ₈ H ₁₈	10,611
n-nonane(l)	C ₉ H ₂₀	10,587
n-decane(l)	C ₁₀ H ₂₂	10,567
Jet A(l)	CH _{1.94}	10,333
JP-4(l)	CH _{2.0}	10,389
JP-5(l)	CH _{1.92}	10,277

different fuels is presented. One should note that n-decane closely represents Jet-A, JP-4, and JP-5.

Example 9.3: Kerosene, which can be approximated as liquid *n*-decane, is to be burned in a combustor. The inlet total temperature of the fuel is $T_{t1} = 444.44$ K (800 °R), and the fuel burns with 100-percent air (stoichiometric condition), which is at $T_{t2} = 666.67$ K (1200 °R). What is the exit total temperature if dissociation of the compounds is negligible?

Thus, using the stoichiometrically balanced chemical equation from Example 9.1 and the energy equation (Eq. 9.4.3), in which oxygen and fuel are not a part of the products, one can write

$$\begin{aligned}
 & 11[\Delta h_f^\circ + (h_{T_t} - h_{298})]_{\text{H}_2\text{O}} + 10[\Delta h_f^\circ + (h_{T_t} - h_{298})]_{\text{CO}_2} \\
 & + 3.76 \times 15.5[\Delta h_f^\circ + (h_{T_t} - h_{298})]_{\text{N}_2} \\
 & = 1[\Delta h_f^\circ + (h_{T_{t1}} - h_{298})]_{\text{C}_{10}\text{H}_{22}} + 15.5[\Delta h_f^\circ + (h_{T_{t2}} - h_{298})]_{\text{O}_2} \\
 & + 3.76 \times 15.5[\Delta h_f^\circ + (h_{T_{t2}} - h_{298})]_{\text{N}_2}.
 \end{aligned}$$

Thus, one must find T_t . However, to find T_t , it must be possible to evaluate $(h_{T_t} - h_{298})_i$ for each product. This can best be done with tables. For simplicity, however, each term will be evaluated based on

$$(h_{T_t} - h_{298})_i = \int_{298}^{T_t} c_{pi} dT.$$

And, for this example each c_{pi} will be assumed to approximate the form

$$c_{pi} = a_i + b_i T.$$

Thus, $(h_{T_t} - h_{298}) = \left[a_i T + b_i \frac{T^2}{2} \right]_{298}^{T_t} = a_i T_t + b_i \frac{T_t^2}{2} - a_i(298) - b_i \frac{298^2}{2}$. Thus, for each constituent

$$h_i = \Delta h_{if}^\circ + (h_{T_t} - h_{298}) = \Delta h_{if}^\circ + a_i T_t + b_i \frac{T_t^2}{2} - a_i(298) - b_i \frac{298^2}{2}.$$

Using Table 9.4, one finds the following for each constituent:

$$\begin{aligned}
 \text{C}_{10}\text{H}_{22}: & \quad a = 296 \quad b = 0.000 \\
 \text{O}_2: & \quad a = 27.0 \quad b = 0.0079 \\
 \text{N}_2: & \quad a = 27.6 \quad b = 0.0051 \\
 \text{H}_2\text{O}: & \quad a = 30.5 \quad b = 0.0103 \\
 \text{CO}_2: & \quad a = 28.8 \quad b = 0.0280,
 \end{aligned}$$

where the resulting c_p is in kJ/kg-mole-K.

Thus, the total enthalpies of each of the reactants are

$$\begin{aligned} h_{\text{C}_{10}\text{H}_{22}} &= -294366 + 296 \times 444 + 0 - 296 \times 298 - 0 \\ &= -251,150 \text{ kJ/kg-mole} \end{aligned}$$

$$\begin{aligned} h_{\text{O}_2} &= 0 + 27 \times 667 + 0.0079 \frac{667^2}{2} - 27 \times 298 - 0.0079 \frac{298^2}{2} \\ &= 11,370 \text{ kJ/kg-mole} \end{aligned}$$

$$\begin{aligned} h_{\text{N}_2} &= 0 + 27.6 \times 667 + 0.0051 \frac{667^2}{2} - 27.6 \times 298 - 0.0051 \frac{298^2}{2} \\ &= 11,092 \text{ kJ/kg-mole.} \end{aligned}$$

Thus,

$$\begin{aligned} \sum (N_i h_{i,\text{reactants}}) &= N_{\text{C}_{10}\text{H}_{22}} h_{\text{C}_{10}\text{H}_{22}} + N_{\text{O}_2} h_{\text{O}_2} + N_{\text{N}_2} h_{\text{N}_2} \\ \sum (N_i h_{i,\text{reactants}}) &= 1(-251,150) + 15.5(11,370) + 15.5 \times 3.76(11,092) \\ &= 571,527 \text{ kJ.} \end{aligned}$$

Now one must find the total enthalpies of each of the products. Thus,

$$\begin{aligned} h_{\text{H}_2\text{O}} &= -241,820 + 30.5 \times T_{\text{products}} + 0.0103 \frac{T_{\text{products}}^2}{2} - 30.5 \times 298 \\ &\quad - 0.0103 \frac{298^2}{2} \text{ kJ/kg-mole} \end{aligned}$$

$$\begin{aligned} h_{\text{CO}_2} &= -393,520 + 28.8 \times T_{\text{products}} + 0.028 \frac{T_{\text{products}}^2}{2} - 28.8 \times 298 \\ &\quad - 0.028 \frac{298^2}{2} \text{ kJ/kg-mole} \end{aligned}$$

$$\begin{aligned} h_{\text{N}_2} &= 0 + 27.6 \times T_{\text{products}} + 0.0051 \frac{T_{\text{products}}^2}{2} - 27.6 \times 298 \\ &\quad - 0.0051 \frac{298^2}{2} \text{ kJ/kg-mole.} \end{aligned}$$

Because the equation is essentially quadratic with only one unknown variable due to the assumed form of the specific heats, one could solve directly for T_{products} . However, in general, the problem is iterative if tables are used. Thus, the iterative approach is used for this example. First, the total exit temperature is assumed to be 2531 K, which will be checked later. Thus, the total enthalpies of the products are:

$$\begin{aligned} h_{\text{H}_2\text{O}} &= -241,820 + 30.5 \times 2531 + 0.0103 \frac{2531^2}{2} \\ &\quad - 30.5 \times 298 - 0.0103 \frac{298^2}{2} = -141,180 \text{ kJ/kg-mole} \end{aligned}$$

$$\begin{aligned} h_{\text{CO}_2} &= -393,520 + 28.8 \times 2531 + 0.028 \frac{2531^2}{2} \\ &\quad - 28.8 \times 298 - 0.028 \frac{298^2}{2} = -240,769 \text{ kJ/kg-mole} \end{aligned}$$

$$\begin{aligned} h_{\text{N}_2} &= 0 + 27.6 \times 2531 + 0.0051 \frac{2531^2}{2} \\ &\quad - 27.6 \times 298 - 0.0051 \frac{298^2}{2} = 77,740 \text{ kJ/kg-mole.} \end{aligned}$$

Thus,

$$\begin{aligned}\sum (N_i h_i)_{products} &= N_{\text{H}_2\text{O}} h_{\text{H}_2\text{O}} + N_{\text{CO}_2} h_{\text{CO}_2} + N_{\text{N}_2} h_{\text{N}_2} \\ \sum (N_i h_i)_{products} &= 11(-141,180) + 10(-240,769) + 15.5 \times 3.76(77,740) \\ &= 570,127 \text{ kJ}.\end{aligned}$$

Therefore, $\sum (N_i h_i)_{products} \cong \sum (N_i h_i)_{reactants}$ and a good guess was made on T_1 . Thus, the adiabatic flame temperature is $T_1 = 2531 \text{ K}$ (4556 °R).

For a second, less accurate method, one can also solve for the total temperature using the simpler, earlier heating value method and compare the results with those for the adiabatic flame temperature. That is, if one assumes that all of the gas into the burner is air and all of the gas out of the burner is air,

$$\dot{m}_f \Delta H = \dot{m} c_p (T_{t4} - T_{t3}) + \dot{m}_f c_p T_{t4},$$

or

$$T_{t4} = \frac{f \Delta H + c_p T_{t4}}{(1 + f)c_p}.$$

For n-decane $\Delta H = 10,567 \text{ cal/g}$ (44,230 kJ/kg); thus,

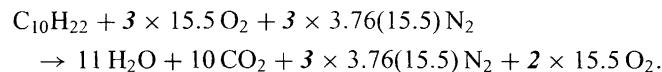
$$T_{t4} = \frac{0.0667 \times 44,230 + 666.67 c_p}{1.0667 c_p} = \frac{2766}{c_p} + 625.0.$$

The value of c_p is a function of the average temperature, and so the problem is iterative. Iterating, one finds

$$T_{t4} = 2778 \text{ K and } c_p = 1.284 \text{ kJ/kg-K}.$$

Thus, this total temperature is in error by 247 K, as well as the temperature rise, and the percent error in the temperature rise is $247/(2531 - 667) = 13.2$ percent.

If this exercise were to be repeated for 300-percent air (three times the air needed for the stoichiometric condition, $f = 0.0222$), it would be necessary to include the unburned oxygen and added nitrogen in the products in both the chemical and thermodynamic equations. For example, the chemical equation for 300-percent air becomes



Because the excessive oxygen and more nitrogen are heated during the combustion process, the final temperature will be lower, resulting in an adiabatic flame temperature of 1453 K. The simple heating value analysis would yield $T_{t4} = 1489 \text{ K}$ ($c_p = 1.147 \text{ kJ/kg-K}$). This is an error of 36 K or a percent error in the temperature rise of only 4.6 percent. Details are left as an exercise to the reader. Solutions can also be obtained using the software, "KEROSENE".

As was shown in Example 9.3, as the fuel ratio decreases, the accuracy of the simple analysis increases. The main reason for this improvement is that, for the simple analysis, all of the gas is assumed to be air. For the adiabatic flame temperature analysis, the incoming gas is air, but the exiting gas is water vapor, carbon dioxide, nitrogen, and oxygen. As the fuel ratio decreases, however, more of the exiting gas becomes air in the adiabatic flame temperature method. Thus, as f decreases, the assumption of pure air in the simple analysis becomes increasingly reasonable. Furthermore, when the fuel ratio is large, and the resulting adiabatic flame temperature is large, significant dissociation of the compounds into elements can occur. This reduces the adiabatic flame temperature. Thus, for a second reason, as f decreases the simple method becomes more accurate.

9.5. Pressure Losses

Undesired losses in total pressure occur in the primary burners and afterburners. These losses are due to three different effects. First, irreversible and nonisentropic heating or combustion of the gas takes place; this is essentially Rayleigh line flow. Second, friction losses occur due to the cans and liners being scrubbed by the gas as it flows through small orifices; this is essentially Fanno line flow. Third, drag mechanisms in the form of flameholders are used that generate turbulence and separation, which are both dissipative mechanisms, again increasing the entropy of the flow. Each effect is addressed separately in this section and then all three effects are discussed in a more general approach.

9.5.1. Rayleigh Line Flow

As discussed in the previous paragraph, several mechanisms exist for pressure drops and total pressure losses in burners. The first to be analyzed is heat addition to the flow. This is analyzed based on Rayleigh line flow, which is flow with heat addition but no friction. The process is a constant area process. The flow is analyzed with a control volume approach in Appendix H. Ten independent equations are derived and 14 variables are in these equations. Therefore, if one specifies 4 variables, one can solve for the remaining 10. Typically, the inlet conditions M_1 , p_{t1} , T_{t1} are known as well as the exit condition T_{t2} , and thus the remaining exit conditions can be found.

Example 9.4: Flow with an incoming Mach number of 0.3 and an inlet total pressure of 300 psia is heated from a total temperature of 1200 °R to 2400 °R. What is the total pressure ratio if the specific heat ratio is 1.30?

SOLUTION:

From the Rayleigh line tables for a Mach number of 0.3, the temperature and pressure ratios can be found as follows:

$$\frac{T_{t1}}{T_t^*} = 0.3363$$

$$\frac{p_{t1}}{p_t^*} = 1.1909.$$

Therefore, the total pressure and temperature at the sonic condition, which is not present but used as a reference, are

$$p_t^* = 300/1.1909 = 251.9 \text{ psia}$$

$$T_t^* = 1200/0.3363 = 3568 \text{ °R.}$$

Thus, the exit temperature ratio is

$$\frac{T_{t2}}{T_t^*} = \frac{2400}{3568} = 0.6726.$$

From the tables for this total temperature ratio,

$$M_2 = 0.495.$$

And for this Mach number,

$$\frac{p_{t2}}{p_t^*} = 1.1131;$$

thus, the total pressure at the exit is

$$p_{t2} = 1.1131 \times 251.9 = 280.4 \text{ psia.}$$

Finally, the total pressure ratio due only to heat addition (Rayleigh line flow) is

$$\pi = \frac{p_{t2}}{p_{t1}} = \frac{280.4}{300} = 0.935.$$

9.5.2. Fanno Line Flow

Again, several mechanisms exist for pressure drops and total pressure losses to occur in burners. The second cause to be analyzed is due to friction in the flow. This is analyzed based on Fanno line flow, which is flow with friction but no heat addition. The process is a constant area process. The flow is analyzed with a control volume approach in Appendix H. One now has 11 equations and 17 variables, and so 6 must be specified. For example, if the inlet conditions M_1 , T_1 , and p_{t1} and duct parameters L , D , and f are specified, one can find the exit conditions, including p_{t2} .

Example 9.5: Flow with an incoming Mach number of 0.3 and an inlet total pressure of 300 psia enters a channel 18 in. long with a 5 in. diameter and a Fanning friction factor of 0.040. What is the total pressure ratio if the specific heat ratio is 1.30?

SOLUTION:

From the tables for a Mach number of 0.30, one can find the nondimensional length-to-diameter and pressure parameters

$$\left. \frac{4fL^*}{D} \right]_1 = 5.7594$$

and

$$\frac{p_{t1}}{p_t^*} = 2.0537;$$

thus, one can find the total pressure at the sonic condition, which is a reference condition (that might not occur in the actual conditions) as follows:

$$p_t^* = 300/2.0537 = 146.2 \text{ psia.}$$

Next, from the duct geometry one can find the parameter

$$\left. \frac{4fL}{D} \right]_{1-2} = \frac{4 \times 0.040 \times 18}{5} = 0.576;$$

thus, one can find the corresponding length-to-diameter parameter at the exit,

$$\left. \frac{4fL^*}{D} \right]_2 = \left. \frac{4fL^*}{D} \right]_1 - \left. \frac{4fL}{D} \right]_{1-2} = 5.7594, - 0.576 = 5.1834,$$

and so from the tables, the exit Mach number can be found as follows:

$$M_2 = 0.312.$$

Therefore, owing to friction the Mach number increased about 10 percent. Next, from the tables at this Mach number, one finds that

$$\frac{p_{t2}}{p_t^*} = 1.9829,$$

and so the exit total pressure can be found by $p_{t2} = 1.9829 \times 146.2 = 289.8$ psia. Hence, the pressure ratio for the burner due only to friction (Fanno line flow) is

$$\pi = \frac{p_{t2}}{p_{t1}} = \frac{289.8}{300} = 0.966$$

9.5.3. Combined Heat Addition and Friction

In Sections 9.5.1 and 9.5.2, heat addition and friction are treated separately. However, in a burner the two effects occur simultaneously. Thus, in this section an analysis whereby both are included is conducted. The technique that will be used is the so-called generalized one-dimensional flow method, and this is described in Appendix H. In general, differential equations are derived that must be numerically integrated between two end states to obtain the drop in total pressure due to both friction and heat addition.

Example 9.6: Flow with an incoming Mach number of 0.3 and an inlet total pressure of 300 psia enters a channel 18 in. long with a 5 in. diameter and a friction factor of 0.040. The total temperature increases from 1200 °R to 2400 °R. What is the total pressure ratio if the specific heat ratio is 1.30? Note that this example is a combination of Examples 9.4 and 9.5 in which both heat addition and friction are included.

SOLUTION:

This problem will be solved by numerically integrating Eqs. H.13.3 and H.13.4. One hundred incremental steps are used, and heat addition and friction are assumed to be uniform; thus $\Delta x = 18/100 = 0.18$ in. and $\Delta T_t = 1200/100 = 12$ °R. A forward difference method is used. Hence, for the first step from Eq. H.13.1, the change in the square of the Mach number is

$$\Delta(M^2) = M^2 \left[(1 + \gamma M^2) \frac{\left(1 + \frac{\gamma-1}{2} M^2\right) \Delta T_t}{1 - M^2} \frac{1}{T_t} + 4f\gamma M^2 \frac{\left(1 + \frac{\gamma-1}{2} M^2\right) \Delta x}{1 - M^2} \frac{1}{D} \right]$$

and so that the square of the Mach number at the end of the first incremental step is

$$M_i^2 = M_{i-1}^2 + \Delta(M^2)$$

$$M^2 = 0.3^2 + 0.3^2 \left[(1 + 1.3 \times 0.3^2) \frac{\left(1 + \frac{1.3-1}{2} 0.3^2\right) 12}{1 - 0.3^2} \frac{1}{1200} \right. \\ \left. + 4 \times 0.04 \times 1.3 \times 0.3^2 \frac{\left(1 + \frac{1.3-1}{2} 0.3^2\right) 0.18}{1 - 0.3^2} \frac{1}{5} \right]$$

$$M^2 = 0.091187,$$

or the Mach number at the end of the first incremental step is

$$M = 0.3020$$

From Eq. H.13.2 the change in total pressure for the incremental step is

$$\Delta p_t = p_t \left(-\frac{\gamma M^2 \Delta T_t}{2} \frac{1}{T_t} - \frac{4f\gamma M^2 \Delta x}{2} \frac{1}{D} \right),$$

or the total pressure at the end of the first incremental step is

$$p_{ti} = p_{ti-1} + \Delta p_t$$

$$p_t = 300 + 300 \left(-\frac{1.3 \times 0.3^2}{2} \frac{12}{1200} - \frac{4 \times 0.04 \times 1.3 \times 0.3^2}{2} \frac{0.18}{5} \right)$$

$$p_t = 299.7234 \text{ psia.}$$

This is repeated for all 100 incremental steps, and the previous step is always used for the initial conditions for the following step. Thus, one finds after 100 steps that

$$M_2 = 0.550$$

$$p_{t2} = 261.55 \text{ psia;}$$

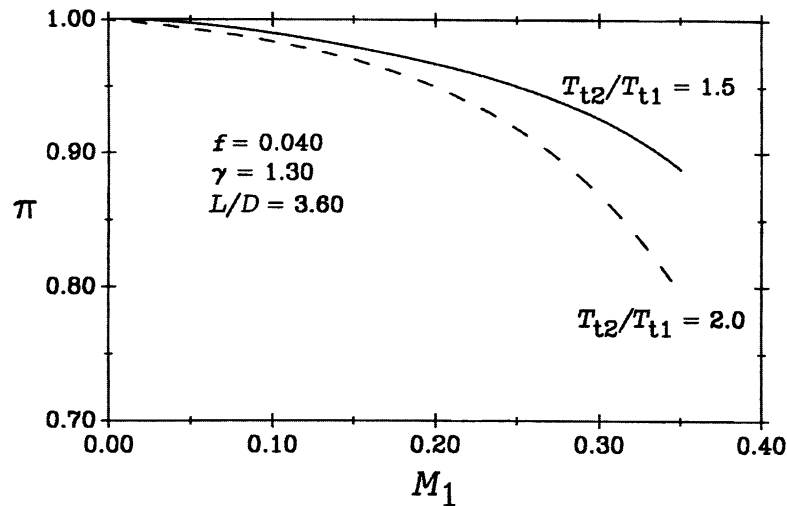


Figure 9.10 Variation of total pressure ratio with Mach number and total pressure for Example 9.6 (frictional flow with heat transfer).

thus,

$$\pi = p_{t2}/p_{t1} = 261.55/300 = 0.872.$$

This total pressure ratio is lower than is obtained by multiplying the results from the previous examples ($0.935 \times 0.966 = 0.903$) and is more accurate.

In Figure 9.10, results for other incoming Mach numbers and one other total temperature ratio are shown. As can be seen, as the Mach number increases, the total pressure ratio quickly decreases from unity. Also, as the total temperature ratio increases (i.e., as the fuel ratio increases), the total pressure ratio decreases.

9.5.4. Flow with a Drag Object

When an obstruction is in the flow, the total pressure is also reduced because of the friction from the added turbulence and separation. Many primary burners and most afterburners contain such obstructions in the form of flameholders to keep the local velocity less than the flame speed. Thus, a method of including such losses is needed. In Appendix H, a method is described in which a control volume approach is used for a constant area flow and uniform properties are assumed at the entrance and exit. In summary, one has 16 variables and 11 equations. Thus, if five variables are specified the problem can be solved. Typically, the inlet conditions M_1 , p_{t1} , and T_{t1} and flameholder geometry parameters A_d/A , and C_d , are known, and thus the exit conditions can be found, including the total pressure.

Example 9.7: Flow with an incoming Mach number of 0.30, an inlet total pressure of 2069 kPa, and a total temperature of 666.7 K enters a channel with a flameholder. The drag coefficient of the flameholder is 0.5 and it occupies 10 percent of the total flow area. What is the total pressure ratio if the specific heat ratio is 1.30?

SOLUTION:

First, for the given inlet Mach number and total conditions, one can find the static conditions

$$T_1 = 657.8 \text{ K}$$

$$p_1 = 1952 \text{ kPa,}$$

and so for the sound speed at the inlet,

$$a_1 = 495.3 \text{ m/s},$$

and from the Mach number the inlet velocity is

$$V_1 = 148.6 \text{ m/s}.$$

Also, from the ideal gas equation for the temperature and pressure, above the inlet density is

$$\rho_1 = 10.34 \text{ kg/m}^3,$$

and so from Eq. H.9.8,

$$\begin{aligned} p_1 + \rho_1 V_1^2 - \frac{1}{2} C_d \rho_1 V_1^2 \frac{A_d}{A} &= \rho_1 V_1 \left[\frac{\mathcal{R}T_2}{\sqrt{2c_p(T_{11} - T_2)}} + \sqrt{2c_p(T_{11} - T_2)} \right] \\ 1952 \text{ kPa} \times \frac{1000 \text{ N}}{\text{m}^2 \text{ kPa}} \times \frac{\text{kg-m}}{\text{N-s}^2} + 10.34 \frac{\text{kg}}{\text{m}^3} \times 148.6^2 \frac{\text{m}^2}{\text{s}^2} \\ &- \frac{1}{2} \times 0.5 \times 10.34 \frac{\text{kg}}{\text{m}^3} \times 148.6^2 \frac{\text{m}^2}{\text{s}^2} \times 0.10 \\ &= 10.34 \frac{\text{kg}}{\text{m}^3} \times 148.6 \frac{\text{m}}{\text{s}} \left[\frac{287.1 \frac{\text{J}}{\text{kg-K}} \times \frac{\text{N-m}}{\text{J}} \times \frac{\text{kg-m}}{\text{N-s}^2} \times T_2(\text{K})}{\sqrt{2 \times 1.244 \frac{\text{kJ}}{\text{kg-K}} \times \frac{1000 \text{ J}}{\text{kJ}} \times \frac{\text{N-m}}{\text{J}} \times \frac{\text{kg-m}}{\text{N-s}^2} \times (666.7 - T_2) \text{K}}} \right. \\ &\quad \left. + \sqrt{2 \times 1.244 \frac{\text{kJ}}{\text{kg-K}} \times \frac{\text{N-m}}{\text{J}} \times \frac{1000 \text{ J}}{\text{kJ}} \times \frac{\text{kg-m}}{\text{N-s}^2} \times (666.7 - T_2) \text{K}} \right] \\ 2,174,000 &= 1537 \left[\frac{287.1 T_2}{\sqrt{2488(666.7 - T_2)}} + \sqrt{2488(666.7 - T_2)} \right]. \end{aligned}$$

Iteratively solving for the exit static temperature T_2 , one finds

$$T_2 = 657.7 \text{ K};$$

hence, the exit velocity is

$$\begin{aligned} V_2 &= \sqrt{2c_p(T_{11} - T_2)} \\ &= \sqrt{2 \times 1.244 \frac{\text{kJ}}{\text{kg-K}} \times \frac{\text{N-m}}{\text{J}} \times \frac{1000 \text{ J}}{\text{kJ}} \times \frac{\text{kg-m}}{\text{N-s}^2} \times (666.7 - 657.7) \text{ K}} = 149.1 \text{ m/s}, \end{aligned}$$

and the exit speed of sound is $a_2 = 495.3 \text{ m/s}$. The exit Mach number is thus $M_2 = 0.3010$.

Also, the exit density is $\rho_2 = \rho_1 V_1 / V_2 = 10.34 \times 148.6 / 149.1 = 10.30 \text{ kg/m}^3$,

and so from the ideal gas law for the temperature and density, $p_2 = 1945 \text{ kPa}$.

Finally, for $M_2 = 0.3010$ and the p_2 , above the exit total pressure is

$$p_{t2} = 2062 \text{ kPa},$$

and the total pressure ratio due only to the blockage of the flameholder is

$$\pi = p_{t2}/p_{t1} = 2062/2069 = 0.997.$$

One can see that this loss in total pressure is much smaller than the losses due to the other effects. Note also that, with the generalized analysis, the total pressure loss due to the heat addition, friction, and drag could be calculated simultaneously.

9.6. Performance Maps

9.6.1. Dimensional Analysis

Performance curves or “maps” are usually used to provide a working medium for a burner engineer. These provide a quick and accurate view of the conditions at which the combustor is operating and what can be expected of the burner if the flow conditions are changed. Of primary concern are the total pressure ratio and burn efficiency of a burner; that is, p_{t4}/p_{t3} (or π_b) and η_b for a primary burner and π_{ab} and η_{ab} for an afterburner. For a primary combustor, the total pressure ratio is a function of many variables, and the functional relationship f_1 can be written as

$$p_{t4}/p_{t3} = \mathcal{F}_1\{\dot{m}, T_{t3}, A, p_{t3}, f, \Delta H, \gamma, \mathcal{R}\}. \quad 9.6.1$$

Dimensionless parameters can be used to reduce the number of independent variables. Using the Buckingham Pi theorem, one finds the following for a given value of γ :

$$p_{t4}/p_{t3} = \mathcal{F}_1\left[\frac{\dot{m}\sqrt{\mathcal{R}T_{t3}}}{Ap_{t3}}, f, \frac{\Delta H}{\mathcal{R}T_{t3}}\right]. \quad 9.6.2$$

This form is rarely used to document the performance of a burner, however. Next if both Fanno and Rayleigh line flows or generalized one-dimensional flow with heat addition and friction are *independently* considered, one finds, for a given burner diameter, length, and friction factor that the pressure ratio is a function (\mathcal{F}_2) of the entering Mach number and total temperature ratio; that is,

$$p_{t4}/p_{t3} = \mathcal{F}_2\left[M_3, \frac{T_{t4}}{T_{t3}}\right], \quad 9.6.3$$

or, using the definition of Mach number,

$$p_{t4}/p_{t3} = \mathcal{F}_2\left[\frac{V_3}{\sqrt{\gamma\mathcal{R}T_3}}, \frac{T_{t4}}{T_{t3}}\right]. \quad 9.6.4$$

Next, using continuity yields

$$p_{t4}/p_{t3} = \mathcal{F}_2\left[\frac{\dot{m}_3}{\rho_3 A_3 \sqrt{\gamma\mathcal{R}T_3}}, \frac{T_{t4}}{T_{t3}}\right], \quad 9.6.5$$

but since T_{t3}/T_3 and p_{t3}/p_3 are strictly functions of Mach number, one can write

$$p_{t4}/p_{t3} = \mathcal{F}_2\left[\frac{\dot{m}_3}{\rho_3 A_3 \sqrt{\gamma\mathcal{R}T_{t3}}}, \frac{T_{t4}}{T_{t3}}\right], \quad 9.6.6$$

or, using the ideal gas law,

$$p_{t4}/p_{t3} = \mathcal{F}_2\left[\frac{\dot{m}_3 \mathcal{R} T_{t3}}{p_{t3} A_3 \sqrt{\gamma \mathcal{R} T_{t3}}}, \frac{T_{t4}}{T_{t3}}\right]. \quad 9.6.7$$

Thus,

$$p_{t4}/p_{t3} = \mathcal{F}_2\left[\frac{\dot{m}_3 \sqrt{\mathcal{R} T_{t3}}}{p_{t3} A_3 \sqrt{\gamma}}, \frac{T_{t4}}{T_{t3}}\right], \quad 9.6.8$$

or, for a given value of γ ,

$$p_{14}/p_{13} = \mathcal{F}_2 \left[\frac{\dot{m}_3 \sqrt{\mathcal{R} T_{13}}}{p_{13} A_3}, \frac{T_{14}}{T_{13}} \right] \quad 9.6.9$$

Hence, the first term of Eq. 9.6.9 matches that of Eq. 9.6.2. Next, if a small fuel ratio with the simplified burner analysis (heating value) is considered, one can use Eq. 3.2.24 to yield

$$\frac{\eta_b f \Delta H}{c_p T_{13}} = \frac{T_{14}}{T_{13}} - 1. \quad 9.6.10$$

Thus, for a given γ and given η_b , one can write

$$p_{14}/p_{13} = \mathcal{F}_2 \left[\frac{\dot{m}_3 \sqrt{\mathcal{R} T_{13}}}{p_{13} A_3}, \frac{f \Delta H}{\mathcal{R} T_{13}} \right]. \quad 9.6.11$$

Next, by reexamining the results from the dimensional analysis, the last two terms in Eq. 9.6.2 can be directly related and thus combined. Furthermore, for a given fuel, one can write

$$p_{14}/p_{13} = \mathcal{F}_2 \left[\frac{\dot{m}_3 \sqrt{\mathcal{R} T_{13}}}{p_{13} A_3}, \frac{f}{T_{13}} \right]. \quad 9.6.12$$

Substituting into Eq. 9.6.9 and “nondimensionalizing” or correcting, as is done for compressors and turbines, one finds the general expression

$$p_{14}/p_{13} = \mathcal{F} \left[\frac{\dot{m} \sqrt{\theta_{13}}}{\delta_{13}}, \frac{f}{\theta_{13}} \right] = \mathcal{F} \left[\dot{m}_{c3}, \frac{f}{\theta_{13}} \right], \quad 9.6.13$$

where again

$$\delta_{13} = p_{13}/p_{\text{stp}} \quad 9.6.14$$

and

$$\theta_{13} = T_{13}/T_{\text{stp}} \quad 9.6.15$$

and f is the usual fuel ratio. Note again that the two independent parameters are not truly dimensionless. The first is called the “corrected” mass flow and has dimensions of mass flow, whereas the second is dimensionless. Thus, since they both are not dimensionless, the resulting function cannot be used to correlate or compare different combustors, fuels, or both. The function can be used for one particular burner and fuel, however, as is the usual case. Similarly, for the burner efficiency, one finds

$$\eta_b = \mathcal{G} \left[\frac{\dot{m} \sqrt{\theta_{13}}}{\delta_{13}}, \frac{f}{\theta_{13}} \right] = \mathcal{G} \left[\dot{m}_{c3}, \frac{f}{\theta_{13}} \right], \quad 9.6.16$$

where the function \mathcal{G} is different from that of \mathcal{F} . A similar analysis can be performed for an afterburner. The functions \mathcal{F} and \mathcal{G} usually are derived from a combination of empiricism and modeling. As is done for compressors and turbines, the maps can be found for one set of conditions and applied to other conditions using the corrected parameters.

9.6.2. Trends

Typical trends of p_{14}/p_{13} and η_b are shown in Figures 9.11 and 9.12. As can be seen, the total pressure ratio drops as the corrected mass flow rate increases and as the fuel ratio increase. By comparison with Figure 9.10 one can see that the trends are the same. Also a

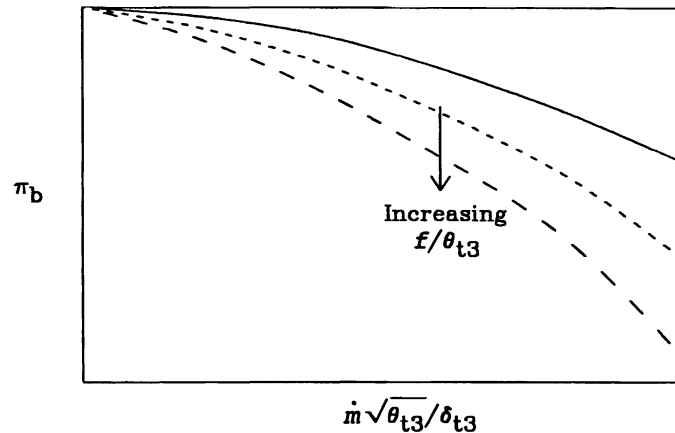


Figure 9.11 General performance map (p_4/p_{13}) for a primary burner.

relative maximum in the burn efficiency can be seen in Figure 9.12, although this trend is strongly dependent on burner design, including the injection nozzles and mixing methods. Thus, the shape and trends of the efficiency map vary greatly from burner to burner. Note that mapping conventions are the same for both primary burners and afterburners.

9.7. Fuel Types and Properties

Up to this point, the fundamental fuel consideration has been the heating value. However, different characteristics are considered and controlled in fuel refining and mixing. On the basis of chemical characteristics, compositions, and chemical structure, hydrocarbon fuels can generally be classified as paraffins (C_nH_{2n+2}), olefins (C_nH_{2n}), diolefins (C_nH_{2n-2}), naphthenes (C_nH_{2n}), and aromatics (C_nH_{2n-6} or C_nH_{2n-12}). Fuel is also classified for military use or commercial use. Military grades are JP1, . . . , JP5(USN), . . . JP8(USAF), . . . JP10. Commercial grades are Jet A, Jet A-1, and Jet B. The characteristics are selected based on the particular engine and flight conditions, including altitude and geographic locations. All are kerosene based but have different characteristics. First, a fuel is a mix of the different hydrocarbons. A fuel that is a kerosene is considered to have n between 8 and 16. Thus,

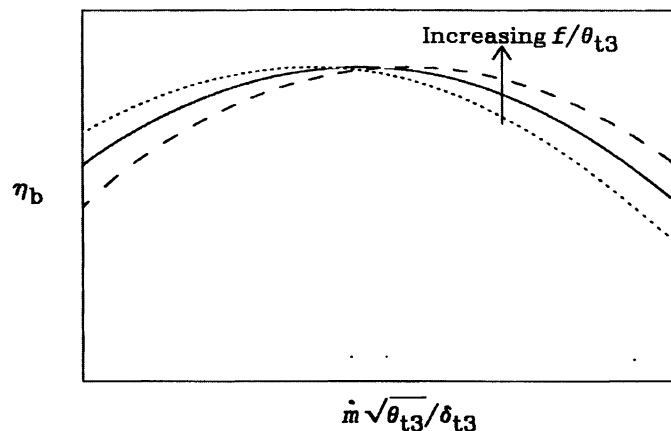


Figure 9.12 General performance map (η_b) for a primary burner.

Table 9.3. Notes on Commercial Fuels

Fuel	Type	Comments
A	Kerosene	Used domestically in the United States
A-1	Kerosene	Used internationally outside of the United States Has a lower freezing point than A
B	Wide-cut	Used in geographies with very low temperatures Has a lower freezing point than A-1

kerosene is not a single compound but a mixture and has the characteristics of a mixture. For example, to find the mixture viscosity one would mass average the viscosities of each constituent. Also, for example, each constituent has an individual vapor pressure, and so some constituents can evaporate before others. In Section 9.4, kerosene was approximated to be $C_{10}H_{22}$, which is an accurate estimation in the middle of the n range. On the other hand, a “wide-cut” fuel is a mixture of more compounds and is not refined as much as kerosene; as a result it is less expensive. For such a mixture, the value of n is between 5 and 16. Such a fuel includes compounds of the gasoline class and is usually referred to as a mixture of kerosene and gasoline; it is much more volatile. Such wide-cut fuels are not generally used in the United States owing to the increased danger of fire during handling and crashes. Some comparative notes on commercial and military fuels are presented in Tables 9.3 and 9.4.

The characteristics of commercial fuels are specified by ASTM, whereas those for military fuels are set and monitored by the government. Regardless of the application, the different characteristics are measured (most by ASTM standards, as described by Bacha et al. 2000) and are identified as accelerated gum content (a measure of nonvolatile material formed at high temperature), acidity (standard definition), aromatics level (part of constituent makeup), color (a general inspection – should be clear white to clear light yellow), corrosivity (to metals such as aluminum and engine materials), distillation level (constituent makeup or profile of the fuel), existent gum content (a “clogging” nonvolatile impurity), flash point (temperature at which burning is possible), freezing point (will be different for the different constituents), lubricity (lubricating characteristic for elastohydrodynamic lubrication such as rolling element bearings), luminometer number (an indicator of flame

Table 9.4. Notes on Military Fuels

Fuel	Type	Comments
JP-1	Kerosene	Original fuel in the United States, NLU
JP-2	Wide-cut	Experimental fuel – never used
JP-3	Wide-cut	About 1/3 kerosene, 2/3 gasoline, NLU
JP-4	Wide-cut	USAF fuel (limited use), Very low freezing point Much like Jet-B
JP-5	Kerosene	USN fuel High flash point due to carrier applications and safety
JP-6	Wide-cut Kerosene	Low freezing point, NLU
JP-7	Kerosene	For SR-71, low volatility
JP-8	Kerosene	USAF fuel (primary fuel) Much like A-1
JP-8+100	Kerosene	USAF fuel – has a thermal stability additive
JP-9	NA	Developmental, pure high-energy fuel
JP-10	NA	Developmental, pure high-energy fuel

NLU – No longer used

radiation heat transfer), mercaptan sulfur level (certain sulfur compound impurities), naphthalene content (part of constituent makeup and can cause carbon deposits), net heating value (value does not change greatly regardless of mixture), olefin content (part of constituent makeup), pour point (lowest temperature at which fuel is fluid), specific gravity or density (standard definition), smoke point (a measure of flame size), thermal stability (susceptibility to particulate formation that clogs parts of the system), sulfur content (amount of pure sulfur in the fuel, which can cause toxicity when burned), vapor pressure (partial pressure at which constituent vaporizes at a given temperature; 100 °F is a standard), viscosity (kinematic viscosity usually used), water reaction level (mixing capabilities of water in the fuel), and water separability (ease at which undesired water can be removed from fuel).

In addition, some other characteristics are monitored, including microbial growth (amount of bacterial, fungi, or other micro-organism growth in a stored fuel; this contamination increases with time), electrical conductivity (standard definition – can be potentially hazardous if a large current traverses fuel), and coefficient of thermal expansion (standard definition – affects fuel tank size and pressure). Furthermore, several additives are sometimes or often used, including, but not limited to, antioxidants, antifreezing materials, leak detectors (leave trails to help track down system fuel leaks), anticorrosives, lubrication improvers, and biocides. More details on fuel properties can be found in Bacha et al. (2000) and Boyce (1982).

9.8. Summary

This chapter has addressed the chemistry, thermodynamics, and gas dynamics of primary combustors and afterburners. The purpose of the primary combustor is to add thermal energy to the propulsion system by increasing the total temperature of the fluid, of which a part is removed by the turbine and the remainder of which is converted to high-kinetic-energy fluid in the nozzle. The purpose of an afterburner is to add thermal energy, all of which is converted to high-kinetic-energy fluid. First, the geometries were defined and important design considerations were summarized. The design of a primary burner is much more complex than that of an afterburner. The three varieties of primary burners are can, annular, and cannular. Primary combustors operate with larger fuel efficiency and lower total pressure ratios than do afterburners. The burning zone in a combustor is fuel rich with a low velocity. Good mixing is needed to ensure high burner efficiencies; on the other hand, low total pressure losses are desired, which are associated with high turbulence levels. Thus, a trade-off or balance of these two conflicting design concepts is needed in the design of a burner. Afterburners operate with much higher exit temperatures than do primary burners, and the nozzle material limits the temperature. Flammability and flame speed were shown to be fundamentally critical to the stability of the burner. In general, the design of a burner is not as straightforward as for a compressor or turbine. Next, the ignition process and different engine starting methods were discussed, for the shaft must be rotating before the burner can be ignited. The chemistry was covered, and the balancing of the chemical equation for stoichiometric (no fuel or oxygen in the products) and other conditions was discussed. The thermodynamics of the adiabatic flame temperature was next covered, and the heating value was derived from this method. Differences between the simple heating value method of burner analysis and the adiabatic flame method were discussed, and it was shown that, as the fuel-to-air mixture becomes lean, the heating value method becomes more viable. Typically, the stoichiometric fuel-to-air mixture ratio is 0.06 to 0.07 for jet fuels, but if such ratios were used for an engine, the operating temperatures would be too high. Locally, however, burners operate internally near the stoichiometric condition for stability. Next, total pressure losses were discussed and the losses were shown to be due to the heat addition, friction,

and flow obstructions (flameholders). One-dimensional Rayleigh line flow and Fanno line flow processes were reviewed and shown to be methods to predict pressure losses. More advanced predictions can be made with generalized one-dimensional frictional flow with heat addition and flow restrictions. In general, the largest loss is due to heat addition, and very little loss is due to flow obstructions. Typical types of burner performance curves or maps and trends were next presented again based on dimensional analysis and empiricism. Finally, different important fuel characteristics and fuel types were identified.

List of Symbols

A	Area
c_p	Specific heat at constant pressure
C_d	Drag coefficient
D	Diameter
F	Force
f	Fuel ratio
f	Fanning friction factor
h	Specific enthalpy
Δh_f°	Standard enthalpy of formation
ΔH	Heat of formation
L	Length
\dot{m}	Mass flow rate
M	Mach number
M	Molecular weight
N	Number of moles
p	Pressure
\dot{Q}	Heat transfer rate
\mathcal{R}	Ideal gas constant
s	Entropy
T	Temperature
V	Velocity
\mathcal{V}	Combustion volume
\dot{W}	Power
γ	Specific heat ratio
δ	Ratio of pressure to standard pressure
η	Efficiency
θ	Ratio of temperature to standard temperature
π	Total pressure ratio
ρ	Density

Subscripts

air	Air
c	Corrected
d	Drag
f	Fuel
i	Counter
i	ith constituent
stp	Standard conditions
t	Total (stagnation)
T	At temperature T

- 1,2 Positions for process analysis
- 3 Inlet to burner

Superscripts

- * Choked

Problems

- 9.1 Balance the chemical equation for n-nonane for the stoichiometric condition and 300-percent air.
- 9.2 Find the adiabatic flame temperature of liquid n-decane for 250-percent air if the fuel inlet total temperature is 900 °R and the air inlet total temperature is 1350 °R. What is the fuel-to-air mixture ratio?
- 9.3 If air enters a combustor at 1300 °R total temperature with a specific heat ratio of 1.3 and a total pressure of 200 psia, find the total pressure ratio across the burner as a function of entrance Mach number if the exit total temperature is 2500 °R. Plot the results.
- 9.4 If air enters a combustor at 1300 °R total temperature with a specific heat ratio of 1.3 and a total pressure of 200 psia, find the total pressure ratio across the burner as a function of inlet Mach number if the friction factor is 0.035, the burner length is 13 in., and the can diameter is 4 in. Plot the results.
- 9.5 If air enters a combustor at 1300 °R total temperature with a specific heat ratio of 1.3 and a total pressure of 200 psia, find the total pressure ratio across the burner as a function of entrance Mach number if the friction factor is 0.035, the burner length is 13 in., the can diameter is 4 in., and the exit total temperature is 2500 °R. Plot the results.
- 9.6 If air enters an afterburner with flameholders at 1600 °R total temperature with a specific heat ratio of 1.3 and a total pressure of 60 psia, find the total pressure ratio across the afterburner as a function of inlet Mach number if the drag coefficient is 0.45 and the area ratio of flameholder to total area is 0.15. Plot the results.
- 9.7 If air enters a combustor with flameholders at 1300 °R total temperature with a specific heat ratio of 1.3 and a total pressure of 200 psia, find the total pressure ratio across the burner as a function of entrance Mach number if the friction factor is 0.035, the burner length is 13 in., the can diameter is 4 in., the drag coefficient of the flameholders is 0.55, the area ratio of flameholder to total area is 0.12, and the exit total temperature is 2500 °R. Plot the results.
- 9.8 The adiabatic flame temperature of liquid n-decane is 2750 °R. The fuel inlet total temperature is 900 °R and the air inlet total temperature is 1350 °R. What is the fuel-to-air mixture ratio?
- 9.9 If air enters a combustor at 1230 °R total temperature with a specific heat ratio of 1.35 and a total pressure of 200 psia, find the total pressure ratio across the burner as a function of exit total temperature if the inlet Mach number is 0.38. Plot the results.
- 9.10 If air enters a combustor at 1230 °R total temperature with a specific heat ratio of 1.35 and a total pressure of 200 psia, find the total pressure ratio across the burner as a function of exit total temperature if the friction factor

is 0.030, the burner length is 15 in., the can diameter is 5 in., and the entrance Mach number is 0.38. Plot the results.

- 9.11** If air enters a combustor with flameholders at 1230 °R total temperature with a specific heat ratio of 1.35 and a total pressure of 200 psia, find the total pressure ratio across the burner as a function of exit total temperature if the friction factor is 0.030, the burner length is 15 in., the can diameter is 5 in., the drag coefficient of the flameholders is 0.50, the area ratio of flameholder to total area is 0.13, and the entrance Mach number 0.38. Plot the results.
- 9.12** Balance the chemical equation for n-octane for the stoichiometric condition and 350-percent air.
- 9.13** Find the adiabatic flame temperature of liquid n-decane for 350-percent air if the fuel inlet total temperature is 1020 °R and the air inlet total temperature is 1150 °R. What is the fuel-to-air mixture ratio?
- 9.14** If air enters an afterburner with flameholders at 1670 °R total temperature with a specific heat ratio of 1.36 and a total pressure of 73 psia, find the total pressure ratio across the burner as a function of entrance Mach number if the drag coefficient of the flameholders is 0.53, the area ratio of flameholder to total area is 0.18, and the exit total temperature is 3450 °R. Plot the results.
- 9.15** Find the adiabatic flame temperature of liquid n-octane for 300-percent air if the fuel inlet total temperature is 935 °R and the air inlet total temperature is 1040 °R. What is the fuel-to-air mixture ratio?
- 9.16** Using the enthalpies of formation, find the heating value of liquid n-octane at 298 K.
- 9.17** You are given kerosene (n-decane) at 950 °R burning with air at 1400 °R.
- What is the temperature of the products for 100-, 200-, 350-, and 1000-percent air?
 - Accurately plot T_{prod} versus % air.
 - What is the fuel-to-air mass flow ratio f for these conditions?
 - Plot T_{prod} versus f .
- 9.18** You have a combustion chamber with an incoming Mach number M_3 , an incoming total pressure of 275 psia, an incoming air total temperature of 1400 °R, and an inlet area of 0.30 ft². The exiting total temperature is T_{14} . Assume $\gamma = 1.30$. What is the burner total pressure ratio (π_b) for the conditions below?
- $T_{14} = 2490$ °R; $M_3 = 0.1, 0.22, 0.42$
Plot π_b versus M_3 .
Plot π_b versus \dot{m} (lbm/s).
 - $M_3 = 0.42, T_{14} = 1400, 2060, 2490$ °R
Plot π_b versus T_{14} .
Plot π_b versus f if the fuel is kerosene
(see Problem 9.17 to determine how f varies with T_{14}).
- 9.19** A burner has an inlet Mach number of 0.35, an inlet total pressure of 250 psia and an inlet total temperature of 1100 °R. The exit total temperature is 2300 °R. The chamber is 18 in. long, is 3.5 in. in diameter, and has a friction factor of 0.037. You are to find the total pressure ratio for the burner. Assume

friction and heat addition can be treated separately and the specific heat ratio is 1.30.

- 9.20** You are given kerosene (n-decane) at 1100 °R burning with air at 1200 °R.
- What is the temperature of the products for 100-, 200-, and 400-percent air?
 - Accurately plot T_{prod} versus % air.
 - What is the fuel-to-air mass flow ratio f for these conditions?
 - Plot T_{prod} versus f .
- 9.21** You have a combustion chamber with an incoming Mach number M_3 , an incoming total pressure of 250 psia, an incoming air total temperature of 1200 °R, and an inlet area of 0.40 ft². The exiting total temperature is T_{t4} . Assume $\gamma = 1.32$. Determine the map for the given set of conditions; that is, what is the burner total pressure ratio (π_b) for the conditions below?
- $T_{t4} = 2500$ °R; $M_3 = 0.1, 0.25, 0.37$
Plot π_b versus M_3 .
Plot π_b versus \dot{m} (lbm/s).
 - $M_3 = 0.37, T_{t4} = 1200, 2000, 2500$ °R
Plot π_b versus T_{t4} .
Plot π_b versus f if the fuel is kerosene
(see Problem 9.20 to determine how f varies with T_{t4}).
- 9.22** A burner has an inlet Mach number of 0.25, an inlet total pressure of 250 psia, and an inlet total temperature of 1100 °R. The exit total temperature is 2300 °R. The chamber is 18 in. long, is 3.5 in. in diameter, and has a friction factor of 0.037. You are to find the total pressure ratio for the burner. Assume friction and heat addition can be treated separately and the specific heat ratio is 1.30.
- 9.23** You are given kerosene (n-decane) at 1000 °R burning with air at 1250 °R.
- What is the temperature of the products for 100-, 200-, 400-, and 800-percent air?
 - Accurately plot T_{prod} versus % air.
 - What is the fuel-to-air mass flow ratio f for these conditions?
 - Plot T_{prod} versus f .
- 9.24** You have a combustion chamber with an incoming Mach number M_3 , an incoming total pressure of 260 psia, an incoming air total temperature of 1250 °R, and an inlet area of 0.42 ft². The exiting total temperature is T_{t4} . Assume $\gamma = 1.31$. Determine the map for the given set of conditions; that is, what is the burner total pressure ratio (π_b) for the conditions below?
- $T_{t4} = 2700$ °R; $M_3 = 0.15, 0.25, 0.35$
Plot π_b versus M_3 .
Plot π_b versus \dot{m} (lbm/s).
 - $M_3 = 0.35, T_{t4} = 1700, 2200, 2700$ °R
Plot π_b versus T_{t4} .
Plot π_b versus f if the fuel is kerosene
(see Problem 9.23 to determine how f varies with T_{t4}).
- 9.25** You are given n-decane at 1100 °R burning with air at 1200 °R. What is the temperature of the products for 300-percent air? For simplicity, you may assume that the specific heats are not functions of temperature and are equal

to 33.19, 54.37, 30.20, 41.26, 32.70, 34.88, and 296.0 kJ/kg-mole-K for CO, CO₂, H₂, H₂O, N₂, O₂, and C₁₀H₂₂, respectively.

- 9.26** You are given *n*-decane at 611 K (1100 °R) burning with air at 667 K (1200 °R). What percentage of air will result in an exit temperature of 1465 K (2637 °R)? For simplicity you may assume that the specific heats are not functions of temperature and are equal to 33.19, 54.37, 30.20, 41.26, 32.70, 34.88, and 296.0 kJ/kg-mole-K for CO, CO₂, H₂, H₂O, N₂, O₂, and C₁₀H₂₂, respectively.
- 9.27** You are given *n*-decane at 667 K (1200 °R) burning with air at 556 K (1000 °R). What percentage of air will result in an exit temperature of 1502 K (2704 °R)? For simplicity you may assume that the specific heats are not functions of temperature and are equal to 33.4, 57.7, 30.3, 41.1, 32.9, 35.2, and 296.0 kJ/kg-mole-K for CO, CO₂, H₂, H₂O, N₂, O₂, and C₁₀H₂₂, respectively.
- 9.28** You are given *n*-decane at 444 K (800 °R) burning with air at 556 K (1000 °R). What percentage of air will result in an exit temperature of 1358 K (2444 °R)? For simplicity, you may assume that the specific heats at constant pressure are not functions of temperature and are equal to 55.7, 40.4, 32.5, 34.6, and 296.0 kJ/kg-mole-K for CO₂, H₂O, N₂, O₂, and C₁₀H₂₂, respectively.
- 9.29** Air enters a combustor at total conditions of 200 psia and 1250 °R and at a Mach number of 0.25. The gas is heated to 2760 °R. Find the pressure at the exit of the burner if friction is negligible and the exit Mach number. Assume the specific heat ratio is 1.350.

Ducts and Mixers

10.1. Introduction

Two remaining components that affect the overall performance of a turbofan engine are the bypass duct and mixer, as shown in Figure 10.1. These are relatively simple compared with the other components but should be included because they both generate losses in total pressure. Because the length-to-flow-width ratio of the bypass duct is moderate, the duct can incur significant losses. Also, it is desirable to have a uniform temperature gas entering the afterburner or nozzle so that these components operate near peak efficiency. Mixing of two fluid streams at different temperatures is a highly irreversible process, and a mixer consists of three-dimensional vanes in both the radial and circumferential (annular) directions. Thus, with good mixing of the low-temperature bypassed air and high-temperature primary air, further significant losses can occur. Owing to the temperatures exiting from the turbine, mixers are generally fabricated from a nickel-based alloy. This chapter covers total pressure losses in these two components.

10.2. Total Pressure Losses

Three irreversible mechanisms exist for pressure drops and total pressure losses to occur in ducts and mixers. The first is frictional flow in the duct primarily due to the viscous effects in the boundary layer. The second is the irreversible mixing process of two gas streams with different properties in the mixer. The third is the loss incurred by the mixer because it is a drag obstacle in the flow used to promote good “folding” and mixing of the two streams; this loss is similar to the loss due to a flameholder. Each of the losses are treated and analyzed independently in this chapter, although in Appendix H, a numerical methodology is presented (generalized one-dimensional compressible flow) whereby several effects can simultaneously be included.

10.2.1. Fanno Line Flow

The first effect to be analyzed is due to friction in the flow. This friction is generated by the wall friction in the boundary layer as well as freestream turbulence, which causes viscous dissipation. This will be analyzed based on Fanno line flow, which is flow with friction but no heat addition. The process is a constant area irreversible process. The flow is analyzed with a control volume approach in Appendix H. Eleven equations are involved in the analysis. Seventeen variables are present, and so six must be specified. For example, if the inlet conditions M_1 , T_1 , and p_{t1} and duct information L , D , and f are specified, one can find p_{t2} and thus the resulting total pressure drop or total pressure ratio. Solutions can also be obtained using the software, “FANNO.”

Example 10.1: Flow with an incoming Mach number of 0.50 and an inlet total pressure of 25 psia enters the bypass duct approximating the size of an older engine

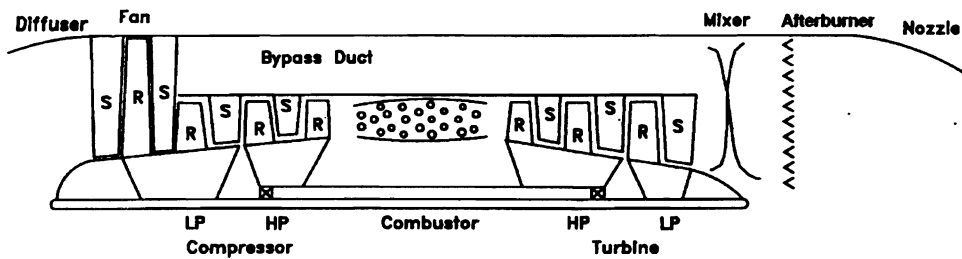


Figure 10.1 Turbofan engine with bypass duct and mixer.

duct. The duct is 110 in. long with an average outside diameter of 19 in. and an average inside diameter of 13 in., yielding a hydraulic diameter of 6 in. The duct has a Fanning friction factor of 0.003. What is the total pressure ratio if the specific heat ratio is 1.40?

SOLUTION:

From the tables for a Mach number of 0.50, one can find the nondimensional length-to-diameter and pressure parameters:

$$\left. \frac{4fL^*}{D} \right]_1 = 1.0691$$

and

$$\frac{p_{t1}}{p_t^*} = 1.3398;$$

thus, the total pressure can be found at the sonic condition, which is a reference condition (that might not occur in the actual conditions) as follows:

$$p_t^* = 25/1.3398 = 18.659 \text{ psia.}$$

Next, from the duct geometry, one can find the parameter

$$\left. \frac{4fL}{D} \right]_{1-2} = \frac{4 \times 0.003 \times 110}{6} = 0.2200;$$

thus, one can find the corresponding length-to-diameter parameter at the exit

$$\left. \frac{4fL^*}{D} \right]_2 = \left. \frac{4fL^*}{D} \right]_1 - \left. \frac{4fL}{D} \right]_{1-2} = 1.0691 - 0.2200 = 0.8491.$$

Hence, the exit Mach number can be found from the tables or equations as follows:

$$M_2 = 0.5301.$$

Thus, as the result of friction the Mach number increased about 6 percent. Next, from the tables, at this Mach number

$$\frac{p_{t2}}{p_t^*} = 1.2863,$$

and so the exit total pressure can be found: $p_{t2} = 1.2863 \times 18.659 = 24.00$ psia. The pressure ratio for the duct is therefore

$$\pi = \frac{p_{t2}}{p_{t1}} = \frac{24.00}{25} = 0.960.$$

This is a significant loss and should be minimized further (if possible) by reducing the friction factor or Mach number.

10.2.2. Mixing Process

A second process that results in total pressure losses is the irreversible mixing process. For this occurrence, two streams (one from the bypass duct and one from the turbine exit) at different temperatures, total temperatures, Mach numbers, flow rates, velocities, total pressures, and so on are irreversibly mixed to form one (hopefully) uniform stream. Note that the mixing process is ideally frictionless, although in actuality friction is involved as discussed in the next section. Thus, in reality, two mechanisms generate a loss in total pressure for a mixer. This mixing process is also analyzed in Appendix H. From this analysis, 27 unknowns are present. However, 19 independent equations are available. Thus, if 8 variables are specified, one can find the remaining 19. For example, if the inlet conditions \dot{m}_1 , \dot{m}_2 , T_{t1} , T_{t2} , p_{t1} , p_{t2} , M_1 , and M_2 are known, the exit conditions can be found, including the total pressure. Solutions can also be obtained using the software, "GENERAL1D."

Example 10.2: Two streams at different total temperatures mix. The stream from the fan bypass duct has a total temperature (T_{t1}) of 444.4 K (800 °R), and the stream from the turbine exit has a total temperature (T_{t2}) of 888.9 K (1600 °R). The bypass flow rate (\dot{m}_1) is 45.35 kg/s (100 lbm/s), and the primary flow rate (\dot{m}_2) is 90.70 kg/s (200 lbm/s). The Mach number of both streams is 0.5546, and the total pressure of both streams is 160.6 kPa (23.29 psia). Assume the specific heat ratio is 1.400 and find the fully mixed conditions.

SOLUTION:

First, from Eqs. H.10.13 and H.10.14, one finds the static temperatures

$$T_1 = \frac{T_{t1}}{\left[1 + \frac{\gamma-1}{2}M_1^2\right]} = \frac{444.4}{\left[1 + \frac{0.4}{2}0.5546^2\right]} = 418.8 \text{ K (753.6 }^\circ\text{R)}$$

$$T_2 = \frac{T_{t2}}{\left[1 + \frac{\gamma-1}{2}M_2^2\right]} = \frac{888.9}{\left[1 + \frac{0.4}{2}0.5546^2\right]} = 837.4 \text{ K (1507.3 }^\circ\text{R)}$$

From Eqs. H.10.16 and H.10.17, one obtains the static pressures

$$p_1 = p_{t1} \left\{ \frac{1}{\left[1 + \frac{\gamma-1}{2}M_1^2\right]} \right\}^{\frac{\gamma}{\gamma-1}} = 160.6 \left\{ \frac{1}{\left[1 + \frac{0.4}{2}0.5546^2\right]} \right\}^{\frac{1.4}{0.4}}$$

$$= 130.3 \text{ kPa (18.90 psia)}$$

$$p_2 = p_{t2} \left\{ \frac{1}{\left[1 + \frac{\gamma-1}{2}M_2^2\right]} \right\}^{\frac{\gamma}{\gamma-1}} = 160.6 \left\{ \frac{1}{\left[1 + \frac{0.4}{2}0.5546^2\right]} \right\}^{\frac{1.4}{0.4}}$$

$$= 130.3 \text{ kPa (18.90 psia)}$$

from the temperatures calculated above as follows: The sound speeds can also be found

$$a_1 = \sqrt{\gamma \mathcal{R} T_1} = \sqrt{1.4 \times 287.1 \frac{\text{J}}{\text{kg}\cdot\text{K}} \times 418.7 \text{ K} \times \frac{\text{N}\cdot\text{m}}{\text{J}} \times \frac{\text{kg}\cdot\text{m}}{\text{N}\cdot\text{s}^2}}$$

$$= 410.3 \text{ m/s (1345.7 ft/s)}$$

$$a_2 = \sqrt{\gamma \mathcal{R} T_2} = \sqrt{1.4 \times 287.1 \frac{\text{J}}{\text{kg}\cdot\text{K}} \times 837.4 \text{ K} \times \frac{\text{N}\cdot\text{m}}{\text{J}} \times \frac{\text{kg}\cdot\text{m}}{\text{N}\cdot\text{s}^2}}$$

$$= 580.0 \text{ m/s (1903.1 ft/s)}$$

For the given Mach numbers the velocities of the incoming streams are thus

$$V_1 = M_1 a_1 = 0.5546 \times 410.3 = 227.5 \text{ m/s (746.31 ft/s)}$$

$$V_2 = M_2 a_2 = 0.5546 \times 580.0 = 321.7 \text{ m/s (1055.4 ft/s)}.$$

Next, for an ideal gas for the temperatures and pressures given above the densities are

$$\rho_1 = 0.2229 \text{ kg/m}^3 \text{ (0.002104 slug/ft}^3\text{)}$$

$$\rho_2 = 0.5423 \text{ kg/m}^3 \text{ (0.001052 slug/ft}^3\text{)}.$$

Hence, from Eqs. H.10.2 and H.10.3 the inlet areas can be found as follows:

$$A_1 = \frac{\dot{m}_1}{\rho_1 V_1} = \frac{45.35 \frac{\text{kg}}{\text{s}}}{1.085 \frac{\text{kg}}{\text{m}^3} \times 227.5 \frac{\text{m}}{\text{s}}} = 0.1839 \text{ m}^2 \text{ (1.9797 ft}^2\text{)}$$

$$A_2 = \frac{\dot{m}_2}{\rho_2 V_2} = \frac{90.70 \frac{\text{kg}}{\text{s}}}{0.5423 \frac{\text{kg}}{\text{m}^3} \times 321.7 \frac{\text{m}}{\text{s}}} = 0.5201 \text{ m}^2 \text{ (5.5993 ft}^2\text{)}.$$

From eq. H.10.1, the exit area is therefore

$$A_3 = A_1 + A_2 = 0.1839 + 0.5201 = 0.7040 \text{ m}^2 \text{ (7.5790 ft}^2\text{)}.$$

From Eqs. H.10.4 and H.10.5, one finds the total mass flow from the exit by

$$\dot{m}_3 = \dot{m}_1 + \dot{m}_2 = 45.35 + 90.70 = 136.1 \text{ kg/s (300 lbm/s)},$$

and from Eq. H.10.9 the total temperature at the exit is (all of the specific heats are the same and thus cancel)

$$\begin{aligned} T_{t3} &= \frac{\dot{m}_1 c_p T_{t1} + \dot{m}_2 c_p T_{t2}}{\dot{m}_3 c_p} = \frac{45.35 \times 444.4 + 90.70 \times 888.9}{136.1} \\ &= 740.7 \text{ K (1333.3 }^\circ\text{R)} \end{aligned}$$

Next, using Eq. H.10.25 yields

$$\begin{aligned} (p_1 + \rho_1 V_1^2) A_1 + (p_2 + \rho_2 V_2^2) A_2 &= \dot{m}_3 \left[\frac{\mathcal{R} T_3}{\sqrt{2c_p(T_{t3} - T_3)}} + \sqrt{2c_p(T_{t3} - T_3)} \right] \\ \left[130.3 \text{ kPa} \times 1000 \frac{\text{N/m}^2}{\text{kPa}} + 1.085 \frac{\text{kg}}{\text{m}^3} \times 227.5^2 \frac{\text{m}^2}{\text{s}^2} \times \frac{\text{N}}{\frac{\text{kg}\cdot\text{m}}{\text{s}^2}} \right] &\times 0.1839 \text{ m}^2 \\ + \left[130.3 \frac{\text{lbf}}{\text{in}^2} \times 1000 \frac{\text{N/m}^2}{\text{kPa}} + 0.5423 \frac{\text{kg}}{\text{m}^3} \times 321.7^2 \frac{\text{m}^2}{\text{s}^2} \times \frac{\text{N}}{\frac{\text{kg}\cdot\text{m}}{\text{s}^2}} \right] &\times 0.5201 \text{ m}^2 \\ = 136.1 \frac{\text{kg}}{\text{s}} \times \left[\frac{287.1 \frac{\text{J}}{\text{kg}\cdot\text{K}} \times T_3(\text{K})}{\sqrt{2 \times 1.005 \frac{\text{kJ}}{\text{kg}\cdot\text{K}} \times (740.7 \text{ K} - T_3(\text{K})) \times 1000 \frac{\text{J}}{\text{kJ}} \times \frac{\text{N}\cdot\text{m}}{\text{J}} \times \frac{\text{kg}\cdot\text{m}}{\text{N}\cdot\text{s}^2}}} \right. \\ &+ \left. \sqrt{2 \times 1.005 \frac{\text{kJ}}{\text{kg}\cdot\text{K}} \times (740.7 \text{ K} - T_3(\text{K})) \times 1000 \frac{\text{J}}{\text{kJ}} \times \frac{\text{N}\cdot\text{m}}{\text{J}} \times \frac{\text{kg}\cdot\text{m}}{\text{N}\cdot\text{s}^2}} \right]. \end{aligned}$$

Thus, by iteration one finds the static temperature at the exit as

$$T_3 = 695.7 \text{ K (1252.2 }^\circ\text{R)},$$

and so from Eq. H.10.24 the velocity at the exit is

$$V_3 = \sqrt{2c_p(T_{t3} - T_3)}$$

$$= \sqrt{2 \times 1.005 \frac{\text{kJ}}{\text{kg-K}} \times (740.7 \text{ K} - 695.7 \text{ K}) \times 1000 \frac{\text{J}}{\text{kJ}} \times \frac{\text{N-m}}{\text{J}} \times \frac{\text{kg-m}}{\text{N-s}^2}}$$

$$V_3 = 300.9 \text{ m/s (987.26 ft/s)}.$$

From eq. H.10.4 the exit density is

$$\rho_3 = \frac{\dot{m}_3}{V_3 A_3} = \frac{136.1 \frac{\text{kg}}{\text{s}}}{300.9 \frac{\text{m}}{\text{s}} \times 0.7040 \text{ m}^2}$$

$$\rho_3 = 0.6515 \text{ kg/m}^3 (0.001246 \text{ slug/ft}^3).$$

From Eq. H.10.21, one finds the Mach number at the exit by

$$M_3 = \frac{V_3}{\sqrt{\gamma \mathcal{R} T}} = \frac{300.9 \frac{\text{m}}{\text{s}}}{\sqrt{1.4 \times 287.1 \frac{\text{J}}{\text{kg-K}} \times 695.7 \text{ K} \times \frac{\text{N-m}}{\text{J}} \times \frac{\text{kg-m}}{\text{N-s}^2}}}$$

$$M_3 = 0.5692,$$

and for an ideal gas (Eq. H.10.12) with the static temperature and density, the static pressure at the exit is

$$p_3 = 128.3 \text{ kPa (18.60 psia)}.$$

Finally, from Eq. H.10.18, the total pressure at the exit is

$$p_{t3} = p_3 \left[\frac{T_{t3}}{T_3} \right]^{\frac{\gamma}{\gamma-1}} = 128.3 \left[\frac{740.7}{695.7} \right]^{\frac{1.4}{0.4}}$$

$$p_{t3} = 159.8 \text{ kPa (23.171 psia)}.$$

Finally, the total pressure ratio due only to irreversible mixing is

$$\frac{p_{t3}}{p_{t1}} = \left[\frac{159.8}{160.6} \right] = 0.9949.$$

That is, less than 1 percent of the total pressure was lost as a result of the mixing process.

10.2.3. Flow with a Drag Object

When an obstruction is in the flow, the total pressure is also reduced because of the boundary layer friction around the obstruction and from the added wake turbulence, separation, and shearing of the fluid, which results in viscous dissipation. Mixers contain such obstructions to enhance the folding and mixing of the two streams. Thus, a method of including such losses is needed to complement the pure mixing process. A control volume approach is used for a constant area flow for which uniform properties are assumed at the entrance and exit. Details are covered in Appendix H. For the end result, there are 16 variables and 11 equations. Thus, if five variables are specified the problem can be solved. Typically, if the mixer inlet conditions M_1 , p_{t1} , and T_{t1} and mixer geometry parameters A_d/A and C_d are known, the exit conditions can be found, including the total pressure loss. Solutions can also be obtained using the software, "GENERAL1D."

Example 10.3: Flow exiting the mixing process of Example 10.2 enters the mix enhancer. Thus, flow with an incoming Mach number of 0.5692, an inlet total pressure of 23.171 psia, and a total temperature of 1333.33 °R enters the enhancer.

The drag coefficient of the mixer is 0.4, and it occupies 8 percent of the total flow area. What is the total pressure ratio if the specific heat ratio is 1.40?

SOLUTION:

First, for the given inlet Mach number and total conditions, one can find the static conditions:

$$T_1 = 1252.2 \text{ }^\circ\text{R}$$

$$p_1 = 18.600 \text{ psia,}$$

For this value of T_1 the sound speed is

$$a_1 = 1734.57 \text{ ft/s,}$$

and from the Mach number the inlet velocity is

$$v_1 = 987.32 \text{ ft/s.}$$

Also for T_1 and p_1 , from the ideal gas equation the inlet density is

$$\rho_1 = 0.001246 \text{ slug/ft}^3;$$

thus, from Eq. H.9.8,

$$\begin{aligned} p_1 + \rho_1 V_1^2 - \frac{1}{2} C_d \rho_1 V_1^2 \frac{A_d}{A} &= \rho_1 V_1 \left[\frac{\mathcal{R} T_2}{\sqrt{2c_p(T_{11} - T_2)}} + \sqrt{2c_p(T_{11} - T_2)} \right] \\ 18.600 \times 144 + 0.001246 \times 987.32^2 - \frac{1}{2} \times 0.4 \times 0.001246 \times 987.32^2 \times 0.08 \\ &= 0.001246 \cdot 987.32 \left[\frac{53.35 \times 32.17 T_2}{\sqrt{2 \times 0.2400 \times 32.17 \times 778.16 \times (1333.3 - T_2)}} \right. \\ &\quad \left. + \sqrt{2 \times 0.2400 \times 32.17 \times 778.16 \times (1333.3 - T_2)} \right]. \end{aligned}$$

Iteratively solving for the exit static temperature T_2 , one finds

$$T_2 = 1250.4 \text{ }^\circ\text{R.}$$

Thus, from Eq. H.9.7 the exit velocity is

$$\begin{aligned} V_2 &= \sqrt{2c_p(T_{12} - T_2)} \\ &= \sqrt{2 \times 0.2400 \frac{\text{Btu}}{\text{lbm } ^\circ\text{R}} \times 778.16 \frac{\text{ft-lbf}}{\text{Btu}} \times 32.17 \frac{\text{lbm}}{\text{slug}}} \\ &\quad \times \sqrt{(1333.3 \text{ }^\circ\text{R} - 1250.4 \text{ }^\circ\text{R}) \times \frac{\text{slug-ft}}{\text{lbf sec}^2}} \\ &= 998.1 \text{ ft/s.} \end{aligned}$$

The sound speed at the exit is $a_2 = 1733.3 \text{ ft/s}$;

thus, the exit Mach number is $M_2 = 0.5758$,

and the exit density is

$$\rho_2 = \rho_1 V_1 / V_2 = 0.001246 \times 987.32 / 998.10 = 0.001233 \text{ slug/ft}^3.$$

From the ideal gas law the exit pressure is $p_2 = 18.3727 \text{ psia}$.

Finally, for $M_2 = 0.5758$ and the p_2 above, the total pressure at the exit is

$$p_{02} = 23.002 \text{ psia,}$$

and the total pressure ratio due to the friction from the mix enhancer is

$$\pi = p_{02} / p_{01} = 23.002 / 23.171 = 0.9927.$$

One can see that this loss in total pressure is small owing to the drag obstacle and that it is of the same order of magnitude as that due to the mixing process found in Example 10.2. Thus, with the result from Example 10.2 the total pressure ratio for the entire mixer can conservatively be estimated by multiplying the two ratios:

$$\pi = 0.9949 \times 0.9927 = 0.9876.$$

The loss in total pressure is therefore less than 2 percent from the two mechanisms.

10.3. Summary

This chapter has covered total pressure losses in the bypass duct and mixer of a turbofan engine. The duct delivers air from the fan to the mixer. The mixer folds the bypassed air into the core airflow so that the flow into the afterburner or nozzle has nearly uniform properties. Although simple components, they both induce total pressure losses. Frictional flow (Fanno line) was used to model the flow in the duct; losses are due to wall friction and turbulent shear. Separate, irreversible mixing and drag obstacles (mixer vanes) models (and resulting fluid shear) were used to predict the total pressure losses in the mixer. Moderate losses occur in the frictional flow in the duct. Other losses are due to the mixing process and also due to the added drag of the obstacles used to enhance good mixing of the flow. Reduction of the frictional loss is achieved by using smooth boundaries to minimize the friction factor. One must use a trade-off in minimizing the mixing loss because, to obtain maximum mixing, moderate total pressure losses can occur. However, if good mixing is not achieved, uniform flow will not enter the afterburner and nozzle and they will not perform at near peak efficiency.

List of Symbols

A	Area
c_p	Specific heat at constant pressure
C_d	Drag coefficient
D	Diameter
F	Force
f	Fanning friction factor
h	Specific enthalpy
L	Length
\dot{m}	Mass flow rate
M	Mach number
p	Pressure
\mathcal{R}	Ideal gas constant
s	Entropy
T	Temperature
V	Velocity
γ	Specific heat ratio
π	Total pressure ratio
ρ	Density

Subscripts

d	Drag
t	Total (stagnation)
1,2,3	Positions for process analysis

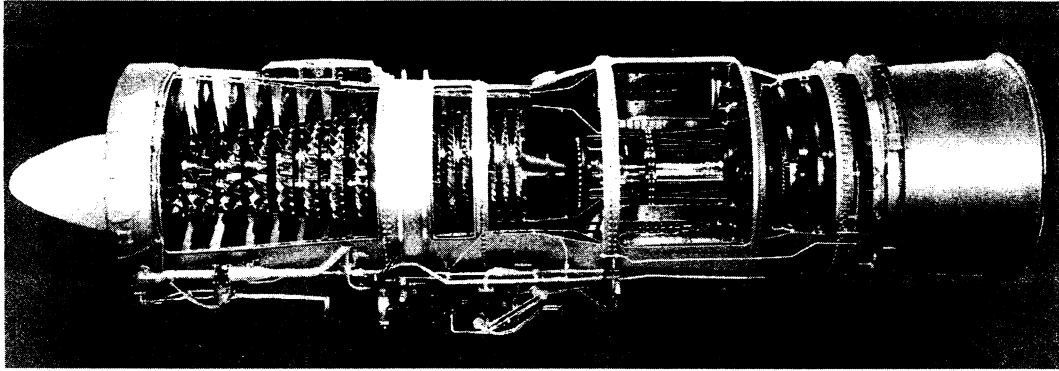
Superscripts

* Choked

Problems

- 10.1** A mixer is to be analyzed. The duct flow rate from the fan is 200 lbm/s and is at a Mach number of 0.45, whereas the primary flow rate is 75 lbm/s and is at a Mach number of 0.75. The total temperatures of the bypassed and primary air are 900 and 1500 °R, respectively. The static pressures of the two streams are 15 psia. Find the exit conditions of only the mixing process. That is, find the total temperature, static pressure, total pressure, and Mach number. Assume $\gamma = 1.40$.
- 10.2** A mixer is to be analyzed. The duct flow rate from the fan is 200 lbm/s and is at a Mach number of 0.45, whereas the primary flow rate is 75 lbm/s and is at a Mach number of 0.75. The total temperatures of the bypassed and primary air are 900 and 1500 °R, respectively. The static pressures of the two streams are 15 psia. A structural member in the flow is used to promote mixing of the two streams. The member has a drag coefficient of 0.60, and the frontal area of the member is 7 percent of the total flow area. Find the exit conditions of the combined mixing process and flow around the drag object. That is, find the total temperature, static pressure, total pressure, and Mach number. Assume $\gamma = 1.40$.
- 10.3** Flow in a bypass duct is to be analyzed. Air enters the duct at a Mach number of 0.4 and a total temperature of 900 and total pressure of 20 psia. The length of the duct is 4.5 ft, and the average effective diameter is 0.35 ft. The Fanning friction factor is 0.035. Find the exit conditions, including the Mach number and total pressure. Assume $\gamma = 1.40$.
- 10.4** A mixer is to be analyzed. The duct flow rate from the fan is 60 lbm/s and is at a Mach number of 0.55, whereas the primary flow rate is 120 lbm/s and is at a Mach number of 0.85. The total temperatures of the bypassed and primary air are 1000 and 1700 °R, respectively. The static pressures of the two streams are 20 psia. The mixer has a drag coefficient and occupies 6 percent of the flow area. Find the exit conditions of only the mixing process for the two conditions that follow. That is, find the total temperature, static pressure, total pressure, and Mach number. Assume $\gamma = 1.40$. (a) Drag coefficient is 0.00, (b) Drag coefficient is 0.60.
- 10.5** A mixer is to be analyzed. The duct flow rate from the fan is 100 lbm/s and is at a Mach number of 0.60, whereas the primary flow rate is 100 lbm/s and is at a Mach number of 0.80. The total temperatures of the bypassed and primary air are 900 and 1800 °R, respectively. The static pressures of the two streams are 24 psia. The mixer has a drag coefficient and occupies 8 percent of the flow area. Find the exit conditions of only the mixing process for the two conditions that follow. That is, find the total temperature, static pressure, total pressure, and Mach number. Assume $\gamma = 1.38$. (a) Drag coefficient is 0.00, (b) Drag coefficient is 0.70.

System Matching and Analysis



PWJ57
(courtesy of Pratt & Whitney)



Matching of Gas Turbine Components

11.1. Introduction

In the previous seven chapters, much emphasis has been placed on the analysis and design of individual components of gas turbines. On the other hand, in Chapters 2 and 3 cycle analyses are presented for ideal and nonideal engines as a whole in which the different components are integrated into a system. However, in Chapter 3, component efficiencies and some characteristics are assumed or assigned a priori for the overall cycle analyses. In general, however, the previous seven chapters demonstrate, through the use of either theoretical analyses or empirical characteristic curves (or “maps”), that component efficiencies and other operating characteristics change significantly at different conditions – for example, at different flow rates and rotational speeds.

To understand the overall effects of changing operating conditions, one can consider an engine initially at some steady-state operating condition. However, as the fuel injection rate in the burner is changed, the turbine inlet temperature and pressure are changed. Thus, the turbine will change rotational speeds. Because the turbine and compressor are on the same shaft, however, this change in rotational speed in turn changes the ingested mass flow rate and pressure ratio developed by the compressor, which influences the burner inlet pressure and the turbine inlet pressure, and so on. Eventually, the engine will again reach a different steady-state operating condition. In other words, the different components interact and influence each other as an engine changes flight conditions. These interactions dictate the overall engine characteristics, including parameters such as mass flow rate, rotational speed, pressure ratios, thrust, derived power, and so forth. The ways in which the components interact and how their individual characteristics dictate the engine steady state operating point are termed component matching and form the topic of this chapter.

Up to this point, the components have been treated as being independent of each other; this is not the case, for they can interact strongly. Yet, this interaction or matching between the components dictates the overall performance of a gas turbine, as discussed by El-Masri (1988), Johnsen and Bullock (1965), Kurzke (1995, 1998), Mirza-Baig and Saravanamuttoo (1991), and Saito et al. (1993). Not only should each component operate individually with a high efficiency, but a gas turbine as a system must operate efficiently so that the maximum power is derived. Thus, components must be chosen so that they can operate near peak efficiency as a unit.

The overall objective of this chapter is first to present a method whereby the steady-state matching point of the compressor, burner, and turbine (which are as a combination called a gas generator) can be determined if individual component performance characteristic curves or maps are known. The gas generator can then be coupled with the other gas turbine components to determine the matching point of the entire engine or power plant. Mathematical models for the diffuser, compressor, combustor, turbine, nozzle, inlet, and exhaust that can be used to represent available maps or data are presented to accomplish this objective. Such modeling allows the matching process to be accomplished relatively easily using computer analyses. The individual component models are then assembled to

determine the overall matching point of a gas turbine. The matching point can be found for different fuel flows and, thus, the engine operating line can be predicted. Both on-design and off-design operating points can be analyzed. The analysis represents a relatively simple method whereby a large and complex database can be condensed to the operating condition of a gas turbine. In this chapter, the methodology is applied only to a simple turbojet without an afterburner (Fig. 2.40) and to a simple power-generation gas turbine or turboshaft (Fig. 2.61). In general, however, the approach can be applied to any of the previously covered engine or power-generation gas turbine types. As a last step, determining the matching points of a jet engine(s) with an airframe is discussed so that aircraft speed can be predicted as the fuel rate is varied.

11.2. Component Matching

Because each component of a gas turbine cannot act independently of the other components, the general procedure by which the gas turbine matching point is determined must be developed. This is done for three cases. The first case is a single-shaft gas generator (compressor, burner, and turbine). The second case is for an entire single-spool turbojet engine (diffuser, gas generator, and nozzle) as discussed by Flack (1990). The third case is for an entire single-spool power gas turbine (inlet, gas generator, exhaust, and load) as discussed by Flack (2002). Simulations of the engine operating conditions can be made if individual component performance characteristic curves or maps are known. Because most of the concepts of maps are covered in previous chapters, they will not be discussed in great detail in this chapter but will be reviewed and summarized. Kurzke (1996) also presents a method of estimating maps.

11.2.1. Gas Generator

a. Compressor

Dimensional analysis, which is discussed in Chapter 6, shows that the developed total pressure ratio and efficiency of a compressor are functions of only two parameters: the “corrected” mass flow and “corrected” speed, regardless of altitude, absolute speed, and so on. The general functional relationships for a compressor map (Fig. 6.14) namely, pressure ratio and efficiency – are specified in Chapter 6 as

$$\pi_c = \phi_c(\dot{m}_{c2}, N_{c2}) \quad 11.2.1$$

$$\eta_c = \psi_c(\dot{m}_{c2}, N_{c2}), \quad 11.2.2$$

where ϕ_c and ψ_c represent empirical functions that are either predicted or determined experimentally for a given compressor and can be in graphical, tabular, or equational form. Similar notation is used for the functions of other components. Recall that the corrected values of mass flow and speed for the compressor are defined by

$$\dot{m}_{c2} \equiv \dot{m}_2 \frac{\sqrt{T_{t2}/T_{stp}}}{p_{t2}/p_{stp}} = \dot{m} \frac{\sqrt{T_{t2}/T_{stp}}}{p_{t2}/p_{stp}} \quad 11.2.3$$

$$N_{c2} \equiv \frac{N}{\sqrt{T_{t2}/T_{stp}}}. \quad 11.2.4$$

The subscript stp denotes standard conditions ($p_{\text{stp}} = 14.69$ psia or 101.33 kPa and $T_{\text{stp}} = 518.7$ °R or 288.2 K), total conditions are evaluated at the compressor inlet, the true mass flow rate into the compressor is \dot{m} , and N is the true rotational speed of the shaft. Corrected mass flow rate and speed are similarly defined for the other components.

As shown in Chapters 3 and 6 (Eq. 3.2.8) from a thermodynamics analysis, the compressor total pressure ratio is related to the total temperature ratio as follows:

$$\pi_c = [1 + \eta_c(\tau_c - 1)]^{\frac{\gamma}{\gamma-1}}. \quad 11.2.5$$

As in previous chapters, specific heats are evaluated at the average temperature of a given component and will not be subscripted here for the sake of brevity.

b. Turbine

Similarly, in Chapter 8 a turbine map is discussed (Fig. 8.12). Although the map has a much different shape than that for a compressor, the total pressure ratio and efficiency are functions of only two parameters: the “corrected” turbine mass flow and “corrected” turbine speed regardless, again, of altitude, absolute speed, and so on. These general functional relationships are as follows:

$$\pi_t = \phi_t(\dot{m}_{c4}, N_{c4}) \quad 11.2.6$$

$$\eta_t = \psi_t(\dot{m}_{c4}, N_{c4}). \quad 11.2.7$$

Again, these functions can be predicted or measured and can be in graphical, tabular, or equational form. From Chapters 3 and 8 (Eq. 3.2.19), the turbine total pressure ratio is related to the total temperature ratio by

$$\pi_t = \left[1 + \frac{(\tau_t - 1)}{\eta_t} \right]^{\frac{\gamma}{\gamma-1}}. \quad 11.2.8$$

c. Combustor

In Chapter 3, a simple energy balance from the first law of thermodynamics (Eq. 3.2.24) for the burner is expressed as

$$f(\eta_b \Delta H - c_p T_{i3} \tau_b) = c_p T_{i3} (\tau_b - 1), \quad 11.2.9$$

where ΔH is the enthalpy of reaction and f is the fuel-to-air flow ratio. Note that this can be replaced by a more accurate adiabatic flame temperature calculation, as is done in Chapter 9. In that chapter, characteristics for a combustor are covered and a typical burner map is shown in Figures 9.11 and 9.12. The burner efficiency and total pressure are shown there to be a result of both friction and the combustion process; they are functions of basically only two parameters:

$$\eta_b = \psi_b \left(\dot{m}_{c3}, \frac{f}{T_{i3}/T_{\text{stp}}} \right) \quad 11.2.10$$

$$\pi_b = \phi_b \left(\dot{m}_{c3}, \frac{f}{T_{i3}/T_{\text{stp}}} \right). \quad 11.2.11$$

d. Closure Equations

Some of the component parameters must be related so that matching can be accomplished. Using the definitions of the corrected flows and speeds for the turbine and compressor, the two corrected mass flows and speeds can be related if it is assumed that mass flow is conserved, any bleeds ($\dot{m}_4 = (1 + f) \times \dot{m}_2$) are ignored, and that the compressor and turbine are on the same shaft ($N_2 = N_4$); thus,

$$\dot{m}_{c2} = \frac{\dot{m}_{c4} \pi_b \pi_c}{(f + 1) \sqrt{\tau_b \tau_c}} \quad 11.2.12$$

$$N_{c2} = N_{c4} \sqrt{\tau_b \tau_c}. \quad 11.2.13$$

Similarly, the corrected mass flows for the burner and compressor can be related on the assumption, once again, that mass flow is conserved ($\dot{m}_3 = \dot{m}_2$) as follows:

$$\dot{m}_{c2} = \frac{\dot{m}_{c3} \pi_c}{\sqrt{\tau_c}}. \quad 11.2.14$$

By executing an energy balance on the shaft without any external power load – that is, all of the turbine power is used to drive the compressor except for bearing and damper losses (Eq. 3.2.22) – one finds

$$c_{pc}(\tau_c - 1) = \eta_m(1 + f)c_{pt} \tau_b \tau_c(1 - \tau_t), \quad 11.2.15$$

where the mechanical shaft efficiency accounts for shaft losses and is directly a function of the shaft speed:

$$\eta_m = \psi_m(N). \quad 11.2.16$$

Lastly, the burner inlet total temperature is related to the compressor total temperature by the definition of the total temperature ratio of the compressor τ_c :

$$T_{t3} = \tau_c T_{t2}. \quad 11.2.17$$

Thus, there are 17 equations (11.2.1 to 11.2.17) and 20 variables (\dot{m} , \dot{m}_{c2} , \dot{m}_{c3} , \dot{m}_{c4} , N , N_{c2} , N_{c4} , π_c , π_b , π_t , τ_c , τ_b , τ_t , η_c , η_b , η_t , η_m , f , T_{t2} , and T_{t3}). Three variables can be specified for a gas generator (typically T_{t2} , f , and N_{t2}) and the remaining 15 can be found. Section 11.2.5.a presents a solution method.

11.2.2. Jet Engine

Section 11.2.1 has just specified the principal equations for the components of a gas generator (compressor, burner, and turbine). The complementary equations for the diffuser and nozzle of a jet engine are presented in this section.

a. Diffuser

The flow for a diffuser is adiabatic, and thus the total temperature is given by (Eq. 8.2.9):

$$T_{t2} = T_a \left[1 + \frac{\gamma - 1}{2} M_a^2 \right], \quad 11.2.18$$

where M_a is the freestream Mach number. Owing to internal and external losses as discussed in Chapter 4, the diffuser total pressure ratio is related to the freestream Mach number as

follows:

$$\pi_d = \phi_d(M_a). \quad 11.2.19$$

Thus, the diffuser exit total pressure is (on the basis of Eqs. 8.2.13 and 3.2.1) as follows:

$$p_{t2} = p_a \pi_d \left[1 + \frac{\gamma - 1}{2} M_a^2 \right]^{\frac{\gamma}{\gamma - 1}}. \quad 11.2.20$$

b. Nozzle

In Chapter 5, the general nozzle characteristics are shown to be functions of only two parameters. The nozzle characteristics (map Fig. 5.19) are expressed in that chapter as

$$\eta_n = \psi_n(p_{t5}/p_a) \quad 11.2.21$$

$$\dot{m}_{c5} = \phi_n(\eta_n, p_{t5}/p_a) \quad 11.2.22$$

c. Closure Equations

As is the case for the gas generator, some equations are necessary to relate the component characteristics. For example, the total pressure at the inlet of the nozzle can be related to the diffuser exit total pressure by

$$p_{t5} = p_{t2} \pi_c \pi_b \pi_t. \quad 11.2.23$$

The corrected mass flow for the nozzle is related to that of the turbine on the assumption that mass is conserved ($\dot{m}_4 = \dot{m}_5$) as expressed by

$$\dot{m}_{c4} = \frac{\dot{m}_{c5} \pi_t}{\sqrt{\tau_t}}. \quad 11.2.24$$

Thus, seven additional equations are now included and eight new variables (T_a , p_a , M_a , π_d , p_{t2} , η_n , \dot{m}_{c5} , and p_{t5}) have been added. Therefore, we have a total of 24 equations with 28 variables. Fortunately, three of these variables are flight conditions (p_a , T_a and M_a). Therefore, for any given flight condition we have 23 unknown variables and 22 equations. Hence, one variable (usually f) can be specified and the remaining parameters can be determined. For example, for specific flight conditions for given components (and accompanying maps), the fuel ratio can be varied and the pressure ratios, efficiencies, corrected rotational speeds, corrected mass flow rates, dimensional rotational speed, mass flow rate, and so on, at which the engine will operate can be found. One solution method of determining the unknown variables is discussed in Section 11.2.5.b.

Moreover, once the matching problem has been solved to find the component operating points, the methods developed in Chapters 2 and 3 can be used to find the important overall engine characteristics – namely, engine thrust and *TSFC*. For example, the dimensional thrust is given by (from Eq. 1.6.10)

$$F = \dot{m} [(1 + f) u_8 - u_a] + A_8 (p_8 - p_a). \quad 11.2.25$$

As a reminder, note that empirical functions representing component maps are recognized in 10 of the preceding equations (ϕ_c , ψ_c , ϕ_b , ψ_b , ϕ_t , ψ_t , ψ_m , ϕ_d , ϕ_n , and ψ_n). These must be specified to solve the matching problem – they can be graphical, tabular, or mathematical. Furthermore, they can be derived from empirical data or theoretical predictions. In

Section 11.2.4, mathematical models are presented that can be used to curve fit the different functions for the maps.

11.2.3. Power-Generation Gas Turbine

Section 11.2.1 specifies the governing equations for the gas generator. In this section, the accompanying matching equations for the inlet, exhaust, and load system of a gas power turbine are discussed. Although the gas generator of a power-generation gas turbine is essentially the same as that of a jet engine, some subtle differences in the operating characteristics of the components exist. Flack (2002) includes component matching for a power-generation unit with regeneration.

a. Inlet

For an inlet, the flow is adiabatic and velocities are very low far from the inlet ($M_a = 0$); thus, the exit total temperature of the inlet is given by

$$T_{t2} = T_a. \quad 11.2.26$$

Furthermore, the frictional losses in total pressure of the inlet are directly related to the freestream inlet velocity. Thus, the total pressure ratio for an inlet can be written as

$$\pi_i = \phi_i (\dot{m}_{c1}). \quad 11.2.27$$

The total exit pressure of the inlet therefore is (again on the fact that $M_a = 0$ and thus that $p_a = p_{ta}$):

$$p_{t2} = p_a \pi_i. \quad 11.2.28$$

b. Exhaust

The total pressure loss for an exhaust is due to viscous effects and is, consequently, a function of the flow speed. Thus, the total pressure ratio can be written as

$$\pi_e = \phi_e (\dot{m}_{c5}). \quad 11.2.29$$

The velocity at the exhaust exit is very low ($p_{ta} = p_a = p_e = p_{te}$), and so the total inlet pressure of the exhaust can be found from

$$p_{t5} = \frac{p_a}{\pi_e}. \quad 11.2.30$$

c. Load System

Furthermore, when an external load is applied to the shaft by, for example, a ship propeller, this power load is directly related to rotational speed and can be found from

$$\mathcal{P}_\ell = \phi_\ell (N) \quad 11.2.31$$

One should realize that this load, \mathcal{P}_ℓ , is an actuality the net useful or output power of the power gas turbine system. For the case of electric generation, the unit typically runs at a constant rotational speed. As a result, this power load equation would be replaced by another taking into account that the shaft speed N is known and that the generator power load is adjusted to maintain a constant shaft speed. Or, as another example, the generator and free turbine may be on a different shaft, which would necessitate additional modeling.

d. Closure Equations

As is the case for the jet engine, some equations are necessary to relate the component characteristics. For example, the corrected mass flow for the inlet can be related to that of the compressor using conservation of mass ($\dot{m}_1 = \dot{m}_2$) as follows:

$$\dot{m}_{c1} = \dot{m}_{c2}\pi_i. \quad 11.2.32$$

The total pressure at the inlet of the exhaust can also be related to the inlet total pressure to the compressor ($\pi_c = \frac{p_{t5}}{p_{t2}}$, $\pi_b = \frac{p_{t4}}{p_{t3}}$, and $\pi_t = \frac{p_{t5}}{p_{t4}}$) by

$$p_{t5} = p_{t2}\pi_c\pi_b\pi_t. \quad 11.2.33$$

The corrected mass flow for the exhaust can be related to that of the turbine, again using conservation of mass ($\dot{m}_4 = \dot{m}_5$), by

$$\dot{m}_{c4} = \frac{\dot{m}_{c5}\pi_t}{\sqrt{\tau_t}}. \quad 11.2.34$$

Performing an energy balance on the shaft with an external power load – that is, all of the turbine power is used to drive the compressor and external load except for bearing and damper losses – yields

$$c_{p_c}(\tau_{c-1}) + \frac{\mathcal{P}_\ell}{\dot{m}T_{t2}} = \eta_m(1+f)c_{p_t}\tau_b\tau_c(1-\tau_t), \quad 11.2.35$$

which replaces Eq. 11.2.15. As a result, the preceding 10 equations add 9 new variables (T_a , p_a , p_{t2} , p_{t5} , π_i , π_e , \dot{m}_{c1} , \dot{m}_{c5} , and \mathcal{P}_ℓ). Thus, 26 equations result with 29 variables. However, two of these are ambient conditions (p_a and T_a). Therefore, for any given ambient condition, 27 variables and 26 equations are present. One can specify one variable (usually f) and determine the remaining parameters. For example, for given ambient conditions in given component maps, one can vary the fuel ratio and determine the load or output power, rotational speed, mass flow rate, and so on at which the power turbine will operate. The solution method of determining the unknown variables is discussed in Section 11.2.5.c. Once the matching problem has been solved to find the component operating points, one can find the power turbine thermodynamic efficiency and *SFC*, as described in Chapters 1, 2 and 3.

Empirical functions representing component maps are identified in 10 of the preceding equations (ϕ_c , ψ_c , ϕ_b , ψ_b , ϕ_t , ψ_t , ψ_m , ϕ_i , ϕ_e , and ϕ_ℓ). As before, these must be available or specified to solve the matching problem, and they can be graphical, tabular, or mathematical. Furthermore, they can be derived from empirical data or theoretical predictions.

11.2.4. Component Modeling

Nine components are considered for the overall gas turbine jet engine or power-generation gas turbine: compressor, combustor, turbine, shaft, diffuser, nozzle, inlet, exhaust, and load. A mathematical model for each is described in this section that can be used to curve fit data by the appropriate choice of curve-fitting parameters, as partially presented by Flack (1990). Functional relationships have been developed that match typical experimental data and trends but do not necessarily match all data accurately. They have developed based on known physical dependence of characteristics, deviations from optimal values by variations of known characteristics, and simple curve fitting. It is most important to note that modeling each component mathematically is not necessary for the general matching solution method; models are presented for convenience and to accelerate a solution using commercial math solvers.

a. Compressor

A model for a corrected speed line on a generalized compressor map is

$$\pi_c = 1 + c_1 \dot{m}_{c2} \sqrt{\frac{\frac{\dot{m}_{c2}}{c_2 N_{c2}} - 1}{c_3 - 1}}. \quad 11.2.36$$

If one considers any particular speed line (at N_{c2}), the flow rate at $\pi_c = 1$ is defined as \dot{m}_{c2_0} and the flow rate at which surge occurs is \dot{m}_{c2_s} . The three curve-fitting parameters in Eq. 11.2.36 are now found. First, mass flow is approximately proportional to speed; thus,

$$c_2 = \dot{m}_{c2_0} / N_{c2} \quad 11.2.37$$

$$c_3 = \dot{m}_{c2_s} / \dot{m}_{c2_0}. \quad 11.2.38$$

Also, the surge line over a range is approximately a straight line:

$$c_1 = \frac{\pi_{c_s} - 1}{\dot{m}_{c2_s}}. \quad 11.2.39$$

Knowing that the efficiency drops from the maximum value as both speed and mass flow are changed, one can model the compressor efficiency by

$$\eta_c = \eta_{c_d} - c_4 |N_{c2_d} - N_{c2}| - \frac{c_5}{N_{c2}} [\dot{m}_{c2_d} - \dot{m}_{c2}]^2. \quad 11.2.40$$

At the maximum efficiency point on speed line N_{c2} , the corrected flow is \dot{m}_{c2_d} :

$$\dot{m}_{c2_d} = c_6 \dot{m}_{c2_0} = c_6 c_2 N_{c2}. \quad 11.2.41$$

The curve-fitting parameter c_6 can be related to a measure of the surge margin (μ),

$$c_6 = c_3(\mu + 1), \quad 11.2.42$$

where this is defined as

$$\mu = \frac{\dot{m}_{c2_d}}{\dot{m}_{c2_s}} - 1. \quad 11.2.43$$

The maximum efficiency on the map is η_{c_d} and occurs at corrected speed N_{c2_d} . The values of c_4 and c_5 are both chosen to best fit experimental test data or predictions.

b. Combustor

Knowing that, as the mass flow rate and or heat addition increases the pressure drops faster than either of these two quantities increase, and from Fanno and Rayleigh line analyses, one can model the total pressure ratio map by

$$\pi_b = 1 - b_1 \dot{m}_{c3}^2 \left[\frac{f}{T_{i3}/T_{stp}} \right]^2, \quad 11.2.44$$

and the model for the combustion efficiency η_b is

$$\eta_b = \eta_{b_d} - \frac{b_2}{\left[\frac{\dot{m}_{c3} f}{T_{i3}/T_{stp}} \right]^2}. \quad 11.2.45$$

The maximum combustion efficiency is η_{b_d} , and b_1 and b_2 are found from experimental test data or predictions.

c. Turbine

A turbine map is modeled as

$$\dot{m}_{c4} = \dot{m}_{c4c} \left\{ 2 \left[\frac{1}{\pi_t} - 1 \right]^n - \left[\frac{1}{\pi_t} - 1 \right]^{2n} \right\} \quad 11.2.46$$

The parameter π_{tc} is the pressure ratio at which the flow chokes, and \dot{m}_{c4c} is the corrected mass flow rate at that limit. The parameter n is given by

$$n = \frac{N_{c4}}{2N_{c4d}}. \quad 11.2.47$$

The corrected speed at which the maximum efficiency occurs is defined as N_{c4d} . A model for the turbine efficiency is

$$\eta_t = \eta_{td} \left\{ 1 - k_1 \left[\frac{1}{\pi_t} - \frac{1}{\pi_{tc}} \right]^2 - k_2 \left[\frac{\dot{m}_{c4c} N_{c4d} - \dot{m}_{c4} N_{c4}}{\dot{m}_{c4c} N_{c4d}} \right]^2 \right\}. \quad 11.2.48$$

The maximum efficiency is η_{td} , and the parameters k_1 and k_2 are selected to best fit experimental data or predictions.

d. Shaft

Experimental data and predictions both show that the mechanical shaft efficiency can effectively be modeled as

$$\eta_m = 1 - s_1 N^{s_2}, \quad 11.2.49$$

where for antifriction or rolling bearings s_2 is approximately 1, whereas for fluid film bearings, the quantity is around 2. The parameter s_1 is dependent on the a particular bearing design and is found from data or predictions.

e. Diffuser

In Chapter 4, the recovery factor is modeled by (Eq. 4.4.2):

$$\pi_d = \pi_{d0} [1 - d(M_a - 1)^{1.35}] \quad 11.2.50$$

The maximum pressure recovery is π_{d0} and the constant d is 0.0 for subsonic operation and typically 0.075 for supersonic operation.

f. Nozzle

Four nozzle types are considered, as in section 5.7.2, and operating characteristics are predicted for each. A general map is shown in Figure 5.19, and all nozzle types can be modeled as

$$\dot{m}_{c5} = \dot{m}_n a_2 M_8 \frac{p_8}{p_{t5}} \sqrt{1 + \frac{\gamma - 1}{2} M_8^2}, \quad 11.2.51$$

where \dot{m}_n is a characteristic flow rate. Knowing that, as the Mach number increases so do frictional losses, as in Fanno line flow, one can model the nozzle efficiency η_n by

$$\eta_n = \eta_{nd} - a_1 M_8^2, \quad 11.2.52$$

where η_{nd} is the maximum efficiency and a_1 is chosen to match experimental data. The exit Mach number M_8 is given by (Eq. 3.2.37):

$$M_8 = \sqrt{\frac{2 \left[\frac{1}{\eta_n \left[\frac{p_8}{p_{t5}} \right]^{\frac{\gamma-1}{\gamma}} + 1 - \eta_n} \right]}{\gamma - 1}} \quad 11.2.53$$

Fixed Converging: The map for this nozzle type is shown in Figure 5.16. The maximum Mach number at the exit is unity for this nozzle type. As discussed in Chapter 5, to analyze this type of nozzle for a given pressure ratio p_{t5}/p_a , one must first check for choking. If the nozzle is choked, the exit Mach number is unity. If the nozzle is not choked, then p_8 is equal to p_a and then M_8 can be found from Eq. 11.2.53. For this geometry (from Eq. 5.7.8),

$$\dot{m}_n = \rho_{stp} a_{stp} A_8 \quad 11.2.54$$

Also, a_2 is given by (from Eq. 5.7.8)

$$a_2 = \sqrt{\frac{\gamma}{\gamma_{stp}} \frac{\mathcal{R}_{stp}}{\mathcal{R}}} \quad 11.2.55$$

Variable C-D with Fixed Exit Area: This nozzle is of variable geometry, and thus the exit pressure matches the ambient pressure with a fixed exit area (the minimum area varies with operating conditions). This nozzle type can operate supersonically. Equations 11.2.51 to 11.2.55 again apply.

Variable C-D with Fixed Minimum Area: Figure 5.18 depicts a map of this nozzle type. It has a variable geometry, and thus again the exit pressure matches the ambient pressure and has a fixed minimum area, where the exit area varies with operating conditions. Equations 11.2.51 to 11.2.53 again apply, except now

$$\dot{m}_n = \rho_{stp} a_{stp} A^* \quad 11.2.56$$

and from Eqs. 5.7.15 and 5.7.16,

$$a_2 = \frac{\sqrt{\frac{\gamma+1}{2+(\gamma-1)M_8^2}} \sqrt{\frac{\gamma}{\gamma_{stp}} \frac{\mathcal{R}_{stp}}{\mathcal{R}}}}{M_8 \left\{ \frac{1}{\eta_n} \left[\frac{\eta_n}{\frac{2}{\gamma+1} - 1 + \eta_n} \right] \left[\frac{1}{1 + \frac{\gamma-1}{2} M_8^2} - 1 + \eta_n \right] \right\}^{\frac{\gamma}{\gamma-1}}} \quad 11.2.57$$

As shown in Chapter 5, \dot{m}_{c5} is constant for all conditions for this nozzle type.

g. Inlet (Power Gas Turbine)

The only parameter that must be simulated for the inlet of a power gas turbine is the total pressure loss due to boundary layers, turbulence, and so on. The pressure recovery factor π_i can be found based on geometrical considerations similar to those for a subsonic diffuser (Chapter 4, Section 11.2.4) and is directly related to velocity or mass flow rate.

Table 11.1. Summary of Empirical Component Parameters

Component	Number of Parameters	Parameters
Compressor	8	$c_1 c_2 c_3 c_4 c_5 N_{c2d} \mu \eta_{cd}$
Combustor	3	$b_1 b_2 \eta_{bd}$
Turbine	6	$k_1 k_2 \dot{m}_{c4c} N_{c4d} \eta_{td} \pi_{tc}$
Shaft	2	$s_1 s_2$
Diffuser	2	$\pi_{dd} d$
Nozzle	3	$a_1 \dot{m}_n \eta_{nd}$
Inlet (turboshaft)	1	z_1
Exhaust (turboshaft)	1	z_2
Power load (turboshaft)	2	$z_3 z_4$

Knowing that the losses are similar to Fanno line flow, one can model this loss as

$$\pi_i = 1 - z_1 \dot{m}_{c1}^2. \quad 11.2.58$$

In Eq. 11.2.58, z_1 is specified to match the mathematical model to experimental or predicted data. Such a model can also sometimes be used for a subsonic jet engine diffuser.

h. Exhaust (Power Generation Gas Turbine)

The only parameter that must be simulated for the exhaust of a power gas turbine is the total pressure loss due to viscous flow. The pressure recovery factor π_e can be found based on geometrical considerations similar to those for a subsonic diffuser or inlet and, as for the inlet in the preceding paragraph, is directly related to velocity or mass flow rate. Again, knowing that the losses are similar to Fanno line flow, one can model this loss as

$$\pi_e = 1 - z_2 \dot{m}_{c5}^2. \quad 11.2.59$$

The value of z_2 in Eq. 11.2.59 is specified to match the mathematical model to experimental or predicted data.

i. Shaft Load (Power-Generation Gas Turbine)

In the presence of an external and significant load (ship propeller, tank drive, etc.) power is derived from the shaft for auxiliary purposes. A general model for the load on the shaft is

$$\mathcal{P}_\ell = z_3 N^{z_4}. \quad 11.2.60$$

The value of z_4 is typically between 1 and 2, and z_3 is strongly dependent on the particular type of load.

j. Application of Models to Matching

Mathematical models of the compressor, burner, turbine, shaft, diffuser, nozzle, inlet, exhaust, and load maps are presented in this section for gas turbines. These models can be used to curve fit data to facilitate matching calculations such as those presented in the previous section. In general, using these component models requires 24 parameters to be specified for a jet engine and 23 for a power gas turbine as summarized in Table 11.1.

It cannot be emphasized strongly enough that such modeling is not necessary for the general problem solution, however. The reader should realize that these models serve only to facilitate the matching calculations – for example by computer math solvers. Furthermore, if the preceding curve-fitting equations cannot be used to match component maps accurately, look-up tables or other equations can be used for the general solution methods.

11.2.5. Solution of Matching Problem

Section 11.2 discusses three cases: a single-shaft gas generator, a complete single-spool turbojet engine, and a single-spool power gas turbine or turboshaft. The gas generator has 15 governing equations with 18 variables, the complete jet engine is associated with 22 equations involving 26 variables, and the power turbine has 26 equations and 29 variables. Generalized relationships were presented for component maps. Section 11.2.4 offers curve-fitting correlations for the maps. In this section, one possible solution method is presented for cases with known components. Because the equations are nonlinear and performance curves may not be in equation form, the solution is iterative. The step-by-step process of obtaining a solution is set forth. The same general solution method applies regardless of whether one has numerical curve-fitted models of the components as presented in Section 11.2.4, graphical maps, or tabular look-up maps for components.

a. Gas Generator

For a gas generator, three parameters must be specified for a solution to be obtainable. These are typically chosen to be T_{12} , N_{c2} , and f . A flowchart outlining the solution is shown in Figure 11.1.

- (1) Using N_{c2} and T_{12} , one can find N from eq. 11.2.4.
- (2) An estimate of \dot{m}_{c2} must be used to initiate the iteration.
- (3) On the basis of N_{c2} and \dot{m}_{c2} , compressor maps can be used to find π_c from predictions, data using the graphical or tabular form (Eq. 11.2.1, Fig. 6.14), or modeling Eq. 11.2.36. The efficiency, η_c , can be found from data in graphical/tabular form (Eq. 11.2.2, Fig. 6.14) or modeling Eq. 11.2.40.
- (4) The temperature ratio τ_c can then be found from the compressor pressure ratio, temperature ratio, and efficiency equation (Eq. 11.2.5) because π_c and η_c are known.
- (5) By knowing T_{12} , one can find T_{13} from Eq. 11.2.17.
- (6) The combustor corrected flow \dot{m}_{c3} can now be found using the compressor corrected mass flow (Eq. 11.2.14).
- (7) Through \dot{m}_{c3} with f , η_b and π_b can be found from combustor maps using the graphical or tabular forms (Eqs. 11.2.10 and 11.2.11, Figs. 9.11 and 9.12) or models (Eqs. 11.2.45 and 11.2.44).
- (8) Since η_b and T_{13} are known, τ_b can be found from the energy balance in the burner (Eq. 11.2.9).
- (9) The turbine corrected flow and speed, \dot{m}_{c4} and N_{c4} , can be related to corresponding quantities for the compressor and found through Eqs. 11.2.12 and 11.2.13.
- (10) Because \dot{m}_{c4} and N_{c4} are known, the turbine pressure ratio π_t and efficiency η_t can be found from the turbine maps graphically or tabularly (Eqs. 11.2.6 and 11.2.7, Fig. 8.12) or through the use of models (Eqs. 11.2.46 and 11.2.48).
- (11) The graphical or tabular shaft map (Eq. 11.2.16) or model (Eq. 11.2.49) can be used with N to determine the mechanical efficiency η_m .
- (12) Equation 11.2.15, which represents the power balance on the shaft and applies for no external power load, can be used with f , η_m , τ_b , and τ_c to find τ_t .
- (13) One can calculate π_t from the turbine pressure ratio, temperature ratio, and efficiency equation by using τ_t and η_t (Eq. 11.2.8).
- (14) Therefore, two values of π_t are found independently; if the two are the same within a tolerance, the correct value of \dot{m}_{c2} was used. If the two are significantly different, a new value of \dot{m}_{c2} should be used and the process must be repeated. The Regula Falsi method (Appendix G) or another numerical method can be used to reduce the number of iterations. Such a method is used for following examples.

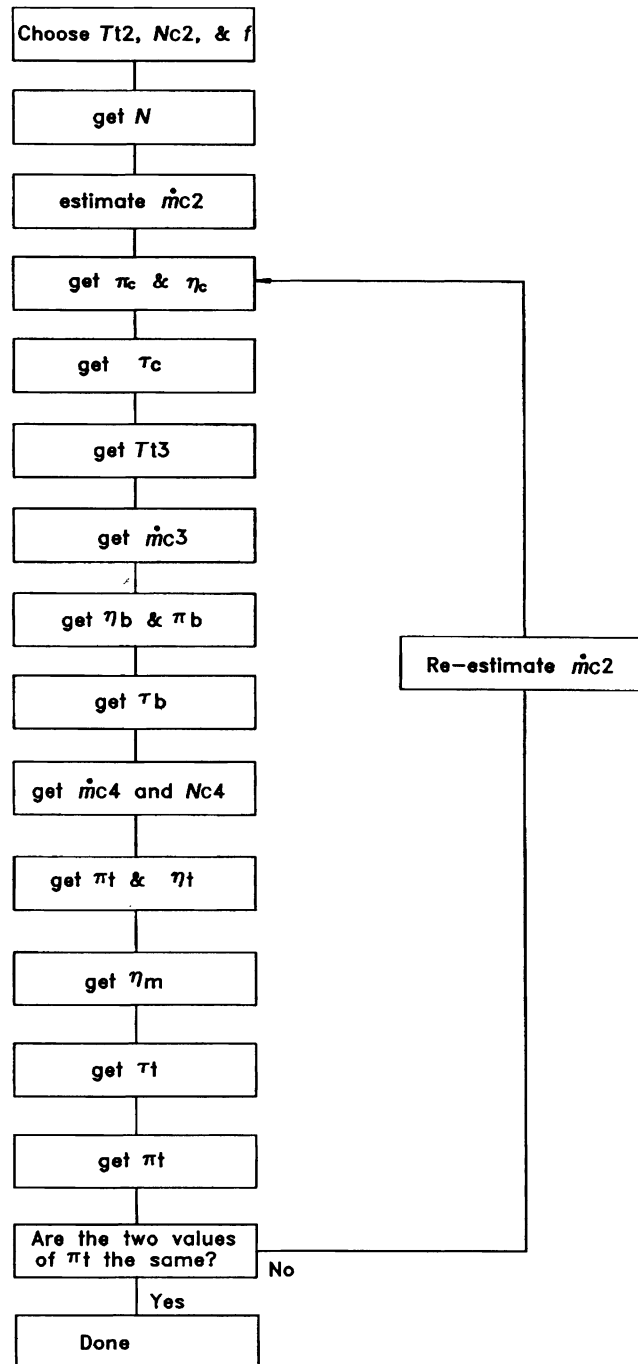


Figure 11.1 Flow chart for solution of gas generator.

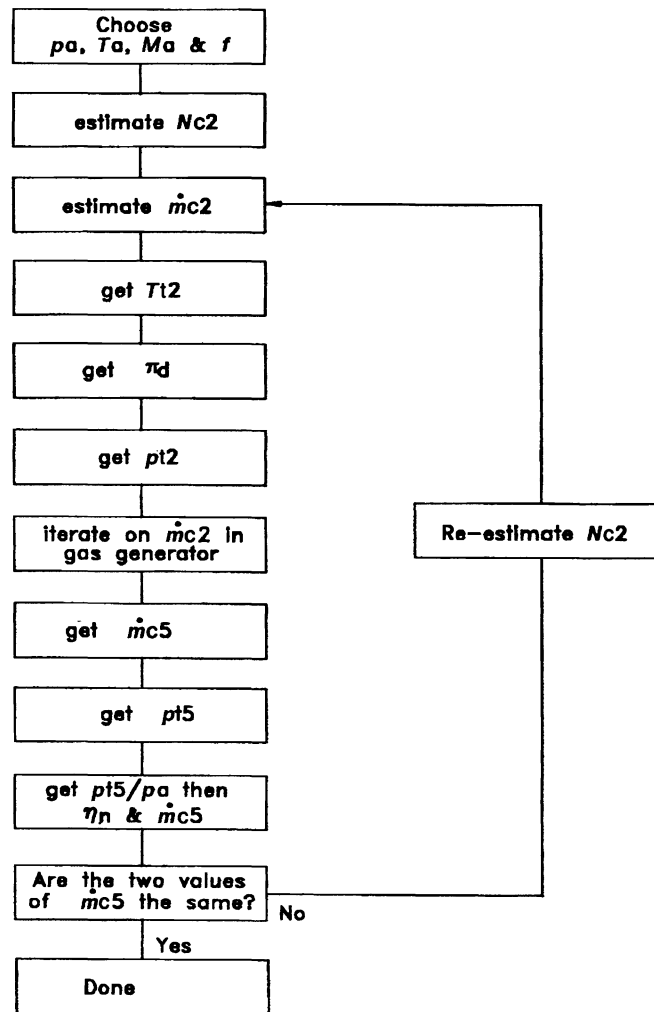


Figure 11.2 Flow chart for solution of jet engine.

b. Jet Engine

For a turbojet, four parameters must be specified. These are p_a , T_a , M_a , and f . The solution method chosen for this case is a two-nested loop iteration. A flow chart outlining the solution is shown in Figure 11.2.

- (1) First, one must estimate N_{c2} .
- (2) Second, \dot{m}_{c2} must be estimated.
- (3) By means of M_a , the value of T_{t2} is calculated from the adiabatic diffuser equation (Eq. 11.2.18).
- (4) From M_a , the pressure ratio for the diffuser, π_d , is found through map predictions or data, from graphical or tabular information (Eq. 11.2.19), through or modeling (Eq. 11.2.50).
- (5) Knowing M_a , π_d , and p_a , one finds the total pressure into the compressor, p_{t2} , from Eq. 11.2.20.

- (6) Iteration on the corrected mass flow rate for the compressor, \dot{m}_{c2} , in the gas generator for the given N_{c2} is necessary (as outlined in the preceding section for a gas generator) until a converged solution is found. This can obviously be a lengthy step.
- (7) The corrected mass flow for the nozzle, \dot{m}_{c5} , is related to the corrected mass flow for the turbine and found from Eq. 11.2.24.
- (8) Knowing p_{t2} , π_b , and π_c , one can relate the value of p_{t5} to the total pressure into the compressor and calculate it through Eq. 11.2.23.
- (9) One can first find p_{t5}/p_a and then η_n and \dot{m}_{c5} from predicted or experimental nozzle maps, from graphical or tabulated information (Eqs. 11.2.21 and 11.2.22, Fig. 5.19), or through modeling (eqs. 11.2.54, 11.2.52, and 11.2.51).
- (10) Thus, two values of \dot{m}_{c5} are found independently. The solution is converged if these two values are within a tolerance. However, if they are not, iteration on N_{c2} is necessary and the preceding process must be repeated. The Regula Falsi method for both loops can be used to facilitate convergence. In all cases, the average total temperature of a component is used to evaluate the ratio of specific heats for that component, as is done in Chapter 3.

By applying the method to different fuel ratios it is possible to predict the operating line of the gas turbine. Thus, both on-design and off-design operating points will be found. Optimally, all of the components will reach peak efficiency for the same on-design operating point. If they do not, the method will indicate which component should be changed so that a better overall engine efficiency can be obtained.

c. Power-Generation Gas Turbine

For the case of power generation with a speed-dependent load, three parameters must be specified and have been chosen to be p_a , T_a , and f . The solution for this case again is a two-nested loop iteration. A flow chart outlining the solution is shown in Figure 11.3.

- (1) First, an estimate of N_{c2} is needed.
- (2) The value of T_{t2} is found from T_a (Eq. 11.2.26).
- (3) Next, an estimate of corrected mass flow for the inlet, \dot{m}_{c1} , is used.
- (4) From \dot{m}_{c1} , the inlet pressure ratio π_i is found through predictions or data (Eq. 11.2.27), or modeling (Eq. 11.2.58).
- (5) Next, the inlet total pressure to the compressor p_{t2} is found from π_i and p_a and Eq. 11.2.28.
- (6) Knowing the corrected mass flow and total pressure ratio for the inlet, one finds the corrected mass flow into the compressor, \dot{m}_{c2} , from Eq. 11.2.32.
- (7) The true mass flow rate \dot{m} can be found from \dot{m}_{c2} , T_{t2} , and p_{t2} by means of Eq. 11.2.3.
- (8) One can also find the true shaft speed, N , from N_{c2} and T_{t2} by means of Eq. 11.2.4.
- (9) Using N , one can find the external resulting power load P_ℓ from predictions or data (Eq. 11.2.31), or modeling (Eq. 11.2.60).
- (10) The graphical or tabular shaft map (Eq. 11.2.16) or model (Eq. 11.2.49) can be used with N to determine the mechanical efficiency η_m .
- (11) Iteration on the corrected mass flow for the inlet \dot{m}_{c1} and resulting \dot{m}_{c2} for the gas generator (using Eq. 11.2.35 for the shaft power balance) for the given N_{c2} is necessary until the solution is converged. Again, this can be a lengthy step.
- (12) Next, the corrected mass flow for the exhaust \dot{m}_{c5} is found from Eq. 11.2.34 by knowing \dot{m}_{c4} , and the total pressure ratio and temperature ratio for the turbine.

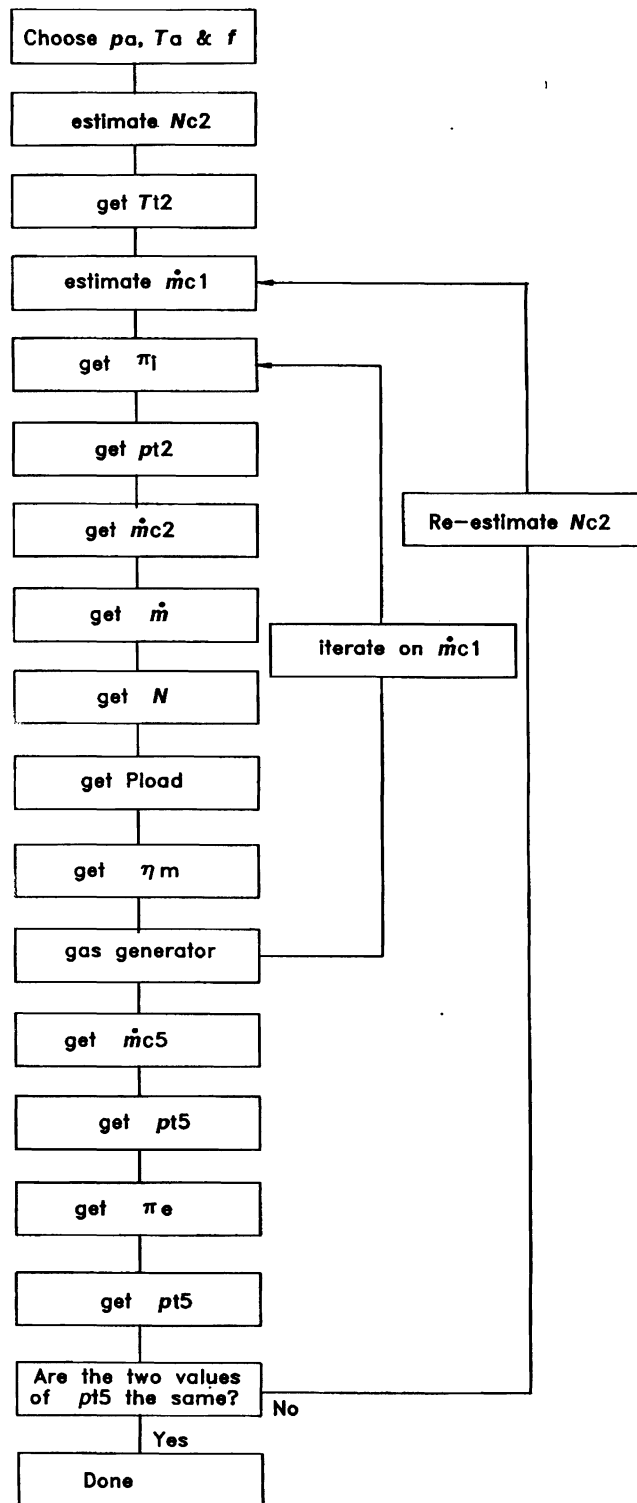


Figure 11.3 Flow chart for solution of power-generation gas turbine (speed-dependent load).

- (13) Knowing p_{t2} , π_c , π_b , and π_t one can calculate the total pressure into the exhaust, p_{t5} , from Eq. 11.2.33.
- (14) Knowing \dot{m}_{c5} , one can find the pressure ratio for the exhaust, π_e , from predictions or data (Eq. 11.2.29), or modeling (Eq. 11.2.59).
- (15) Then p_{t5} is calculated from p_e and π_e from Eq. 11.2.30.
- (16) Thus, two values of p_{t5} are independently calculated. If these two values are within a tolerance, the solution is converged. If they are not, one must iterate on N_{c2} and repeat the preceding process. As is the case for the jet engine, the average total temperature of a component is used to evaluate the ratio of specific heats for that component as is done in Chapter 3.

In the case of power generation running at a constant speed (for example, for electric generation), three parameters must be specified and have been chosen to be p_a , T_a , and f . The solution for this case is a single-loop iteration and is somewhat more straightforward because the shaft speed is known. A flow chart outlining the solution is shown in Figure 11.4.

- (1) First, N is specified.
- (2) The value of T_{t2} is found from T_a (Eq. 11.2.26).
- (3) Next, an estimate of corrected mass flow for the inlet, \dot{m}_{c1} , is used.
- (4) Using \dot{m}_{c1} , one can find the inlet pressure ratio π_i from predictions or data (Eq. 11.2.27), or through modeling (Eq. 11.2.58).
- (5) Next, the inlet total pressure to the compressor, p_{t2} , is found from π_i and p_a and Eq. 11.2.28.
- (6) Knowing the corrected mass flow and total pressure ratio for the inlet, one finds the corrected mass flow into the compressor, \dot{m}_{c2} , from Eq. 11.2.32.
- (7) The true mass flow rate \dot{m} can be found from \dot{m}_{c2} , T_{t2} , and p_{t2} with Eq. 11.2.3.
- (8) One can also find the corrected shaft speed N_{c2} from N and T_{t2} with Eq. 11.2.4.
- (9) Next, by knowing N_{c2} and \dot{m}_{c2} , one can use compressor maps to find π_c either from predictions or data using the graphical or tabular form (Eq. 11.2.1, Fig. 6.14) or modeling (Eq. 11.2.36) as well as the efficiency η_c from the graphical or tabular form (Eq. 11.2.2, Fig. 6.14) or through modeling (Eq. 11.2.40).
- (10) The temperature ratio τ_c can be found from the compressor pressure ratio, temperature ratio, and efficiency equation (Eq. 11.2.5) because π_c and η_c are known.
- (11) By knowing T_{t2} , one can find T_{t3} from Eq. 11.2.17.
- (12) The combustor corrected flow \dot{m}_{c3} can now be found from the compressor corrected mass flow (Eq. 11.2.14).
- (13) One can use \dot{m}_{c3} with f to find η_b and π_b from combustor maps by means of the graphical or tabular forms (Eqs. 11.2.10 and 11.2.11, Figs. 9.11 and 9.12) or models (Eqs. 11.2.45 and 11.2.44).
- (14) Next, τ_b can be found from the energy balance in the burner (Eq. 11.2.9) because η_b and T_{t3} are known.
- (15) The turbine corrected flow and speed, \dot{m}_{c4} and N_{c4} , can be related to corresponding quantities for the compressor and found by means of Eqs. 11.2.12 and 11.2.13.
- (16) Now, the turbine pressure ratio π_t and efficiency η_t can be found from the turbine maps graphically or tabularly (Eqs. 11.2.6 and 11.2.7, Fig. 8.12) or through models (Eqs. 11.2.46 and 11.2.48) because \dot{m}_{c4} and N_{c4} are known.
- (17) One can then calculate τ_t from the turbine pressure ratio, temperature ratio, and efficiency equation by using π_t and η_t (Eq. 11.2.8).
- (18) Next, the graphical or tabular shaft map (Eq. 11.2.16) or model (Eq. 11.2.49) can be used with N to determine the mechanical efficiency η_m .

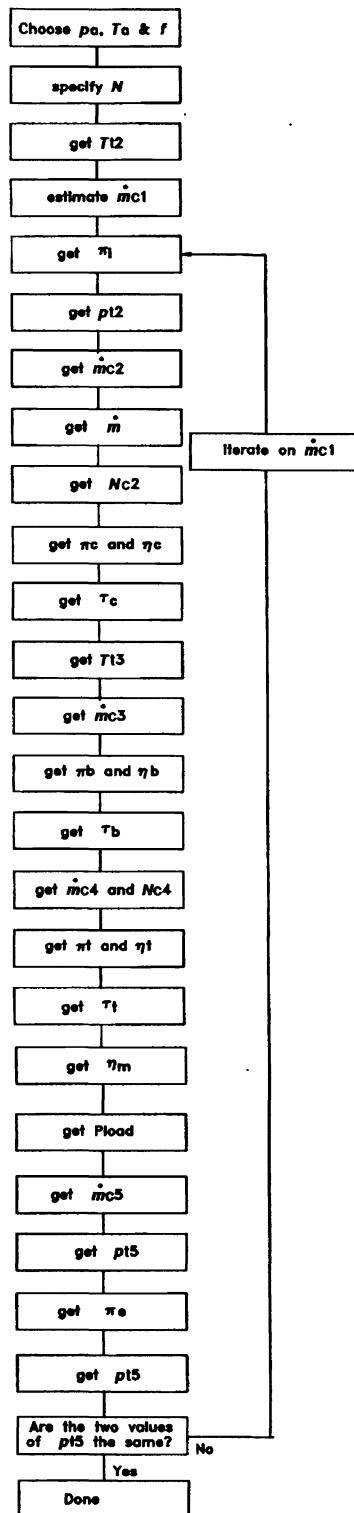


Figure 11.4 Flow chart for solution of power-generation gas turbine (constant speed).

- (19) With Eq. 11.2.35, which is the power balance on the shaft, one can use f , η_m , τ_b , τ_t , and τ_c to find the external power load \mathcal{P}_e , which is used for electric generation.
- (20) The corrected mass flow for the exhaust, \dot{m}_{c5} , is found from Eq. 11.2.34 by knowing \dot{m}_{c4} and the total pressure ratio and temperature ratios for the turbine.
- (21) Knowing p_{12} , π_c , π_b , and π_t one can calculate the total pressure into the exhaust, p_{t5} , from Eq. 11.2.33.
- (22) Next, knowing \dot{m}_{c5} , one can find the pressure ratio for the exhaust, π_e , from predictions or data (Eq. 11.2.29) or through modeling (Eq. 11.2.59).
- (23) Then p_{t5} is calculated from p_e and π_e by means of Eq. 11.2.30.
- (24) Thus, two values of p_{t5} are independently calculated. If these two values are within a tolerance, the solution is converged. If they are not, one must iterate on \dot{m}_{c1} and repeat the preceding process. As before, the average total temperature of a component is used to evaluate the ratio of specific heats for that component.

By applying the method to different fuel ratios, one can predict the operating line of a power-generation gas turbine. As is the case for a jet engine, both on-design and off-design operating points will be found. Optimally, all of the components will reach peak efficiency for the same on-design operating point. If they do not, the method will indicate which component should be changed so that a better overall engine efficiency can be obtained.

11.2.6. Other Applications

Thus far, only single-shaft gas turbines have been discussed, which has necessitated matching six components for a jet engine and seven for a power-generation gas turbine. The method can also be applied to more complex engines. For example, a similar analysis can be applied to a twin-spool turbofan or turbojet. For a twin-spool turbofan with an exhausted fan and afterburner, 12 components (and their corresponding maps) will have to be matched (diffuser, fan, low-pressure compressor, high-pressure compressor, primary burner, high-pressure turbine, low-pressure turbine, afterburner, primary nozzle, fan nozzle, and two shafts). As a result, although the same approach can be used, the solution method becomes much more cumbersome and requires several more levels of nested iterations and much longer solution times (Flack, 2004). As a result, performing such matching requires computer methods.

11.2.7. Dynamic or Transient Response

Thus far, the matching analysis has been for strictly steady-state performance. That is, the fuel ratio is specified and the steady-state operating point is found. Nothing in the analysis allows the determination of the time period needed for the gas turbine to reach this point. The largest influence is the rotor polar moment of inertia, I , although the fuel injection and combustion, flow inertia through a gas turbine, and fluid compressibility all induce dynamics as well. For a jet engine, the equation that governs the rotational inertial effect is

$$T_t - T_c - T_m = I \frac{\partial \omega}{\partial t}, \quad 11.2.61$$

where T_t , T_c , and T_m are the torques of the turbine, compressor, and mechanical losses, respectively. To apply such an analysis, observe the following procedures

1. Consider the gas turbine operating at some known condition.
2. The fuel ratio can be changed and the instantaneous turbine inlet temperature can be found if it is assumed the conditions into the burner have not yet changed.

3. The turbine torque can be found based on the new instantaneous turbine inlet temperature.
4. The net torque can be found, and the angular acceleration or rate of change of the shaft rotation can be found.
5. A discretized form of Eq. 11.2.61 can be used over a selected discrete (short) time interval to find the new rotational speed at the end of this period.
6. The new speed can be used as in Sections 11.2.5.a through 11.2.5.c find parameters such as the mass flow, compressor total pressure ratio, and so on.
7. The new conditions can be used to find the new burner exit temperature and the preceding process repeated for a new time increment, and continually repeated, until steady-state conditions are attained.

The steady-state solution will be the same as discussed in Section 11.2.5; however, in this analysis, the time required will be predicted as a part of the transient response. Such an analysis has been used by Kurzke (1995) and Reed and Afjeh (2000).

Example 11.1: A single-spool turbojet engine with given components is to be assembled. Because this case represents an engine, the diffuser, compressor, combustor, turbine, shaft, and nozzle are all included. For this example, the components have been modeled using equations presented in Section 11.2.4. The maps for the compressor, burner, and turbine are shown in Figures 11.5 through 11.7, and the different model parameters, which fit the data, are presented in Table 11.2. The nozzle has a fixed minimum area and a variable exit area, and thus the exit pressure matches the ambient pressure. The engine is to be operated at a Mach number of 0.5 and at $T_a = 289$ K (520 °R) and $p_a = 101.3$ kPa (14.69 psia). Find the operating characteristics of the engine as the fuel ratio is parametrically varied from 0.010 to 0.035 in increments of 0.005.

SOLUTION:

As a representative case, $f = 0.02$ is chosen to demonstrate the solution. The first estimate on N_{c2} is 10,954 rpm and the first estimate on \dot{m}_{c2} of 88.12 kg/s (194.3 lbm/s) are chosen.

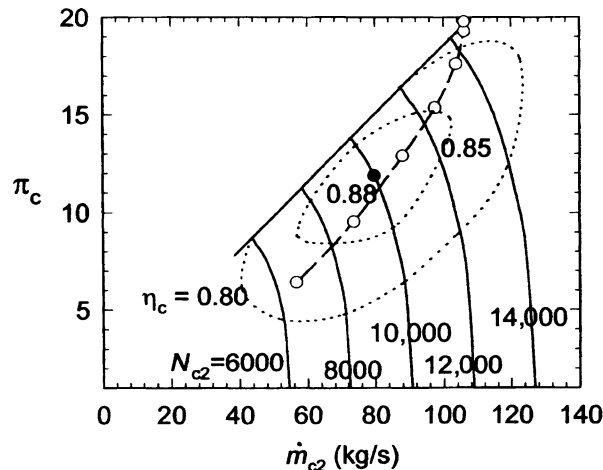


Figure 11.5 Compressor map for Example 11.1.

Table 11.2. Parameters for Example 11.1

<i>Diffuser</i>	<i>Turbine</i>
$\pi_{d_1} = 1$	$k_1 = 1.0$
$d = 0$	$k_2 = 0.20$
	$N_{c4d} = 4000 \text{ rpm}$
<i>Compressor</i>	$\dot{m}_{c4c} = 15.87 \text{ kg/s (35 lbm/s)}$
$c_1 = 0.1764 \text{ s/kg (0.08 s/lbm)}$	$\eta_{t_d} = 0.90$
$c_2 = 0.00907 \text{ kg/s/rpm (0.02 lbm/s/rpm)}$	$\pi_{t_c} = 0.28$
$c_3 = 0.80$	
$c_4 = 0.00001/\text{rpm}$	<i>Shaft</i>
$c_5 = 9.724 \text{ rpm s}^2/\text{kg}^2 \text{ (2.0 rpm s}^2/\text{lbm}^2)$	$s_1 = 0$
$N_{c2d} = 10,000 \text{ rpm}$	$s_2 = 0$
$\eta_{c_d} = 0.88$	
$\mu = 0.10$	<i>Nozzle – Converging–Diverging, Fixed A*</i>
<i>Combustor</i>	$a_1 = 0$
$b_1 = 9.068 \text{ s}^2/\text{kg}^2 \text{ (1.865 s}^2/\text{lbm}^2)$	$\dot{m}_n = 88.08 \text{ kg/s (194.2 lbm/s)}$
$b_2 = 0.0 \text{ s}^2/\text{kg}^2 \text{ (0.0 s}^2/\text{lbm}^2)$	$\eta_{n_d} = 0.98$
$\Delta H = 10,000 \text{ kcal/kg (18,000 B/lbm)}$	
$\eta_{b_d} = 0.91$	<i>Performance</i>
	$T_a = 289 \text{ K (520 }^\circ\text{R)}$
	$p_a = 101.3 \text{ kPa (14.69 psia)}$
	$M_a = 0.50$

From Eq. 11.2.18 for $T_a = 289 \text{ K (520 }^\circ\text{R)}$, for $M_a = 0.5$, and for $\gamma = 1.401$, one can find the total temperature exiting the diffuser from

$$T_{t2} = T_a \left[1 + \frac{\gamma - 1}{2} M_a^2 \right] = 303 \text{ K (546 }^\circ\text{R)}.$$

Since the Mach number and the ambient temperature are known, one can find the airspeed as follows:

$$u_a = M_a \sqrt{\gamma \mathcal{R} T_a} = 170.4 \text{ m/s (559.1 ft/s)}.$$

For the diffuser, because the freestream Mach number is subsonic, one can find the pressure recovery factor from the modeling equation (Eq. 11.2.50) as follows:

$$\begin{aligned} \pi_d &= \pi_{d_1} [1 - d(M_a - 1)^{1.35}] \\ \pi_d &= 1(1 - 0.0) = 1.00. \end{aligned}$$

Thus, one can find the total pressure exiting the diffuser from Eq. 11.2.20 for $\gamma = 1.401$:

$$p_{t2} = p_a \pi_d \left[1 + \frac{\gamma - 1}{2} M_a^2 \right]^{\frac{\gamma}{\gamma - 1}}$$

$$p_{t2} = 120.2 \text{ kPa (17.43 psia)}.$$

Now, one can solve the gas generator portion of the problem can be solved. Using Eqs. 11.2.3 and 11.2.4,

$$\dot{m}_{c2} \equiv \dot{m} \frac{\sqrt{T_i/T_{stp}}}{P_t/P_{stp}}$$

$$N_{c2} \equiv \frac{N}{\sqrt{T_i/T_{stp}}},$$

for $\dot{m}_{c2} = 88.12 \text{ kg/s}$ (194.3 lbm/s) and $N_{c2} = 10,954 \text{ rpm}$, one can find the true mass flow rate and rotational speed:

$$\dot{m} = 102.0 \text{ kg/s} \text{ (224.9 lbm/s)} \text{ and } N = 11,225 \text{ rpm.}$$

One can also find the compressor total pressure ratio by using $\dot{m}_{c2} = 88.12 \text{ kg/s}$ and $N_{c2} = 10,954 \text{ rpm}$ with Figure 11.5 or the modeling equation (Eq. 11.2.36):

$$\pi_c = 12.69.$$

From Figure 11.5 or the modeling equation (Eq. 11.2.40), again using \dot{m}_{c2} and N_{c2} , one can find the compressor efficiency:

$$\eta_c = 0.870.$$

Because π_c is known, Eq. 11.2.5 can be used to find the total temperature ratio for the compressor as follows:

$$\pi_c = [1 + \eta_c(\tau_c - 1)]^{\frac{\gamma}{\gamma-1}}.$$

One can solve for the total temperature ratio of the compressor as $\tau_c = 2.177$ for $\gamma = 1.384$, and from Eq. 11.2.17 the total temperature exiting the compressor can be found as follows:

$$T_{t3} = \tau_c T_{t2}$$

$$T_{t3} = 661 \text{ K (1189 }^\circ\text{R)}.$$

Using Eq. 11.2.14,

$$\dot{m}_{c2} = \frac{\dot{m}_{c3} \pi_c}{\sqrt{\tau_c}},$$

one can solve for the corrected mass flow for the burner because \dot{m}_{c2} and τ_c are known:

$$\dot{m}_{c3} = 10.25 \text{ kg/s (22.60 lbm/s)}.$$

Next, since f and T_{t3} are known, one can find the quantity $f/(T_{t3}/T_{stp}) = 0.00872$. For the burner, the efficiency is given as $\eta_b = 0.91$, and using $\dot{m}_{c3} = 10.25 \text{ kg/s}$ and $f/(T_{t3}/T_{stp}) = 0.00872$, one can find the total pressure ratio for the burner from Figure 11.6 or the modeling equation (Eq. 11.2.44):

$$\pi_b = 0.927.$$

Next, using the energy equation for the burner, Eq. 11.2.9,

$$f(\eta_b \Delta H - c_p T_{t3} \tau_b) = c_p T_{t3} (\tau_b - 1),$$

since f , η_b , ΔH , and T_{t3} are known, one can solve for the total temperature ratio for the burner as

$$\tau_b = 1.982 \text{ for } \gamma = 1.341;$$

therefore, the exit total temperature for the combustor is $T_{t4} = \tau_b T_{t3} = 1309 \text{ K}$ (2357 °R).

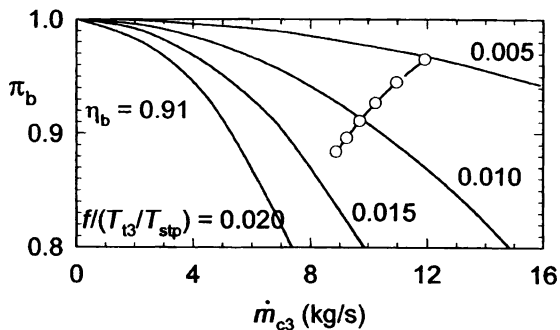


Figure 11.6 Burner map with four values of $f/(T_{t3}/T_{stp})$ for Example 11.1.

Thus, using Eq. 11.2.12,

$$\dot{m}_{c2} = \frac{\dot{m}_{c4} \pi_b \pi_c}{(f + 1) \sqrt{\tau_b \tau_c}}$$

because \dot{m}_{c2} , π_c , τ_c , π_b , and τ_b are known, one can find the corrected mass flow for the turbine:

$$\dot{m}_{c4} = 15.87 \text{ kg/s (35.00 lbm/s)}$$

Using Eq. (11.2.13),

$$N_{c2} = N_{c4} \sqrt{\tau_b \tau_c}$$

one finds the corrected speed for the turbine $N_{c4} = 5273$ rpm.

Next, for the turbine, using $\dot{m}_{c4} = 15.87$ kg/s and $N_{c4} = 5273$ rpm, one finds the total pressure ratio for the turbine from Figure 11.7 or the modeling equation (Eq. 11.2.46):

$$\pi_t = 0.280.$$

From Figure 11.7 or the modeling equation (Eq. 11.2.48), again using $\dot{m}_{c4} = 15.87$ kg/s and $N_{c4} = 5273$ rpm, one finds the turbine efficiency $\eta_t = 0.882$.

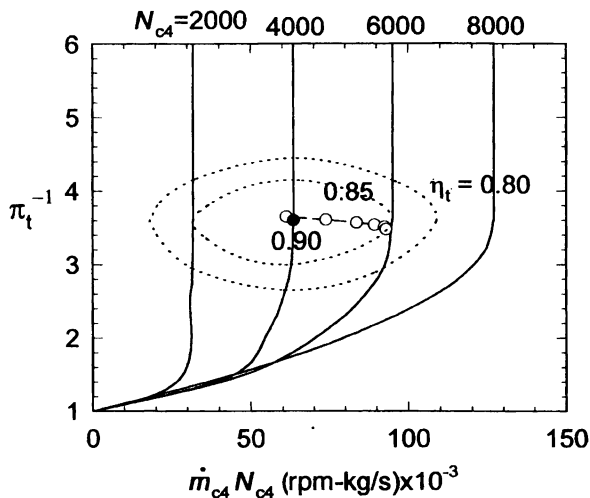


Figure 11.7 Turbine map for Example 11.1.

For the shaft, from the modeling equation (Eq. 11.2.49), the mechanical efficiency is given by

$$\eta_m = 1 - s_1 N^{s_2},$$

and so $\eta_m = 1.00$.

Thus, using the power balance on the shaft, Eq. 11.2.15,

$$c_{p_c}(\tau_c - 1) = \eta_m(1 + f)c_{p_t}\tau_b\tau_c(1 - \tau_t),$$

since f , τ_c , and τ_b are known, one can solve for the total temperature ratio of the turbine for specific heat ratios of 1.384 and 1.328 for the compressor and turbine, respectively:

$$\tau_t = 0.762.$$

Thus, the total exit temperature of the turbine is $T_{t5} = \tau_t T_{t4} = 998 \text{ K}$ (1797 °R). Hence, from Eq. 11.2.8 for $\gamma = 1.328$, the second (and independent) calculation for the total pressure ratio of the turbine yields (τ_t and η_t are known)

$$\pi_t = \left[1 + \frac{(\tau_t - 1)}{\eta_t} \right]^{\frac{\gamma}{\gamma-1}}$$

$$\pi = 0.280.$$

This value of π_t agrees with the previously calculated value of π_t . Thus, the initial guess on \dot{m}_{c2} was good. If the two values of π_t had not been in agreement, a new value of \dot{m}_{c2} would have been tried and the preceding process repeated. This ends the solution for the gas generator. Now one must determine if the initial guess on N_{c2} was valid. Since the corrected mass flow for the turbine, total pressure ratio, and total temperature ratio for the turbine are known, using Eq. 11.2.24,

$$\dot{m}_{c4} = \frac{\dot{m}_{c5}\pi_t}{\sqrt{\tau_t}},$$

one finds the corrected mass flow for the nozzle: $\dot{m}_{c5} = 49.51 \text{ kg/s}$ (109.2 lbm/s). The total pressure exiting the turbine from Eq. 11.2.23 can be found because p_{t2} , π_c , π_b , and π_t are known:

$$p_{t5} = p_{t2} \pi_c \pi_b \pi_t$$

$$p_{t5} = 395.9 \text{ kPa (57.41 psia)}.$$

Thus, one can find the nozzle parameter $p_{t5}/p_a = 3.906$.

For the nozzle the efficiency is given as $\eta_n = 0.98$.

Next, using Eq. 11.2.52,

$$M_8 = \sqrt{\frac{2 \left[\frac{1}{\eta_n \left[\frac{p_8}{p_{t5}} \right]^{\frac{\gamma-1}{\gamma}} + 1 - \eta_n} \right]}{\gamma - 1}},$$

for $\gamma = 1.340$, $p_{t5}/p_a = 3.906$, and $p_8 = p_a$, one finds the nozzle exit Mach number $M_8 = 1.537$.

For adiabatic flow $T_{t5} = T_8 \left[1 + \frac{\gamma-1}{2} M_8^2 \right]$, and since $T_{t5} = 998 \text{ K}$, one can solve for the nozzle exit static temperature:

$$T_8 = 712 \text{ K (1282 °R)}.$$

The speed of sound at the exit is $a_8 = \sqrt{\gamma \mathcal{R} T_8} = 523.3 \text{ m/s}$ (1717 ft/s).

Hence, the gas velocity at the nozzle exit is $u_8 = M_8 a_8 = 804.2 \text{ m/s}$ (2639 ft/s).

From modeling equations (Eqs. 11.2.51 and 11.2.57),

$$a_2 = \frac{\sqrt{\frac{\gamma + 1}{2 + (\gamma - 1)M_8^2}} \sqrt{\frac{\gamma}{\gamma_{\text{stp}}} \frac{\mathcal{R}_{\text{stp}}}{\mathcal{R}}}}{M_8 \left\{ \frac{1}{\eta_n} \left[\frac{\eta_n}{\frac{2}{\gamma+1} - 1 + \eta_n} \right] \left[\frac{1}{1 + \frac{\gamma-1}{2}M_8^2} - 1 + \eta_n \right] \right\}^{\frac{\gamma}{\gamma-1}}}$$

$$\dot{m}_{c5} = \dot{m}_n a_2 M_8 \frac{p_8}{p_{t5}} \sqrt{1 + \frac{\gamma-1}{2}M_8^2},$$

and using the preceding values of p_{t5} , p_8 , M_8 , and η_n , one finds from a second (and independent calculation method) the corrected mass flow for the nozzle to be

$$\dot{m}_{c5} = 49.51 \text{ kg/s (109.2 lbm/s)}.$$

This value of \dot{m}_{c5} agrees with the earlier calculated value of \dot{m}_{c5} . Thus, the initial guess on N_{c2} was also good. It must have been the author's lucky day. If the two values of \dot{m}_{c5} had not been in agreement, a new value of N_{c2} would have been tried and the preceding process repeated (including the nested iteration on \dot{m}_{c2}). Thus, the solution for $f = 0.02$ has been found. Now that the component operating points have been found, the thrust can be found from Eq. 11.2.25:

$$F = \dot{m}[(1 + f)u_8 - u_a] + A_8(p_8 - p_a).$$

The thrust is 66,310 N (14,907 lbf), which results in a *TSFC* of 0.1108 kg/(h-N) (1.086 lbm/(h-lbf)).

Other values of f (ranging from 0.010 to 0.035) were selected, and a series of calculations were completed using the procedure above. Net results for these other values of f are presented as operating lines (dashed lines) as f varies on the maps in Figures 11.5 through 11.7. As can be seen on Figure 11.5, the case for $f = 0.02$ results in an engine operating condition near the compressor maximum efficiency point. Also, as can be seen in Figure 11.5, over the given range of fuel ratios, the compressor efficiency ranged from 82.7 to 87 to 77.7 percent and the compressor total pressure ratio monotonically increased. The operating line passed close to the maximum efficiency point. At a fuel ratio of 0.037, the compressor surged, which, as discussed in Chapter 6, would be accompanied by violent vibrations and possibly a combustor flameout, resulting in total loss of thrust.

In Figure 11.6, the burner pressure ratio decreases from 0.965 to 0.884 as the corrected mass flow decreases from 11.92 to 8.89 kg/s. The turbine (Fig. 11.7) changes characteristics minimally as the efficiency ranges from 0.899 to 0.860 and the pressure ratio varies from 0.274 to 0.287. Note that the operating line passes through the maximum efficiency point for the turbine, indicating that the turbine and compressor are well matched.

In Figure 11.8, other resulting parameters are presented for this fuel ratio range. One can easily see that the turbine inlet temperature, exit Mach number, and compressor corrected speed all increase with rising fuel ratio. For high fuel ratios, the turbine inlet temperature is excessive. The compressor corrected flow rate generally increases but tends toward a constant as the compressor approaches surge.

Finally, in Figure 11.8 the thrust and *TSFC* are shown as functions of the fuel ratio. As can be seen, the thrust always increases with f . However, the *TSFC* reaches a minimum at a fuel ratio of 0.014. Optimally, this combination of components

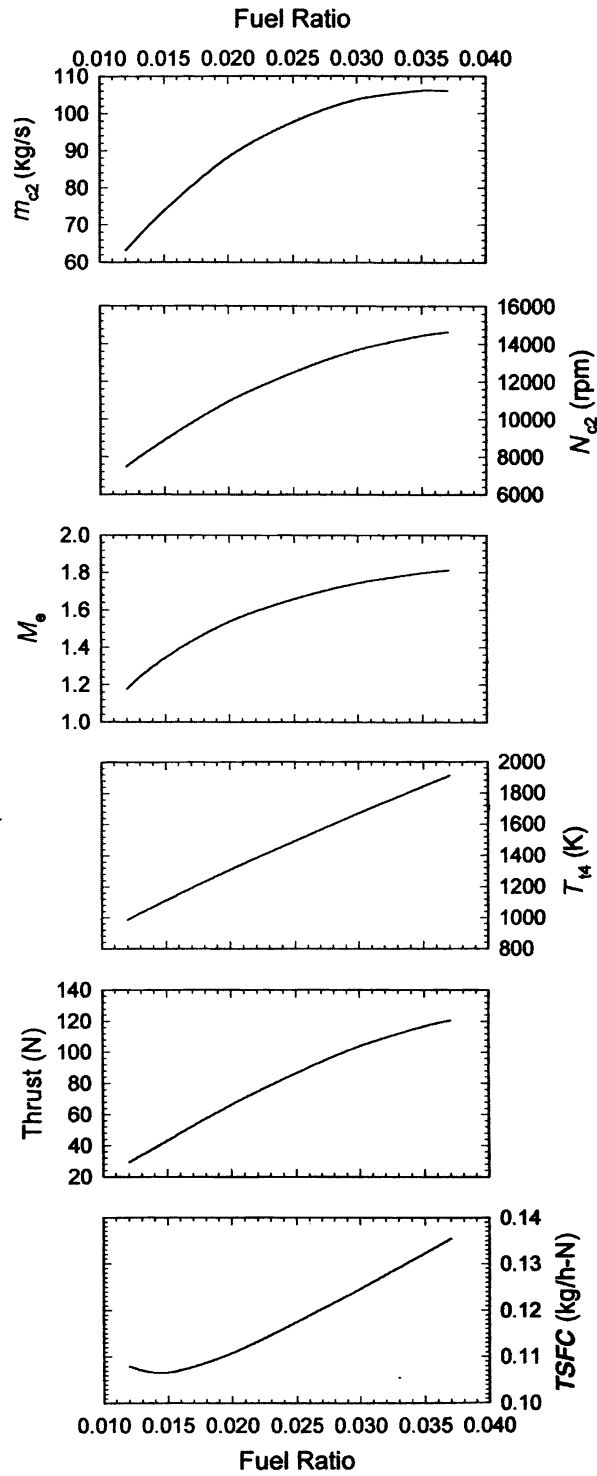


Figure 11.8 Operating conditions versus fuel ratio for Example 11.1.

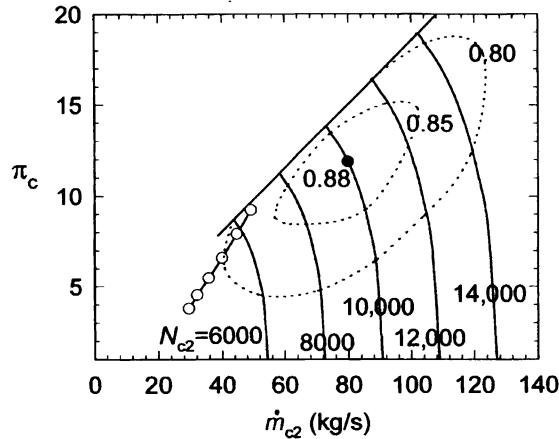


Figure 11.9 Compressor map with operating line for Example 11.1.a.

should be run at a fuel ratio of 0.014 for the best fuel economy. Other results also influence the chosen operating point, however.

Example 11.1.a: As an extension of the previous example, an analysis on a second single-spool turbojet engine with given components was performed. Again maps for the diffuser, compressor, combustor, turbine, shaft, and nozzle are all included. All of the maps are the same as before except for the turbine map. For this case the turbine has been designed to operate at a larger pressure drop (π_t at the choking condition is smaller) and to run at a higher rotational speed. The maps for the compressor and turbine are shown in Figures 11.9 and 11.10. The operating characteristics of the engine were again found, and the operating lines are shown on the maps. In Example 11.1, the turbine and compressor are noted as being well matched. In this example, however, the resulting operating line for both components is well away from the maximum efficiency points. Clearly, the compressor and turbine are not well matched. Thus, this example is presented to

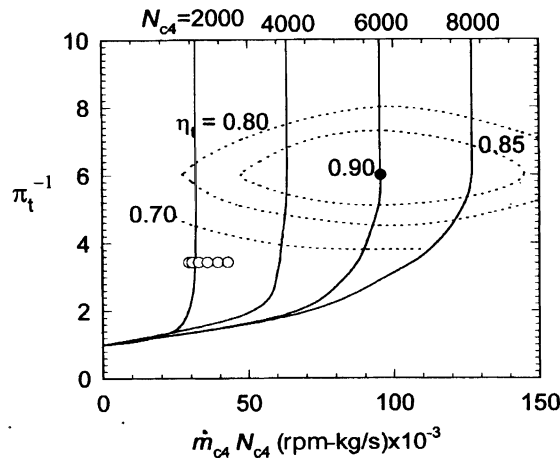


Figure 11.10 Turbine map with operating line for Example 11.1.a.

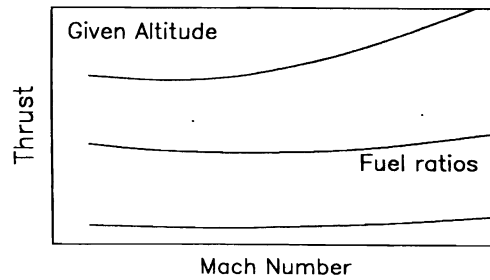


Figure 11.11 General overall operating characteristic map for an engine at a given altitude.

show one possible scenario in which an inappropriate combination of a compressor and turbine are “assembled.” This could represent, for example, an initial iteration in a design process for a new engine design. Example 11.1 would, for that case, represent the last iteration. More on the design phase is discussed in Section 11.4.

11.3. Matching of Engine and Aircraft

Up to this point in the text, the performance of the engine has been treated separately from that of the aircraft. However, just as a turbine must be matched to a compressor, an engine must be matched to an aircraft. For example, if an aircraft has two engines and each engine produces a given value of thrust, at a given altitude the aircraft will cruise at only one Mach number. That is, a pilot governs the cruise speed by adjusting the thrust level.

The previous sections describe the interactions among engine components. The fuel ratio and Mach numbers are treated independently. Thus, for a given engine with known components, an operating characteristic map, as shown in Figure 11.11, can be generated for an engine at various altitudes. This figure indicates how the developed thrust varies with inlet Mach number and fuel ratio for a given engine with given components (and maps). For example, one point of such a map has been calculated in Example 11.1. Similar calculations for ranges of both Mach number and fuel ratios could be used to generate such a figure.

If only the airframe is considered, the thrust required to power an aircraft at a given altitude will become greater as the aircraft speed increases. That is, the total thrust from one or more engines will balance the aircraft drag. These airframe drag characteristics will be determined from, for example, wind tunnel tests. A general variation is shown in Figure 11.12. Therefore, by combining Figures 11.11 and 11.12, one can determine the required engine conditions for a given Mach number. Mathematically, from these two figures, four

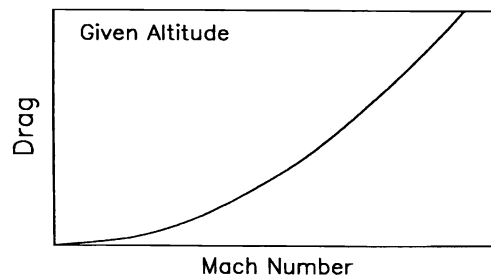


Figure 11.12 General drag characteristics for an airframe.

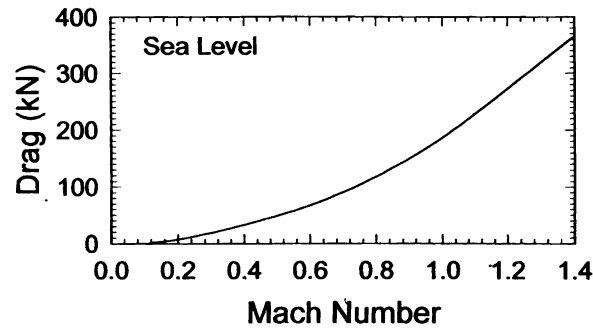


Figure 11.13 Drag characteristics for the airframe in Example 11.2.

variables are obtained (Mach number, fuel ratio, thrust, and altitude). Furthermore, with these two figures there are two equations. For the engine,

$$F = \mathcal{f}(M, f, \text{altitude}). \quad 11.3.1$$

And for the airframe,

$$F = \mathcal{g}(M, \text{altitude}). \quad 11.3.2$$

Therefore, if two variables are specified (namely the flight altitude and Mach number), the other two are determinable (namely, fuel ratio and thrust). As a result of this engine and airframe matching, for a given engine (or set of engines) on a given airframe, once the Mach number and altitude are specified, the required fuel ratio is set.

A model that can often be applied for a given airframe and that can be used in a computerized matching solution is

$$F_{\text{airframe}} = C_{\text{dm}} M_a^2. \quad 11.3.3$$

Note, however, in that C_{dm} is a modeling parameter rather than a conventional nondimensional drag coefficient and has the units of force.

Example 11.2: A single-spool turbojet engine with given components is to be assembled for a given airframe. Since this case represents an engine, the diffuser, compressor, combustor, turbine, shaft, and nozzle are all modeled. The maps for the compressor, burner, and turbine are shown in Figures 11.5 through 11.7, and the different model parameters, which fit the data, are presented in Table 11.2. The nozzle has a fixed minimum area and a variable exit area. The aircraft has drag characteristics shown in Figure 11.13. The aircraft with two engines is to be operated near standard temperature and pressure at a Mach number of 0.90. Find the required fuel ratio and resulting *TSFC* at this condition. Also determine how the fuel ratio and *TSFC* vary as the flight Mach number changes from 0.4 to 1.2 at $T_a = 289 \text{ K}$ (520°R) and $p_a = 101.3 \text{ kPa}$ (14.69 psia).

SOLUTION:

Note that this is the same engine as in Example 11.1. Thus, the detailed calculations of the engine component matching will not be performed. However, Figure 11.14 was generated for this engine (solid lines) by following the same method as in Example 11.1 and by parametrically varying the Mach number and fuel ratio and solving the engine matching problem many times. Also, the required thrust per

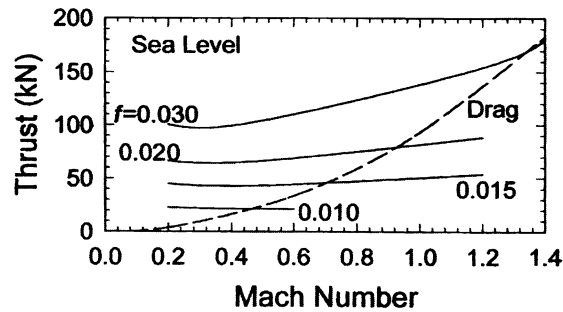


Figure 11.14 Overall operating characteristic map for the engine in Example 11.2 at sea level.

engine (total drag/two engines) is superimposed on this figure (dashed line). Where the two curves intersect determines the operating conditions of the engines. For example, for Mach numbers of 0.47, 0.71, and 0.91, the required fuel ratios are 0.01, 0.015, and 0.02, respectively.

In particular, at a Mach number of 0.90, the required thrust per engine is 75,800 N (17,040 lbf). By iterating on the Mach number and repeating the methodology from Example 11.1, the required fuel ratio for these conditions was found to be 0.0199. Other conditions at a Mach number of 0.90 are presented in Table 11.3.

Furthermore, the fuel ratio (from Fig. 11.14) and the resulting values of $TSFC$ are plotted versus the Mach number in Figure 11.15 to determine the overall performance for different flight Mach numbers. As can be seen, the required fuel ratio varies almost linearly with Mach number. The value of $TSFC$ appears to be approaching a minimum well below the design condition, which is not desirable

Table 11.3. Detailed Results for Example 11.2 for $M_a = 0.90$

Diffuser	Turbine
$\pi_d = 1.0$	$\dot{m}_{c4} = 15.87 \text{ kg/s (35.00 lbm/s)}$
$\gamma_d = 1.400$	$\gamma_t = 1.326$
	$N_{c4} = 5070 \text{ rpm}$
Compressor	$T_{t4} = 1342 \text{ K (2416 }^\circ\text{R)}$
$\dot{m}_{c2} = 82.63 \text{ kg/s (182.2 lbm/s)}$	$\pi_t = 0.280$
$\eta_c = 0.876$	$\eta_t = 0.876$
$N_{c2} = 10140 \text{ rpm}$	
$\gamma_c = 1.381$	Nozzle
$\pi_c = 11.38$	$\dot{m}_{c5} = 49.52 \text{ kg/s (109.2 lbm/s)}$
	$A_8/A^* = 1.393$
Combustor	$M_8 = 1.700$
$\dot{m}_{c3} = 10.50 \text{ kg/s (23.15 lbm/s)}$	$p_5/p_a = 5.029$
$\gamma_b = 1.338$	$\eta_n = 0.98$
$\pi_b = 0.933$	$\gamma_n = 1.338$
$\eta_b = 0.91$	
$f = 0.0199$	Overall
	$F = 75,790 \text{ N (17,040 lbf)}$
Shaft	$N = 10,929 \text{ rpm}$
$\eta_m = 1.00$	$TSFC = 0.1227 \text{ kg/h-N (1.203 lbm/h-lbf)}$
	$\dot{m} = 129.8 \text{ kg/s (286.1 lbm/s)}$

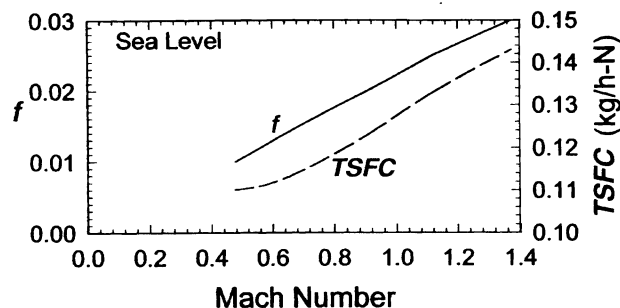


Figure 11.15 Variation of fuel ratio and *TSFC* with flight Mach number for the engines and aircraft in Example 11.2.

and indicates that a better design is likely attainable. If one would like to improve the design, new maps could be attempted – especially the compressor map – to increase the pressure ratio and thus reduce the *TSFC*.

11.4. Use of Matching and Cycle Analysis in Second-Stage Design

So far in this chapter the concept of component matching has been presented and used in examples as a method of directly analyzing engines or gas turbines with given maps. In fact, the method in practice is used to perform a second-stage design analysis (often called an advanced design analysis) of a new or proposed engine or gas turbine. The preliminary (or first-stage) design has been outlined in Chapter 3, which basically set the engine type and “sized” the engine. For this second-stage jet engine design, a set of overall engine design conditions, including both on-design and off-design conditions, are given to an engine manufacturer by a military group or commercial enterprise, including, but not exclusively, thrusts and *TSFCs* at different altitudes. A group of system design engineers then uses a component matching analysis to vary the engine types parametrically and *iteratively vary the component maps* to accomplish the overall design goals and to ensure that all of the components fit together. For instance, in Example 11.1.a, which might represent an initial matching analysis, the resulting operating points for the engine indicate that the components are clearly not matched well. The compressor is designed to operate at a rotational speed (or mass flow) that is too high and with a pressure ratio that is too high, or the initial turbine is designed to operate with a value of π_t that is too low and a rotational speed that is too high, or both the compressor and turbine are not well designed. The maps should be adjusted accordingly until the best efficiency points of all components are at the best performance point of the engine, the derived turbine power matches the compressor power requirements, required thrust is delivered, and so on. For the maps shown in Example 11.1.a, this would mean that the compressor should be designed for a lower rotational speed and either the flow deflection angles of the blades or vanes should be reduced or number of stages should be reduced. For the turbine, it means that reducing the blade or vane deflection angles or number of stages and reducing the running speed are in order. The final sets of component maps (i.e., example 11.1) optimize overall performance. The maps determined by this systems group during this design phase then become the detailed design goals of the more focused or specific component design groups. For example, compressor design or turbine design groups then design the blades and vanes and stages to produce these maps. Then, detailed analyses and designs of the components are undertaken to obtain components

with the required maps by using the methods presented in the previous seven chapters as well as more advanced techniques. Such design methodology is a part of an inverse system design; that is, one starts with the overall design goals and works backward to determine the component maps that will accomplish the goals. Once the maps are determined, the geometries that produce these maps are designed in detail. This is therefore the second step in an industrial engine or gas turbine design.

11.5. Summary

A method of matching gas turbine components has been presented in this capstone chapter. At the end of a complicated and expensive design and development process, an engine must operate at high (and known) performance over a range of conditions. Matching is the process by which components are integrated to allow predictions of overall engine performance. First, the fundamental method of matching components with generalized characteristic maps was described. Three cases were considered: gas generator (compressor, burner, turbine), a single-shaft turbojet engine (diffuser, gas generator, nozzle), and a single-shaft power-generation gas turbine (inlet, gas generator, exhaust, load). Second, curve-fit functional mathematical models for the different maps of the components were developed so that the component maps could be defined by assigning values to parameters. Although convenient for computer analyses, such modeling is not necessary for the matching process; it merely eases the solution process. Third, steady-state matching was accomplished for both single-spool jet engines and power gas turbines by simultaneously solving the mathematical models of the component maps or graphical data along with the matching equations. The method was demonstrated in an example for a single-spool turbojet engine with given component maps. For the example, a range of fuel ratios was used and the compressor was shown to increase in speed and eventually surge as the fuel ratio was increased. The technique is a tool through which one can select components to optimize overall engine performance and predict off-design performance of an engine. The method was only applied to a simple turbojet engine or a simple power-generation gas turbine in this chapter. The method can be extended to include more complex engines, including twin-spool turbopumps with afterburners, as well. For these cases more maps and equations are needed and all of the components are matched. Furthermore, the method can be extended to find the dynamic or transient response of a gas turbine during shaft acceleration or deceleration.

In previous chapters the influence of components on each other was not considered. Chapters 2 and 3 consider the entire engine through cycle analyses; however, component parameters (efficiency, pressure ratios, flow rates, etc.) are specified. In Chapters 4 through 10 the individual components are analyzed and, for example, the pressure ratios and efficiencies of the components have been found to be strong functions of component geometries, flow rates, and rotational speeds. This chapter thus integrates all of the previous chapters in as much as cycle analysis of the engine is once again performed; however, in this chapter the component interaction and varying efficiencies are included.

As a final step, engine and airframe matching was accomplished. The performance characteristics of an engine (or set of engines) must be matched to an aircraft. For this matching, the total thrust from the engines must match the total aerodynamic drag of the airframe for a cruise condition to result. Thus, when both the engine and aircraft are matched, the fuel ratio and speed cannot be independently varied. As a result, when the drag characteristics of an airframe are coupled with an engine for which all of the component maps are known, by varying the fuel ratio (as performed by a pilot), one can determine the operating points of all engine components and airframe speed.

At the conclusion of this chapter, the reader, if given a set of engine design goals (both on- and off-design), has a significant package of analyses that can be used for the inverse design of an engine as a system. One can study the effects of parametrically changing component maps and engine types for ranges of operating conditions until the engine design goals are accomplished. Thus, the engine can be treated as a system, and realistic engine predictions can be made. Through this methodology, an inverse design process can be used to specify the desired operating characteristics, namely maps, of the different components to accomplish the overall design goals. Once the design maps are determined, the components can be designed to realize these maps. This is the second step in real industrial engine design.

List of Symbols

A	Area
a	Speed of sound
c_p	Specific heat at constant pressure
F	Force or thrust
f	Fuel ratio
ΔH	Heating value
I	Rotor polar moment of inertia
m	Mass flow rate
M	Mach number
N	Rotational speed
p	Pressure
\mathcal{P}	Power
\mathcal{R}	Ideal gas constant
T	Temperature
T	Torque
$TSFC$	Thrust specific fuel consumption
γ	Specific heat ratio
η	Efficiency
π	Total pressure ratio
τ	Total temperature ratio
ϕ	General function
ψ	General function
ω	Rotational speed

Subscripts

a	Freestream or ambient
b	Primary burner
c	Compressor
c	Corrected
d	Diffuser
e	Exhaust
f	Fuel
i	Inlet
l	Load
m	Mechanical (shaft)
n	Nozzle
stp	Standard conditions
t	Total (stagnation)

t	Turbine
1	Inlet to diffuser
2	Exit of diffuser, inlet to compressor
3	Exit of compressor, inlet to combustor
4	Exit of combustor, inlet to turbine
5	Exit of turbine, inlet to nozzle
8	Exit of nozzle or exhaust

Superscripts

* Choked

Modeling Parameters

c_1	Compressor
c_2	Compressor
c_3	Compressor
c_4	Compressor
c_5	Compressor
N_{c2d}	Compressor
μ	Compressor
η_{c_d}	Compressor
b_1	Combustor
b_2	Combustor
η_{b_d}	Combustor
k_1	Turbine
k_2	Turbine
\dot{m}_{c4_c}	Turbine
N_{c4_d}	Turbine
η_{t_d}	Turbine
π_{d_c}	Turbine
s_1	Shaft
s_2	Shaft
d	Diffuser
π_{d_d}	Diffuser
a_1	Nozzle
\dot{m}_n	Nozzle
η_{n_d}	Nozzle
z_1	Inlet (power gas turbine)
z_2	Exhaust (power gas turbine)
z_3	Power load (power gas turbine)
z_4	Power load (power gas turbine)
C_{dm}	Airframe

Problems

11.1 A turbojet engine with given maps for the compressor, turbine, burner, and converging nozzle is to be assembled. The engine is to operate at sea level and at a Mach number of 0.75. The maps are shown in Figures 11.P.1 through 11.P.4. The shaft mechanical efficiency is 0.995, the burner efficiency is 0.91, the fuel has a heating value of 17,800 Btu/lbm, the diffuser total

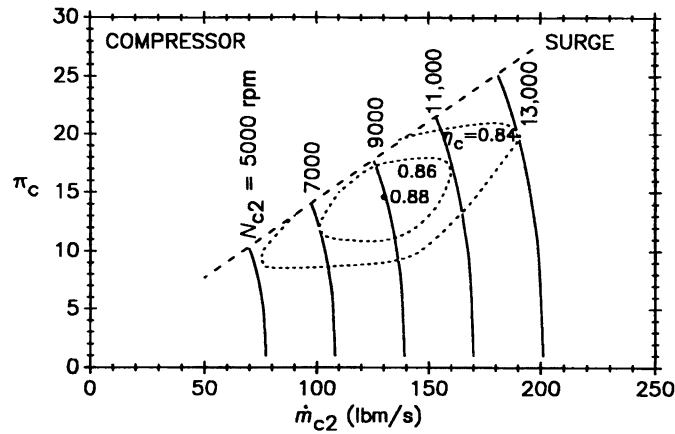


Figure 11.P.1 Compressor performance map for Problems 11.1, 11.2, and 11.3.

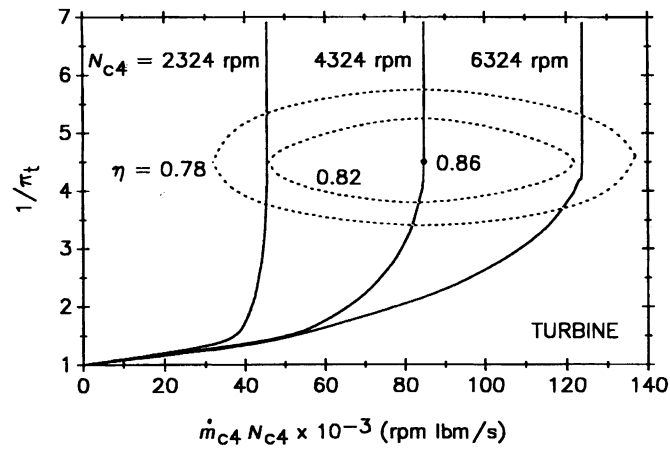


Figure 11.P.2 Turbine performance map for Problems 11.1, 11.2, and 11.3.

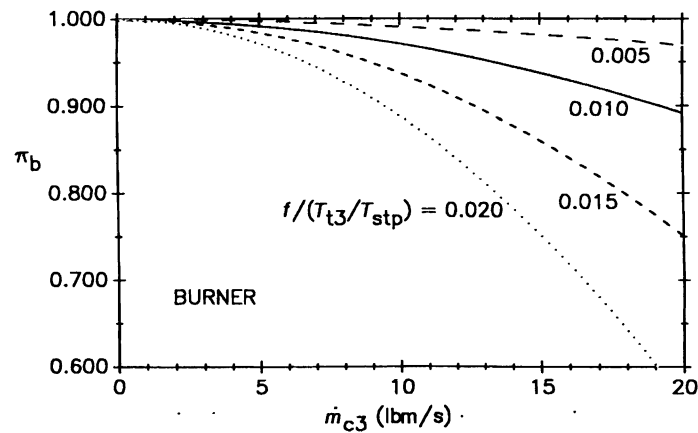


Figure 11.P.3 Burner performance map for Problems 11.1, 11.2, and 11.3.

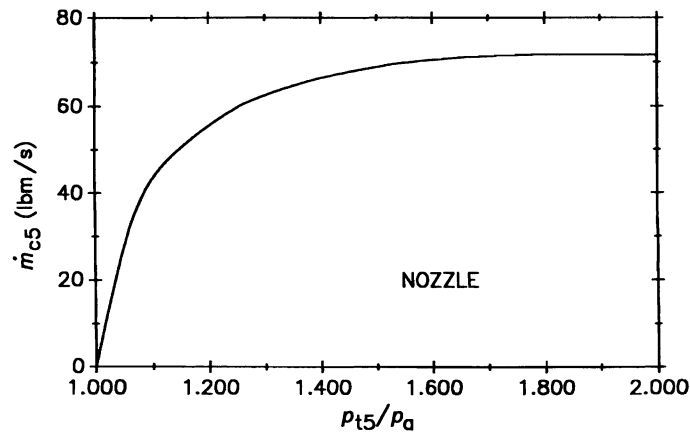


Figure 11.P.4 Nozzle performance map for Problems 11.1 and 11.3.

recovery factor is 0.92, and the nozzle efficiency is 0.96. If the fuel ratio is 0.03, find the thrust, *TSFC*, engine air mass flow rate, and shaft speed. Indicate the operating point on the figures.

- 11.2 A gas generator for a turbojet engine with given maps for the compressor, turbine, and burner is to be assembled. The maps are shown in Figures 11.P.1 through 11.P.3. The shaft mechanical efficiency is 0.995, the burner efficiency is 0.91, and the fuel has a heating value of 17,800 Btu/lbm. If the fuel ratio is 0.020, the corrected speed of the compressor is 9000 rpm, and the total temperature at the inlet to the compressor is 577 °R, find the corrected compressor air mass flow rate, compressor total pressure ratio, and shaft speed. Indicate the operating point on the figures.
- 11.3 Three identical turbojet engines with given maps for the compressors, turbines, burners, and converging nozzles are to be assembled and used on a given aircraft. The aircraft is to operate at sea level. The engine maps are shown in Figures 11.P.1 through 11.P.4, and the drag characteristics for the airframe are shown in Figure 11.P.5. The shaft mechanical efficiency is 0.995, the burner efficiency is 0.91, the fuel has a heating value of 17,800

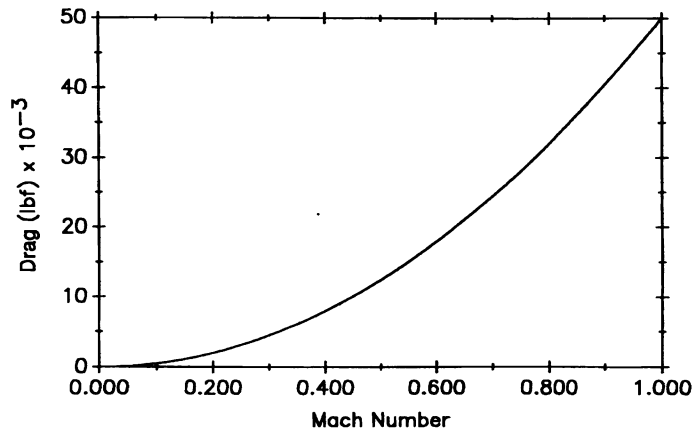


Figure 11.P.5 Drag on airframe for Problem 11.3.

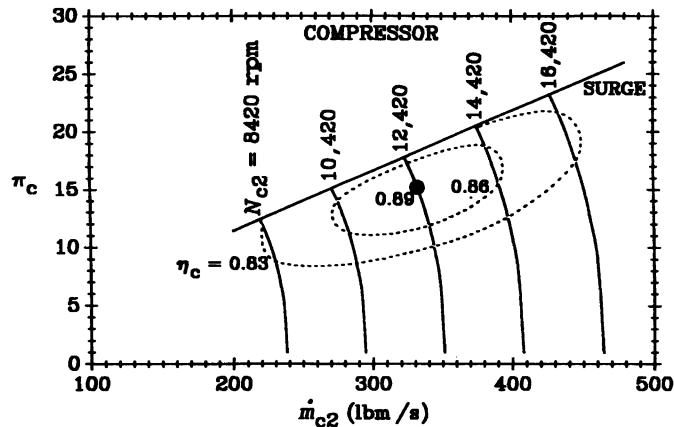


Figure 11.P.6 Compressor performance map for Problems 11.4 and 11.5.

Btu/lbm, the diffuser total recovery factor is 0.92, and the nozzle efficiency is 0.96. If the fuel ratio is 0.021, find the operating Mach number and for each engine find the thrust, $TSFC$, engine air mass flow rate, and shaft speed. Indicate the operating point on the figures.

- 11.4 A turbojet engine with given maps for the compressor, turbine, burner, converging nozzle, and shaft is to be assembled. The engine is to operate at 27,000 ft. The maps are shown in Figures 11.P.6 through 11.P.10. The fuel has a heating value of 17,800 Btu/lbm, and the maximum diffuser total recovery factor is 0.96, which decreases as found empirically with increasing Mach numbers above unity.
- If the fuel ratio is 0.026 and the Mach number is 0.85, find the thrust, $TSFC$, engine air mass flow rate, and shaft speed. Indicate the operating point on the figures. Compare this analysis to that in Problem 3.34.
 - If the Mach number is 0.85, find the operating line on the compressor and turbine maps.
 - If the Mach number is 0.60, find the operating line on the compressor and turbine maps.

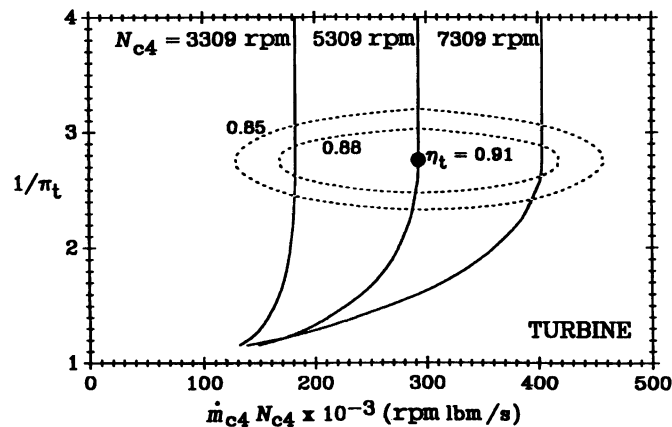


Figure 11.P.7 Turbine performance map for Problems 11.4 and 11.5.

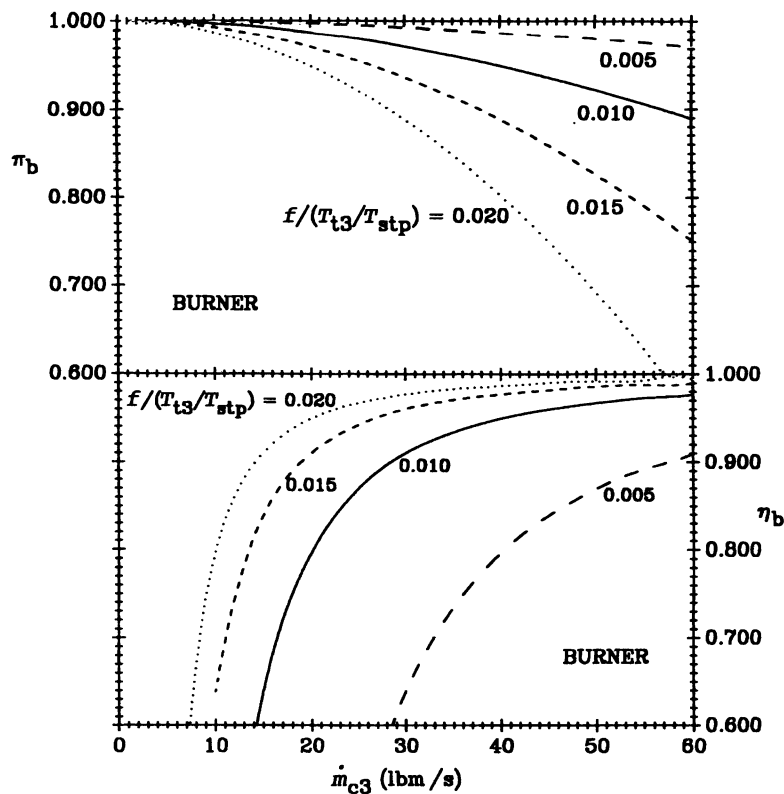


Figure 11.P.8 Burner performance map for Problems 11.4 and 11.5.

- (d) If the Mach number is 1.10, find the operating line on the compressor and turbine maps.
- 11.5 Three identical turbojet engines with given maps for the compressors, turbines, burners, converging nozzles, and shafts are to be assembled and used on a given aircraft. The aircraft is to operate at 27,000 ft. The engine maps are shown in Figures 11.P.6 through 11.P.10, and the drag characteristics for the airframe are shown in Figure 11.P.11. For each engine the fuel has a heating value of 17,800 Btu/lbm and the maximum diffuser total recovery factor is 0.96, which decreases as found empirically with increasing Mach numbers above unity.
- (a) If the fuel ratio is 0.026, find the operating Mach number and for each engine find the thrust, $TSFC$, engine air mass flow rate, and shaft speed. Indicate the operating point on the figures.
- (b) Find the dependence of operating Mach number on the fuel ratio for turbine total temperatures ranging from 1900 to 3900 °R.
- 11.6 A power gas turbine with given maps for the compressor, turbine, burner, inlet, exhaust, and electric generator load is to be assembled. The unit is to operate at standard sea level. The maps are shown in Figures 11.P.12 through 11.P.16. The shaft mechanical efficiency is 0.995, the burner efficiency is 0.91, and the fuel has a heating value of 10,000 kCal/kg. If the fuel ratio ranges from 0.012 to 0.032, find the net output power, thermal efficiency,

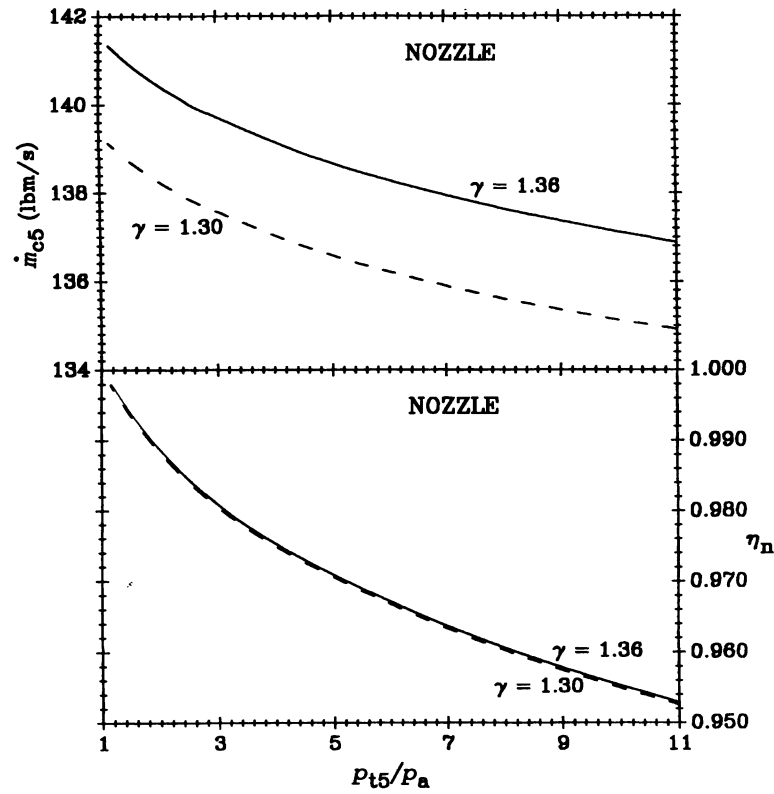


Figure 11.P.9 Nozzle performance map for Problems 11.4 and 11.5.

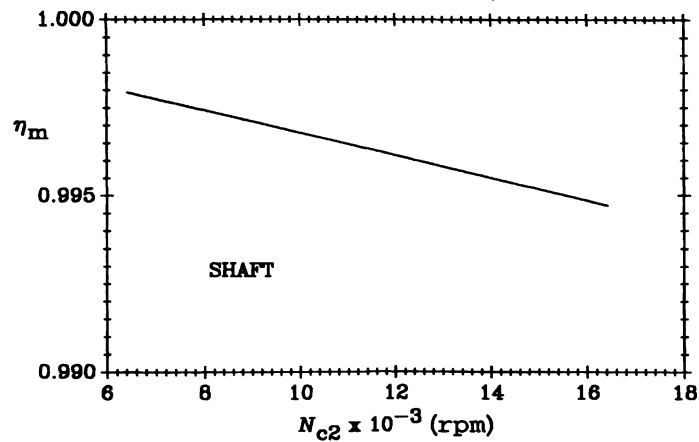


Figure 11.P.10 Shaft performance map for Problems 11.4 and 11.5.

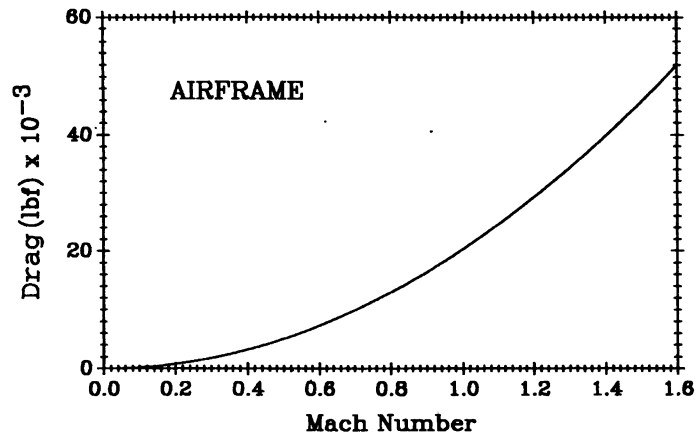


Figure 11.P.11 Drag on airframe for Problem 11.5.

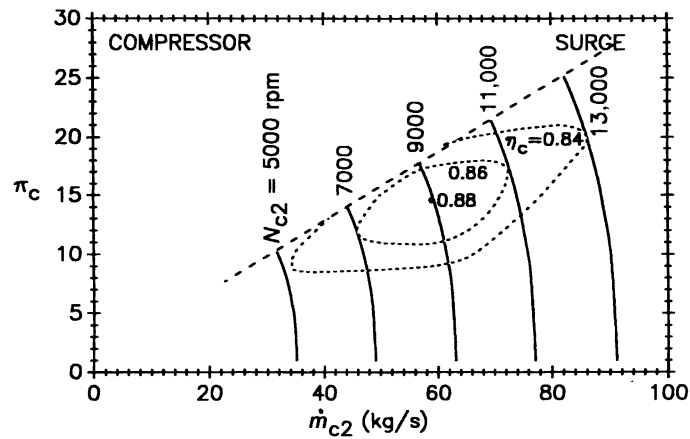


Figure 11.P.12 Compressor performance map for Problem 11.6.

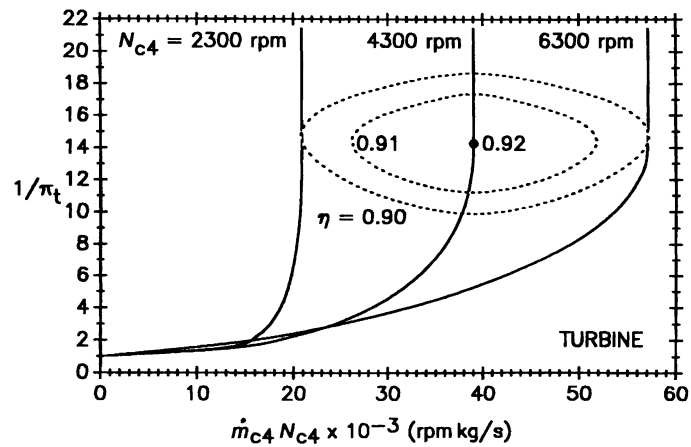


Figure 11.P.13 Turbine performance map for Problem 11.6.

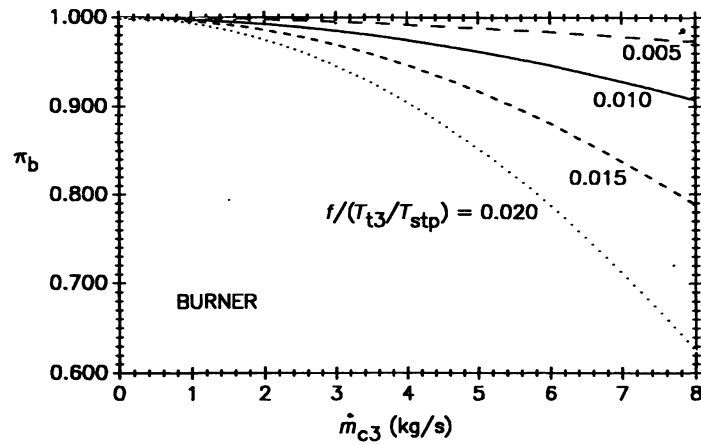


Figure 11.P.14 Burner performance map for Problem 11.6.

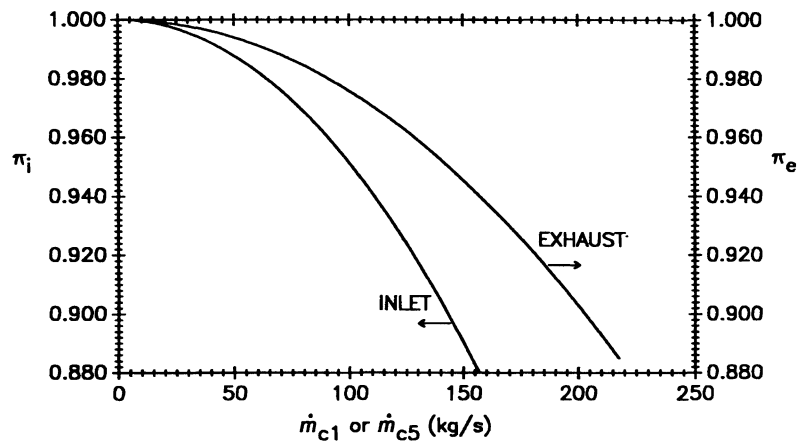


Figure 11.P.15 Inlet and exhaust performance maps for Problem 11.6.

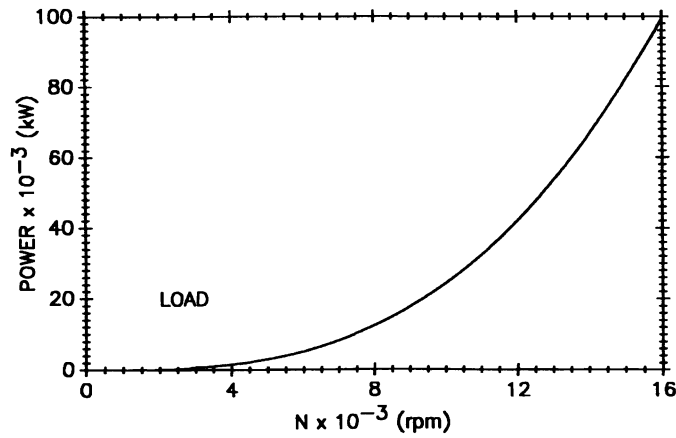


Figure 11.P.16 Load characteristics for Problem 11.6.

air mass flow rate, and shaft speed. Indicate the operating points on the figures.

- 11.7** An aircraft is to be outfitted with three engines. Drag on the airframe at STP is tabulated below. Components of the engines have been matched so that engine maps at STP are available as tabulated below. If a fuel ratio of 0.020 is used, what is the operating Mach number of the aircraft?

Airframe Drag	
Mach Number	Drag (lbf)
0.00	0.0
0.20	3000
0.40	10,000
0.60	23,000
0.80	40,000
1.00	63,000

Single Engine Thrust (lbf)			
Mach Number	$f = 0.015$	$f = 0.020$	$f = 0.025$
0.40	5700	7800	10800
0.60	5000	7300	10200
0.80	5200	7500	10300

- 11.8** An aircraft is to be outfitted with two turbofan engines. Drag on the airframe at STP is tabulated below. Components of the engines have been matched so that engine maps at STP are available as tabulated below. If a fuel ratio of 0.022 is used, what is the operating Mach number of the aircraft?

Airframe Drag	
Mach Number	Drag (lbf)
0.0	0.0
0.2	4000
0.4	16,000
0.6	36,000
0.8	64,000
1.0	10,0000

Single Engine Thrust (lbf)			
Mach Number	$f = 0.016$	$f = 0.020$	$f = 0.024$
0.40	18,000	29,000	40,000
0.60	17,000	28,000	39,000
0.80	18,000	29,000	40,000
1.00	20,000	31,000	42,000

One-Dimensional Compressible Flow

H.1. Introduction

The basic concepts of compressible flow are applied in all of the chapters in this book. Specifically, in Chapters 4 (diffusers), 5 (nozzles), 9 (combustors), and 10 (mixers), analyses of fundamental, compressible, steady-state, one-dimensional flow are used to predict total pressure losses and other characteristics in the different components. Thus, to avoid repetition of material, this appendix is presented to summarize different fundamental processes. Included in the processes are the stagnation process, ideal gas properties, isentropic flow with area changes, frictional adiabatic with constant area (Fanno) flow, flow with heat addition and constant area (Rayleigh), normal and oblique shocks, flow with drag objects, mixing flows, and generalized one-dimensional flow, which allows the combination of two or more different fundamental phenomena. In all of the preceding analyses a control volume approach is used and the flow is assumed to be steady and uniform at the different cross-sectional flow surfaces. Such processes are covered in detail in fundamental gas dynamics texts such as Anderson (1982), Liepmann and Roshko (1957), Shapiro (1953), and Zucrow and Hoffman (1976). The flow is assumed to be one-dimensional. Although flow can be two- or three-dimensional in components, a one-dimensional analysis can lead to reasonable results for many cases. For all cases the gas is assumed to be ideal.

H.2. Ideal Gas Equation and Stagnation Properties

First, one can relate the different pressures, temperatures, and densities by the ideal gas equation

$$pv = p/\rho = \mathcal{R}T, \quad \text{H.2.1}$$

where \mathcal{R} is the ideal gas constant and is equal to 1545 ft-lbf/(lb-mole-°R) (or 8.315 kJ/(kg-mole K)). For air with a molecular weight of 28.97 lbm/lb-mole, one finds that the ideal gas constant is 1545/28.97 or 53.35 ft-lbf/(lbm-°R) (or 0.2871 kJ/kg-K). Furthermore, one can relate the specific heat at constant pressure to the ideal gas constant by

$$c_p = \frac{\gamma \mathcal{R}}{\gamma - 1}, \quad \text{H.2.2}$$

where γ is the specific heat ratio

$$\gamma = \frac{c_p}{c_v} \quad \text{H.2.3}$$

and c_v is the specific heat at constant volume. Also, one can relate the ideal gas constant to the specific heats by

$$\mathcal{R} = c_p - c_v. \quad \text{H.2.4}$$

Table H.1.a Specific Heat at Constant Pressure, c_p (Btu/lbm-°R)

T (°R)\Pressure (atm)	1	4	7	10	40	70	100
360	0.2405	–	–	0.2499	–	–	0.4170
492	0.2403	–	–	0.2446	–	–	–
540	0.2405	–	–	0.2439	–	–	0.2776
720	0.2424	–	–	0.2441	–	–	0.2599
900	0.2462	0.2465	0.2469	0.2476	0.2506	–	–
1080	0.2513	0.2515	0.2517	0.2520	0.2542	–	–
1440	0.2626	0.2627	0.2629	0.2630	0.2642	0.2653	–
1800	0.2730	0.2731	0.2732	0.2733	0.2739	0.2746	–
2160	0.2819	0.2820	0.2820	0.2820	0.2825	0.2830	0.2833
2520	0.2902	0.2902	0.2902	0.2903	0.2906	0.2910	0.2912
2880	0.2986	0.2985	0.2985	0.2985	0.2987	0.2989	0.2992
3600	0.3198	0.3173	0.3167	0.3165	0.3158	0.3159	0.3159
5400	0.6835	0.5217	0.4796	0.4613	0.4052	0.3895	0.3843

Table H.1.b Specific Heat Ratio, γ (dimensionless)

T (°R)\Pressure (atm)	1	4	7	10	40	70	100
360	1.3987	–	–	1.3781	–	–	1.1968
492	1.3992	–	–	1.3895	–	–	–
540	1.3987	–	–	1.3910	–	–	1.3280
720	1.3944	–	–	1.3906	–	–	1.3583
900	1.3859	1.3853	1.3844	1.3829	1.3766	–	–
1080	1.3752	1.3748	1.3744	1.3737	1.3693	–	–
1440	1.3533	1.3531	1.3528	1.3526	1.3504	1.3485	–
1800	1.3353	1.3352	1.3350	1.3349	1.3339	1.3327	–
2160	1.3214	1.3212	1.3212	1.3212	1.3205	1.3197	1.3193
2520	1.3093	1.3093	1.3093	1.3092	1.3088	1.3082	1.3079
2880	1.2980	1.2982	1.2982	1.2982	1.2979	1.2976	1.2973
3600	1.2729	1.2756	1.2763	1.2765	1.2773	1.2772	1.2772
5400	1.1115	1.1513	1.1668	1.1746	1.2037	1.2136	1.2171

Adapted from *Handbook of Supersonic Aerodynamics*, Vol. 5, Bureau of Ordnance, Dept. of the U.S. Navy, Washington, DC, 1953.

Or using Eq. H.2.9, one can define the total or stagnation pressure p_t :

$$p_t = p \left[1 + \frac{\gamma - 1}{2} M^2 \right]^{\frac{\gamma}{\gamma - 1}} \quad \text{H.2.13}$$

Recall again that this is for an isentropic process that is more restrictive than the definition for the total temperature (Eq. H.2.9), which is only an adiabatic process.

H.3. Variable Specific Heats

In Table H.1 (from Department of the U.S. Navy (1953)) values of c_p and γ are presented for air between 360 and 5400 °R and between 1 and 100 atm. As can be seen, c_p

In Chapter 3 and others, the specific heats are assumed to be across each component but have different values based on component temperatures. To justify the assumption of constant specific heats across each component, one should consider the evaluation of $h_i - h_j$, where i and j are any two states. This must be considered because large temperature differences can exist across components. In general, an enthalpy change is given by

$$\Delta h = \int_{T_j}^{T_i} c_p dT. \quad \text{H.3.3}$$

One should determine if the best approximation of Δh is $\bar{c}_p \Delta T$, where \bar{c}_p is evaluated at the average temperature ($\bar{T} = (T_i + T_j)/2$) or if the best approximation is $c_{p_i} T_i - c_{p_j} T_j$, where the specific heats are evaluated at the end states. As an approximation to determine which method is best, one can model the dependence of c_p on T , and thus

$$c_p = C + BT. \quad \text{H.3.4}$$

Therefore,

$$\bar{c}_p = C + B\bar{T}. \quad \text{H.3.5}$$

Now, substituting Eq. 3.1.4 into 3.1.3 and evaluating yield

$$\Delta h = C(T_i - T_j) + B \left[\frac{T_i^2 - T_j^2}{2} \right], \quad \text{H.3.6}$$

but this can be factored to become

$$\Delta h = \left[C + B \left(\frac{T_i + T_j}{2} \right) \right] (T_i - T_j). \quad \text{H.3.7}$$

By comparing this to Eq. H.3.5, one sees that

$$\Delta h = \bar{c}_p \Delta T. \quad \text{H.3.8}$$

Thus, the conclusion is that one should use the value of c_p evaluated at the average temperature and the temperature difference to calculate the change in enthalpy.

To further demonstrate the point, one can consider a numerical example of air between the temperatures of 1000 and 2000 °R. From tables for air, one finds that at these two temperatures the enthalpies are 241.0 and 504.7 Btu/lbm, respectively. Also at these temperatures, the values of c_p are 0.249 and 0.277 Btu/lbm-°R, respectively. The value of c_p at the average temperature (1500 °R) is 0.264 Btu/lbm-°R. Thus, the actual change in enthalpy is $504.7 - 241.0 = 263.7$ Btu/lbm. By comparison, $c_{p_i} T_i - c_{p_j} T_j = 0.277 \text{ Btu/lbm-}^\circ\text{R} \times 2000 \text{ }^\circ\text{R} - 0.249 \text{ Btu/lbm-}^\circ\text{R} \times 1000 \text{ }^\circ\text{R} = 305$ Btu/lbm. When using the value of c_p at the average temperature, one finds $\bar{c}_p (T_i - T_j) = 0.264 \text{ Btu/lbm-}^\circ\text{R} \times (1000 \text{ }^\circ\text{R}) = 264$ Btu/lbm. Clearly, using the value of c_p at the average temperature to evaluate Δh is best.

H.4. Isentropic Flow with Area Change

The cross-sectional area can change axially in several components, and ideally the flow is without friction or heat transfer. The nozzle and diffuser are the two most obvious components in which the area changes. As the area changes, so do the Mach number, velocity, and other properties. In this section the dependence of the variables is discussed. The diagram of the model is shown in Figure H.2, including the control volume. Uniform

where a is the sound speed. For an ideal gas,

$$p_1 = \rho_1 \mathcal{R} T_1 \quad \text{H.4.8}$$

$$p_2 = \rho_2 \mathcal{R} T_2, \quad \text{H.4.9}$$

and from the definition of stagnation pressure,

$$p_{t1} = p_1 \left[1 + \frac{\gamma - 1}{2} M_1^2 \right]^{\frac{\gamma}{\gamma - 1}} \quad \text{H.4.10}$$

$$p_{t2} = p_2 \left[1 + \frac{\gamma - 1}{2} M_2^2 \right]^{\frac{\gamma}{\gamma - 1}}. \quad \text{H.4.11}$$

Thus, one can utilize Eqs. H.4.1 through H.4.11 and therefore have 11 equations. Sixteen variables are present, and so 5 must be specified. For example, if M_1 , T_1 , p_1 , A_1 , and A_2 are specified, one can find M_2 . Thus, these equations define the process on the h - s diagram. For subsonic internal flow (the usual case for a diffuser), the Mach number decreases as the area increases. For supersonic flow, however, the Mach number increases owing to an increase in area – for example, in the diverging section of a nozzle.

To aid in the solution of these equations, many gas dynamics and fluid mechanics texts present tables of M , T/T_t , p/p_t , A/A^* , and other variables versus Mach number, where the superscript * indicates reference conditions at the sonic condition. Such tables are presented in this text in Appendix B for three values of γ . Solutions can also be obtained using the software, “ISENTROPIC”.

H.5. Fanno Line Flow

Boundary layers and other viscous flows are the primary means by which total pressure losses occur within diffusers and ducts. Such flow is also important in burners and afterburners owing to viscous flow through small orifices or holes in a burner wall. This flow will be analyzed based on Fanno line flow, which is flow with friction but no heat addition or loss. The Fanno line process is a constant area process, which does not necessarily represent a diffuser, duct, or burner exactly. However, for a diffuser, for example, when the exit to inlet area ratio is near unity so that the flow does not separate, the mechanism can be used to predict the total pressure losses reasonably. The diagram of the model is shown in Figure H.3 with the control volume, and the h - s diagram is shown in Figure H.4. For the Fanno process line of the h - s diagram, the continuity and energy equations are used. Many of the equations from the previous section can be used because this process is also adiabatic ($T_{t1} = T_{t2}$).

For example, the continuity equation above yields for $A_1 = A_2$:

$$\rho_1 V_1 = \rho_2 V_2. \quad \text{H.5.1}$$

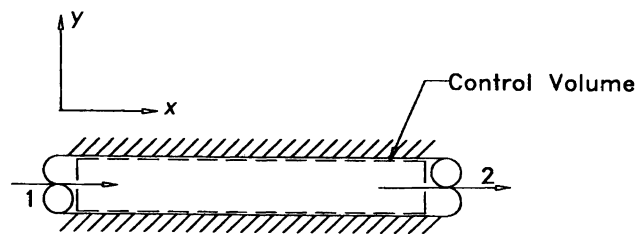


Figure H.3 Geometry for frictional and adiabatic flow (Fanno line).

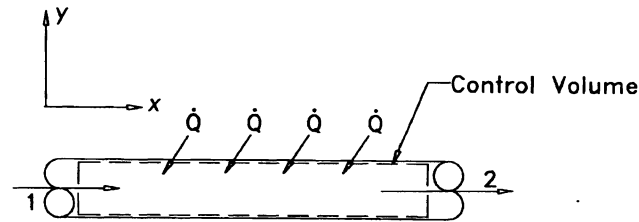


Figure H.5 Geometry for frictionless flow with heat transfer (Rayleigh line).

The flow is analyzed with a control volume approach for an ideal gas, and the first equation to be used is the momentum equation, which yields

$$p_1 A - p_2 A = V_1(-\rho_1 V_1 A) + V_2(\rho_2 V_2 A). \quad \text{H.6.1}$$

Thus, using the continuity equation (Eq. H.5.1) yields

$$p_1 - p_2 = \rho_1 V_1 (V_2 - V_1). \quad \text{H.6.2}$$

Thus, 10 independent equations are listed above (Eqs. H.6.4 through H.6.11, H.5.1 and H.6.2). Fourteen variables are in these equations. Therefore, if one specifies four variables, it is possible to solve for the remaining ten. Typically, M_1 , p_{t1} , T_{t1} , and T_{t2} are known. Note that the energy equation was not used, although if T_{t1} and T_{t2} are known the energy equation gives the total heat addition to the flow.

These equations generate the h - s diagram. For subsonic flow, as heat is added to the flow (the total temperature T_t increases) the exit Mach number increases. For supersonic flow, however, as heat is added, the Mach number decreases. One interesting phenomenon occurs as heat is added for the subsonic case. The static temperature T increases until the Mach number reaches $1/\sqrt{\gamma}$, at which point the temperature decreases. As noted above, the energy equation was not utilized. However, for the case of a burner, it can be used (and usually is) to relate the change in total temperature to fuel flow rate.

To aid in the solution of these equations, many gas dynamics and fluid mechanics texts present tables of T/T^* , p_t/p_t^* , and other variables versus Mach number, where * indicates reference conditions at the sonic point. Such tables are presented in this text in Appendix D. Solutions can also be obtained using the software, "RAYLEIGH".

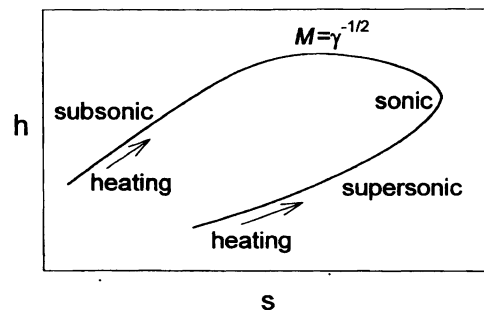


Figure H.6 h - s diagram for Rayleigh line flow.

$$\frac{p_2}{p_1} = \frac{2\gamma}{\gamma + 1} M_1^2 - \frac{\gamma - 1}{\gamma + 1} \quad \text{H.7.3}$$

$$\frac{p_{t2}}{p_{t1}} = \frac{\left[\frac{\frac{\gamma+1}{2} M_1^2}{1 + \frac{\gamma-1}{2} M_1^2} \right]^{\frac{\gamma}{\gamma-1}}}{\left[\frac{2\gamma}{\gamma-1} M_1^2 - \frac{\gamma-1}{\gamma+1} \right]^{\frac{1}{\gamma-1}}} \quad \text{H.7.4}$$

$$T_2 = T_1 \quad \text{H.7.5}$$

$$\frac{T_2}{T_1} = \frac{1 + \frac{\gamma-1}{2} M_1^2}{1 + \frac{\gamma-1}{2} M_2^2} \quad \text{H.7.6}$$

H.8. Oblique Planar Shocks

As discussed in Chapter 4, oblique shocks incur lower losses in total pressure than do normal shocks. In this section, planar two-dimensional shocks are analyzed. Although the flow is truly two-dimensional, it has many characteristics of one-dimensional flow. Flow before the shock is uniformly parallel to the axis, and behind the planar shock, flow is *uniformly* parallel to the wedge.

Figure H.9 shows an oblique shock. A wedge with an angle of δ forms the shock. A control volume is drawn around the shock as shown. Also, the velocity vectors are broken down into components normal to, and parallel to, the shock, as shown. First from continuity,

$$\rho_1 u_{n1} = \rho_2 u_{n2}. \quad \text{H.8.1}$$

Next, from the momentum equation parallel to the shock,

$$(\rho_1 u_{n1}) u_{t1} = (\rho_2 u_{n2}) u_{t2}. \quad \text{H.8.2}$$

Thus, from Eq. H.8.1, very simply,

$$u_{t1} = u_{t2}. \quad \text{H.8.3}$$

Next, from the momentum equation normal to the shock,

$$p_1 - p_2 = \rho_2 u_{n2}^2 - \rho_1 u_{n1}^2, \quad \text{H.8.4}$$

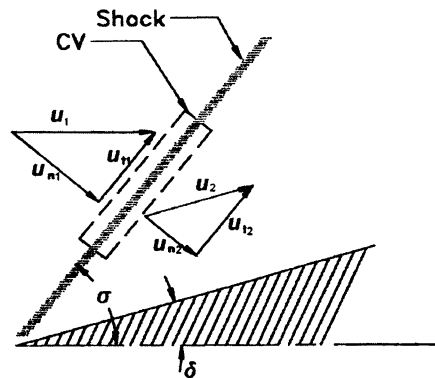


Figure H.9 Oblique shock with control volume.

$$u_{t2} = u_2 \cos(\sigma - \delta) \quad \text{H.8.18}$$

$$u_{n2} = u_2 \sin(\sigma - \delta), \quad \text{H.8.19}$$

where σ is the shock angle relative to the incoming flow and δ is the flow turning angle relative to the incoming flow. Next, from Eqs. H.8.3, H.8.16, and H.8.18, one finds

$$\frac{u_1}{u_2} = \frac{\cos(\sigma - \delta)}{\cos \sigma}, \quad \text{H.8.20}$$

and with Eqs. H.8.1, H.8.17, and H.8.19,

$$\rho_1 u_1 \sin \sigma = \rho_2 u_2 \sin(\sigma - \delta). \quad \text{H.8.21}$$

Thus,

$$\frac{\rho_2}{\rho_1} = \frac{u_1 \sin \sigma}{u_2 \sin(\sigma - \delta)}, \quad \text{H.8.22}$$

and using Eq. H.8.20, one sees that

$$\frac{\rho_2}{\rho_1} = \frac{\tan \sigma}{\tan(\sigma - \delta)}. \quad \text{H.8.23}$$

Next, using Eqs. H.8.10 and H.8.17, one obtains

$$p_2 - p_1 = \rho_1 u_1^2 \sin^2 \sigma \left[1 - \frac{\rho_1}{\rho_2} \right]. \quad \text{H.8.24}$$

Now, since for an ideal gas $M = \frac{u}{a} = \frac{u}{\sqrt{\frac{\gamma p}{\rho}}}$, one finds

$$\frac{p_2}{p_1} = 1 + \gamma M_1^2 \sin^2 \sigma \left[1 - \frac{\rho_1}{\rho_2} \right]. \quad \text{H.8.25}$$

Similarly, using Eqs. H.8.11 and H.8.17,

$$\frac{p_1}{p_2} = 1 + \gamma M_2^2 \sin^2(\sigma - \delta) \left[1 - \frac{\rho_2}{\rho_1} \right], \quad \text{H.8.26}$$

and, finally, using Eq. H.2.12 yields

$$\frac{p_{t2}}{p_{t1}} = \frac{p_2}{p_1} \left[\frac{1 + \frac{\gamma-1}{2} M_2^2}{1 + \frac{\gamma-1}{2} M_1^2} \right]^{\frac{\gamma}{\gamma-1}}. \quad \text{H.8.27}$$

Thus, if one considers Eqs. H.8.14, H.8.23, H.8.25, H.8.26, and H.8.27, there are seven independent variables: σ , δ , M_1 , M_2 , p_2/p_1 , p_{t2}/p_{t1} , and ρ_2/ρ_1 . Therefore, if two are specified, the remaining five can be determined. For example, for a given incoming Mach number (M_1) and a given turning angle (δ), one can find the shock angle, exit Mach number, total pressure ratio, and all of the other variables. These equations can easily be programmed in a commercial math solver. A set of figures are presented herein for $\gamma = 1.40$ to aid in the theoretical solution and are presented in Figure 4.6. Solutions can also be obtained using the software, "SHOCK".

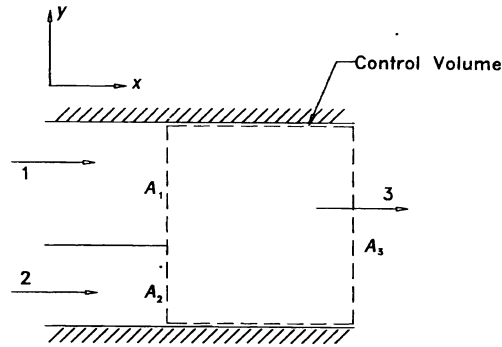


Figure H.11 Geometry for mixing process.

Next, from the adiabatic energy equation between the stagnation and static states (t_2 and 2) at station 2, the gas velocity is

$$V_2 = \sqrt{2 c_p (T_{t2} - T_2)}. \quad \text{H.9.7}$$

Therefore, from Eqs. H.9.6, H.9.7 and H.4.1 and realizing that $T_{t2} = T_{t1}$ (the process is adiabatic), one obtains

$$p_1 + \rho_1 V_1^2 - \frac{1}{2} C_d \rho_1 V_1^2 \frac{A_d}{A} = \rho_1 V_1 \left[\frac{\mathcal{R} T_2}{\sqrt{2 c_p (T_{t1} - T_2)}} + \sqrt{2 c_p (T_{t1} - T_2)} \right]. \quad \text{H.9.8}$$

Thus, if the inlet conditions are known, the preceding equation can be used to solve for T_2 iteratively, after which all other exit conditions can be found. Solutions can also be obtained using the software, "GENERAL1D".

H.10. Mixing Process

Another process that results in total pressure losses is the highly irreversible mixing process. For this occurrence, two streams (for example, one from the bypass duct and one from the turbine exit) at different temperatures, total temperatures, Mach numbers, flow rates, velocities, total pressures, and so on are irreversibly mixed to form one (it is hoped) uniform stream. A diagram of this is shown in Figure H.11, which includes the control volume. Two streams enter with properties 1 and 2, and one uniform stream leaves with all properties at 3 (for example p_3 , T_3 , V_3 , M_3 , etc.). One must be able to find the exiting conditions based on the two inlet conditions. For this process the continuity, momentum, and energy equations are once again used.

First of all, one can consider the areas at the inlet and exit:

$$A_1 + A_2 = A_3. \quad \text{H.10.1}$$

Next, the mass flows are given by

$$\dot{m}_1 = \rho_1 V_1 A_1 \quad \text{H.10.2}$$

$$\dot{m}_2 = \rho_2 V_2 A_2 \quad \text{H.10.3}$$

$$\dot{m}_3 = \rho_3 V_3 A_3; \quad \text{H.10.4}$$

thus, from continuity,

$$\rho_3 V_3 A_3 = \rho_1 V_1 A_1 + \rho_2 V_2 A_2. \quad \text{H.10.5}$$

To aid in the solution, one can use Eqs. H.10.8 and H.10.12 to show that

$$(p_1 + \rho_1 V_1^2) A_1 + (p_2 + \rho_2 V_2^2) A_2 = \rho_3 \mathcal{R} T_3 A_3 \frac{V_3}{V_3} + \dot{m}_3 V_3, \quad \text{H.10.22}$$

or using Eq. H.10.4 results in

$$(p_1 + \rho_1 V_1^2) A_1 + (p_2 + \rho_2 V_2^2) A_2 = \frac{\dot{m}_3 \mathcal{R} T_3}{V_3} + \dot{m}_3 V_3. \quad \text{H.10.23}$$

Using the adiabatic energy equation again between states t3 and 3 to find the gas velocity at station 3 results in

$$V_3 = \sqrt{2 c_p (T_{t3} - T_3)}; \quad \text{H.10.24}$$

thus, from Eqs. H.10.23 and H.10.24, one finds:

$$\begin{aligned} & (p_1 + \rho_1 V_1^2) A_1 + (p_2 + \rho_2 V_2^2) A_2 \\ &= \dot{m}_3 \left[\frac{\mathcal{R} T_3}{\sqrt{2 c_p (T_{t3} - T_3)}} + \sqrt{2 c_p (T_{t3} - T_3)} \right]. \end{aligned} \quad \text{H.10.25}$$

Therefore, examining Eq. H.10.25, one can see that the left-hand side is usually known. Also, T_{t3} and \dot{m}_3 can easily be found from Eqs. H.10.9 and H.10.5, respectively, and thus the only remaining unknown in Eq. H.10.25 is T_3 , which can be found iteratively. Solutions can also be obtained using the software, "GENERAL1D".

H.11. Generalized One-Dimensional Compressible Flow

In the preceding sections, area changes, friction, heat addition, and drag were treated separately. However, for example, in an engine component several effects can occur simultaneously. Thus, in this section an analysis is introduced that includes several effects. The technique used is the so-called generalized one-dimensional flow method derived in many gas dynamics texts such as Shapiro (1953). It is a differential equation analysis from which influence coefficients are derived. These coefficients relate changes of one variable on another. In this book, the general method will not be derived.

Figure H.12 illustrates the generalized geometry. Included in the differential analysis are area changes, changes in total temperature by heat addition, friction, and drag objects. Shapiro (1953) also includes gas mass addition for which the gas is injected into the

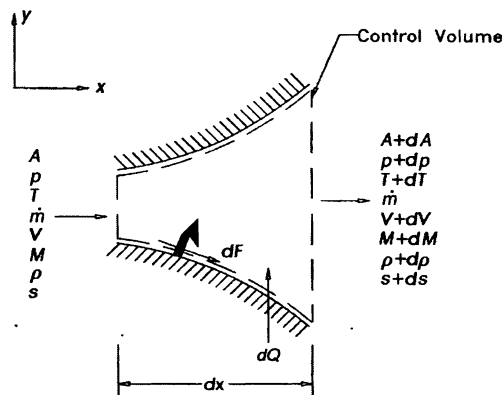


Figure H.12 Geometry for generalized one-dimensional compressible flow.

The two most important equations for the present applications are those for the Mach number and total pressure (other property changes can easily and similarly be found from Table H.2), and these can be found from Table H.2. That is,

$$\frac{dM^2}{M^2} = -2 \left[\frac{\left(1 + \frac{\gamma-1}{2} M^2\right)}{1 - M^2} \right] \frac{dA}{A} + 4f\gamma M^2 \left[\frac{\left(1 + \frac{\gamma-1}{2} M^2\right)}{1 - M^2} \right] \frac{dx}{D} \quad \text{H.12.1}$$

$$\frac{dp_t}{p_t} = -\frac{1}{2} 4f\gamma M^2 \frac{dx}{D} \quad \text{H.12.2}$$

Note that the area variation does not directly affect the total pressure. The area change does indirectly affect the total pressure variation, however, since the Mach number changes due to area variations and the Mach number affects the total pressure loss. In general, the two equations above cannot be analytically integrated but can be numerically integrated between two end states to obtain the drop in total pressure due to both friction and area change (and resulting diameter change). That is, between any two states 1 and 2,

$$M_2^2 - M_1^2 = -2 \int_{A_1}^{A_2} M^2 \left[\frac{\left(1 + \frac{\gamma-1}{2} M^2\right)}{1 - M^2} \right] \frac{dA}{A} + 4f\gamma \int_0^L M^4 \left[\frac{\left(1 + \frac{\gamma-1}{2} M^2\right)}{1 - M^2} \right] \frac{dx}{D} \quad \text{H.12.3}$$

$$p_{t2} - p_{t1} = -2f\gamma \int_0^L p_t M^2 \frac{dx}{D}. \quad \text{H.12.4}$$

To integrate Eq. H.12.4 numerically one must also evaluate Eq. H.12.3 to obtain the Mach number variation and incorporate the diameter change. Note that, if $A_2 = A_1$, the method reverts to Fanno line flow. On the other hand, if $f = 0$, the method reverts to isentropic flow with area changes. Thus, these two known solutions can provide a valuable check on the general method. Details of the numerical integration technique are presented in Example 4.3 in Chapter 4. Solutions can also be obtained using the software, "GENERAL1D".

H.13. Combined Heat Addition and Friction

Sections H.6 and H.5 treat heat addition and friction separately. However, for example, in a burner the two effects occur simultaneously. Thus, in this section the analysis includes both. The generalized one-dimensional compressible flow technique is used again. Results of the method are used in this section to determine the governing differential equations for flows with combined heat addition and friction.

Again, the two most important equations for the present application are those for the Mach number and total pressure, and these can be found from Table H.2. That is,

$$\frac{dM^2}{M^2} = (1 + \gamma M^2) \left[\frac{1 + \frac{\gamma-1}{2} M^2}{1 - M^2} \right] \frac{dT_t}{T_t} + 4f\gamma M^2 \left[\frac{1 + \frac{\gamma-1}{2} M^2}{1 - M^2} \right] \frac{dx}{D} \quad \text{H.13.1}$$

$$\frac{dp_t}{p_t} = -\frac{\gamma M^2}{2} \frac{dT_t}{T_t} - \frac{1}{2} 4f\gamma M^2 \frac{dx}{D}. \quad \text{H.13.2}$$

possible). That is, between any two states 1 and 2,

$$\begin{aligned}
 M_2^2 - M_1^2 = & -2 \int_{A_1}^{A_2} M^2 \left[\frac{1 + \frac{\gamma-1}{2} M^2}{1 - M^2} \right] \frac{dA}{A} \\
 & + \int_{T_{t1}}^{T_{t2}} (1 + \gamma M^2) M^2 \left[\frac{1 + \frac{\gamma-1}{2} M^2}{1 - M^2} \right] \frac{dT_t}{T_t} \\
 & + 4f\gamma \int_0^L M^4 \left[\frac{1 + \frac{\gamma-1}{2} M^2}{1 - M^2} \right] \frac{dx}{D}
 \end{aligned} \tag{H.14.3}$$

$$p_{t2} - p_{t1} = -\frac{1}{2}\gamma \int_{T_{t1}}^{T_{t2}} p_t M^2 \frac{dT_t}{T_t} - 2f\gamma \int_0^L p_t M^2 \frac{dx}{D}. \tag{H.14.4}$$

To integrate Eq. H.14.4 numerically one must also evaluate Eq. H.14.3 to obtain the Mach number variation. Solutions can also be obtained using the software, "GENERAL1D".

List of Symbols

a	Sound speed
A	Area
C	Drag coefficient
c_p	Specific heat at constant pressure
D	Diameter
f	Fanning friction factor
F	Drag force
h	Specific enthalpy
L	Axial length
M	Mach number
\dot{m}	Mass flow rate
p	Pressure
\dot{Q}	Heat transfer rate
\mathcal{R}	Ideal gas constant
s	Entropy
T	Temperature
U	Velocity
V	Velocity
x	Axial position
y	Velocity ratio
δ	Turning angle
γ	Specific heat ratio
ρ	Density
μ	Viscosity
σ	Shock angle

Turbomachinery Fundamentals

I.1. Introduction

This book discusses six basic types of turbomachines directly: axial flow compressors, axial flow pumps, radial flow compressors, centrifugal pumps, axial flow gas turbines, and axial flow hydraulic turbines. Two other basic types are used in practice that are not covered in this text because of their limited application in propulsion: radial inflow gas turbines and radial inflow hydraulic turbines. The basic derivations of the equations for each machine type are covered in this appendix rather than in the chapters in which the machines are discussed. As will be shown, the resulting fundamental equations apply to all types of turbomachines, regardless of categorization. Application of the equations with complementing velocity polygons is, however, different for the different turbomachines. Advanced details can be found in texts, including Balje (1981), Cohen et al. (1996), Dixon (1998, 1975), Hah (1997), Hill and Peterson (1992), Howell (1945a, 1945b), Japikse and Baines (1994), Logan (1993), Osborn (1977), Shepherd (1956), Stodola (1927), Turton (1984), Vavra (1974), Wallis (1983), Whittle (1981), and Wilson (1984). Furthermore, Rhie et al. (1998), LeJambre et al. (1998), Adamczyk (2000), and Elmendorf et al. (1998) show how modern computational fluid dynamic (CFD) tools can effectively be used for the complex three-dimensional analysis and design of turbomachines.

I.2. Single-Stage Energy Analysis

In this section, the equations are derived so that the internal fluid velocities can be related to the pressure change, power, and other important turbomachine characteristics. This is done for a general single-stage (rotor and stator for an axial machine or impeller and diffuser for a centrifugal machine). A control volume approach is used for the derivation. In Figure I.1, a single stage is shown for an axial flow turbomachine, whereas Figure I.2 shows a single stage for a radial flow turbomachine. Regardless of the type of machine, two different oblique cylindrical control volumes are drawn around the rotating element (rotor or impeller) in this stage – one stationary and one rotating. For the case of an axial flow machine, a second stationary control volume is drawn around the stator. All control volumes cut through the case and rotor shaft as shown. The objective is to relate the inlet and exit conditions to the property changes. As is shown in the following sections, the same control volume analysis applies to axial flow compressors, centrifugal compressors, and axial flow turbines. The same basic equations result from the analysis; however, the application of the equations for the three different machines is somewhat different.

I.2.1. Total Pressure Ratio

The three basic equations to be used are the continuity, moment of momentum, and energy equations. The first to be discussed is the general continuity equation applied to a control volume:

for a control volume is

$$\begin{aligned} \dot{Q} + \dot{W}_{\text{sh}} + \dot{W}_{\text{loss}} &= \frac{\partial}{\partial t} \iiint_{\text{CV}} \left[(u + V^2/2 + gz) \right] \rho d\mathcal{V} \\ &+ \iint_{\text{CS}} \left[(u + pv + V^2/2 + gz) \right] \rho \mathbf{V} \cdot d\mathbf{A}. \end{aligned} \quad \text{I.2.3}$$

where \dot{Q} is the heat transfer rate, \dot{W}_{sh} is an applied or derived shaft power to or from the control volume, \dot{W}_{loss} is a power loss within the control volume, v is the specific volume, and u is the specific internal energy.

One must now make a few realistic assumptions so that these equations become manageable. First, the flow is assumed to be steady. Second, the control volumes are assumed to be free of any body forces (which will affect the potential energy) as well as surface forces. The control volumes are assumed to be adiabatic. Next, the power loss term is assumed to be negligible, although losses will eventually be included in the form of an efficiency. The flow in and out of the control volumes is assumed to be uniform as well. The flow is also assumed to be planar two-dimensional, and a “mean line” or “meridional” analysis is used. That is, for an axial machine and for the inlet of a centrifugal machine a point located midway between the hub and tip will be used to evaluate the radii, fluid properties and velocities. Also, in the case of an axial machine this implies that no radial component of velocity will be present. For the case of a radial flow machine, this implies that no radial component of velocity will be present in the inlet plane and that no axial component of velocity will be present in the exit plane. Lastly, the gas is assumed to be ideal. Although the assumptions may look restrictive, the analysis yields very realistic results for many applications. The list of assumptions is as follows:

- | | |
|-----------------------|---------------------------------|
| (1) Steady | (5) No power losses |
| (2) No body forces | (6) Uniform flow |
| (3) No surface forces | (7) Planar two-dimensional flow |
| (4) Adiabatic | (8) Ideal gas |

Thus, by assumption (1), Eq. I.2.1 becomes

$$0 = \iint_{\text{CS}} \rho \mathbf{V} \cdot d\mathbf{A}. \quad \text{I.2.4}$$

By the use of assumptions (1), (2), and (3), Eq. I.2.2 becomes

$$\mathbf{T}_{\text{sh}} = \iint_{\text{CS}} (\mathbf{r} \times \mathbf{V}) \rho \mathbf{V} \cdot d\mathbf{A}. \quad \text{I.2.5}$$

Next, by the use of assumptions (1), (2), (4), and (5), Eq. I.2.3 reduces to

$$\dot{W}_{\text{sh}} = \iint_{\text{CS}} \left[(u + pv + V^2/2) \right] \rho \mathbf{V} \cdot d\mathbf{A}. \quad \text{I.2.6}$$

Now, by applying Eq. I.2.4 with assumptions (6) and (7) to the stationary control volume around the rotor or impeller, one quickly finds that

$$\rho_1 c_{a1} A_1 = \rho_2 c_{e2} A_2, \quad \text{I.2.7}$$

Again, if the application is a turbine, the power will be negative, indicating that power is derived from the fluid. Equation I.2.6 can be used for the stationary rotor or impeller control volume with assumptions (6) and (7) to yield

$$\dot{W}_{\text{sh}} = \dot{m}_2 (u_2 + p_2 v_2 + 1/2 c_2^2) - \dot{m}_1 (u_1 + p_1 v_1 + 1/2 c_1^2), \quad \text{I.2.18}$$

where c is the absolute velocity. The enthalpy can be related to the internal energy by

$$h = u + pv \quad \text{I.2.19}$$

Thus, by using Eqs. I.2.8, I.2.18, and I.2.19, one obtains

$$\dot{W}_{\text{sh}} = \dot{m} (h_2 + 1/2 c_2^2 - h_1 - 1/2 c_1^2). \quad \text{I.2.20}$$

Remembering the definition of total enthalpy from Eq. H.2.5, however, one finds

$$\dot{W}_{\text{sh}} = \dot{m}(h_{t2} - h_{t1}). \quad \text{I.2.21}$$

Thus, the transferred power is equal to the change in total enthalpy. In the case of a compressor, the power delivered to the rotor stage by the shaft is equal to the increase in the total enthalpy. For a turbine, the power removed from the rotor stage by the shaft is equal to the decrease in the total enthalpy. Up to this point in the derivation, the nonideal power loss has been neglected. Using a definition of efficiency similar to that applied to an entire turbomachine, one finds that

$$\dot{W}_{\text{sh}} = \mathcal{E} \dot{m}(h'_{t2} - h_{t1}), \quad \text{I.2.22}$$

where h'_{t2} is the ideal total enthalpy at station 2 (for the same total pressure increase as in the nonideal case). Also, for a compressor, \mathcal{E} is equal to $1/\eta_{12}$, and for a turbine \mathcal{E} is equal to η_{12} (η_{12} is the aerodynamic efficiency of the rotor or impeller). Note that the ideal work or power is less than actually encountered for a compressor but larger than for the actual case of a turbine. For an ideal gas (assumption [8]), Eq. I.2.22 becomes

$$\dot{W}_{\text{sh}} = \mathcal{E} \dot{m} c_p T_{t1} \left[\frac{T'_{t2}}{T_{t1}} - 1 \right]. \quad \text{I.2.23}$$

For isentropic flow, one can use Eq. H.2.11 to find

$$\dot{W}_{\text{sh}} = \mathcal{E} \dot{m} c_p T_{t1} \left[\left[\frac{p_{t2}}{p_{t1}} \right]^{\frac{\gamma-1}{\gamma}} - 1 \right]. \quad \text{I.2.24}$$

Next, one can solve for p_{t2}/p_{t1} and find

$$\frac{p_{t2}}{p_{t1}} = \left[\frac{\dot{W}_{\text{sh}}}{\mathcal{E} c_p T_{t1} \dot{m}} + 1 \right]^{\frac{\gamma}{\gamma-1}}. \quad \text{I.2.25}$$

Using the results from the moment of momentum equation (Eq. I.2.17), one obtains

$$\frac{p_{t2}}{p_{t1}} = \left[\frac{U_2 c_{u2} - U_1 c_{u1}}{\mathcal{E} c_p T_{t1}} + 1 \right]^{\frac{\gamma}{\gamma-1}}, \quad \text{I.2.26}$$

which is greater than unity for the case of a compressor but less than unity for the case of a turbine. Thus, knowing the velocity information of a rotor and the efficiency, one can find the total pressure ratio. As a reminder, because of a subtle difference, for the case of a compressor, \mathcal{E} is equal to $1/\eta_{12}$, and for a turbine \mathcal{E} is equal to η_{12} . Note that Eq. I.2.26 applies to axial or radial flow machines. However, the application of the equation will be

Equation (I.2.17) also applies. That is,

$$\dot{W}_{sh} = \dot{m}[U_2 c_{u2} - U_1 c_{u1}]. \quad \text{I.2.34}$$

Next, Eq. I.2.30 can be compared with the Bernoulli equation ($pv + w^2/2 = \text{constant}$). One can see that they are similar except for the $\Delta u = u_2 - u_1$ term. Thus, for reversible flow, u_2 is equal to u_1 . As a result, for ideal flow,

$$p_2 - p_1 = \frac{\rho}{2} [w_1^2 - w_2^2]. \quad \text{I.2.35}$$

For incompressible flow, however, the total pressure is

$$p_t = p + 1/2 \rho c^2. \quad \text{I.2.36}$$

Therefore, using Eqs. I.2.33, I.2.34, and I.2.36, one finds

$$p_{t2} - p_{t1} = \frac{\rho}{\mathcal{E}_c} [U_2 c_{u2} - U_1 c_{u1}], \quad \text{I.2.37}$$

where the efficiency parameter ($\mathcal{E}_c = 1/\eta_{12}$ and $\mathcal{E}_t = \eta_{12}$) accounts for nonideal effects. Also, using Eqs. I.2.35 and I.2.36 one finds

$$p_{t2} - p_{t1} = \frac{\rho}{2} (w_1^2 - w_2^2 + c_2^2 - c_1^2). \quad \text{I.2.38}$$

For comparison, it may be desirable to find percent reaction of an axial flow turbomachine with an incompressible fluid. Once again, the percent reaction is given by Eq. I.2.27, which again becomes

$$\%R = \frac{1}{1 + \left[\frac{c_2^2 - c_1^2}{w_1^2 - w_2^2} \right]}. \quad \text{I.2.39}$$

One can compare this equation with that for compressible flow and see that they are identical. Also, using Eqs. I.2.18 and I.2.28, one finds for an incompressible fluid that

$$\%R = \frac{u_2 + \frac{p_2}{\rho} - u_1 - \frac{p_1}{\rho}}{u_{t3} + \frac{p_{t3}}{\rho} - u_{t1} - \frac{p_{t1}}{\rho}}. \quad \text{I.2.40}$$

Ideally, u_2 and u_1 are identical, as shown above, and likewise the total internal energies u_{t3} and u_{t1} , are the same. Thus, the percent reaction for incompressible and ideal flow reduces to

$$\%R = \frac{p_2 - p_1}{p_{t3} - p_{t1}}. \quad \text{I.2.41}$$

For example, ideal axial flow turbomachine stages have percent reactions of about 0.45 to 0.55. For a nonideal pump or hydraulic turbine, the percent reaction indicates that approximately half of the enthalpy change occurs in the rotor and half in the stator. For an ideal pump or hydraulic turbine this also means that half of the pressure change occurs in the rotor and half in the stator. This implies that the force “loads” on the rotor and stator blades are about the same. For a compressor, if the pressure rises across the rotor blades and stator vanes are equal, the percent reaction tends to be somewhat higher owing to the compressibility of the flow and radial variations. For a compressible flow turbine, radial variations also influence the design reaction. For a compressor, if a large pressure rise in either the rotor blades or stator vanes occurs, separation or partial separation of the cascade is likely. As a result of the associated losses, the efficiency will be less than optimum. On the other hand, for a turbine, if a large pressure drop occurs

and

$$N_{ci} = \frac{N}{\sqrt{\theta_{ti}}}, \quad \text{I.3.8}$$

Note that these two independent parameters are not truly dimensionless. The first is called the “corrected” mass flow and has dimensions of mass flow, whereas the second is called the “corrected” speed and has dimensions of rotational speed. As a result,

$$p_{te}/p_{ti} = \mathcal{f}\{\dot{m}_{ci}, N_{ci}\} \quad \text{I.3.9}$$

and

$$\eta = \mathcal{g}\{\dot{m}_{ci}, N_{ci}\}. \quad \text{I.3.10}$$

The functions \mathcal{f} and \mathcal{g} can be determined from modeling, experimental data, or a combination of empiricism and modeling. The corrected mass and corrected speed are also often referred to as a percent of the design conditions. For example 100 percent speed and 100 percent mass flow would be the design condition or point of maximum efficiency. These equations can be in the form of analytical equations, curve fits, tables, or graphs.

Thus, since the two parameters are not dimensionless, the resulting functions cannot be used to correlate or compare different compressible turbomachines. One can use the functions for one particular turbomachine, however, as is the usual case. The functions \mathcal{f} and \mathcal{g} retain most of the nondimensional characteristics. Therefore, raw data can be obtained under one set of conditions (for example, at STP) but applied over a wider range of conditions if “corrected” parameters are used. That is, the map is applicable regardless of altitude, speed, atmospheric conditions, and so on. Thus, obtaining raw data is not necessary for all possible conditions.

List of Symbols

A	Area
c	Absolute velocity
c_p	Specific heat at constant pressure
ε	Efficiency parameter
g	Gravitational constant
h	Specific enthalpy
\dot{m}	Mass flow rate
N	Rotational speed
p	Pressure
\dot{Q}	Heat transfer rate
\mathcal{R}	Ideal gas constant
r, R	Radius
$\%R$	Percent reaction
T	Temperature
T	Torque
U	Blade velocity
u	Specific internal energy
v	Specific volume
V	Velocity
w	Relative velocity
\dot{W}	Power

References

- Abbott, I. H., and von Doenhoff, A. E. (1959). *Theory of Wing Sections*, Dover Publications, New York, NY.
- Adamczyk, J. J. (2000). Aerodynamic analysis of multistage turbomachinery flows in support of aerodynamic design. *ASME Transactions, Journal of Turbomachinery*. **122** (2), 189–217.
- Adler, D. (1980). Status of centrifugal impeller internal dynamics, parts I and II. *Transactions ASME, Journal of Engineering for Power*. **102** (3), 728–746.
- Ainley, D. G., and Mathieson, G. C. R. (1951). A method of performance estimation for axial flow turbines. *Aeronautical Research Council, R&M No. 2974*.
- Anderson, J. D. (1982). *Modern Compressible Flow with Historical Perspective*. McGraw-Hill, New York.
- Ashley, S. (1997). Turbines on a Dime. *Mechanical Engineering*. **119** (10), 78–81.
- ASME International History and Heritage (1997). *Landmarks in Mechanical Engineering*. Purdue University Press, West Lafayette, IN.
- Aungier, R. H. (2000). *Centrifugal Compressors – A Strategy for Aerodynamic Design and Analysis*. ASME Press, New York, NY.
- Bacha, J., Barnes, F., Franklin, M., Gibbs, L., Hemighaus, G., Hogue, N., Lesnini, D., Lind, J., Maybury, J., and Morris, J. (2000). *Aviation Fuels Technical Review*. Chevron Products Company, FTR-3.
- Balje, O. E. (1981). *Turbomachines*. Wiley, New York, NY.
- Billington, D. P. (1996). *The Innovators*. Wiley, New York, NY.
- Boyce, M. P. (1982). *Gas Turbine Engineering Handbook*. Gulf Publishing Co., Houston, TX.
- Brennen, C. E. (1994). *Hydrodynamics of Pumps*. Concepts ETI & Oxford, Norwich, VT.
- Busemann, A. (1928). Das Förderhöhenverhältnis radialer Kreiselpumpen mit logarithmischspiraligen Schaufeln. *Zeitschrift für Angewandte Mathematik und Mechanik*. **8**, 372–384.
- Caruthers, J. E., and Kurosaka, M. (1982). *Flow Induced Vibration of Diffuser Excited Radial Compressors*. NASA NAG No. 3–86.
- Chase, M. W. (1998), NIST-JANAF Thermochemical Tables, 4th Edition, *Journal of Physical and Chemical Reference Data Monographs & Supplements, Monograph No. 9*, AIP Press, New York, NY.
- Cohen, H., Rogers, G. F. C., and Saravanamuttoo, H. I. H. (1996). *Gas Turbine Theory*, 4th ed. Longman Group, Essex, UK.
- Cumpsty, N. (1997). *Jet Propulsion*. Cambridge, Cambridge, UK.
- Cumpsty, N. A. (1977). Critical review of turbomachinery noise. *Transactions of ASME, Journal of Fluids Engineering*. **99**(2), 278–293.
- Cumpsty, N. A. (1988). *Compressor Aerodynamics*. Longman Group, Essex, UK.
- Department of the U.S. Navy (1953). *Handbook of Supersonic Aerodynamics*, Vol. 5. Bureau of Ordnance, Washington, DC.
- Dixon, S. L. (1975). *Worked Examples in Turbomachinery*. Pergamon Press, Oxford, UK.
- Dixon, S. L. (1998). *Fluid Mechanics and Thermodynamics of Turbomachinery*, 4th ed. Butterworths, Boston, MA.
- Dring, R. P., Joslyn, H. D., Hardin, L. W., and Wagner, J. H. (1982). Turbine rotor-stator interaction. 27th ASME International Gas Turbine Exposition. *ASME Paper No. 82-GT-3*.
- Dunham, J. (2000). A. R. Howell – Father of the British axial compressor. ASME TURBOEXPO 2000, May 8–11, Munich, Germany. *ASME Paper No. 2000-GT-8*.
- Dunn, M. G. (2001). Convective heat transfer and aerodynamics in axial flow turbines. ASME TURBO EXPO 2001, New Orleans, LA. *ASME Paper No. 2001-GT-0506*.
- Eckardt, D. (1975). Instantaneous measurements in the jet-wake discharge flow of a centrifugal compressor impeller. *ASME Transactions, Journal of Engineering for Power*. **91** (3), 337–345.

- Kercher, D. M. (1998). A film cooling CFD bibliography: 1971–1996. *International Journal of Rotating Machinery*. **4** (1), 61–72.
- Kercher, D. M. (2000). Turbine airfoil leading edge film cooling bibliography: 1972–1998. *International Journal of Rotating Machinery*. **6** (5), 313–319.
- Kerrebrock, J. L. (1992). *Aircraft Engines and Gas Turbines*, 2d ed. MIT Press, Cambridge, MA.
- Kurzke, J. (1995). Advanced user-friendly gas turbine performance calculations on a personal computer. ASME TURBOEXPO 1995, June 5–8, Houston, TX. *ASME Paper No. 95-GT-147*.
- Kurzke, J. (1996). How to get component maps for aircraft gas turbine performance calculations. ASME TURBOEXPO 1996, June 10–13, Birmingham, UK. *ASME Paper No. 96-GT-164*.
- Kurzke, J. (1998). Gas turbine cycle design methodology: A comparison of parameter variation with numerical optimization. ASME TURBOEXPO 1998, June 2–5, Stockholm, Sweden. *ASME Paper No. 98-GT-343*.
- Lefebvre, A. H. (1983). *Gas Turbine Combustion*. Hemisphere Publishing, New York, NY.
- LeJambre, C. R., Zacharias, R. M., Biederman, B. P., Gleixner, A. J., and Yetka, C. J. (1998). Development and application of a multistage Navier–Stokes solver: Part II – Application to a high-pressure compressor design. *ASME Transactions, Journal of Turbomachinery*. **120** (2), 215–223.
- Liepmann, H. W., and Roshko, A. (1957). *Elements of Gas Dynamics*. Wiley, New York, NY.
- Lloyd, P. (1945). Combustion in the gas turbine. *Proceedings of the Institution of Mechanical Engineers*. **153** (12), 462–472.
- Logan, E. (1993). *Turbomachinery – Basic Theory and Applications*, 2d ed. Marcel Dekker, New York, NY.
- Maccoll, J. W. (1937). The conical shock wave formed by a cone moving at high speed. *Proceedings of the Royal Society of London, Series A*. **159**, 459–472.
- Malecki, R. E., Rhie, C. M., McKinney, R. G., Ouyang, H., Syed, S. A., Colket, M. B., and Madabhushi, R. K. (2001). Application of an advanced cfd-based analysis system to the pw6000 combustor to optimize exit temperature distribution – Part I: Description and validation of the analysis tool. TURBO EXPO 2001, New Orleans, LA. *ASME Paper No. 2001-GT-0062*.
- Mattingly, J. D. (1996). *Elements of Gas Turbine Propulsion*. McGraw-Hill, New York, NY.
- Mattingly, J. D., Heiser, W. H., and Daley, D. H. (1987). *Aircraft Engine Design*. AIAA Education Series, Reston, VA.
- Meher-Homji, C. B. (1996). The development of the Junkers Jumo 004B – The world’s first production turbojet. ASME TURBO EXPO 1996, June 10–13, Birmingham, UK. *ASME Paper No. 96-GT-457*.
- Meher-Homji, C. B. (1997a). The development of the Whittle turbojet. ASME TURBO EXPO 1997, Orlando, Florida. *ASME Paper No. 97-GT-528*.
- Meher-Homji, C. B. (1997b). Anselm Franz and the Jumo 004. *Mechanical Engineering*. **119** (9), 88–91.
- Meher-Homji, C. B. (1999). Pioneering turbojet developments of Dr. Hans von Ohain – From the IICs 1 to the HeS 011. ASME TURBO EXPO 1999, June 7–10, Indianapolis, IN. *ASME Paper No. 99-GT-228*.
- Merzkirch, W. (1974). *Flow Visualization*. Academic Press, New York, NY.
- Miner, S. M., Beaudoin, R. J., and Flack, R. D. (1989). Laser velocimeter measurements in a centrifugal flow pump. *ASME Transactions, Journal of Turbomachinery*. **111** (3), 205–212.
- Mirza-Baig, F. S., and Saravanamuttoo, H. I. H. (1991). Off-design performance prediction of turbofans using gasdynamics. 36th ASME International Gas Turbine Exposition, 1991, June 3–6, Orlando, FL. *ASME Paper No. 91-GT-389*.
- Moody, L. F. (1944). Friction factors for pipe flow. *Transactions of the ASME*. **66** (8), 671–684.
- Oates, G. C. (1997). *Aerothermodynamics of Gas Turbine and Rocket Propulsion*, 3d ed. AIAA Education Series, Reston, VA.
- Oates, G. C. (ed.) (1985). *Aerothermodynamics of Aircraft Engine Components*. AIAA Education Series, Reston, VA.
- Oates, G. C. (ed.) (1989). *Aircraft Propulsion Systems Technology and Design*. AIAA Education Series, Reston, VA.
- Olson, W. T., Childs, J. H., and Jonash, E. R. (1955). The combustion-efficiency problem of the turbojet at high altitude. *Transactions of the ASME*. **77**, 605–615.
- Osborn, W. C. (1977). *Fans*, 2d ed. Pergamon Press, Oxford, UK.
- Peters, J. E. (1988). Current gas turbine combustion and fuels research and development. *AIAA Journal of Propulsion*. **4** (3), 193–206.

www.geae.com/
www.gepower.com/dhtml/aeroenergy/en.us/
www.pratt-whitney.com/
www.pwc.ca
www.rolls-royce.com/
www.snecma-moteurs.com/
www.V2500.com/
www.jet-engine.net

The publisher has endeavored to ensure that the URLs for external Web sites referred to in this book are correct and active at the time of going to press. However, the publisher has no responsibility for the Web sites and can make no guarantee that a site will remain live or that the content is, or will, remain appropriate.

- 3.60 $T_{15} = 1987^\circ\text{R}$, $T_{16} = 3975^\circ\text{R}$, $\eta_f = 90.0$ percent
 $M_8 = 1.00$, $TSFC = 0.865$ lbm/h-lbf
- 3.62 (a) $\eta_{th} = 0.358$, $\mathcal{P} = 26,627$ hp, 0.394 lbm/hp-h
 (b) $\eta_{th} = 0.369$, $\mathcal{P} = 29,642$ hp, 0.383 lbm/hp-h
- 4.2 (a) $\pi_d = 0.997$ (b) $\pi_d = 0.460$
- 4.6 $\pi_d = 0.977$
- 4.10 (a) $\pi_d = 0.970$, $A^*/A_1 = 0.800$
 (b) $\pi_d = 0.744$
- 4.12 (a) 4690 lbf, 2.10 lbm/h-lbf
 (c) 5617 lbf, 1.75 lbm/h-lbf
- 4.14 $\pi_d = 0.911$
- 4.16 (a) $\pi_d = 0.943$, $A^*/A_1 = 0.803$
 (b) $\pi_d = 0.6155$
- 4.18 (a) 1681 lbf, 2.16 lbm/h-lbf
 (b) 2413 lbf, 1.50 lbm/h-lbf
- 4.20 $\pi_d = 0.484$ $M = 0.513$
- 4.24 $\delta = 40.5^\circ$, $\pi_d = 0.737$
- 4.26 (a) $\delta = 23.3^\circ$, $M = 1.89$, $\pi_d = 0.932$
 (b) $\delta = 46.8^\circ$, $M = 0.74$, $\pi_d = 0.53$
- 4.28 $M = 0.668$, $p_t = 19.02$ psia, $\pi_d = 0.877$
- 4.30 $M = 1.15$, $\sigma = 55.6^\circ$, $M_{min} = 1.90$
- 4.34 $\pi_d = 0.53$, $C_p = 0.976$
- 5.4 $p_{16}/p_a = 1.185$: $M_8 = 0.498$, $\dot{m}_{c6} = 71.72$ lbm/s
 $p_{16}/p_a = 4.465$: $M_8 = 1.601$, $\dot{m}_{c6} = 71.72$ lbm/s
 $p_{16}/p_a = 1.064$: $M_8 = 0.300$, $\dot{m}_{c6} = 47.31$ lbm/s
- 5.12 (a) $p_a = 3.196$ psia (b) $p_a = 6.456$ psia
- 5.14 $M_8 = 1$, $\dot{m} = 26.71$ lbm/s
- 5.16 $\dot{m}_c = 90.2$ lbm/s
- 5.18 $\dot{m} = 79.8$ lbm/s, $\dot{m}_c = 53.0$ lbm/s
- 5.20 $p_8 = 59.3$ psia, $\eta_n = 98.2$ percent
- 5.24 $M = 1.00$, $\dot{m} = 76.7$ lbm/s, $\dot{m}_c = 65.9$ lbm/s
- 5.26 $\dot{m} = 222$ lbm/s, $\dot{m}_c = 171.4$ lbm/s, $F = 26,347$ lbf
- 5.28 (a) $\dot{m} = 261.1$ lbm/s, $\dot{m}_c = 268.3$ lbm/s, $M_8 = 0.588$
 (b) $\dot{m} = 251.6$ lbm/s, $\dot{m}_c = 268.3$ lbm/s
- 5.30 $p_8 = 53.63$ psia, $T_8 = 1277^\circ\text{R}$
- 5.32 $p_8 = 52.9$ psia, $T_8 = 1192^\circ\text{R}$, $M_6 = 0.1922$
- 5.34 $A/A = 1.111$, $M_8 = 1.339$, $\dot{m} = 70.4$ lbm/s, $\dot{m}_c = 57.6$ lbm/s
- 6.2 $\pi = 1.205$, 2390 hp
- 6.4 (a) $\pi = 1.212$ (c) (i) $\Delta = 18.2^\circ$
- 6.10 $\%R = 0.502$
- 6.14 $\alpha_2 = 61.63^\circ$, $\%R = 0.553$, $\pi = 1.540$, π too large—will surge — $C_p = 0.707$
- 6.18 $\%R = 0.122$, $\delta_{23} = -15.3^\circ$, poor—stator heavily loaded
- 6.24 $\alpha_2 = 59.20^\circ$, $\%R = 0.531$, $\pi = 1.262$
- 6.28 $\%R = 72.6$ percent, $\pi = 1.215$, $\delta_{23} = -26.7^\circ$

Index

- adiabatic processes, 46–50, 592–593
- adiabatic flame temperatures, 61, 146, 449, 453, 454, 455, 483
 - enthalpy and, 454
 - fuel ratios and, 450, 455
 - stoichiometric condition and, 450, 453, 455
 - See also specific components*
- aeroderivative, 31
- afterburners, 19, 90, 146, 166, 167–168, 440, 445, 462–463
 - chemistry and, 450
 - efficiency and, 146–147
 - enthalpy and, 451–452
 - fuel ratios and, 63
 - ideal, 61
 - ideal characteristics of, 46–47
 - ignition of, 449
 - isobaric processes in, 61
 - materials in, 447
 - objective of, 19, 445
 - pressure ratios and, 147
 - ramjets and, 446
 - screech, 447
 - stoichiometric condition and, 450
 - thermodynamics of, 451
 - thrust-*TSFC* and, 168, 445
 - turbofans and, 25, 98–102, 106–108, 112, 113
 - turbojets and, 19, 84
- airfoils, 51, 331–332, 378. *See also* propellers;
compressors; turbines
- altitude, 83, 258–259, 264
- area changes
 - friction and, 608, 610
 - heat addition and, 610
 - See also specific components*
- atmosphere, standard, 527
- blades, 141
 - angle of, 56, 58
 - attachment methods, 279
 - camber, 281
 - cascade, 277
 - chord, 281
 - cooling of, 142, 428
 - data for, 332
 - disk and, 277, 279
 - materials in, 277–279
 - resonance and, 281
 - rotor, 51, 277, 407
 - stator, 51, 277, 407
 - See also* compressors; impellers; mixers; *specific components*
- boundary layer
 - compressors and, 137
 - diffusers and, 135–136, 209
 - See also* separation
- Brayton cycle, 10
 - intercooling and, 14
 - regeneration and, 13
- Buckingham Pi theorem, 261, 461, 620
- burners, 88, 118, 145, 440
 - adiabatic flame temperature and, 61, 146
 - CFD method for, 440
 - chemistry and, 450
 - component matching and, 483
 - counter-flow, 374
 - design criteria for, 440–441
 - dimensional analysis and, 461
 - drag and, 456, 459
 - efficiency and, 145–146, 461, 462, 483
 - enthalpy and, 451–452
 - exit pressure from, 157
 - exit temperatures from, 75–76
 - Fanno line flow and, 456, 457, 461
 - flame speed, 448
 - flame holders. *See* flame holders
 - flame stability, 447
 - friction and, 456, 458
 - fuel mass-flow rate, 60, 146
 - fuel ratios and, 61, 447, 462, 483
 - fuel types, 463
 - gas velocities and, 448
 - generalized flow method, 461
 - geometries of, 441
 - heat addition and, 458
 - heating value method, 60, 146
 - ideal, 59
 - ideal characteristics of, 46–47
 - ignition, 449
 - imperfect combustion and, 145
 - materials for, 445
 - modeling of, 488
 - percent air, 450
 - performance maps for, 461
 - pressure losses and, 145, 146, 456, 483
 - pressure ratios, 146, 157, 445, 461, 462
 - primary, 59, 61–62, 145
 - Rayleigh line flow, 456, 461

- mean line control volume approach, 286
- multiple spool engines and, 280–281, 312
- operating line, 302
- percent reaction, 287, 289, 294, 342, 343
- performance, by stages, 331
- performance maps, 299
- pressure changes in, 283
- pressure coefficient, 305
- pressure ratios, 276, 277, 281, 287, 289, 299, 300–301, 302, 307
- pressure ratio limits, 306
- pressure ratios, by stages, 299
- radial equilibrium and, 316
- rotational speed and, 290, 299–301, 302
- rotor blades, 277
- separation and, 281
- single stage energy analysis, 286
- single stage performance predictions, 354
- solidity parameter, 281, 346–347
- speed, corrected, 299–302
- stator vanes, 277, 307, 312
- streamline analysis method, 320
- surge, 283, 299, 301–303, 306
- testing, 301
- thermodynamic efficiency and, 276
- trends, 300
- TSFC* and, 276
- turbines and, 406–407, 409
- variable stators, 307
- velocity polygons and, 283, 287, 289, 332
- compressors, centrifugal, 374
 - blade geometries, 377
 - blade number, 386
 - blade stresses, 392
 - cross over, 377
 - diffusers, 375–378, 394, 396
 - dimensional analysis and, 390
 - durability of, 374
 - efficiency, 374, 383, 385, 391, 392–393, 395
 - geometry of, 374
 - impellers, 378–380, 391, 392, 396–397
 - incompressible flow, 381
 - inducers and, 375
 - Mach numbers and, 396–397
 - mapping conventions for, 390
 - percent reaction and, 381, 396
 - performance maps, 390
 - pre-swirl, 375, 379, 383, 385
 - pressure ratios and, 381, 384, 386, 390–391, 395
 - resonance and, 395
 - rotors and, 380
 - scroll and, 376–377
 - separation and, 395
 - single stage energy analysis, 380
 - slip factor, 382, 385, 386, 392
 - surge and, 390, 391
 - swept blades, 377, 392
 - swirl free, 378
 - vaned diffusers, 394
 - velocity polygons and, 378, 386
- computational fluid dynamics (CFD) method, 209, 227, 231–232, 276, 320, 321, 332, 350, 440
- cycle analysis, 10
 - example problems of, 156
 - general approach of, 155
 - ideal, 46
 - non-ideal, 134
- de Laval, Carl, 5
- diffusers, 48, 135, 209, 380, 394
 - additive drag and, 227, 229, 232
 - adiabatic processes and, 209
 - area changes and, 215, 216
 - area ratios and, 210–211, 212–213, 214, 225, 226, 227–228
 - boundary layers and, 135–136, 209, 210, 214, 230
 - CFD method and, 216, 227, 231–232
 - compressors and, 135–136, 137, 209, 281–283
 - conical ramps and, 220
 - conical shocks and, 220
 - critical condition, 227
 - enthalpy and, 135, 209, 211
 - external flow patterns, 210
 - Fanno line flow and, 214, 215, 216, 236
 - free stream air, 209
 - friction and, 215
 - ideal, 48
 - ideal characteristics of, 46–47
 - incompressible flow, 213
 - internal area of, 225
 - internal diffuser recovery factor, 217
 - isentropic processes and, 209, 211, 213
 - lambda shocks, 226
 - Mach numbers and, 210, 212, 213, 216–217, 218–220, 221–223, 224
 - mass flow ratio, 227
 - modeling of, 489
 - non-ideal, 135
 - normal shocks and, 216, 217
 - objectives of, 209
 - oblique-conical shocks and, 220
 - oblique-planar shocks and, 218, 227
 - oblique shocks and, 225, 226, 232
 - off-design operation of, 227
 - one-dimensional flow method, 215
 - operation modes of, 226
 - performance map of, 235
 - pressure coefficient, 211, 213
 - pressure losses and, 209, 210, 214, 215, 217
 - pressure ratios and, 213, 214, 217, 235
 - pressure recovery factor, 135–137, 209, 210, 236
 - pressure rise limits, 211
 - separation and, 210, 211–212, 213
 - sonic condition, 232
 - spikes, 220

- pressure losses and, 471
 - See also* bypass mixer, by pass duct
- multiple spool engines, 18, 78, 91, 499
 - burners and, 448
 - compressors and, 312
 - critical speeds, 314
 - mechanical implementation of, 314
 - off-design operation and, 312
 - power and, 314
 - three spooled, 315
 - turbines and, 407
 - turbofans and, 20, 22
- Newton, Isaac, 4
- nozzles, 63, 65, 147, 150, 244
 - adiabatic processes and, 63–65, 147
 - afterburners and, 446
 - altitude and, 258–259, 264
 - area ratios, 245
 - choked, 149–150, 233–234, 245–246, 252–254
 - converging, 150, 245–246, 259
 - converging-diverging, 150, 161–163, 247, 259
 - converging-diverging, variable, 258, 262, 263, 490
 - corrected mass flow, 260
 - dimensional analysis and, 260
 - efficiency and, 148–149, 150, 245
 - engine performance and, 256
 - equations for, 244, 245
 - exit area, fixed, 262, 490
 - exit pressure, 147
 - fan, 65, 150, 245
 - fixed-converging, 261, 490
 - fixed minimum area, 263, 490
 - ideal, 63, 65
 - ideal characteristics of, 46–47
 - iris type, 258–259
 - isentropic processes and, 63–65
 - lambda shocks and, 249
 - Mach numbers and, 260, 261, 262, 263
 - mass flow and, 149, 260–262
 - materials used in, 244
 - modeling of, 489
 - overexpanded, 248–249
 - performance maps for, 260
 - performance of, 245
 - performance trends, 261
 - plug type, 258–260
 - pressure losses and, 148
 - pressure ratios and, 245, 256
 - schedules, 262–264
 - shock diamonds, 249
 - sonic conditions, 149
 - sonic line, 251
 - specific heats and, 245–246, 262
 - underexpanded, 247
 - See also* fan nozzles; thrust reversers; vectoring
- Ohain, Hans von, 6
- Papin, Denis, 4
- percent reaction, 618. *See also specific components*
- performance maps, 482
 - burners, 461
 - compressors, axial, 299
 - compressors, centrifugal, 390
 - diffusers, 235
 - nozzles, 260
 - turbines, 425
- performance measures, 41
- power generation gas turbines, 30, 119
 - component matching and, 486
 - compressor pressure ratio, 124
 - exhaust, 68, 153, 486
 - fuel ratios and, 499
 - inlet, 119, 486, 490
 - load system, 486
 - modeling of, 490, 491, 495
 - power of, 120
 - shaft loading and, 491
 - specific fuel consumption and, 121–122
 - thermal efficiency of, 121–122
- power generation measures, 42
- power turbine exhaust, ideal, 68
 - non-ideal, 153
- pressure ratios. *See specific components*
- propellers, 55, 143
 - advance ratio, 144
 - efficiency and, 143–144
 - fixed blades and, 144
 - flow direction, 143
 - ideal, 56
 - ideal characteristics of, 46–47
 - Mach numbers and, 58, 144
 - nonideal, 143
 - power coefficient, 58, 144
 - reversible pitch, 265
 - schedules for, 56
 - stresses on, 56
 - thrust and, 144
 - thrust coefficients and, 58
 - work coefficient and, 57
 - variable blades, 144
- propulsion performance measures, 41
- propulsive efficiency, 41
- pumps, 286, 288, 381, 384
 - slip and, 384
- ramjets, 16
 - afterburners and, 446
 - ideal, 71
- Rankine cycle, 15–16
- Rankine-Hugoniot equations, 602
- Rayleigh line flow, 456, 461, 598, 600
- Regula Falsi method, 585

- thermodynamic efficiency, 427
- turning angles, 410
- velocity polygons, 413, 419
- viscous shear, 409
- turbofans, 20, 25, 91, 471
 - afterburners and, 25, 98–102, 106–108
 - bypass ratios, 53, 93, 94, 95–98, 105–106
 - compressor pressure ratio, 93, 94–96, 105
 - efficiency of, 22
 - fan exhausted, 20, 25, 38, 91–102
 - fan mixed, 24, 25, 102–108
 - fan total pressure ratio, 94–98
 - fuel economy, 25
 - high bypass and, 406
 - ideal, 91
 - ideal thrust, 93, 94, 98, 102, 103–105, 107, 108, 111, 113
 - ideal *TSFC* and, 93–102, 105, 108–111, 113
 - Mach numbers, 94, 98–99, 103–105
 - mass flow and, 105
 - mixed-exhausted comparisons, 108
 - nonafterburning, 92–98, 102–106
 - pressure ratios and, 108
 - turbojets, compared, 108
- turbojets, 17
 - afterburners and, 84
 - altitude and, 83
 - compressor pressure ratio, 81–84, 86–87
 - fuel economy, 25
 - ideal, 78
 - ideal thrust, 81, 89–91
 - ideal *TSFC* and, 86–87, 89–91
 - inlet temperatures, 82–83
 - Mach numbers and, 83–84
 - mass flow and, 81
 - nonafterburning, 79
 - ramjets and, 84, 86–87
 - turbofans, compared, 108
- turbomachines
 - fundamentals of, 613
 - history of, 3
- turboprops, 27, 40, 113, 374
 - compressor pressure ratio, 116
 - gearboxes, 27, 56, 58, 374
 - ideal, 58
 - ideal thrust for, 113–116, 119
 - ideal *TSFC* and, 116, 119
 - reversible pitch propellers, 265
 - specific fuel consumption and, 116
 - work coefficient for, 115–116, 119
- turboshafts, 29, 374
- UDF. *See* unducted fan
- unducted fan (UDF), 29, 58, 113
- V2 rocket, 8
- vectoring, thrust, 267
- velocity polygons
 - compressors and, 283, 289, 332, 378, 386
 - turbines and, 413, 419
 - See also specific components*
- Whittle, Sir Frank, 6
- windmills, 3
- wind tunnels, 231–232, 234, 508